

Volume 7 No 2 2007

ISSN 1473-6691

Journal of the ICRU

ICRU REPORT 78

**Prescribing, Recording, and Reporting
Proton-Beam Therapy**



OXFORD UNIVERSITY PRESS

INTERNATIONAL COMMISSION ON
RADIATION UNITS AND
MEASUREMENTS

Journal of the ICRU

ISSN 1473-6691

Commission Membership

P. M. DeLuca (Chairman)
A. Wambersie (Vice Chairman)
S. M. Seltzer (Secretary)
P. Dawson
K. Doi
R. A. Gahbauer
M. Inokuti
D. T. L. Jones
H.-G. Menzel
B. D. Michael
H. G. Paretzke
H. Tatsuzaki
G. F. Whitmore
A. Allisy (Honorary Chairman)

Executive Secretary

P. L. Russell

Assistant Executive Secretary

L. J. Atwell

Managing Editors: ICRU Website and ICRU News

R. A. Gahbauer
D. T. L. Jones

Honorary Editor ICRU News

H. G. Ebert

Honorary Counsel

W. R. Ney

Journal of the ICRU Scientific Editor

M. Inokuti

SUBSCRIPTIONS

A subscription to Journal of the ICRU comprises 2 issues (Reports). All prices include postage, and for subscribers outside the UK delivery is by Standard Air.

Annual Subscription Rate (Volume 7, 2 issues, 2007)

Institutional

Print edition and site-wide online access: £194/\$350/€291

Print edition only: £184/\$332/€276

Site-wide online access only: £184/\$332/€276

Personal

Print only: £100/\$180/€150

Please note: £ Sterling or € Euro rates apply in Europe, US\$ elsewhere

Reports are available for purchase as single issues. Please see the Journal homepage: <http://jicru.oxfordjournals.org/>, and go to 'Purchase back reports of the ICRU'.

Full prepayment, in the correct currency, is required for all orders. Orders are regarded as firm and payments are not refundable. Subscriptions are accepted and entered on a complete volume basis. Claims cannot be considered more than FOUR months after publication or date of order, whichever is later. All subscriptions in Canada are subject to GST. Subscriptions in the EU may be subject to European VAT. If registered, please supply details to avoid unnecessary charges. For subscriptions that include online versions, a proportion of the subscription price may be subject to UK VAT. Personal rate subscriptions are only available if payment is made by personal cheque or credit card and delivery is to a private address.

Visit www.jicru.oxfordjournals.org for complete listing of previous reports available from Oxford University Press.

For further information, please contact: Journals Customer Service Department, Oxford University Press, Great Clarendon Street, Oxford OX2 6DP, UK. Email: jnlscust.serv@oxfordjournals.org. Tel (and answerphone outside normal working hours): +44 (0)1865 353907. Fax: +44 (0)1865 353485. **In the US, please contact:** Journals Customer Service Department, Oxford University Press, 2001 Evans Road, Cary, NC 27513, USA. Email: jnlorders@oxfordjournals.org. Tel (and answerphone outside normal working hours): 800 852 7323 (toll-free in USA/Canada). Fax: 919 677 1714. **In Japan, please contact:** Journals Customer Services, Oxford University Press, 1-1-17-5F, Mukogaoaka, Bunkyo-ku, Tokyo, 113-0023, Japan. Email: okudaoup@po.ijjnet.or.jp. Tel: (03) 3813 1461. Fax: (03) 3818 1522.

Methods of payment. Payment should be made: by cheque (to Oxford University Press, Cashiers Office, Great Clarendon Street, Oxford, OX2 6DP, UK); by bank transfer [to Barclays Bank Plc, Oxford Office, Oxford (bank sort code 20-65-18) (UK); overseas only Swift code BARC GB22 (GB£ Sterling Account no. 70299332, IBAN GB89BARC20651870299332; US\$ Dollars Account no. 66014600, IBAN GB27BARC20651866014600; EU€ EURO Account no. 78923655, IBAN GB16BARC20651878923655]; or by credit card (Mastercard, Visa, Switch or American Express).

Journal of the ICRU is published twice a year by Oxford University Press, Oxford, UK. Annual subscription price is £184/\$332/€276. Journal of the ICRU is distributed by Mercury International, 365 Blair Road, Avenel, NJ 07001, USA. Periodicals postage paid at Rahway, NJ and at additional entry points.

US Postmaster: send address changes to Journal of the ICRU, c/o Mercury International, 365 Blair Road, Avenel, NJ 07001, USA.

Permissions

For information on how to request permissions to reproduce articles/information from this journal, please visit www.oxfordjournals.org/jnls/permissions.

Dosage disclaimer

The mention of trade names, commercial products or organizations, and the inclusion of advertisements in the journal does not imply endorsement by the ICRU, the editors, the editorial board, Oxford University Press or the organization to which the authors are affiliated. The editors and publishers have taken all reasonable precautions to verify dosage, the results of experimental work and clinical findings published in the journal. The ultimate responsibility for the use and dosage of drugs mentioned in the Journal and in interpretation of published material lies with the medical practitioner, and the editors and publishers cannot accept liability for damages arising from any errors or omissions in the journal. Please inform the editors of any errors.

Legal Notice

This report was prepared by the International Commission on Radiation Units and Measurements, Inc. (ICRU). The Commission strives to provide accurate, complete and useful information in its reports. However, neither the ICRU, the members of the ICRU, Oxford University Press, other persons contributing to or assisting in the preparation of this report, nor any person acting on behalf of any of these parties: (a) makes any warranty or representation, express or implied, with respect to the accuracy, completeness or usefulness of the information contained in this report, or that the use of any information, method or process disclosed in this report may not infringe on privately owned rights; or (b) assumes any liability with respect to the use of, or for damages resulting from the use of any information, method or process disclosed in this report.

© International Commission on Radiation Units and Measurements 2007

All rights reserved; no part of this publication may be reproduced, stored in a retrieval system, or transmitted in any form or by any means, electronic, mechanical, photocopying, recording, or otherwise without prior written permission of the Publishers, or a licence permitting restricted copying issued in the UK by the Copyright Licensing Agency Ltd, 90 Tottenham Court Road, London W1P 9HE, or in the USA by the Copyright Clearance Center, 222 Rosewood Drive, Danvers, MA 01923. For those in the USA or Canada not registered with CCC, articles can be obtained by fax in 48 hours by calling: WISE for Medicine™ 1-800-667-WISE.

Typeset by Techset Composition (P) Ltd
Printed by Bell & Bain, Glasgow, UK

ICRU REPORT No. 78

PREScribing, RECORDing, AND REPORTING PROTON-BEAM THERAPY

**THE INTERNATIONAL COMMISSION ON
RADIATION UNITS AND
MEASUREMENTS**

Prepared jointly with the INTERNATIONAL ATOMIC ENERGY AGENCY
December 2007

Journal of the ICRU Volume 7 No 2 2007
ISBN 9780199543489
Published by Oxford University Press

ICRU 2015 -- All rights reserved.
AAPM Member Copy
Single use only, copying and networking prohibited.

PRESCRIBING, RECORDING, AND REPORTING PROTON-BEAM THERAPY

Report Committee

D. T. L. Jones (Co-Chair), iThemba LABS, Somerset West, South Africa
H. D. Suit (Co-Chair), Massachusetts General Hospital, Boston, Massachusetts, USA
Y. Akine, Proton Medical Radiation Center, Tsukuba, Japan
G. Goitein, Paul Scherrer Institute, Villigen, Switzerland
M. Goitein, Ankerstrasse 1, Windisch AG, Switzerland
N. Kanematsu, National Institute of Radiological Sciences, Chiba, Japan
R. L. Maughan, University of Pennsylvania, Philadelphia, Pennsylvania, USA
H. Tatsuzaki, National Institute of Radiological Sciences, Chiba, Japan
H. Tsujii, National Institute of Radiological Sciences, Chiba, Japan
S. M. Vatnitsky, International Atomic Energy Agency, Vienna, Austria

Commission Sponsors

P. M. DeLuca, Jr, University of Wisconsin, Madison, Wisconsin, USA
R. A. Gahbauer, A. James Cancer Hospital, Ohio State University, Columbus, Ohio, USA
A. Wambersie, Université Catholique de Louvain, Brussels, Belgium
G. F. Whitmore, Ontario Cancer Institute, Toronto, Ontario, Canada

International Atomic Energy Agency Sponsors

P. Andreo, International Atomic Energy Agency, Vienna, Austria
J. H. Hendry, International Atomic Energy Agency, Vienna, Austria

Consultants to the Report Committee

G. Coutrakon, Loma Linda University Medical Center, Loma Linda, California, USA
A. Lomax, Paul Scherrer Institute, Villigen, Switzerland
H. Paganetti, Massachusetts General Hospital, Boston, Massachusetts, USA
E. Pedroni, Paul Scherrer Institute, Villigen, Switzerland

The Commission wishes to express its appreciation to the individuals involved in the preparation of this report, for the time and efforts which they devoted to this task and to express its appreciation to the organizations with which they are affiliated.

All rights reserved. No part of this book may be reproduced, stored in retrieval systems or transmitted in any form by any means, electronic, electrostatic, magnetic, mechanical photocopying, recording or otherwise, without the permission in writing from the publishers.

British Library Cataloguing in Publication Data. A Catalogue record of this book is available at the British Library.

ISBN 9780199543489

THE INTERNATIONAL COMMISSION ON RADIATION UNITS AND MEASUREMENTS

INTRODUCTION

The International Commission on Radiation Units and Measurements (ICRU), since its inception in 1925, has had as its principal objective the development of internationally acceptable recommendations regarding:

- (1) quantities and units of radiation and radioactivity,
- (2) procedures suitable for the measurement and application of these quantities in clinical radiology and radiobiology, and
- (3) physical data needed in the application of these procedures, the use of which tends to assure uniformity in reporting.

The Commission also considers and makes similar types of recommendations for the radiation protection field. In this connection, its work is carried out in close cooperation with the International Commission on Radiological Protection (ICRP).

POLICY

The ICRU endeavors to collect and evaluate the latest data and information pertinent to the problems of radiation measurement and dosimetry and to recommend the most acceptable values and techniques for current use.

The Commission's recommendations are kept under continual review in order to keep abreast of the rapidly expanding uses of radiation.

The ICRU feels that it is the responsibility of national organizations to introduce their own detailed technical procedures for the development and maintenance of standards. However, it urges that all countries adhere as closely as possible to the internationally-recommended basic concepts of radiation quantities and units.

The Commission feels that its responsibility lies in developing a system of quantities and units having the widest possible range of applicability. Situations may arise from time to time when an expedient solution of a current problem may seem advisable. Generally speaking, however, the Commission feels that action based on expediency

is inadvisable from a long-term viewpoint; it endeavors to base its decisions on the long-range advantages to be expected.

The ICRU invites and welcomes constructive comments and suggestions regarding its recommendations and reports. These may be transmitted to the Chairman.

CURRENT PROGRAM

The Commission recognizes its obligation to provide guidance and recommendations in the areas of radiation therapy, radiation protection, and the compilation of data important to these fields, and to scientific research and industrial applications of radiation. Increasingly, the Commission is focusing on the problems of protection of the patient and evaluation of image quality in diagnostic radiology. These activities do not diminish the ICRU's commitment to the provision of a rigorously defined set of quantities and units useful in a very broad range of scientific endeavors.

The Commission is currently engaged in the formulation of ICRU reports treating the following subjects:

- Approaches to the Dosimetry of Low-Dose Exposures to Ionizing Radiation*
Assessment of Image Quality in Mammography
Design of a Voxel Phantom for Radiation Protection
Dose and Volume Specifications for Reporting Intra-Cavity Therapy in Gynecology
Dose Distributions in Normal Tissues Distant from the PTV in Radiation Therapy
Doses from Cosmic-Ray Exposures of Aircrew
Dosimetry Systems for Use in Radiation Processing
Fundamental Quantities and Units
Harmonization of Reporting Patient Diagnostic Doses
Image Quality and Patient Dose in Computed Tomography
Key Data for Measurement Standards in the Dosimetry of Ionizing Radiation
Prescribing, Recording, and Reporting Intensity-Modulated Photon-Beam Radiation Therapy (IMRT)
Prescribing, Recording, and Reporting Ion-Beam Therapy

PRESCRIBING, RECORDING, AND REPORTING PROTON-BEAM THERAPY

Quantitative Aspects of Bone Densitometry ROC (Receiver Operator Characteristic) Analysis in Medical Imaging

In addition, the ICRU is evaluating the possibility of expanding its program to encompass nonionizing radiation, particularly the quantities and units aspects.

The Commission continually reviews radiation science with the aim of identifying areas where the development of guidance and recommendations can make an important contribution.

THE ICRU'S RELATIONSHIP WITH OTHER ORGANIZATIONS

In addition to its close relationship with the ICRP, the ICRU has developed relationships with other organizations interested in the problems of radiation quantities, units, and measurements. Since 1955, the ICRU has had an official relationship with the World Health Organization (WHO), whereby the ICRU is looked to for primary guidance in matters of radiation units and measurements and, in turn, the WHO assists in the worldwide dissemination of the Commission's recommendations. In 1960, the ICRU entered into consultative status with the International Atomic Energy Agency (IAEA). The Commission has a formal relationship with the United Nations Scientific Committee on the Effects of Atomic Radiation (UNSCEAR), whereby ICRU observers are invited to attend annual UNSCEAR meetings. The Commission and the International Organization for Standardization (ISO) informally exchange notifications of meetings, and the ICRU is formally designated for liaison with two of the ISO technical committees. The ICRU also enjoys a strong relationship with its sister organization, the National Council on Radiation Protection and Measurements (NCRP). In essence, these organizations were founded concurrently by the same individuals. Presently, this long-standing relationship is formally acknowledged by a special liaison agreement. The ICRU also corresponds and exchanges final reports with the following organizations:

Bureau International de Métrologie Légale
Bureau International des Poids et Mesures
European Commission
Council for International Organizations of Medical Sciences
Food and Agriculture Organization of the United Nations
International Committee of Photobiology
International Council for Science
International Electrotechnical Commission
International Labor Organization
International Organization for Medical Physics

International Radiation Protection Association
International Union of Pure and Applied Physics
United Nations Educational, Scientific and Cultural Organization

The Commission has found its relationship with all of these organizations fruitful and of substantial benefit to the ICRU program.

OPERATING FUNDS

In recent years, principal financial support has been provided by the European Commission, the National Cancer Institute of the US Department of Health and Human Services and the International Atomic Energy Agency. In addition, during the last 10 years, financial support has been received from the following organizations:

American Association of Physicists in Medicine
Belgian Nuclear Research Centre
Canadian Nuclear Safety Commission
Eastman Kodak Company
Electricité de France
Fuji Medical Systems
Helmholtz Zentrum München
Hitachi, Ltd.
International Radiation Protection Association
International Society of Radiology
Ion Beam Applications, S.A.
Italian Radiological Association
Japan Industries Association of Radiological Systems
Japanese Society of Radiological Technology
MDS Nordin
National Institute of Standards and Technology
Nederlandse Vereniging voor Radiologie
Philips Medical Systems, Incorporated
Radiation Research Society
Radiological Society of North America
Siemens Medical Solutions
Varian Medical Systems

In addition to the direct monetary support provided by these organizations, many organizations provide indirect support for the Commission's program. This support is provided in many forms, including, among others, subsidies for (1) the time of individuals participating in ICRU activities, (2) travel costs involved in ICRU meetings, and (3) meeting facilities and services.

In recognition of the fact that its work is made possible by the generous support provided by all of the organizations supporting its program, the Commission expresses its deep appreciation.

Paul M. DeLuca
Chairman, ICRU
Madison, Wisconsin, USA
AAPM Member Copy
Single use only, copying and networking prohibited.

PRESCRIBING, RECORDING, AND REPORTING PROTON-BEAM THERAPY

CONTENTS

ACKNOWLEDGMENTS	i
PREFACE	1
ABSTRACT	3
EXECUTIVE SUMMARY	5
1 INTRODUCTION	11
1.1 Principles of proton therapy	11
1.1.1 Physical characteristics	11
1.1.2 Biological effects	15
1.1.3 Clinical evaluations	15
1.2 History of proton therapy	16
1.3 Present status	17
2 RADIATION BIOLOGY CONSIDERATIONS	21
2.1 Introduction	21
2.2 Microdosimetry and linear energy transfer	21
2.3 Review of published proton RBE values	21
2.3.1 RBE values determined using <i>in vitro</i> and <i>in vivo</i> systems	23
2.3.2 RBE versus depth for 60–250 MeV beams	24
2.3.2.1 60–85 MeV	24
2.3.2.2 160–250 MeV	25
2.3.2.3 RBE on the declining distal edge of the SOBP	25
2.4 Use of a generic RBE value	26
2.5 Dose specification	27
2.5.1 The RBE-weighted absorbed dose (D_{RBE})	28
3 BEAM DELIVERY AND PROPERTIES	29
3.1 Proton-therapy facilities	29
3.2 The treatment-delivery system	29
3.2.1 The beam nozzle and snout	29
3.2.1.1 Passive beam-delivery techniques	29
3.2.1.2 Dynamic beam-delivery techniques	32
3.2.1.2.1 Wobbled beams	35
3.2.1.2.2 Repainting	35
3.2.2 Patient support and positioning	36
3.2.3 Special treatment techniques	36

3.2.3.1	<i>Eye treatments</i>	36
3.2.3.2	<i>Stereotactic radiosurgery and stereotactic radiotherapy</i>	37
3.2.4	<i>Rotating gantries</i>	37
3.3	Accelerators	38
3.3.1	<i>Linear accelerators</i>	39
3.3.2	<i>Cyclotrons, isochronous cyclotrons, and synchrocyclotrons</i>	39
3.3.3	<i>Synchrotrons</i>	41
3.3.4	<i>Typical accelerator operating parameters</i>	42
3.4	The properties of proton beams	43
3.4.1	<i>Proton interactions with matter</i>	43
3.4.2	<i>Definition and specification of beam properties and beam parameters</i>	43
3.4.2.1	<i>Beam properties</i>	44
3.4.2.2	<i>Beam parameters</i>	44
3.5	Radiation quality	46
4	DOSIMETRY	49
4.1	General considerations	49
4.2	Reference dosimetry with a Faraday cup	50
4.3	Reference dosimetry with a calorimeter	54
4.4	Reference dosimetry with ionization chambers having ^{60}Co calibration coefficients	57
4.4.1	<i>ICRU proton dosimetry protocol (ICRU 59)</i>	57
4.4.1.1	<i>Physical quantities for ICRU 59</i>	58
4.4.2	<i>IAEA proton dosimetry code of practice (TRS 398)</i>	59
4.4.2.1	<i>Physical quantities for TRS 398</i>	61
4.4.3	<i>Considerations concerning dry and humid air</i>	62
4.4.4	<i>The value of w/e in air for proton beams</i>	64
4.4.4.1	<i>Definitions</i>	64
4.4.4.2	<i>Determination of the $w(E)$ value</i>	65
4.4.5	<i>Comparison of proton dosimetry protocols</i>	66
4.4.6	<i>Relation between absorbed dose to water and air-kerma calibration coefficients</i>	68
4.5	Reference dosimetry for scanned beams	69
4.6	Ionization-chamber dosimetry comparisons	69
4.7	Beam monitoring	70
4.7.1	<i>Ionization chambers</i>	71
4.7.2	<i>Position and dose uniformity</i>	72
4.7.3	<i>Considerations for scanned beams</i>	73
4.7.4	<i>Secondary-emission monitors</i>	73
4.7.5	<i>Range/energy measurements</i>	74
4.8	Relative dosimetry	74
4.8.1	<i>Phantom materials</i>	74
4.8.2	<i>Detectors for dose-distribution measurements</i>	75
4.8.2.1	<i>Single ionization chambers</i>	76
4.8.2.2	<i>Silicon diodes</i>	76
4.8.2.3	<i>Radiographic films</i>	77
4.8.2.4	<i>Alanine</i>	77
4.8.2.5	<i>Other detectors</i>	78
4.8.3	<i>Determination of dose distributions</i>	80
4.8.3.1	<i>Range and depth-dose characteristics</i>	80
4.8.3.2	<i>Beam profiles and penumbrae</i>	81
5	GEOMETRIC TERMS, AND DOSE AND DOSE–VOLUME DEFINITIONS	83
5.1	Anatomic volumes relating to the tumor	83

CONTENTS

5.1.1	<i>Gross tumor volume (GTV)</i>	83
5.1.2	<i>Clinical target volume (CTV)</i>	84
5.1.2.1	<i>The dose intention for the CTV</i>	84
5.1.3	<i>Internal target volume (ITV)</i>	85
5.1.4	<i>Planning target volume (PTV)</i>	85
5.1.4.1	<i>Margins for the different types of variations and uncertainties</i>	85
5.1.4.2	<i>Delineating the PTV</i>	86
5.1.4.3	<i>Multiple PTVs</i>	86
5.1.4.4	<i>Proton-specific issues regarding the PTV</i>	86
5.2	Anatomic volumes relating to unininvolved normal tissues and organs	87
5.2.1	<i>Organ at risk (OAR)</i>	87
5.2.2	<i>Planning organ at risk volume (PRV)</i>	87
5.2.3	<i>Remaining volume at risk (RVR)</i>	88
5.3	Generic geometric terms	88
5.3.1	<i>Volume of interest (VOI)</i>	88
5.3.2	<i>Target volume (TV)</i>	88
5.3.3	<i>Surface of interest (SOI)</i>	88
5.3.4	<i>Point of interest (POI)</i>	88
5.4	Nomenclature	89
5.4.1	<i>Multiple GTVs, CTVs, and PTVs</i>	89
5.4.1.1	<i>One GTV plus a surrounding volume intended to receive the same dose</i>	89
5.4.1.2	<i>One GTV plus a surrounding volume intended to receive a lower dose</i>	89
5.4.1.3	<i>No GTV</i>	89
5.4.1.4	<i>Two spatially separated GTVs</i>	90
5.4.1.5	<i>Two nested GTVs plus a region of possible microscopic disease</i>	90
5.4.1.6	<i>Reduced tumor dose in a region closely adjacent to an OAR</i>	91
5.4.2	<i>Multiple OARs and PRVs</i>	91
5.4.3	<i>Number of RVRs</i>	91
5.4.4	<i>Qualification of geometric terms</i>	91
5.4.4.1	<i>Tumor, nodal, or metastatic basis for a target volume</i>	91
5.5	Variation of geometry with time	91
5.6	Dose and dose-volume related definitions	92
5.6.1	<i>One-dimensional dose and dose-volume summarization</i>	92
5.6.1.1	<i>The volume receiving at least a specified dose (V_D)</i>	92
5.6.1.2	<i>The least dose received by a specified volume (D_V)</i>	93
5.6.1.3	<i>Other dose measures</i>	93
5.6.2	<i>Two-dimensional dose-volume summarization</i>	93
5.6.2.1	<i>Two-dimensional dose displays</i>	93
5.6.2.2	<i>Dose-volume histograms (DVH)</i>	93
5.6.2.3	<i>Dose-area histograms (DAH)</i>	93
5.6.3	<i>Prescribed dose</i>	93
5.6.3.1	<i>Prescribed dose for multiple PTVs</i>	94
5.6.3.2	<i>Prescribed dose for multiple treatment segments (segment dose)</i>	94
5.6.4	<i>Relative dose</i>	94
5.6.5	<i>Treated volume</i>	94
5.6.6	<i>Conformity index (CI)</i>	94
5.6.7	<i>Irradiated volume (at a specified dose)</i>	94
6	TREATMENT PLANNING	95
6.1	Introduction	95
6.2	What is different about planning proton-beam therapy?	95
6.2.1	<i>Heterogeneities</i>	95
6.2.2	<i>Beam-delivery techniques</i>	96

6.2.3	<i>Single beams</i>	96
6.2.3.1	<i>Inverse beam design</i>	96
6.2.3.2	<i>Selection of beam directions</i>	96
6.2.3.3	<i>The PTV</i>	96
6.2.3.4	<i>The proton RBE</i>	97
6.2.3.5	<i>The design of beam-modifying devices</i>	97
6.2.3.6	<i>Repainting</i>	97
6.2.3.7	<i>Dose algorithms</i>	97
6.2.4	<i>Plans</i>	97
6.2.4.1	<i>Number of beams</i>	97
6.2.4.2	<i>Intensity-modulated proton therapy (IMPT)</i>	98
6.2.4.3	<i>Imaging</i>	98
6.2.4.4	<i>Positioning accuracy, immobilization, and localization</i>	98
6.2.4.5	<i>Uncertainty analysis</i>	98
6.2.4.6	<i>Target volume size</i>	99
6.2.5	<i>Quality assurance</i>	99
6.3	The patient's anatomy	99
6.4	Heterogeneities	100
6.4.1	<i>Introduction</i>	100
6.4.2	<i>Interactions of protons in matter</i>	100
6.4.2.1	<i>Mass thickness</i>	100
6.4.2.2	<i>Energy loss</i>	100
6.4.2.2.1	<i>Water-equivalent density</i>	100
6.4.2.3	<i>Multiple Coulomb scattering</i>	101
6.4.3	<i>Bulk heterogeneity intersecting the full beam</i>	101
6.4.4	<i>Bulk heterogeneity partially intersecting the beam</i>	102
6.4.5	<i>Complexly structured heterogeneities</i>	102
6.4.6	<i>Compensation for heterogeneities</i>	103
6.4.6.1	<i>Conversion from CT Hounsfield number to water-equivalent density</i>	103
6.4.6.1.1	<i>Direct-fit method</i>	104
6.4.6.1.2	<i>Stoichiometric method</i>	104
6.4.6.1.3	<i>Confirmation of calibration</i>	104
6.4.6.1.4	<i>Accuracy</i>	105
6.4.6.2	<i>Design of compensators</i>	105
6.4.6.2.1	<i>Choice of range</i>	106
6.4.6.2.2	<i>Compensator design close to, and outside, the projected target boundary</i>	106
6.4.6.2.3	<i>Real and virtual compensators</i>	107
6.4.6.2.4	<i>The effect of an air gap between compensator and patient</i>	107
6.4.6.2.5	<i>High-Z heterogeneities</i>	107
6.5	Design of individual proton beams	108
6.5.1	<i>Compensation for heterogeneities</i>	108
6.5.1.1	<i>Choosing beam directions</i>	108
6.5.1.2	<i>Tangential irradiation</i>	108
6.5.2	<i>Categories of models for dose computation</i>	108
6.5.2.1	<i>Uniform-intensity beam algorithms</i>	109
6.5.2.2	<i>Pencil-beam algorithms</i>	109
6.5.2.3	<i>Monte Carlo algorithms</i>	109
6.5.3	<i>Normalization and the calculation of monitor units</i>	110
6.6	Design of groups of beams: the treatment plan	110
6.6.1	<i>Treatment goals and constraints</i>	110
6.6.1.1	<i>Setting goal(s) and constraints</i>	110
6.6.1.2	<i>Establishing a score combining target-volume and normal-tissue effects</i>	110

CONTENTS

6.6.1.3	<i>Target-volume goals and constraints</i>	111
6.6.1.4	<i>Normal-tissue constraints</i>	111
6.6.2	<i>Approaches to treatment design</i>	111
6.6.2.1	<i>Uniform-intensity radiation therapy</i>	111
6.6.2.2	<i>Intensity-modulated radiation therapy (IMRT)</i>	112
6.7	Plan assessment	112
6.7.1	<i>Inspection of the dose distribution</i>	112
6.7.2	<i>Clinical feasibility</i>	113
6.7.3	<i>Dose-summarizing quantities</i>	113
6.8	Plan comparison	113
6.8.1	<i>Plan comparison by inspection</i>	114
6.8.2	<i>Automated plan comparison</i>	114
6.9	Plan optimization	115
6.10	Comparison of uniform-intensity versus IMPT treatment plans	115
6.11	Special techniques	118
6.11.1	<i>Intraocular treatments with protons</i>	118
6.11.1.1	<i>Model of the patient anatomy</i>	118
6.11.1.2	<i>Beam simulation</i>	118
6.11.1.3	<i>Output of the planning process</i>	118
6.11.1.4	<i>Presentation of results</i>	118
6.11.1.5	<i>Treatment example</i>	118
6.11.2	<i>Stereotactic treatments with protons</i>	119
6.11.2.1	<i>Immobilization</i>	119
6.11.2.2	<i>Imaging</i>	121
6.11.2.3	<i>Planning</i>	121
6.11.2.4	<i>Treatment</i>	122
7	MOTION MANAGEMENT	123
7.1	Motion of, and within, the patient	123
7.2	Support and immobilization	123
7.2.1	<i>Proton-specific aspects of immobilization</i>	123
7.2.2	<i>Immobilization techniques</i>	124
7.3	Localization	124
7.3.1	<i>Localization based on skin marks</i>	124
7.3.2	<i>Localization based on bony anatomy</i>	124
7.3.3	<i>Localization relative to the immobilization device</i>	125
7.3.4	<i>Localization based on identification of target-volume markers or the tumor itself</i>	125
7.4	Verification	125
7.4.1	<i>Verification using radiography</i>	125
7.4.2	<i>Verification using positron emission tomography</i>	125
7.5	Organ motion	126
7.5.1	<i>The measurement of organ motion</i>	126
7.5.2	<i>Organ motion in the absence of special measures</i>	126
7.5.3	<i>Organ motion under conditions of respiration gating</i>	126
7.5.4	<i>Organ motion with tumor tracking</i>	127
7.6	Compensation for patient and organ motion	127
7.6.1	<i>Margins at the periphery of the CTV or OARs: lateral margins</i>	127
7.6.2	<i>Margins at the periphery of the CTV or OARs: margin in depth</i>	128
7.6.3	<i>Dose variation within the CTV and OARs: interplay effects</i>	128
7.6.3.1	<i>Experimental observation of interplay effects</i>	129
7.6.3.2	<i>Repainting to reduce the influence of interplay effects</i>	130
7.7	Conclusion	130

8 ESTIMATION AND PRESENTATION OF UNCERTAINTY IN THE DELIVERED DOSE	131
8.1 The inevitability of uncertainty	131
8.2 The estimation of uncertainty	131
8.3 The presentation of uncertainty	132
8.4 Recommendations for the consideration and reporting of uncertainty	134
9 QUALITY ASSURANCE	135
9.1 Proton beam-delivery systems	135
9.2 Patient positioning and immobilization	137
9.3 Treatment-planning systems	137
9.4 Examples of periodic checks	139
10 PRESCRIBING, RECORDING, AND REPORTING TREATMENT	141
10.1 Introduction	141
10.2 General recommendations for prescribing, recording, and reporting	141
10.2.1 The components of prescribing, recording, and reporting a patient's treatment	141
10.2.2 Planning aims	141
10.2.2.1 Specifying planning aims	141
10.2.2.2 Normal-tissue constraints	142
10.2.2.3 Selection of treatment approach: the treatment plan	143
10.3 Prescribing proton-beam therapy	143
10.3.1 General approaches to prescribing	143
10.3.2 The prescription	143
10.3.3 General recommendations for prescribing	143
10.3.4 Approval of the prescription and technical data	143
10.4 Additional aspects of prescribing, recording, and reporting	149
10.4.1 Therapy equipment	149
10.4.2 Beam-shaping techniques	149
10.4.3 Techniques for dealing with heterogeneities	149
10.4.4 Margins	149
10.5 Recording proton-beam therapy	149
10.5.1 The treatment record	149
10.5.2 The patient's record	149
10.6 Reporting the treatment of a single patient	149
10.6.1 Reporting proton-beam therapy	149
10.6.2 Patient-specific reports	150
10.6.2.1 The initial medical note	150
10.6.2.2 The completion note	150
10.6.2.3 Summary report to the referring physician	150
10.6.2.4 Case report	150
10.6.2.5 Detailed report to a physician	150
10.7 Reporting proton-beam therapy for a series of patients	150
APPENDIX A IMPLEMENTATION OF THE TRS 398 CODE OF PRACTICE FOR IONIZATION CHAMBER DOSIMETRY	151
A.1 Calibration of ionization chambers	151
A.1.1 Calibration in a ^{60}Co beam	151
A.2 Reference dosimetry in the user proton beam	153
A.2.1 Determination of the absorbed dose to water	153
A.2.2 Practical considerations for measurements in the proton beam	153
A.2.3 Corrections for influence quantities	153

CONTENTS

A.2.3.1 <i>Temperature, pressure, and humidity</i>	153
A.2.3.2 <i>Electrometer calibration</i>	154
A.2.3.3 <i>Polarity effect</i>	154
A.2.3.4 <i>Ion recombination</i>	154
A.3 Dosimetry worksheet (IAEA, 2000)	157
APPENDIX B CLINICAL EXAMPLES	159
Case number B.1 Uveal melanoma	160
<i>General patient information</i>	160
<i>Medical evaluation of presenting lesion</i>	160
<i>General medical evaluation</i>	160
<i>Treatment intent</i>	160
<i>Treatment planning</i>	161
<i>Patient immobilization and positioning</i>	161
<i>Treatment prescription</i>	161
<i>Treatment technique</i>	162
<i>Quality assurance</i>	162
<i>Equipment</i>	162
<i>Total doses delivered</i>	163
<i>Patient status at completion of treatment</i>	163
<i>Addendum: technical information</i>	163
Case number B.2 Adenocarcinoma of prostate	164
<i>General patient information</i>	164
<i>Medical evaluation of presenting lesion</i>	164
<i>General medical evaluation</i>	164
<i>Treatment intent</i>	164
<i>Treatment planning</i>	164
<i>Patient immobilization and positioning</i>	164
<i>Treatment prescription</i>	165
<i>Treatment technique</i>	165
<i>Quality assurance</i>	165
<i>Equipment</i>	165
<i>Total doses delivered</i>	166
<i>Patient status at completion of treatment</i>	167
<i>Addendum: technical information</i>	167
Case number B.3 Carcinoma of lung	168
<i>General patient information</i>	168
<i>Medical evaluation of presenting lesion</i>	168
<i>General medical evaluation</i>	168
<i>Treatment intent</i>	168
<i>Treatment planning</i>	168
<i>Patient immobilization and positioning</i>	169
<i>Treatment prescription</i>	169
<i>Treatment technique</i>	169
<i>Quality assurance</i>	170
<i>Equipment</i>	171
<i>Total doses delivered</i>	171
<i>Patient status at completion of treatment</i>	171
<i>Addendum: technical information</i>	171
Case number B.4 Acoustic neuroma	172
<i>General patient information</i>	172
<i>Medical evaluation of presenting lesion</i>	172
<i>General medical evaluation</i>	172
<i>Treatment intent</i>	172

<i>Treatment planning</i>	172
<i>Patient immobilization and positioning</i>	174
<i>Treatment prescription</i>	174
<i>Treatment technique</i>	175
<i>Quality assurance</i>	175
<i>Equipment</i>	175
<i>Total doses delivered</i>	175
<i>Patient status at completion of treatment</i>	175
<i>Addendum: technical information</i>	176
Case number B.5 Medulloblastoma (pediatric)	177
<i>General patient information</i>	177
<i>Medical evaluation of presenting lesion</i>	177
<i>General medical evaluation</i>	177
<i>Treatment intent</i>	177
<i>Treatment planning</i>	177
<i>Patient immobilization and positioning</i>	178
<i>Treatment prescription</i>	179
<i>Treatment technique</i>	181
<i>Quality assurance</i>	181
<i>Equipment</i>	181
<i>Total doses delivered</i>	181
<i>Patient status at completion of treatment</i>	182
<i>Addendum: technical information</i>	183
Case number B.6 Skull-base chordoma	185
<i>General patient information</i>	185
<i>Medical evaluation of presenting lesion</i>	185
<i>General medical evaluation</i>	185
<i>Treatment intent</i>	185
<i>Treatment planning</i>	185
<i>Patient immobilization and positioning</i>	186
<i>Treatment prescription</i>	186
<i>Treatment technique</i>	186
<i>Quality assurance</i>	186
<i>Equipment</i>	186
<i>Total doses delivered</i>	187
<i>Patient status at completion of treatment</i>	188
<i>Addendum: technical information</i>	188
REFERENCES	189

ACKNOWLEDGEMENTS

The International Commission on Radiation Units and Measurements gratefully acknowledges the generous contributions to the production of the present report by:

Hitachi, Ltd.

7-2-1 Omika-cho

Hitachi-shi

Ibaraki-ken

319-1221 JAPAN

Ion Beam Applications S.A.

Chemin du Cyclotron 3

B-1348 Louvain-la-Neuve

BELGIUM

Siemens Medical Solutions

Henkestrasse 127

D-91052 Erlangen

FEDERAL REPUBLIC OF GERMANY

PREFACE

The current report on proton therapy is the latest in a series of ICRU reports dealing with prescribing, recording, and reporting of external-beam radiation therapy. This joint report of the ICRU and the IAEA highlights the long and effective collaboration between the two organizations.

Robert R. Wilson was the first to recognize the potential advantage of protons and light ions for external-beam radiation (Wilson, 1946). In this benchmark publication, Wilson outlined all the advantages that protons and light ions would offer due in large part to their physical dose distributions. At the energies used for therapy, protons interact almost exclusively with atomic electrons in Coulomb force collisions yielding nearly straight trajectories culminating in a rapid increase in energy loss near the end of range, and thus forming the so-called Bragg peak. Essentially, no energy is deposited beyond the end of range and there is a very sharp distal dose fall-off. Despite these significant physical dose-distribution advantages, the initial clinical use of protons was modest as accelerators capable of producing 200–300 MeV/u protons were limited to large physics laboratories. Even so, the clinical experience grew systematically, facilitated by the advent of accelerators suitable for hospital-based installations in the mid 1990s.

Anticipating the wider clinical use of protons, the ICRU published Report 59, *Clinical Proton Dosimetry Part I: Beam Production, Beam Delivery and Measurement of Absorbed Dose*, in 1998. Report 59 noted that, while protons require some definitions and approaches that emphasize the advantages of the physical dose distribution, for the most part proton therapy could be and was delivered in a manner typical of conventional radiation therapy. Radiation treatment of solid tumors has advanced dramatically since ICRU published Report 59. Advances in image science have had an enormous impact. Four-dimensional data, time plus three-dimensional high-resolution volume information, largely from computerized tomography (CT) and magnetic resonance imaging (MRI), provide finely resolved anatomical detail. MRI, positron-emission tomography (PET), and

PET/CT image sets provide complementary physiological information.

The use of these dramatic advances to effect the desired improvements in radiation therapy requires similar advances in the delivery of absorbed dose. Photon treatment from a narrow range of beam directions with a limited selection of field shapes can never achieve the desired outcome. Only with the use of large numbers of small, variable-intensity beamlets delivered from multiple directions can three-dimensional absorbed dose distributions approach the resolution of the imaging data. This technique is called intensity-modulated radiation therapy (IMRT). Protons, by virtue of their physical dose distributions, can produce three-dimensional dose distributions similar to typical IMRT treatment regimes using beam-delivery schemes less complex than photon IMRT. Much of the justification for using protons is the relative ease of creating three-dimensional dose distributions that are highly conformal to the tumor volume with a concomitant reduction in total dose. With some increase in beam-delivery complexity, protons can also be used for IMRT. In this changed environment, the specification of appropriate therapeutic volumes for reporting treatments requires new approaches and more elaborate interpretations.

Recognizing these advances and their implications, ICRU initiated the creation of the present report dealing with proton therapy and a related report dealing with high-energy photon IMRT. Throughout the process of report creation, the committees worked closely to ensure a consistent and coordinated scientific approach.

Compared with high-energy photons and electrons, protons exhibit a modest increase in relative biological effectiveness (RBE) related to their somewhat higher linear energy transfer (LET) values. The LET values for swift protons are similar to photons, but increase somewhat near the end of range. Thus, for equivalent doses and dose distributions, the response of tissues is similar, in fact almost clinically indistinguishable from conventional photon therapy. However, in several locations in the clinical proton beam, *e.g.*, on the distal edge of the spread-out Bragg peak (SOBP) and in the lateral penumbra, slow protons create mean LET

values well in excess of $10 \text{ keV } \mu\text{m}^{-1}$, introducing a different biological response to protons compared with conventional low-LET radiations. Significant numbers of these higher LET protons are limited to a small-volume irradiated region. While their significance is still a matter of debate from a clinical viewpoint, this report, based on long clinical experience and biological evidence, suggests the use of a uniform RBE value of 1.10 throughout the treatment volume. This is a core recommendation of this report. This RBE value is assumed to be independent of dose fractionation, fraction size, and other routine variations in the clinical treatment strategy. Although these assumptions are not strictly correct, they are of modest clinical significance as the RBE value is near unity.

In this report, the product of the absorbed dose and RBE is called the RBE-weighted absorbed dose with the special unit of gray (Gy). Historically, proton therapy centers have often used the annotation of CGE, GyE, or Gy(E) to indicate the RBE-weighted absorbed dose, *e.g.*, ‘...the RBE-weighted dose was 70 GyE’. Such modifications of a fundamental or special unit are not acceptable in the SI context. Moreover, the use of the symbol E with the connotation of ‘equivalent’ can easily lead to confusion as to what equivalence is being discussed or specified. In the present report, when indicating the absorbed dose the explicit language such as ‘the absorbed dose was 63 Gy’ or ‘ $D = 63 \text{ Gy}$ ’ is appropriate. When RBE-weighted dose is expressed, the ICRU recommends the use of: ‘the RBE-weighted dose was 70 Gy (RBE)’ or ‘ $D_{\text{RBE}} = 70 \text{ Gy (RBE)}$ ’. In each case, the unit is Gy and the RBE weighting is indicated by explicit language or subscripting and by appending ‘(RBE)’, which is clearly separated from the base unit. The language is unambiguous as to whether physical dose or RBE-weighted dose is used. When possible and important for clarity, both RBE-weighted and physical dose should be specified. This situation highlights the issue that RBE corrections are only one of a variety of modifications to the physical dose needed to account for other therapeutic features such as dose fractionation or total treatment time if one wishes to refer back to a standard therapeutic regime.

Over time, the ICRU has systematically defined various volumes essential for the reporting and recording of external-beam radiation treatments, seen, for example, in ICRU Reports 50, 62, and 71. Some volumes relate to the tumor and various critical organs, whereas others relate to the uncertainties of position of anatomic volumes with respect to treatment beams. Recognizing the limitation of reporting dose at a point, the present report recommends the use, recording, and reporting of

dose-volume metrics derived from dose-volume histograms. Such reporting is essential when the physical-absorbed dose distribution includes steep dose gradients and the therapeutic treatment plans are fully three-dimensional in scope. In fact, clinically-valid comparisons between different therapeutic regimes, *e.g.*, protons, heavy ions, and IMRT with high-energy photons, require this sophisticated three-dimensional and even four-dimensional recording and reporting. In an appendix, this report gives several examples of clinical reporting that are comprehensive, detailed, and based on recommendations contained in the present report.

Subsequent to the publication of ICRU Report 59, several issues surrounding dosimetry protocols and values of various physical parameters arose. In some ways, proton dosimetry protocols are more simplistic than those for energetic photons or electrons. Many of the complex issues of secondary charged-particle transport that affect cavity theory are dramatically reduced. However, these issues are replaced with greater uncertainty in three fundamental quantities, proton-stopping power, either relative or absolute, proton range, and the mean proton energy loss needed to create an ion-pair, W/e . As discussed in this report, adoption of the IAEA dosimetry protocol described in the IAEA Technical Reports Series No. 398, *Absorbed Dose Determination in External Beam Therapy. An International Code of Practice for Dosimetry Based on Standards of Absorbed Dose to Water* (2000) is recommended. This protocol was developed subsequent to the publication of Report 59 and is suitable for use in most proton applications. Besides the dosimetry protocol, the treatment of the W/e value is discussed in detail. For a proton SOBP of the type used in typical therapeutic applications, a range of protons with different energies, E , is present at different locations in the SOBP. Since the proton differential $w(E)/e$ value is not independent of E , $W(E)/e$ is not constant and increases for lower proton speeds. The choice of the most appropriate $W(E)/e$ value is a challenge. These considerations and improved measurements of W/e based on calorimetric techniques subsequent to the publication of ICRU Report 59, led to improved recommendations of W/e for proton clinical dosimetry. These recommendations have been fully adopted in the present report. At the present moment, proton physical-absorbed dose can be determined with an absolute uncertainty of <3 percent for relevant clinical conditions.

Paul M. DeLuca Jr
André Wambersie
Gordon Whitmore

ABSTRACT

Proton therapy is a fast-expanding modality and the number of new facilities is rapidly increasing. The advantage of proton beams relative to conventional photon beams for radiation therapy lies in their superior dose distributions. The efficacy of proton therapy is well established for several tumor categories. The present report provides information necessary to standardize techniques and procedures and to harmonize the clinical descriptions of proton treatments with those of other modalities. The concepts and recommendations in other ICRU reports concerning radiation therapy are extended to proton therapy.

The topics covered here include the rationale for as well as the history of proton therapy, proton radiation biology, proton-beam delivery and properties, dosimetry, geometric and dose–volume terms, treatment planning, uncertainties in dose delivery, motion management, quality assurance, and prescribing, recording, and reporting treatment. In addition, six clinical examples of proton-beam

therapy are provided to illustrate the application of the recommendations contained in this report.

Recommendations in the report include the use of a generic relative biological effectiveness (RBE) value of 1.1 and the adoption of the IAEA TRS (Technical Report Series) 398 code of practice as the standard proton dosimetry protocol. The concept of RBE-weighted absorbed dose (D_{RBE} , the product of proton-absorbed dose, D , and proton RBE) is introduced to estimate the photon dose that would produce the same therapeutic effect as the proton-absorbed dose, D , given under identical conditions.

As the present report describes in some detail the radiobiological, physical, technical, treatment-planning, and clinical aspects of proton beam therapy, it should be a useful reference for current practitioners and should also provide new and potential users, as well as other interested readers, with the basic background to enable them to understand the techniques involved in proton therapy.

EXECUTIVE SUMMARY

The rationale for using protons for radiation therapy lies in their physical properties (*i.e.*, near-zero dose distal to the target volume and the resultant capability of conforming the planned dose more closely to the specified target volume than is feasible by photon techniques). The biological effects of proton beams have no known or predicted advantages. The depth-dose curve for a monoenergetic proton beam exhibits a relatively flat low-dose entrance region (the plateau) followed by a sharp high-dose peak (the Bragg peak), just beyond which the particles lose the remainder of their energy in a few millimeters. For planning of conventional proton-beam therapy, the distribution of proton energies is designed to provide a near-uniform dose across the volume of interest, *i.e.*, in the spread-out Bragg peak (SOBP). There is an additional dose-distribution advantage of protons, *viz.*, for depths typically up to \sim 17–18 cm in tissue, the lateral dose fall-off is steeper than for photon beams. This provides an additional gain for the treatment of lesions of intermediate depth, sited close to critical and radiosensitive structures. The well-defined limit of penetration in tissue depends on the incident proton-beam energy and the density of the tissue transited. To irradiate deep-seated lesions in adult patients, and depending on the clinical application, proton beam energies of 200–250 MeV (corresponding to ranges in tissue of 26–38 cm) are required. Proton accelerators providing 60–75 MeV beams (with ranges of 3–4.5 cm) are used almost exclusively for the treatment of ocular lesions.

The clinical outcomes of proton-beam therapy in terms of local control confirm its efficacy for the treatment of several types of lesions, *e.g.*, uveal melanomas, chordomas and chondrosarcomas of the skull base and axial spine, small tumors of

non-small-cell lung cancer, hepatic cancers, paranasal sinus carcinomas, and solid tumors in pediatric patients. The probable efficacy of proton-beam therapy with respect to other treatment modalities is being assessed by the method of comparative treatment planning combined with biomathematical modeling. Although proton therapy is a relatively new external-beam modality, it is a rapidly proliferating field. More than 53 000 patients have been treated to date (December 2007) with great success; the greatest number of patients being those with uveal melanoma, prostate cancer, and benign intracranial lesions. Proton therapy is now firmly established in the radiation oncologists' armamentarium. However, at present, there are no recognized uniform standards for dose prescription and treatment description for proton therapy. Such standards are essential for the design of clinical trials, for the evaluation of clinical data from the various proton therapy facilities, and for assessing the efficacy of proton radiation therapy relative to photon or other radiation treatments. These include conventional therapies and the newly emerging techniques such as intensity-modulated radiation therapy (IMRT) and tomotherapy. Such comparisons are essential for assessing the efficacy of proton therapy for the treatment of new sites. Important aspects to ensure uniform standards of proton dose prescription include the adoption of a uniform dosimetry protocol and the specification of a generic clinical relative biological effectiveness (RBE).

The present report provides information necessary to standardize techniques and procedures and to harmonize the clinical descriptions of proton treatments with those of other modalities, recommends the adoption of a uniform dosimetry protocol, proposes the use of a generic clinical RBE, and describes the radiobiological, physical, technical, treatment-planning, and clinical aspects so as to provide new users with the basic background to enable them to understand the techniques involved in proton therapy.

ICRU Reports 50 and 62 (ICRU, 1993b; 1999) described the prescribing, recording, and reporting of photon-beam therapy, whereas ICRU Report 71

NOTE: Sections of the text of ICRU Reports 50, 59, 62, and 71 (ICRU, 1993b; 1998; 1999; 2004) and IAEA Report TRS 398 (IAEA, 2000) are quoted verbatim or in summary form in the present report. Figures and tables from these reports have also been copied or adapted. These extracts are not always specifically referenced or acknowledged but are used with permission.

(ICRU, 2004) described electron-beam therapy. A similar ICRU report is presently being prepared on conformal photon therapy and IMRT. The definitions of geometric and other therapy terms in the present report are consistent with the definitions given in these reports. ICRU Report 59 (ICRU, 1998) and IAEA Report TRS 398 (IAEA, 2000) on proton dosimetry were considered in making recommendations regarding a uniform international proton dosimetry protocol. Throughout the present report, the differences between the processes involved in proton-beam therapy and conventional therapies are highlighted.

Radiation biology

Although it has been shown that the RBE (relative biological effectiveness) relative to high-energy photons is slightly, but significantly, greater than unity in nearly all studies, the radiobiological characteristics of proton beams provide no known clinical advantages. Nevertheless, the statement of proton doses and the choice of an appropriate RBE value to relate proton and photon doses are important issues.

- The RBE for proton beams is defined in the present report as the ratio of the photon dose to the proton dose required to give the same biological effect under identical irradiation conditions.
- RBE is a function of LET (linear energy transfer). The LET of a monoenergetic 250 MeV proton beam is $\leq 8 \text{ keV } \mu\text{m}^{-1}$ for depths of penetration of 2.5 cm to 27 cm. There is very slight dependence of RBE on LET over that range. The LET increases steeply at the end of range, *i.e.*, in the Bragg peak, with an accompanying rise in RBE to about 1.5 at its maximum.
- RBE determinations have been made in the clinical energy range for a wide variety of *in vitro* and *in vivo* systems for diverse end points. The mean RBE from the published studies is 1.1. Available data are consistent with a tissue-independent generic RBE value of 1.1.
- The available data reveal no variation in RBE with depth from the plateau and across the SOBP, excepting for the terminal 5 mm to 10 mm of the SOBP. Over that narrow range, the RBE is some 8 percent to 10 percent higher.
- On the declining distal edge of the SOBP sharp relative increments (up to 50 percent) in the RBE have been observed. This results in an effective increase in range of $\sim 1 \text{ mm}$ and $\sim 2 \text{ mm}$ for proton beams in the energy ranges below 75 MeV and above 150 MeV, respectively.

- There are no proton RBE determinations for human tissues. Clinical RBE values must therefore be derived from laboratory investigations. No clinical experience has been reported indicating an RBE different from 1.1. Accordingly, the recommendation is that proton radiation therapy be planned using a generic RBE value and that value be 1.1.
- Absorbed dose [in units of gray (Gy)] is a fundamental quantity in all therapeutic applications, but it is not a sufficient predictor of therapeutic outcome. All relevant treatment parameters such as absorbed dose, fractionation schedule, overall treatment time, beam quality, *etc.* should be specified. Previously the quantity "equivalent dose" with a variety of units [CGE, GyE, Gy(E), *etc.*] has been used to describe the product of the proton absorbed dose and the proton RBE. "Equivalent dose" is a quantity reserved for radiation protection purposes while the employment of modified unit symbols is not permitted in the SI (*Le Système International d'Unités/The International System of Units*). In order to overcome these problems it is recommended in the present report that the quantity RBE-weighted absorbed dose, D_{RBE} [in units of Gy (RBE)] be used to describe the product of proton absorbed dose, D , and the proton RBE. D_{RBE} [Gy (RBE)] is therefore the photon absorbed dose that would produce the same therapeutic effect as a proton absorbed dose of D (Gy), given under identical conditions. Throughout the present report all doses are explicitly given as absorbed dose (Gy) or RBE-weighted absorbed dose [Gy (RBE)].

Beam delivery and properties

A proton therapy facility consists of three main equipment components, *viz.* an accelerator, a beam transport system, and a treatment delivery system. In the latter system the proton beam is tailored to suit the lesion being treated. If the aim of the facility is to irradiate safely any lesion in the body of an adult with tumoricidal doses, proton ranges of at least 26–38 cm in tissue (corresponding to proton energies of 200–250 MeV) are required. Intensities of the order of $(3 \text{ to } 6) \times 10^{10}$ particles per second (5 nA to 10 nA) are required to deliver absorbed doses of about 2 Gy uniformly to a target volume of one liter in one minute. The exact requirements of beam energy and intensity depend on details of the beam-delivery system used. Both passive and active beam-delivery systems are employed to deliver the required dose to the target. Proton

EXECUTIVE SUMMARY

ranges are adjusted by the use of degraders (with a cyclotron) or by changing the beam energy (with a synchrotron).

- A typical passive beam-modification arrangement employs a double-scattering system (to spread the beam laterally), a rotating variable-thickness propeller (or ridge filter) to spread out the Bragg peak in depth, and a field-specific collimator.
- Dynamic beam-scanning systems can be used to achieve the desired lateral dose distribution at specific depths by magnetically deflecting the beam across the target. Several different techniques can be used to change the beam penetration depth. The advantages of beam scanning are flexibility (no patient-specific devices required), IMPT (intensity-modulated proton therapy) can be undertaken, there is better dose conformation to the target volume, and the background dose to the patient and the activation of beam-line elements are reduced. However, there are specific problems related to patient and organ motion, which can, however, be minimized by multiple “repainting” of the target volume. Scanning beams are not suitable for treating small lesions.
- To achieve the potential precision of proton-dose delivery, support and immobilization of the patient is of primary importance. However, the techniques used are, in most cases, very similar to those used in conventional high-technology therapy.
- Dedicated beam-delivery systems are required for special treatment techniques, such as eye treatments (proton energies < 70 MeV), and stereotactic radiosurgery and radiotherapy.
- A rotating gantry provides flexible beam delivery. Several different types of gantries are in use, and they typically weigh about 200 tons. For accurate beam delivery, rotation about a mechanical isosphere with a diameter of less than 2 mm is required.
- Linear accelerators, cyclotrons, synchrocyclotrons, and synchrotrons can be used for accelerating protons to the required therapeutic energies. To date linear accelerators have not been used. Both room-temperature and superconducting cyclotrons are in use. Synchrotrons are the most flexible machines in terms of energy variation, which can be accomplished pulse by pulse, but beam intensities are limited.
- Protons lose their energy in a medium primarily through interactions with atomic electrons. Because of their large mass relative to the electron mass, protons lose only a small fraction of energy in each interaction. Although nuclear interactions increase with energy,

electromagnetic interactions dominate at therapeutic energies.

- Many definitions of beam properties and beam parameters are the same for proton beams as for photon beams. Specific proton-beam definitions are required for describing scanning beams and depth-dose characteristics.
- The radiation quality of a proton beam is determined by the energy distribution, which can affect various beam characteristics such as the entrance (plateau) dose, distal dose fall-off, penumbrae, and the radiation dose outside the treatment field. The latter is particularly important for the treatment of pediatric cases. The dose outside the treatment field is critically dependent on details of the beam-delivery system for passively modified beams. The dose outside the treatment field is typically more than an order of magnitude less for scanned beams.

Dosimetry

Accurate absorbed-dose determination is a fundamental prerequisite for any radiation therapy treatment, as tumor control and normal tissue complication probabilities are steep functions of absorbed dose. Relative accuracy and reproducibility of 3 percent and 2 percent respectively, are desirable. Beam monitors are required in the beam-delivery system to control the dose in the patient. Measurement of dose distributions is necessary for treatment planning purposes.

- Since calorimeters are absolute dosimeters they are the instruments of choice for determining reference absorbed dose in proton therapy beams. However, they are not suited for routine use, and ionization chambers remain the practical instruments for proton dosimetry. There are currently no primary standards for absorbed doses in proton beams and ionization chambers have to have calibration coefficients traceable to a primary standard in a ^{60}Co beam. Alternatively, they can be calibrated with a calorimeter in the user's proton beam.
- Two proton dosimetry protocols are in current use, *viz.*, ICRU Report 59 (ICRU, 1998) and IAEA TRS 398 (IAEA, 2000). It is recommended in the present report that the TRS 398 code of practice be adopted as the standard proton dosimetry protocol as it is very simple to use, harmonizes with other modalities' codes of practice (also given in TRS 398), which are being universally adopted, and has a more robust and rigorous formalism than that of ICRU Report 59.

- There is little difference between reference dosimetry for passively modified beams and for scanned beams.
- Parallel-plate ionization chambers are the most common and well-proven detectors for proton beam monitoring. Non-saturating secondary emission monitors (SEM) and multiwire ionization chambers (MWIC) are also used. MWICs or pixel ionization chamber arrays can be used for monitoring the beam position of scanning beams.
- Detectors for relative dose-distribution measurements include ionization chambers, silicon diodes, radiographic films, alanine, diamond detectors, radiochromic film, and gel detectors. Ionization chambers are often the instruments of choice as they are the simplest to use and do not require specific calibration for such relative measurements. Radiographic films, scintillator screens, or two-dimensional pixel detectors can be used to measure the dose distributions of scanned beams.

Geometry and dose-volume definitions

Previous reports (ICRU, 1993b; 1999; 2004) have introduced and defined a variety of terms and acronyms to standardize the identification of a number of volumes of clinical interest. These include the gross tumor volume (GTV), the clinical target volume (CTV), the planning target volume (PTV), the organ at risk (OAR), and the planning organ at risk volume (PRV), *etc.* With the exception of the PTV and PRV, these terms remain unaltered in the context of proton beam therapy. Indeed their definitions and delineations should be modality independent.

- The PTV and PRV serve two functions: they are planning tools, and they are used to report doses. Regarding the first, protons differ from photons in that the design of a proton beam requires different margins lateral to, and distal and proximal to the CTV. As a result, a different PTV in principle, would have to be used for each possible beam direction. This is cumbersome, and some centers design their proton beams without reference to a PTV, but purely based on the CTV using appropriate lateral and distal and proximal margins. Nevertheless, it is recommended in the present report that PTVs be used in proton planning for dose reporting purposes, allowing for all but distal and proximal margins due to range uncertainties.
- It is recommended that neither the PTV nor the PRVs be compromised in order to guide dose

planning. If needed, additional volumes should be used for this purpose.

- Some nomenclatures to standardize the geometric terms when multiple volumes are required for complex situations are suggested in the present report.
- The terms: volume of interest (VOI), surface of interest (SOI), and point of interest (POI) as generic terms are introduced in the present report.
- A number of dose and dose-volume terms are defined in the present report. These include:

D_V	the least dose received by a volume, V , of a specified VOI
V_D	the largest volume of a specified VOI which receives more than or equal to the dose, D
$D_{\text{near-min}}$	the least dose received by at least 98 percent of a VOI. It equals $D_{98\%}$
$D_{\text{near-max}}$	the greatest dose which all but 2 percent of a VOI receives. It equals $D_{2\%}$.

- The term ‘prescribed dose’, or equivalently ‘prescription dose’, is defined differently from previous ICRU reports. It was previously defined as a goal dose at a specified point (*e.g.*, the ICRU reference point). It is now proposed that the prescribed dose be referred to a specified volume. For example, one could prescribe that 95 percent of the PTV should receive within -5 and $+7$ percent of the prescribed dose.

Treatment planning

The present report focuses on the main differences between the planning of proton-beam therapy and photon-beam therapy, namely:

- The depth-dose properties of protons and photons are quite different. A monoenergetic proton beam loses energy slowly until near the end of range where the rate of energy loss increases sharply, resulting in the formation of the narrow (several millimeters) Bragg peak, beyond which no appreciable energy is deposited. Consequently, protons deliver less integral dose outside the target volume, by a factor of 2 to 3, than do photons.
- Protons scatter within the patient. This has the consequence that the width of a proton-beam penumbra depends on depth and this must be taken into account in planning proton-beam therapy. Scattering also affects the behavior of protons in regions of sharply changing density

EXECUTIVE SUMMARY

(along the direction of the proton beam) when anatomic displacement occurs, so that additional care is needed when protons are directed nearly tangent to an inhomogeneity such as the external skin surface.

- The penetration of a proton beam is very sensitive to inhomogeneities of tissue density within the patient. These can affect the depth of penetration and the sharpness of the terminal Bragg peak. Inhomogeneities must therefore be measured and allowed for. Their influence is much greater than it is on photon beam distributions.
- The measurement of internal densities, and their conversion to '*water-equivalent*' densities, is thus particularly important for protons. This is usually done using conventional kilovoltage CT (computed tomography) together with a measured look-up table relating Hounsfield numbers to water-equivalent density. However, CT using megavoltage photons has the potential to minimize the effects of artifacts from embedded metallic objects.
- Intensity-modulated radiation therapy (IMRT) is feasible with protons (where it is termed intensity-modulated proton therapy or IMPT) just as it is with x rays (intensity-modulated x-ray therapy or IMXT). The main difference is that protons have an additional dimension that can be manipulated (depth of penetration), which in principle increases the flexibility and improves the likelihood of achieving the desired result.

Motion management

As with photons, motion of the patient and his or her internal anatomy must be accounted for in the planning and delivery of therapy. However, because of the sharp lateral and distal dose fall-offs, there are some differences in proton-beam therapy:

- The motion of regions of inhomogeneous density potentially upsets the dose distribution, if it is planned without regard to motion. This has two consequences: 1) the effect of motion should be reduced to the extent possible through, for example, immobilization of the patient and respiration gating; 2) the residual uncertainties must be taken into account, for example, through the use of appropriate margins, both lateral and distal to the PTV.
- Motion causes a specific problem in scanned-beam therapy due to what are termed 'interplay effects'. These occur when a scanned pencil beam is moved throughout the target volume ("painted") while the internal anatomy is moving.

Small regions within the target volume might either escape being irradiated by moving away from the pencil beam as it passes through them, or be overdosed by moving in synchrony with, and within, a moving pencil beam. This gives rise to dose fluctuations within the target volume - so-called 'dose mottle'.

- Interplay effects cannot be entirely eliminated (they occur in IMXT as well, but to a lesser extent), but they can be reduced to a tolerable level. The most straightforward approach is to undertake what is called 'repainting'. With repainting, one delivers the entire dose pattern multiple times - with a fraction of the dose delivered at each repainting. The individual repaintings need to be at times greater than or comparable to the period of motion (typically, a few seconds for respiration motion).

Uncertainty

Uncertainty is inevitable in planning and delivering radiation therapy. In this, protons are no different from other radiations. However, protons do have additional sources of uncertainty. These include the effects of motion, additional dosimetric uncertainties with protons, and issues of relative biological effectiveness. The present report recommends the following for all procedures and for each patient:

- The sources of uncertainty should be analyzed and minimized to the extent possible or practicable.
- The magnitude of the remaining unavoidable uncertainties should be documented.
- Treatment planning programs should provide tools to aid in this analysis. In this regard, some approaches to the display of uncertainty are presented.
- For normal reporting purposes, in uncomplicated cases, it would be sufficient to report a generic level of uncertainty, tailored when necessary to the individual circumstances of the particular patient.
- For cases where exceptionally large uncertainties might exist, the uncertainties in the dose distributions, as well as in the summarizing statistics, should be estimated (together with their corresponding confidence levels).

Quality assurance

A rigorous QA (quality assurance) program is required to ensure reproducible, accurate, and safe fulfillment of the treatment prescription. QA checks are often technology- and equipment-

specific and focus principally on various aspects of dose delivery, patient positioning and treatment planning as well as radiation protection.

- The positioning and alignment of hardware components in the treatment nozzle are checked by the measurement of depth doses and lateral beam profiles, the parameters of which should be within predetermined tolerance limits. Beam monitors and the settings of beam-modification devices also require routine checking. Additional specific tests are required for scanning beam-delivery systems.
- Regular checks of the patient-positioning system with respect to the treatment isocenter and beam axis should be undertaken to ensure that the patient can be positioned accurately in the beam.
- Comprehensive acceptance testing and QA programs are required for treatment-planning systems. These systems should be validated by comparing calculated with measured doses over a range of clinical situations. Regular calibration of the planning CT scanner is also required to ensure the integrity of the dose calculations. Proton treatment-planning QA procedures are similar to those for conventional therapies and are fully documented in various publications.

Prescribing, recording, and reporting treatment

The procedures for prescribing and documenting patient treatments are an important part of the treatment process, which begins with an initial examination and assessment of the patient and determination of the therapeutic goals (radical or palliative), and continues to the follow-up

procedures after completion of treatment. The procedures include the following:

- Completing the initial medical note in which all relevant clinical information is recorded.
- Specifying the planning aims, *i.e.*, detailing all the information needed to plan the intended treatment.
- Creating an acceptable treatment plan; this may be the result of an iterative process if the initial planning aims cannot be met.
- Providing a treatment prescription according to the specifications in the treatment plan; this specifies the dose at specified points or within delineated volumes, and how the patient is to be treated.
- Specifying the treatment data necessary to execute the treatment plan.
- Compiling the treatment record in which all data relevant to the patient's treatment are recorded.
- Writing reports of the treatment, including the completion note, report(s) to referring physician(s) and other involved medical personnel, and publication of the results of the treatment.

Six clinical examples of reporting proton beam therapy from several proton treatment facilities are presented to illustrate how to interpret the concepts and how to apply the recommendations developed in this report. The clinical examples are for treatments of uveal melanoma, adenocarcinoma of the prostate, carcinoma of the lung, acoustic neuroma (radiosurgical case), medulloblastoma (pediatric case), and skull-base chordoma. These clinical examples should not be interpreted as ICRU recommendations for selecting particular treatment strategies.

1 INTRODUCTION

Many reviews of proton therapy have been published over the years. These studies have discussed the physical, biological, technical, and clinical aspects, as well as considerations of its efficacy and speculations concerning the future role of protons in radiation therapy (Archambeau *et al.*, 1974; Bonnett, 1993; Breuer and Smit, 2000; Chu, 1995a; Fowler, 1981; Goitein, 1995; Goitein *et al.*, 1985; 2002; Graffmann, 1975; Jones, 1999; 2001a; 2001b; 2001c; Koehler and Preston, 1972; Kogelnik, 1997; Miller, 1995; Munzenrider *et al.*, 1981; Nahum *et al.*, 1994; Petti and Lennox, 1994; Raju, 1980; 1994; 1995a; 1995b; 1996; Smith, 2006; Suit, 2002; Suit and Krengli, 1997; Suit and Urie, 1992; Suit *et al.*, 1992; 2003; Verhey and Munzenrider, 1982; Wambersie and Battermann, 1995; Wambersie *et al.*, 1999; 2002; 2004b).

In the present section first the principles of, and rationale for, proton therapy are summarized. Then follows a brief history of the development and use of proton therapy, after which a description of the present status of this treatment is given. The scope and goals of the present report and its relationship to the existing reports are then discussed.

1.1 PRINCIPLES OF PROTON THERAPY

1.1.1 Physical characteristics

The rationale for the use of proton beams in radiation therapy is remarkably simple. It is based on the physical characteristics of energy loss by protons when they penetrate matter, namely, (i) protons have a finite depth of penetration in material, the magnitude of which depends on their energy and on the density of the irradiated material; (ii) protons exhibit a relatively low ionization density (energy loss per unit path length) at the surface that slowly increases to near the end of the beam range at which point there is a narrow region of high ionization density, termed the Bragg peak, with negligible dose deposited beyond the peak; and (iii) the dose from a proton beam falls off sharply both laterally and distally. These characteristics are illustrated in Figs 1.1 and 1.2. The

relationship between the incident proton-beam energy and its maximum penetration in tissue is shown in Fig. 1.3. To be able to irradiate all possible target volumes in adult patients, proton ranges of 26–38 cm in tissue (corresponding to proton energies of 200–250 MeV) are required. This allows for energy losses in beam-modifying devices, in diagnostic and dosimetry equipment in the beam line, and in the air gap between the accelerator vacuum system and the patient surface. Proton accelerators producing energy beams with energies of 60–75 MeV (with proton ranges of ~3.0–4.5 cm in water) are used principally for the treatment of ocular lesions (Goitein and Miller, 1983; Goitein *et al.*, 1983a).

Accelerated protons are near-monoenergetic and form a beam of small (relative to typical target volumes) lateral dimension and angular divergence; they need to be modified for practical use. There are two approaches to form a desired dose distribution for a proton-therapy beam, *viz.*, passive scattering and modulation (referring to the method of spreading the beam laterally and with the desired dose distribution in depth), or dynamic scanning of a pencil beam both laterally and in depth.

In passive scattering, the lateral dose distribution is formed by placing the scattering material in the beam together with an occluding aperture to shape the beam laterally so as to provide a near-uniform dose across the field (Koehler *et al.*, 1977). The distribution of dose in depth is formed either by layering suitably weighted proton beams of different energies (ranges), usually using a variable-thickness propeller that rotates in the beam (Chu *et al.*, 1993; Koehler *et al.*, 1975; Wilson, 1946), or by a ridge filter made up of multiple ridges of variable-thickness absorber placed in the beam (Kostjuchenko *et al.*, 2001; Larsson, 1961).

The second approach to form the dose distribution involves scanning of a pencil beam both laterally and in depth (by changing its energy), in which case a near-arbitrary distribution of dose is possible laterally, and considerable dose shaping can be achieved in depth (Bacher *et al.*, 1989;

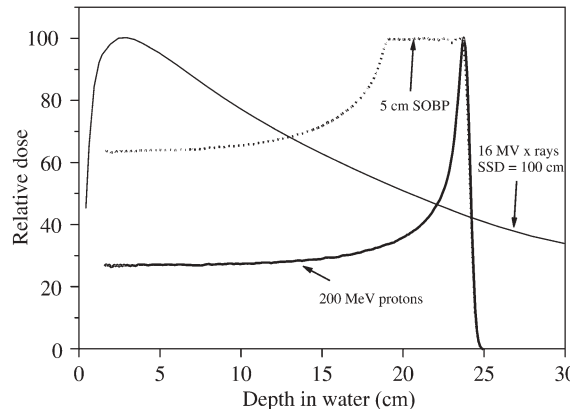


Figure 1.1. Depth-dose curves for a 200 MeV proton beam: both unmodulated and with a 5 cm spread-out Bragg peak (SOBP), compared with a 16 MV x-ray beam (for $10 \times 10 \text{ cm}^2$ fields). The curves are normalized in each case to 100 at maximum dose. (Adapted from Jones, 1999; reproduced with permission).

Pedroni *et al.*, 1989; 1995; 2005). The lateral distribution for any proton energy is determined by the lateral positions and weights of each pencil beam of a chosen energy, and the distribution in depth is determined by weighting the pencil beams at each position within the field.

In either method, the beam range is changed either by inserting absorbers in the beam path (in the case of cyclotrons) or by changing the beam energy (in the case of synchrotrons). When the

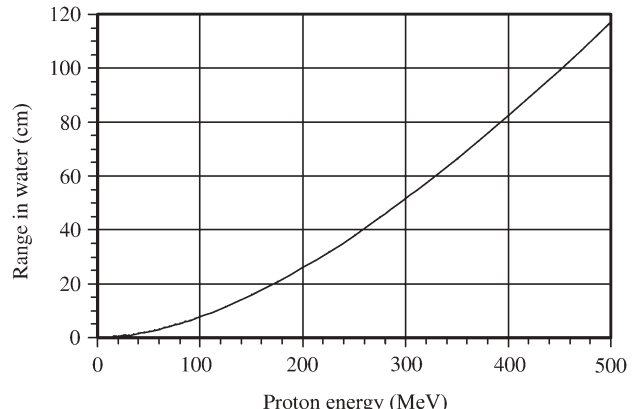


Figure 1.3. Proton range in water as a function of energy. Compiled from data given in ICRU (1993a).

distribution of energies is designed to provide a uniform dose over some depth, the resultant distribution is designated as the spread-out Bragg peak (SOBP) as shown in Figs 1.1 and 1.4. The SOBP is the segment of the depth-dose curve characterized by an essentially flat dose region. Thus, for each beam, the SOBP is designed to cover the tissue volume of interest in depth with virtually no dose at greater depths. Layering of proton beams of graded energies has the effect of increasing the entrance dose relative to a monoenergetic beam. This effect increases with the length of the SOBP.

Beam scanning can achieve a closer conformation of the high-dose region to the PTV than can passive beam-modification systems (ICRU, 1993b; 1999; Urie and Goitein, 1989); specifically the dose proximal to the PTV is less in most cases. Beam scanning is the only practical technique that enables

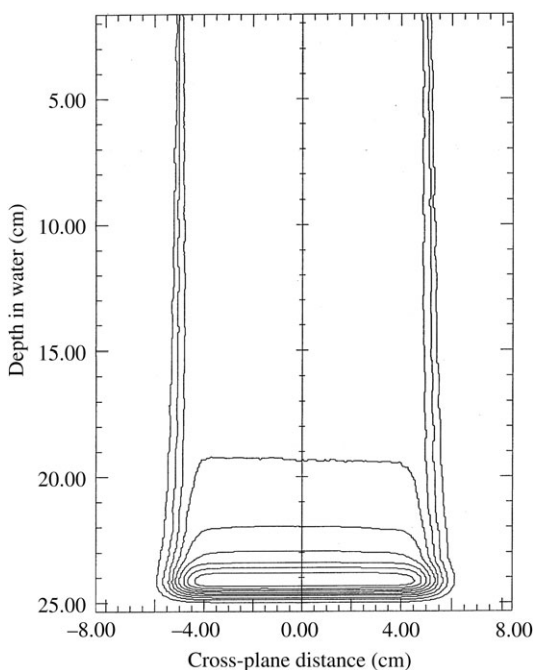


Figure 1.2. Isodose distribution for a 100 mm diameter unmodulated 200 MeV proton beam. The isodoses in 10 percent steps from 10 percent to 90 percent are shown (Jones, 1995; reproduced with permission).

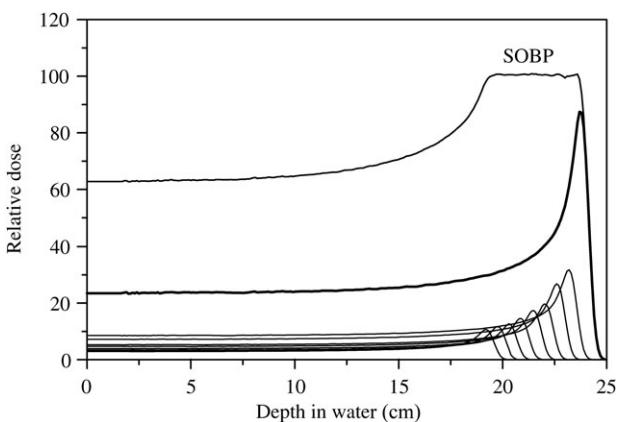


Figure 1.4. Depth-dose curve for a monoenergetic 200 MeV clinical proton beam (thick line) showing the Bragg peak at the end of the range. The superposition of suitably weighted proton beams (thin lines) of different energies (ranges) results in a spread-out Bragg peak (SOBP) that provides a uniform depth dose over the target region (Jones and Schreuder, 2001; reproduced with permission).

INTRODUCTION

intensity-modulated proton therapy (IMPT) to be performed. There are further potential advantages in that activation of beam line components and the secondary scattered dose, predominantly due to neutrons, to the patient might be substantially reduced (Hall, 2006), and fewer or no patient-specific treatment devices are required. These factors are the principal bases for the current trend to employ beam scanning in the clinical situation. However, the effects of anatomical motion are more severe than with passively modified beams, and might result in the creation of regions of high dose outside, and low dose inside the target volume, and the reduction of scattered dose is often not the deciding factor in prescribing the treatment. Beam-modification techniques are described in more detail in Section 3.

Figure 1.5 emphasizes the dose sparing achieved proximally and distally to the target volume by a single range-modulated proton beam in comparison with a single high-energy x-ray beam. The clinical advantages of the proton beam are obvious: in strong contrast to photon beams, there is a very little dose distal to the SOBP (which encloses the target volume) and, for all except the most superficial lesions, there is a lower dose proximal to the target volume. The excess dose from photons for each beam path is shown in black for emphasis. These dose-distribution advantages of protons are obtained for all techniques of dose delivery. Importantly, the flexibility in choosing the number of beams, beam orientation, beam weighting, beam scanning, the use of intensity-modulation techniques (Hong *et al.*, 2005; Pedroni *et al.*, 1995), four-dimensional image-guided treatment (tracking or gated) (Sheng *et al.*, 2005;

Yamada *et al.*, 2005), and tomotherapy techniques (Welsh *et al.*, 2002) is as great for proton as for photon treatments. The significant skin-sparing effect with high-energy photon beams, due to dose build-up resulting from electronic disequilibrium near the surface, is much reduced with proton beams. However, for deep lesions treated with multi-field techniques, skin dose is rarely a clinical problem.

For a given dose to the target volume, protons deposit substantially less dose outside the target volume than do photons. In this situation, the tolerance of patients to proton treatments is increased over that experienced with photon treatments. The result is a decreased frequency and severity of injury to uninvolved normal tissues for a specified dose to the target. Alternatively, one can take advantage of the improved dose distribution of the proton irradiation to increase the dose delivered to the target volume and hence to increase the probability of local control of the tumor for a given complication probability. In accordance with these predictions, the efficacy of proton therapy has been demonstrated for several tumor types, as shown in Table 1.1. Further, for patients whose tumors are to be treated by combined radiation and chemotherapy, the lesser radiation dose to chemotherapy-sensitive normal tissues may permit an increment in drug dose and, hence, augment response frequency and/or duration.

Tissue inhomogeneity has a greater effect on proton dose distributions than on photon dose distributions. While planning for proton therapy, the density of tissue along the proton path must be precisely determined and accounted for in order to obtain the required proton energy distribution to achieve the planned dose distribution in the patient. Failure to allow for a zone of higher density could result in a near-zero dose in a distal segment of the target volume due to the reduced range of the protons. In contrast, for photons, because of their different energy loss processes, an increased density would cause only a modest lowering of the dose distal to the higher density region (Fig. 1.6). Conversely, neglecting to account for an air cavity upstream of the target volume would, for proton beams, result in a high dose being deposited in distal normal structures, while only a modestly increased dose would be deposited in the case of photon beams.

Proton beams have a sharp lateral penumbra, but that sharpness decreases with increasing beam energy and, hence, depth of penetration (Jones, 1995; Larsson, 1961). The width of the penumbra (80–20 percent isodose levels) is narrower for proton than for photon beams for penetrations up

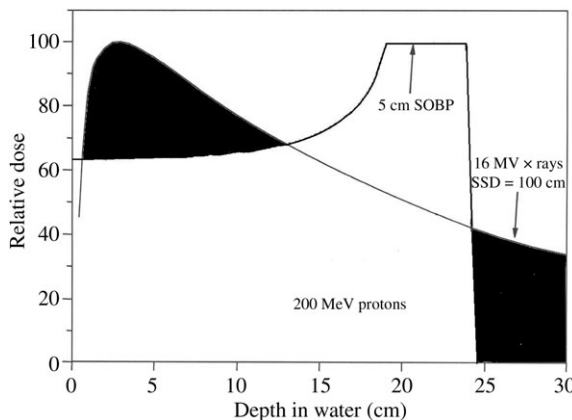


Figure 1.5. Depth-dose curves for a modulated proton beam and a high-energy photon beam normalized to the same maximum dose. The black areas highlight the regions where the photon dose drastically exceeds the proton dose (adapted from Fig. 1.1).

Table 1.1. Selected clinical results of proton and high-technology photon radiation therapy.

Primary tumor	Proton (+ photon) dose ^a , D_{RBE} [Gy (RBE)]	Photon dose ^b , D (Gy)	Number of patients	Local control	Reference
Uveal melanoma	70 in 5 fractions		2069	95 % at 15 y	Gragoudas <i>et al.</i> (2002b)
	60 in 4 fractions		2435	92 % at 10 y	Egger <i>et al.</i> (2001)
	60–70 in 4 fractions		1406	96 % at 5 y	Dendale <i>et al.</i> (2006)
		60–70 in 5 fractions	158	98 % at 33 m	Dieckman <i>et al.</i> (2006)
Chondrosarcoma	72 in ~38 fractions		200	98 % at 10 y	Rosenberg <i>et al.</i> (1999)
	67 in ~34 fractions		26	92 % at 36 m	Noel <i>et al.</i> (2004)
Chordoma	69 in ~36 fractions		132	44 % at 10 y	Terahara <i>et al.</i> (1999)
	67 in 37 fractions		100	54 % at 4 y	Noel <i>et al.</i> (2005)
		67 in 37 fractions	45	50 % at 5 y	Debus <i>et al.</i> (2000)
Prostate (TIII–TIV)	67.2 versus 75.6 (Phase III trial)		202	60 versus 77 % ^c at 8 y	Shipley <i>et al.</i> (1995)
Prostate (TIIa–TII)	74 in 37 fractions		1255	73 % ^c at 8 y	Slater <i>et al.</i> (2004)
Prostate (TII–TII)	70.2 versus 79.2 (Phase III trial)		393	61.4 versus 80.4 % at 5 y	Zietman <i>et al.</i> (2005)
Prostate (TIIc–TIIc)		81 in 45 fractions	255	78 % ^{c,d} at 8 y	Zelefsky <i>et al.</i> (2006)
Lung (TII–TII)	51–60 in 10 fractions		29 (TII)	87 % at 3 y	Bush <i>et al.</i> (2004a)
Lung (TII)		45 in 3 fractions	40	39 % at 3 y	
Glioblastoma multiforme	90 in 5 fractions ^e		23	18 % survival at 3 y	Fitzek <i>et al.</i> (1999)
Adenocystic carcinoma of paranasal sinus	76 in ~38 fractions		23	93 % at 5 y	Pommier <i>et al.</i> (2006)
Paranasal sinus		63 in ~32 fractions	85	62 % at 5 y	Hoppe <i>et al.</i> (2007)
Axial skeleton chondrosarcoma	72.2 in 40 fractions		6	100 % at 5 y	Hug <i>et al.</i> (1995)
Liver: primary	72 in 16 fractions		162	87 % at 5 y	Chiba <i>et al.</i> (2005)
	63 in 15 fractions		34	75 % at 2 y	Bush <i>et al.</i> (2004b)
Liver: primary and metastatic		26 in 1 fraction	28	82 % at 24 m	Wulf <i>et al.</i> (2006)
		37 in 3 fractions			
		25 in 5 fractions	45	82 % at 2 y	Mendez-Romero <i>et al.</i> (2006)
		30 in 10 fractions	lesions		
		60 in 3 fractions ^f	21	93 % at 18 m	Kavanaugh <i>et al.</i> (2006)

^aProton (+ photon) RBE-weighted dose. Protons were delivered alone or in combination with photons. A proton RBE of 1.10 was employed. Mean or median doses are quoted as stated in the original papers. Neither the proton (+ photon) or the photon series are notated for combined surgery or chemotherapy.

^bPhotons were delivered by either IMRT or a stereotactic technique. Mean or median doses are quoted as stated in the original papers.

^cBiochemical-relapse free.

^dIntermediate risk group.

^eTwo fractions per day.

^fStereotactic body radiotherapy.

to intermediate depths, ~17–18 cm. Figure 1.7 shows an example of penumbra widths versus depth of penetration for a 200 MeV proton beam, a ^{60}Co beam, and an 8 MV linear accelerator beam. For these conditions, the proton-beam penumbra is narrower than the 8 MV beam up to a depth of

~18 cm. For both these beams, the penumbrae are narrower than for the ^{60}Co beam. For a given incident-beam energy, the proton-beam penumbra is widest in the Bragg-peak region, where the proton energy is least (see Fig. 1.2). Because primary protons are scattered out of the beam,

INTRODUCTION

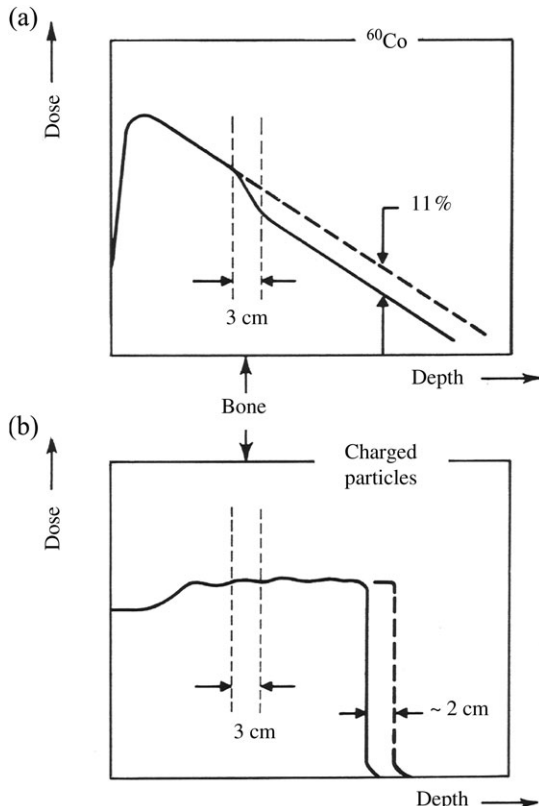


Figure 1.6. Effect of a 3 cm thick slab of bone placed in: (a) a ^{60}Co beam (a); and in the spread-out Bragg peak (SOBP) of a proton beam (b). The ^{60}Co beam is reduced in intensity but still penetrates deeply, whereas the penetration of the proton beam is reduced, but the magnitude of the dose in the high-dose region is unaffected (Goitein, 1982b; reproduced with permission).

proton beams have progressively lower central axis Bragg peaks as the beam diameter is decreased below about 10 mm (Hong *et al.*, 1996; Larsson, 1967). This effect is illustrated in Fig. 1.8. This series of curves was derived by calculation, supported by a depth-dose measurement for the 2.4 mm radius beam.

1.1.2 Biological effects

The biological effects of proton beams in the therapeutic energy range have been extensively studied in various experimental settings and reviewed by Paganetti *et al.* (2002) and Skarsgard (1998) and are discussed in detail in Section 2. These experiments have employed a wide variety of biological systems (both *in vivo* and *in vitro*), response end points, proton energies, dose levels, and fractionation protocols. The relative biological effectiveness (RBE) values for the diverse *in vivo* systems for proton energies between 60 and 250 MeV are consistent with a mean RBE of 1.1 (see Section 2). This is applicable for both acute- and late-responding tissues and for the range of dose/

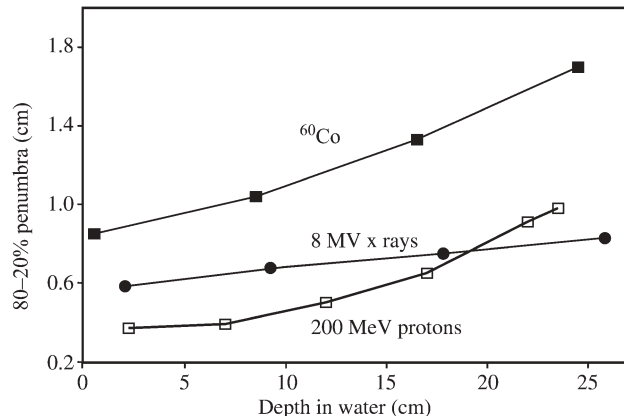


Figure 1.7. Measured lateral penumbrae (80–20 percent dose levels) as a function of depth for a 200 MeV proton beam compared with other radiation beams. For these conditions the penumbrae for 8 MV x rays are narrower than for protons at depths >18 cm. (Figure courtesy of D.T.L. Jones, iThemba Laboratory for Accelerator-Based Sciences, Somerset West, South Africa.)

fractionation schemes employed clinically. Although none of the available RBE values are based on human tissue response, the recommendation in the present report is that a RBE of 1.10 be employed as a generic value, *i.e.*, a value that is independent of dose, tissue type, fractionation, *etc.* (Section 2).

1.1.3 Clinical evaluations

As noted earlier, the available clinical outcome data (see Table 1.1) support the contention that proton therapy is effective for the treatment of a number of types of lesions. This is evident in the local control results achieved for chondrosarcoma of the skull base, uveal melanoma (the results given

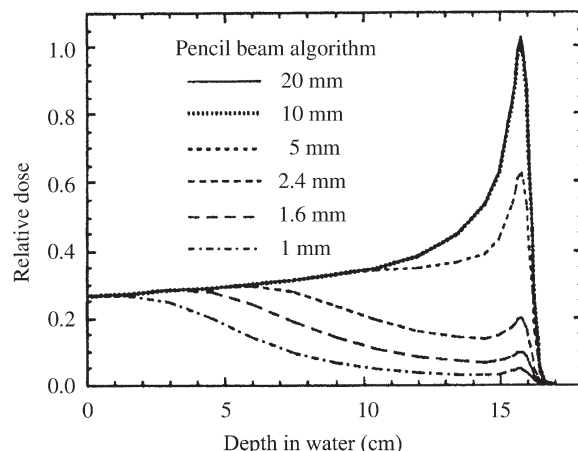


Figure 1.8. Depth-dose curves for a 160 MeV proton beam as a function of collimator radius, calculated using a pencil beam algorithm (Hong *et al.*, 1996; reproduced with permission).

were obtained for lesions of a wide spectrum of sizes and sites within the globe), hepatocellular carcinoma, stage T1 non-small-cell lung cancer, paranasal sinus carcinoma, and sarcomas of the axial spine. The evaluation of a gain in local control probability by charged-particle radiation therapy at long follow-up has been assessed in Phase III clinical trials for only two tumor categories, *viz.*, uveal melanomas [helium ions versus ^{125}I brachytherapy] (Char *et al.*, 1993) and prostate cancer (Shipley *et al.*, 1995; Zietman *et al.*, 2005). In the case of prostate cancer each of the two trials was designed to assess local control probability for two proton dose levels used as boost doses.

Effective and alternative forms of evaluation of the probable efficacy of proton-beam therapy are the comparison of treatment plans in terms of dose distributions and possibly including biomathematical-model predictions of tumor control probabilities (TCP) and normal tissue complication probabilities (NTCP) (Baumert *et al.*, 2001, 2004; Bölsi *et al.*, 2003; Deasy *et al.*, 2001; Drzymala *et al.*, 1991; Fogliata *et al.*, 2002; Goitein and Schultheiss, 1985; Hsiung-Stripp *et al.*, 2001; Lin *et al.*, 2000; Lomax *et al.*, 2003; Miralbell *et al.*, 2002; Mock *et al.*, 2004; Nahum and Glimelius, 2001; Nahum and Sanchez-Nieto, 2001; Niemierko and Goitein, 1993; Stavrev *et al.*, 2001; Suit *et al.*, 2003; van Luijk *et al.*, 2003; Weber *et al.*, 2004; Zurlo *et al.*, 2000). Further references and a summary table are given in Glimelius *et al.* (2005).

1.2 HISTORY OF PROTON THERAPY

Robert Wilson first proposed the use of protons and heavier ions for radiation therapy in 1946 (Wilson, 1946). At that time, accelerators capable of generating proton beams with sufficient energy for proton radiation therapy were under construction. He noted that the large mass of the proton would cause it to travel in a nearly straight path through tissue and that the energy deposition pattern of a proton beam would produce high radiation doses near the end of the range in a relatively narrow region, referred to as the Bragg peak. He proposed the irradiation of localized regions within the body with proton beams, thereby providing significant sparing of surrounding tissues. He also explained how rotating modulator propellers could spread the Bragg peak over large targets, transmission ionization chambers could be employed to monitor patient dose, and ionization chambers could provide absolute dose-calibration coefficients for the beam monitors.

The first studies of the biological effects of charged-particle beams were conducted on the

184 in. synchrocyclotron at the University of California, Berkeley. Tobias *et al.* (1952) reported LD₅₀ values for whole-body irradiation of mice by 340 MeV protons and for the rat pituitary by 190 MeV deuterons. Larsson *et al.* (1958; 1959), Leksell *et al.* (1960), and Rexed *et al.* (1960) described radiation injury to the spinal cord and brain of experimental animals by high-energy proton beams. Robertson *et al.* (1975) reported a comprehensive RBE study of mammalian cells *in vitro* using loss of colony-forming ability as the end point. Subsequently, there has been extensive laboratory research to determine the biological effectiveness of protons relative to photon irradiation (Paganetti *et al.*, 2002; Skarsgard, 1998). This is considered further in Section 2.

The first use of proton beams in the management of human patients was at the University of California, Berkeley. This work was directed principally at the suppression of hormone production by the pituitary gland by very high-dose and highly localized proton irradiation. The rationale was that a high proportion of human breast cancers are hormone dependent. Extensive animal studies using proton and deuteron beams preceded the clinical work. The first 'patient' was a dog with an extensive ulcerated breast tumor. Tobias and co-workers irradiated the pituitary gland with deuterons (Lawrence, 1957; Tobias *et al.*, 1954; 1955) and found a substantial reduction in size of the lesion.

On the basis of this good response and prior demonstrated marked suppression of hormonal levels following high-dose irradiation of the rat pituitary, the Berkeley team decided to proceed with patient treatment. They commenced a Phase-I clinical trial of dose escalation of proton irradiation of the pituitary of women with breast carcinoma. The radiation was administered in three fractions per week for \sim 2 weeks; the total dose was 140–300 Gy. The crossfire technique was employed, in which multiple small, unmodulated 340 MeV proton beams intersected at the pituitary and exited the skull, *i.e.*, the pituitary was irradiated by the plateau region of each beam. The first patient was treated in 1954, only 8 years after the publication of Wilson's paper (Wilson, 1946). Several of the 26 patients experienced good clinical responses (Lawrence, 1957; Tobias *et al.*, 1958). In 1957, the accelerator was upgraded and the Berkeley team commenced a long-term clinical and laboratory investigation with 910 MeV helium ions and then with heavier ions, *e.g.*, C and Ne (Castro *et al.*, 1980). The treatment facilities were closed in 1992.

The first proton clinical treatments in Europe were conducted in 1957 using the 185 MeV synchrocyclotron at the University of Uppsala,

INTRODUCTION

Sweden. Pilot studies of the efficacy of fractionated irradiation (between 1 and 10 fractions) of malignant tumors were undertaken. A few patients with glioblastoma multiforme and tumors of the uterine cervix, nasopharynx, head and neck, and other sites were treated. For several patients in the study, the tumor responses were judged to be good (Falkmer *et al.*, 1962). In the late 1950s, a program of stereotactic radiosurgery with narrow proton beams for the treatment of Parkinson's disease and intractable pain was also started in Uppsala (Graffman *et al.*, 1985; Larsson *et al.*, 1963).

Following the change from proton to helium ion beams by the Berkeley program in 1957, proton therapy recommenced in the USA in 1961 on the 160 MeV synchrocyclotron at the Harvard University Cyclotron Laboratory. Kjellberg and co-workers undertook single-dose stereotactic treatments of pituitary adenomas and intracranial tumors (Kjellberg, 1979; Kjellberg *et al.*, 1962a; 1962b; 1968) and later proton treatment of arteriovenous malformations (AVM) (Kjellberg, 1979; Kjellberg *et al.*, 1983). They used irradiation techniques in which the Bragg peaks of multiple narrow beams stopped in the lesion. Good success rates were realized for the ablation of pituitary adenomas and AVMs (Kjellberg, 1979).

Proton therapy began in Russia (Dubna) in 1967, in Japan (Chiba) in 1979, and in the Southern Hemisphere (Somerset West, South Africa) in 1993 (Sisterson, 2005). All the early proton-treatment facilities were established in the existing accelerator laboratories. iThemba LABS (South Africa) is the only accelerator laboratory designed *ab initio* for particle therapy. The first hospital-based facility became operational in 1990 at the Loma Linda University Medical Center, CA, and included the first proton-beam isocentric gantries (Coutrakon *et al.*, 1994; Slater *et al.*, 1995).

In 1973, Suit and co-workers instituted a program at the Harvard Cyclotron Laboratory to evaluate the efficacy of highly fractionated radiation therapy of malignant tumors. The first patients were treated mainly for sarcomas at several sites, with special emphasis on sarcomas of the skull base (Suit and Goitein, 1974; Suit *et al.*, 1975; 1982). These initial studies were rapidly expanded to tumors at several other sites. Following initial experiments on monkey eyes (Constable *et al.*, 1976), the first program involving the treatment of uveal melanomas was initiated in 1976 at the Harvard Cyclotron Laboratory (Gragoudas *et al.*, 1977; 1980; 2002a; 2002b).

In 1975, Koehler *et al.* first described the detailed design of a rotating propeller of variable thickness which, when placed in the beam, achieved the

required SOBP (Koehler *et al.*, 1975). Later, in 1977, they described a double-scattering technique to provide uniform lateral proton-dose distributions (Koehler *et al.*, 1977). Techniques for distal-edge compensation (Goitein, 1978a; Urie *et al.*, 1984; Wagner, 1982) were also developed at the Harvard Cyclotron Laboratory. These latter beam-modification systems and techniques or variants thereof are still widely used in broad-beam energy-modulated proton beam therapy. The use of ridge filters to form SOBPs was first described by Larsson (1961), and these filters are used at several centers.

Magnetic beam scanning was also first used in Uppsala for broad-beam SOBP treatments with the 187 MeV proton beam (Larsson, 1961). Kanai *et al.* (1980; 1983) used scanned beams with the 70 MeV proton beam in Chiba, Japan. Extensive clinical use of high-energy scanned proton beams has been undertaken at the Paul Scherrer Institute, Villigen, Switzerland (Pedroni *et al.*, 1995; 2005). Such beams are required for IMPT (Cella *et al.*, 2001; Lomax, 1999; Lomax *et al.*, 2001; Oelfke and Bortfeld, 2001).

Detailed dosimetric methods for proton therapy were first formulated by Verhey *et al.* (1979), and techniques for accurate patient positioning (Verhey *et al.*, 1982) were developed at the Harvard Cyclotron Laboratory. Goitein developed the first three-dimensional treatment-planning systems used in radiation therapy, one specifically for eye treatments (Goitein and Miller, 1983) and another for general use. He also introduced dose-volume histograms (DVHs), digitally reconstructed radiographs (DRRs), and the display of uncertainty bands around isodose contours (Goitein, 1978a; 1980; 1982a; Goitein and Abrams, 1983; Goitein *et al.*, 1983b).

1.3 PRESENT STATUS

A summary of the clinical outcomes of proton and photon radiation therapy for selected tumor types is presented in Table 1.1. These results, together with the physical rationale for proton therapy, have generally been accepted as very positive and constitute the bases for the substantial and increasing interest in the use of proton beams for radiation treatment of patients with both benign and malignant lesions. Local control is comparable for proton therapy and high-technology photon therapy for those cases for which similar RBE-weighted absorbed doses were administered. Proton therapy achieved no gain in the long-term local control in the treatment of patients with glioblastoma multiforme. Of the 23 patients in the study, only one patient survived 5 years (Fitzek

PRESCRIBING, RECORDING, AND REPORTING PROTON-BEAM THERAPY

Table 1.2. Proton therapy facilities (December 2007).

Institute	Location	Accelerator	Max. clinical energy MeV		Beam direction	First treatment	Patients treated
Crocker Nuclear Laboratory (operated by the University of California, San Francisco)	Davis, CA, USA	C	60	3.1	Horizontal	1994	920
Clatterbridge Centre for Oncology Centre	Clatterbridge, UK	C	62	3.3	Horizontal	1989	1 701
Antoine-Lacassagne National Institute of Radiological Sciences	Nice, France	C	65	3.6	Horizontal	1991	3 129
Centro di Adro Terapia e Applicazioni Nucleari Avanzate	Chiba, Japan	C	70	4.1	Vertical	1979–2002	145
Centro di Adro Terapia e Applicazioni Nucleari Avanzate	Catania, Italy	C	70	4.1	Horizontal	2002	151
Paul Scherrer Institute	Villigen, Switzerland	C	72	4.3	Horizontal	1984	4 875
Tri-University Meson Factory	Vancouver, Canada	C	72	4.3	Horizontal	1995	130
Hahn-Meitner-Institut	Berlin, Germany	C	72	4.3	Horizontal	1998	1 014
Université Catholique de Louvain	Louvain-la-Neuve, Belgium	C	90	6.4	Horizontal	1991–1993	21
Harvard Cyclotron Laboratory	Cambridge, MA, USA	SC	160	17.7	Horizontal	1961–2002	9 116
The Svedberg Laboratory (1)	Uppsala, Sweden	SC	185	22.8	Horizontal	1957–1976	73
The Svedberg Laboratory (2)	Uppsala, Sweden	SC	200	26.0	Horizontal	1989	738
Institute for Theoretical and Experimental Physics	Moscow, Russia	S	200	26.0	Horizontal	1969	4 024
iThemba Laboratory for Accelerator Based Sciences	Somerset West, South Africa	C	200	26.0	Horizontal	1993	500
Midwest Proton Radiotherapy Institute	Bloomington, IN, USA (1)	C	200	26.0	Horizontal	1993–1999	34
Midwest Proton Radiotherapy Institute	Bloomington, IN, USA (2)	C	200	26.0	Iso, Horiz	2004	379
Centre de Protonthérapie de l'Institut Curie	Orsay, France (1)	SC	200	26.0	Horizontal	1991	3 766
Joint Institute for Nuclear Research	Dubna, Russia (1)	SC [↓]	200	26.0	Horizontal	1967–1996	124
Joint Institute for Nuclear Research	Dubna, Russia (2)	SC [↓]	200	26.0	Horizontal	1999	402
Wakasa Wan Energy Research Center	Tsuruga, Japan	S	200	26.0	Vert, Horiz	2002	49
Paul Scherrer Institute	Villigen, Switzerland (1)	C ^{↓*}	230	32.9	Isocentric	1996	320
Hyogo Ion Beam Medical Center	Nishi-Harima, Japan	S	230	32.9	Is, Ve, Ho, 45°	2001	1 658
University of Florida Proton Therapy Institute	Jacksonville, FL, USA	C	230	32.9	Iso, Horiz	2006	15
National Cancer Center	Kashiwa, Japan	C	235	34.2	Iso, Horiz	1998	552
Francis H Burr Proton Therapy Center	Boston, MA, USA	C	235	34.2	Iso, Horiz	2001	2 710

Continued

INTRODUCTION

Table 1.2. Continued

Institute	Location	Accelerator	Max. clinical energy MeV	Beam direction	First treatment	Patients treated	
Shizuoka Cancer Center	Mishima, Japan	S	235	34.2	Iso, Horiz	2003	570
Wanjie Proton Therapy Center	Wanjie, China	C	235	34.2	Iso, Horiz	2004	537
National Cancer Center	Ilsan, South Korea	C	235	34.2	Iso (2), Horiz(1)	2007	
Proton Medical Research Center	Tsukuba, Japan (1)	S [↓]	250	37.9	Vert, Horiz	1983–2000	700
M D Anderson Cancer Center	Houston, TX, USA	S	250	37.9	Iso, Horiz	2006	527
Paul Scherrer Institute	Villigen, Switzerland (2)	sC*	250	37.9	Iso (2), Horiz(1)	2007	
Loma Linda University Medical Center	Loma Linda, CA, USA	S	270	43.2	Iso, Horiz	1990	11 414
Proton Medical Research Center	Tsukuba, Japan (2)	S	270	43.2	Isocentric	2001	1 188
Lawrence Berkeley National Laboratory	Berkeley, CA, USA	SC	340	63.3	Horizontal	1954–1957	30
Petersburg Nuclear Physics Institute	St. Petersburg, Russia	S	1 000	325.4	Horizontal	1975	1 327
				Total number of patients	1954–2007	53 439	

Accelerators: C = Cyclotron; SC = Synchrocyclotron; S = Synchrotron

Beam directions: Is(o) = Isocentric; Ve(rt) = Vertical; Ho(riz) = Horizontal; 45° = Inclined at 45° to horizontal

Symbols: ↓ = degraded beam; * = scanned beam

Facilities with energies less than 100 MeV (above the horizontal line) are used principally for the treatment of ocular lesions

et al., 1999), following twice daily delivery of RBE-weighted doses of 1.8 Gy (RBE) to a total of 90 Gy (RBE) in 5 weeks.

A critical requirement is the demonstration of an increment in tumor-control probability for a similar or reduced normal tissue-control probability. When considering local control, attention must be paid to the length of follow-up, and the assessment of the frequency and severity of radiation injury. No attempt has been made in the latter regard in the present report. It is not feasible at present because of lack of long-term follow-up data, especially in the case of high-technology photon treatments.

Table 1.2 provides a full list of proton-therapy facilities at which patients have been treated, including the number of patients treated at the time of writing. Thirty-three centers have been established. Four have been closed (those at Berkeley, CA, Cambridge, MA, Louvain-la-Neuve, and Chiba). Several of the older centers have undergone major upgrades of their original facilities (Uppsala, Dubna, Bloomington, IN, and Tsukuba). In the latter case, a completely new accelerator was installed. In addition, a new dedicated cyclotron for proton therapy has been commissioned at the Paul Scherrer Institute (PSI), Villigen. There are

currently 26 active clinical facilities. As noted above, all the early facilities were based on accelerators in physics laboratories. Recently, commercial proton accelerators and ancillary equipment have become available, and most new facilities are now hospital-based and feature 360°-rotating gantries. The growth of proton-therapy facilities is shown in Fig. 1.9. The sites of the currently active centers

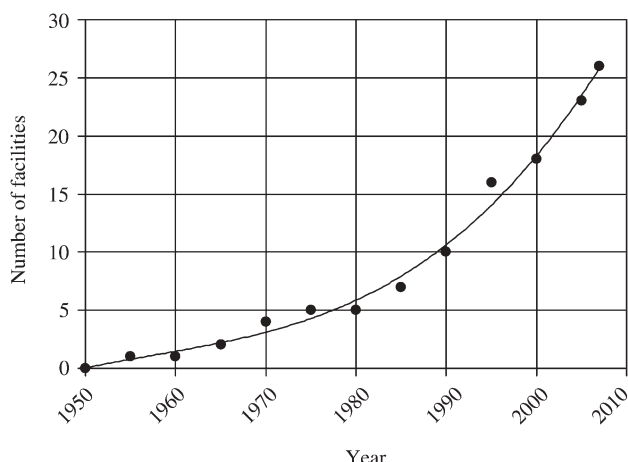


Figure 1.9. Number of operating proton therapy facilities given at 5 year intervals from 1950 to 2005. The number for 2007 is also shown. The curve is drawn to guide the eye.

Table 1.3 Dedicated proton therapy facilities under construction or funded (December 2007).

Institute	Location	Accelerator	Max. clinical energy (MeV)	Range in water (g cm^{-2})	Beam direction	Scheduled first treatment
Wesdeutsche Protontherapiezentrum	Essen, Germany	C	230	32.9	Iso (3), Horiz (1)	2009?
Roberts Proton Therapy Center	Philadelphia, PA, USA	C	230	32.9	Iso (4), Horiz (1)	2009?
Oklahoma ProCure Treatment Center	Oklahoma City, OK, USA	C ^a	230	32.9	Iso (1), Horiz (1), Dual fixed (2)	2009?
Centre de Protonthérapie de l'Institut Curie	Orsay, France (2)	C	230	32.9	Iso (1), Horiz (4)	2010?
Hampton University Proton Beam Therapy Center	Hampton, VA, USA	C	230	32.9	Iso (4), Horiz (1)	2010?
Sino-Japanese Friendship Hospital	Beijing, China	C	235	34.2	Iso (1), Horiz (1)	2007?
Rinecker Proton Therapy Center	Munich, Germany	sC ^a	250	37.9	Iso (4), Horiz (1)	2007?

Accelerators: C, cyclotron; sC, superconducting cyclotron. Beam directions: Iso, isocentric; Horiz, horizontal; Dual fixed, two fixed beam directions intersecting at single isocenter.

^aScanned beam.

are: Europe, 8; USA, 6; Japan, 5; Russia, 3; South Africa, 1; Canada, 1; China, 1; and South Korea, 1. The accelerators used in these active centers are cyclotrons in 15 centers, synchrocyclotrons in 3 centers, and synchrotrons in 8 centers. Of the 15 cyclotrons, 7 produce beams with energies between 60 and 72 MeV and are used principally for the treatment of ocular lesions. A further seven proton-therapy facilities are currently under construction or fully funded (Table 1.3). In addition, there are six new carbon-ion therapy facilities under development (Heidelberg and Marburg, Germany; Pavia, Italy; Lanzhou, China; Wiener Neustadt, Austria; and Maebashi, Japan) that will also provide therapeutic proton beams.

As shown in Table 1.2, more than 53 000 patients are recorded as having been treated with protons up to December 2007. The growth in patient treatments to December 2003 is shown in Fig. 1.10. As shown, a substantial fraction of proton treatments up to then had been for eye lesions (41 percent) and for prostate cancer (16 percent). Although proton therapy is a relatively new teletherapy modality, it is clearly in a rapid growth phase.

Proton therapy is judged likely to become an increasingly important component of the radiation oncology armamentarium.

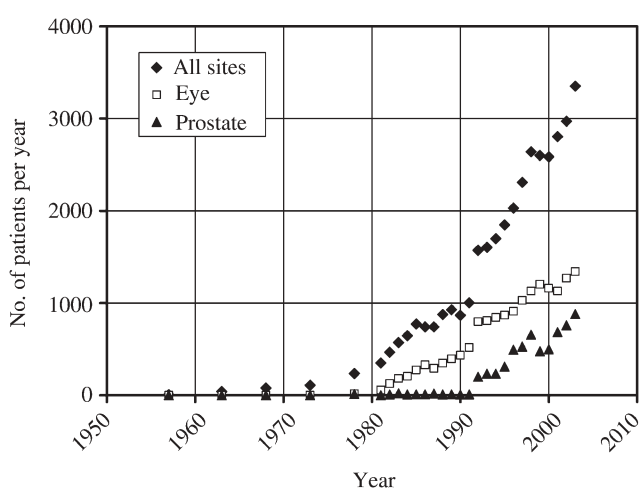


Figure 1.10. Number of patients treated annually with protons up to 2003. The data for 1957, 1963, 1968, 1973, and 1978 are annual averages for the periods 1954–1960, 1961–1965, 1966–1970, 1971–1975, and 1976–1980, respectively.

2 RADIATION BIOLOGY CONSIDERATIONS

2.1 INTRODUCTION

The rationale for proton therapy relates primarily to improved physical dose selectivity. Little clinical benefit is to be expected from selective radiobiological effects. Nevertheless, the relative biological effectiveness (RBE) of protons relative to high-energy (1–30 MeV) photons is significantly greater than unity. This fact immediately poses two questions: what is the best RBE estimate to be used in any calculation relating proton and photon doses, and how should proton doses be prescribed, recorded, and reported? Both of these subjects are discussed in the present section beginning with a discussion of the role of microdosimetry as a predictor of RBE. This will be followed by an evaluation of the available *in vitro* and *in vivo* information on proton RBE values, which leads to a suggestion to use a generic RBE for all therapeutic applications of protons. Finally, the section ends with a discussion of the impact of RBE on the issue of dose specification in proton therapy.

2.2 MICRODOSIMETRY AND LINEAR ENERGY TRANSFER

The microdosimetric characteristics of the proton beam have a strong influence on the RBE for each biological system. Linear energy transfer (LET) has been adopted as an approximation to the microdosimetric quantity \bar{y}_D (dose mean lineal energy) (ICRU 1977; 1989). LET is a descriptor of the energy transferred from the beam to the irradiated material, per unit of particle path length (in units of $\text{keV } \mu\text{m}^{-1}$, for example). For protons, the LET increases slowly along the particle path and then quite rapidly at the end of the particle range, resulting in the formation of the Bragg peak (see Fig. 1.1). The variation in LET with depth in mono-energetic and energy-modulated proton beams is illustrated in Figs 2.1a and 2.1b, respectively.

The rate of absorption of energy from an energy-modulated proton beam, producing a spread-out Bragg peak (SOBP), varies only to a modest degree with depth from the entrance to near the beginning

of the SOBP. There the absorption of energy becomes increasingly rapid. This is illustrated in Fig. 2.2, which presents the cumulative fractional absorption of energy per unit of LET (in $\text{keV } \mu\text{m}^{-1}$) from an energy-modulated 250 MeV proton beam at four depths, *viz.*, 2.5, 14.5 and 27.5 cm, and on the distal edge of an 8 cm SOBP.¹ As discussed earlier, there are very modest differences in energy absorbed per unit LET over the extended range in depth from 2.5 to 27.5 cm. Approximately 50 percent of the dose is absorbed at $3\text{--}4 \text{ keV } \mu\text{m}^{-1}$. However, at the distal edge of the SOBP, the curve is displaced sharply to the right and 50 percent of the dose is absorbed at $\sim 18 \text{ keV } \mu\text{m}^{-1}$. This is associated with an increased RBE, *vide infra*. The consequence of both LET and RBE increasing as dose is decreasing on the distal edge of the Bragg peak is to extend the biologically effective range of the proton beam by $\sim 2 \text{ mm}$ for 160–250 MeV beams and $\sim 1 \text{ mm}$ for 60–85 MeV proton beams, *vide infra*.

Linear energy transfer has proven useful in understanding the variation in biological effectiveness of different segments of the range of a particular particle beam in an individual biological system. However, LET does not predict biological response with high accuracy for different cell or tissue systems. For example, Weyrather *et al.* (1999) determined cell survival curves and the ratio of α -values in ^{12}C and x-ray beams for exponential phase V79, CHO-K1, and xrs5 cell lines growing as monolayers. They observed substantial differences in the ratio of the α -values versus LET relations for the three cell lines, as illustrated in Fig. 2.3.

2.3 REVIEW OF PUBLISHED PROTON RBE VALUES

The present report is concerned with protons of clinical utility in radiation oncology, *viz.*, 60–250 MeV beams. RBE values for low-energy protons, *viz.*, $< 10 \text{ MeV}$, exhibit significant energy dependence and are substantially higher than

¹Calculated from Coutrakon *et al.* (1997).

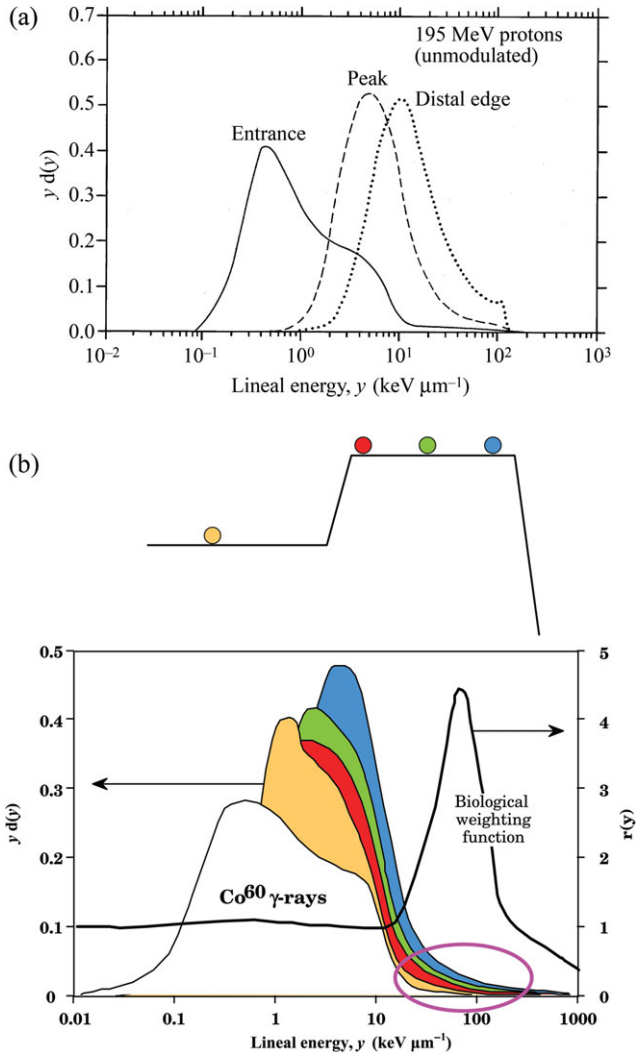


Figure 2.1. (a) Microdosimetric (lineal energy, y) spectra measured at different depths in a 200 MeV monoenergetic proton beam, *viz.*, on the entrance plateau, on the Bragg peak, and on the declining distal edge of the Bragg peak (Binns *et al.*, 1993; reproduced with permission). (b) Microdosimetric (lineal energy, y) spectra measured in a 90 MeV energy-modulated proton beam at the Université Catholique de Louvain. Measurements were performed in the initial plateau (yellow), and at the proximal (red), middle (green), and distal (blue) parts of the SOBP, as indicated on the schema at the top of the figure. The y spectrum for ^{60}Co is given for comparison. Compared with ^{60}Co , the four proton spectra are slightly shifted toward high y values, which might explain the 10 percent relative difference in RBE. In addition, there is a progressive shift, with depth, of the proton spectra toward higher y values that could be responsible for the slight additional RBE increase of 5–10 percent at the end of the SOBP compared with the initial plateau and other shallower depths in the proton beam. The right ordinate is the biological weighting function that expresses the RBE variation as a function of y for the case of intestinal crypt cell regeneration. Only a small proportion of the proton spectra overlaps with the ascending part (RBE > 1) of the biological weighting function (as indicated by the pink oval). Adapted from Gueulette, Université Catholique de Louvain, redrawn from the data of Gueulette *et al.* (2004), Loncol *et al.* (1994), and Menzel *et al.* (1990). Reproduced with permission.

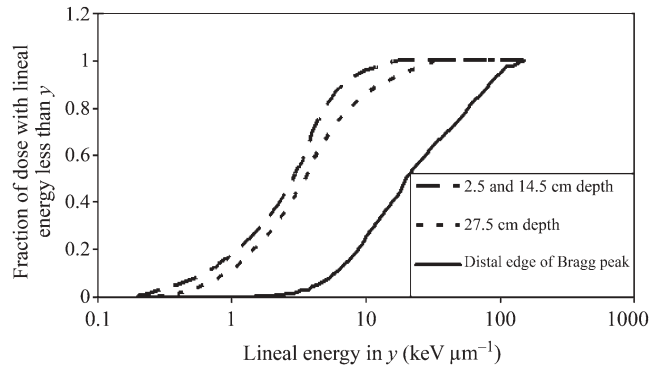


Figure 2.2. Plot of the cumulative energy absorbed per unit lineal energy from a 250 MeV proton beam with an 8 cm SOBP at depths of 2.5, 14.5, 27.5 cm and at the distal edge of the terminal Bragg peak. Adapted from Coutrakon, Loma Linda University Medical Center, using data from Coutrakon *et al.* (1997). Reproduced with permission.

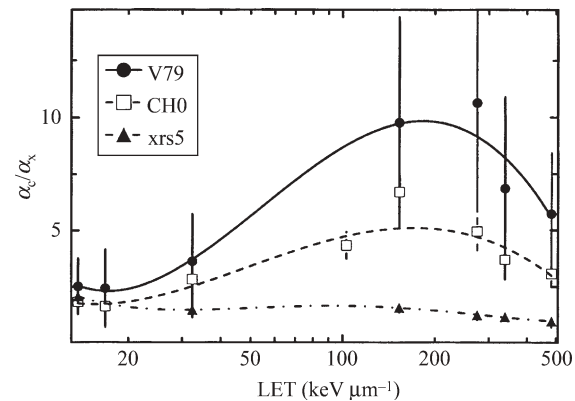


Figure 2.3. Ratio of α -values for ^{12}C ions and x rays as a function of LET for three cell lines. The range in LET was obtained by use of ^{12}C ion track segment irradiation (Weyrather *et al.*, 1999; reproduced with permission).

RBEs of clinical proton beams (Belli *et al.*, 1993; Cox *et al.*, 1977; Raju, 1995b). There is no proposed clinical utility of beams of this low energy.

RBE values have been determined for a broad array of mammalian cell lines *in vitro* using loss of colony-forming capacity as the endpoint and for *in vivo* experimental systems employing diverse cell and tissue responses as endpoints. For these experiments, cells or tissues were positioned in the mid-point of the SOBP. The reference radiations were ^{60}Co or other high-energy photon beams. The resultant RBE values have been collated and reviewed by Paganetti *et al.* (2002) and are pooled here with the more recent values by Kagawa *et al.* (2002). In the assessment of these experimental data, special attention was given to the relationship between RBE and dose. For higher LET radiations, *e.g.*, fast neutrons, RBE has been shown to increase inversely with dose, especially for doses less than about 10 Gy (Field, 1977).

2.3.1 RBE values determined using *in vitro* and *in vivo* systems

All known published RBE values at all dose levels for mammalian cell lines studied *in vitro* in proton beams in the clinical energy range are presented in Figs 2.4a–c. The majority of values are for V79 cells. The mean RBE is 1.19 (1.13–1.24).² There is no apparent increase in RBE as dose is decreased to <10 Gy. RBE values are presented separately for V79 (Fig. 2.4b) and non-V79 cells (Fig. 2.4c). The mean RBE value for the V79 cells is 1.24 (1.04 to 1.44), while for the non-V79 cells it is 1.12 (0.98 to 1.22). Note that V79 cells exhibit a larger shoulder on survival curves than do other cell lines.

RBE values for a variety of *in vivo* systems are presented in Fig. 2.5a. The animal tissues and organs studied include skin (acute reaction and late contraction), lung, jejunal crypts, tail, vertebrae, testis, lens, and bone marrow. Mean RBE for all proton energies, dose levels, and tissue systems is 1.10 (1.09–1.12). This value is significantly less than the mean value for all *in vitro* RBE values. Also, for the *in vivo* studies, there is no evidence of an increase in RBE as dose is reduced from 10 to 0.7 Gy. Furthermore, there is no evident difference in RBE among the tissue systems investigated at any dose level. As discussed earlier, several of the RBE values were <1.0. Figure 2.5b and c shows the RBE values for acute-reacting and late-reacting tissues, respectively. No significant difference was detected.

There are three determinations of RBE for *in vivo* systems at the mid-SOBP positions of 60–85 MeV proton beams. Gueulette *et al.* (1996) determined the RBE of mouse jejunal crypt cell survival for single-dose irradiation by an 85 MeV proton beam versus ^{60}Co photons. The resultant RBE was 1.08³ at a photon-absorbed dose of 13.3 Gy resulting in 20 surviving crypts per intestinal circumference. Ando *et al.* (1985) employed inactivation of mouse fibrosarcoma micro-colony forming cells in lung and measured RBE values for absorbed doses of 5–6 Gy in a 70 MeV beam. The RBE values in three experiments were 1.01, 1.14, and 1.02. For the second and third experiments, assays were also performed using a 250 MeV beam. The RBE values were 1.09 and 0.99, respectively.⁴ Nemoto *et al.* (1998) found the RBE for 80 MeV protons to be 1.20⁵ at a

²The confidence bands given here and throughout the present section are the 95 percent limits unless otherwise stated.

³This value was significantly higher than 1.00 ($p = 0.005$).

⁴Confidence limits for the RBE values were not given and could not be computed from the paper.

⁵95 percent confidence limits were given as 1.06–1.62.

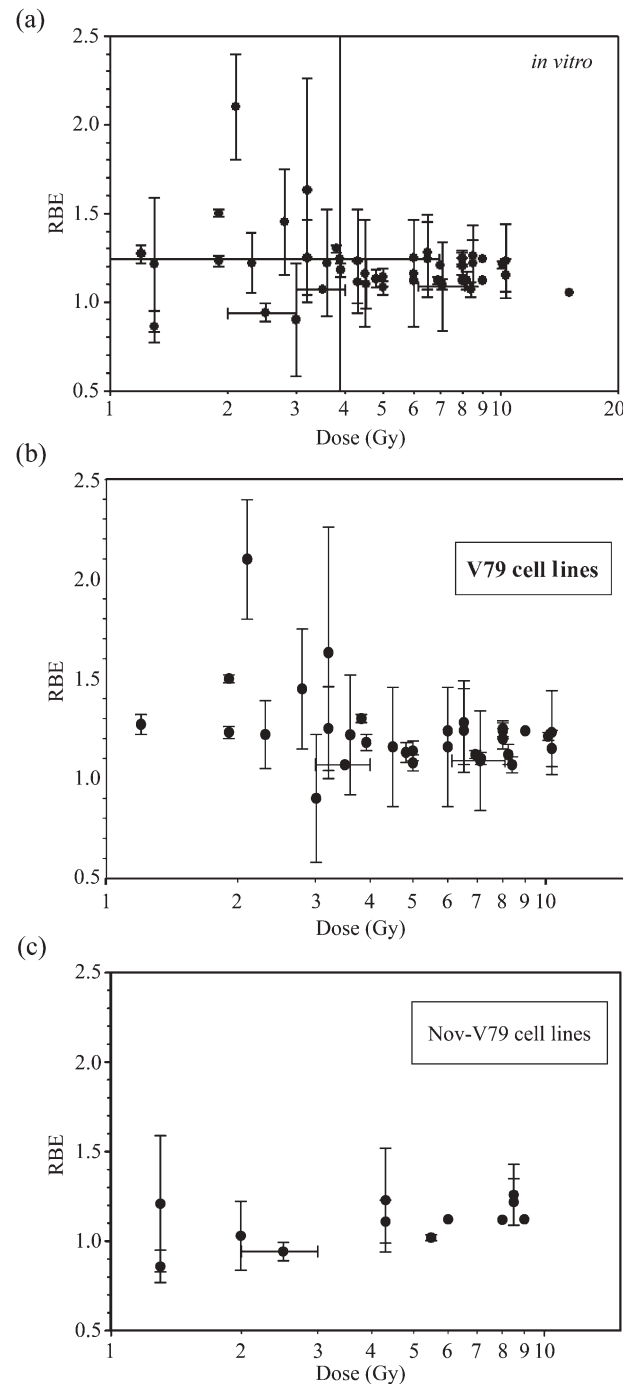


Figure 2.4. (a) RBE versus absorbed dose for all cell lines irradiated *in vitro* and using colony formation as the endpoint (Paganetti *et al.*, 2002; reproduced with permission). (b, c) RBE versus dose for V79 cells (b) and for non-V79 cells (c) irradiated *in vitro*, both using colony formation as the endpoint. Data derived from (a) (Paganetti *et al.*, 2002).

photon-absorbed dose of 8.5 Gy for acute skin reactions. They also reported the RBE value to be 1.15, 1.24, and 1.15 at photon-absorbed doses of 33.7, 20.7, and 13.0 Gy, respectively. All these values are consistent with an average RBE of 1.1.

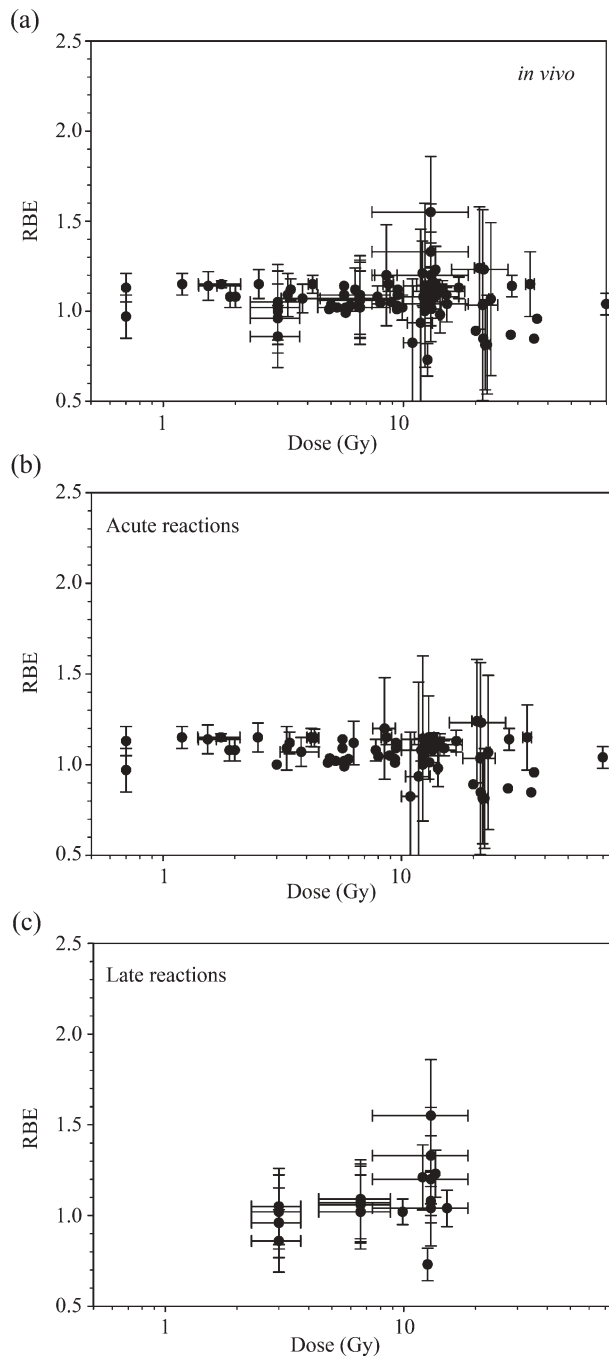


Figure 2.5. (a) All RBE versus dose values for acute- and late-reacting experimental animal-tissue systems. The tissues studied include jejunal crypt cells, lung, skin (acute reaction and late contraction), vertebral growth, bone marrow, testis, lens, and tumor (Paganetti *et al.*, 2002; reproduced with permission). (b, c) RBE versus absorbed dose for acute (b) and late (c) reactions in experimental animal-tissue systems. Data derived from (a) (Paganetti *et al.*, 2002), supplemented with data from Kagawa *et al.* (2002).

Special mention is made of the findings of two studies on late-reaction endpoints. These are the only published RBE values for late tissue injury, despite the high clinical interest in risk of

late-radiation injury. RBE values were determined for 200 MeV proton irradiation of the lungs of Balb/c mice using LD_{50} (the dose lethal to 50 percent of animals) as the endpoint (Guelette *et al.*, 2000). Radiation was delivered using a 3 cm high beam in 1, 3, and 10 dose fractions, with 12 h between fractions; the mice were positioned in the mid-portion of a 7 cm SOBP. RBE values for the 10-fraction schedule were 0.86, 0.95, 1.05, and 1.02 for LD_{50} values at 180, 210, 240, and 270 d, respectively. The absorbed doses per fraction for the latter schedule were 2.3–3.7 Gy (^{60}Co) and 2.0–3.2 Gy (proton). The mean RBE for the 10-fraction irradiation was significantly lower than the mean RBE of the single-fraction assays ($p < 0.05$). Tatsuzaki *et al.* (1991) irradiated the legs of ICR mice using 250 MeV protons or ^{60}Co photons in 10 fractions over 11 d and scored skin contraction at 250 d. The RBE was found to be 1.02–1.03.⁶ There are no reported RBE determinations of late reactions in central nervous system tissues after proton irradiation.

In summary, the available data on *in vitro* and *in vivo* systems (including acute- and late-reacting tissues) are consistent with a tissue-independent mean RBE value of 1.10. Further, there is no suggestion from studies on *in vivo* systems of an increase in RBE as absorbed dose is reduced to < 3 –4 Gy. This finding for protons of no dose dependence of RBE is in contrast with those for fast neutrons, where RBE increases steeply as absorbed dose is decreased below 4 Gy (Field, 1977). The fact that the proton RBE data do not conform to the expectations from the neutron data may, in part, reflect the difficulty in demonstrating the modest changes in relatively small RBE values. The available experimental studies (Fig. 2.5a) do not extend into the absorbed dose range (< 1.0 Gy) where hypersensitivity has been demonstrated (Chandna *et al.*, 2002).

2.3.2 RBE versus depth for 60–250 MeV beams

A clinically important radiobiological question is the magnitude of change, if any, of RBE along the plateau, across the SOBP, and on the distal portion of the terminal Bragg peak.

2.3.2.1 60–85 MeV

For proton beams of this energy range, the SOBPs are ~ 14 –30 mm in depth. Eight reported *in vitro* measurements of RBE values versus depth in the SOBP for 60–85 MeV beams are summarized in

⁶No confidence limits were provided for these RBE values.

Table 2.1. These results are consistent with an increase in RBE along the 14–30 mm SOBP of 60–85 MeV proton beams, but with clear variability in the magnitude of the change in RBE between the different studies. The very detailed study of Wouters *et al.* (1996) reported an increase of 7 percent across the 24 mm SOBP. Bettega *et al.* (2000) determined the RBE at 3–12 mm from the beginning of a 14 mm SOBP of a 65 MeV beam. For one cell system, there was a 16 percent relative increase and in the second cell system a 6 percent relative decrease in RBE over those 9 mm. Blomquist *et al.* (1993) found no increase in RBE between 2 and 17 mm along a 17 mm SOBP for the V79–379A cell line. From five studies, there was evidence of an increase in the RBE over these short lengths of SOBP, *viz.*, relative increments of 7–23 percent. In one study, it was shown that there was no change in RBE values at 9 and 14 mm along a 14 mm SOBP (Matsumura *et al.*, 1999).

2.3.2.2 160–250 MeV

Robertson *et al.* (1975) employed the H4 (rat hepatoma) cell line with 160 MeV protons and ^{60}Co photons in their determination of the RBE as a function of position in a 5 cm SOBP.⁷ They found that the mean of 78 RBE values determined at absorbed doses of ≥ 3 Gy for positions proximal to the final Bragg peak was 1.00 ± 0.01 .⁸ Additionally, for 102 determinations at absorbed doses of 2–3 Gy, the mean RBE was ~ 1.0 . Further, RBE values were not significantly different from 1.0 at five positions over the 3 mm proximal to the center of the final Bragg peak. That is, there was no evidence for an RBE above 1.0 over the entire SOBP. The values for the distal 3 mm and beyond are shown in Fig. 2.6a. Slabbert *et al.* (1994) reported RBE values for V79 cells irradiated by a 200 MeV proton beam relative to a ^{60}Co beam. They made measurements for absorbed doses between 2 and 12 Gy at depths of 43.5 (initial plateau) and 141.5, 167.5, and 191.5 mm in a 7 cm SOBP; the 191.5 mm depth was at 1 cm proximal to the distal peak. The resultant mean RBE values were 1.00, 1.04, 1.07, and 1.16,⁹ respectively.

Coutrakon *et al.* (1997) employed V79 cells and determined α and β values¹⁰ at 2.5 cm intervals from the entrance to the distal portion of 8 cm SOBPs of 155, 200, and 250 MeV proton beams.

⁷The endpoint for the RBE determinations was SF (surviving fraction) = 0.1.

⁸The standard error.

⁹These were not significantly >1.00 .

¹⁰ α and β are parameters in the linear quadratic model for cell survival.

RBEs versus depth computed for surviving fractions (SF) of 0.1 and their 95 percent confidence limits are presented in Fig. 2.7.¹¹ There were no increases in RBE with depth from the entrance through the SOBP until the final 1 cm proximal to the end of range for the 155 and 200 MeV beams, *viz.*, at 12.2 and 19.9 cm, respectively. This increase was significant for the 155 MeV beam. In contrast, for the 250 MeV beam, there was no increase in RBE with depth including the point at about 1.4 cm proximal to the final Bragg peak, *i.e.*, at 30.0 cm depth. The endpoint range was 31.4 cm. In a subsequent experiment, Robertson extended these studies to examine RBE at 5 mm beyond the midportion of the final peak. His finding was that the ratio of the RBE at the declining edge point to that at the entrance for the 200 MeV beam was ~ 1 . Raju *et al.* (1978) investigated the response of V79 cells and found that the surviving fractions at absorbed doses of 3, 4, and 8 Gy were constant over the full depth of the 9 cm SOBP of a 160 MeV beam.

2.3.2.3 RBE on the declining distal edge of the SOBP

The studies in a 5 cm SOBP of a 160 MeV beam by Robertson *et al.* (1975) included measurement of the variation (in ~ 0.5 mm intervals) of RBE from 3 mm before, to 6.5 mm beyond, the midpoint of the distal Bragg peak contributing to the SOBP. The RBE increased from ~ 1.0 –1.4 from the midpoint to 6 mm beyond the distal Bragg peak (Fig. 2.6a). No RBE variation was observed in the 3 mm proximal to this midpoint.

In Fig. 2.6b, the absorbed dose curve is compared with the experimentally determined RBE-weighted absorbed dose curve (absorbed dose \times experimentally determined RBE). In the region between ~ 1 and 4 mm beyond the distal Bragg peak, the RBE-weighted absorbed dose is ~ 8 percent greater than the RBE-weighted absorbed dose in the SOBP. The effect of the rather large increment in RBE is primarily to extend the RBE-weighted dose curve along the declining edge of the final Bragg peak by ~ 2 mm as the relative dose decreases from ~ 100 –85 percent and by ~ 1 mm at the 50 percent dose level.

Slabbert *et al.* (1994) determined the RBE for monolayers of V79 cells at the distal end and on the declining edge of the SOBP in a 200 MeV beam. Increased RBE values of 1.3, 1.4, and 1.5 were obtained at the end of the SOBP and at the 35 and 32 percent isodose levels, respectively. In contrast to

¹¹RBE values were computed as the ratios of dose to yield an SF of 0.1 at the surface, to the dose to yield the same SF at each specified depth.

Table 2.1. *In vitro* RBE values versus depth in the SOBP of 60–85 MeV proton beams.

Energy (MeV)	Reference beam	Cell line	End point	SOBP width (mm)	RBE			RBE ratio distal/proximal	Reference
					SOBP proximal	SOBP middle	SOBP distal		
85	⁶⁰ Co	CHO	SF = 0.5	30	0.94	1.22	1.16	1.23	Guelette <i>et al.</i> (1996)
70	⁶⁰ Co	V79	SF = 0.5	24	1.28	1.30	1.38	1.07	Wouters <i>et al.</i> (1996)
67	⁶⁰ Co	V79 379A	SF = 0.5	20	1.63	1.63	1.63	1.00	Blomquist <i>et al.</i> (1993) ^a
65	⁶⁰ Co	SCC25	SF at 2 Gy	14	1.05		1.22	1.16	Bettega <i>et al.</i> (2000)
65	⁶⁰ Co	SCC25	SF at 2 Gy	14	1.13		1.05	0.94	Bettega <i>et al.</i> (2000)
			progeny ^b						
65	¹³⁷ Cs	CHO	SF = 0.67	18	1.19	1.23	1.37	1.15	Tang <i>et al.</i> (1997)
65	¹³⁷ Cs	V79	SF = 0.5	14		1.35	1.34	1.00	Matsumura <i>et al.</i> (1999)
65	Proton beam plateau	CAL4	SF = 0.01	28	1.09	1.12	1.27	1.16	Courdi <i>et al.</i> (1994)

SF, surviving fraction.^a In this paper Blomquist *et al.* (1993) also reported that the RBE values for the LS-174T cells tended towards higher values with dose, *viz.* the RBEs were 1.21, 1.23, and 1.26 for SFs of 0.5, 0.12, and 0.001, respectively. This was the opposite of the results for the V79 cells, *viz.* the RBE for those SFs were 1.63, 1.28, and 1.15, respectively.^b These experiments were performed on the progeny of irradiated SCC25 cells.

Robertson *et al.*'s (1975) experiment, there was an increase in RBE in the distal half of the SOBP.

Bettega *et al.* (2000), using a 65 MeV beam and human SCC25 cells, determined RBE at 15.6, 25.0, 27.2, and 27.8 mm depths; the latter two positions were at the 91 and 52 percent depth–dose levels, respectively, on the declining edge of the SOBP. The RBE values obtained were 1.05, 1.22, 1.39, and 2.05, respectively. These higher RBEs on the declining edge of the SOBP have the effect of extending the RBE-weighted range by ~1 mm.

Paganetti and Goitein (2000), using a biomathematical model, concluded that the extension in depth of the RBE-weighted range is a function of the proton energy and energy spread.

2.4 USE OF A GENERIC RBE VALUE

There are no proton RBE values based on human-tissue response data, despite clinical experience of the treatment of more than 50 000 patients. All of the available proton RBE values on tissue systems with usefully narrow confidence limits have been derived from data on laboratory experimental systems. Estimates of RBE require data from a range of doses for both the photon and proton arms delivered to relatively homogeneous subjects treated in a defined protocol. This condition is not really feasible in clinical medicine but is readily achieved in laboratory experiments. Accordingly, the RBE value to be applied clinically must be derived from laboratory-based investigations, preferably using *in*

vivo systems, and then 'validated' clinically. Clinical experience has not been interpreted as indicating that the RBE is different from 1.10.

The literature on RBE values indicates that there are no experimental data from *in vivo* systems that support the use of a tissue-, dose-, dose per fraction-, or energy- (60–250 MeV) specific proton RBE for murine tissues.

Accordingly, the use of a generic RBE in proton-radiation therapy is judged to be clinically appropriate and is therefore recommended. A generic proton RBE means the use of a single value, independent of the tissue irradiated, dose per fraction, total dose, proton energy, and position on the physical depth–dose curve up to the midpoint of the terminal Bragg peak. The RBE value to be employed should be that which best fits pooled RBE values from *in vivo* studies, *e.g.*, 1.1. This applies to all tissues in the direct beam path.

In addition to increasing the level of the RBE-weighted absorbed dose (relative to the absorbed dose), the application of a generic RBE of 1.1 to a computed absorbed depth–dose curve slightly increases the range of the RBE-weighted absorbed depth dose.

While the use of a generic value of 1.1 to convert the absorbed dose to a RBE-weighted absorbed dose in a proton beam is recommended in the present report, several experimental data suggest that the RBE might increase by 5–10 percent in the deepest part of the SOBP relative to the middle of the SOBP. There is also evidence (see Section 2.3.2.3) that the RBE does increase significantly

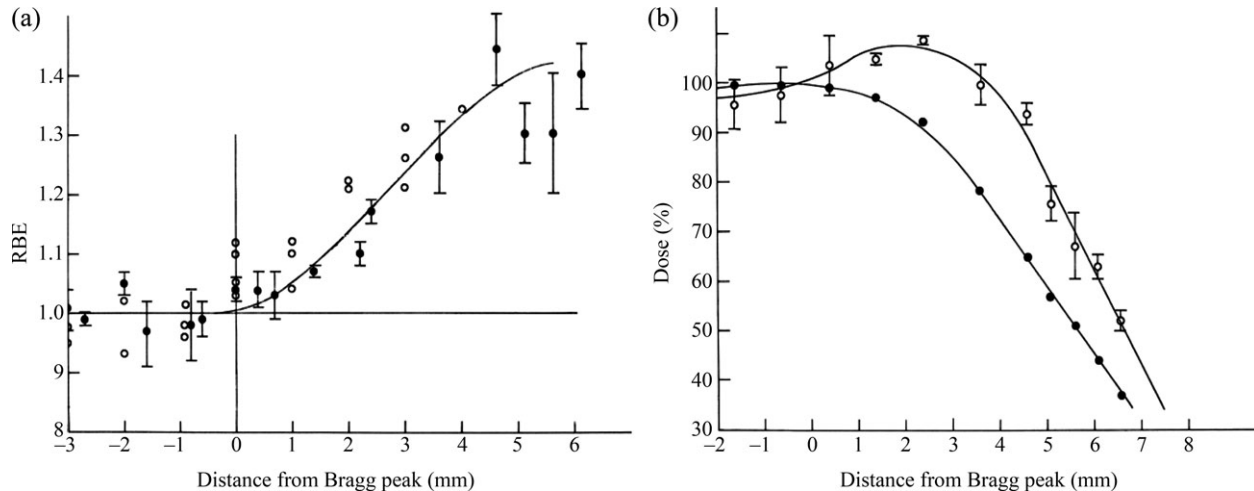


Figure 2.6. RBE determination for H4 cells at $SF_{0.1}$ (surviving fraction of 0.1) in an unmodulated 160 MeV proton beam and in the distal region of a 5 cm SOBP produced by the same beam. The measurements cover a range from 3 mm proximal to 6.5 mm distal to the Bragg peak (Robertson *et al.*, 1975; reproduced with permission). (a) RBE as a function of depth normalized to the RBE at the midpoint of the distal Bragg peak contributing to the SOBP. Open circle represents RBE for unmodulated beam. Filled circle represents RBE for modulated beam. (b) Variation with depth of the absorbed dose and the RBE-weighted absorbed dose. The two curves are normalized to their values at the depth of the midpoint of the distal Bragg peak. Open circle represents RBE-weighted absorbed dose. Filled circle represents absorbed dose.

over the initial few millimeters of the declining edge of the SOBP relative to the RBE at the depth of the distal Bragg peak. This yields an increase in the range of the RBE-weighted absorbed dose by 1–2 mm (see Fig. 2.6). These effects might need to be considered in treatment planning, especially for single-field treatments and when organs at risk are located at these positions.

2.5 DOSE SPECIFICATION

Absorbed dose is a fundamental quantity used in all therapeutic applications of ionizing radiation. Measurement and reporting of absorbed dose is crucial to the understanding of any radiation effects (BIPM, 2006; ICRU, 1993b; 1998). As a general recommendation and in line with ICRU Reports 50, 62, and 71 (ICRU, 1993b; 1999; 2004), the absorbed dose should be specified at a certain number of relevant points and/or in specific volumes. However, absorbed dose alone is not a sufficient predictor of therapeutic outcome. Therefore, all relevant parameters such as absorbed dose, fractionation, overall time, and radiation quality should be reported. In radiation therapy, when comparing, combining, or exchanging information for treatments performed under different conditions, weighting of absorbed dose is often useful and sometimes necessary (Grégoire *et al.*, 2004; Wambersie *et al.*, 2004a; 2006).

To account for the fact that protons exhibit a RBE significantly different from unity, it has been

common practice to report, in addition to absorbed dose, the ‘equivalent’ or ‘cobalt-equivalent’ dose. This ‘equivalent’ dose was defined as the product of the absorbed dose and the proton RBE. It thus represents the photon dose that would give the same therapeutic effect as the actual proton dose, assuming all irradiation conditions including the number of fractions and overall treatment time, are the same for both radiation qualities.

The use of the term ‘equivalent dose’ as defined above cannot be recommended for therapeutic applications. The term ‘equivalent dose’ has previously been defined for radiation protection purposes (ICRP, 1991) and is already used in several important national and international regulatory documents. Moreover, the term ‘equivalent’ could, in any case, be misleading to the extent that the equivalence is only relative to photons delivered under the same conditions as the protons. When comparing two proton treatments delivered with different fractionation schemes, the therapeutic effects of equal ‘equivalent’ doses could be different if the respective reference photon treatments were delivered with a different fractionation scheme.

It has been common practice to report ‘equivalent dose’ in units of ‘gray equivalent’ or ‘cobalt gray equivalent’ using symbols such as CGE, GyE, or Gy(E). However, the SI (*Système International d’Unités*/International System of Units) does not permit the use of arbitrary units nor the addition of words, subscripts, asterisks, *etc.* to the unit; hence, the use of CGE, GyE, or Gy(E) is not recommended (BIPM, 2006).

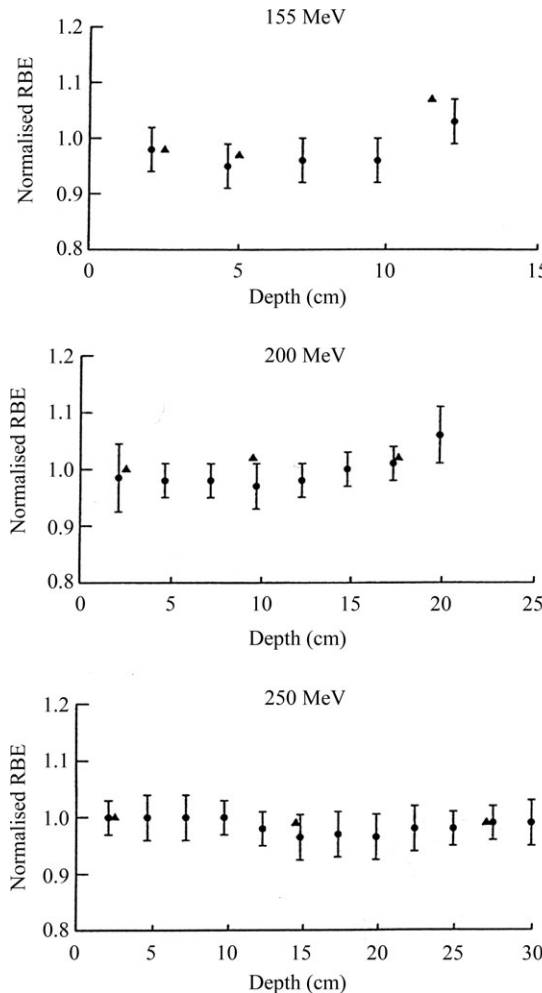


Figure 2.7. RBE versus depth (solid circles) for 155, 200, and 250 MeV proton beams (see text). The data are normalized to an RBE of 1.0 at 2.5 cm depth for the 250 MeV beam. The circles are values determined from V79 cell survival curves. The triangles are values derived from microdosimetry measurements (Coutrakon *et al.*, 1997; reproduced with permission).

2.5.1 The RBE-weighted absorbed dose (D_{RBE})

To replace the term equivalent dose and its units Gy(E), GyE, or CGE, the quantity RBE-weighted absorbed dose, D_{RBE} , will be used in the present report to designate the product of the total proton-absorbed dose, D , and the proton RBE, with respect to photons delivered under the same conditions. The symbol d_{RBE} will denote the RBE-weighted absorbed dose per fraction. The special name of the unit of both absorbed dose and RBE-weighted dose is gray (Gy).

In the case of protons, where use of a generic RBE of 1.1 is recommended:

$$D_{\text{RBE}} = 1.1 \times D. \quad (2.1)$$

- Symbol D represents the proton absorbed dose (in Gy).
- Symbol D_{RBE} (in Gy) is the RBE-weighted proton absorbed dose and is the dose of photons that would produce the same therapeutic effect as a proton-absorbed dose, D , given under identical circumstances.

Because RBE is dimensionless, D and D_{RBE} are both expressed in Gy. The use of a single unit for two quantities may be seen as a source of confusion. To avoid this confusion it is recommended that the quantity, either D or D_{RBE} , be always explicitly specified. For example, one can write 'the absorbed dose to the PTV was 63 Gy (or $D_{\text{PTV}} = 63$ Gy) and/or the RBE-weighted absorbed dose to the PTV was 70 Gy (or $D_{\text{RBE,PTV}} = 70$ Gy) assuming an RBE of 1.1'. To further reduce the possibility of confusion, it is recommended that the quantity D_{RBE} be expressed in Gy, followed by a space and the parenthetical descriptor '(RBE)'. The RBE-weighted absorbed dose specification would read ' $D_{\text{RBE}} = 70$ Gy (RBE)'. This notation will be used throughout the remainder of the present report. Other sections of the present report will elaborate on a variety of quantities such as $D_{\text{RBE,PTV,98\%}}$, an RBE-weighted absorbed dose encompassing 98 percent of a PTV. In every case, the quantities $D_{98\%}$ or $D_{\text{RBE},98\%}$, representing absorbed or RBE-weighted absorbed doses, respectively, and the chosen RBE value used should be clearly specified.

In summary, the concepts of absorbed and RBE-weighted absorbed doses serve different purposes. Absorbed dose is a physical quantity derived from measurement or calculation, whereas RBE-weighted dose is a biologically weighted quantity designed to define doses of protons that would produce identical biological effects as doses of photons if administered under identical conditions. As such, the absorbed dose will have a primary role in dosimetry protocols and a prominent role in any clinical protocol and final report. The RBE-weighted dose is better suited to a comparison of the effects of photon versus proton therapy, for the selection of appropriate proton doses, and the prediction of therapeutic outcomes based on previous experience with photons. Whether the quantities absorbed dose and/or RBE-weighted absorbed dose should be used in clinical practice in the different steps of treatment preparation and planning procedures is a matter of experience and local policy. It is, however, important and obligatory that the quantities involved be clearly specified to avoid any risk of confusion.

3 BEAM DELIVERY AND PROPERTIES

3.1 PROTON-THERAPY FACILITIES

A typical proton-therapy facility, shown in Fig. 3.1, comprises several main components: (i) an accelerator with an energy-selection system to produce energetic protons, (ii) a beam-transport system to steer the beam to the treatment-delivery system, and (iii) a treatment-delivery system. The latter comprises several subsystems and may include some or all of the following: a gantry, a beam nozzle, a snout, a volume-tracking and beam-gating device, and a patient-positioning and immobilization system. The final component of the proton-therapy facility is a shielded enclosure to separate the accelerator and beam-transport system from the treatment rooms, in order to protect patients and to allow personnel to move freely between treatment rooms while the beam is in use within adjacent restricted areas. The accelerator and its energy-selection, beam-transport, and treatment-delivery systems need to interact to produce the desired treatment. For example, energy changes are necessary to scan the beam through the target volume, which may require changes in the accelerator cycle or an energy-selection system, the beam-transport system and the beam nozzle and snout. From the perspective of the patient treatment, the treatment-delivery system is the most significant component of the overall facility. Therefore, in the present section, the patient support, immobilization, and positioning system are considered first, followed by discussion of the gantry or fixed beam line, the beam-transport system, the accelerator, and energy-selection requirements.

The overall aim of the facility is to deliver therapeutic doses of proton beams to tumor sites anywhere in the human body. This aim requires a proton beam of sufficient energy to penetrate past the centerline in the thickest region of the body (*i.e.*, in the pelvis) potentially at an oblique angle. In practice, the beam penetration must be 26–38 cm in human tissue, which requires an accelerator capable of producing proton energies of 200–250 MeV. In addition, the beam must have sufficient intensity to allow therapeutic doses to be

delivered within a reasonable time. Typically beam intensities of between 1.8×10^{11} and 3.6×10^{11} particles per minute are required if doses of 2 Gy min^{-1} are to be delivered uniformly to target volumes of one liter. The exact energy and intensity requirements depend critically on the mode of beam delivery (either scattering or scanning) that is actually used.

3.2 THE TREATMENT-DELIVERY SYSTEM

The treatment-delivery system comprises several major subsystems: the beam nozzle, snout, the patient support, immobilization, and positioning system, and the gantry.

3.2.1 The beam nozzle and snout

Beam-delivery techniques are commonly categorized as passive or dynamic. This categorization refers to the method used to spread out the beam laterally. The spreading out of the beam in depth is often done dynamically (*i.e.*, in a time sequence of steps) or passively using a ridge filter. The spreading of the beam in depth is used with both scattering systems (passive beam delivery) and uniform scanning systems (dynamic beam delivery). These beam-spreading devices are incorporated in the nozzle and snout, together with patient-specific beam-modifying devices.

3.2.1.1 Passive beam-delivery techniques

Passive beam delivery involves ‘scattered beams’ and is a method of achieving a spatially uniform dose distribution by scattering and degrading the primary proton beam in a set of distributed absorbers to create the beam diameter, maximum energy, and energy spread needed to deliver uniform dose to the target at all depths. An example of such a system is a rotating propeller with variable-thickness blades, as first discussed by Wilson (1946) in combination with a separated pair of scatterers (ICRU, 1998; Koehler *et al.*, 1977). The field shape is determined by a block or aperture, the shape of which is determined by the

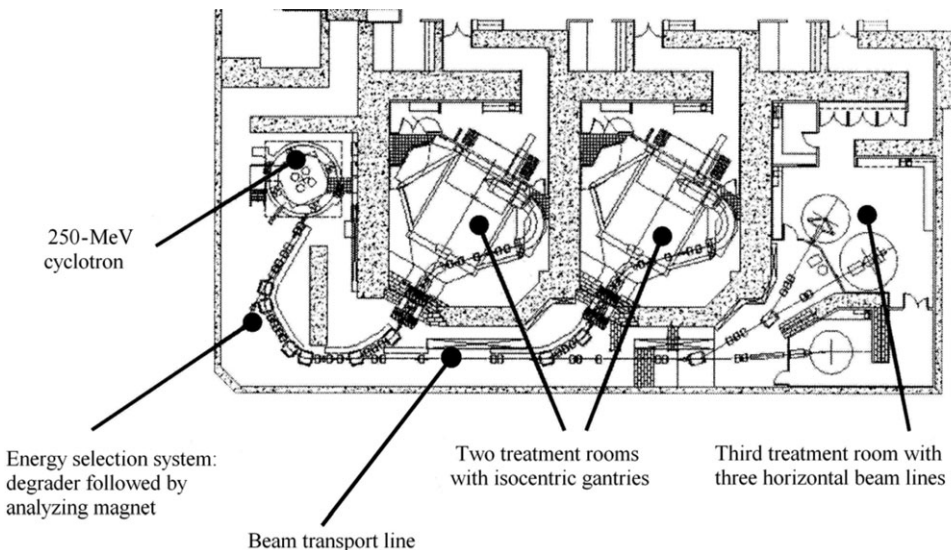


Figure 3.1. Proton-therapy facility layout at Massachusetts General Hospital (Francis H. Burr Proton Therapy Center). For a synchrotron-based facility, the layout is similar. Facilities can have as many as six treatment rooms. (Adapted from Goitein *et al.*, 2002; reproduced with permission.)

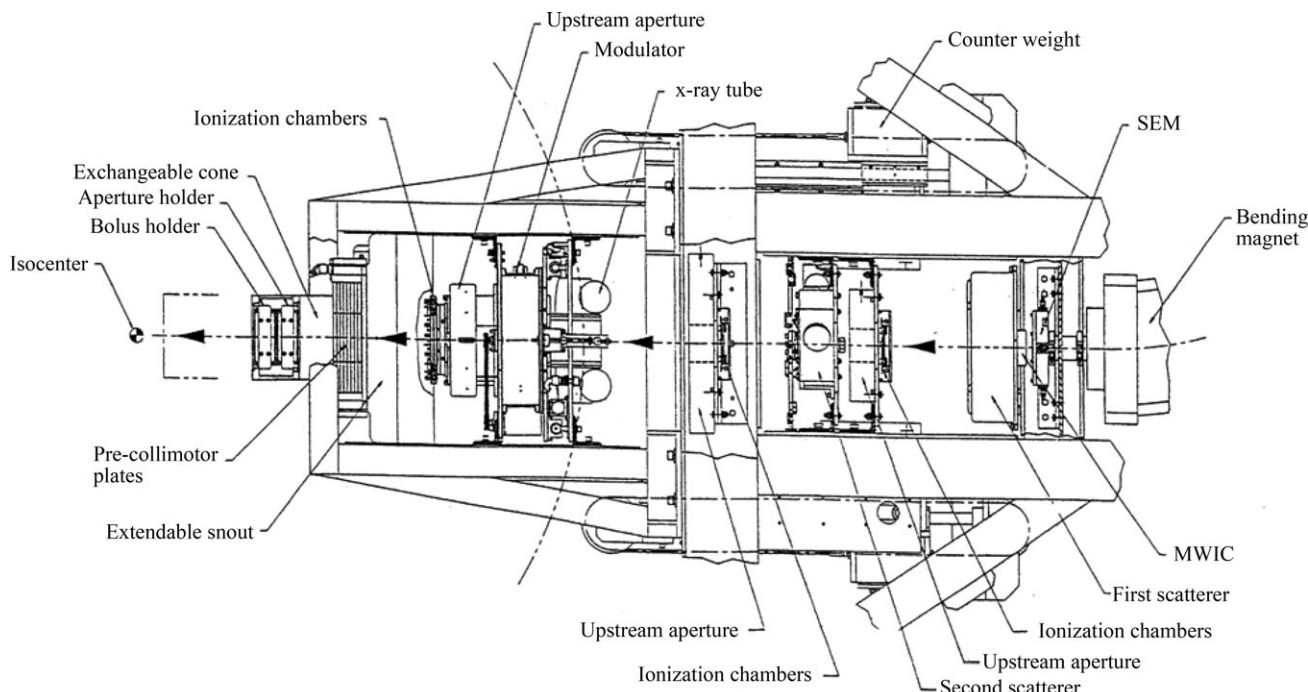


Figure 3.2. Schematic diagram of the components of the passive scattering nozzle used for proton-therapy treatment at Loma Linda University Medical Center. MWIC, multi-wire ionization chamber; SEM, secondary-electron monitor (Moyers, 1999; reproduced with permission).

projected target volume. The major components of a passive scattering system are shown in Fig. 3.2.

Uniformity of intensity over the useful cross-section of the beam can be obtained by selecting only the central portion of the Gaussian distribution of a singly scattered beam. This would require a large drift distance between the scatterer

and the patient and would result in a low efficiency of the beam in use. Double scattering by a pair of separated scatterers can increase the area of uniform fluence in the central area at the treatment position (Koehler *et al.*, 1977). With this technique, developed at Harvard University Cyclotron Laboratory, the first scattering foil results in a

Gaussian dose distribution at the treatment position with a high intensity in the center of the field. A second composite scatterer, placed between the first scatterer and the treatment position, typically has an occluding ring on the beam axis followed by a thin, high-*Z* scatterer (*Z* is the atomic number of the element). This combination reduces the dose in the center and uses the scattered protons to increase the dose outside the center. This technique results in a larger homogeneous, circular dose distribution at a specific distance from the two scatterers and a more efficient use of the particles, although a large drift distance is still necessary. The homogeneous dose distribution must be substantially larger in each direction than the target volume, and collimators (blocks or apertures) are needed to shape the proton field to the projected target cross-section. A drift distance of at least 3 m is recommended between scatterer and patient. This is not a problem for a fixed, horizontal beam line, but would result in a large diameter for a gantry beam-delivery system when the scatterers are placed after the last bending magnet. Smaller drift distances of 1.5–2 m would yield an undesirable increase in surface dose relative to dose at depth (Rabin, 1987). The gantry designed for the Loma Linda facility has a diameter of 12 m, but economizes on the cost of shielding by arranging most of the magnets in one plane (ICRU, 1998).

A refinement of the double-scattering technique uses a contoured second scatterer made of a combination of a high-*Z* and a low-*Z* material. The high-*Z* scatterer provides the main scattering and is combined with a plastic counterpart, thinner at the center and with increasing thickness at increasing radii to ensure the same energy loss of the protons over the entire surface of the scatterer (Grussell *et al.*, 1994). If, in addition to using a contoured scatterer, the scattering and range-shifting elements are placed far upstream of the patient, a sharper dose fall-off and a higher beam-usage efficiency of ~46 percent result. Beam spreading can also be achieved by passive magnetic dispersion into a circular or linear shape (Blosser *et al.*, 1991; ICRU, 1998).

In order to achieve optimum beam shaping with passive scattering techniques, most beam-modifying devices are patient- and/or field-specific, as shown schematically in Fig. 3.3. However, it is customary to use a discrete set of non-patient-specific range shifters and modulators. Range modulation is achieved by varying the thickness of absorber material traversed by the protons. This can be done spatially by using an absorber plate with ridge-shaped elevations, called a 'ridge filter', or in time, with a rotating absorber propeller with

different thickness sectors. The resulting dose distribution can be made essentially uniform in depth over a distance determined by the thickness of the volume to be irradiated. Together with collimation of the beam, this results in a single-field dose distribution that can be conformed to the distal surface of the target volume contour by the use of a patient- and beam-specific compensator (ICRU, 1998). A limitation of a passive scattering system is that the compensator is designed to shape the dose distribution to the distal surface of the planning target volume (PTV, defined in Section 5.1.4) and, hence, this shape is also imposed on the proximal PTV surface, so that one cannot avoid exposure of volumes of normal tissue in the proximal region to approximately the full target dose. For large, irregular target volumes, the unnecessary exposure of normal tissues adjacent to the target volume can be reduced with the use of a dynamic multi-leaf collimator in combination with a compensating bolus and a step-wise reduction in the range of the protons (Chu *et al.*, 1993; ICRU, 1998).

The field-shaping device and compensator should be as close to the patient's skin as possible to minimize the scattering, which degrades the lateral penumbra (LP). In order to achieve this, these components are mounted so that they may be moved along the central beam axis, toward or away from the patient. These retractable components are mounted on a movable snout, which is carried on the nozzle, where the fixed components of the last part of the beam line are supported.

In a passive system, beam modulation is a problem because a specific range modulator is required for each energy and each spread-out Bragg peak (SOBP) length, if variation in dose throughout the SOBP is to be minimized. This requires a large number of modulator wheels or ridge filters, and in practice the dose uniformity in the SOBP may be dictated by the variety of beam modulators available. In modern high-patient-throughput proton-therapy facilities, efficient solutions are required to the problem of patient-specific beam modifiers for beam modulation without sacrificing dose uniformity. Precise control of the beam intensity and beam-on time with fast switching, such as is achievable in cyclotrons by controlling the beam at the ion source, or during the first few turns of acceleration, provide a method for beam-intensity modulation. In principle, a single modulator wheel can be used to spread out the Bragg peak to any desired extent if the beam can be switched on and off in synchrony with selected segments of a modulator wheel and if the beam intensity can be controlled. In synchrotrons, using radiofrequency (RF)-driven

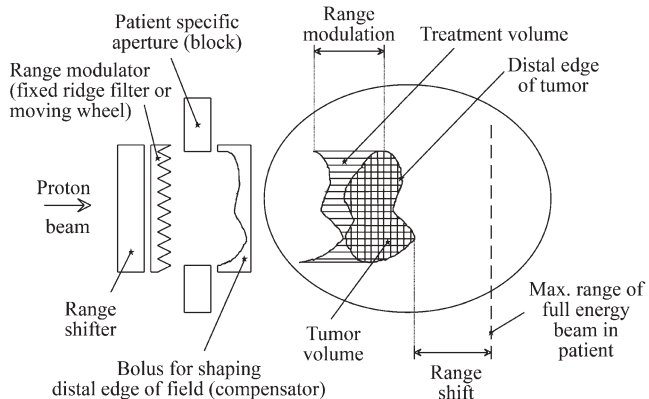


Figure 3.3. Schematic diagram showing how patient-specific beam-modifying devices (range shifter, range modulator, aperture, and bolus) are used to shape a passively scattered proton beam to conform to the tumor position, dimensions, and distal edge.

extraction, the beam can be switched on and off in $\sim 200\text{--}250\ \mu\text{s}$ within a single spill, which may be sufficient for accurate synchrony (Hiramoto and Nishi, 1992). In addition, recent advances in beam-intensity control might allow a reduction in the number of modulator wheels to be used with synchrotron beams (see Section 3.2.1.2 for more details of beam intensity control).

In principle, range shifters should not be necessary in scattering systems with either a synchrotron (where it should be relatively easy to vary the exact energy from pulse to pulse), or with a cyclotron (where energy selection is available). The use of computer-controlled multi-leaf collimators can further simplify the situation by eliminating the need for individualized blocks or apertures for each field treated. Thus, the number of individually manufactured patient-specific beam modifiers required in passive scattering can be reduced to one per field per patient (a set of compensators to shape the dose distribution to the distal surface of the PTV).

The passive beam-dispersal techniques, which simultaneously irradiate the entire target volume, have many advantages such as safety, simplicity, and a lower sensitivity to the time structure of the proton beam than any of the dynamic techniques. However, passive scattering techniques tend to be sensitive to variations in beam position relative to the scatterer. For monitoring and dosimetry, passive beam spreading results in less stringent conditions on time and spatial resolution. The reduced flexibility in shaping the dose distribution in three dimensions is less important for small or regularly shaped target volumes. However, dynamic techniques can reduce the dose to normal tissue and may be preferred in some situations (ICRU, 1998).

One disadvantage of beams that feature the use of a double-scattering system is that they have considerably larger penumbra due to the large effective source size produced by the two scatterers. This is one reason why dynamic beam-delivery techniques (providing wobbled and scanned beams) are thought to be advantageous.

3.2.1.2 Dynamic beam-delivery techniques

Dynamic beam scanning is a time-dependent method of achieving a desired dose distribution by magnetically moving the beam across the target cross-section while dynamically changing the energy of the beam and, consequently, the depth of penetration (ICRU, 1998). A scanned beam is composed of a number of finite pencil beams, delivered in time sequence, which together result in the desired three-dimensional dose distribution. There are two main approaches to delivering a scanned beam, together with an intermediate variant:

- (1) Discrete scanning (spot or voxel scanning) is a method in which the dose is delivered by pencil beams applied in discrete steps. After each pencil beam is delivered, the proton source is interrupted, the beam-steering elements (magnets and/or mechanical positioning devices) are changed to deliver protons at a different position and/or energy, and the beam is then turned back on until the desired number of protons has been delivered. While it is not essential, the Bragg peaks of the pencil beams are generally delivered in a regular Cartesian grid for reasons of technical simplicity. Their spacing is chosen to avoid non-uniformity (ripple) in the dose profile.

- (2) Continuous scanning (raster scanning) is a method in which a pencil beam of protons is scanned continuously across the cross-section of the beam in a raster pattern. Variation in intensity as a function of beam position is achieved by continuous control of the proton-beam intensity and/or the scanning speed. Once one 'layer' of protons of a particular energy has been laid down, the proton source is interrupted, the beam energy is changed by a usually small increment, and the beam is then turned back on to irradiate the next layer.
- (3) Quasi-discrete scanning, a possible variant of discrete scanning, which has been used with a carbon-ion beam, is a method in which the ion source is not turned off during the move to the next pencil beam position but is allowed to continue to deliver particles between grid points of the scan (Haberer *et al.*, 1993). The dose thus delivered between grid points is accounted for in the dose delivered by the next pencil beam. This approach works well only when the time to move to a new position is small compared with the dwell time and the pencil beams are delivered in a spatially contiguous manner.

In order to prevent unintended ripple in the dose profile in discrete and quasi-discrete scanning, the inter-pencil beam spacing of near-Gaussian profile beams needs to be ≤ 80 percent of the pencil beam's full width at half maximum (fwhm). In the carbon-ion beam implementation described in Haberer *et al.* (1993), the spacing was chosen to be ~ 20 percent of the pencil beam's fwhm, making the beam delivery much less sensitive to possible fluctuations in the pencil-beam positions.

The advantage of dynamic beam shaping using beam scanning is that it can overcome all the problems associated with custom-made beam-modifying devices by potentially controlling the position of a pencil beam precisely within the patient using electronic or electronic/electromechanical control. More importantly, dynamic methods can be used to implement intensity-modulated proton therapy (IMPT) to better conform dose distributions to the proximal surface of the PTV as well as the distal surface, while avoiding normal-tissue structures. Several dynamic methods of varying complexity can be used to raster scan or scan a pencil beam throughout the PTV as described above. The principle of spot scanning is illustrated schematically in Fig. 3.4.

Discrete scanning deposits dose in a voxel and switches the beam off during the change of parameters for the next voxel (Kanai *et al.*, 1980). As a three-dimensional conformal treatment of a 11

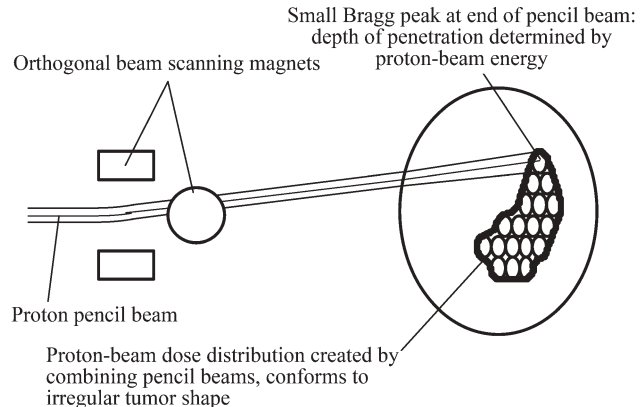


Figure 3.4. Schematic diagram showing how a variable-energy pencil beam can be spot scanned in three dimensions through a target volume to produce a dose distribution that conforms to the shape of the target volume.

volume with a voxel size of $5 \times 5 \times 5 \text{ mm}^3$ needs $\sim 10\,000$ spots and as the treatment time should be comparable to treatment times for photons, *e.g.*, several minutes, it requires either fast ramping of the magnet current or a fast switching magnet, depending on the time structure of the beam of the accelerator (ICRU, 1998). Discrete voxel or spot scanning for charged-particle therapy is presently in use at the Paul Scherrer Institute (PSI) for proton-beam scanning (Pedroni *et al.*, 1995) and at the Gesellschaft für Schwerionenforschung (GSI) with a ^{12}C ion beam (Haberer *et al.*, 1993). Scanning techniques are under development in Uppsala (Lorin *et al.*, 2000) and by major proton-therapy accelerator vendors.

Continuous scanning, first used at Uppsala in 1960s (Graffman *et al.*, 1985) and later developed at Berkeley for heavy ions (Chu *et al.*, 1989), is a flexible technique to yield large homogeneous dose distributions for different shapes. The scanning is done on a rectangular grid with a higher scanning frequency in one direction and a lower scanning frequency in the direction perpendicular to it. Rectangular fields of different shapes and sizes can be scanned in this way, giving a field shape more closely related to the target volume projection, therefore, reducing the beam particle losses. Up to $40 \times 40 \text{ cm}^2$ fields could be scanned at Berkeley with scanning rates of 40 and 1 Hz for the two axes, respectively. The lateral shape of the target volume was still tailored by an individual collimator (ICRU, 1998).

In synchrotrons, pulse-to-pulse energy variation is possible. In cyclotrons, which operate at a fixed energy, energy variation requires energy degradation by a variable-thickness absorber. This produces a large energy spread in the beam that must

be limited by magnetic energy selection; this technique uses a magnet to spread the degraded beam energy spectrum across an energy-defining slit. The slit selects the required energy range and a second magnet refocuses the beam into the beam transport system. For the lowest energies, this process is very inefficient and a large amount of beam is lost on the energy-defining slits leading to activation and shielding problems.

Scanning, whether discrete or continuous, requires range control and a controllable and sufficiently intense beam output in order to deliver well-defined dose throughout the target volume safely, with sufficient accuracy, and within a reasonable time. The beam intensity as a function of time for cyclotrons and synchrotrons is shown in Fig. 3.5. Cyclotrons have a continuous and inherently higher beam output (Fig. 3.5a). Synchrotrons

have slow pulse-repetition rate (Fig. 3.5b) that can extend treatment times if multiple scanning of dose voxels ('repainting') is required in order to ensure that doses are delivered throughout the target volume with sufficient uniformity (better than ± 2.5 percent) or to overcome the effects of intra-fraction tumor motion. This is also a problem with scanned beams produced in cyclotrons, although the continuous beam output from a cyclotron (*i.e.*, higher duty cycle) gives a two or three times higher dose rate. For synchrotrons, the radio-frequency-driven extraction (RFDE) system used in the Tsukuba facility has improved the control of beam extraction, *i.e.*, the ability to switch the beam on and off multiple times on a 200–250 μ s time-scale, during a single spill stretched up to 5–7 s in length (Fig. 3.5c and d). It effectively increases the beam duty cycle from 83 to 87 percent in

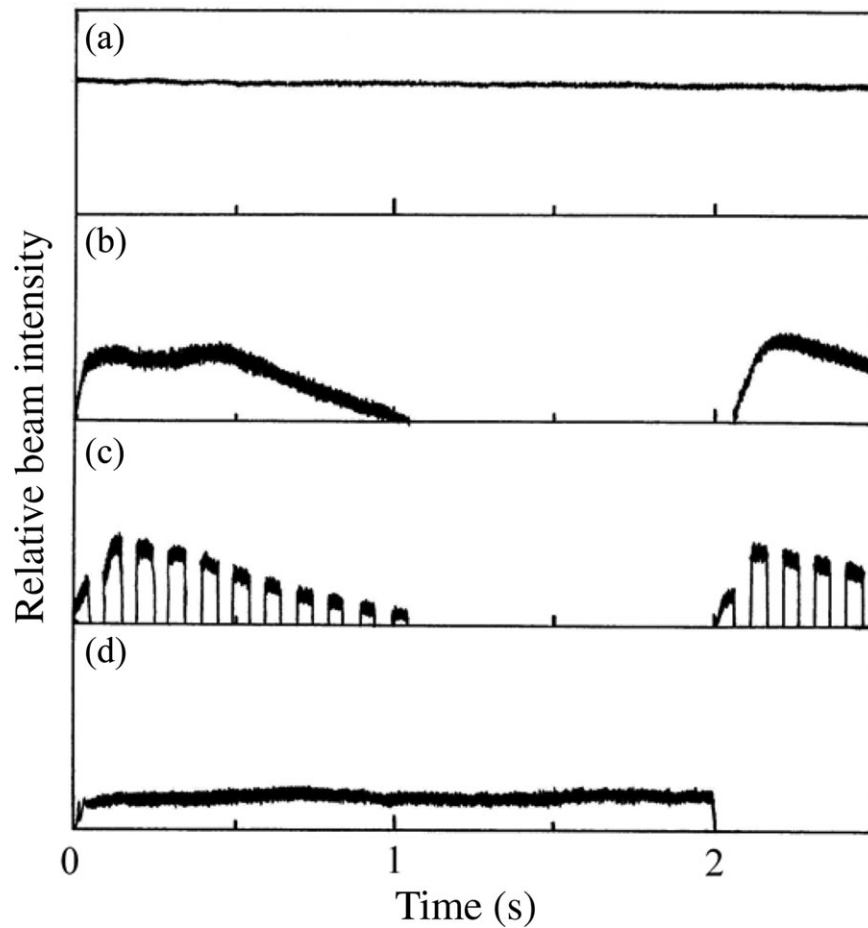


Figure 3.5. Beam intensity as a function of time for (a) an isochronous cyclotron and (b), (c), and (d) for a synchrotron. (a) The cyclotron gives a continuous output stable to within a few percent; the beam can be switched on and off in ~ 50 μ s. (b) The synchrotron produces pulsed output; with conventional extraction (magnetic deflection) pulses (spills) may be typically 0.2–1 s long with a repetition rate of between ~ 0.5 and 2 Hz. (c) In a synchrotron with RF-driven extraction (RFDE), the beam can be switched on and off in ~ 200 μ s, at any time within the spill envelope, producing a large number of short pulses within a single spill. (d) In RFDE, the extraction RF amplitude may be adjusted to control the extracted beam intensity, allowing a more uniform beam intensity during the spill ('flat-top'). In RFDE, the spill may be stretched to be up to 5–7 s in length.

synchrotrons (Hiramoto and Nishi, 1992). Raster scanning has the further requirement that the beam intensity be stable and known. In cyclotrons, fluctuations in beam intensity can be controlled at, or close to, the ion source with a fast time response (10–50 μ s) feedback loop. Recent developments in synchrotron beam extraction enable a more uniform extraction of the beam during a single spill (Fig. 3.5d). Reproducible beam pulses of this type might allow for continuous scanning.

3.2.1.2.1 Wobbled beams. A ‘wobbled beam’ is a scanned beam whose finite pencil beams have a large lateral size that is greater than that of a pristine pencil beam (which typically has a Gaussian lateral profile with a fwhm of 5–10 mm) by a factor of 2 or 3, but nevertheless is small compared with the field width. A scatterer is used to adjust the lateral size of the pencil beam. This technique has been considered only for the delivery of uniform-intensity dose distributions. Wobbled beams have the advantage over scattered beams in that: (i) it is estimated that protons are used two to three times more efficiently; (ii) consequently a lower neutron background is expected to be produced; and (iii) almost the identical equipment as scanned beams is used, thus allowing for the implementation of full scanning capability. However, such beams usually require the use of a patient collimator and compensator.

In principle, wobbled beams could be delivered using a sequence of static pencil beams. However, in practice, they have been implemented using continuous scanning, for which a variety of scan patterns is possible. ‘Wobbling’ was developed at the Lawrence Berkeley National Laboratory for heavy ion beams at the BEVALAC (Chu *et al.*, 1985; 1989). By wobbling, the particles of a beam pulse are smeared out on rings by the use of a pair of dipole magnets with fields which vary sinusoidally with time, with a phase difference of 90°. Several rings of different radii and doses are added, depending on the desired field size, to obtain flat fields of up to 30 cm diameter with <5 percent dose variation. This technique economizes on the use of particles, as does double scattering, but strongly depends on stable pulse intensities unless large numbers of pulses are used for each ring. This system was in routine use for heavy-ion radiotherapy at Berkeley from 1985 to 1992 and could equally well be used for protons (ICRU, 1998). The original wobbling technique has been simplified by Kanai *et al.* (1999) at the National Institute for Radiological Sciences, Chiba, Japan. The simplified technique uses a single wobbling ring with a stronger scatterer, rather than multiple rings; this

technique reduces the sensitivity of the beam uniformity to the time structure of the beam pulse, especially when beam gating is used for respiratory synchronization. This single-ring wobbling system is widely used in Japanese particle-therapy centers.

Wobbling uses beam-modifying techniques similar to those used for passive beam scattering; the techniques include fixed-range modulation and may include patient- and beam-specific modifying devices. As with passive scattering, dose conformation at the proximal edge of the target volume can be improved using a dynamic multi-leaf collimator in combination with a compensating bolus and step-wise reduction in the range of the protons (Chu *et al.*, 1989).

3.2.1.2.2 Repainting. The rationale for ‘repainting,’ *i.e.*, the delivery during scanning of at least some of the pencil beams multiple times, is discussed in Section 7.6.3. In the limit of scanning that is either very much faster or very much slower than the motion under consideration repainting is not required. For repainting to be most effective in delivering a uniform dose to a given volume, the volume must be repainted multiple times within the period of the organ motion, or the repainting should occur on a time scale greater than the period of the motion and out of synchrony with that motion.

Presently proposed commercial systems use spot scanning or continuous scanning, but have relatively slow energy-switching times. In a typical commercial regime for spot scanning a cubic volume of 1 liter, a proton pencil beam with a Gaussian profile of 10 mm fwhm ($\sigma = 4.5$ mm) may be used to laterally scan an area of $10 \times 10 \text{ cm}^2$ using a 15×15 array of spots at a single depth. If depth layers are 5 mm apart, a total of 4 500 spots are required to scan the volume once. In both a synchrotron and a cyclotron, the position of an individual spot can be verified and the specified dose delivered in about 5 ms with between 1 s and 1.5 s required to change energy. Thus, 1.1 s are required to scan a single layer, and the total time for a single scan of all layers is about 45 s. Continuous scanning offers the advantage that there is no dead time between spots associated with spot-position adjustment and verification, but while energy-switching times remain a significant factor, these efficiency advantages are limited to about 25 percent. The distal layers can be repainted more frequently than the proximal layers, since the proximal layers receive dose from protons in the plateau region of the distal pencil-beam Bragg peaks, thus, reducing the number of repaintings required.

Lomax *et al.* (2004) have documented the Paul Scherrer Institute (PSI) experience in proton-beam

spot scanning using a cyclotron with an energy-selector system. In this system, lateral scanning is achieved by a combination of magnetic scanning and patient-couch motion. The PSI proton pencil beam has a Gaussian profile of 8 mm fwhm ($\sigma = 3.5$ mm), and beam spots are spaced 5 mm apart orthogonal to the beam direction and 4.5 mm apart in depth. With this arrangement approximately 10 000 spots are required to irradiate a volume of 1 liter and approximately 3 000 spots can be delivered per minute. In analyzing the spot weights and energies for practical proton fields, Lomax *et al.* (2004) have shown that there is a relatively broad spread of low- and high-weighted Bragg peaks over all energy steps, *i.e.*, high-weighted Bragg peaks are not concentrated in a single distal layer. This indicates that there is only a limited relationship between the pencil-beam weighting and depth of penetration, which implies that systematically repainting using more distal-layer than proximal-layer repaintings, as suggested above, may not be sufficient to overcome the effects of motion in practice. Thus effective repainting of moving targets in times less than two or three minutes is not feasible at present.

At the Paul Scherrer Institute continuous scanning strategies are under development (Meer *et al.*, 2006; Pedroni, E., Personal communication, 2007), which use fast scanning (1 cm s⁻¹ to 2 cm s⁻¹) combined with beam intensity modulation at the ion source and a newly-developed fast energy-switching system (switching time ~ 90 ms). Such innovations should allow a 1 liter volume to be scanned in approximately 5 s. Thus, with the development of more advanced scanning and repainting strategies it should be possible to adequately over-paint large-volume moving targets in times of one minute or less.

Other methods for overcoming target motion, such as motion tracking and beam gating are described in Sections 7.5 and 7.6.

3.2.2 Patient support and positioning

The function of the patient support and immobilization system is to hold the patient in a stable position during treatment. The patient support can be a couch or a chair. Several institutions use patient couch tops or chairs mounted on robotic arms (Noel *et al.*, 2003). Immobilization devices are used to 'fix' the patient to the treatment couch or chair (see Section 3.2.3).

Once the immobilized patient has been positioned using lasers and skin marks, the position of the treatment volume relative to the beam is checked using a suitable imaging method immediately prior to treatment. Orthogonal radiographs

have so far been the main technique employed. Cone-beam CT, conventional CT, or ultrasound equipment available in the treatment room is also used. The patient can be repositioned if necessary; a treatment couch or chair with six degrees of freedom provides the maximum flexibility for the accurate repositioning of the patient.

An alternative method of patient positioning is the use of modern couches that feature easily removable, precision-mounted couch tops. By using multiple couch tops or whole-body pods, patients can be pre-positioned in a positioning suite outside the treatment room. Using a specially designed transporter, the couch top or pod is moved into the treatment room, where it is fixed to the couch base and accurately positioned in the treatment beam (Pedroni *et al.*, 1995). The purpose of such systems is to increase the efficiency and patient throughput.

3.2.3 Special treatment techniques

The first applications of charged particles in radiation therapy were the use of finely collimated beams to treat small well-defined lesions to high dose in a single or few fractions using the techniques of stereotactic surgery. These special techniques are still used with proton beams for the treatment of malignant and benign diseases, including uveal melanomas, pituitary adenomas, brain tumors, and arteriovenous malformations.

3.2.3.1 Eye treatments

Proton beams for ocular tumor treatment require energy of about 70 MeV, *i.e.*, a penetration in water of 4 cm (Goitein *et al.*, 1983b), although a beam with energy as low as 62 MeV has been used. The methods for treating ocular lesions with proton beams were developed at Massachusetts General Hospital and the Harvard Cyclotron Laboratory (Goitein and Miller, 1983; Gragoudas *et al.*, 1977). A typical proton-beam irradiation arrangement for the treatment of ocular lesions is shown in Fig. 3.6. Patients are commonly treated in the seated position, and a custom-made facemask and bite block are used for immobilization. The eye is fixated on an external light source that can be adjusted to control the direction of the gaze during the treatment. Tantalum rings are usually sutured around the perimeter of the tumor and are used for radiological set up; otherwise, the set up is achieved using a light field projected through the treatment aperture on to the eye (Munzenrider, 1999).

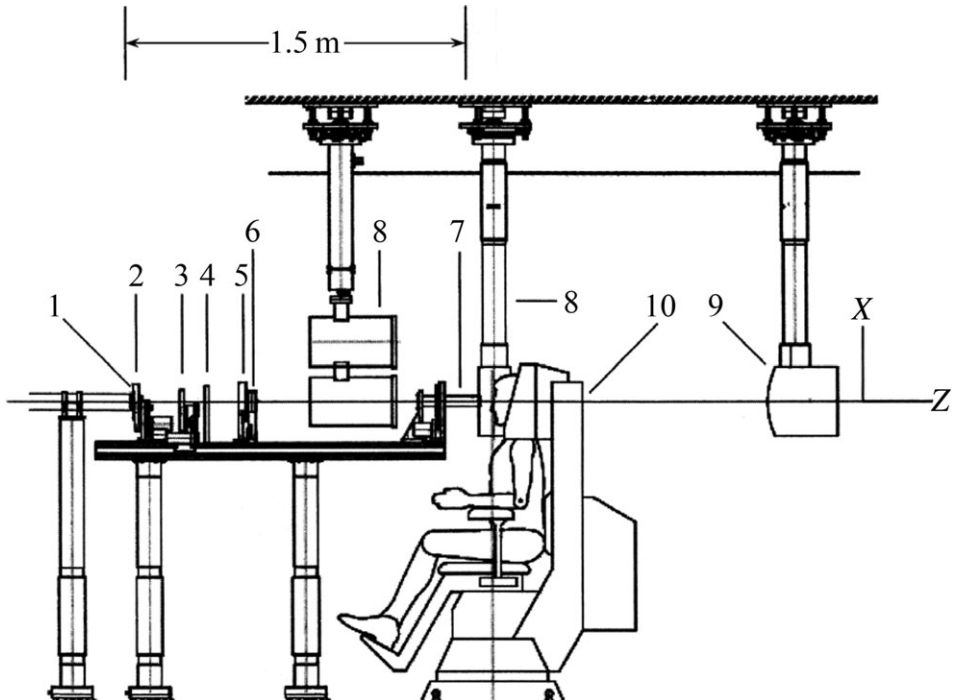


Figure 3.6. A typical proton-beam arrangement for eye irradiations as was installed at the Hahn-Meitner Institute, Berlin. The beam enters from the left. After a $100 \mu\text{m}$ Kapton foil (1), which acts as a vacuum exit window, a computer-controlled variable range shifter (2) and a range modulator (3) are mounted close together. The beam passes a collimator (4), a segmented ionization chamber (5), and two transmission ion chambers (6). Directly in front of the patient is mounted the nozzle (7), *i.e.*, a pipe that can hold a collimator, an aperture, a compensator, or a phantom for dosimetry experiments. An on-line x-ray imaging system (8 and 9) is mounted from the ceiling and can be removed during treatment. The patient sits in a chair with multiple degrees of freedom (10). (Adapted from Paganetti, 1998; reproduced with permission.)

3.2.3.2 Stereotactic radiosurgery and stereotactic radiotherapy

The techniques of stereotactic radiosurgery (SRS), in which the head is held rigidly in a metal ring attached directly to the patient's skull and aligned with a radiation source, were first investigated by Leksell and co-workers (Larsson *et al.*, 1958; Leksell, 1951). Tumors were irradiated with cross-fired proton beams using the plateau region of the Bragg curve to deliver dose to the target volume, rather than using the Bragg peak.

Modern stereotactic therapy uses multi-slice CT images for three-dimensional planning. Treatments are delivered in a single fraction or sometimes in three or four fractions in SRS, or with conventional fractionation in stereotactic radiotherapy. For use in multifraction treatments, more convenient methods for immobilization and repositioning have been developed, one of which uses stainless-steel microsphere fiducials implanted in the skull (Gall *et al.*, 1993b). The microspheres can be detected on the CT used for treatment planning and on the radiographs used for patient positioning. This system was used with a sophisticated patient-positioning device, shown in Fig. 3.7, which allows

patients to be treated supine while stereotactically aligned with a fixed, horizontal proton beam (Chapman *et al.*, 1993).

Another alignment technique employs an automatic positioning and monitoring system that uses real-time stereophotogrammetry. In this technique, reflective fiducials are placed on the surface of the patient's molded facemask, which is rigidly fixed to the treatment chair. These fiducials are detected in three dimensions by video cameras and the data are used to control the motion of the computerized adjustable chair with five degrees of freedom (Jones *et al.*, 1995).

The introduction of proton-therapy centers with rotational gantries allows for the supine stereotactic treatment of patients from multiple non-coplanar directions, using combinations of couch and gantry angles, without the need for specialized patient-alignment apparatus of the type shown in Fig. 3.7. A more detailed description of available immobilization techniques is given in Section 7.2.2.

3.2.4 Rotating gantries

For the greatest flexibility in beam delivery, the passive scattering nozzle or scanning system

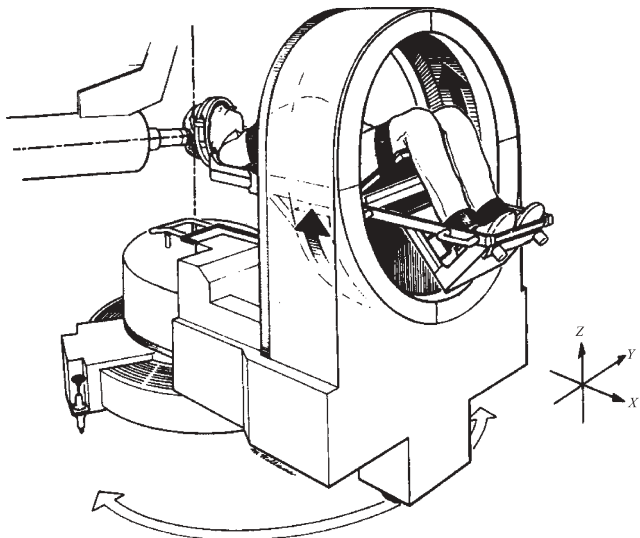


Figure 3.7. An apparatus for StereoTactic Alignment for Radiosurgery (STAR). The patient's head is held in a fixation ring and can be moved into different positions relative to the fixed proton beam (Harsh *et al.*, 2002; reproduced with permission).

should be mounted on a gantry that allows the beam to rotate through a 360° around the treatment couch as shown in Fig. 3.8. The simplest gantry requires magnets that can bend the maximum-energy proton beam through a total of 180° bend; one 45° bend followed by a 135° bend. In addition, some quadrupole focusing elements are required between these magnets. The magnets weigh up to 100 Mg (~ 100 tons) and must be supported so that the intersection of the central beam axis and the axis of rotation of the gantry is contained within a 1 or 2 mm diameter sphere as the gantry rotates. Furthermore, the gantry needs to be ~ 5 m in radius to accommodate the scattering or scanning nozzle. This requires a rigid structure of ~ 10 m diameter, 10 m length and with a total weight, including the magnets, of up to 200 Mg (~ 200 tons). Gantry designs have been developed to reduce the size requirements of the shielded room. Koehler (1987) proposed a 'corkscrew' bending magnet arrangement (Fig. 3.8), which can reduce the overall length of the gantry. At the Paul Scherrer Institute (PSI), a compact gantry was created by mounting the treatment couch eccentrically on the gantry structure, thus allowing a reduction in the overall diameter (Pedroni *et al.*, 1995). Most recently, it has been proposed at PSI that a gantry allowing only 190° rotation should be used in conjunction with a 180° couch rotation, thus reducing the room size requirements significantly and allowing easy access to the patient (Pedroni *et al.*, 2004).

3.3 ACCELERATORS

Proton accelerators for therapy need to produce beams with sufficient energy to reach the distal edges of the deepest tumors and with beam currents adequate to achieve treatment times comparable with (or better than) the conventional x-ray treatment facilities for the range of field sizes and doses used in radiotherapy (ICRU, 1998). Incident beam energy of 215 MeV is required to obtain beam penetration to a depth of 30 g cm^{-2} on the patient surface. This requires a beam energy emerging from an accelerator of between 225 and 250 MeV depending on the beam-modifying elements required for the treatment. To achieve dose rates of 2 Gy min^{-1} in a volume of 1000 cm^3 , a beam current of $\sim 8 \text{ nA}$, equivalent to $>5 \times 10^{10}$ protons per second extracted from the accelerator, is required.

Particle accelerators are normally built with either a straight or a circular arrangement of the components. To produce high-energy protons, it is

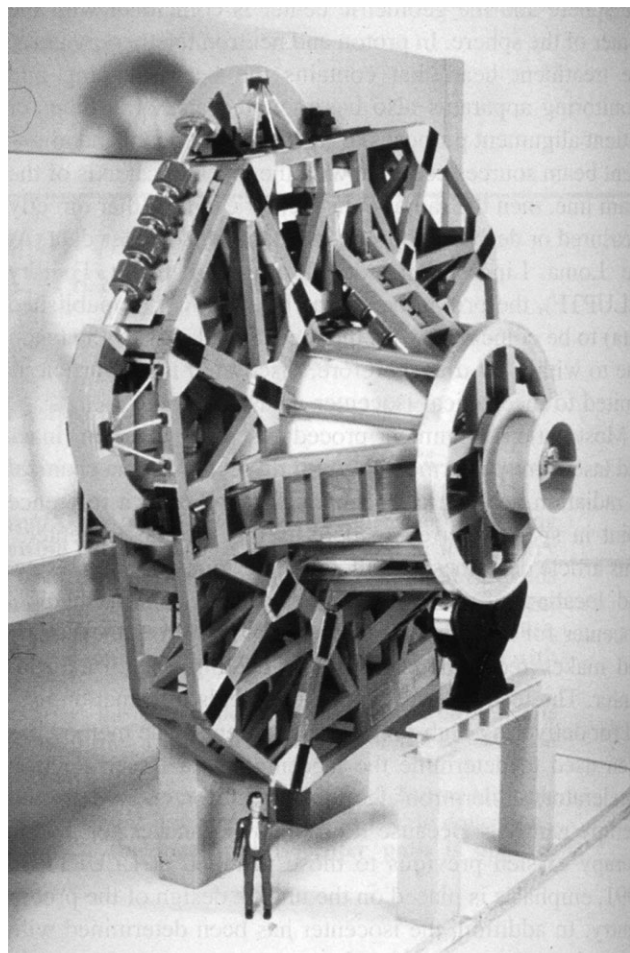


Figure 3.8. Model of a corkscrew-type gantry, viewed from the rear (Moyers and Lesyna, 2004; reproduced with permission).

necessary to accelerate them in stages. Rather than accelerating the particles through a single large potential, the simplest arrangement for achieving this is the linear accelerator, in which a number of accelerating cavities, driven by an RF power supply, are connected in series along a linear path. In a linear accelerator, each particle generally traverses the acceleration cavity only once and, consequently, linear accelerators for producing high-energy protons are long. The problem of length is overcome in cyclic accelerators using a magnet to constrain the particles to move in a closed path and traverse a single RF-powered accelerating structure multiple times. The original cyclic accelerator was the cyclotron developed by Lawrence and co-workers in the early 1930s.

In a cyclotron, the particles are accelerated in the gap between the pole pieces of a large magnet using a fixed magnetic field and a fixed RF. The particles start at the center of the magnet with zero energy and spiral outwards as they gain energy. They are extracted from the accelerator at the periphery of the magnetic field by deflecting them from the circular path into a beam-transport system. In a later development of the cyclic accelerator, the synchrotron, particles from a low-energy accelerator are injected into a fixed-radius ring of magnets; each particle traverses the same path repeatedly during the acceleration cycle, with an increasing magnetic field keeping the particles in a fixed orbit.

At present, the only accelerators being used in dedicated hospital-based proton-therapy facilities are either cyclotrons or synchrotrons.

3.3.1 Linear accelerators

Linear accelerators are typically characterized by high energy consumption and a very high beam intensity, which could produce a potential safety problem. Nevertheless, a few authors have proposed this type of accelerator for proton radiotherapy (Boyd *et al.*, 1982; Hamm *et al.*, 1991). A versatile proton linear accelerator was designed at Los Alamos for pion therapy and was subsequently calculated to be able to produce proton beam currents of up to 100 μ A at 650 MeV (Boyd *et al.*, 1982). Protons of \sim 200 MeV energy could be produced with an accelerator length of 40 m. Commercial klystrons from radar equipment could be used to produce RF power for acceleration (ICRU, 1998).

A version of a linac more tailored to the needs of proton therapy in terms of energy and beam current was proposed by Hamm *et al.* (1991). By using side-coupled linac sections for accelerating

protons from 70 to 250 MeV and RF power systems from medical electron linacs, the facility would be better adapted for hospital installation and its price could be reduced (ICRU, 1998).

3.3.2 Cyclotrons, isochronous cyclotrons, and synchrocyclotrons

In these machines, the acceleration process depends on a magnetic resonance condition, in which the resonant frequency of the RF acceleration voltage is determined by the magnetic field and the charge-to-mass ratio of the particle. As mentioned above, the particles in a cyclotron are accelerated by a high-voltage high-frequency electric field between two D-shaped hollow electrodes (dees), which are supported in a vacuum tank between the poles of a large electromagnet. The particles move in the gap between the pole pieces of the magnet. In classical cyclotrons, the magnetic field and the frequency of the accelerating RF field are constant. In practice, a small gap is left between the opposing edges of the electrodes and a source of ions is located in this gap at the center of the magnet pole pieces as shown in Fig. 3.9. A low-velocity ion emerging from the ion source is

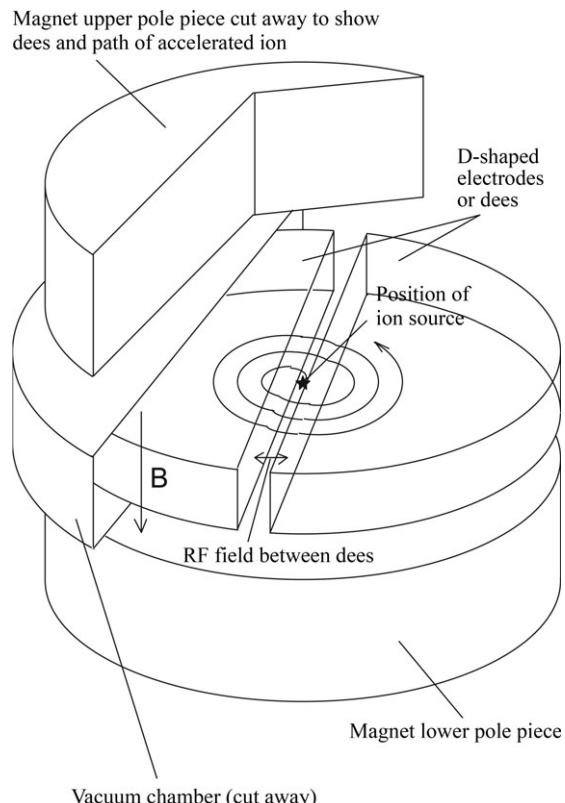


Figure 3.9. Schematic diagram showing the main components of a classical cyclotron and the path of the accelerated ions.

accelerated toward the electrode and enters the electric field-free space within the hollow electrode, continuing its path on a semi-circular arc. When it reaches the gap between the electrodes, it receives a further acceleration because of the synchrony between the RF and the particles' orbital frequency. As the particle gains energy crossing the electrode gap, it spirals outward until it reaches a maximum energy determined by the radius of the magnet pole pieces.

A classical cyclotron can be used to accelerate protons to only 10–15 MeV, which is much lower than the energy required for therapy. Above this limit the relativistic mass increase of the proton causes the resonant condition to fail. The problem of the relativistic mass increase can be overcome using an isochronous cyclotron, in which the relativistic mass increase is compensated by increasing the magnetic field with radius, thus maintaining the resonance condition, *i.e.*, there is a constant orbital frequency. When the magnetic field strength increases with radius, axial defocusing of the beam occurs. This would cause the beam to stray from the median plane and to strike the magnet pole pieces. Compensation for this defocusing can be achieved by introducing an azimuthal variation in the magnetic field (Thomas, 1938): the magnetic field is allowed to increase with radius, and vertical focusing is obtained by including radial or spiral hills and valleys on the pole pieces in order to create alternate high- and low-field sectors, as shown in Fig. 3.10. In this design the dees (within which the charged particles move in circular orbits in perpendicular magnetic fields) may be in three or four sections. On crossing the field boundaries between these magnetic field sectors, the ions experience focusing forces that restore them to the median plane. Isochronous cyclotrons are fixed-field and fixed-frequency accelerators; modern machining techniques allow the magnetic-field profiles to be engineered with high precision ensuring a high degree of isochronicity with no necessity for magnet trim coils.

An isochronous cyclotron using a high field strength in a narrow pole gap has been designed (Beeckman *et al.*, 1991), which reduces the magnet weight and energy consumption. A 230 MeV cyclotron built to this design is used at Massachusetts General Hospital for proton therapy (ICRU, 1998). The magnet is 4.34 m in diameter, 2.1 m high, and weighs 180 Mg (200 tons). Total magnet power consumption is 220 kW.

A 250 MeV isochronous cyclotron, which uses a superconducting magnet, has been designed by Blosser *et al.* (1993). Machines based on this design are installed at the PSI and the Rinecker Proton

Therapy Center in Munich as dedicated proton-therapy facilities. The magnet is 3.09 m in diameter, 1.65 m high, and weighs 80 Mg (90 tons). The cryogenic magnet's coil is cooled by four cryo-cooler units, each with a rated cooling power of 1.5 W (total 6 W). The coils are contained in a sealed cryostat and remain sealed and cold when the magnet pole caps are raised for service or repair. The use of low-maintenance cryo-cooler units considerably simplifies cryostat operation and maintenance. The magnet requires 2.5 W of cooling to maintain its operating temperature; therefore, at any time two cryo-coolers can be shut down for maintenance, if necessary.

The capability of accurate machining intricately shaped pole pieces allows the construction of large isochronous cyclotrons, which have displaced the synchrocyclotron as the accelerator of choice in the energy range from ~100 MeV to 1 GeV. In the synchrocyclotron, also called a frequency-modulated cyclotron, the increase in the relativistic mass of

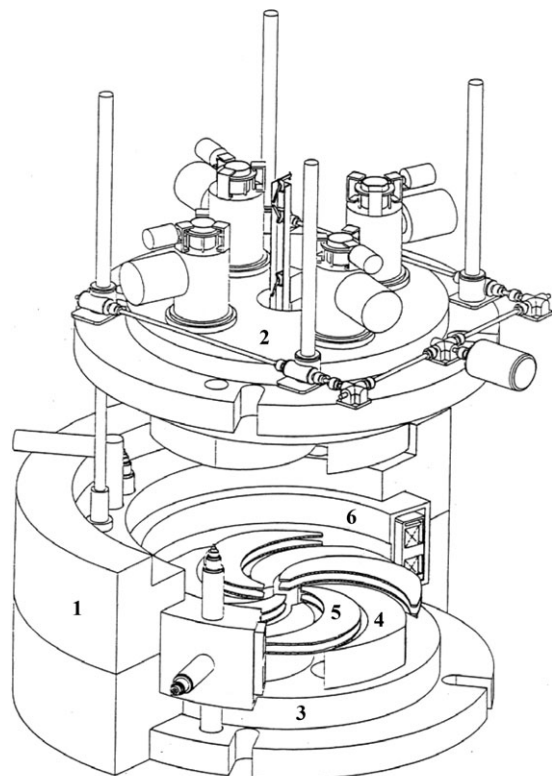


Figure 3.10. Cut-away diagram of a 250 MeV superconducting cyclotron showing: (1) the magnet yoke, (2) the upper pole piece, (3) the lower pole piece, (4) the spiral hill on the magnet pole piece, (5) the spiral shaped RF dee positioned in the pole piece valley, and (6) the magnet coil. The outer diameter of the magnet yoke is 3.2 m. The construction of modern room-temperature isochronous cyclotrons follows a similar design, but significantly larger (Blosser *et al.*, 1993; reproduced with permission).

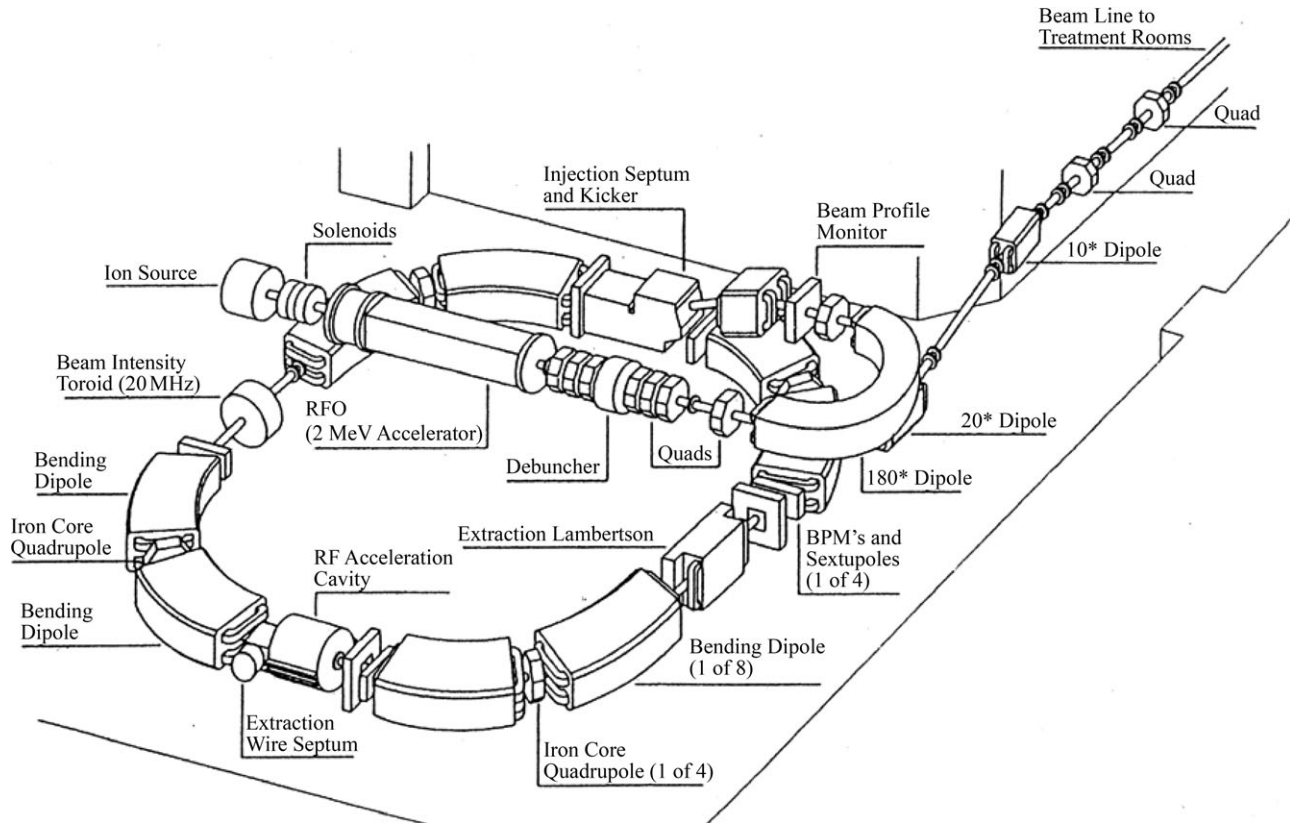


Figure 3.11. A schematic view of the Loma Linda University Medical Center 250 MeV proton-therapy synchrotron showing the major components of the accelerator. The outer diameter of the synchrotron ring is 6.71 m (Courtralon *et al.*, 1994; reproduced with permission).

the protons with energy is compensated by a decrease in the frequency of the accelerating voltage, while the magnetic field strength remains constant. This acceleration method requires pulsed operation, since one proton bunch must exit the synrocyclotrons before the acceleration of the next bunch begins. Synrocyclotrons with conventional magnets are large in size and mass. In principle, they can be tuned for different energies, but currently operating machines of this type have fixed energies. The extraction efficiency of the synrocyclotron is of the order of 90 percent and the extracted proton-beam intensity is normally more than adequate for therapy. The synrocyclotron is considered a very reliable accelerator, with no stringent tolerances on the magnetic field shape. This assertion is verified by the experience with the Harvard synrocyclotron that was operated for proton therapy with a very high reliability between 1961 and 2002 (ICRU, 1998; Sisterson *et al.*, 1991).

3.3.3 Synchrotrons

In a synchrotron, bending magnets keep a bunch of protons in a fixed orbit during the acceleration cycle. The frequency of the high-voltage acceleration system, installed in straight sections between the

bending magnets, is increased with increasing speed of the particle and is closely coupled with an increase in the magnetic field in the bending magnets. The protons can be extracted at any energy by either single turn extraction or by slow extraction to achieve longer pulses. Both room-temperature and superconducting proton synchrotrons have been considered as well as H^- synchrotrons. Only room-temperature designs will be discussed below (ICRU, 1998). The layout of the components of a typical synchrotron is shown in Fig. 3.11.

Low-energy particles are injected into the accelerator ring. To achieve acceleration, the magnetic field and the frequency of the accelerating electric field must be increased in synchrony. Because of the finite time required to cycle the magnets, synchrotrons produce a pulsed output. Typically, the beam acceleration cycle takes ~ 200 ms to 1 s and beam extraction occurs over a similar period. The pulse repetition rate is therefore typically 0.5–2 Hz. The use of numerous small magnets around the accelerator ring, positioned so that the magnetic-field radial vectors alternate in direction between successive magnets, creates net radial and vertical focusing in a small magnet aperture further reducing magnet cost. This principle of alternating gradient focusing (Courant *et al.*, 1952)

Table 3.1 Typical operating parameters of some accelerators in use in proton-therapy facilities.

Parameter	Cyclotrons		Synchrotrons	
	MGH	PSI	LLUMC	PMRC
Magnet ring or magnet max. diameter (m)	4.34	3.198	6.71	7.00–7.82
Magnet weight (tons) or number of magnets in ring	165 tons	90 tons	8 magnets	6 magnets
Energy at extraction (MeV)	230	250	70 to 260	70 to 250
Beam current (nA) or particles per pulse (ppp)	300 nA	500 nA	3.4×10^{10} ppp	7.5×10^{10} ppp
Pulse repetition rate (s)	CW	CW	2.2 s cycle	2 s to 7 s spill length 0.2 s to 0.5 s between spills
Extraction system	Electrostatic deflection 70 kV	Electrostatic deflection	Lambertson magnet	RFDE
RF cavity frequency (MHz)	106.1	74	0.974 to 9.713	1.5 to 2.0
Field strength (T) Hill	2.9	≈3.6		
Valley maximum	0.9	≈2.0	1.52	1.814
Average power consumption (kW)	446	350	350	?
Ion source or injector type	Cold cathode	Cold Cathode	2 MeV RFQ	7 MeV linac
RF voltage (kV)	130 peak	100 peak	0.3	1.3

MGH, Massachusetts General Hospital, Boston, MA, USA; PSI, Paul Scherrer Institute, Villigen, Switzerland; LLUMC, Loma Linda University Medical Center, Loma Linda, CA, USA; PMRC, Proton Medical Research Center, Tsukuba, Japan; CW, continuous wave.

has enabled the construction of very large synchrotrons for high-energy physics research. When applied to the relatively low energy, 250–300 MeV, machines required for proton therapy, the alternating gradient principle results in reduced size, weight, and total cost of the synchrotron.

The first hospital-based proton radiotherapy facility was installed at the Loma Linda University Medical Center and is based on a room-temperature synchrotron (Cole *et al.*, 1987). Purpose-built hospital-based particle-therapy synchrotrons have also been installed at Tsukuba University (Fukumoto *et al.*, 1989) and at the Hyogo Ion Beam Medical Center, Japan (Kagawa *et al.*, 2002). The latter accelerator can also produce a ¹²C beam. More recently, such synchrotrons have also been installed at the Wakasa Wan Energy Research Center, Tsuruga, Japan, The Shizuoka Cancer Center, Mishima, Japan, and the M D Anderson Cancer Center, Houston, TX, USA.

The synchrotron is highly flexible in terms of energy variation. With a synchrotron, it is feasible to use energy variation of the beam instead of range shifting with a variable thickness absorber to modulate the energy for depth control of the proton beam. A possible limitation for this accelerator is the maximum current per bunch that can be extracted. This is due to space-charge effects that depend on the injection energy. The injector at Loma Linda is an RF-quadrupole (RFQ) linear accelerator (linac) (Kapchinskii and Teplyakov, 1970) of 2 MeV, whereas at Tsukuba, a 7 MeV RFQ linac is used (ICRU, 1998).

Synchrotrons with conventional magnets using H[−] ions have been proposed by Martin (1987) and at ITEP in Moscow (Khoroshkov *et al.*, 1991), and are being considered for hospital use in northern Italy (Amaldi *et al.*, 1994). The primary argument for the construction of an H[−] machine is the simplicity of beam extraction, which is accomplished by stripping the electrons off the H[−] ions in a very thin foil target. This leads to a very small beam divergence, permitting transport of the extracted beam with narrow-gap magnets. However, H[−] machines have stringent requirements for the vacuum in the accelerator, due to the possibility of electron stripping by residual gas molecules in the beam pipe. Magnetic electron stripping is another potential problem for the H[−] machine, resulting in a maximum allowable field strength of slightly over 0.5 T, thus requiring a large diameter accelerator ring. The average beam current could also be rather low for clinical use (ICRU, 1998).

3.3.4 Typical accelerator operating parameters

At present, isochronous cyclotrons or slow-cycling synchrotrons are commonly used for proton-beam therapy. Both of these types of accelerators can provide proton beams that are well suited to applications in the clinical environment, and are commercially available. The typical operating parameters of some isochronous cyclotrons and slow-cycling synchrotrons for use in proton-therapy facilities are listed in Table 3.1. For a proton-therapy

facility capable of treating deep-seated tumors, energies in the range of 225–250 MeV are required. If ranges in excess of 37 cm are required due to highly oblique beam entries, or if proton radiography is planned, energies of ≥ 300 MeV are needed. All the machines described in Table 3.1 operate at well below 300 MeV.

3.4 THE PROPERTIES OF PROTON BEAMS

3.4.1 Proton interactions with matter

Proton interactions with matter have been described in detail in ICRU (1998) and only some of the main features will be repeated here.

Protons lose their energy in a medium primarily through numerous electromagnetic interactions with atomic electrons (ICRU, 1993a; 1998). They have a mass that is large compared with the mass of electrons, hence they lose only a small fraction of their energy in each interaction (at most $4m/M = 0.0022$, where m is the electron mass and M is the proton mass) and they are deflected by only small angles in each interaction.

The proton mass electronic stopping power in a material, $S(E)/\rho$, is defined as

$$\frac{S(E)}{\rho} = \left(\frac{1}{\rho}\right) \left(\frac{dE}{dx}\right), \quad (3.1)$$

where S is the linear stopping power (note that the nomenclature $s = S/\rho$ is used interchangeably), dE is the mean energy lost by a proton in electronic collisions while traversing a distance dx in a material of density ρ . Frequently, the unit $\text{MeV cm}^2 \text{ g}^{-1}$ is used, where the mass thickness, or areal density, (in g cm^{-2}) is defined as the product of density ρ and absorber thickness [ρdx in Eq. (3.1)]. The quantity S/ρ ($=s$) depends on the physical and chemical composition and density of the material and on the energy of the proton.

In the continuous-slowing-down approximation (csda), the range R of a particle is given by

$$R = \int [S(E)]^{-1} dE. \quad (3.2)$$

Because each particle experiences a different set of interactions, a group of particles of the same initial energy has a distribution of energies after traversing a thickness of absorber (energy straggling) and a resulting distribution of depths at which the particles stop (range straggling) (ICRU, 1998). The rate of energy loss of a charged particle is proportional to the square of its charge and approximately inversely

proportional to the square of its velocity. Thus, as a particle traverses matter, its rate of energy loss increases until, at very low velocities, it captures an electron, decreasing its effective charge. The average rate of energy loss consequently decreases at very low velocities. The foregoing explains the formation of the Bragg dose peak (ICRU, 1998).

At increasing energy, nuclear interactions (Chadwick *et al.*, 1999; ICRU, 2000) become more important (Laitano *et al.*, 1996; Medin, 1997; Medin and Andreo, 1997a; Paganetti, 2002; Wroe *et al.*, 2005). In the therapeutic energy range, the probability of nuclear events is small compared with the probability of electron interactions, although each nuclear reaction can transfer a significant portion of the proton energy to the medium. Nuclear interactions essentially remove primary protons from the beam and result in the production of secondary particles. These particles may be important from the biological point of view because of their higher RBE values (ICRU, 1998). Among the nuclear processes that occur, neutron production has a non-negligible impact due to the production of heavy charged particles generated by subsequent neutron interactions. In addition to the potential biological effect due to nuclear secondaries, protons slowing down near the Bragg peak may also be expected to produce an enhanced biological effect (ICRU, 1998; Paganetti, 2002; Paganetti and Goitein, 2000) (see Section 2).

3.4.2 Definition and specification of beam properties and beam parameters

In practice, a number of definitions of the proton beam characteristics are required. Some of these relate to the beam models used in treatment planning and others relate to the physical characteristics of the beam as determined by measurement. To draw a distinction between these sets of definitions, the following section discusses 'Beam properties' that relate to the treatment-planning system and 'Beam parameters' that are defined for measurement purposes.

From the perspective of treatment planning, a 'beam' consists of directed radiation characterized by a number of physical factors that identify: the type and quality of the radiation source; the direction from which radiation comes and the point within the patient to which it is directed; and the 'shape' (lateral to the beam and, in the case of protons, in depth) of the high-dose region (treated volume). At any point, the directional properties of a beam may be characterized by its angular divergence and angular emittance (Section 3.4.2.1).

The physical characteristics of the clinically acceptable treatment beams produced by passive scattering or dynamic methods must be defined in terms of a set of beam parameters. The beam characteristics should be defined in terms of a set of measurable and calculable parameters, which can be used to assess the clinical acceptability of the beams, to benchmark the treatment-planning algorithms used to calculate patient isodose distributions and for routine quality-assurance purposes. These parameters differ for beams produced by passive scattering or by dynamic methods, and are discussed in Section 3.4.2.2.

3.4.2.1 Beam properties

Field. The ‘field’ of a beam is the area of intersection of the beam with a plane normal to the beam direction and at any distance from the effective source. Thus, it is a two-dimensional structure and it is, for example, possible to refer to the fluence distribution within a field (often termed the beam’s intensity profile).

Uniform-intensity beam. A ‘uniform-intensity beam’ is used to irradiate a volume within the patient with near-uniformity. A uniform-intensity beam can be produced by either passive or dynamic beam-delivery techniques.

Intensity-modulated beam. Intensity-modulated therapy is a technique of treatment in which the individual beams do not irradiate the PTV uniformly—indeed are likely to do so in a highly non-uniform manner. The intent of intensity-modulated therapy is that the set of beams that constitute the plan generate a conformal and usually uniformly-treated volume within a PTV that has concavities, and/or achieve ‘conformal avoidance’ of particular organs. The beams are, then, termed ‘intensity-modulated beams’ (to contrast them with uniform-intensity beams). In proton-beam therapy, an intensity-modulated beam is generally produced using some method of beam scanning.

Angular divergence and angular emittance. There are two distinct aspects to the angular distribution of the particles in a beam. The first, ‘angular divergence’, describes the correlation of the mean direction of the particles in the beam with their position within the field. This effect is typically due to the spreading out of a beam that emanates from a source, which is a finite distance from the patient. It gives rise, for example, to the inverse-square effect in which dose falls off for purely geometric reasons as the square of the distance from the source. On the other hand, the ‘angular emittance’ describes the distribution of particle directions around their mean direction at a

given point (on, say, the patient’s skin surface). Owing to multiple scattering of charged particles within matter, all proton beams acquire angular ‘confusion’ at depth within the patient and this is a major contribution to the beam penumbra.

Infinitesimal pencil beam. An ‘infinitesimal pencil beam’ is a beam which, at the place that it is incident on the patient, has infinitesimal lateral extent, infinitesimal angular emittance, and is monoenergetic.

Finite pencil beam. A ‘finite pencil beam’ is analogous to an infinitesimal pencil beam except that, at the place that it is incident on the patient, it has: finite (but, nevertheless, small) lateral extension, finite (but, nevertheless, small) angular emittance, and finite (but, nevertheless, small) energy spread.

Pencil beam. The general term ‘pencil beam’ may be employed when no distinction between infinitesimal and finite initial conditions needs to be made.

3.4.2.2 Beam parameters

Passively scattered beams. For passively scattered beams, the parameter set should include the profile of the beam in depth (*i.e.*, the profile of the SOBP), the lateral profile of the beam, and data on the beam penetration and width, flatness, symmetry, lateral penumbra and distal dose fall-off. The variation in these parameters with beam energy, length and depth of the SOBP, and the field size should be documented. Gall *et al.* (1993a) defined a set of beam parameters that has been widely used and is illustrated in Fig. 3.12. More recently, an alternative set of beam parameters for characterizing the SOBP (Fig. 3.13) has been proposed (Gottschalk, 2003).

The parameter definitions given by Gall *et al.* were as follows:

Depth of penetration (d'_{90}), or *range* in Gall’s nomenclature, is defined as the depth (in g cm^{-2}) along the beam central axis in water to the distal 90 percent point of the maximum dose value.

Distal-dose fall off (DDF) is defined as the distance (in g cm^{-2}) in which the dose, measured in water along the beam central axis, decreases from 80 to 20 percent of the maximum dose value.

SOBP length (m'_{90}) is defined as the distance in water between the distal and proximal 90 percent points of the maximum dose value.

Lateral penumbra (LP) is defined at a given depth as the distance (in mm) in which the dose, measured along the line perpendicular to the beam central axis, decreases from 80 to 20 percent of the maximum dose value at that depth.

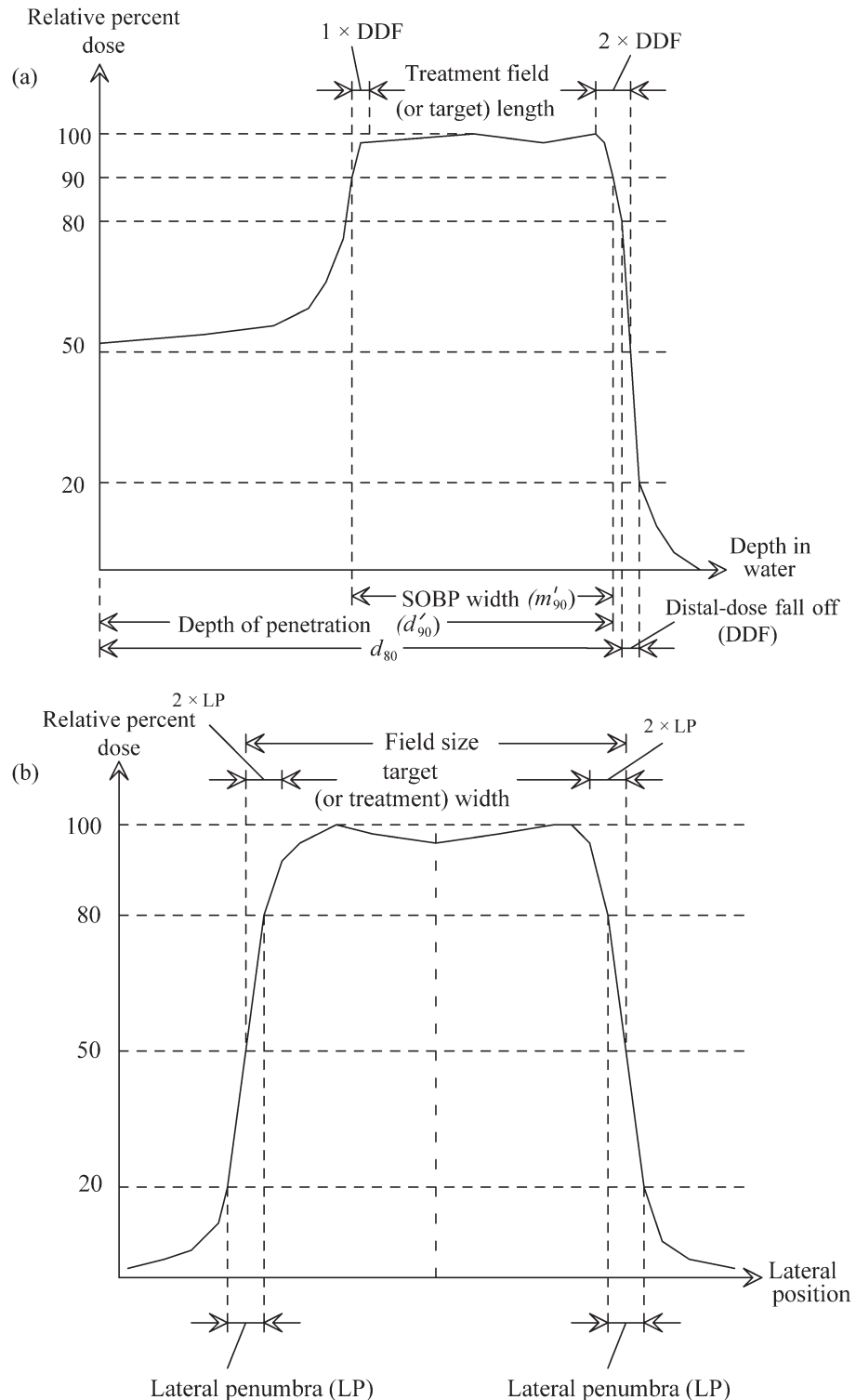


Figure 3.12. (a) Depth-dose curve for an SOBP and (b) a lateral proton-beam profile in the Bragg peak showing some parameters commonly used to characterize the proton dose distribution as defined by Gall *et al.* (1993).

Field size is defined as the distance (in mm) between the 50 percent points of the maximum dose value, measured along the line perpendicular to the beam central axis, on the isocenter plane in air.

Target (or treatment) length is defined as the distance between two DDF lengths ($2 \times \text{DDF}$) proximal to the distal 50 percent isodose level of the SOBP, and one DDF length ($1 \times \text{DDF}$) distal to the

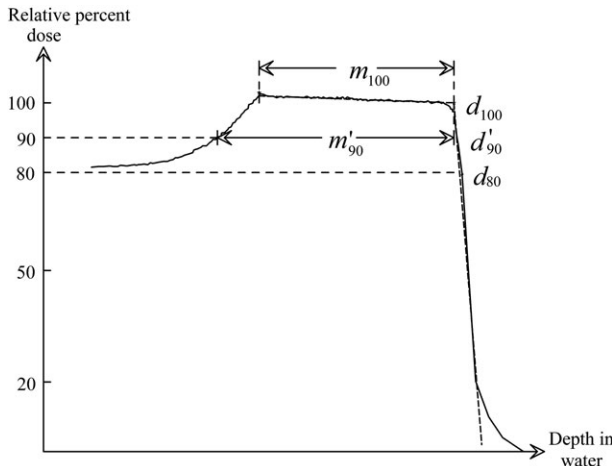


Figure 3.13. Model SOBP showing the quantities defined by Gottschalk, d_{100} and m_{100} , and the commonly used quantities d'_{90} , m'_{90} , and d_{80} .

proximal 90 percent isodose level of the SOBP (Fig. 3.12a).

Target (or treatment) width is defined as the distance between two LP widths ($2 \times \text{LP}$) from the 50 percent isodose levels of the lateral-beam profile (Fig. 3.12b).

The following additional parameters can be used to define the dose uniformity: lateral symmetry and lateral flatness.

Lateral flatness (in percent) is defined as

$$F_{\text{lp}} = \left(\frac{d_{\text{lp max}} - d_{\text{lp min}}}{d_{\text{lp max}} + d_{\text{lp min}}} \right) \times 100, \quad (3.3)$$

where $d_{\text{lp max}}$ and $d_{\text{lp min}}$ are the maximum and minimum absorbed dose values in the beam profile measured in the target width.

Lateral symmetry (in percent) is defined as

$$S_{\text{lp}} = \left(\frac{D_1 - D_2}{D_1 + D_2} \right) \times 100, \quad (3.4)$$

where D_1 and D_2 are the integrated absorbed doses in each half of the field about the central axis.

In the SOBP parameterization proposed by Gottschalk (see Fig. 3.13), the terms depth and modulation are used in preference to depth of penetration and target (or treatment) length defined above. Gottschalk uses a model-independent analysis of SOBP data to determine beam parameters (Gottschalk, 2003). The beam is divided into three separate segments along the depth axis, namely proximal rise, flat top, and distal drop, and each segment is fitted with a separate polynomial. The break points between segments are parameters of the fit in addition to three sets of polynomial coefficients. The

intersections of the best-fit polynomials provide a robust definition of two points and based on these points the depth at full dose (d_{100}) and the modulation at full dose (m_{100}) are defined. The procedure can be used to define the 100 percent dose level, the range-equivalent depth (d_{80}), the gradient of the DFF, the slope of the SOBP 'flat top', the entrance dose and the goodness of the fit (rms). Gottschalk argues that the parameters d_{100} and m_{100} are more convenient definitions of penetration and extent of modulation than the commonly used definitions of d'_{90} and m'_{90} (see Figs 3.12 and 3.13). He argues that d'_{90} is an arbitrary choice and if the intention is to take the target volume to full dose then d_{100} is more appropriate.

The term 'range' has often been used loosely to define beam penetration. The use of this term should be restricted to describe calculated or tabulated csda particle ranges as derived from Eq. (3.2) above and as discussed in ICRU Report 49 (ICRU, 1993a). The depth of penetration may be defined in several different ways (d_{80} , d_{90} , or d_{100}) as discussed above and as illustrated in Figs 3.12 and 3.13. It is important, in reporting the depth of penetration of a proton beam, to carefully specify which of these definitions is being used.

It is recommended that the dose-distribution parameterization of Gall *et al.* (1993a) be used to characterize lateral-dose distributions, and that the parameterization of Gottschalk (2003) be used to characterize depth-dose distributions.

Dynamically scanned beams. For scanned beams, the characterization parameters defined above are not appropriate. Scattered-beam data are generally collected in an extended water phantom using a small-volume ionization chamber or diode. With a spot-scanned beam, the integrated-beam dose distribution is produced by superimposing a large number of individual pencil beams. More importantly, treatment-planning systems for scanned proton beams perform their calculations by summing individual pencil beams. Thus, beam-scanning systems require the measurement of depth-dose curves and lateral profiles of finite pencil beams, requiring small-field dosimetry equipment with a good spatial resolution (Pedroni *et al.*, 2005).

If the dose distribution in a three-dimensional volume resulting from beam scanning is to be measured, then some multi-channel or integrating detector is required. These measurements are discussed in more detail in Section 4.

3.5 RADIATION QUALITY

The radiation quality of the beam as it enters the patient is determined by the energy distribution of

the scattered beam, or of the pencil beam in scanning applications, and the degree of scattering that the beam has experienced in transit through beam-line components and beam-modifying devices. Radiation quality can affect the distal fall-off of the Bragg peak, the lateral-beam penumbra, and the low-level dose to the patient outside the field at large off-axis distances, including the secondary neutron and photon doses. The mode of beam production and delivery can considerably affect the radiation quality. Secondary radiation can also be produced in the patient.

An experimental study of the factors affecting proton-beam penumbra has been made by Oozeer *et al.* (1997) for a passively scattered proton beam. They found that for the system under investigation the beam penumbra as it enters a phantom (the 'entrance' penumbra) is little affected by the range shifter but is influenced by the final collimator, the bolus thickness, and the air gap between the bolus and the entrance to the phantom. At a given depth in the phantom, the LP depends on the 'entrance' penumbra, the range, and the depth. As depth increases, the fractional contribution of the 'entrance' penumbra to the total penumbra decreases.

Paganetti and co-workers used Monte Carlo calculations to investigate the influence of various beam-modifying devices on the beam characteristics for an ocular melanoma treatment beam line, but these methods are also well suited to applications for the treatment of deep-seated tumors (Paganetti, 1998; Paganetti and Goitein, 2000). The effects of different beam-line arrangements on beam penumbra, the depth-dose distributions and the distal fall-off of the Bragg peak can be studied. There are two contributions to the slight variation in relative biological effectiveness (RBE) within the irradiated volume: the first is that the linear energy transfer (LET) of the primary protons increases as they slow down and only becomes significant at the end of their range; the second contribution is from secondary particles (charged particles and neutrons), particularly those originating from non-elastic nuclear interactions, which can have high LET and can affect all parts of the Bragg curve. These small RBE variations are consistent with a generic RBE value of 1.1 and are usually ignored.

In addition to affecting the dose distribution within the target volume, secondary particles, especially neutrons from nuclear interactions, can deliver dose outside the target volume, both laterally and beyond the distal edge of the Bragg peak. In passive beam delivery, the secondary neutron dose results from neutrons produced by proton

interactions with material in the treatment head or nozzle (scatterer, range shifter, range modulator, collimator aperture, and beam-shaping bolus), and to a very much lesser extent from those from proton interactions with nuclei of patient tissue in the beam path. In dynamic beam delivery, the neutron dose is produced almost entirely by proton interactions with nuclei of patient tissue in the beam path. Hence, the secondary neutron scattering in the treatment head can theoretically lead to an increased risk of radiation-induced secondary cancer for scattered proton beams compared with scanned proton beams. However, it must be noted that: (i) there is limited clinical experience with scanned beams, which have only been used at one center; (ii) there is no published evidence of increased risk of secondary cancers in patients who have undergone proton therapy; and (iii) the available data on doses outside the treatment field in proton therapy have large uncertainties and (where comparable) are not in good agreement.

The energy distribution of the secondary neutrons contributing significantly to dose is in the range from zero to the maximum initial energy of the proton beam. The radiation-weighting factors, or quality factors, of neutrons, as function of neutron energy, recommended by the International Commission on Radiological Protection (ICRP, 1991) are: 5, 10, 20, 10, and 5 for energies of <10, 10–100 keV, 100 keV to 2 MeV, 2–20 MeV, and >20 MeV, respectively. It is suggested that 10 is a reasonable quality factor to be used for scattered radiation from 150 to 250 MeV proton beams. These quality factors are used only for calculating the risk of secondary cancers and should not be used for therapeutic dose calculations.

There are limited data on secondary doses to proton therapy patients outside the treatment field. Binns and Hough (1997) and Yan *et al.* (2002) made measurements in 200 and 160 MeV beams, respectively. Binns and Hough measured a dose equivalent of 33–80 mSv per treatment Gy at distances of 50–120 cm off-axis of a prototype beam designed for treating small intracranial lesions and skull-base tumors at the National Accelerator Centre (now iThemba LABS). To reduce this background additional shielding was installed in the beam line prior to commissioning for clinical use. Yan *et al.* measured dose equivalents in the range of ~1–15 mSv per treatment Gy around the passive scattering nozzle at the Harvard Cyclotron Laboratory at a distance of 50 cm. Recently, Wroe *et al.* (2007) determined the dose equivalents outside a 225 MeV proton therapy prostate treatment field at the Loma Linda University Medical Center. The dose equivalents on the surface of a

phantom decreased from 3.9 to 0.18 mSv per treatment Gy as the distance from the proton field edge increased from 2.5 to 60 cm. Data from Monte Carlo calculations are also available (Agosteo *et al.*, 1998; Fontenot *et al.*, 2005; Jiang *et al.*, 2005; Polf and Newhauser, 2005; Polf *et al.*, 2005). The data from Polf *et al.* show good agreement with the measured data of Yan *et al.* (2002), with the Monte Carlo calculations of the dose equivalent being within a factor of 2–3 of the measurements. Jiang *et al.* (2005) calculated organ-specific patient-effective dose due to secondary neutrons for two simulated treatment plans in the lung and paranasal sinus. The total whole-body effective dose was calculated to be 0.162 and 0.0266 Sv, with 0.058 and 0.0042 Sv contributions from neutrons produced internally in the patient, for the lung and paranasal sinus treatments, respectively. The work of Fontenot *et al.* (2005) showed that Monte Carlo simulations give values of the dose-equivalent 2.6 times those from measurements. Roy and Sandison (2004) and Mesolaras *et al.* (2006) focused on determining the fetal dose

equivalent during proton therapy of the mother in the passively scattered 205 MeV beam at the Midwest Proton Radiotherapy Institute. They measured fetal dose equivalents of between (0.10 and 0.26) and (0.025 and 0.450) mSv per treatment Gy, respectively. The excess risk to the fetus of radiation-induced cancer death in the first 10 years of life was estimated to be 17.4 percent per 10 000 children.

These data show that the scattered neutron dose for a passively scattered beam is highly dependent on the energy and on the specific design features of the beam line and machine head. Monte Carlo simulations differ substantially from measurements, which have relatively large uncertainties. The measurements of Schneider *et al.* (2002b) show that with scanned beams the neutron dose equivalent outside the treatment field is less than for most passively scattered beams. However, the recent measurements by Mesolaras *et al.* (2006) in a passively scattered beam are substantially lower than those by Schneider *et al.* (2002b).

4 DOSIMETRY

4.1 GENERAL CONSIDERATIONS

Absorbed-dose determination must be accurate and reproducible as tumor-control and normal-tissue complication probabilities are steep functions of absorbed dose. Dosimetry techniques at any facility must be consistent with those at other facilities if clinical data are to be compared. At the level of one standard deviation (1 SD), relative accuracy of 3 percent is desirable, although 5 percent is often accepted, while relative precision (reproducibility) of 2 percent is required. If the latter cannot be achieved in clinical practice, the cause should be investigated. The determination of range is an important issue in proton therapy and is addressed in Sections 4.7 and 4.8.

The specifications for the design of a dosimeter depend on the requirements for:

1. the accuracy of the absorbed-dose determination;
2. the sensitivity of the measuring system;
3. the energy dependence of the dosimeter response;
4. the spatial resolution.

Calorimeters are absolute dosimeters as they measure directly the energy deposited in a sensing element by a temperature rise. No radiation calibration is necessary and the measurements have a relatively small uncertainty (Laitano, 1997; 1998; Seuntjens and DuSautoy, 2002). They have been recommended as the instruments of choice for determining the absorbed dose in proton beams under reference conditions (AAPM, 1986; Vynckier *et al.*, 1991; 1994). However, they are not commercially available and are cumbersome and difficult to use routinely. Nevertheless, they are finding increasing use in all types of therapy beams (ICRU, 2001; Palmans *et al.*, 2004; Seuntjens and DuSautoy, 2002).

Faraday cups can also be used at high energies (ICRU, 1998; Laitano, 1997; Verhey *et al.*, 1979). However, their use is based on fluence determinations in air and requires accurate knowledge of the effective area, energy spectrum of the proton beam, and knowledge of secondary-particle production. The measurements have to be converted to absorbed dose using appropriate stopping-power ratios. Although reasonable agreement has been found in some studies (*e.g.*, Newhauser *et al.*, 2002a; 2002b),

ionization chambers calibrated with Faraday cups have given problematic results, yielding proton-absorbed doses that have been found in some cases to be in excess of 10 percent lower than doses determined with ionization chambers calibrated with a calorimeter or with a ^{60}Co beam (Delacroix *et al.*, 1997; Palmans and Vynckier, 2002; Vatnitsky *et al.*, 1996b; Vynckier, 2004). However, the problems can be reduced by careful design, and accurate measurements are achievable (Grusell *et al.*, 1995; Jones *et al.*, 1999). Nevertheless, the use of Faraday cups for clinical proton dose measurements is not recommended (see Section 4.2). However, as mentioned in Section 4.7, multilayer Faraday cups (MLFCs) are very useful instruments for making in-beam range measurements (Gottschalk *et al.*, 1999; Paganetti and Gottschalk, 2003).

Carbon activation can also be used for proton-beam dosimetry. This technique is based on the activation of ^{11}C (half-life = 20.4 min) via the $^{12}\text{C}(p,pn)^{11}\text{C}$ reaction (Cumming, 1963; Kostjuchenko and Nichiporov, 1993; Larsson and Sarby, 1987; Larsson *et al.*, 1965; Nichiporov, 2003; Nichiporov *et al.*, 2004). It is essentially an off-line method involving irradiation of a carbon sample in the beam and subsequent $4\pi \beta-\gamma$ coincidence counting. ^{11}C emits a positron (β) (with maximum energy of 968 keV) that annihilates with an electron, the result of which is the emission of two oppositely directed 0.511 MeV quanta. The counting system requires the detection of the three particles (a β and two 0.511 MeV quanta) in coincidence. The technique is not suitable for routine applications as the experimental set-up is quite complicated, but it can be used for independent verification of ionization-chamber dosimetry. A recent study showed relative agreement of 1.7 percent between doses measured using carbon activation and ionization chambers (Nichiporov, 2003).

The practical instruments for absorbed-dose determination are ionization chambers (Boag, 1966; Chu, 1995b), which are readily available, cheap, robust, easy to use, and require little ancillary equipment. However, there are no primary standards for proton beams, and ionization chambers have to be calibrated, either by means of

a calorimeter in the user's proton beam, or have calibration coefficients traceable to a primary standard ^{60}Co beam (Andreo, 2002; ICRU, 2001). In the latter case, the knowledge of physical data and constants is required to determine appropriate correction factors for the use in clinical proton beams.

Protocols for proton-therapy dosimetry have been published by the American Association of Physicists in Medicine (AAPM) (AAPM, 1986) and the European Clinical Heavy Particle Dosimetry Group (ECHED) (Vynckier, 1995; Vynckier *et al.*, 1991; 1994) and were consolidated into ICRU Report 59 (ICRU, 1998; Jones, 2001d). In ICRU Report 59, it is recommended that the reference absorbed-dose measurements in the clinical situation be made with cylindrical ionization chambers having ^{60}Co calibration coefficients traceable to standards laboratories. The calibration coefficients should be checked, preferably with a calorimeter (ICRU, 1998). The calibration coefficients can be given in terms of air kerma, exposure, or absorbed dose to water. The latter is preferred as the uncertainties in the chamber-dependent factors used to convert the measurements to absorbed dose are less, and the formalism is simpler and easier to interpret (Andreо, 1992; Hohlfield, 1988; Medin *et al.*, 1995; Rogers, 1992). Recently the International Atomic Energy Agency (IAEA) has published (Technical Reports Series—TRS 398) a code of practice for radiotherapy dosimetry (including proton therapy) based solely on absorbed dose to water standards using ^{60}Co -calibrated ionization chambers (IAEA, 2000).

Comparisons of dose measurements among different centers are important for establishing uniform standards and for verifying the integrity of the dosimetry (Fukumura *et al.*, 2002; Jones *et al.*, 1992; Kacperek *et al.*, 2002; Vatnitsky *et al.*, 1996b; 1999b). Such studies are essential in order to establish the relative doses delivered if pooling or comparing clinical results from different institutes. Comparisons are especially important for unconventional beams such as protons, and have revealed problems with dosimetry strategies (Vatnitsky *et al.*, 1996b) (see Sections 4.2 and 4.6). If a single dosimetry protocol is used, inter-institutional consistency is usually excellent (Vatnitsky *et al.*, 1999b) and is independent of what the calibration coefficients for that specific protocol are based on.

Medin and Andreo (1992) reviewed and evaluated the stopping-power ratios of interest for proton-beam dosimetry in use at that time. Subsequently, new mass total stopping-power data were published by the ICRU (ICRU, 1993a). More recently, calculations of the water-to-air stopping-power ratios, which are specifically required for ionization chamber-based proton dosimetry, have

been made (Medin, 1997; Medin and Andreo, 1997b). These latter calculations were based on the ICRU (ICRU, 1993a) stopping powers, but included the contributions from secondary electrons and nonelastic nuclear collisions.

The densities and atomic compositions of a variety of materials relevant to proton dosimetry are given in Table 4.1 (ICRU, 1984; 1993a). Proton mass total stopping powers (including nuclear stopping power) and continuous slowing-down approximation (csda) ranges for these materials are given in Tables 4.2 and 4.3, respectively (ICRU, 1993a). The contribution of nuclear stopping power is negligible in the therapeutic proton energy range and amounts to $<10^{-3}$ of the electronic stopping power >1 MeV (ICRU, 1993a).

In the present section, reference dosimetry with Faraday cups and calorimeters is first discussed. Faraday-cup dosimetry is not recommended and is only included here for completeness. The two recent protocols (IAEA, 2000; ICRU, 1998) for ionization-chamber dosimetry in proton beams, based on ^{60}Co calibrations traceable to standards laboratories (IAEA, 2000; ICRU, 2001), are then described and compared. The importance of dry versus humid (ambient) air in interpreting ionization-chamber response is also considered. The energy required to form an ion pair in air (w -value) for protons contributes potentially the largest uncertainty to the determination of absorbed dose, and is considered in Section 4.4.4. Because it is recommended that the IAEA protocol (IAEA, 2000) be adopted, its features are covered in full. Implementation details are given in Appendix A. A worksheet for determining the absorbed dose to water in a proton beam using this protocol is also provided in Appendix A. Dosimetry comparisons, beam monitoring, and relative dosimetry are also described in some detail.

The descriptions in the present section concern mainly the dosimetry of static (passively modified) proton beams, but in many cases apply equally to the dosimetry of active (scanned) beams. Special requirements for scanned beams are elucidated where applicable. The main differences in the dosimetry of passive and active systems are in beam monitoring and relative dosimetry.

4.2 REFERENCE DOSIMETRY WITH A FARADAY CUP

A Faraday cup is a device that can be used to determine the number of protons in a beam. Protons that reach the thick absorber inside the Faraday cup produce a net charge proportional to the number of protons. The electrically insulated and conducting

DOSIMETRY

Table 4.1. Density and composition of materials for which proton stopping powers (Table 4.2) and ranges (Table 4.3) are given (ICRU, 1984; 1993a).

Material	Density, ρ (g cm $^{-3}$)	Atomic composition/fraction by mass				
		H	C	N	O	Others
Water	1.0000	0.111894			0.888106	
TE gas (propane) ^a	1.8263×10^{-3}	0.102672	0.568940	0.035022	0.293366	
Polystyrene	1.0600	0.077418	0.922582			
PMMA	1.1900	0.080538	0.599848		0.319614	
ICRU muscle	1.0400	0.101997	0.123000	0.035000	0.729003	0.011000 (Na, Mg, P, S, K)
Graphite	2.2200		1.000000			
Air, dry ^a (near sea level)	1.20484×10^{-3}		0.000124	0.755267	0.231781	0.012827 (Ar)
A-150 plastic	1.1270	0.101327	0.775501	0.035057	0.052316	0.017422 (F) 0.018378 (Ca)

^aAt standard temperature and pressure.

proton-beam absorber must be thick enough to stop all primary protons and proton-produced secondary-charged particles in the absorber. A potential error in this measurement can occur because of the collection of secondary-charged particles such as spallation products and electrons produced upstream that can add to, or subtract from, the charge due to primary protons. Charged particles generated in the sensing absorber, usually electrons, can escape the absorber and modify the response. Appropriate use of thin entrance foils, vacuum environs, and trapping electromagnetic fields surrounding the sensing absorber minimizes the effects due to the escape of secondary electrons (Cambria *et al.*, 1997; Jones *et al.*, 1999; Kacperek and Bonnett, 1990; Lin *et al.*, 1994; Verhey *et al.*, 1979; Vynckier *et al.*, 1984; Ziegler *et al.*, 1996). Another problem concerns energetic protons and other heavier charged particles produced near the periphery of the absorber by fast neutrons that are generated by proton interactions in the upstream portion of the sensing absorber. The use of non-hydrogenous high-Z absorbers with concomitantly small particle-production cross-sections minimizes this effect (ICRU, 1998).

Faraday-cup-based dosimetry is more sensitive to the energy distribution of the proton beam than ionization chambers or calorimeters and, therefore, caution is recommended when using fluence determination as a basis for clinical dosimetry. A fluence measurement in a proton beam of known fluence distribution (as a function of energy) can be used to calibrate a transfer ionization chamber for use in a clinical beam. If one assumes that a transmission ionization chamber is used to monitor the beam fluence, the dose to water¹ D_w can be obtained by a

fluence measurement followed by a charge measurement with an ionization chamber at the same point. If the proton beam is monoenergetic with energy E and is of small enough cross-section to be completely accepted by the aperture of the cup, then the dose to water D_w is given by

$$D_w = (1.602 \times 10^{-10}) \left(\frac{N}{a} \right) \left[\frac{S(E)}{\rho} \right]_w, \quad (4.1)$$

where $1 \text{ eV} = 1.602 \times 10^{-19} \text{ J}$, N is the number of protons per monitor unit collected in the Faraday cup, a is the effective area of the beam (in cm 2 ; assuming uniformity), $[S(E)/\rho]_w$ is the mass electronic stopping power of the protons of energy E in water (in MeV cm 2 g $^{-1}$), D_w is then expressed in Gy (monitor unit) $^{-1}$.

When the calibrating beam is composed of a mixture of protons of various energies, the mass electronic stopping power in Equation (4.1) must be replaced with an integral over the proton spectrum:

$$D_w = (1.602 \times 10^{-10}) \int \Phi_E(E) \left[\frac{S(E)}{\rho} \right]_w dE, \quad (4.2)$$

where $\Phi_E(E)$ is the fluence of protons of energy E per monitor unit.

The mass stopping power to be used depends critically on accurately known beam energy. The presence of a small admixture of low-energy scattered protons can lead to significant errors in absorbed-dose determination (Verhey *et al.*, 1979). Monte Carlo calculations may be helpful in estimating the effect of low-energy contaminants on the calibration. A monoenergetic proton beam constructed without collimators has been reported to be capable of avoiding the production of low-energy scattered protons (Grusell *et al.*, 1995). The effect of nuclear interactions is to increase the apparent mean deposited

¹For consistency the dosimetry nomenclature of IAEA Report TRS 398 (IAEA, 2000) is used throughout the present report. Specifically, the use of italics in some subscripts of symbols for dosimetric quantities follows IAEA Report TRS 398.

Table 4.2. Proton mass total stopping powers in various materials (ICRU, 1993a).

Energy, E (MeV)	Proton mass total stopping power, S_{tot}/ρ (MeV cm 2 g $^{-1}$)							
	Water	TE gas (propane)	Polystyrene	PMMA	ICRU muscle	Graphite	Air (dry)	A-150 plastic
1.00	260.8	273.7	257.7	253.2	258.5	229.7	222.9	268.1
1.25	222.9	233.4	220.5	216.8	221.0	196.8	191.2	229.0
1.50	195.7	204.5	193.7	190.5	194.0	173.1	168.3	200.9
1.75	174.9	182.6	173.3	170.5	173.5	155.1	150.9	179.6
2.00	158.6	165.3	157.2	154.6	157.3	140.9	137.1	162.7
2.25	145.4	151.4	144.0	141.8	144.2	129.3	125.8	149.1
2.50	134.4	139.8	133.2	131.1	133.3	119.6	116.5	137.7
2.75	125.1	130.0	123.9	122.1	124.1	111.5	108.6	128.2
3.00	117.2	121.7	116.1	114.3	116.2	104.5	101.8	120.0
3.50	104.2	108.0	103.2	101.7	103.4	93.01	90.68	106.6
4.00	94.04	97.38	93.06	91.79	93.29	83.99	81.97	96.10
4.50	85.86	88.80	84.92	83.79	85.17	76.71	74.92	87.66
5.00	79.11	81.74	78.20	77.19	78.47	70.69	69.09	80.70
5.50	73.43	75.80	72.54	71.64	72.84	65.62	64.17	74.85
6.00	68.58	70.74	67.72	66.90	68.02	61.30	59.97	69.86
6.50	64.38	66.37	63.56	62.80	63.86	57.55	56.33	65.55
7.00	60.71	62.55	59.91	59.21	60.22	54.28	53.15	61.78
7.50	57.47	59.18	56.70	56.05	57.00	51.39	50.33	58.46
8.00	54.60	56.19	53.84	53.24	54.15	48.81	47.83	55.51
8.50	52.02	53.51	51.29	50.73	51.59	46.52	45.59	52.87
9.00	49.69	51.10	48.99	48.45	49.28	44.44	43.57	50.49
9.50	47.59	48.91	46.90	46.40	47.19	42.56	41.73	48.34
10.0	45.67	46.92	45.00	44.52	45.29	40.84	40.06	46.37
12.5	38.15	39.14	37.56	37.19	37.84	34.13	33.51	38.70
15.0	32.92	33.73	32.39	32.08	32.64	29.45	28.94	33.36
17.5	29.05	29.74	28.57	28.31	28.81	25.99	25.55	29.42
20.0	26.07	26.67	25.62	25.39	25.85	23.32	22.94	26.38
22.5	23.69	24.22	23.28	23.08	23.49	21.19	20.85	23.96
25.0	21.75	22.22	21.36	21.18	21.56	19.46	19.15	21.99
27.5	20.13	20.56	19.77	19.61	19.96	18.01	17.73	20.34
30.0	18.76	19.15	18.42	18.27	18.60	16.78	16.53	18.95
35.0	16.56	16.90	16.26	16.13	16.42	14.82	14.60	16.73
40.0	14.88	15.17	14.60	14.49	14.75	13.31	13.12	15.02
45.0	13.54	13.80	13.28	13.18	13.42	12.11	11.94	13.66
50.0	12.45	12.68	12.21	12.12	12.34	11.14	10.99	12.56
55.0	11.54	11.76	11.32	11.24	11.45	10.33	10.19	11.64
60.0	10.78	10.98	10.57	10.50	10.69	9.645	9.517	10.87
65.0	10.13	10.31	9.926	9.858	10.04	9.060	8.942	10.21
70.0	9.559	9.727	9.369	9.306	9.477	8.553	8.443	9.634
75.0	9.063	9.221	8.882	8.823	8.986	8.109	8.006	9.133
80.0	8.625	8.774	8.452	8.397	8.552	7.717	7.620	8.691
85.0	8.236	8.376	8.070	8.018	8.166	7.368	7.277	8.297
90.0	7.888	8.020	7.728	7.678	7.820	7.056	6.970	7.945
95.0	7.573	7.699	7.420	7.372	7.509	6.775	6.693	7.628
100	7.289	7.409	7.140	7.095	7.227	6.520	6.443	7.341
125	6.192	6.290	6.064	6.027	6.139	5.538	5.475	6.233
150	5.445	5.528	5.331	5.300	5.398	4.868	4.816	5.479
175	4.903	4.976	4.800	4.772	4.861	4.382	4.338	4.932
200	4.492	4.558	4.397	4.372	4.453	4.014	3.976	4.518
225	4.170	4.230	4.081	4.058	4.134	3.724	3.691	4.193
250	3.911	3.966	3.827	3.806	3.877	3.492	3.462	3.932
275	3.698	3.749	3.618	3.599	3.666	3.300	3.275	3.717
300	3.520	3.568	3.444	3.426	3.490	3.140	3.118	3.538
350	3.241	3.284	3.170	3.154	3.213	2.889	2.871	3.257
400	3.032	3.072	2.966	2.951	3.006	2.700	2.687	3.046
450	2.871	2.908	2.808	2.794	2.846	2.554	2.544	2.884
500	2.743	2.778	2.683	2.670	2.720	2.438	2.431	2.755

DOSIMETRY

Table 4.3. Proton continuous slowing down approximation (csda) ranges in various materials (ICRU, 1993a).

Energy, E (MeV)	Proton csda range, r_0 (g cm $^{-2}$)							
	Water	TE gas (propane)	Polystyrene	PMMA	ICRU muscle	Graphite	Air (dry)	A-150 plastic
1.00	0.00246	0.00227	0.00244	0.00247	0.00247	0.00275	0.00287	0.00230
1.25	0.00350	0.00326	0.00349	0.00354	0.00352	0.00393	0.00408	0.00331
1.50	0.00470	0.00441	0.00470	0.00477	0.00473	0.00529	0.00548	0.00448
1.75	0.00605	0.00571	0.00607	0.00616	0.00609	0.00682	0.00705	0.00580
2.00	0.00756	0.00715	0.00759	0.00770	0.00761	0.00851	0.00879	0.00726
2.25	0.00920	0.00873	0.00925	0.00939	0.00927	0.0104	0.0107	0.00887
2.50	0.0110	0.0105	0.0111	0.0112	0.0111	0.0124	0.0128	0.0106
2.75	0.0129	0.0123	0.0130	0.0132	0.0130	0.0145	0.0150	0.0125
3.00	0.0150	0.0143	0.0151	0.0153	0.0151	0.0169	0.0174	0.0145
3.50	0.0195	0.0187	0.0197	0.0200	0.0197	0.0219	0.0226	0.0189
4.00	0.0246	0.0236	0.0248	0.0252	0.0248	0.0276	0.0284	0.0239
4.50	0.0302	0.0289	0.0304	0.0309	0.0304	0.0338	0.0348	0.0294
5.00	0.0362	0.0348	0.0366	0.0371	0.0365	0.0406	0.0417	0.0353
5.50	0.0428	0.0412	0.0432	0.0438	0.0431	0.0480	0.0493	0.0417
6.00	0.0498	0.0480	0.0503	0.0510	0.0502	0.0559	0.0573	0.0487
6.50	0.0574	0.0553	0.0580	0.0588	0.0578	0.0643	0.0659	0.0561
7.00	0.0654	0.0631	0.0661	0.0670	0.0659	0.0733	0.0751	0.0639
7.50	0.0738	0.0713	0.0747	0.0756	0.0744	0.0827	0.0847	0.0722
8.00	0.0828	0.0800	0.0837	0.0848	0.0834	0.0927	0.0949	0.0810
8.50	0.0922	0.0891	0.0932	0.0944	0.0929	0.103	0.106	0.0902
9.00	0.102	0.0986	0.103	0.105	0.103	0.114	0.117	0.0999
9.50	0.112	0.109	0.114	0.115	0.113	0.126	0.129	0.110
10.0	0.123	0.119	0.125	0.126	0.124	0.138	0.141	0.121
12.5	0.183	0.178	0.186	0.188	0.185	0.205	0.209	0.180
15.0	0.254	0.247	0.258	0.260	0.256	0.284	0.290	0.250
17.5	0.335	0.326	0.340	0.344	0.338	0.375	0.382	0.330
20.0	0.426	0.415	0.432	0.437	0.430	0.476	0.486	0.420
22.5	0.527	0.513	0.535	0.540	0.531	0.589	0.600	0.519
25.0	0.637	0.621	0.647	0.654	0.642	0.712	0.725	0.628
27.5	0.757	0.738	0.769	0.776	0.763	0.846	0.861	0.747
30.0	0.885	0.864	0.900	0.909	0.893	0.990	1.01	0.874
35.0	1.17	1.14	1.19	1.20	1.18	1.31	1.33	1.16
40.0	1.49	1.46	1.52	1.53	1.50	1.66	1.69	1.47
45.0	1.84	1.80	1.87	1.89	1.86	2.06	2.09	1.82
50.0	2.23	2.18	2.27	2.29	2.25	2.49	2.53	2.20
55.0	2.64	2.59	2.69	2.72	2.67	2.96	3.00	2.62
60.0	3.09	3.03	3.15	3.18	3.12	3.46	3.51	3.06
65.0	3.57	3.50	3.64	3.67	3.60	3.99	4.05	3.54
70.0	4.08	4.00	4.16	4.19	4.12	4.56	4.63	4.04
75.0	4.62	4.53	4.71	4.74	4.66	5.16	5.24	4.58
80.0	5.18	5.09	5.28	5.32	5.23	5.79	5.88	5.14
85.0	5.78	5.67	5.89	5.93	5.83	6.46	6.55	5.73
90.0	6.40	6.28	6.52	6.57	6.45	7.15	7.25	6.34
95.0	7.05	6.92	7.18	7.24	7.11	7.87	7.98	6.98
100	7.72	7.58	7.87	7.93	7.78	8.63	8.74	7.65
125	11.5	11.3	11.7	11.8	11.6	12.8	13.0	11.4
150	15.8	15.5	16.1	16.2	15.9	17.6	17.9	15.7
175	20.6	20.3	21.1	21.2	20.8	23.1	23.3	20.5
200	26.0	25.5	26.5	26.7	26.2	29.0	29.4	25.8
225	31.7	31.2	32.4	32.6	32.0	35.5	35.9	31.5
250	37.9	37.4	38.7	39.0	38.3	42.4	42.9	37.7
275	44.5	43.8	45.5	45.7	44.9	49.8	50.3	44.2
300	51.5	50.7	52.6	52.9	51.9	57.6	58.2	51.1
350	66.3	65.3	67.7	68.1	66.9	74.2	74.9	65.9
400	82.3	81.1	84.0	84.5	83.0	92.1	92.9	81.8
450	99.2	97.8	101	102	100	111	112	98.7
500	117	115	120	120	118	131	132	116

energy per proton. This increases the predicted dose to water per proton, depending on proton energy, by several percent (Seltzer, 1993). The uncertainties introduced by nuclear effects and by the sensitivity of the calibration to the energy and type of the beam particles combine to make ionization-chamber calibrations based on fluence potentially less accurate than those based on calorimetry and ^{60}Co .

Several studies in clinical proton beams, comparing doses deduced directly from Faraday-cup measurements or with ionization chambers calibrated with Faraday cups, and with ionization chambers calibrated with calorimeters or ^{60}Co beams, have shown consistently large relative discrepancies (5–20 percent), with the Faraday-cup dose determinations usually being lower (Cambria *et al.*, 1997; Cuttone *et al.*, 1999; Delacroix *et al.*, 1997; Gall *et al.*, 1994; Jones *et al.*, 1994a; 1994b; Schreuder *et al.*, 1994; Vatnitsky *et al.*, 1996b; Verhey *et al.*, 1979). The magnitudes of these discrepancies depend to some extent on which protocols and physical constants were used to determine the absorbed dose with ionization chambers having ^{60}Co calibration coefficients, and on the stopping powers used for the Faraday-cup measurements. However, variations in these latter values do not account for the large differences in absorbed dose that are frequently observed. Better relative agreement (<4 percent) was found in some studies (Grusell *et al.*, 1995; Jones *et al.*, 1999; Kacperek and Bonnett, 1990; Kacperek *et al.*, 1991; Newhauser *et al.*, 2002a; 2002b). These latter results can possibly be ascribed to improved Faraday-cup construction, and more accurate determination of the beam area and correction for secondary-particle absorption.

Doses have been determined in a 250 MeV clinical beam at the Paul Scherrer Institute (PSI) with a Faraday cup and an ionization chamber using pencil beams (used for beam scanning). For residual energies between 138 and 214 MeV, the ratio of the doses measured with the ionization chamber to those measured with the Faraday cup varied from 0.978 to 1.008 (Coray *et al.*, 2002; Pedroni *et al.*, 2005). This illustrates that with care relatively good agreement between the two dosimetry systems can be obtained. Nevertheless, the Faraday-cup primary monitor at PSI is corrected to the ionization-chamber dose values.

In view of the large differences frequently observed, but not sufficiently understood, between absorbed doses obtained using Faraday cups and ^{60}Co -calibrated ionization chambers or calorimeters, the sole use of such fluence-based techniques is not currently recommended for proton-therapy dosimetry.

4.3 REFERENCE DOSIMETRY WITH A CALORIMETER

Unlike measurements based upon the products produced by the interaction of ionizing radiation with matter, *e.g.*, ionizations, a calorimetric measurement is a direct determination of the energy imparted to a sensing element as indicated by the temperature change. Under the assumption that all the deposited energy is thermalized, absorbed dose may thus be directly determined in a calorimetric measurement. In principle, no knowledge of any radiation parameters is required. Ideally, absorbed-dose standards for therapeutic proton beams should be calorimeters. A calorimetric absorbed-dose determination can also provide an independent confirmation of ionization-chamber determinations. Detailed discussions of calorimetric techniques are given in Attix (1986), Daires *et al.* (1994), Domen (1987), Palmans and Vynckier (2002), Palmans *et al.* (2004), Ross and Klassen (1996), Schulz *et al.* (1987), Seuntjens and DuSautoy (2002), and Seuntjens *et al.* (1994).

Calorimetric determination involves the measurement of the temperature change in a mass of material resulting from energy imparted by ionizing radiation. The temperature change is typically of the order of the $10^{-3}\text{ }^{\circ}\text{C Gy}^{-1}$. Thermistors are metal-oxide semi-conductors with a negative temperature coefficient, which can be used in conjunction with a Wheatstone bridge to conveniently determine this temperature change with great precision (Domen, 1987; ICRU, 1998; Kubo and Brown, 1984; 1986; Kubo *et al.*, 1989; Laughlin and Jenna, 1966).

Many calorimeters operate in an adiabatic manner. One or more insulating jackets surround a core of material. In an adiabatic or isothermal operation mode, the core and jacket are maintained at equal temperature. If a temperature difference exists, then the calorimeter response needs to be corrected for heat transfer between the core and jacket. The net core temperature change, relative to the pre-irradiation period, is then proportional to the energy deposited by the incident ionizing radiation. To ensure that the signal derives from the material of interest, even for large imparted energy density, a core mass of several grams is usually employed. The imparted energy per unit mass is then representative of the average absorbed dose to the core material. Conversion of the measured temperature change to energy imparted is accomplished by knowledge of the mass of the core, combined either with calibration of the temperature response of the core with resistive heating, or with knowledge of the specific heat of the core material. Adiabatic calorimeters usually use homogeneous

DOSIMETRY

core and jacket materials such as graphite (Domen and Lamperti, 1974; Palmans *et al.*, 2004) or A-150 tissue-equivalent plastic (Delacroix *et al.*, 1997; McDonald *et al.*, 1976; Verhey *et al.*, 1979).

Although calorimetry avoids difficulties associated with determination or knowledge of radiation-specific parameters, technical problems can limit the accuracy of the measurement. Perhaps, the most significant is the conversion of the deposited energy into non-thermal processes such as chemical reactions. These reactions may create or absorb heat, *i.e.*, they can be either exothermic or endothermic. One can define a heat excess (exothermic case) or heat defect (endothermic case) as the fraction of the energy imparted that creates or absorbs heat, respectively, in the calorimeter material.

Calorimeters provide the most direct method of absorbed-dose determination and are an excellent choice for a primary standard. However, calorimeters are not generally available at proton facilities and are more difficult to use than ionization chambers, and therefore they have not been chosen as routine reference dosimeters for proton therapy. They are, however, in use as reference dosimeters at national and international standards laboratories. Appropriate examples of calorimeters have been constructed of graphite (McDonald, 1987; McEwen and Duane, 2000; Palmans *et al.*, 2004), A-150 tissue-equivalent (TE) plastic (Caumes *et al.*, 1984; Delacroix *et al.*, 1997; McDonald and Domen, 1986), and water (Brede *et al.*, 2000; Domen, 1980; 1994; Schulz *et al.*, 1987; Seuntjens and Palmans, 1999). The use of an ice calorimeter has even been reported in Rosser (1994). When available, calorimeters should be used as primary standards or, alternatively, to confirm the proton calibration coefficient of the reference ionization chamber (ICRU, 1998).

A calorimeter can be used to determine the absorbed dose to water D_w in a proton beam as

$$D_w = \Delta T c (1 + T_D)^{-1} k_i s_{w,cal}, \quad (4.3)$$

where ΔT is the temperature rise due to radiation (in K), c the specific heat of the sensitive element (in $\text{J kg}^{-1} \text{K}^{-1}$), T_D is the heat defect (or excess) due to deposited energy which does not result in a temperature increase (see below), k_i is the product of several correction factors (excluding the heat defect) that depend on the construction of the calorimeter and its core material (see below), and $s_{w,cal}$ is the ratio of the mass electronic stopping power of water to the calorimeter material. Of

course, this latter factor does not apply if a water calorimeter is used.

The heat defect T_D is given by

$$T_D = \frac{E_a - E_h}{E_a}, \quad (4.4)$$

where E_a is the energy imparted to the material and E_h is the energy appearing as heat. A positive heat defect means that some deposited energy is lost in rearrangement of the lattice structure and the temperature rise is therefore too small.

The factors k_i for calorimetry include corrections for heat transfer (convection and conduction), absorption and scattering (presence of other materials), and dose gradient (difference between measured dose and dose at reference point). For calorimetry with solid materials, convective heat transfer does not apply. The core can be thermally insulated by a vacuum or air cavity, and a correction factor is required to account for the presence of the cavity (Boutillon, 1989; McEwen and Duane, 2000; Palmans and Vynckier, 2002; Seuntjens and DuSautoy, 2002). If conduction and convection heat losses are minimal, the temperature rise is directly related to the energy imparted per unit mass near the measurement point. Any possible heat defect has to be considered and taken into account.

As mentioned above, the value of ΔT is normally determined with the help of a Wheatstone bridge that is used to measure the change in resistance of a thermistor in thermal contact with the calorimeter. The specific heat c can be measured by passing an accurately known current through a heating resistor that is in thermal contact with the calorimeter, and measuring the temperature change for a known amount of dissipated energy. In the case of water, c is well known (Wagner and Pruss, 2002). These techniques are discussed elsewhere (Domen, 1987; McDonald and Domen, 1986; Seuntjens and DuSautoy, 2002). The mass electronic stopping powers needed are energy dependent, but the ratio required for the calorimetric dose determination in water is only weakly dependent on proton energy for energies above ~ 1 MeV (ICRU, 1998). Properties of common materials used for calorimetry are given in Table 4.4.

Graphite calorimeters have a longer history than water calorimeters as national laboratory absorbed-dose standards (Chauvenet *et al.*, 1997; DuSautoy, 1996; Guerra *et al.*, 1996; McEwen and Duane, 2000), and the heat defect and convection effects are assumed to be negligible (ICRU, 1998; Schulz *et al.*, 1990; Seuntjens and DuSautoy, 2002). In addition, the specific heat of graphite is a factor of

Table 4.4. Properties of materials used for calorimetry (adapted from Palmans and Vynckier, 2002; reproduced with permission).

Property	Water (4°C)	Graphite	A-150
Heat defect (T_D) (%)	0.0 ± 0.5	0.0 ± 0.3	4.0 ± 1.5
Specific heat (c) (J kg $^{-1}$ K $^{-1}$)	4205	710	1720
Thermal diffusivity (α) (m 2 s $^{-1}$)	1.44×10^{-7}	0.80×10^{-4}	2.72×10^{-7}
Temperature rise per unit dose ($\Delta T/D$) (mK Gy $^{-1}$)	0.24	1.41	0.58

6 lower than that of water, giving rise to an increased signal-to-noise ratio of potentially the same magnitude compared with water calorimetry. Difficulties with both water (Ross and Klassen, 1996) and graphite (McEwen and Duane, 2000; Seuntjens and DuSautoy, 2002) calorimetry are understood and have largely been solved. However, the use of a graphite calorimeter to derive the absorbed dose to water requires knowledge of conversion factors that can increase the uncertainty.

Water calorimeters have been developed to provide a more direct determination of absorbed dose to water (Domen, 1980; 1994; Ross and Klassen, 1996; Seuntjens *et al.*, 1994). These devices are usually operated in a non-adiabatic manner, and the temperature in a small region (the 'core') of the water calorimeter surrounding the thermistor temperature-sensing element is directly measured. For water calorimeters operated near room temperature, convection currents can be a recurring problem.

Several water-based portable calorimeters have been developed for absorbed-dose determinations in various therapy (including proton) beams (Brede *et al.*, 2000; 2006; Medin *et al.*, 2005; 2006; Schulz *et al.*, 1987; 1991; 1992). Palmans *et al.* (2004) have also recently developed a portable graphite-based instrument with which measurements were made in a low-energy (62 MeV) ocular-treatment proton beam line.

Although the heat defect in water is sensitive to the amount of dissolved gases and absorbed impurities, dose rate, and accumulated dose (ICRU, 1998; Klassen and Ross, 1991; Ross *et al.*, 1989), for practical irradiation conditions, the heat defect due to dissolved impurities is approximately constant. Investigations by Domen (1994) and Schulz *et al.* (1992) indicate that by using nitrogen-purged high-resistivity water, the heat defect can be made negligibly small for low linear energy transfer (LET) beams. Similar results are found with argon- and hydrogen-saturated water (Palmans and Vynckier, 2002; Palmans *et al.*, 1996; Seuntjens *et al.*, 1994). For pure (hypoxic) water at 4°C, the heat defect is assumed to be zero (Schulz

et al., 1991) for low-LET beams. The latter result is consistent with later measurements by Brede *et al.* (1994; 1997), Palmans *et al.* (1996), and Seuntjens *et al.* (1994). It is recommended that the heat defect be determined for each water-calorimetric system used.

The heat defect for A-150 plastic is usually taken as 0.04 ± 0.015 (Brede *et al.*, 1997; Fleming and Glass, 1969; McDonald and Goodman, 1982; Säbel *et al.*, 1973; Schulz *et al.*, 1990). Because A-150 plastic is a mixture of several materials, the heat defect may be sensitive to the manufacturing and curing process (Brede *et al.*, 1997) as well as the radiation history of the sample. Therefore, it is desirable to measure the heat defect of individual batches of A-150 prior to any dosimetry investigations. Using low-energy protons, deuterons, and α -particles of different energies, Brede *et al.* (1997) have demonstrated an LET dependence of the heat defect in A-150 plastic and pure water. However, for low-LET radiations such as high-energy protons, this effect is negligible.

The uncertainties of the mass electronic stopping-power ratio and the heat defect give a combined relative uncertainty of $\sim 2\text{--}3$ percent in calorimetric dose determinations in A-150 plastic; but in the case of graphite or water, that uncertainty can be reduced due to a smaller uncertainty in the heat defect (Palmans *et al.*, 1996; Schulz *et al.*, 1987). Typical uncertainties for dose determination with a water calorimeter in a high-energy photon beam are shown in Table 4.5 (Seuntjens and DuSautoy, 2002). Similar uncertainties are applicable to proton beams.

Several absorbed-dose measurements have been made with calorimeters in clinical proton beams. Most of these measurements involved water calorimeters (Brede *et al.*, 1999; 2006; Hashemian *et al.*, 2003; Jones *et al.*, 1999; Medin *et al.*, 2005; 2006; Palmans *et al.*, 1996; Seuntjens *et al.*, 1994; Schulz *et al.*, 1992; Siebers *et al.*, 1995), while two involved A-150 plastic calorimeters (Delacroix *et al.*, 1997; Verhey *et al.*, 1979), and one involved a graphite calorimeter (Palmans *et al.*, 2004). The doses measured were compared with those measured

Table 4.5. Typical relative standard uncertainties, u_c , for an absorbed dose to water (D_w) determination with a water (pure or saturated with H_2) calorimeter in a high-energy photon beam (adapted from Seuntjens and DuSautoy, 2002; reproduced with permission).

Quantity	u_c (%)
Thermistor calibration	0.20
Repeatability	0.15
Specific heat capacity	0.05
Conduction heat loss correction	0.15
Field perturbation correction	0.02
Profile uniformity	0.02
Positioning	0.10
Water density	0.02
Heat defect	0.30
Combined relative standard uncertainty in D_w	0.43

using other instruments. The proton energies required to create an ion pair in air (w -values) could be deduced by comparison of calorimetric with ionization-chamber dose determinations.

4.4 REFERENCE DOSIMETRY WITH IONIZATION CHAMBERS HAVING ^{60}Co CALIBRATION COEFFICIENTS

When proton absorbed dose is determined, it is usually measured in some material that differs from the material of interest. For example, measurements are usually made in a water phantom using a gas-filled ionization chamber constructed with walls of some other material such as plastic or graphite. The absorbed dose to water is then inferred from the response of the dosimeter, which is not composed of water. In this case, the ionization produced in the filling gas must be related to the absorbed dose in the material of interest. Interactions in the chamber walls and surrounding media produce little direct response in the gas. The relationship between absorbed dose in the gas and absorbed dose in the medium of interest is determined by the ratio of the mass electronic stopping powers for the two materials (ICRU, 1998).

The response of a radiation detector to a proton beam is also influenced by the geometry of the detector. This is because the energy deposited by a particle in the detector depends on both the effective stopping power of the medium and the path length of the particle in the medium. As an example, the response of cylindrical and parallel plate ionization chambers of the same volume would be expected to differ because of differences in mean path length (Bichsel, 1995).

The Bragg–Gray theory was developed in order to calculate the absorbed dose to a medium from ionization measurements in a gas cavity placed in the medium. The following two conditions need to be satisfied in order for the theory to hold (ICRU, 1977; 1989):

1. A cavity in the measuring medium does not perturb the charged-particle field, *i.e.*, the charged-particle energy fluence in the cavity is identical to that in the medium, and the cavity has no effect on this energy fluence distribution.
2. The energy deposited in the cavity is due entirely to the charged particles crossing it.

Under the above conditions, the ratio of the absorbed dose in the adjacent medium to the absorbed dose in the cavity is equal to the ratio of the mass collision electronic stopping powers of the respective materials.

4.4.1 ICRU proton dosimetry protocol (ICRU 59)

The ICRU dosimetry protocol (ICRU, 1998), which is restated here, recommends that ambient-air-filled cylindrical ionization chambers with graphite or A-150 TE plastic walls with traceable ^{60}Co calibration factors be used. The emphasis is on prescribing the techniques for absorbed-dose measurements with ionization chambers having air-kerma calibration coefficients. Chambers with volumes of 0.5 cm^3 or greater should be used for large beams ($\geq 5 \text{ cm}$ diameter). For smaller beams, chambers with volumes of $\sim 0.1 \text{ cm}^3$ should be used. Absorbed dose should be measured in a water phantom or in other materials that are close to tissue in electron density. When measuring in materials other than water, the depth of measurement should be scaled to the equivalent depth in water using measured equivalent depths (Schneider *et al.*, 2002a) or the csda ranges given in ICRU (1993a). The effective beam energy should be determined from the residual csda range, which is defined for this purpose as the distance in water between the point of measurement and the practical range, *i.e.*, the depth beyond the Bragg peak at which the dose falls to 10 percent of its maximum value (see Fig. 4.1). The preferred reference point for calibration is the center of the modulated spread-out Bragg peak (SOBP).

The absorbed dose to water in a proton beam, $D_{w,p}$, measured with an ambient air-filled ionization chamber having an air-kerma calibration coefficient [assuming constant values for $(s_{w,\text{air}})_p$ and

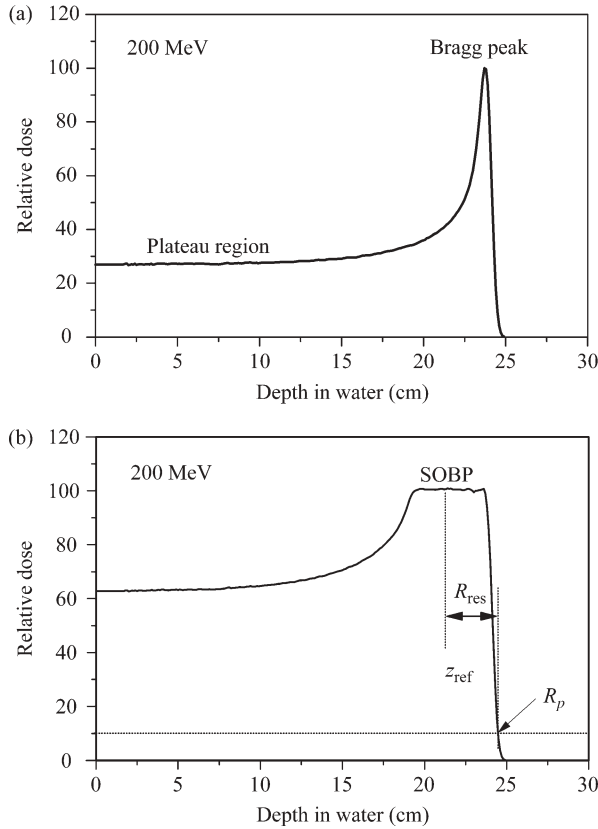


Figure 4.1. (a) Percentage depth-dose distribution for a 200 MeV proton beam, illustrating the 'plateau' region and the Bragg peak; (b) percentage depth-dose distribution for a modulated proton beam. Indicated on the figure are the reference depth z_{ref} (middle of the SOBP), the residual range at z_{ref} used to specify the quality of the beam R_{res} and the practical range R_p . Adapted from IAEA (2000).

$(w_{\text{air}}/e)_p$] is given (ICRU, 1998) by

$$D_{w,p} = M_p^{\text{corr}} N_{D,g} C_p, \quad (4.5)$$

$$N_{D,g} = \frac{N_K (1-g) A_{\text{wall}} A_{\text{ion}}}{s_{\text{wall,air}} (\mu_{\text{en}}/\rho)_{\text{air,wall}} K_{\text{hum}}}, \quad (4.6)$$

$$C_p = (s_{w,\text{air}})_p \frac{(w_{\text{air}}/e)_p}{(W_{\text{air}}/e)_c}, \quad (4.7)$$

where M_p^{corr} is the product of the electrometer reading M corrected for ion recombination, temperature, pressure, and all the factors that produce a modified response relative to the calibration conditions (IAEA, 1997a), $N_{D,g}$ is the absorbed-dose calibration coefficient, N_K is the air-kerma calibration coefficient for ^{60}Co uncorrected for ion recombination, g is the fraction of kinetic energy of secondary charged particles that is lost to radiative processes (bremsstrahlung) in air [0.003 for ^{60}Co (Boutillon, 1987)], A_{wall} is the correction factor for

attenuation and scatter in the wall and build-up cap in the ^{60}Co calibration beam, A_{ion} is the correction factor for ion recombination in the gas of the ionization chamber when exposed in air in the ^{60}Co calibration beam, $s_{\text{wall,air}}$ is the mean ratio of restricted mass stopping powers of the wall material to air for the secondary electrons generated by the ^{60}Co calibration photons, $(\mu_{\text{en}}/\rho)_{\text{air,wall}}$ is the mean ratio of air-to-wall mass energy absorption coefficients for the calibration ^{60}Co gamma rays, K_{hum} is the correction factor to account for the difference in response between ambient air and dry air, $(s_{w,\text{air}})_p$ is the ratio of water-to-air mass electronic stopping powers in the proton beam, $(w_{\text{air}}/e)_p$ is the mean energy to form an ion pair in the ionization-chamber gas for protons, and $(W_{\text{air}}/e)_c$ is the mean energy to form an ion pair in the ionization-chamber gas for the calibration ^{60}Co beam (see Section 4.4.4 below for full discussion and definitions of w and W).

If an exposure calibration factor (N_X) is used, N_K can be calculated from

$$N_K = N_X \left(\frac{W_{\text{air}}}{e} \right)_c (1-g)^{-1} (2.58 \times 10^{-4} \text{ CR}^{-1} \text{ kg}^{-1}). \quad (4.8)$$

If the ionization chamber is calibrated in terms of absorbed dose to water in the calibration ^{60}Co beam ($N_{D,w,c}$), the dose to water, $D_{w,p}$, is then given (ICRU, 1998) by

$$D_{w,p} = M_p^{\text{corr}} N_{D,w,c} k_p, \quad (4.9)$$

where

$$k_p = \frac{(s_{w,\text{air}})_p}{(s_{w,\text{air}})_c} \frac{(w_{\text{air}}/e)_p}{(W_{\text{air}}/e)_c}. \quad (4.10)$$

The errors and omissions in the ICRU 59 dosimetry protocol are addressed in Section 4.4.5.

4.4.1.1 Physical quantities for ICRU 59

The largest uncertainty in absorbed-dose determination is in the value of $(w_{\text{air}}/e)_p$. This issue is discussed fully in Section 4.4.4. AAPM (AAPM, 1986) and ECCHED (Vynckier *et al.*, 1991; 1994) used two different values: 34.3 J C^{-1} and 35.2 J C^{-1} , respectively. A compromise value of $(34.8 \pm 0.7) \text{ J C}^{-1}$ for ambient air was recommended in ICRU Report 59 (ICRU, 1998). This value is consistent with both direct measurements and those inferred from comparison between ionization chamber and calorimetric measurements. For $(W_{\text{air}}/e)_c$, a value of

(33.97 ± 0.05) J C $^{-1}$ for dry air is recommended (Boutillon and Perroche-Roux, 1987; CCMERI, 1985; Niatel *et al.*, 1985). However, if humid (ambient) air is used in the ionization chamber in the ^{60}Co beam, this value should be reduced to 33.77 J C $^{-1}$ (ICRU, 1998; Rogers and Ross, 1988; Schulz *et al.*, 1986) with an uncertainty of ± 0.05 J C $^{-1}$ (0.15 percent) (Boutillon and Perroche-Roux, 1987). When using humid air in the ionization chamber in the ^{60}Co beam, a correction factor of $K_{\text{hum}} = 0.997$ (CCMERI, 1977; ICRU, 1979; Schulz *et al.*, 1986) [Equation (4.6)] must be applied. The ratio $(w_{\text{air}}/e)_p/(W_{\text{air}}/e)_c$ for humid air is 1.031 ± 2.0 percent (ICRU, 1998; Jones, 2001d). The ratio of the water-to-air mass electronic stopping powers for protons is taken from ICRU (1993a) and can be considered constant within 1.2 percent (ICRU, 1998) in the energy range of interest here. A value of 1.133 can be assumed (Jones, 2001d). The values of the other physical quantities and their relative uncertainties are given in Table 4.6 (Jones, 2001d; Vynckier, 1995). Quantities not given in the table (e.g., A_{ion}) are assumed to have values of 1 with negligible uncertainties. For ionization chambers calibrated in terms of absorbed dose to water, the value of $(s_{w,\text{air}})_c$ is taken as 1.134 (ICRU, 1998).

4.4.2 IAEA proton dosimetry code of practice (TRS 398)

This code of practice (IAEA, 2000) is based solely upon the use of ionization chambers having calibration coefficients specified in terms of absorbed dose to water in a reference beam of quality Q_0 (^{60}Co). The absorbed dose to water at the reference depth, z_{ref} , in water for a reference calibration

beam of quality Q_0 and in the absence of the chamber is given by

$$D_{w,Q_0} = M_{Q_0} N_{D,w,Q_0}. \quad (4.11)$$

The absorbed dose to water at the reference depth z_{ref} in water, in a proton beam of quality Q and in the absence of the chamber, is given by

$$D_{w,Q} = M_Q N_{D,w,Q_0} k_{Q,Q_0}, \quad (4.12)$$

where M is the reading of the dosimeter with the reference point of the chamber positioned at z_{ref} , corrected for the influence quantities pressure and temperature, electrometer calibration, polarity effect and ion recombination (IAEA, 1997a; 2000), N_{D,w,Q_0} is the calibration coefficient in terms of absorbed dose to water for the dosimeter at the reference quality Q_0 (^{60}Co), k_{Q,Q_0} is the chamber specific factor that corrects for differences between the reference beam quality Q_0 and the actual quality being used Q . Reference conditions for the determination of absorbed dose in proton beams are given in Table 4.7. Water is recommended as the reference medium for the determination of absorbed dose and for beam-quality measurements.

The beam-quality correction factor k_{Q,Q_0} is defined as the ratio, at the qualities Q and Q_0 , of the calibration coefficients in terms of absorbed dose to water of the ionization chamber:

$$k_{Q,Q_0} = \frac{N_{D,w,Q}}{N_{D,w,Q_0}} = \frac{D_{w,Q}/M_Q}{D_{w,Q_0}/M_{Q_0}}. \quad (4.13)$$

Field sizes should be $10 \times 10 \text{ cm}^2$ and the phantom should extend at least 5 cm beyond all four sides of the field size employed at the depth of

Table 4.6. Physical quantities and relative standard uncertainties for absorbed dose determinations using A-150/air ionization chambers with ^{60}Co air-kerma calibration coefficients [Jones (2001d), using data from AAPM (1983), Gastorf *et al.* (1986), IAEA (1997a), Nath and Schulz (1981), Vynckier (1995), and Vynckier *et al.* (1991, 1994)].

Quantity	Symbol	Value	Relative standard uncertainty (%)
Electrometer reading	M	0.1	
Product of electrometer reading correction factors		0.2	
Air-kerma calibration coefficient	N_K	1.0	
Absorption and scattering correction factor in A-150 in calibration ^{60}Co beam	A_{wall}	0.983–0.992	0.1
Mean ratio of mass electronic stopping powers in calibration ^{60}Co beam (A-150/air)	$s_{\text{wall},g}$	1.145	0.1
Mean ratio of mass energy absorption coefficients in calibration ^{60}Co beam (air/A-150)	$[(\mu_{\text{en}}/\rho)_{\text{air,wall}}]_c$	0.906	0.1
Mean ratio of mass electronic stopping powers in proton beam (water/air)	$(s_{w,\text{air}})_p$	1.133 ^a	1.2
Ratio of energy required to produce an ion pair in ambient air	$(w_{\text{air}}/e)_p/(W_{\text{air}}/e)_c$	1.031	2.0
Humidity correction factor	K_{hum}	0.997	0.1
Combined relative standard uncertainty		2.6	

^aAssuming a constant value.

Table 4.7. Reference conditions for the determination of absorbed dose in proton beams (IAEA, 2000).

Quantity	Reference value or reference characteristics
Phantom material	Water
Chamber type	For $R_{\text{res}} \geq 0.5 \text{ g cm}^{-2}$, cylindrical and plane parallel chambers For $R_{\text{res}} < 0.5 \text{ g cm}^{-2}$, plane parallel chambers
Measurement depth, z_{ref}	Middle of the SOBP ^a
Reference point of the chamber	For plane-parallel chambers, on the inner surface of the window at its centres For cylindrical chambers, on the central axis at the center of the cavity volume
Position of the reference point of the chamber	For plane-parallel and cylindrical chambers, at the point of measurement depth z_{ref}
SSD	Clinical treatment distance
Field size at the phantom surface	$10 \times 10 \text{ cm}^2$, or that used for normalization of the output factors whichever is larger For small field applications (<i>i.e.</i> , eye treatments), $10 \times 10 \text{ cm}^2$ or the largest field clinically available

^aThe reference depth can be chosen in the 'plateau region', at a depth of 3 g cm^{-2} , for clinical applications with monoenergetic proton beams (*e.g.*, for plateau irradiations).

measurement and also extend to at least 5 g cm^{-2} beyond the maximum depth of measurement. Kanai *et al.* (2004) have assessed these field- and phantom-size requirements in a 235 MeV clinical beam with a 6 cm SOBP. They found that the lateral dimensions of the water phantom need not exceed the field size. Indeed, there was a discrepancy of only 0.5 percent if a phantom of $5 \times 5 \text{ cm}^2$ cross-section is used in a $10 \times 10 \text{ cm}^2$ field. Nevertheless, the 5 cm margin should be adhered to as these latter measurements were made under specific conditions.

For horizontal beams, the water phantom entrance window should be made of 2–5 mm thick poly(methyl methacrylate) (PMMA) or polystyrene. To calculate the water-equivalent thickness, mass densities of 1.19 and 1.06 g cm^{-3} , respectively (ICRU, 1984), should be used (IAEA, 2000). If required, a close-fitting waterproofing cover of PMMA with a thickness not exceeding 1 mm should be used. There should be an air gap of 0.1–0.3 mm between the chamber and the cover to allow the air pressure and temperature in the chamber to equilibrate (IAEA, 2000).

The proton-beam quality index is the residual range R_{res} (g cm^{-2}) in water and is defined (Fig. 4.1) as

$$R_{\text{res}} = R_p - z_{\text{ref}}. \quad (4.14)$$

where R_p is the practical range (g cm^{-2}), namely, the depth of the 10 percent level of the peak dose on the distal edge of the Bragg peak, and z_{ref} is the reference depth for the measurement (middle of SOBP). Reference conditions for the determination of proton-beam quality are given in Table 4.8.

Laitano *et al.* (1996) and Laitano and Rosetti (2000) have calculated stopping powers in water and TE materials averaged over the proton energy spectra at various positions in unmodulated and range-modulated proton beams of the same maximum energies (50–300 MeV). They found relative differences of up to 20 percent between *absolute* stopping powers calculated at the same depth in modulated and unmodulated beams. They also found negligible differences in the case of stopping-power *ratios*, which have little energy dependence. Medin and Andreo (1992) and Palmans and Verhaegen (1998) calculated the differences in stopping-power ratios between a modulated beam and a monoenergetic proton beam with the same residual range. The effects are small and can safely be neglected (Palmans and Vynckier, 2002). The use of residual range or energy is therefore an appropriate beam-quality specifier for ionization-chamber-based proton dosimetry.

Ideally k_{Q,Q_0} should be obtained from Eq. (4.13) by direct measurement of the absorbed dose at the qualities Q and Q_0 . However, as no primary standards of absorbed dose to water for protons are available, all values of k_{Q,Q_0} are derived by

Table 4.8. Reference conditions for the determination of proton beam quality: residual range (R_{res}) (IAEA, 2000).

Quantity	Reference value or reference characteristics
Phantom material	Water
Chamber	Cylindrical and plane parallel
Reference point of the chamber	For plane-parallel chambers, on the inner surface of the window at its center For cylindrical chambers, on the central axis at the center of the cavity volume
Position of the reference point of the chamber	For plane-parallel and cylindrical chambers, at the point of interest
SSD	Clinical treatment distance
Field size at the phantom surface	$10 \text{ cm} \times 10 \text{ cm}$ For small field applications (<i>i.e.</i> , eye treatments), $10 \text{ cm} \times 10 \text{ cm}$ or the largest field clinically available

calculation (IAEA, 2000). These calculations are based on ^{60}Co gamma radiation as the reference-beam quality Q_0 (Andreo, 1992; Medin *et al.*, 1995):

$$k_{Q,Q_0} = \frac{(s_{w,\text{air}})_Q}{(s_{w,\text{air}})_{Q_0}} \frac{(w_{\text{air}}/e)_Q}{(W_{\text{air}}/e)_{Q_0}} \frac{p_Q}{p_{Q_0}}, \quad (4.15)$$

where $s_{w,\text{air}}$ is the water-to-air stopping-power ratio, w_{air}/e and W_{air}/e are the differential and integral mean energies, respectively, expended in dry air per ion pair formed (see Section 4.4.4 for full discussion and definitions of w and W), p is the product of ionization-chamber perturbation factors, which includes all departures from the behavior of an ideal Bragg–Gray detector:

$$p = p_{\text{cav}} p_{\text{cel}} p_{\text{dis}} p_{\text{wall}}, \quad (4.16)$$

where p_{cav} is the factor that corrects the response of an ionization chamber for effects related to the air cavity, predominantly the in-scattering of electrons and heavy charged particles that makes the particle fluence inside the cavity different from that in the medium in the absence of the cavity, p_{cel} is the factor that corrects the response of an ionization chamber for the effect of the central electrode (lack of air equivalence) during in-phantom measurements (for plane-parallel ionization chambers, p_{cel} is not applicable), p_{dis} is the factor that accounts for the effect of replacing a volume of water with the detector cavity when the reference point of the chamber is taken to be at the chamber center—it is the alternative to the use of an effective point of measurement of the chamber (for plane-parallel ionization chambers, p_{dis} is not applicable), and p_{wall} is the factor that corrects the response of an ionization chamber for the non-water equivalence of the chamber wall and any waterproofing material.

4.4.2.1 Physical quantities for TRS 398

For proton dosimetry, the calculated beam-quality correction factors given in TRS 398 (IAEA, 2000) are based on a calibration in ^{60}Co . The values for $(s_{w,\text{air}})_Q$ are described as a function of the proton beam-quality specifier R_{res} (Fig. 4.2):

$$(s_{w,\text{air}})_Q = a + bR_{\text{res}} + \frac{c}{R_{\text{res}}}, \quad (4.17)$$

where $a = 1.137$, $b = -4.265 \times 10^{-5}$, and $c = 1.840 \times 10^{-3}$ (IAEA, 2000).

This equation is derived as a fit to the monoenergetic stopping-power ratios calculated using the Monte Carlo code PETRA (Medin and Andreo,

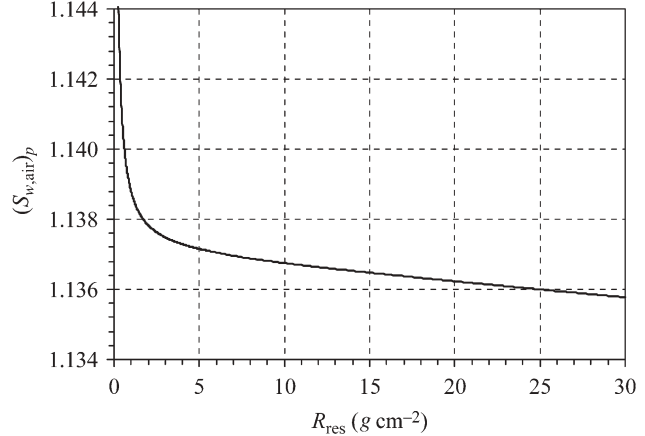


Figure 4.2. Water-to-air stopping-power ratios for proton beams as a function of beam quality index, R_{res} , calculated using Eq. (4.17). The curve is a fit (IAEA, 2000) to monoenergetic stopping-power ratios (Medin and Andreo, 1997a; 1997b). The data include the transport of secondary electrons and nuclear inelastic processes, and the basic stopping powers are taken from ICRU (1993a).

1997a; 1997b). The basic proton stopping powers are taken from ICRU (1993a). The PETRA stopping-power ratios include the transport of secondary electrons and heavy charged particles produced in nuclear non-elastic processes, which is not the case for the ICRU stopping powers. The statistical uncertainty of $(s_{w,\text{air}})_Q$ is estimated to be 0.2 percent (Medin and Andreo, 1997b). The relative uncertainty of the stopping-power ratios at the reference depth in a clinical proton beam is estimated to be 1 percent. The value of $(s_{w,\text{air}})_{Q_0}$ for ^{60}Co is taken as 1.133 ± 0.5 percent (IAEA, 1997a; 1997b), which was calculated by Andreo *et al.* (1986) using Monte Carlo methods and the monoenergetic electron stopping-power data tabulated in ICRU (1984). An additional uncertainty of ± 0.1 percent is assigned to account for spectrum differences among ^{60}Co beams.

To assess $(w_{\text{air}}/e)_Q$ for dry air in TRS 398 (IAEA, 2000), only the values of $(W_{\text{air}}/e)_Q$ and $(w_{\text{air}}/e)_Q$ given in ICRU (1998) were considered (Section 4.4.4). A procedure using weighted medians, taking into account the statistical uncertainty of each value (Müller, 2000a; 2000b), yielded the value of $(w_{\text{air}}/e)_Q = 34.23 \text{ J C}^{-1}$, with a relative standard uncertainty of 0.4 percent. The consistency of the data used in the evaluation (Müller, 2000a) is discussed in Jones (2006). The value of W_{air}/e for dry air in ^{60}Co is 33.97 J C^{-1} with a relative uncertainty of ± 0.2 percent, although the uncertainty quoted in the original publication (Boutillon and Perroche-Roux, 1987) is $\pm 0.05 \text{ J C}^{-1}$ (± 0.15 percent).

The range of values of the ionization-chamber perturbation factors p and their relative uncertainties

Table 4.9. Range of perturbation factors and relative standard uncertainties for cylindrical and plane-parallel ionization chambers (IAEA, 2000).

Factor	Beam quality		Q/p (protons)	
	Q_0/c (^{60}Co)		Value	Relative standard uncertainty (%)
	Value	Relative standard uncertainty (%)		
p_{cav}	1.000	<0.1	1.000	0.3
	0.993 ^b	0.2	1.000	0.4
	1.000			
p_{dis}^a	0.981–0.993 (cc)	0.3	1.000	0.2
	1.000 (ppc)	0.2		
p_{wall}	0.977–1.013 ^c (cc)	0.5	1.000	0.6
	0.989–1.024 (ppc)	1.5		

cc, cylindrical chamber; ppc, plane-parallel chamber.

^aNot applicable to plane-parallel chambers.

^bFor cylindrical chambers with 1 mm diameter aluminum central electrodes.

^cIncludes a 0.5 mm thick PMMA waterproofing sleeve.

in ^{60}Co and proton beams are given in Table 4.9. All the factors for proton beams are taken as 1.000, but uncertainties are assigned to these values.

Calculated values of k_{Q,Q_0} for proton beams, for various cylindrical and plane-parallel ionization chambers, and for selected values of the beam quality R_{res} are given in Table 4.10 (IAEA, 2000). Values of k_{Q,Q_0} for some common ionization chambers are plotted in Fig. 4.3. In Table 4.11, the uncertainty estimates are summarized and show a combined standard relative uncertainty in k_{Q,Q_0} for proton beams of 1.7 and 2.1 percent for cylindrical and plane-parallel ionization chambers, respectively. The largest components of this uncertainty are the uncertainties of $s_{w,\text{air}}$ and p_{wall} for ionization chambers in the proton beam. Estimated relative uncertainties in absorbed-dose determinations are given in Table 4.12. The combined relative standard uncertainties for cylindrical and plane-parallel ionization chambers at the reference depth for clinical proton beams are 2.0 and 2.3 percent, respectively.

Values of k_{Q,Q_0} or $N_{D,w,Q}$ can be obtained for different ionization chambers in proton beams by ‘cross-calibration’ techniques. The respective values for a reference ionization chamber are calculated or derived from calorimetric measurements in the user’s proton beam. By comparing measurements at the reference point, values for other chambers can be deduced (Kanai *et al.*, 2004; Vatnitsky *et al.*, 1996a; 2002).

4.4.3 Considerations concerning dry and humid air

Medin *et al.* (2000) have discussed in detail the importance of the consistency in the use of

w -values related to humid (ambient) air or dry air conditions and the humidity correction for air-kerma-based determinations of absorbed dose to water. In ICRU 59 (ICRU, 1998), the recommended value of $W_{\text{air}/e}$ in the ^{60}Co calibration beam is $(33.77 \pm 0.05) \text{ J C}^{-1}$ (ICRU, 1998; Schulz *et al.*, 1986), corresponding to humid air, which is based on a $W_{\text{air}/e}$ value of $(33.97 \pm 0.05) \text{ J C}^{-1}$ for dry air (Boutillon and Perroche-Roux, 1987). Note that the uncertainties are incorrectly given in ICRU 59 (ICRU, 1998) as 0.15 J C^{-1} .

The W - or w -value (see Section 4.4.4) for air at the standard temperature and pressure (STP) of 20°C , 101.325 kPa and 50 percent relative humidity is 0.6 percent lower than that for dry air at the same temperature and pressure (ICRU, 1979; Niatel, 1969). It is assumed that this ratio is the same for all radiations. Thus, for the same amount of energy available for creating charge, 0.6 percent more charge will be created in air at 50 percent relative humidity than in dry air at STP. However, the response of a cavity ionization chamber will also depend on the degree to which the incident charged particles deposit energy, *i.e.*, on the stopping power, which is different for humid air than for dry air. For the secondary electrons generated in a ^{60}Co beam, the combined effect is that 0.3 percent more charge is created in air at STP and 50 percent relative humidity than in dry air at STP. Thus, for ^{60}Co , the humidity correction factor K_{hum} that corrects the ambient air ionization current I_{hum} to the dry-air ionization current I_{dry} is 0.997 (ICRU, 1979; 1998; Schulz *et al.*, 1986).

Usually standards laboratories provide air-kerma (N_K) calibration coefficients for ionization chambers

DOSIMETRY

Table 4.10. Calculated values of $k_{Q,Q}$ for proton beams, for various cylindrical and plane-parallel ionization chambers as a function of beam quality R_{res} (IAEA, 2000).

Ionization chamber type ^a	Beam quality, R_{res} (g cm ⁻²)														
	0.25	0.5	1	1.5	2	2.5	3	3.5	4	4.5	5	7.5	10	15	20
Cylindrical chambers															
Capintec PR-05P mini	–	1.046	1.045	1.044	1.044	1.044	1.043	1.043	1.043	1.043	1.043	1.043	1.042	1.042	
Capintec PR-05 mini	–	1.046	1.045	1.044	1.044	1.043	1.043	1.043	1.043	1.043	1.043	1.042	1.042		
Capintec PR-06C/G Farmer	–	1.038	1.037	1.036	1.036	1.036	1.036	1.035	1.035	1.035	1.035	1.035	1.034	1.034	
Exradin A2 Spokas	–	1.057	1.055	1.054	1.054	1.054	1.054	1.054	1.054	1.054	1.053	1.053	1.053	1.052	
Exradin T2 Spokas	–	1.020	1.018	1.018	1.017	1.017	1.017	1.017	1.017	1.017	1.017	1.016	1.016		
Exradin A1 mini Shonka	–	1.045	1.043	1.043	1.042	1.042	1.042	1.042	1.042	1.042	1.042	1.041	1.041		
Exradin T1 mini Shonka	–	1.009	1.007	1.007	1.006	1.006	1.006	1.006	1.006	1.005	1.005	1.005	1.004		
Exradin A12 Farmer	–	1.043	1.042	1.041	1.041	1.041	1.040	1.040	1.040	1.040	1.040	1.039	1.039		
Far West Tech IC-18	–	1.007	1.006	1.005	1.005	1.004	1.004	1.004	1.004	1.004	1.004	1.003	1.003		
FZH TK 01	–	1.032	1.031	1.030	1.030	1.030	1.029	1.029	1.029	1.029	1.029	1.028	1.028		
Nuclear Assoc 30-750	–	1.037	1.035	1.034	1.034	1.034	1.034	1.033	1.033	1.033	1.033	1.033	1.032		
Nuclear Assoc 30-749	–	1.041	1.039	1.039	1.038	1.038	1.038	1.038	1.038	1.037	1.037	1.037	1.036		
Nuclear Assoc 30-744	–	1.041	1.039	1.039	1.038	1.038	1.038	1.038	1.038	1.037	1.037	1.037	1.036		
Nuclear Assoc 30-716	–	1.041	1.039	1.039	1.038	1.038	1.038	1.038	1.038	1.037	1.037	1.037	1.036		
Nuclear Assoc 30-753	–	1.041	1.040	1.039	1.039	1.038	1.038	1.038	1.038	1.038	1.038	1.037	1.037		
Farmer shortened	–	1.037	1.036	1.035	1.035	1.035	1.034	1.034	1.034	1.034	1.034	1.033	1.033		
Nuclear Assoc 30-751 Farmer	–	1.044	1.042	1.041	1.041	1.041	1.041	1.040	1.040	1.040	1.040	1.040	1.039		
Nuclear Assoc 30-752 Farmer	–	1.033	1.032	1.031	1.031	1.031	1.031	1.030	1.030	1.030	1.030	1.029	1.029		
NE 2515	–	1.043	1.041	1.041	1.040	1.040	1.040	1.040	1.040	1.039	1.039	1.039	1.038		
NE 2515/3	–	1.043	1.041	1.041	1.040	1.040	1.040	1.040	1.040	1.039	1.039	1.039	1.038		
NE 2577	–	1.043	1.041	1.041	1.040	1.040	1.040	1.040	1.040	1.039	1.039	1.039	1.038		
NE 2505 Farmer	–	1.033	1.032	1.031	1.031	1.031	1.031	1.030	1.030	1.030	1.030	1.030	1.029		
NE 2505/A Farmer	–	1.021	1.019	1.019	1.018	1.018	1.018	1.018	1.018	1.017	1.017	1.017	1.016		
NE 2505/3, 3A Farmer	–	1.043	1.041	1.041	1.040	1.040	1.040	1.040	1.040	1.039	1.039	1.039	1.038		
NE 2505/3, 3B Farmer	–	1.025	1.023	1.023	1.022	1.022	1.022	1.022	1.022	1.021	1.021	1.021	1.020		
NE 2571 Farmer	–	1.043	1.041	1.041	1.040	1.040	1.040	1.040	1.040	1.039	1.039	1.039	1.038		
NE 2581 Farmer	–	1.020	1.018	1.017	1.017	1.017	1.017	1.016	1.016	1.016	1.016	1.016	1.015		
NE 2561/2611 Sec. Standard	–	1.040	1.038	1.038	1.037	1.037	1.037	1.037	1.037	1.037	1.036	1.036	1.036		
PTW 23323 micro	–	1.027	1.025	1.025	1.024	1.024	1.024	1.024	1.024	1.024	1.023	1.023	1.023		
PTW 23331 rigid	–	1.037	1.035	1.034	1.034	1.034	1.034	1.033	1.033	1.033	1.033	1.033	1.032		
PTW 23332 rigid	–	1.031	1.029	1.028	1.028	1.028	1.028	1.027	1.027	1.027	1.027	1.027	1.026		
PTW 23333	–	1.033	1.031	1.031	1.030	1.030	1.030	1.030	1.030	1.029	1.029	1.029	1.028		
PTW 30001/30010 Farmer	–	1.033	1.031	1.031	1.030	1.030	1.030	1.030	1.030	1.029	1.029	1.029	1.028		
PTW 30002/30011 Farmer	–	1.036	1.035	1.034	1.034	1.034	1.034	1.033	1.033	1.033	1.033	1.032	1.032		
PTW 30004/30012 Farmer	–	1.044	1.042	1.041	1.041	1.041	1.041	1.041	1.041	1.040	1.040	1.040	1.039		
PTW 30006/30013 Farmer	–	1.033	1.032	1.031	1.031	1.031	1.030	1.030	1.030	1.030	1.029	1.029	1.029		
PTW 31002 flexible	–	1.032	1.030	1.029	1.029	1.029	1.029	1.029	1.029	1.028	1.028	1.028	1.027		
PTW 31003 flexible	–	1.032	1.030	1.029	1.029	1.029	1.029	1.029	1.029	1.028	1.028	1.028	1.027		
PTW 31006 PinPoint	–	1.027	1.025	1.024	1.024	1.024	1.024	1.024	1.024	1.024	1.023	1.023	1.023		
PTW 31014 PinPoint	–	1.028	1.026	1.025	1.025	1.025	1.025	1.025	1.024	1.024	1.024	1.024	1.023		
SNC 100700-0 Farmer	–	1.033	1.031	1.031	1.030	1.030	1.030	1.030	1.030	1.029	1.029	1.029	1.028		
SNC 100700-1 Farmer	–	1.044	1.042	1.042	1.042	1.041	1.041	1.041	1.041	1.041	1.041	1.040	1.040		
Victoreen Radocon III 550	–	1.031	1.030	1.029	1.029	1.028	1.028	1.028	1.028	1.028	1.028	1.027	1.027		
Victoreen Radocon II 555	–	1.014	1.012	1.012	1.011	1.011	1.011	1.011	1.011	1.011	1.010	1.010	1.010		
Victoreen 30-348	–	1.023	1.022	1.021	1.021	1.021	1.020	1.020	1.020	1.020	1.020	1.019	1.019		
Victoreen 30-351	–	1.026	1.024	1.023	1.023	1.023	1.023	1.023	1.022	1.022	1.022	1.022	1.021		
Victoreen 30-349	–	1.030	1.028	1.027	1.027	1.027	1.027	1.027	1.026	1.026	1.026	1.026	1.025		
Victoreen 30-361	–	1.023	1.021	1.020	1.020	1.020	1.020	1.020	1.020	1.020	1.019	1.019	1.018		
Scdx-Wellhöfer CC01	–	1.042	1.040	1.040	1.039	1.039	1.039	1.039	1.039	1.039	1.039	1.038	1.038		
Scdx-Wellhöfer CC04/IC04	–	1.037	1.035	1.035	1.034	1.034	1.034	1.034	1.034	1.034	1.033	1.033	1.032		
Scdx-Wellhöfer CC08/IC05/IC06	–	1.041	1.039	1.039	1.038	1.038	1.038	1.038	1.038	1.038	1.038	1.037	1.037		
Scdx-Wellhöfer CC13/IC10/IC15	–	1.041	1.039	1.039	1.038	1.038	1.038	1.038	1.038	1.038	1.038	1.037	1.037		
Scdx-Wellhöfer CC25/IC25	–	1.041	1.039	1.039	1.038	1.038	1.038	1.038	1.038	1.038	1.038	1.037	1.037		
Scdx-Wellhöfer FC23-C/IC28	–	1.042	1.040	1.039	1.039	1.039	1.039	1.039	1.038	1.038	1.038	1.038	1.037		
Farmer shortened	–	1.037	1.036	1.035	1.035	1.035	1.034	1.034	1.034	1.034	1.034	1.033	1.033		
Scdx-Wellhöfer FC65-P/IC69 Farmer	–	1.044	1.042	1.041	1.041	1.041	1.041	1.041	1.041	1.040	1.040	1.040	1.039		
Scdx-Wellhöfer FC65-G/IC70 Farmer	–	1.044	1.042	1.041	1.041	1.041	1.041	1.041	1.040	1.040	1.040	1.040	1.039		

Continued

Table 4.10. Continued

Ionization chamber type ^a	Beam quality, R_{res} (g cm^{-2})														
	0.25	0.5	1	1.5	2	2.5	3	3.5	4	4.5	5	7.5	10	15	20
Plane-parallel chambers															
Attix RMI 449	0.995	0.992	0.990	0.989	0.989	0.989	0.989	0.989	0.989	0.989	0.988	0.988	0.988	0.988	0.987
Capintec PS-033	1.029	1.026	1.024	1.024	1.023	1.023	1.023	1.023	1.023	1.023	1.022	1.022	1.022	1.022	1.021
Exradin P11	1.000	0.997	0.995	0.994	0.994	0.994	0.994	0.994	0.994	0.994	0.993	0.993	0.993	0.993	0.992
Holt (Memorial)	1.014	1.010	1.009	1.008	1.008	1.008	1.008	1.008	1.007	1.007	1.007	1.007	1.007	1.007	1.006
NACP/Calcum	0.994	0.991	0.989	0.989	0.988	0.988	0.988	0.988	0.988	0.988	0.987	0.987	0.987	0.987	0.986
Markus	1.009	1.005	1.004	1.003	1.003	1.003	1.003	1.003	1.002	1.002	1.002	1.002	1.002	1.002	1.001
Roos	1.008	1.004	1.003	1.002	1.002	1.002	1.002	1.002	1.001	1.001	1.001	1.001	1.001	1.001	1.000

^aSome of the chambers listed in this table fail to meet some of the main requirements of the code of practice (IAEA, 2000). However, they have been included in this table because of their current clinical use.

filled with air at 50 percent relative humidity. Medin *et al.* (2000) have drawn attention to the fact that Eqs. (4.5)–(4.7) used here (ICRU, 1998) for the determination of absorbed dose to water, using an N_K calibration coefficient that is referred to air at 50 percent relative humidity, contain physical constants that are all referred to dry air. The humidity correction factor in the proton beam cancels, at least to first order, with the humidity correction factor in ^{60}Co . Consequently, the use of the humidity correction factor in Equation (4.6) is not needed.

The approximate cancellation of humidity correction factors is the reason why IAEA codes of practice (IAEA, 1997a; 1997b; 2000) do not include a humidity correction in the chamber factor

$N_{D,\text{air}}$ when N_K refers to air at 50 percent relative humidity. When N_K is referred to dry air, as already stated, K_{hum} in Equation (4.6) is omitted and the only remaining humidity correction is for the ionization current measured in the proton beam.

Further detailed information on the effect of air humidity in ionization-chamber dosimetry in photon and electron beams is given by Mijnheer and Williams (1985) and by Rogers and Ross (1988).

4.4.4 The value of w/e in air for proton beams

For the purposes of simplicity in the present section, the subscripts c and p are used to denote the reference (^{60}Co) and proton-beam qualities, respectively, even though the corresponding subscripts Q_0 and Q are used in IAEA (2000).

Knowledge of w or W (or w/e and W/e) is required for conversion of the charge collected in an ionization chamber to deposited energy. The value of (w_{air}/e) is an important factor in determining the absorbed dose with ionization chambers in proton-therapy beams. As described below, the various dosimetry protocols recommend the use of significantly different (w_{air}/e) values. Most importantly, the values recommended in the two most recent protocols, ICRU 59 (ICRU, 1998) and TRS 398 (IAEA, 2000) differ by more than 2 percent.

4.4.4.1 Definitions

The value of $W(E)$ (in J C^{-1}) for charged particles of energy E in a gas is the mean energy required to create an electron-ion pair by an ionizing particle that imparts all its energy to the gas. Another interpretation of $W(E)$ arises from recognizing that $E/W(E)$ is the mean number of ion pairs formed

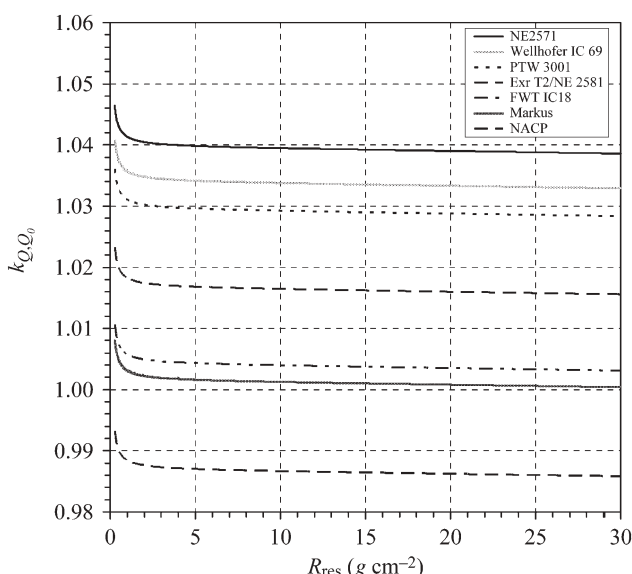


Figure 4.3. Calculated values of k_{Q, Q_0} for various cylindrical and plane-parallel ionization chambers commonly used for reference dosimetry, as a function of proton beam quality Q (R_{res}). Adapted from IAEA (2000).

Table 4.11. Estimated relative standard uncertainties, u_c , of the calculated values for k_{Q,Q_0} for proton beams (IAEA, 2000).

Chamber type	Cylindrical		Plane parallel	
	Protons, u_c (%)	^{60}Co + protons, u_c (%)	Protons, u_c (%)	^{60}Co + protons, u_c (%)
$s_{w,\text{air}}$	1.0	1.1	1.0	1.1
Assignment of $s_{w,\text{air}}$ to beam quality	0.3	0.4	0.3	0.4
$W_{\text{air}/e}$	0.4	0.5	0.4	0.5
p_{cav}	0.3	0.3	0.3	0.3
p_{dis}	0.2	0.4	0.2	0.3
p_{wall}	0.6	0.8	0.6	1.6
p_{cel}	0.4	0.5	—	—
Combined relative standard uncertainty in k_{Q,Q_0}	—	1.7	—	2.1

when particles of energy E dissipate all their energy in the gas.

For indirectly ionizing radiation such as photons or neutrons, or when directly ionizing particles dissipate all their energy in the gas, $W(E)$ is the correct dosimetric conversion coefficient from ionization to energy imparted to the gas. Secondary particles of all energies less than that of the indirectly ionizing radiation are generated and interact with the gas and make $W(E)$ the proper choice (ICRU, 1998; Verhey and Lyman, 1992).

As protons, even for range-modulated beams, lose only a fraction of their energy in traversing the gas, the proper conversion coefficient is the differential value, $w(E)$. Here $\Delta E/w(E)$ is the mean number of ion pairs formed when a particle of energy E expends ΔE in the gas. Use of w is appropriate even for protons with energies as low as 500 keV, as their range in air at standard temperature and pressure is >1 cm, significantly larger

than the dimensions of a typical ionization chamber. Values of $w(E)$ and $W(E)$ are largely independent of energy for particle speeds that are well in excess of outer-orbital electron speeds. When $w(E)$ is constant, $W(E) = w(E)$ (ICRU, 1998).

4.4.4.2 Determination of the $w(E)$ value

Values of w (w/e) in air for protons recommended in the different dosimetry protocols are given in Table 4.13. Also given are the corresponding dry-air or humid-air W_c -values for ^{60}Co used in the respective protocols. As can be seen, the w_p -values recommended differ both in absolute values and in quoted uncertainties, and in whether the values refer to dry or humid air. Furthermore, the w_p -values given are derived from a variety of sources. Specifically, the recommended values in the most recent protocols (IAEA, 2000; ICRU, 1998) differ significantly: ICRU Report 59 (ICRU, 1998) recommends a w_p -value of

Table 4.12. Estimated typical relative standard uncertainty of the absorbed dose to water, $D_{w,p}$, at the reference depth in water for a clinical proton beam, based on a chamber calibration in ^{60}Co (IAEA, 2000).

Physical quantity or procedure	Relative standard uncertainty (%)	
	Cylindrical	Plane parallel
Step 1: Standards laboratory		
$N_{D,w}$ calibration of secondary standard at SSDL	0.5	0.5
Long-term stability of secondary standard	0.1	0.1
$N_{D,w}$ calibration of the user dosimeter at the standards laboratory	0.4	0.4
Combined uncertainty in Step 1	0.6	0.6
Step 2: User proton beam		
Long term stability of the user dosimeter	0.3	0.4
Establishment of reference conditions	0.4	0.4
Correction for influence quantities k_i	0.4	0.5
Beam quality correction k_{Q,Q_0}	1.7	2.0
Combined uncertainty in Step 2	1.9	2.2
Combined relative standard uncertainty in $D_{w,Q}$ (Steps 1 + 2)	2.0	2.3

SSDL, Secondary Standard Dosimetry Laboratory.

If the calibration of the user dosimeter is performed at a Primary Standard Dosimetry Laboratory (PSDL) then the combined uncertainty in Step 1 is lower. The combined standard uncertainty in $D_{w,Q}$ should be adjusted accordingly.

Table 4.13. Recommended w_p -values in air for protons for different dosimetry protocols. The corresponding W_e values in air for ^{60}Co are shown in brackets.

Protocol	w_p (W_e) (J C^{-1})	Source of w_p	Reference
AAPM	34.3 \pm 1.4 (33.73 ± 0.04) ^a (humid air)	Measured value (Verhey <i>et al.</i> , 1979) ^b	AAPM (1986)
ECBED	35.2 \pm 1.4 (33.97 ± 0.07) (dry air)	Measured value (ICRU, 1979)	Vynckier <i>et al.</i> (1991; 1994)
ICRU 59	34.8 \pm 0.7 (33.77 ± 0.05) ^c (humid air)	Compromise between values measured directly and those inferred from comparisons with calorimetry	ICRU (1998)
IAEA TRS 398	34.23 \pm 0.13 (33.97 ± 0.07) (dry air)	Statistical analysis using weighted medians (Müller, 2000a)	IAEA (2000)

^aFrom Verhey *et al.* (1979).^bVerhey *et al.* (1979) reference Myers (1968) in which a value of $(36.0 \pm 1.1\%) \text{ J C}^{-1}$ is actually given (Hayakawa and Schechtman, 1988).^cThe value of $(33.97 \pm 0.15) \text{ J C}^{-1}$ given in ICRU (1998) is incorrect.

$(34.8 \pm 0.7) \text{ J C}^{-1}$ in humid air, whereas IAEA Report TRS 398 (IAEA, 2000) recommends a $w_Q(w_p)$ -value of $(34.23 \pm 0.13) \text{ J C}^{-1}$ in dry air.

The ICRU value was a compromise among values measured directly and those obtained from comparisons of ionization chamber and calorimeter measurements (ICRU, 1998). The IAEA value was obtained by performing a statistical analysis using weighed medians (Müller, 2000a; 2000b) on a modified version of the same original dataset (IAEA, 2000). The ICRU value converted to the equivalent value for dry air becomes 35.0 J C^{-1} , which is 2.3 percent higher than the IAEA value.

Jones (2006) undertook a comprehensive analysis of all available $(W_{\text{air}}/e)_p$ and $(w_{\text{air}}/e)_p$ data for protons with energies $\geq 1 \text{ MeV}$. Apart from the w -values derived from the comparison of ionometric and calorimetric measurements [Brede *et al.*, 2006 (the same data are given in Brede *et al.*, 1999); Delacroix *et al.*, 1997; Hashemian *et al.*, 2003; Palmans *et al.*, 1996; 2004; Schulz *et al.*, 1992; Siebers *et al.*, 1995] and one other measurement (Moyers *et al.*, 2000), none of the data were obtained under clinical conditions. The calorimetric technique also gives a w -value that is averaged over all charged particles in the beam at the point of measurement (therefore, indicating the use of stopping powers that include the effects of secondary electrons and nuclear recoils). Furthermore, similar experimental techniques have been used and evaluations of uncertainties have probably been more uniformly assessed. In addition, the uncertainties are relatively small compared with other measurements in the clinical energy range. Jones (2006), therefore, recommended that the w -value in air for clinical proton dosimetry be derived only from evaluation of calorimetric data. Analysis of these data gave a mean value for $(w_{\text{air}}/e)_p$ that is consistent with the TRS 398 recommended value of $(34.2 \pm 0.1) \text{ J C}^{-1}$.

Subsequently, Medin *et al.* (2006) determined absorbed doses with a sealed water calorimeter operated at 4°C and compared the results with those obtained using ionization chambers and the IAEA TRS-398 code of practice. Measurements were made in a 175 MeV clinical proton beam at a depth corresponding to a residual range of 14.7 cm and energy of 144 MeV. A value for $(w_{\text{air}}/e)_p$ of $33.6 \pm 0.6 \text{ J C}^{-1}$ (1 SD) was derived using ionization-chamber perturbation factors of 1.00. Inclusion of this datum in the calorimetric-derived w -value analysis did not affect the conclusion by Jones (2006) that the TRS 398 value should continue to be used. The data used in the analysis are shown in Fig. 4.4.

4.4.5 Comparison of proton dosimetry protocols

As discussed above, one of the main differences between the two protocols (IAEA, 2000; ICRU, 1998) lies in the w_{air}/e value recommended for

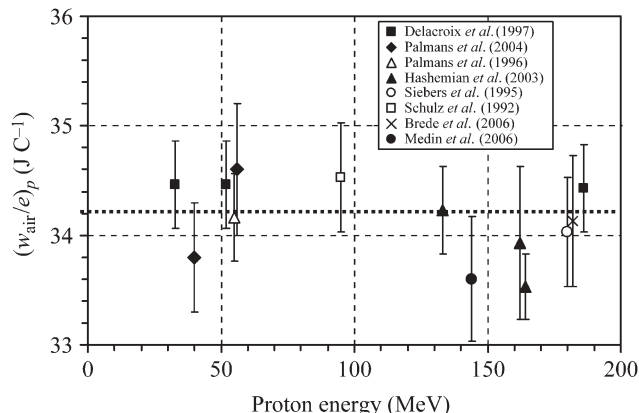


Figure 4.4. Values of w/e in dry air for protons deduced from comparison of ionization chamber and calorimeter measurements. The thick dotted line is the recommended value (34.2 J C^{-1}). [Adapted from Jones (2006); reproduced with permission.]

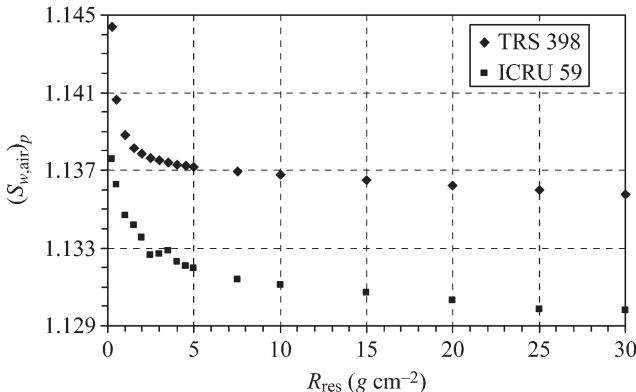


Figure 4.5. Water-to-air stopping-power ratios for protons as a function of residual range for the TRS 398 (IAEA, 2000) and ICRU 59 (ICRU, 1998) dosimetry protocols.

protons. The ratios of w_{air}/e for protons to W_{air}/e for ^{60}Co are 1.0305 (humid air) and 1.0077 (dry air) for the ICRU 59 and TRS 398 protocols, respectively, *i.e.*, the relative TRS 398 value is 2.3 percent lower than the ICRU 59 value.

Both protocols use proton stopping powers given in ICRU Report 49 (ICRU, 1993a), but TRS 398 includes secondary electron transport and nuclear interactions (Medin and Andreo, 1997b). The respective water-to-air stopping-power ratios are shown in Fig. 4.5. The relative TRS 398 (IAEA, 2000) water-to-air stopping-power ratios are at most 0.6 percent higher (Medin *et al.*, 2000) than the corresponding ICRU values (ICRU, 1993a; 1998). TRS 398 provides a formula, Eq. (4.17), to calculate $s_{w,\text{air}}$ for protons. Chamber perturbation factors and uncertainties in ^{60}Co and in proton beams are specified in TRS 398, while ICRU 59 does not specify any chamber perturbation factors in its dose-to-water calibration formalism. As shown in Table 4.9, the perturbation factors given in TRS 398 can be significantly different from unity in ^{60}Co for a variety of ionization chambers (IAEA, 2000; Medin *et al.*, 2000). The total perturbation factor in ^{60}Co can differ from unity by up to 3 percent (Medin *et al.*, 2000). Chamber-perturbation factors in proton beams are assumed to be unity in TRS 398. Monte Carlo simulations (Palmans and Verhaegen, 1998; Verhaegen and Palmans, 2001), analytical calculations (Medin *et al.*, 2006), and experimental measurements (Palmans *et al.*, 1999; 2001; 2002a) support this assumption within uncertainties of ~ 1 percent.

As discussed in Section 4.4.3, ICRU 59 includes a humidity correction factor in calculating the chamber response, but this is problematical as the physical constants refer to values for dry air. The factor $K_{\text{hum}} = 0.997$, Eq. (4.6), should not be used. However, its use would only result in a

relative increase in absorbed dose of 0.3 percent. This issue is discussed fully by Medin *et al.* (2000).

ICRU 59 does not take into account the possibility of the ionization-chamber wall and build-up cap being constructed of different materials. In such cases, the relative calculated correction factor for the non-air-equivalence of the chamber wall and build-up cap during calibration in ^{60}Co (IAEA, 1997a; 2000) can be up to 1.1 percent higher (Medin *et al.*, 2000) than those values calculated according to ICRU 59 (ICRU, 1998). The $s_{\text{wall,air}}$ stopping-power ratios are used to calculate wall-attenuation correction factors in ^{60}Co . The ratios given in ICRU 59 are the same as in the AAPM TG-21 photon and electron dosimetry protocol (AAPM, 1983). The IAEA uses Monte Carlo calculated data from Andreo *et al.* (1986) based on data given in ICRU (1984). The relative IAEA graphite-to-air-stopping power ratio is 0.8 percent higher (Medin *et al.*, 2000) than given in ICRU (1998). For A-150 plastic, the relative difference is 0.3 percent (Medin *et al.*, 2000).

Overall relative uncertainties in proton-absorbed-dose determinations are 2.6 percent (ICRU 59) (Table 4.6) and 2.0 percent (TRS 398) (Table 4.12) for cylindrical ionization chambers. The relative ratios of proton-absorbed doses measured using the TRS 398 formalism to those measured using the ICRU 59 formalism differ by up to 3.1 percent depending on chamber type and residual range (Fukumura *et al.*, 2002; Medin *et al.*, 2000; Vatnitsky *et al.*, 2002). These differences can largely be ascribed to the different proton (w_{air}/e) values used and to the chamber perturbation factors not being applied for ^{60}Co calibrations in the ICRU 59 protocol. The main features of the two protocols (IAEA, 2000; ICRU, 1998) are summarized in Table 4.14.

It is recommended that the TRS 398 code of practice (IAEA, 2000) be adopted as the standard proton dosimetry protocol: it is simple to use; it provides tabulated beam-quality correction factors for a wide range of common cylindrical and plane-parallel ionization chambers; it provides a formula for calculating $s_{w,\text{air}}$ for proton beams in terms of the beam-quality parameter (residual range); it harmonizes with the protocols for conventional radiotherapy and heavy-ion beams (also given in TRS 398), which are being adopted in many institutes; the uncertainties in the dose determinations are less; more recent and accurate physical constants are used; and the formalism is more robust and rigorous than that of ICRU Report 59 (Medin *et al.*, 2000; Vatnitsky and Andreo, 2002). As discussed in Section 4.4.4, the recommended w -value for protons in dry air remains 34.2 J C^{-1} with a relative standard uncertainty of 0.4 percent.

Table 4.14. Comparison of ICRU 59 (ICRU, 1998) dosimetry protocol and TRS 398 (IAEA, 2000) dosimetry code of practice for clinical proton beams.

Feature/quantity	ICRU 59 (ICRU, 1998)	TRS 398 (IAEA, 2000)
Ionization chamber	Cylindrical	Cylindrical and plane-parallel ($R_{\text{res}} \geq 0.5 \text{ g cm}^{-2}$) Plane-parallel ($R_{\text{res}} < 0.5 \text{ g cm}^{-2}$)
Wall material	Graphite or A-150 plastic	Graphite for cylindrical chambers
Gas filling	Ambient air	Ambient air
Chamber volume	$>0.5 \text{ cm}^3$ for beams $\geq 5 \text{ cm}$ diameter $\sim 0.1 \text{ cm}^3$ for beams $< 5 \text{ cm}$ diameter	–
Water proof sleeve	–	$\leq 1 \text{ mm}$ thick PMMA
Dose specification	Water	Water
Calibration beam	^{60}Co	^{60}Co
Calibration coefficient	Primarily N_K , also $N_X, N_{D,w}$	$N_{D,w}$ only
Beam quality	Residual range (to distal 10 % level)	Residual range (to distal 10 % level)
Phantom material	Water (or other materials which match electron density of water)	Water
Reference point for measurement	Middle of SOBP	Middle of SOBP
Field size	–	Depth of 3 g cm^{-2} for plateau irradiations
SSD	–	$10 \times 10 \text{ cm}^2$
Stopping powers	ICRU (ICRU, 1993a)	Clinical treatment distance
$(w_{\text{air}}/e)_p \text{ (J C}^{-1}\text{)}$	34.8 ± 0.7 (ambient air)	PETRA (Medin and Andreo, 1997b)
$(w_{\text{air}}/e)_{^{60}\text{Co}} \text{ (J C}^{-1}\text{)}$	33.77 ± 0.05 (ambient air)	34.23 ± 0.13 (dry air)
$(s_{w,\text{air}})_{^{60}\text{Co}}$	1.134	33.97 ± 0.07 (dry air)
Chamber perturbation factors	No	1.133
Relative uncertainty in absorbed dose (1σ)	2.6 % (Jones, 2001d)	Yes 2.0 % (cylindrical chambers) 2.3 % (plane-parallel chambers)

4.4.6 Relation between absorbed dose to water and air-kerma calibration coefficients

The relation between the N_K – $N_{D,\text{air}}$ formalism [used in IAEA (1997a) and in ICRU (1998)] and the $N_{D,w}$ formalism [used in IAEA (2000)] is relatively straightforward (IAEA, 2000). The quantity $N_{D,\text{air}}$ is given (IAEA, 2000) by

$$N_{D,\text{air}} = N_K(1 - g)k_{\text{att}}k_mk_{\text{cel}}, \quad (4.18)$$

where N_K is the air-kerma calibration coefficient, g is the fraction 0.003 (Boutillon, 1987) of the kinetic energy of secondary-charged particles that is lost in radiative processes (bremsstrahlung), k_{att} is the factor that corrects for the absorption and scattering in the walls of an ionization chamber irradiated in the calibration ^{60}Co beam, k_m is the factor that corrects for the non-air equivalence of the ionization-chamber wall and buildup-cap materials in the calibration ^{60}Co beam, and k_{cel} is the factor that corrects for the non-air equivalence of the central electrode of a cylindrical ionization chamber in the calibration ^{60}Co beam (IAEA, 1997a; 1997b). Note that $N_{D,\text{air}}$ corresponds to N_{gas} of the AAPM protocol (AAPM, 1983).

It is assumed that the $N_{D,\text{air}}$ factor derived at the ^{60}Co quality, Q_0 , is also valid for the user-

beam quality. The factor $N_{D,\text{air}}$ then allows the determination of the mean absorbed dose within the air cavity for the user-proton-beam quality Q :

$$D_{\text{air},Q} = M_Q N_{D,\text{air}}. \quad (4.19)$$

The absorbed dose to water $D_{w,Q}$ at the reference point in a phantom at the center of the chamber is obtained from the dose to air using the Bragg–Gray principle as

$$D_{w,Q} = M_Q N_{D,\text{air}} (s_{w,\text{air}})_Q p_Q, \quad (4.20)$$

where M_Q is the dosimeter reading in the proton beam corrected for influence quantities, $(s_{w,\text{air}})_Q$ is the proton water-to-air stopping-power ratio, p_Q is the overall perturbation factor of the ionization chamber for in-phantom measurements in the proton beam (see Section 4.4.2).

Comparing Eqs. (4.11) and (4.20) for the same beam quality Q_0 , one obtains

$$N_{D,w,Q_0} = N_{D,\text{air}} (s_{w,\text{air}})_{Q_0} p_{Q_0}. \quad (4.21)$$

Alternatively, from Eqs. (4.16), (4.18), and (4.20) one obtains in expanded form

$$N_{D,w,Q_0} = [N_K(1-g)k_{\text{att}}k_m k_{\text{cel}}]_{Q_0}(s_{w,\text{air}})_{Q_0} \times [p_{\text{cav}} p_{\text{cel}} p_{\text{dis}} p_{\text{wall}}]_{Q_0}, \quad (4.22)$$

The symbols and their meaning correspond to those given in IAEA (1997b) and IAEA (2000). Details of the required stopping-power data and perturbation correction factors are given in Sections 4.4.2 and 4.4.2.1. Factors related to the determination of $N_{D,\text{air}}$ can be found in IAEA (1997a; 1997b).

4.5 REFERENCE DOSIMETRY FOR SCANNED BEAMS

Although the first proton-beam scanning system was developed in the late 1970s on a 70 MeV beam (Kanai *et al.*, 1980; 1983), practical clinical experience with such systems has been acquired only on the 270 MeV proton beam at the PSI (Bacher *et al.*, 1989; Lomax, 1999; Lomax *et al.*, 2001; 2004; Pedroni *et al.*, 1990; 1995; 2005). There are few differences in principle between reference dosimetry in scanned beams and passively scattered beams, and the calibration techniques are similar (Coray *et al.*, 2002; Pedroni *et al.*, 2005).

The dose delivered is calculated by the treatment-planning system. Because the scanning system does not require patient-specific hardware, the scanned beam is quite clean (*i.e.*, it does not contain particles scattered from collimators and other beam-modifying elements). Therefore, an absolute dose model based on calculated stopping powers (see Section 3) and the number of protons delivered during the scan can be used. However, the modeling of nuclear interactions must be included in the dose-calculation algorithm; otherwise the calculated dose distributions do not agree with measurements (Pedroni *et al.*, 2005). The importance of taking nuclear interactions into account, including the transport of secondary protons, was emphasized by Medin and Andreo (1997a). Specifically, considerations of nuclear interactions are required to account for the attenuation of the primary proton fluence and for the beam halo around the primary pencil beam. If they are not included relative differences between calculation and measurement of the order of 5 percent are found. The number of protons delivered is controlled in practice by the beam-fluence monitors calibrated against Faraday-cup measurements. In the case of passively modified beams, the dose

calculation model is often based on dose distribution measurements, which include the effects of nuclear interactions.

Reference dosimetry is based on the use of cylindrical ionization chambers calibrated in ^{60}Co using the TRS 398 code of practice (IAEA, 2000). For the calibration, a $10 \times 10 \times 10 \text{ cm}^3$ water volume ('dose box') is irradiated to give a homogeneous dose distribution to an assumed dose of 1 Gy. A reference ionization chamber is placed in the water phantom and the dose is measured at the center of the field at a residual range of 5 g cm^{-2} . At PSI, the ratio between these measurements and those determined with a Faraday cup varies from 0.978 at a proton energy of 138 MeV to 1.008 at a proton energy of 214 MeV. These values are used to correct the dose model in the treatment-planning system (Pedroni *et al.*, 2005).

4.6 IONIZATION-CHAMBER DOSIMETRY COMPARISONS

The ICRU has long recognized the importance of dosimetry comparisons for non-conventional therapy beams. In the early 1970s, it sponsored an International Neutron Dosimetry Intercomparison (INDI) (ICRU, 1978), which followed an earlier European Neutron Dosimetry Intercomparison Project (ENDIP) (Broerse *et al.*, 1978) and several small-scale comparisons (Almond and Smathers, 1977; Broerse *et al.*, 1979). Fourteen groups participated in the INDI and the results highlighted many shortcomings in neutron dosimetry practices. No dosimetry protocols were available at that time and most groups used 'in-house' methods. These comparisons led to the development of the American (AAPM, 1980) and European (Broerse *et al.*, 1981) neutron dosimetry protocols and finally to the publication of a uniform protocol (Mijnheer *et al.*, 1987b), which remains the accepted standard 20 years later. This latter protocol was endorsed by the ICRU (ICRU, 1989).

The situation with proton dosimetry is rather different. Protocols have existed for 15 years and more (AAPM, 1986; Vynckier *et al.*, 1991; 1994). However, no proton absorbed-dose standards are yet available, and dose comparisons are extremely useful in confirming the integrity of the dosimetry techniques used at different institutes.

Dosimetry comparisons between ionization-chamber measurements, and Faraday-cup and calorimetric measurements have been discussed above (Sections 4.2 and 4.3, respectively). Many comparisons involving ionization chambers (both cylindrical and plane-parallel) have been undertaken in the last 15 years or so by various groups

Table 4.15. Proton dosimetry comparisons with ionization chambers. The relative maximum measured dose differences are given in the last column.

Reference	Protocol	Number of chambers	Beam energy (MeV)	Max. difference (%)
Kacperek <i>et al.</i> (1991)	ECBED	8	60	4.5
Jones <i>et al.</i> (1992)	ECBED	7	60–80	2.5
Jones <i>et al.</i> (1994a)	ECBED	7	200	1.8
Schreuder <i>et al.</i> (1994)	AAPM/ECBED	7	135–185	1.4
Medin <i>et al.</i> (1995)	TRS 277	7	170	1.5
Jones (1996)	ECBED	6	58–168	2.3
Palmans <i>et al.</i> (1996)	ECBED	10	85	1.2
Vatnitsky <i>et al.</i> (1996b)	AAPM/ECBED	23	100–250	5.8
Hiraoka <i>et al.</i> (1997)	-	5	70	0.8
Cuttone <i>et al.</i> (1999)	ECBED	3	28–62	2.1
Vatnitsky <i>et al.</i> (1999b)	ICRU 59	11	155	2.9
Nohtomi <i>et al.</i> (2001)	ICRU 59	5	250	1.5
Palmans <i>et al.</i> (2001)	TRS 398	17	75	1.5
Fukumura <i>et al.</i> (2002)	TRS 398	8	150	0.9
Kacperek <i>et al.</i> (2002)	ICRU 59	10	63	3.2
Vatnitsky <i>et al.</i> (2002)	ICRU 59/TRS 398	6	100–155	3.1

AAPM, AAPM (1986); ECBED, Vynckier *et al.* (1991; 1994); TRS 277, IAEA (1997a); ICRU 59, ICRU (1998); TRS 398, IAEA (2000).

in different clinical beams. A summary of the details of these studies is given in Table 4.15. The results are very satisfactory with a few exceptions. In most cases, the relative maximum differences between measured doses are less than ~ 2 percent. The standard deviations of the means are ~ 0.3 –0.5 of the maximum differences. The maximum relative difference of 5.8 percent (standard deviation of the mean: 1.8 percent) occurred in a large-scale study in which two different dosimetry protocols were used.

It is clear from these data that proton dosimetry is on a relatively good footing. However, comparison studies are still extremely useful, especially for new facilities, but also for existing facilities, in order to detect and eliminate any possible systematic errors occurring in the dosimetry process. They also serve as an independent check on the entire dosimetry chain. This chain starts at the standards laboratory and ends at the delivery of absorbed dose to a reference point in a phantom in the user's clinical beam. Such studies are also important for institutes that wish to pool or compare clinical data. Clearly, the adoption of a single dosimetry protocol will go a long way toward standardizing clinical proton dosimetry and reducing the magnitude of the differences in dose determinations by different centers.

4.7 BEAM MONITORING

Beam monitors in beam-delivery systems (nozzles) and elsewhere are required for accurate control of

dose and fluence in the patient. Parallel-plate ionization chambers (Boag, 1966) are the most common and well-proven detectors for this purpose. Their low mass, high sensitivity, large dynamic range, and ease of construction make them well suited to the task of dose monitoring and control. Other types of monitors include gas-scintillation counters (Coutrakon *et al.*, 1991a) and secondary-emission monitors (SEMs) (Section 4.7.4). For safety reasons, at least two independent dose monitors, which are calibrated daily, are recommended. For passively modified beams employing scattering systems for lateral beam spreading, beam-centering systems (including segmented ionization chambers), which are capable of detecting misalignments between the central axes of the beam and the scattering devices, are required.

Dose-monitoring detectors can either intercept the entire beam area or just the central portion. The former requires larger detectors and measurements are more reliable as they are less dependent on beam alignment variations. Beam steering is much more sensitive in double- than in single-scatterer beam-modification systems.

Sealed ionization chambers filled with argon gas have been used in conventional electron linear accelerators for many decades and have a long lifetime before replacement or repair is necessary. If the accelerator used is capable of high instantaneous intensities, special care in the design of the monitoring system is required (Coutrakon *et al.*, 1991b). Positive-ion collection times as little as 20 μ s can be achieved, and the capability of handling high instantaneous intensities can be

accommodated using gases such as helium in which ions have higher drift velocities.

Proton nozzles can be divided into two categories: ones that use flat or contoured scatterers (passive systems) (Grusell *et al.*, 1994; Koehler *et al.*, 1977; Nauraye *et al.*, 1995) and ones that use magnetic deflection (scanning or active systems) (Kanai *et al.*, 1980; 1983; Pedroni *et al.*, 1995; 2005) to spread the beam laterally (see Section 3 for details). Scanning systems add additional requirements for the beam monitors and are discussed separately here (see Section 4.7.3). For example, scanning systems require devices capable of monitoring and controlling the position of a small (~ 1 cm diameter) moving beam. Such detectors need to have fast response times ($<< 1$ ms) in order to track the real-time motion of the beam across the target. The requirement for detector bandwidth depends on the scanning speed in the patient, which can be quite high, typically 1 beam diameter per millisecond. Detectors such as strip or segmented ionization chambers (Cirio *et al.*, 2004) can be effective, and multiwire proportional chambers (MWPCs) (Charpak, 1970; Sauli, 1977) can also be used.

Energy or range measurements made anywhere upstream of the treatment position must be calibrated against range measurements made in a water phantom at the treatment position, as these latter measurements pertain to the beam actually entering the patient. This is particularly important because the range attenuation of nozzle materials can be accurately predicted only if adequate knowledge of the material compositions, densities, thicknesses, *etc.*, is available. Furthermore, it is possible that components may have fallen out of, or into, the beam line. A suitable detector for upstream measurements is a multilayer Faraday cup (MLFC) that is constructed of alternate plates of metal and insulating material (Gottschalk *et al.*, 1999; Paganetti and Gottschalk, 2003; Schreuder *et al.*, 2001). The metal plates are connected to charge integrators, the signals from which essentially provide a charged-particle fluence distribution (spectrum) from which the effective proton-beam energy can be obtained. Alternatively, a multiplate ionization chamber can be used to determine the depth-dose distribution from which the range can be determined (Siebers *et al.*, 1988).

Clearly, energy/range monitoring is needed for both active and passive systems, but the accuracy and the frequency of the energy measurements required are much higher for scanning systems because different ranges must be delivered sequentially in layers and with high accuracy to generate the required dose distribution in the target volume.

A solution is to perform upstream range measurements in real time (during patient treatment) by locating suitable detectors just outside the periphery of the beam and upstream of a fixed or variable patient collimator. This requires that some of the beam strike the range detector either continuously or, in the case of scanned beams, periodically as the beam sweeps over the range detector. Relative precision of range measurements should be less than 0.5 mm. If this limit is exceeded, the cause (*e.g.*, beam-energy drifts, movement of beam-line components) should be investigated. Some recommendations for energy/range monitoring during patient treatments are discussed in Section 4.7.5.

4.7.1 Ionization chambers

Parallel-plate ionization chambers are most frequently selected as integral dose monitors. Air- or argon-filled chambers are typical choices for passive beam-spreading systems. An anode-to-cathode spacing, or gap thickness, of 3–10 mm has been used for therapy applications. For monoenergetic protons crossing a gas-filled gap with negligible energy loss (and therefore constant stopping power), the signal strength can be calculated from the charge per proton, Q , produced in the gas:

$$Q = \frac{S_{\text{gas}} t (1.602 \times 10^{-19})}{(w/e)_p}, \quad (4.23)$$

where S_{gas} ($= -dE/dx$) is the linear proton stopping power in the gas filling, t is the gap thickness, and w_p is the proton energy required to form an ion pair in the gas.

For the gases discussed here, the proton stopping power decreases approximately inversely with energy ($1/E$) in the therapy energy range. The charge produced per proton is 2.5 times larger at 70 MeV than at 250 MeV (ICRU, 1993a). Clearly, a larger gap thickness will increase the charge collected per unit dose but will also result in longer ion-collection times and potentially increased detector-saturation effects due to ion recombination at high intensities.

Typical electric field strengths of $3\text{--}5 \text{ kV cm}^{-1}$ can be used for air or argon before breakdown occurs, whereas $1\text{--}2 \text{ kV cm}^{-1}$ are typically maximum field strengths for helium-filled chambers. The goal of chamber design is to keep the collection efficiency at 100 percent for the highest intensities that occur during normal operation. When designing chambers for use in high-intensity beams, helium will be superior to both air and argon (Table 4.16) owing to the fewer ion pairs produced per proton in the gas and the lower

Table 4.16. Data for a parallel-plate ionization chamber with a 5 mm gap filled with air, argon, and helium at STP.

Gas	Field strength (kV cm^{-1})	Positive ion velocity (cm ms^{-1})	Positive ion collection time (μs)	w (eV)	No. of ion pairs per proton	
					$E_p = 70 \text{ MeV}$	$E_p = 230 \text{ MeV}$
Air	4	5	100	34.2 ^a	160	64
Argon	4	6.8	74	26.6 ^b	460	190
Helium	2	20	25	45.2 ^b	18	7

^aIAEA (2000).^bICRU (1979).

ion-collection times (Boag and Wilson, 1952). Once the chamber is built, ion-collection efficiency as a function of high voltage should be measured to ensure 100 percent collection efficiency at the highest intensities. A guard ring should be included in the construction to minimize leakage currents. To allow appropriate corrections to be made, a separate temperature sensor may be required in the nozzle as the temperature here may differ from that in the room or in the phantom in which the doses are measured.

For scanned proton beams, the ionization chambers must detect the ionization in times short compared with the sweep speed of the beam. Typical beam sweep speeds are $1\text{--}3 \text{ cm ms}^{-1}$. Therefore, sub-millisecond integration times are required. For typical ionization chamber gaps of 3–5 mm and electric field strengths of $3\text{--}5 \text{ kV cm}^{-1}$, helium or argon should be used to keep positive-ion-collection times $<1 \text{ ms}$ (the electron-collection times are several orders of magnitude faster and comprise only 50 percent of the signal). Table 4.16 shows data for a chamber with a 5 mm gap filled with air, argon, and helium. Higher electric fields and smaller gaps will decrease collection times proportionately and reduce ion-recombination effects. Helium-filled chambers are capable of operating in higher intensity beams and have faster response times.

If a noble gas is used for filling, gas purity becomes important (ICRU, 1979; Jesse and Sadauskis, 1952; 1953). The so-called Jesse effect results in a large (up to 50 percent) decrease in the w -values (and therefore increases in the number of ion pairs formed) at relatively small concentrations (~ 0.1 percent) of impurities in the noble filling gas. This is due to metastable excited states of the noble gas producing ionization in the contaminant gas by energy transfer. Mediation of the uncertainty in ionization due to the Jesse effect is possible by purposely adding enough contaminant to the gas

mixture in order to maintain a known w -value for the ionization chambers.

4.7.2 Position and dose uniformity

In parallel-plate ionization chambers, one of the electrode planes is held at high voltage, either positive or negative, whereas the other plane is used to collect ions of one polarity. Without segmentation of the collection electrode, the entire beam is intercepted on a single foil and a signal proportional to the total integrated intensity or dose is recorded. Often the electrode is segmented, *e.g.*, into quadrants, to determine the position of the beam relative to the center of the ion chamber, or equivalently, the central axis of the nozzle. The mass of the ion chambers can be kept low by constructing the electrodes from very thin foils with a microscopic layer of gold (or other metal) evaporated onto the surface. Standard photo-etching techniques can be used to segment the electrode into quadrants, concentric rings, or large square arrays. In the case of passively scattered beams, it can be useful to place two quadrant-segmented chambers in the nozzle, one before and one after the scattering system, to monitor the position and inclination of the axis of the beam relative to the central axis of the nozzle. When deviations of the beam position or angle exceed the specified tolerance, the beam must be inhibited to avoid large fluence or dose non-uniformity in the patient. Alternatively, appropriate signals must be fed back to steering magnets to correct automatically the beam position or beam trajectory.

Fast-recycling integrators (Gottschalk, 1983; Renner *et al.*, 1989) are often used to digitize the charge collected on each quadrant and to calculate centering information. Additionally, ionization chambers with large arrays of square segments (from 20×20 up to 80×80 squares) have been considered for a single planar electrode ($40 \times 40 \text{ cm}^2$ area) yielding high resolution when placed

within 0.5 m or so from the patient. Recent results (Cirio *et al.*, 2004) have demonstrated the efficacy of a two-dimensional pixel ionization chamber with a 32×32 matrix of 1024 cylindrical ionization cells arranged in a $24 \times 24 \text{ cm}^2$ area with 1 ms digitization and readout times. The tissue-equivalent thickness of the detector is only 1 mm. For passively modified beams, response uniformity can be determined with respect to known beam profiles, while the absolute dose response for any pixel can be obtained using a standard calibrated cylindrical ionization chamber under reference conditions (Amerio *et al.*, 2004). For scanning beams, detectors with good spatial resolution are also attractive because they can detect and record full two-dimensional dose information at or near the target with real-time tracking of the beam movement.

4.7.3 Considerations for scanned beams

In addition to achieving real-time tracking of the motion of pencil beams across the patient, special attention must be given to the location and mass of the monitors that may contribute to beam enlargement from multiple Coulomb scattering. In the energy range 70–250 MeV, even thin (25 μm) foils of kapton or titanium (used for vacuum windows) can contribute to a significant increase in beam size at the patient if they are placed at a distance of several meters from the target. In addition, 3 m of air in the nozzle will also have noticeable effects on the beam size. Various solutions have been applied to reduce these problems. In general, it is best to keep all beam monitors within a distance of 70–100 cm from the patient and use the lowest mass of material possible for constructing the chamber. Gold-plated kapton foil parallel-plate ionization chambers are ideal for this purpose, but the detector size requirements are large (up to $40 \times 40 \text{ cm}^2$) and necessitate high stretching forces when fixing the foils to a frame in order to keep electrostatic bulging to a minimum. In such cases, the detector response can be calibrated at many different regions of the detector (Sauli, 1977). Similarly, a multiwire proportional counter (MWPC) (Charpak, 1970; Sauli, 1977, 1992) operated in ion-collection mode can be used as an integral intensity monitor when filled with a noble gas, and all the anode wires are connected together to form one readout channel through a recycling integrator. Up to double the signal strength can then be achieved for the same anode-to-cathode spacing as with the parallel-plate chamber described above.

At the PSI, a 1 l volume of tissue is typically filled with 10 000 ‘spots’ with a spacing of 5 mm in 2 min, giving a mean treatment time per spot of

about 10 ms. Integral beam intensity at any position is monitored by parallel-plate ionization chambers with response times of $<100 \mu\text{s}$ (Lin *et al.*, 1994; Pedroni *et al.*, 1995).

In addition to their use as integral monitors with all the anode wires connected together (above), MWPCs can also be used for monitoring the position of scanning beams. These chambers use thin (25–50 μm diameter) tungsten or copper wires with a 1–2 mm pitch and two thin kapton foils for containing the gas. The MWPCs have been built with 2 mm spatial resolution and a 15 kHz data acquisition rate (Brusasco *et al.*, 2000) at the Gesellschaft für Schwerionenforschung (GSI). Two of these MWPCs are part of the beam-monitoring system and provide active feedback to the scanning magnets to ensure correct positioning of the carbon-ion beam. The cathode planes are made of closely-spaced wires strung on an epoxy frame. The disadvantages of MWPCs are that they only give the projection of the beam shape onto the x - or y -axis and not the true two-dimensional beam shape. Nevertheless, GSI and other institutions are pursuing this option because of their ease of construction, high data-acquisition rate capability, and high resolution. Alternatively, two-dimensional pixel detectors, like the one described in Section 4.7.2, or track detectors (Sunaga *et al.*, 1988) can give good position information for scanned beams.

4.7.4 Secondary-emission monitors

Secondary-emission monitors (Chu, 1995b; Karzmark, 1964; Tautfest and Fechter, 1955) have been used at several facilities. These detectors consist of several parallel thin-metal foils mounted in a vacuum. The foils emit electrons from the surfaces when energetic beams pass through them. The bandwidth of these detectors is well above 1 MHz, but they have at least three orders of magnitude fewer ions produced per passing proton than do ionization chambers. These detectors can be calibrated in the same way as ionization chambers. Their advantage is that they cannot saturate when the intensities become accidentally too high and therefore they provide an additional measure of safety that ionization chambers cannot. However, because they are located in vacuum, they are usually several meters from the patient and can add significantly to beam enlargement. This becomes problematic for scanning beams, but not for passive beams.

More recently, the trend has been not to use SEMs, but rather to find a safe way for ionization chambers to inhibit the beam if intensities increase into the saturation region. Note that if passive

beam spreading is employed downstream of the ionization chamber in question, the dose rates or intensities are much lower than a similar chamber located upstream of the beam-spreading devices for the same intensity accelerator beam. If the associated electronics, *e.g.*, recycling integrators, can be used to detect a dose rate that produces saturation, then the beam might be inhibited before an unsafe condition prevails. In a rare case with an electron-therapy linear accelerator, the monitor ionization chambers failed under extremely high intensities before any shut off signal could be generated. Each facility must ensure that such a scenario is not possible with proton-therapy beams. Finally, the ionization chamber should be tested for the high-intensity condition used to abort patient treatment.

4.7.5 Range/energy measurements

Energy measurements can be made in the accelerator, in the beam-transport system, or in the treatment nozzle. At Loma Linda University Medical Center, for example, the beam position and intensity monitors in the synchrotron are used to calculate proton velocity from the frequency and radial position. This information is used to inhibit beam delivery if the derived energy value from this measurement exceeds a tolerance of ± 0.1 MeV. It is measured several times throughout each 0.2 s beam spill.

For a cyclotron that generates fixed proton energies between 200 and 250 MeV, it is most convenient to measure the energy by verifying that the correct amount of range shifter has been inserted in the beam for a treatment field. It is also possible to monitor the field strength of a bending magnet in the beam line after the energy has been selected. In this case, the magnetic field is constrained to be a certain value consistent with the intended proton energy delivered. Only one magnetic field strength (within some tolerance) will be acceptable for the beam to be enabled. A beam with the incorrect energy entering the bending magnet field will be bent at the wrong angle, and therefore will be lost in the beam-transport system or be steered into the nozzle at an incorrect position. Either condition will induce an aborted treatment.

A third scenario for beam-energy monitoring is to include a range detector in the nozzle, but at a location just outside the active field and upstream of a passive collimator, which can detect particles outside the beam aperture. Multiplate ionization chambers or MLFCs can be used for this purpose (see the beginning of Section 4.7).

4.8 RELATIVE DOSIMETRY

Calibrations of proton-therapy systems are carried out in reference conditions as described in Sections 4.2–4.5. Relative dose measurements or measurements in non-reference conditions require no detector calibration other than the verification of the linearity of response within the assumed dynamic range of the measurement conditions. Relative dose measurements are employed for routine daily clinical physics activities, beam-line commissioning, and collecting data for treatment-planning systems, quality assurance, and for research and development.

Measurements made during the commissioning of proton-beam-delivery systems and computerized treatment-planning systems include mapping of the clinical radiation fields involving unmodulated beam depth–dose curves and lateral profiles and dose distributions of pencil beams used for scanning. From these measurements, fundamental beam characteristics such as beam range and symmetry can be determined. These characteristics are necessary for the design and control of the beam-delivery system and for fitting the data for dose calculation algorithms. For example, unmodulated depth–dose data are used to design range modulators; depth–dose distributions for different beam cross-sections, including pencil beams for scanning and lateral profiles, are used as input data for treatment-planning systems. Once the beam-delivery system is ready for patient treatment, clinical beam field-mapping measurements are made for the range of treatment conditions.

Proton patient portals require individual physical calibration measurements of the output factors for computation of the treatment dose-monitor settings from a calibration model. The output factor is determined as the ratio of corrected dosimeter readings at the reference depth z_{ref} measured under a given set of non-reference conditions relative to that measured under reference conditions (as given in Table 4.7). Individual patient calibrations for passive and active beam-delivery systems are usually performed with a dosimetry system having a single ionization chamber, or an array of ionization chambers with a known dose-calibration coefficient relative to the proton facility's primary dose standard. Kooy *et al.* (2003) derived a model that predicted output factors for SOBP proton fields, which agreed with measurements within 2.9 percent.

4.8.1 Phantom materials

The irradiation medium for clinical dosimetry should simulate the patient as closely as possible

in terms of phantom composition, location, and extent. Water is the standard reference medium. The use of plastic phantoms is strongly discouraged because, in general, they are responsible for discrepancies in the determination of absorbed dose (IAEA, 2000). Plastic phantoms should not be used for reference dosimetry in proton beams because the fluence correction factors, h_{pl} , for scaling absorbed dose to water in plastic to absorbed dose to water in water at the same water-equivalent depth are not very well known. The differences in proton fluence distributions are almost entirely due to differences in the non-elastic nuclear cross-sections between the plastic materials and water. Nevertheless, when accurate chamber positioning in water is not possible or when no waterproof chamber is available, their use is permitted for the measurement of depth-dose distributions for low-energy proton beams (below ~ 100 MeV) (IAEA, 2000). It can be assumed that h_{pl} has a constant value of unity at all depths for such low-energy broad beams (Palmans *et al.*, 2002b), as the contributions from non-elastic interactions to the total dose are very small (<1 percent). Note that this does not apply to higher energy or pencil beams (Palmans *et al.*, 2002b; Schneider *et al.*, 2002a) where corrections of 2–5 percent have been found.

The density of the plastic, ρ_{pl} , should be measured for the batch of plastic in use rather than using a nominal value for the plastic type. Each measurement depth in plastic z_{pl} (expressed in g cm^{-2}) must also be scaled (IAEA, 2000) to give the corresponding depth in water z_w (in g cm^{-2}) by

$$z_w = z_{pl} c_{pl}, \quad (4.24)$$

where c_{pl} is a depth-scaling factor. For proton beams, c_{pl} can be calculated, to a good approximation, as the ratio of csda ranges in grams per square centimeter (Table 4.3) (ICRU, 1993a) in water and in plastic. For example, the depth-scaling factor c_{pl} has values of 0.974 for PMMA and 0.981 for clear polystyrene for nominal densities of 1.190 and 1.060 g cm^{-2} , respectively (IAEA, 2000). If a plastic phantom is used to measure the beam-quality index, the measured quantity is the residual range in the plastic, $R_{\text{res},pl}$. The residual range, R_{res} , in water is obtained using the scaling factor c_{pl} given in Eq. (4.24). Palmans and Verhaegen (1997) have performed Monte Carlo calculations of depth-dose distributions for 50–250 MeV proton beams. Allowing for the different material compositions they found excellent agreement between the proton depth-dose

characteristics for PMMA, polystyrene, A-150 plastic, and water.

4.8.2 Detectors for dose-distribution measurements

Detectors employed for relative dosimetry must have the appropriate sensitivity, energy independence, response linearity, and spatial resolution for each clinical dosimetry task. Depending upon the task, ionization chambers, silicon diodes, radiographic films, diamond detectors, gels, scintillators, thermoluminescence dosimeters (TLDs), and radiochromic films can be employed (Chu *et al.*, 1993). The time structure of the beam must also be considered for clinical-dosimetry measurements. A detector must dwell at the same location for many beam cycles to obtain reproducible results. Examples of cyclic behavior that must be considered include the accelerator duty cycle, time structure within a treatment beam pulse, pulsed irradiation of a rotating modulator propeller, and dynamic beam spreading. Dosimetry measurement systems with multiple detectors in one-, two-, or three-dimensional arrays save time in measurements of dose distributions, particularly in dynamic systems. It should also be noted that many relative dose measurements employ a separate detector as a reference monitor to correct for dose-rate variations.

The measurements used for controlling the dose and the shape of the dose distribution delivered with scanning beams differ from those with passive scattering only from the point of view of the longer time needed for the measurements. With a dynamic method one needs to accumulate the time-varying signal of the dosimeter placed at a fixed point in a phantom over the full time of a scan. Obviously, measurements based on dose rates using moving detectors cannot be used in scanned beams. The simultaneous use of several dosimeters is recommended. These should be distributed either at discrete positions in a volume or aligned along arrays (for measuring dose profiles). Alternatively, two-dimensional dosimeters such as films, scintillating screens, or gel dosimeters can be employed. The choice of ionization chambers is a compromise between the sensitive volume and spatial resolution. Smaller chambers accumulate a relatively high noise-to-signal ratio over the duration of the scan. Ionization chambers with volumes of $\sim 0.1 \text{ cm}^3$, which give a relative dose precision of a few percent, can be used, but smaller chambers are not viable.

4.8.2.1 Single ionization chambers

Output factors are measured at reference depths (middle of SOBP or in the plateau). For larger fields, the dose distributions are uniform at the reference positions and larger volume ($0.5\text{--}1\text{ cm}^3$) cylindrical ionization chambers are typically used. Depending on the beam range and field size, smaller chambers might have to be used. The use of parallel-plate extrapolation ionization chambers has also been reported (Zankowski *et al.*, 1998).

For dose-distribution measurements, the chamber must have good resolution in the direction of the distribution being measured because of the sharp distal and lateral dose gradients (Mobit *et al.*, 2000). Parallel-plate chambers are recommended for depth-dose measurements in large fields, whereas small (mini) cylindrical chambers (or other detectors) are recommended for depth-dose measurements in small fields and for all lateral dose-profile measurements.

There are often significant discrepancies between measured Bragg curves and Monte Carlo calculations owing to the complexities of beam transport and of accounting for nuclear interactions and detector geometry (Boon, 1998). This discrepancy increases with detector resolution and is especially significant for proton energies $<100\text{ MeV}$. Bichsel (1995) used an analytic model to interpret these effects. Ulmer and Kaissl (2003) have applied a deconvolution model to depth-dose measurements with different detectors at $80\text{--}180\text{ MeV}$, and the results show excellent agreement with Monte Carlo calculations.

4.8.2.2 Silicon diodes

Semiconductor diodes have routinely been used for absorbed-dose measurements. Because of their small volume, typically $\leq 0.1\text{ mm}^3$, excellent spatial resolution with good sensitivity is achieved. Because of these advantageous features, Si diodes have been widely used in radiation dosimetry (Björk *et al.*, 2000; Bucciolini *et al.*, 2003; Gulbrandsen and Madsen, 1962; Koehler, 1967; Raju, 1966; Rikner, 1985; Smith *et al.*, 1977; Trump and Pinkerton, 1967; Wilkins *et al.*, 1997). In most cases, Si diodes are operated without external bias, in the so-called photovoltaic mode, where the intrinsic depletion regions are used to produce charge flow (Klevenhagen, 1977a; 1977b; Maruhashi, 1977).

As the charge flow is by impurity carrier in the diode junction, very high dose rates, even of low-LET radiation, produce a nonlinear dose response in n-Si diodes (Rikner and Grusell, 1987).

Additionally, because of lattice damage (Knoll, 1989), the sensitivity per unit absorbed dose varies with the magnitude of previous exposure. Such lattice damage is dependent upon the type of particle producing the defects, with greater damage resulting from more massive particles. The relative damage from equal doses of 8 MV x rays, 20 MeV electrons, and 70 MeV protons was measured, and a relative damage ratio of 1:20:40, respectively, was established (Rikner, 1983). For 70 MeV proton bombardment, the damage from a 10 kGy exposure reduces the sensitivity to 30 percent of the value prior to irradiation (ICRU, 1998). Newhauser *et al.* (2002a) showed that the sensitivity of a diode used routinely in an ocular proton beam line decreased to ~ 40 percent because of radiation damage accumulated over a 5 year period.

When Si diodes are used for absorbed-dose determinations for protons, an energy-dependent response, different from that of ionization chambers, is often seen. However, this effect is largely eliminated when Hi-p Si diodes are used (see below). Koehler (1967) and Raju (1966) found a discrepancy between diode response and gas-ionization chamber response near the Bragg-peak region. Such results are consistently observed with both monoenergetic and SOBP proton beams (Coutrakon *et al.*, 1991b; Onori *et al.*, 2000; Schreuder *et al.*, 1997). Figure 4.6 shows plots of depth-dose curves measured with a diode compared with those measured with other detectors for monoenergetic and SOBP beams (Schreuder *et al.*, 1997). The large difference in the diode response compared with the other detectors is not explained by differences in stopping power between air and Si. This would produce a correction increasing the difference. Columnar recombination may contribute to the observed effects. Silicon diodes also exhibit a temperature-dependent response (Koehler, 1967; Newhauser *et al.*, 2002a). This should be taken into account to achieve reproducible measurements.

Case *et al.* (1994) modeled the response of thimble and parallel-plate ionization chambers and silicon diodes using a stochastic proton transport technique. They demonstrated geometry-induced effects in the response of the thimble ionization chamber that they claim might explain part of the difference between the responses of diodes and thimble chambers near the distal portion of the Bragg peak. Geometric effects would not explain the difference in response between plane-parallel ionization chambers and silicon diodes. The use of Hi-p Si diodes reduces these effects and the depth-dose distributions in proton beams are found to

correspond closely to the distributions obtained with plane-parallel ionization chambers (Grusell and Medin, 2000; Pacilio *et al.*, 2002; Vatnitsky *et al.*, 1999a). However, the sensitivity of this type of diode decreases rapidly with accumulated dose. Grusell and Medin (2000) showed that Hi-p Si detectors give a signal that is proportional to the ionization density in the silicon crystal in all parts of the Bragg curve. This is in contrast to detectors based on n-type silicon, or on low-resistivity p-type silicon. After pre-irradiation, these latter detectors exhibit recombination effects that are related to the proton stopping power, yielding an increase in the detector signal per unit dose with increasing LET. This effect leads to an over-response in the Bragg peak, which increases gradually with the accumulated detector dose.

Whatever the explanation, silicon diodes do not all give a response that corresponds to absorbed dose in tissue as measured by ionization chambers at proton energies $<\sim 20$ MeV. To interpret their response as absorbed dose to tissue requires knowledge of the proton-fluence energy spectrum at each point of measurement, particularly for protons with energies $<\sim 20$ MeV. Hence, caution is advised when using silicon diodes for energy-dependent proton dosimetry. However, they can safely be used to measure dose distributions at constant energy (*e.g.*, lateral beam profiles) as shown in Fig. 4.7 (Schreuder *et al.*, 1997).

4.8.2.3 Radiographic films

Radiographic-film dosimetry can be a very convenient method of measuring relative proton doses. The response of film is based on the formation of a latent image in microscopic silver halide crystals (grains) dispersed uniformly on a gelatin base (emulsion). The development process reduces the affected grains to silver, whereas the fixing process removes unirradiated grains. The resulting optical density is proportional to the fluence of particles passing through the emulsion (Dudley, 1966). As a result, changes in optical density across the film can only be interpreted as changes in dose if the energy spectrum of the protons is constant. Therefore, films can be conveniently and safely used to measure the distributions perpendicular to the proton-beam direction, but not along the beam axis to measure depth-dose distributions. In an intermediate situation in which film is to be used to verify the dose distribution of irregularly shaped volumes, and where there is a mixture of protons with different energies, an expected film density distribution should be calculated and compared with the measured dose distribution (Spielberger

et al., 2001; 2002). The calculation is based on the known energy distribution and a measured density-fluence calibration curve of the film. Although film does not necessarily give a response linear in absorbed dose, the simplicity and convenience of film makes it a very useful medium for studying the changing fluence distribution of a proton beam as it passes through matter.

4.8.2.4 Alanine

Small tissue-like integrating dosimeters allow a more precise determination of absorbed dose at high spatial resolution than many other dosimeters. The crystalline amino acid, *L*- α -alanine, is a good example (Bartolotta *et al.*, 1984; 1990; 1993; Ciesielski and Wielopolski, 1994; Waligórska *et al.*, 1989; Wieser *et al.*, 1993). Alanine is a solid hydrocarbon in microcrystalline form that, when bombarded by ionizing radiation, produces free radicals that can subsequently be quantified by electron spin resonance (ESR) spectroscopy. Similar to TLD dosimeters, alanine acts as a single-target system, exhibiting a linear response with absorbed dose until saturation occurs. Regulla and Deffner (1982) report a tissue-like absorbed-dose response to a wide range of photon energies. For 200 mg samples, they observed a linear absorbed-dose response range from 1 to 10^5 Gy. As with other solid-state dosimeters, the absorbed-dose response depends upon LET, *i.e.*, the microscopic spatial pattern of energy depositions by ionizing radiation.

Hansen and Olsen (1985) report integral ESR response values relative to gamma-ray or electron bombardment for 16 and 6 MeV protons and 20 MeV α -particles of 1.00, 0.86, and 0.58, respectively. For these bombardment conditions, the average mass electronic stopping powers in alanine were 38, 119, and $534 \text{ MeV cm}^2 \text{ g}^{-1}$, respectively. While the relative sensitivity per unit absorbed dose varied with stopping power, the observed linearity and saturation dependence was independent of stopping power, *i.e.*, the free-radical production was dependent upon stopping power as a simple scaling factor. Low-LET radiation results in the production of free radicals, which are stable at room temperature.

However, for high-LET radiation, significant fading occurs that depends upon the total absorbed dose delivered. Hansen and Olsen (1989) reported 2.5, 3.2, and 3.7 percent fading at 1000 h following exposure to 16, 6, and 1 MeV protons, respectively. Even for low-LET radiation, Regulla and Deffner (1982) reported 10 percent fading at elevated storage temperatures of 70°C , as well as increased yields for irradiations at elevated temperatures, 20 percent at 90°C and 10^5 Gy. Bradshaw *et al.* (1962)

and Ebert *et al.* (1965) compared the response of alanine powder in low-energy (<8 MeV) proton beams with the response in ^{60}Co .

The use of the alanine dosimeter for absorbed-dose determinations in clinical proton beams requires consideration of the proton energy-fluence spectrum and control of the environment during and subsequent to bombardment. Nichiporov *et al.* (1995) investigated the dose response of alanine in a 169 MeV proton beam using ESR spectroscopy. They found a linear response (± 2 percent) in the dose range from 50 to 300 Gy and a relative inter-detector response of ± 1.5 percent. Depth-dose measurements at a residual proton energy of 50 MeV were indirectly compared with ionization-chamber measurements and found to be in good agreement. Fattibene *et al.* (1996) and Onori *et al.* (1997) found good agreement between depth doses measured with alanine and

parallel-plate ionization chambers in a 62 MeV clinical proton beam. In both investigations, anomalous doses were measured with the alanine detectors distal to the Bragg peak and could not be satisfactorily explained. In a dosimetry comparison in low-energy proton therapy beams, the relative difference between alanine and ionization-chamber dose determinations was ± 2 percent (Cuttone *et al.*, 1999). Recently Palmans (2003) undertook Monte Carlo simulations of the depth-dose curves in alanine pellets in a 60 MeV ocular proton beam. The results showed an underestimation of the Bragg peak intensities for both unmodulated (up to 30 percent) and modulated (up to 15 percent) beams.

4.8.2.5 Other detectors

Other types of dosimeters such as diamond detectors and TLDs have been used for measuring relative doses in a phantom. The potential advantages of diamond detectors for relative dosimetry in radiotherapy have been well documented (Bucciolini *et al.*, 2003; De Angelis *et al.*, 2002; Khrunov *et al.*, 1990; Vatnitsky and Järvinen, 1993; Vatnitsky *et al.*, 1993). They are radiation-resistant, practically TE, have high sensitivity and stability, and are relatively small. Depending on the type of detector used, relative dose measurements have shown good agreement with those of ionization-chamber measurements in high-energy (≥ 200 MeV) proton beams (Schreuder *et al.*, 1997; Vatnitsky *et al.*, 1993; 1995; 1999a). However, the

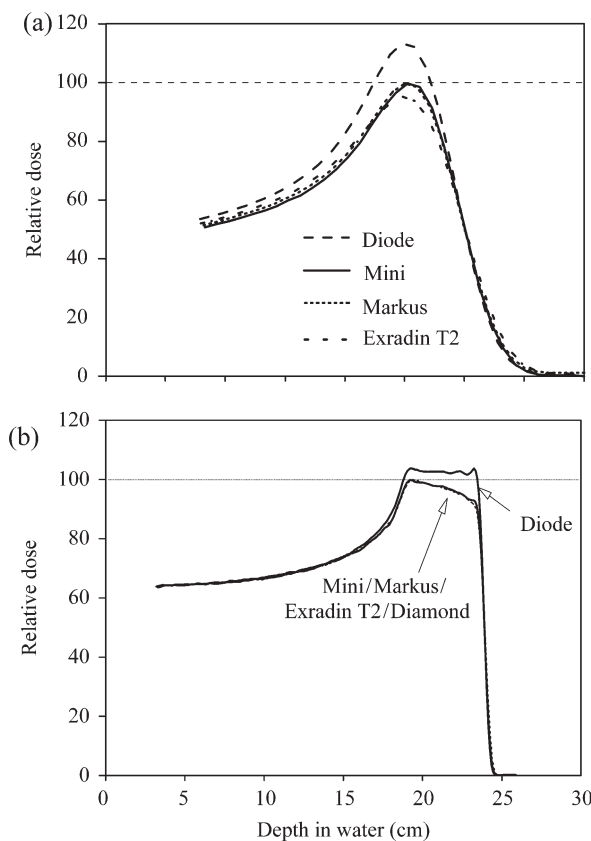


Figure 4.6. Comparison of depth doses measured in a 200 MeV proton beam with a diode, diamond detector, and three different ionization chambers (Markus parallel plate, Exradin 0.5 cm³ cylindrical, and Mini, which is a 0.007 cm³ specially constructed cylindrical ionization chamber). (a) For an unmodulated beam for which only the Bragg-peak region is shown and (b) for a beam with a 5 cm SOBP. In both cases, the data are normalized to the same entrance dose level where the measured dose levels are independent of detector resolution (Schreuder *et al.*, 1997; reproduced with permission).

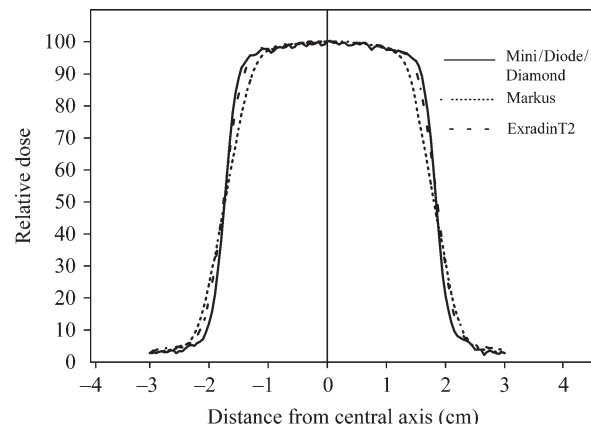


Figure 4.7. Comparison of beam profiles measured in a 200 MeV proton beam with a diode, diamond detector, and three different ionization chambers (see Fig. 4.6) in a 3.5 cm diameter field at a depth of 5 cm in water ($E_p \approx 167$ MeV). The Markus and Exradin T2 chamber measurements are only shown for comparison, and should not be used to measure beam profiles. The data are normalized to 100 on the central axis (Schreuder *et al.*, 1997; reproduced with permission).

DOSIMETRY

results obtained in low-energy beams have been problematic (Onori *et al.*, 2000; Pacilio *et al.*, 2002).

Several experimental investigations of the usefulness of TLDs, mainly LiF (TLD-100), for applications in clinical proton dosimetry have been undertaken (Bilski *et al.*, 1997; Bucciolini *et al.*, 1999; 2000; Carlsson and Carlsson, 1970; Fattibene *et al.*, 1996; Loncol *et al.*, 1996; Vatnitsky *et al.*, 1995; 1999a). Their usefulness is limited by their relatively large water-equivalent thickness and LET-dependent response. However, measurements have shown good agreement with ionization-chamber measurements, particularly in range-modulated beams in which the LET variation is diluted (Fattibene *et al.*, 1996; Vatnitsky *et al.*, 1995). The main application for TLDs in proton therapy is probably for *in vivo* dosimetry. Diamond detectors and TLDs should only be used for relative proton dosimetry once their characteristics have been checked against the characteristics of appropriate ionization chambers in the clinical beam in which they will be used.

The advent of scanning proton beams, as well as intensity-modulated radiation therapy, has brought more demands for dosimeters that can make two- and three-dimensional determinations. Unlike passive beam-delivery systems, in which the entire target volume is continuously filled to uniform dose throughout the irradiation, scanned beams must sequentially deliver layers of dose at discrete proton energies to fill the target volume to a uniform, or prescribed (in the case of intensity modulation) dose. For these treatment prescriptions, the entire treatment with all energies must be delivered for each dose measurement in the target volume. For discrete dosimeters, or even linear ion-chamber arrays, this process can be quite time-consuming.

One of the two-dimensional dosimeters showing promise is radiochromic film (e.g., GafChromic™ MD-55 film) (Butson *et al.*, 2001; Niroomand-Rad *et al.*, 1998) that gives more accurate depth-dose profiles than radiographic film because of reduced saturation effects in the high-LET region of the Bragg peak. The film can be sandwiched, for example, between polystyrene blocks with the beam entering through the edge of the film. This technique can give a two-dimensional dose distribution through the target volume that shows distal-edge boundaries quite well. After optically scanning the film along the depth axis and comparing with ionization-chamber data, saturation in the Bragg-peak region appears to be <10 percent of the peak dose (Daftari *et al.*, 1999; Fidanzio *et al.*, 2002; Luchin *et al.*, 2000; Nichiporov *et al.*, 1995; Piermattei *et al.*, 2000; Vatnitsky, 1997; Vatnitsky

et al., 1997). Two disadvantages of radiochromic film have been its high cost and its low sensitivity. However, given its ease of procurement, long storage life, and high spatial resolution, its use is increasing, while efforts to improve its sensitivity are being made (Geso *et al.*, 2004; Soares, 2006), while cheaper film is becoming available. A new radiochromic film (GafChromic EBT) with improved characteristics (Cheung *et al.*, 2005; Sankar *et al.*, 2006) is being used in clinical dosimetry (Zeidan *et al.*, 2006).

Two-dimensional dosimetry with high spatial resolution can be performed with a scintillating screen viewed through a 45° mirror by a charge-coupled device (CCD) camera (Boon, 1998; Boon *et al.*, 1998; 2000; Coutrakon *et al.*, 1990; Ryneveld, 1998). The same CCD system has also proved to be extremely useful to verify the dose delivery in scanned beams (Lomax *et al.*, 2004). It can also provide the necessary data to describe the dose distribution of the elemental scanned beam (the physical pencil beam). These data are required as input for the dose calculation of extended scanned dose fields in treatment planning. However, the CCD has the problem of having a small amount of quenching of the signal in the Bragg-peak region. This can be accounted for in the calculation of the dose response, but it can be also be corrected by choosing a proper mixture of the phosphors (Safai *et al.*, 2004).

Another class of detectors is liquid and gel detectors. One of the first types, Fricke dosimeters, relies on the conversion of Fe^{2+} to Fe^{3+} in an aqueous ferrous sulfate solution by irradiation. The relative dose can be obtained by determining the number of ferric ions produced, using an optical absorption spectrophotometer with ultraviolet light at 304 nm (Attix, 1986). With Fricke gels, the change in paramagnetic properties can be measured using MRI or optical techniques. The former can provide three-dimensional images of the dose distributions. The MRI of gels containing FeSO_4 has been investigated by several authors (Gore *et al.*, 1984; Hazle *et al.*, 1991; Maryanski *et al.*, 1994; Podgorsak and Schreiner, 1992). A major limitation of Fricke gel systems is the continual post-irradiation diffusion of ions, resulting in a blurred dose distribution.

Polymer gel dosimeters are also under experimentation as three-dimensional dosimeters, e.g., BANG™ gel (Ramm *et al.*, 2000; Uusi-Simola *et al.*, 2003). One of the promising ones, such as the so-called MAGIC (methacrylic and ascorbic acid in gelatin initiated by copper) dosimeter (Fong *et al.*, 2001) can be manufactured and used more easily than other gels and can be imaged by optical

scanning or by MRI. In addition, the gel does not need to be stored in an oxygen-free environment as many other gels do. Gels can also be used with scanning beams, but the experience is very limited. Gels have the advantage of giving a representation of the dose in the entire three-dimensional volume, but the precision of the data is still less than that obtained with a CCD-based system. However, there is only limited practical and theoretical knowledge of gel dosimetry in proton and ion beams (Gustavsson *et al.*, 2004; Hilts *et al.*, 2000; Jirasek and Duzenli, 2002; Ramm *et al.*, 2000). Presently, there are means available for verifying scanning-beam dose delivery with sufficient precision to ensure that the system is safe for patient treatments. However, since the energy (or LET)-dependent responses of gel dosimeters have not been well documented (Gustavsson *et al.*, 2004), their clinical use has thus far been limited. A new type of radiochromic gel material (PRESAGETM) has recently been described (Guo *et al.*, 2006). This material has potential advantages over other gel dosimeters, including insensitivity to oxygen and amenability to machining to arbitrary shapes and sizes, without the need for a container.

An example of a large multiarray detector for three-dimensional dosimetry is a 400 scintillator/fiber system developed at PSI (Safai *et al.*, 2004). The scintillators (sensitive volume of 5 mm³) are optically coupled to the fiber light guides (2 mm diameter by 1 m long). The detectors are embedded at different depths in a polyethylene phantom. The light signals from the scintillators are carried by the bundle of fibers and are mapped on a CCD by means of a lens system. Other novel developments for quasi-three-dimensional dose verification involve the use of stacks of two-dimensional arrays of ionization chambers interleaved with plastic slabs (Amerio *et al.*, 2004; Brusasco *et al.*, 1997; 2000; Cirio *et al.*, 2004).

4.8.3 Determination of dose distributions

The description of the changing energy and spatial characteristics of a proton beam as it passes through matter is critical for predicting the dose deposition of the protons. The relative dosimeters described above can be very helpful in determining these characteristics. The determination and parameterization of the dose distributions in matter is important for the accuracy of dose-calculation algorithms used in computerized treatment-planning systems.

4.8.3.1 Range and depth-dose characteristics

A critical aspect of proton treatment is the possibility of stopping the beam at a specific point within the patient. Accurate control of the stopping point depends on knowledge of the beam range in water and of the water-equivalent path lengths (WEPLs) of materials placed in the beam path and of the tissues traversed. The central-axis beam range in water is measured for the beam energies and range absorbers that are to be used clinically. Depth-dose distributions should be determined for a selection of energy, range modulation, field size, and other treatment parameters that might affect the distributions. The sharpness of the distal-dose fall off depends on the incident-beam energy and energy spread of the accelerated beam, and on the range straggling produced by absorbers in the beam-delivery system and by the patient.

For measurements of depth-dose distributions, the use of plane-parallel chambers is recommended. In principle, a measured depth-ionization distribution should be converted to a depth-dose distribution, using the depth dependence of the stopping-power ratio, $s_{w,\text{air}}$. This is achieved by multiplying the measured ionization charge or current at each depth z by the stopping-power ratio, $s_{w,\text{air}}$, and the perturbation factor at that depth. Values for $s_{w,\text{air}}$ as a function of R_{res} can be calculated from Eq. (4.17). Perturbation factors are assumed to have a value of unity (see Section 4.4.2.1). For practical purposes, these conversion factors are not usually applied, as $s_{w,\text{air}}$ varies by less than ± 0.4 percent from the median value for residual proton ranges in water from 0.25 to 30.00 cm (IAEA, 2000). The influence of ion recombination and polarity effects on the depth-ionization distribution should be investigated and taken into account if there is a variation with depth. If the field size for which measurements are to be performed is smaller than twice the diameter of the cavity of the plane-parallel chamber, then a detector with a better spatial resolution (*e.g.*, minichamber, diode, or diamond) is recommended (see below). The resulting distribution must also be converted, if necessary, using the appropriate stopping-power ratios (*e.g.*, water-to-air, water-to-silicon, or water-to-graphite). For the latter, the necessary stopping-power values can be found in ICRU (1993a). The suitability of such detectors for depth-dose measurements should be verified by test comparisons with a plane-parallel chamber at a larger field size. For scanning beams, measurement times should be long enough compared with the scanning cycle of the field in order to yield reproducible readings.

Accurate depth-dose measurements must be made throughout the Bragg peak region, including the sharp distal fall-off region near the end of the range. This requires a detector with good spatial resolution and with a dose response that is practically independent of the variation of proton energy with depth. As mentioned above parallel-plate ionization chambers (Palmans *et al.*, 2002a) are recommended for depth-dose measurements, but small-volume thimble ionization chambers (mini chambers) (Schreuder *et al.*, 1997), and diamond detectors (Pacilio *et al.*, 2002; Vatnitsky and Järvinen, 1993; Vatnitsky *et al.*, 1999a) can be used. Caution is called for when using silicon diodes since, as was noted above, they have been observed to have up to 10 percent higher response than parallel-plate ionization chambers in the Bragg-peak region (Koehler, 1967; Raju, 1966; Schreuder *et al.*, 1997). However, the use of suitable diodes (and the avoidance of n-doped types) can give good agreement with ionization-chamber measurements (Grusell and Medin, 2000). When using a diamond detector, the response should be corrected for the dose-rate effects (Pacilio *et al.*, 2002). Radiographic film should not be used for depth-dose measurements because of its significant variation in response per unit dose as a function of depth in a proton beam. Accurate depth-dose measurements with radiochromic films can be made if the films are placed perpendicular to the beam axis at different depths.

Water-equivalent path lengths for materials placed in the beam path are measured, and, for purposes of treatment planning, the relationship between WEPL (or proton stopping power) and CT number (based on relative x-ray attenuation coefficients) for body tissues is established (Schaffner and Pedroni, 1998; Schneider *et al.*, 1996; Szymanowski and Oelfke, 2003). The distribution of dose as a function of depth, determined as a basic characteristic of the beam, is also required data for treatment planning. The WEPLs for materials can be measured by submerging samples of known thickness in a water phantom and measuring the effect on beam range. The WEPLs for materials used for patient-specific devices, such as range shifters and tissue compensators, need to be determined. In addition, the WEPLs for tissue-substitute materials should be determined and correlated with observed CT numbers for the same materials.

The shape of the central-axis depth-dose curve varies with field size (Larsson, 1967; Vatnitsky *et al.*, 1999a) and can differ significantly for small fields and at locations within irregularly shaped fields where the lateral extent is less than a few penumbra widths. An understanding of this variation is important for treatment planning and treatment-field

calibration. The depth-dose curve near the surface of treatment fields can be affected by protons scattered from field-shaping apertures. Aperture scatter effects (van Luijk *et al.*, 2001) can also be more pronounced for small and irregularly-shaped fields.

4.8.3.2 Beam profiles and penumbrae

For proton-treatment beams that are produced by passive beam-shaping (scattering) techniques, the lateral uniformity of proton-treatment fields should be comparable or superior to that of conventional photon and electron fields. Uniformity may be expressed in terms of field symmetry for points equidistant from the beam central axis and a flatness variation over some designated portion (e.g., 80 percent) of the field area. Uniformity characteristics should be measured at several depths for a variety of treatment-planning dose distributions.

The shape of the dose distribution at the lateral field edge is extremely important in planning proton-beam treatments. Field placement in proximity to radiation-sensitive normal tissue depends on accurate knowledge of the penumbra as well as consideration of the uncertainty in patient alignment. Penumbra widths are defined (see Section 3.4.2.2) as the distance separating stated dose levels (e.g., 80–20 percent of the central axis dose at that depth). Penumbra characteristics, which can be determined by beam profile scans, will depend on the design of the beam-delivery system and will vary with most treatment parameters, including beam energy, range modulation, depth in the patient, and collimator-to-skin distance (Urie *et al.*, 1986b). These variations should be accurately measured and reproduced in the treatment-planning system. Oozer *et al.* (1997) have developed a model for the lateral penumbrae in water for a 200 MeV clinical proton beam based on beam-profile measurements with a silicon diode. The results show that the lateral penumbrae are essentially independent of beam modulation and collimator diameter. The model has been integrated into a treatment-planning system.

Lateral-uniformity measurements should be made in water or in a water-equivalent phantom with a detector having high spatial resolution in the scan direction. Energy independence for lateral scanning is not as important as for depth scanning. Silicon diodes, diamond detectors, and small ionization chambers are useful. Radiographic film placed in a phantom perpendicular to the beam direction provides results similar to the other detectors. The film should be scanned with a system that has good spatial resolution and a film-density response correction should be made. Radiochromic films also give very high spatial resolution.

5 GEOMETRIC TERMS, AND DOSE AND DOSE-VOLUME DEFINITIONS

In previous ICRU reports (ICRU, 1993b; 1999; 2004), a number of important concepts concerning anatomic volumes of interest were introduced and defined. Among these were: for tumors, the gross target volume (GTV), the clinical target volume (CTV), and the planning target volume (PTV); and, for normal tissues, the concepts of organ at risk (OAR) and planning organ at risk volume (PRV).

Except for the PTV and PRV, these definitions apply to all modalities equally. Both in their delineation and in their use, it is irrelevant as to whether photons, electrons, protons, or any other radiation are to be employed. Indeed, it is important not to let knowledge of the likely radiation modality affect how these volumes are delineated since (i) their definitions are modality independent; and (ii) one might wish to combine or compare or retrospectively analyze treatment plans for more than one modality.

Because the definitions of geometric (and dosimetric) terms are very largely the same for protons as for all other modalities of radiation therapy, the definitions and explanations of previous reports remain largely valid for proton-beam therapy. For this reason, and to harmonize the present report with the preceding reports, portions of ICRU Reports 71 (ICRU, 2004) have been reproduced in the present section. The reader is referred to this report for clarifying diagrams and explanations that are omitted in the present section.

Each of the above-mentioned volumes is discussed below. The GTV and CTV are purely oncological concepts and are independent of any therapeutic approach. They represent volumes with known or suspected tumor involvement. The OAR represents normal tissues. The PTV and PRV are purely geometric concepts, which do not necessarily correspond to tissue or organ borders. The definitions of these concepts and explanations are given in ICRU Report 62 (ICRU, 1999) and can be extended and applied to all forms of external-beam therapy, including conformal therapy (ICRU, 2004).

Volumes should be carefully delineated; for example, contours should not unduly extend into spaces (such as air cavities or the region outside

the body outline) which are not properly part of the volume of interest. All geometric objects should relate to the patient's anatomy under treatment conditions, and at one point in time (see Section 5.5). In the present report, the term *delineation* is used to describe the identification of the spatial extent of an object, regardless of whether it is identified by a manual process of drawing contours on an image, or by an automatic feature extraction technique, or by any other method.

5.1 ANATOMIC VOLUMES RELATING TO THE TUMOR

The volumes relating to the tumor are schematically represented in Fig. 5.1.

5.1.1 Gross tumor volume (GTV)

The GTV is the gross palpable, visible, or clinically demonstrable location and extent of the malignant (or otherwise) growth. It can consist of primary tumor and, if present, metastatic lymphadenopathy, or other metastases. In the GTV, the tumor cell density is always high ($\geq 10^6 \text{ mm}^{-3}$). Hence, an adequate dose must be delivered to the whole GTV for radical therapy. There is no GTV after complete surgical resection.

The shape, size, and location of a GTV can be determined by clinical examination (e.g., inspection, palpation, and endoscopy), and/or various imaging techniques (e.g., x ray, CT, digital radiography, ultrasonography, MRI, magnetic resonance spectroscopy [MRS], PET, and other radionuclide imaging methods). The methods used to determine the GTV should meet the requirements for staging the tumor according to the clinical TNM (UICC, 1997) and AJCC (AJCC, 2002) systems.

The GTV (primary tumor, metastatic lymphadenopathy, and other known metastases) can appear different in size and shape, sometimes significantly, depending on which examination technique is used for evaluation. The radiation oncologists should in each case indicate which technique has been used for the evaluation and for the delineation of the GTV (see Section 5.4.4).

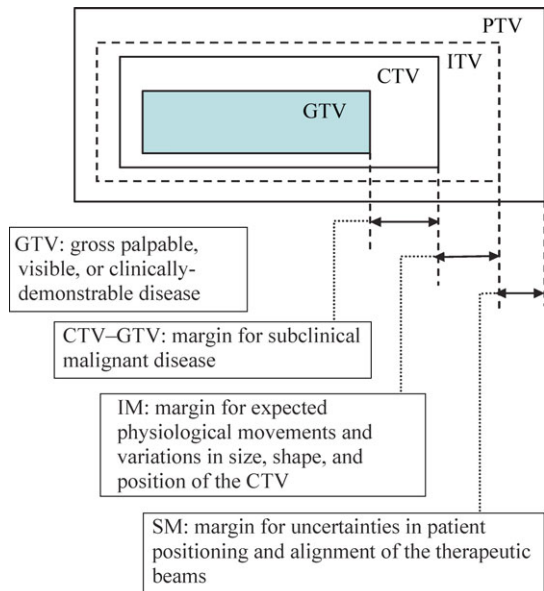


Figure 5.1. Illustration of the volumes and margins relating to the definition of the target volume.

There are at least four reasons to describe and report the GTV in a complete and accurate way. First, as indicated above, it is required for staging, *e.g.*, according to the TNM system. Secondly, an adequate dose must be delivered to the whole GTV in order to obtain local tumor control. Thirdly, evaluation of the GTV regression is needed when redefining the PTV (Section 5.1.4) during the course of treatment. Fourthly, changes in the GTV during treatment can be one of the predictive values for response to treatment.

A GTV can be confined to only part of an organ, can involve a whole organ, or can extend outside the normal borders of the organ or tissue involved.

There can be more than one GTV. This will be the case, for example, when there is more than one volume containing gross palpable, visible, or clinically demonstrable malignant growth, and these volumes are spatially separated. A possible nomenclature for such cases is discussed in Section 5.4.1.

A GTV can change with time because of tumor shrinkage, tumor growth, or therapeutic intervention. In that case, several GTVs can be delineated, and should be qualified, for example, as in GTV (initial), GTV [$D_{RBE} > 30$ Gy (RBE)], GTV [$D_{RBE} > 50$ Gy (RBE)], *etc.* (see Section 5.4.4).

The delineation of the GTV is a required part of the treatment prescription, except in the event that no gross disease is present.

5.1.2 Clinical target volume (CTV)

Macroscopically, tumors might seem relatively well delineated. However, when microscopic examination

of a cancer is performed, one often finds sub-clinical extensions around the GTV, *i.e.*, individual malignant cells, small cell clusters, or micro-extensions, which cannot be detected clinically. The CTV is a tissue volume that contains the GTV(s) and/or sub-clinical malignant disease at a certain probability level. This volume thus has to be treated adequately. Like the GTV, the CTV is a clinical-anatomical concept.

Delineation of the CTV is based (i) on the available data on the probability of (sub-clinical) malignant cells outside the GTV; and (ii) on the judgement of the radiation oncologist. The relevant data to consider concern the probability of microscopic extension at different distances around the GTV, and the probability of sub-clinical invasion of regional lymph nodes or other tissues. The CTV delineation should be based on knowledge of pathways of tumor infiltration in three dimensions.

There might be no macroscopic disease, and hence no GTV, after gross resection or, occasionally, after chemotherapy as the gross tumor might then no longer be evident or even present. In such a case, only a CTV, and not a GTV, would be defined.

The delineation of the CTV is a required part of the treatment prescription. If the CTV is identical with the GTV, then its specific delineation could be useful, but it would be sufficient to state that the CTV and GTV are identical.

The CTV includes the gross lesion (GTV) and the suspected sub-clinical extension of the tumor. After the planned dose to the CTV has been delivered, an additional or 'boost' dose can be administered to the GTV. In some circumstances, the CTV can be coincident with the GTV, for example, in the case of a benign tumor or a well-encapsulated malignant tumor. Nevertheless, for record-keeping reasons, it is preferable to define a CTV in such a case.

5.1.2.1 The dose intention for the CTV

Additional volumes with presumed sub-clinical spread can also be considered for therapy, *e.g.*, regional lymph nodes or metastases. They are also defined as CTVs. Thus, two types of sub-clinical disease (adjacent to the GTV or at a distance, *e.g.*, lymph nodes) can be envisaged. The prescription is then based on the probability that there are cancer cells in some anatomically definable tissues/organs, even though they cannot be detected with present-day techniques: they are sub-clinical. For prescription of treatment, these sub-clinical deposits (or their probability of existence) can be described in terms of frequency of risk for later detectable manifestations if not treated adequately in the sub-clinical stage. The estimate of that probability is based on clinical experience from adequately documented treatment

and follow-up (Grégoire *et al.*, 2000; Martinez-Monge *et al.*, 1999, for head and neck tumors).

5.1.3 Internal target volume (ITV)

The PTV, as discussed in Section 5.1.4, allows for two components of uncertainty, namely, internal uncertainties (e.g., physiologic movements and variations in size, shape, and position of the CTV within the patient) and uncertainties in factors external to the patient (e.g., set-up uncertainties). The volume that includes the CTV plus an allowance for the internal component of uncertainty is termed the internal target volume (ITV). The margin between the ITV and the CTV is termed the internal margin and is more fully described in Section 5.1.4.1. Delineation of the ITV is considered optional.

5.1.4 Planning target volume (PTV)

The concept of PTV was introduced in ICRU Report 50 (ICRU, 1993b). The PTV is a geometrical concept, introduced for treatment planning. It surrounds the CTV with additional margins to compensate for different types of variations and uncertainties of beams relative to the CTV.

The PTV has two functions:

- It is a tool that can be used to help in the selection of the appropriate beam sizes and beam arrangements to ensure that the prescribed dose is actually delivered to all parts of the CTV with a specified probability, qualified by the need to keep the risk of damage to adjacent normal tissues below a clinically acceptable level.
- It is of use in prescription and reporting. For example, a radiation oncologist will usually prescribe dose in terms of the coverage of the PTV: e.g., ‘at least 95 percent of the PTV must receive 70 Gy (RBE)’. [This example can be more concisely written as ‘ $V_{D=70\text{Gy(RBE)}}(\text{PTV}) \geq 95$ percent’ (see Section 5.6.1.1.)]. It should be noted that the estimated distribution of dose within the PTV is an underestimate of the dose distribution in the CTV. This results because the CTV can remain well within the PTV and hence not experience the reduced dose often delivered at the PTV boundary. In addition, the dose distribution within the CTV is, if anything, an over-estimate at each point of the dose the CTV will actually receive because the CTV can well move close to the PTV boundary and hence can receive a lower peripheral dose. Therefore, the computed dose distributions to the PTV and CTV bracket the dose at the specified confidence level that the contents of the CTV are likely to receive, and they can be used to estimate the range of possible doses at that confidence level.

Beams can be designed directly for the CTV, taking into account the need for internal and external margins within the aperture design, without reference to a PTV. This is particularly natural in the case of proton (and other charged particle) beams. Nevertheless, PTVs must be defined since they are required for reporting purposes. These matters are further discussed in Section 5.1.4.4.

Each CTV, and thus GTV, must have a corresponding PTV. The delineation of the PTV is a required part of the treatment prescription.

5.1.4.1 Margins for the different types of variations and uncertainties

As discussed in Section 7, a variety of techniques are available for patient immobilization, assessment, and reduction of organ motion. However, even once the appropriate techniques have been implemented, there always remains some degree of residual motion and some uncertainties about where the patient, GTV, CTV, and OARs are located relative to the treatment equipment. These uncertainties must be taken into account in planning the treatment, and constitute the basis for determining the PTV.

To avoid significant deviation from the prescribed dose in any part of the CTV(s), one must add margins to the CTV(s) to compensate for variations and uncertainties (i) in position, size, and shape of the CTV, and (ii) in patient-beam positioning, both during a given radiation treatment fraction and between successive fractions. To facilitate discussion, and in keeping with previous reports (ICRU, 1993b; 1999), these will be referred to as the internal margin (IM) and the set-up margin (SM), respectively.

Internal margin. This is the margin that must be added to the CTV to compensate for expected physiological movements and variations in size, shape, and position of the CTV during therapy. The IM is often asymmetric around the CTV. Techniques such as breath gating or tumor tracking exist to reduce the IM (see Section 7.5). As mentioned above, the volume encompassed within the IM is termed the ITV. In practice, it might not be necessary to explicitly delineate the ITV, but the IM (as well as the SM) must be taken into account when delineating the PTV.

Set-up margin. To account specifically for uncertainties (inaccuracies and lack of reproducibility) in patient positioning and alignment of the therapeutic beams during treatment planning and through all treatment sessions, an SM for each beam is needed. The uncertainties vary with different anatomical directions, and thus the size of such margins depends on the selection of beam geometries. The inaccuracies depend on such factors as:

- variations in patient positioning;

- mechanical uncertainty of the equipment (e.g., sagging of gantry, collimators, and couch);
- transfer set-up errors from CT and simulator to the treatment unit;
- human factors.

These uncertainties can also vary from center to center, and within a given center from machine to machine. The use of patient immobilization devices, the application of quality assurance programs, and the skill and experience of the radiographers/radiotherapists are important and must be taken into account. The use of different record and verification systems (in real time or not) can also be important and significantly alter the size of the required set-up margins.

5.1.4.2 Delineating the PTV

The procedure for arriving at an overall margin, combining the individual contributions to the uncertainty, is discussed in Section 7.6. The needed margins are likely to differ in different directions. A generally satisfactory approach is to assess them explicitly in the six cardinal directions: AP, PA, left, right, cephalad, and caudad. The PTV can then be delineated by expanding the CTV by those margins. This process can be performed using a computer-based expansion tool. Manual expansion is tedious and prone to error, as the out-of-plane dimension is not easily appreciated while delineating the PTV in any given plane.

5.1.4.3 Multiple PTVs

The intention is usually to deliver an as-uniform-as-possible dose to one specific CTV, subject only to the restrictions of physical achievability and the need to balance tumor control with sparing of adjacent normal tissues. In that case, there will be only one corresponding PTV. However, there are cases in which one specifically wishes to prescribe a non-uniform dose to the target volume(s). It is recommended that the prescription for this be accomplished by defining multiple-nested GTVs and/or CTVs, each with their own PTV to each of which a uniform dose is prescribed (see Section 5.4.1). The circumstances in which more than one PTV might be needed include the following:

- (1) When there is more than one CTV. For example, there might be two spatially separated GTVs, which then have two spatially separated CTVs associated with them, which, in turn, need separate PTVs.
- (2) When it is desired to irradiate a target volume non-uniformly. In this case, the PTVs receiving

the higher or lower doses are nested within the parent PTV. This situation can arise under two circumstances:

- (a) One wishes to 'paint' the dose non-uniformly within the tumor, e.g., to give a higher dose to a region within the tumor that is judged to be of higher radio-resistance than the rest of the tumor.
- (b) The tumor lies close to a sensitive uninvolved organ and therefore a section of the target volume must receive a lower dose than that delivered to the rest of the target volume. Nested PTVs might then be needed if guidance is required for planning purposes.

In general, delineation of the PTV margin should not be compromised even if it overlaps with another PTV, an OAR, or a PRV. In the case of 2(a), if the dose gradient within the target volume can be designed by an automated optimization scheme, there might be no need to define nested PTVs as the computer algorithm itself might determine automatically how the dose should vary within the outermost PTV. However, it should be noted in the prescription that the PTV is intended to receive a non-uniform dose. If nested PTVs are needed for the purposes of 2(a), then the outermost should be delineated without compromises due to overlapping with neighboring volumes of interest (VOIs, see Section 5.3.1).

5.1.4.4 Proton-specific issues regarding the PTV

The material in Section 5.1.4 up to this point would apply equally to any radiation modality. However, there are some differences in the way the PTV is used in proton-beam therapy. For photon beams, the PTV is primarily used to determine the lateral beam margins. In the case of protons (and other charged-particle beams), in addition to the lateral margins, some margin in depth must be left to allow for uncertainties in the knowledge of where the distal (say) 90 percent isodose would fall. The beam energy (*i.e.*, penetration) should be chosen such that the CTV is within the irradiated volume taking into account *both* motion *and* range uncertainties. Thus, for protons, the lateral margins and the margins in depth (relative to the proximal and distal tumor surfaces) solve different problems and will virtually always be numerically different. As a consequence, for each beam orientation being considered, one would, in principle, need a separate PTV with different margins laterally and along the direction of each beam.

An alternative approach is to determine the beam parameters using the CTV, rather than the PTV, and to place the burden of adding appropriate lateral

and range margins to the computer algorithm. That is, both lateral and depth margins are computed in designing each beam. In the case of scattered-beam treatments, the lateral margins would be designed into the aperture in the beam's-eye view, and the depth margins would be designed into the compensator. For scanned beams, and intensity-modulated proton therapy (IMPT) in general, these margins would influence which pencil beams would be used, and each one's depth of penetration.

It is required that the dose distribution within the 'PTV' be recorded and reported. This would be unworkable if there were a separate PTV for each beam employed, and impossible if separate lateral and depth margins were built into the computer's beam-design algorithm. It is therefore proposed that, in proton therapy, the PTV be defined relative to the CTV on the basis of lateral uncertainties alone. An adjustment must then be made within the beam-design algorithm to take into account the differences, if any, between the margins needed to account for uncertainties along the beam direction (*i.e.*, range uncertainties) and those included in the so-defined PTV (*i.e.*, based on lateral uncertainties).

5.2 ANATOMIC VOLUMES RELATING TO UNINVOLVED NORMAL TISSUES AND ORGANS

Just as for volumes associated with tumors, the delineation of normal tissues and organs that are judged to be uninvolved is no different for protons than for any other radiation modality. The volumes relating to the uninvolved normal tissues (OAR and PRV) are schematically represented in Fig. 5.2.

5.2.1 Organ at risk (OAR)

Normal tissues and organs whose radiation sensitivity can significantly influence treatment planning and/or prescribed dose, termed OAR, should be delineated.

It is desirable that the entirety of all OARs be imaged and delineated, even if this involves imaging parts of the OAR that are not expected to be included in the treatment beams. This is useful in order to be able to characterize irradiated parts of the OAR in terms of their fractional volume—a quantity that is often useful in satisfying prescription constraints or estimating normal-tissue complication probabilities. When it is not practical or clinically desirable to image the full organ, its full volume can, for purposes of estimating fractional volumes only, be estimated. If the relative volume is based on such an estimate, it should be clearly so stated.

Often it is infeasible to image in their entirety cylindrical organs such as the spinal cord or

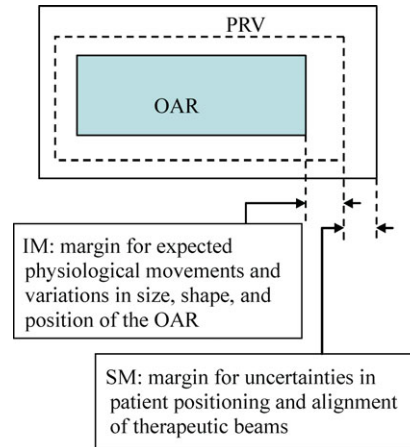


Figure 5.2. Illustration of the volumes and margins relating to the definition of organs at risk.

tubular organs such as the rectum. In this case, the extent of delineation should be carefully reported; *e.g.*, 'the spinal cord was delineated $\pm x$ cm from the cephalad and caudad edges of the PTV', or 'the rectum was delineated up to the sigmoid flexure'.

The delineation of tubular organs, or organs with cavities, for which the organ wall is of interest (*e.g.*, the bladder wall), poses significant technical difficulties. If the organ wall is thick (relative to the voxel size in the imaging study), both the outer and the inner wall can be delineated, and the dose statistics for the difference in these volumes can be computed and reported. If the organ wall is thin, this strategy is prone to error. The best solution then is to define a 'surface of interest' (SOI) (see Section 5.3.3) and compute and report the dose statistics for that surface. A dose–area histogram (see Section 5.6.2.3) would be useful for this purpose.

5.2.2 Planning organ at risk volume (PRV)

In order to ensure with a high probability that adequate sparing of OAR will actually be achieved, an integrated margin has to be added to the OAR, using the same principles of IM and SM as for the PTV. This leads, in analogy with the PTV, to the concept of PRV. The PRV is a tool designed to help treatment planning and evaluation. The design of the necessary margins follows the same principles as for the design of a PTV, and these are discussed in Section 5.1.4, above, and in Section 6.3. For the PRV, the uncertainties that need to be taken into account include:

- movements of the OAR during treatments;
- variations in patient positioning;
- mechanical uncertainty of the equipment (*e.g.*, sagging of gantry, collimators, and couch);
- transfer set-up errors from CT and simulator to the treatment unit;
- human factors.

Each institute should evaluate its own geometrical uncertainties and variations as these depend on clinical procedures, level of skill, *etc.* Evaluation should be representative of routine clinical practice. Uncertainties and variations should be investigated for each patient group (*e.g.*, set-up error), but should also be considered for each individual patient (*e.g.*, respiratory motion). In deciding on the margin to be allowed between OAR and PRV, all uncertainties should be taken into account.

For reporting, it is recommended that, as for the PTV, the PRV be described by including the size of the combined margins of the OAR in different directions. The delineation of the PRV margin should not be compromised even if it overlaps with another PRV, PTV, or OAR.

5.2.3 Remaining volume at risk (RVR)

The volume that is (i) within the imaged region of the patient, and (ii) outside all delineated OARs and CTVs should be identified as the ‘remaining volume at risk’ (RVR). Doses to the RVR should be reported in addition to the doses to specifically-delineated volumes of interest (Section 5.3.1) in order to ensure that attention is paid to all tissues, and not just a selected subset of them. For example, there could be unsuspected regions of high dose within the patient that would go undetected if the RVR were not explicitly evaluated. In addition, the dose to the RVR can be useful in estimating the risk of late effects such as carcinogenesis.

5.3 GENERIC GEOMETRIC TERMS

5.3.1 Volume of interest (VOI)

The VOI is a generic term that can be used to refer to any volume that needs to be identified. The GTV, PTV, and OAR are examples of specifically-named VOIs.

Sometimes the delineation of volumes is useful for technical reasons, *e.g.*, to identify one or more volumes surrounding the PTV to guide dose fall-off in an optimization procedure; or to identify sub-regions of a PTV to allow the patching of proton beams (*i.e.*, the treatment of one part of a target volume by one beam and the remaining part(s) by another beam or beams). The term ‘VOI’ should be used for these volumes, qualified by its use, *e.g.*, ‘VOI (posterior patch for PTV-T1)’.

5.3.2 Target volume (TV)

The term ‘target volume’ has largely been replaced by the more specific terms GTV, CTV, and PTV. However, it is sometimes necessary to refer to the general category of VOIs that are associated with the tumor. In

such a situation, it is permissible to refer to the general term ‘target volume’. It would not be correct to state, say, ‘a mean dose of 75 Gy (RBE) was delivered to the target volume’; rather, one should use the specific term, as in ‘a mean dose of 75 Gy (RBE) was delivered to the PTV’. However, it would be permissible to state, for example, that ‘all target volumes must be delineated before planning can proceed’.

5.3.3 Surface of interest (SOI)

It is sometimes necessary to specify what happens on the surface of a VOI or on a specified curved or planar surface, *e.g.*, to report the dose to the skin, to the surface of the spinal cord, or the dose distribution received by the surface of the rectum (see Section 5.2.1). In such a circumstance, the surface can be designated a surface of interest (SOI). An SOI has no thickness, although in practice it is likely to be represented by the voxels that lie closest to it.

5.3.4 Point of interest (POI)

It is often useful to designate points in space (not necessarily within the patient volume, and not necessarily representing anatomic landmarks). When needed, these can be referred to as points of interest (POIs). Examples of such POIs are:

Internal reference points. These are anatomical landmarks (*e.g.*, bony structures, gas-filled cavities, or surgical clips), which can be used for localization of the GTV, CTV, and OARs and for accurate setup at the imaging unit, simulator, and treatment unit. Often separate reference points must be used for different beams and if there is more than one GTV or CTV.

External reference points. These are palpable or visible points located on or near the surface of the body or on the surface of immobilization devices that fit closely to the body contour (*e.g.*, face masks, bite blocks, and shells). As external reference points, one can also use skin markings or alignment tattoos that are reproducibly related to the body as a whole (*e.g.*, skeletal structures).

ICRU reference point. A particular point of interest is the so-called ICRU reference point introduced in ICRU Report 50 (ICRU, 1993b). It is a point selected according to the following general criteria:

- (1) the dose at the point should be clinically relevant;
- (2) the point should be easy to define in a clear and unambiguous way;
- (3) the point should be selected where the dose can be accurately determined;
- (4) the point should be selected in a region where there is no steep dose gradient. Its use is discussed in Section 5.6.3.

5.4 NOMENCLATURE

Often there are multiple target volumes and, in such situations, a nomenclature (naming convention) is needed. It should be unambiguous, clear, and, where possible, provide insight into the nature of the object being named.

Previous ICRU reports (*e.g.*, ICRU 1993b; 1999; 2004) have addressed the issue of target volume naming conventions. However, because of the increasing complexity of dose prescription in proton beams and other modern therapies, a further clarification is given here, primarily in order to facilitate the distinction between multiple-nested target volumes and multiple spatially-separated target volumes. It is recommended that:

- nested target volumes be labeled with the extensions ‘1’, ‘2’, *etc.*, with the outermost volume being designated ‘1’ (*e.g.*, GTV-1, GTV-2, …, or GTV₁, GTV₂, …);
- spatially-separated target volumes be labeled with the extensions ‘A’, ‘B’, *etc.* (*e.g.*, GTV-A, GTV-B, …, or GTV_A, GTV_B, …)

Alternatively, for nested target volumes, a dose-based nomenclature can be employed whereby each target volume is qualified by a nominal RBE-weighted absorbed dose [*e.g.*, GTV-48 Gy (RBE), GTV-70 Gy (RBE), … or GTV_{48Gy (RBE)}, GTV_{70Gy (RBE)}, …]. The use of this alternative nomenclature has the virtue that it conveys more directly information useful for planning, because different doses are generally planned for different target volumes. However, as target volumes are generally created before planning the treatment, it has the disadvantage that the target volumes would ideally need to be renamed should the iterative planning process (see Section 10.2.2) require a change in the target volume dose(s). Additional qualifiers can be added to these names, as described in Section 5.4.4.

Because the naming of the various VOIs can be rather complex, it is recommended that, for each patient, a drawing be provided to document the relations between the defined VOIs (unless these relationships are self-evident).

5.4.1 Multiple GTVs, CTVs, and PTVs

The examples that follow illustrate the nomenclature and are schematically illustrated in Fig. 5.3 (both alphanumeric- and dose-based nomenclatures are shown in Fig. 5.3, but, for simplicity, only the alphanumeric-based nomenclature is used in the following sub-sections). Of these examples, those of Sections 5.4.1.1 and 5.4.1.2 are the most common,

but the more complex situations described in Sections 5.4.1.3–5.4.1.6 are often encountered.

5.4.1.1 One GTV plus a surrounding volume intended to receive the same dose

In this case, there is a single GTV, and a single CTV and a single PTV are associated with it as illustrated in Fig. 5.3a. The CTV can be identical with the GTV or it can include allowance for undetected disease that is intended to receive the same dose as the GTV.

5.4.1.2 One GTV plus a surrounding volume intended to receive a lower dose

At first glance, the case of a single GTV plus a volume of possible microscopic (*i.e.*, not grossly observable) disease appears the same as the preceding example. However, in this case, the outer region is intended to receive a lower dose, perhaps because it has only a small probability of harboring microscopic disease. For example, it might be intended to deliver a dose of, say, 70 Gy (RBE) to the inner region and a dose of 48 Gy (RBE) to the outer region.

The inner region that is intended to receive the higher dose will include the GTV, and it might also include an allowance for undetected gross disease that is intended to receive the same dose as the GTV. The entirety of this inner region would be defined by a CTV, and the outer region intended to receive a lower dose would be defined by a different, larger CTV. The formal way of describing this situation is to identify the outer region as CTV-1, and to identify the region including the GTV and possible undetected gross disease as CTV-2. The GTV can be identified as GTV-2 as it is associated with CTV-2. Each of these CTVs would then be associated with a corresponding PTV.

Often in such a situation, however, no undetected gross disease is suspected; CTV-2 is coincident with GTV and the higher dose is intended to be delivered to the GTV without extensions. In such a situation, a shorthand prescription such as ‘a RBE-weighted dose of 70 Gy (RBE) to the GTV and 48 Gy (RBE) to the CTV is to be delivered’ would be permissible.

5.4.1.3 No GTV

Figure 5.3c illustrates the nomenclature in the case in which there is a CTV, but no underlying GTV, in one location. This would be the case, for example, if the surgical bed after complete resection were to be irradiated.

5.4.1.4 Two spatially separated GTVs

Figure 5.3d illustrates the case of two spatially-separated GTVs: as, for example, in the case of a

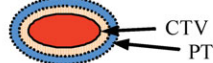
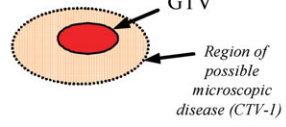
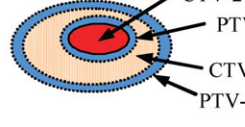
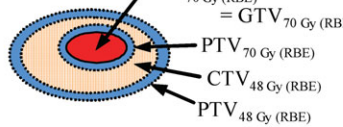
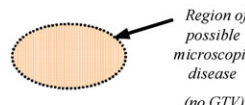
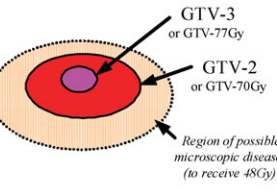
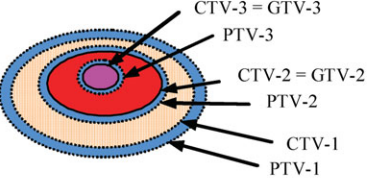
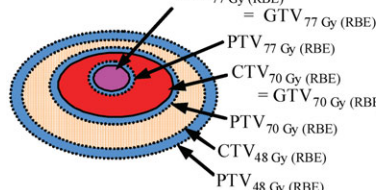
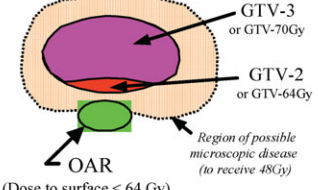
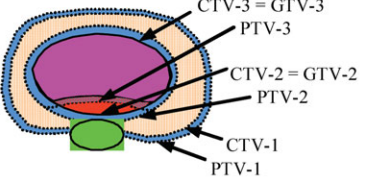
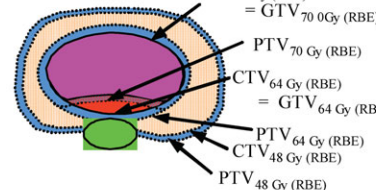
	GTV(s)	CTV(s) and PTV(s)	
		Alphanumeric nomenclature	Dose-based nomenclature
(a)			
(b)			
(c)			
(d)			<i>Use of dose-based nomenclature difficult because more than one GTV, which may receive the same dose</i>
(e)			
(f)			

Figure 5.3. Several scenarios schematically illustrating naming conventions for GTVs, CTVs, and PTVs. Both numerical and dose-based nomenclatures are illustrated. (a) Single GTV; (b) a GTV and surrounding region of possible microscopic (*i.e.*, sub-clinical) disease; (c) a region of suspected disease without gross tumor (*e.g.*, a surgical bed); (d) two spatially separated GTVs; (e) two nested GTVs with the inner one intended to receive a boost dose, plus a surrounding region of possible disease; (f) a neighboring OAR requiring a reduced dose to the tumor in its neighborhood, plus a surrounding region of possible disease. The PRV surrounding the OAR is not shown for reasons of clarity. The RBE-weighted absorbed doses shown in this figure are for purposes of illustration only and would be replaced by the doses relevant to the particular case.

head and neck tumor with a palpable neck node. In such a case, the GTVs are named GTV-A, and GTV-B, respectively, and their corresponding CTVs and PTVs are labeled CTV-A, CTV-B, PTV-A, and PTV-B, respectively, with the obvious extension to the case of more than two GTVs.

It can be useful, for planning purposes, to delineate the union between two or more VOIs so that the dose distribution to the two volumes can be planned and evaluated together. An example is the case in which two CTVs, CTV-A, and CTV-B, overlap and the same dose is desired to be given to each. The union of two such volumes can be referred to as CTV-AB.

5.4.1.5 Two nested GTVs plus a region of possible microscopic disease

Figure 5.3e illustrates the nomenclature in the case in which there are two nested GTVs, with the inner one intended to receive a boost dose, plus a surrounding region of possible microscopic disease. In all, then, there are three regions intended to receive three different dose levels. Formally, a CTV is associated with each of the three regions, but practically, CTVs are likely to be coincident with the GTVs for the two inner regions. In describing such a situation, it would be permissible to omit

mention of the two inner CTVs (data not shown in Fig. 5.3e). All nested GTVs should have at least an associated PTV. The extension to multiple inner GTVs receiving boost doses would require the identification of target volumes with names like GTV-3A, GTV-3B, *etc.*, together with their associated CTVs and PTVs.

5.4.1.6 Reduced tumor dose in a region closely adjacent to an OAR

Figure 5.3f illustrates the case in which a reduced dose is to be given to the part of the target volume that abuts a sensitive OAR and so is divided into two parts with different dose prescriptions (see Section 5.1.4.3). This situation is topologically identical to the boost example illustrated in Fig. 5.3e. It differs only in that the region to receive the ‘boost’ dose is much larger.

5.4.2 Multiple OARs and PRVs

Usually, several OARs are delineated. These could, in principle, be designated OAR-1, OAR-2, *etc.*, and their corresponding PRVs can be named PRV-1, PRV-2, *etc.* However, it is much more helpful to name the OAR according to the anatomic entity it represents, in which case one can have OARs such as ‘prostate’, ‘left kidney’, *etc.*, with the corresponding PRVs being named PRV (prostate), PRV (left kidney), *etc.*

5.4.3 Number of RVRs

Multiple RVRs do not exist. As the RVR represents the volume within the patient in which no anatomic structure has been delineated, it follows that there can be only one RVR.

5.4.4 Qualification of geometric terms

Not infrequently, one wishes to associate one or more pieces of qualifying information with a geometric term. For example, there might be several imaging studies, each one of which indicates an apparently different extent of disease, and, based on these studies, a decision must be made as to what GTV should be treated. In such a case, one would identify a GTV for each imaging study, qualified by the type of study, plus an overall GTV used to plan the treatment.

It is recommended that qualifying information be placed within parentheses immediately following the name of the geometric term and that sufficient information be included as is needed for clarity. For example, one might write: GTV(PET), GTV(contrast CT), GTV(T2-weighted MRI), *etc.* No recommendation is made as to the specific form of the qualifying information. However, if the meaning of the nomenclature used could be unclear, it should be explained. If the

volume to be treated is derived by synthesizing information from several studies with which several GTVs have been delineated, say, GTV(PET) and GTV(contrast CT), then the volume to be treated should be termed simply GTV. If there were two or more spatially separated GTVs, then they could be qualified as GTV-A(CT), GTV-B(PET), *etc.*

5.4.4.1 Tumor, nodal, or metastatic basis for a target volume

There is a value, as emphasized in ICRU Report 71 (ICRU, 2004), in indicating whether a given GTV or CTV represents the primary tumor, or grossly involved nodes, or grossly visible metastases. As that report stated ‘Adding the letters T, N, or M to identify the volumes might better clarify their clinical significance (compared to the identification by numbers only, as used in ICRU Reports 50 and 62)’. For this purpose, that report proposed the nomenclature GTV-T, CTV-T, CTV-N, *etc.*, and CTV-N1, CTV-N2, *etc.* in the case of multiple spatially-separated CTVs. While this nomenclature is unambiguous, and remains entirely valid, the general method for including qualifying information presented in Section 5.4.4 is preferred. It allows the use of names such as CTV(N), CTV-1(N), $PTV_{D_{RBE}} = 70\text{ Gy (RBE)}$ (T), *etc.*, and leaves room for further qualifying information such as GTV [M, PET, 50 Gy (RBE)] for a region of metastatic spread identified by PET and intended to receive a dose of 50 Gy (RBE).

5.5 VARIATION OF GEOMETRY WITH TIME

A patient’s geometry varies with time. Thus, the regions associated with VOIs, AOIs, and POIs vary with time. The variation can be intra-fractional and rapid, as with respiration or heart beat. It can be inter-fractional and slow, as with tumor regression or weight loss. In any event, any representation of geometry must be specific to an identified time. If studies at multiple times (*e.g.*, at different breath phases) are available, the VOIs determined from these studies should be qualified (*e.g.*, by the phase of breathing). The relationship between objects of interest, such as images or VOIs, *etc.*, associated with different times should be referred to one another through a mathematical transformation such as is accomplished by image-registration techniques.

5.6 DOSE AND DOSE–VOLUME RELATED DEFINITIONS

The RBE-weighted absorbed dose to water should be computed and reported. The ultimate description of the dose delivered to the patient is the three-dimensional distribution of absolute (not relative)

dose, superimposed upon a map of the patient's anatomy (e.g., a CT scan). However, such a description is complex and voluminous; a three-dimensional absorbed-dose distribution combined with three-dimensional anatomic information is impossible to appreciate in a static, and hence reportable, view. For this reason, a number of approaches for physical dose summarization are used. These include one-dimensional parameters such as the mean dose delivered to a VOI; and two-dimensional distributions, such as dose–volume histograms (DVHs). In addition, biophysical models such as equivalent uniform dose (EUD), tumor control probability (TCP), and normal tissue complication probability (NTCP) are sometimes employed.

The description of dose and volume poses a problem of units, as they can be expressed as absolute or relative quantities. The term 'absolute' or 'relative' should be used to indicate which of these is intended whenever confusion could arise. The units of any quantity should always be stated. The use of 'ml' or 'Gy (RBE)', for absolute volumes or RBE-weighted absorbed doses, respectively, and the percentage sign (%) for relative volumes or doses provides a sufficient clarification of whether the quantity is absolute or relative (as indicated in Section 5.6.1.1, the value to which the relative dose is normalized should be stated).

5.6.1 One-dimensional dose and dose–volume summarization

The present report introduces a nomenclature for dose–volume specifications (V_D and D_V defined immediately below). Provided DVHs are available, the

estimation of these quantities does not impose any additional computational burden; both can be read from a DVH. Some examples are shown in Fig. 5.4.

5.6.1.1 The volume receiving at least a specified dose (V_D)

The quantity V_D is the largest volume of a specified VOI that receives a dose more than or equal to the RBE-weighted dose, D_{RBE} . Both the volume and the dose can be in absolute or relative units. Which is intended is made clear by the addition of the appropriate units. For example,

- $V_{70\text{Gy (RBE)}} = 142 \text{ cm}^3$ means '142 cm³ of the VOI receives at least 70 Gy (RBE)'.
- $V_{70\text{Gy (RBE)}} = 80 \text{ percent}$ means '80 percent of the VOI receives at least 70 Gy (RBE)'.
- $V_{90\%} = 142 \text{ cm}^3$ means '142 cm³ of the VOI receives at least 90 percent of the prescribed dose'.

For relative volumes, the reference volume should be identified. Usually, it will be the entire volume of the VOI, either as imaged or, if not fully imaged, as estimated (see Section 5.2.1). For relative doses, the reference dose is taken to be the prescribed dose (see Section 5.6.3) unless otherwise stated.

5.6.1.2 The least dose received by a specified volume (D_V)

The quantity D_V is the least dose received by a volume, V , of a specified VOI. Expressed another way, the value D_V indicates that a volume V of a VOI receives at least a dose equal to D_V . Both the dose and the volume can be in absolute or relative units.

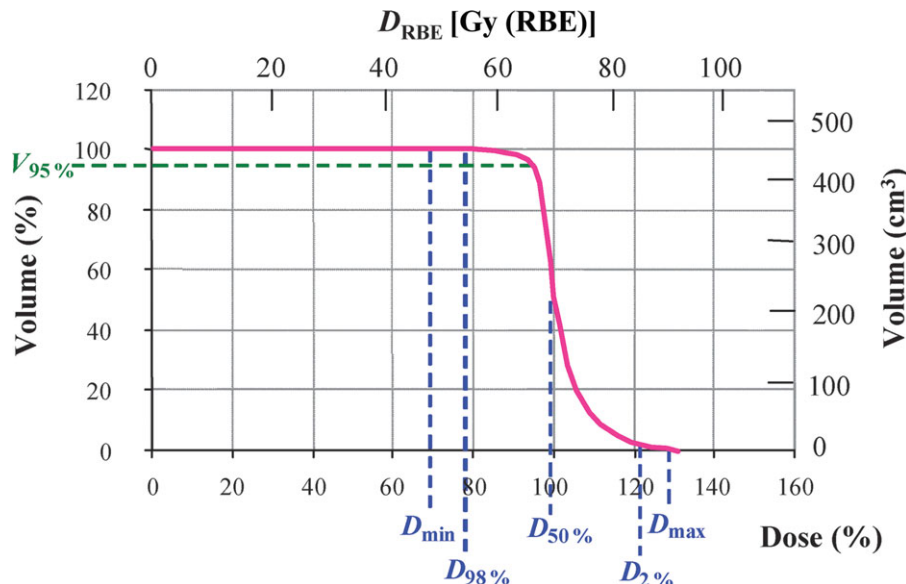


Figure 5.4. A typical dose–volume histogram display, illustrating the use of dual axes (relative and absolute values) for both the dose and volume dimensions (unfortunately, most commercial treatment planning systems do not support this feature), and how a number of volume and dose statistics can be read off from a DVH. $D_{50\%}$ is identical to D_{mean} , and D_{min} and D_{max} are identical to $D_{100\%}$ and $D_{0\%}$, respectively.

ICRU 2015 -- All rights reserved.

Which is intended is made clear by the addition of the appropriate unit to numbers. For example,

- $D_{142\text{ml}} = 70 \text{ Gy (RBE)}$ means ‘at least 70 Gy (RBE) is delivered to 142 ml of the VOI’.
- $D_{80\%} = 70 \text{ Gy (RBE)}$ means ‘at least 70 Gy (RBE) is delivered to 80 percent of the VOI’.
- $D_{142\text{ml}} = 90 \text{ percent}$ means ‘at least 90 percent of the prescribed dose is delivered to 142 ml of the VOI’.

Relative doses and volumes should follow the same rules as for V_D as described in Section 5.6.1.1.

5.6.1.3 Other dose measures

There are a number of other dose-specifying parameters, generally specific to a particular VOI (e.g., the PTV) that can be used to guide or report a treatment. These are the following:

- D_{mean} : the mean dose delivered to the specified VOI. D_{average} can also be used.
- D_{median} : the median dose delivered to the specified VOI. This parameter is used primarily because of the fact that it is easy to estimate, as it can be read directly from a DVH as $D_{50\%}$ (see Fig. 5.4). However, if one wishes to use a single number to characterize the dose distribution, there are radiobiological arguments in favor of using the mean dose for that purpose (Brahme, 1984). This dose statistic is not as readily available as it cannot be read off directly from a DVH (it can, though, be straightforwardly calculated from a DVH).
- D_{min} : the minimum dose delivered to the specified VOI. D_{min} is equivalent to $D_{100\%}$.
- $D_{\text{near-min}}$: the use of $D_{98\%}$ is sometimes used to indicate the near-minimum dose because artifacts in the calculation or display process can yield misleadingly low values of $D_{100\%}$. $D_{98\%}$ can be identified as the ‘near-minimum’ dose.
- D_{max} : the maximum dose delivered to the specified VOI. D_{max} is equivalent to $D_{0\%}$.
- $D_{\text{near-max}}$: the use of $D_{2\%}$ is sometimes used to indicate the near-maximum dose because artifacts in the calculation or display process can yield misleadingly high values of $D_{0\%}$. $D_{2\%}$ can be identified as the ‘near-maximum’ dose.

5.6.2 Two-dimensional dose–volume summarization

5.6.2.1 Two-dimensional dose displays

The display of dose on a two-dimensional plane within the three-dimensional patient is a very common way of inspecting a three-dimensional distribution. However, a single image provides only a sampling, rather than a summarization, of the dose distribution. Nevertheless, the inspection of several

well-chosen two-dimensional sections can give a good appreciation of the three-dimensional dose distribution. Of particular help is the inspection of orthogonal views, such as transverse, sagittal, and coronal views, side by side.

5.6.2.2 Dose–volume histograms (DVH)

A cumulative DVH is a graph of the volume of a specified VOI that receives at least a given dose as a function of that dose, *i.e.*, of V_D versus D (Chen, 1988; Drzymala *et al.*, 1991; Shipley *et al.*, 1979). A differential DVH is an alternative, but less widely used, representation of the same information. It is a histogram of the volume receiving a given dose within a specified, generally small, dose interval, as a function of that dose.

Both forms of DVH can employ either relative or absolute volumes, and relative or absolute doses. It is recommended that two axes be drawn for volume and two for dose, giving respectively, the relative and absolute values of these variables, as illustrated in Fig. 5.4. The DVH is a helpful quantitative tool to summarize the dose distribution to a given VOI. It suffers from the disadvantage that all spatial information is lost. It is recommended that DVHs be prepared for all specifically identified anatomic VOIs of clinical interest, and for the RVR (see Section 5.2.3).

For the RVR, as it can be a large volume of perhaps several liters, and as hot spots can cover only a relatively small volume, it is recommended that its DVH, if dual axes are not available for the display, use the absolute volume and dose, not the relative volume or dose.

5.6.2.3 Dose–area histograms (DAH)

By analogy with DVHs, dose–area histograms (DAHs) can be computed. A cumulative DAH is a graph of the area of a specified SOI that receives at least a given dose as a function of that dose.

5.6.3 Prescribed dose

The ‘prescribed dose’ (or, equivalently, the ‘prescription dose’) is a dose whose value can be used as a reference when prescribing a treatment, and when evaluating the dose distribution achieved. It is valuable, for example, as the reference dose in presenting relative dose distributions, or in computing relative doses for a DVH (see Section 5.6.2.2), in which case, a relative dose of 100 percent would correspond to the prescription dose.

In previous ICRU Reports (ICRU 1993b; 1999; 2004), the prescribed dose was represented by the ‘ICRU Reference Dose’, which is the dose to be delivered to the so-called ‘ICRU Reference Point.’ This usage had the great benefit of simplicity. However, modern radiotherapy has moved towards

a volumetric approach in prescribing and assessing dose, largely because it is uncommon to deliver a completely uniform dose to the entire PTV. For example, it is common to use a dose–volume prescription, *e.g.*, that the entire PTV is required to receive at least 95 percent of the stated prescription dose. The prescription dose, therefore, is a reference dose that can be the dose at the ICRU Reference Point, but is not necessarily so.

5.6.3.1 Prescribed dose for multiple PTVs

It is not uncommon to have nested PTVs (see, for example, Fig. 5.3b and d–f). In this case, the physician will wish to prescribe a different dose level for each PTV. For example, one might wish to prescribe 48 Gy (RBE) for PTV-1, 70 Gy (RBE) for PTV-2, and 77 Gy (RBE) for a small boost region, PTV-3. In such a case, one can speak of a ‘prescribed dose for the particular volume’ and write it ‘prescribed dose (PTV-1)’, ‘prescribed dose (PTV-2)’, *etc.*

5.6.3.2 Prescribed dose for multiple treatment segments (segment dose)

In the example presented in Section 5.6.3.1, the three PTVs could be irradiated simultaneously; for example, by employing non-uniform fields as with IMPT. Frequently, however, what is done is to deliver the treatment in three segments [see Table 10.1 (note 8)] with, for example, the first segment prescribed to deliver 48 Gy (RBE) to PTV-1; the second segment prescribed to deliver an additional 22 Gy (RBE) to PTV-2; and the third segment a further 7 Gy (RBE) to PTV-3. In such a situation, one can speak of the ‘segment dose’. This is the incremental dose delivered in a given segment of the treatment. In the example just given, the segment dose for segment one would be 48 Gy (RBE); for segment two, 22 Gy (RBE); and for segment three, 7 Gy (RBE). The segment dose can be used as a reference dose in the prescription. For example, in the current case one might prescribe the dose for segment two as ‘PTV-2 shall receive at least 95 percent of the prescribed segment dose’.

5.6.4 Relative dose

For all forms of dose reporting, if the dose is presented as a relative rather than absolute value, a reference dose (to which the dose is considered relative) must be chosen. It is recommended that the reference dose be specifically identified, unless it is completely clear from the context. It would be usual that the reference dose would be the prescribed dose, although in some circumstances the segment dose might be used.

5.6.5 Treated volume

Because of the limitations of the irradiation techniques, the volume receiving the prescribed dose might not match the PTV; it might be larger (sometimes much larger) and in general more simply shaped. This leads to the concept of treated volume.

The treated volume is the tissue volume that (according to the approved treatment plan) receives at least the RBE-weighted dose selected as the minimum dose to the PTV (or some specified percentage of the PTV), and specified by the radiation oncology team as appropriate to achieve tumor eradication or palliation, within the bounds of acceptable complications. In proton therapy, $D_{98\%}$ could be selected to determine the treated volume.

The treated volume is the volume enclosed by the isodose surface corresponding to that dose level. When reported, the value of the isodose selected to define the treated volume, should be quoted relative to the prescribed dose (see Section 5.6.3) or in absolute terms.

It is important to identify the shape, size, and position of the treated volume in relation to the PTV for different reasons. One reason is to evaluate causes for local recurrences (inside or outside the treated volume). Another reason is to evaluate and interpret side effects.

5.6.6 Conformity index (CI)

The conformity index (CI) is defined as the ratio of the treated volume to the PTV. Ideally, the treated volume should totally encompass the PTV. If this is not the case, the percentage of the PTV included in the treated volume should be reported.

The CI can be used as part of the optimization procedure, as was proposed by Knöös *et al.* (1998) and van’t Riet *et al.* (1997). However, it is recognized that when optimizing the CI (as close as possible to unity), other optimization parameters might deteriorate, *e.g.*, the size of the irradiated volume or the dose homogeneity in the PTV.

5.6.7 Irradiated volume (at a specified dose)

The irradiated volume is the tissue volume that receives a dose considered significant in relation to normal-tissue damage. The dose level should be explicitly stated, *e.g.*, irradiated volume ($V_{D=25\text{Gy (RBE)}}$).

If the irradiated volume is reported, the significant dose must be explicitly expressed either in absolute values or relative to the prescribed dose to the PTV. The irradiated volume depends on the treatment technique used.

6 TREATMENT PLANNING

6.1 INTRODUCTION

Treatment planning is the process of simulating a number of delivery strategies for a radiation treatment and choosing the best one to use for treatment. The simulation of the patient is based on a reconstruction of the patient's normal anatomy and tumor(s) derived from imaging studies supplemented by delineation of target volumes and organs at risk (OARs). A *plan* consists of an ensemble of beams, together with their weighting factors. The beam properties and weights can be generated manually, automatically, or semi-automatically. The dose within the patient can be calculated for any arrangement of beams using physical models of the beam properties. The resulting dose distributions within the patient can then be compared among rival plans. The judgement of which plan is best is complex, and the experience of the treatment planner and radiation oncologist figures prominently. As described below, this judgement can be aided by methods of dose display and comparison, of dose summarization, and by computation of several model-based measures of dose impact such as tumor control probability (TCP), normal-tissue complication probability (NTCP), and equivalent uniform dose (EUD) (see Section 6.7.3). In intensity-modulated radiation therapy (IMRT), the generation and evaluation of plans is, because of the computational burden, necessarily performed automatically by computer, often with manual iteration of the treatment aims at improving the plan further.

In planning treatments (uniform intensity or intensity modulated) with protons as compared with conventional photons, the features in common far outweigh those that are different. In Section 6.2, some of the more important differences are briefly described—they are treated more fully in the following subsections or elsewhere in the present report. The report concerns itself primarily with proton-beam therapy. However, the present section is equally relevant to light-ion (*e.g.*, carbon or neon) therapy, apart from Section 6.2.3.4, in which relative biological effectiveness (RBE) is discussed.

6.2 WHAT IS DIFFERENT ABOUT PLANNING PROTON-BEAM THERAPY?

The differences between planning proton-beam therapy and photon-beam therapy¹ derive from the differences in the physics of protons and photons, namely,

- that protons have a finite and controllable (through choice of energy) penetration in depth;
- that the penetration of protons is strongly affected by the nature (*e.g.*, density) of the tissues through which they pass, while photons are much less affected (density changes generally give rise to only small intensity changes, except for the lung). Therefore, heterogeneities are much more important in proton-beam therapy than in photon-beam therapy;
- the apparatus for proton-beam delivery is different, and its details affect the dose distributions.

6.2.1 Heterogeneities

Because of the influence of heterogeneities, a map of heterogeneities along the beam path must be made and compensated for (to the extent feasible); finally, the dose distributions must reflect the remaining effects of the heterogeneities. The map of heterogeneities is built up from fine-resolution computed tomography (CT) images converted to water-equivalent densities (see Section 6.4.6.1) in order to compute three-dimensional dose distributions.

The resulting requirements for planning proton-beam therapy imply the following:

- to ascertain the CT Hounsfield number to water-equivalent density conversion table (Section 6.4.6.1);
- to compensate, either physically or virtually, for heterogeneities, including metallic implants when present (Section 6.4.6.2);

¹J. Adams, M. Moyers, P. Petti, S. Rosenthal, B. Schaffner, A. N. Schreuder, and L. Verhey contributed significantly to this section.

- to be aware of, and mitigate the effect of, possible hot-and-cold spots due to lateral scattering effects (Section 6.4.4);
- to take into account uncertainties associated with possible misalignment of the compensator with the patient's tumor, organs, and tissues;
- to take into account uncertainties in proton-beam penetration. For example, it is common practice to avoid, when possible using beam directions for which there would be a tight margin between the planning target volume (PTV) and a sensitive structure lying distal to it (e.g., the spinal cord). One center has a rule that at most one of three beams may allow a tight margin in depth.

6.2.2 Beam-delivery techniques

In proton-beam therapy, a number of different beam-shaping and delivery techniques can be used, and these techniques strongly affect the selection of beams and their resulting dose distributions. The planning software must therefore be able to simulate all techniques of proton-beam delivery available to the user. For example, it might be required to compute the dose distributions of the following:

- | | |
|---|--|
| • Scattered beams | Generally designed to produce a near-uniform dose distribution within the target volume for each beam |
| • Scanned beams
(continuous or discrete) | Can either produce a near-uniform dose distribution or, more usually, a highly non-uniform dose distribution within the target volume for each beam—and are thus suitable for use in intensity-modulated proton therapy (IMPT) |
| • Wobbled beams
(a special case of beam scanning, using relatively wide finite pencil beams) | Generally producing a near-uniform dose within the target volume for each beam |

6.2.3 Single beams

6.2.3.1 Inverse beam design

A fundamental difference between planning with protons and photons is that, in current practice, proton planning has aspects that are *inverse*. For example, on the basis of the knowledge of the target volume and normal anatomy, usually a one-pass calculation is made of the beam settings (e.g., maximum range) and of the real or virtual compensator design (which provide the desired three-dimensional shape of the dose distribution, both laterally and in depth).

6.2.3.2 Selection of beam directions

The finite penetration of protons allows 'distal blocking'—the analogy in depth of the lateral blocking provided by an aperture. As a consequence, with protons, one only needs to be concerned about entrance tissues, except when the beam abuts a critical sensitive structure. With photons, however, one needs to be concerned about both entrance and exit tissues in choosing a beam direction. As a result, a wider range of desirable beam directions is usually available to the planner of proton-beam therapy. In this connection, the use of non-coplanar beam directions, such as vertex beams in treatments of the brain and base of skull, is feasible and often found to be quite advantageous. With photons, in part because of the need to employ near-opposing (or otherwise paired) beam directions, non-coplanar beam arrangements are unusual.

Picking 'good' beam directions is more necessary in proton-beam therapy because of the following:

- the desire to avoid, if possible, beam directions that pass through complex or high-Z heterogeneities, or that lie tangent to a tissue–air interface (see Section 6.5.1). If the latter is unavoidable, the use of a few beams only slightly separated in angle can mitigate the dose perturbations (Goitein, 1977);
- the desire to angle a beam so as to achieve the maximum spatial separation between the PTV and distal critical OARs;
- the desire, due to lack of skin sparing, to avoid superficial or shallow sensitive structures.

The consequence is that, in contrast with IMRT with x rays (IMXT), where one is often able to use equally-spaced angles for the beams, one would select the angles more judiciously for protons.

6.2.3.3 The PTV

The PTV is a volume that is based on an underlying clinical target volume (CTV) to which margins are added to account for internal and external uncertainties in the location of the CTV relative to the radiation beam(s). With protons, different margins are generally required in the depth dimension than in the lateral directions. The consequence is that, if the PTV is to be used to establish the dose margins about the CTV in all directions, a different PTV would have to be designed for each beam direction. In some centers, therefore, the beam is designed relative to the CTV and the implementation of dose margins is built into the beam-design algorithm. However, it is recommended that a PTV always be

delineated as it is needed for dose recording purposes. These matters are discussed in detail in Section 5.1.4.4.

6.2.3.4 The proton RBE

As discussed in Section 2, the RBE-weighted absorbed dose should be used in treatment planning. If, as is usually the case, the treatment-planning program does not take into account the distinction between absorbed dose and RBE-weighted absorbed dose, the planner must do so. Unless otherwise stated, all references here to dose refer to RBE-weighted absorbed dose.

6.2.3.5 The design of beam-modifying devices

The design and placement of the aperture (block) and compensator is more complicated for protons than for photons. First, it must be ascertained that the design of these devices is achievable in practice (e.g., that there is not too abrupt a change in compensator thickness, nor too small a feature in the aperture periphery). Secondly, particular attention must be paid to the distance of closest approach of the aperture and the compensator to the patient, because of the following:

- an air gap between the compensator (or any upstream degrader such as a range shifter) increases the beam penumbra and leads to less satisfactory resolution in compensating for fine heterogeneities. Thus, this distance needs to be minimized, even to the point of designing the compensator so that its downstream face can be placed in contact with the patient. However, mechanical interferences between the nozzle and the patient can force undesirably big air gaps, even to the point of making some beam directions infeasible.
- for reasons of edge sharpness, especially in scattered beams using double scattering that leads to a large effective source size, one wants the aperture as close to the patient as possible. As with the compensator, mechanical interferences can prevent this. On the other hand, there is a small but not negligible beam contamination that comes from protons striking the aperture on or near its edge, leading to a source of low-energy protons, an effect not too dissimilar to the electron contamination which comes from a blocking tray in a photon beam. The aperture needs to be sufficiently distant from the patient's skin surface to allow these low-energy protons to diffuse out.

6.2.3.6 Repainting

Motion of the patient's internal organs and time variation of the beam delivery in IMPT can give rise to local dose fluctuations (dose mottle) due to the so-called interplay effects (see Section 7.6.3). Beam gating on the respiratory cycle or tumor tracking (see Section 7.5) can reduce this effect, but will not eliminate it. The solution is to repaint the target applying the same beam multiple times over many respiration cycles while reducing the dose per application proportionately (see Section 7.6.3.2). This is a technically demanding requirement, but is considered a necessity wherever organ motion is appreciable (e.g., in the thorax and abdomen).

6.2.3.7 Dose algorithms

The dose algorithms in proton-beam therapy require more detailed knowledge of the beam-delivery techniques than is generally required in photon therapy, with the exception of multi-leaf collimator settings in IMXT, which share this problem.

Dose computations also tend to be more demanding of computer performance, especially for IMPT where there is about a 30-fold increase in the number of pencil-beam weights that must be adjusted and optimized.

6.2.4 Plans

6.2.4.1 Number of beams

While, generally, several beams are employed in a patient's treatment, a single proton beam can constitute a satisfactory treatment plan for a deep-seated target (e.g., a para-vertebral sarcoma) as it can give a lower entrance than target dose and no exit dose. However, for a relatively shallow-lying site such as a sacral chordoma treated from the posterior, the skin dose due to protons would be very close to 100 percent and hence, some photon component is often employed.

Typically, fewer proton than photon beams are needed to achieve a satisfactory treatment plan (Lomax *et al.*, 2004). Also, whereas photons tend to necessitate near-opposed beams to compensate for the exponential dose fall-off, or a pair of wedged fields some 90° apart, it is not necessary to use widely separated proton beams; they need only sufficient angular separation that no appreciable overlap of the beams on the skin occurs (Rutz and Lomax, 2005).

6.2.4.2 Intensity-modulated proton therapy (IMPT)

Proton therapy has long used an elementary form of IMRT through the use of beam patching. A pair of beams is designed, with one beam ‘filling in’ a portion of the target volume and the other beam intentionally blocked out. This process is easy to conceive, and can be done manually or using computer tools. There is no analogy of this technique in conventional photon-therapy planning, except in fully automated IMXT.

IMPT is a completely natural extension of broad-beam proton therapy, just as IMXT is a natural extension of conventional three-dimensional conformal radiation therapy (3DCRT). IMPT is computationally more demanding than IMXT, as one has to consider a whole additional dimension of range variability, but otherwise the principles are identical.

6.2.4.3 Imaging

While all modalities of radiation therapy make use of modern imaging techniques, historically proton-beam therapy has particularly emphasized the use of imaging. This is for three main reasons:

- proton therapy, like modern conformal photon therapy, offers additional possibilities for conformality, the delineation of target volumes in three-dimensional space is particularly crucial;
- CT imaging is generally essential for managing heterogeneities;
- proton-beam therapy tends to base patient alignment on bony anatomy, and this must be located by imaging.

In the course of planning a patient’s therapy, a number of different imaging procedures are likely to be employed, both for diagnostic purposes and, with appropriate image registration, for volume of interest (VOI) delineation. However, given the need to evaluate heterogeneities, one CT scan sequence, taken with the immobilized patient in treatment position, is usually required. This sequence is often referred to as the *planning CT*. Because the planning CT is used to compute proton path lengths for use in dose calculations, the calibration of the CT unit is of greater importance in proton-beam therapy than in photon-beam therapy. Because the presence of contrast material can lead to incorrect estimates of the proton path lengths, it is common to perform the planning CT study without contrast media. Alternatively, the Hounsfield numbers (Section 6.4.6.1) in regions containing contrast media might have to be altered to conform to the expected values in that region.

In all forms of therapy, in order to transfer the plan to the patient, the positioning of the patient must be the same for the plan design and the treatment. In proton-beam therapy, owing largely to the tendency to use bony landmarks or physician-inserted fiducial markers for patient (and hence CTV) localization (see Section 7.3.2), DRRs (digitally-reconstructed radiographs) are generally needed so that the setup radiographs obtained from a pair of x-ray tubes located in the treatment room can be verified.

6.2.4.4 Positioning accuracy, immobilization, and localization

Proton-beam therapy generally emphasizes accuracy of beam placement to a greater extent than conventional photon therapy, although modern techniques of conformal photon therapy are tending toward achieving comparable accuracy. The need for accuracy derives from the effort to take full advantage of the superior conformality of dose possible with protons, and the need for good registration between the real or virtual compensator and any heterogeneity within the patient. Placement accuracies of from 2 to 1 mm, or even less, are routinely achieved. It should be emphasized that this accuracy often has less to do with target-volume conformation (the target volumes often cannot be defined so precisely) than with the conformal avoidance of nearby sensitive normal structures, the location, and the extent of which can be more accurately determined.

To achieve such accuracies, excellent immobilization and accurate localization of the patient relative to the treatment equipment is required. The latter is usually accomplished by the localization of bony landmarks as seen in orthogonal radiographs of diagnostic quality. Also, a strategy for dealing with the remaining uncertainties needs to be developed and implemented. These matters are discussed in Sections 7 and 8.

6.2.4.5 Uncertainty analysis

The analysis of uncertainties has tended to be emphasized much more strongly in proton-beam therapy than has been done in photon-beam therapy. The management of uncertainty permeates the entire planning process in proton-beam therapy.

An example of the use of uncertainty analysis is in the design of compensators and the calculation of the maximum proton range (energy) for each beam. These matters are discussed in Section 6.4.6.2. Another example is in the management of abutting proton beams, such as in the patching

technique described in Section 6.2.4.2. Because there are uncertainties in the depth of penetration of proton beams (as well as in their lateral placement), beam ‘feathering’ is often employed, whereby the spatial location of the abutment (the patch line) is varied in space every treatment day over a cycle of three to five fractions. Beam feathering is employed for blurring the lateral edges of abutting photon beams too, but there is no analogy with the depth feathering of protons.

6.2.4.6 Target volume size

Proton-beam therapy is sometimes incorrectly thought of as being useful mainly for small tumors. Experience suggests that the dose-sparing possible with protons is likely to be most valuable for large target volumes for which sparing the remaining volume is likely to be particularly valuable. In this context, ‘large’ refers to the size of the target volume relative to the body compartment of which the target volume is part. Planners must therefore be prepared to plan large as well as small volumes, and to develop techniques for tissue sparing in such instances.

6.2.5 Quality assurance

Variations in dose with depth can be large for proton beams, and therefore quality assurance tools are generally more complex than those needed for photon beams. They have to confirm the machine performance in three dimensions, rather than in two dimensions. Especially in scanned beams, for which it may take many minutes to deliver the entire dose, it is too time-consuming to determine a dose distribution by making measurements at discrete points, and it is not possible to make measurements with a moving detector. Some form of multi-dimensional detector (at least two-dimensional, and ideally, three-dimensional) is therefore required (see Sections 4 and 9).

The process of planning proton-beam therapy is now described in greater detail in the following sections.

6.3 THE PATIENT'S ANATOMY

Even before the decision to use radiation therapy for all or part of a patient's treatment has been taken, a number of imaging studies will have been performed with primarily diagnostic intent. These images are vital, too, for the planning of the radiation treatment as they give essential information as to the anatomic site and extent of disease and

the location of nearby uninvolved normal tissues. Such studies are the following:

- volumetric CT (*i.e.*, multiple thin slices)—with and/or without contrast;
- magnetic resonance imaging (MRI);
- positron emission tomography (PET);
- ultrasound (for some specialized applications);
- other studies appropriate to the situation.

However, to plan radiation therapy, it is important that the information about the patient's anatomy be spatially accurate with respect to the way the patient will be positioned for therapy. For proton-beam therapy, the mapping of tissue densities must also be accurate. In general, this means that a planning CT [a series of CT scans taken with the patient in the immobilization device(s) to be employed, preferably without contrast medium] is needed. Information from other imaging studies may then be superimposed on the planning-CT study through some form of image fusion (either by automatic means, or by a trained observer). This information is further elaborated by delineation of VOIs relating to both tumor and normal tissues. All together, these build up a three-dimensional model of the patient, which is spatially accurate and provides a sufficiently accurate map of the densities of all tissues that may potentially be traversed by protons. In order to maximize resolution, the scanner's field of view should be the minimum possible that nevertheless encompasses any material that could potentially be traversed by the proton beams, including the skin surface where any beam might enter.

In the delineation of normal tissues, all OARs that could potentially be even partially intersected by any radiation beam should be fully imaged and delineated. In addition, the volume within the patient that excludes any delineated PRVs (or OARs, if PRVs are not delineated) and the PTV(s) should be identified as the ‘remaining volume at risk’ (RVR). The RVR is of interest when evaluating plans, as it, too, constitutes irradiated normal tissue and should be examined for regions within it receiving undesirably large doses that might otherwise go undetected.

In some special cases, such as the planning of proton-beam therapy for ocular tumors (see Section 6.11.1) or the treatment of very superficial disease without significant heterogeneities in the beam path(s), a CT study may not be required. Nevertheless, an accurate three-dimensional model of the relevant portion of the patient's anatomy is essential for planning.

6.4 HETEROGENEITIES

6.4.1 Introduction

In heterogeneous media, proton-beam dose distributions are more complex, and often substantially more so, than in a homogeneous medium such as water. Heterogeneities cause two main effects on protons as they penetrate the medium: alterations in the range and alterations in the extent of lateral scattering. In what follows, the dosimetric impacts of these two effects, relative to what occurs in a homogeneous medium (usually water), and for beams with uniform-intensity spread-out Bragg peaks (SOBPs), are discussed.

Given the presence of heterogeneities proximal to, or within, the target volume, it is necessary to take them into account when designing the treatment beams. This could involve calculating their influence and, with very few exceptions, the design of some form of beam modification to correct for the range modification produced by the heterogeneities. This is usually done by means of a real or virtual compensator (as discussed below).

Three situations are discussed in the following sections: (i) a block of material of density different from the rest of the medium that intercepts the entire beam; (ii) a block of material of density different from the rest of the medium that intercepts only part of the beam in the lateral direction; and (iii) complexly structured heterogeneities.

6.4.2 Interactions of protons in matter

The physics of the interactions of protons with matter has been discussed in detail in ICRU (1998) and briefly in Section 3.4.1 of the present report. Here, some general features of the two largest effects are recalled, namely, (i) loss of energy through interaction of protons with electrons, which results in protons having a finite range in matter²; and (ii) multiple scattering of protons through Coulomb interactions with nuclei, which cause a proton's path to deviate from a straight line. The description here is confined to protons in the therapeutic energy range from about 30 to 250 MeV; at other, particularly lower, energies some of the statements below no longer apply.

6.4.2.1 Mass thickness

It is common to characterize a sample of homogeneous material by the product of the length of the sample multiplied by its density. This quantity

is termed as 'mass thickness' or 'areal density' and has the units of grams per square centimeter. When interaction probabilities are expressed in units of mass thickness, rather than physical length, dependence on density is largely removed. The mass thickness of an object composed of slabs of different materials along directions normal to the slabs is the sum of the mass thicknesses of the individual slabs.

6.4.2.2 Energy loss

When penetrating matter, protons lose energy largely due to Coulomb interactions with the atomic electrons. For sections of material thin relative to the proton range, the mass stopping power, S/ρ , describes the average energy loss of a proton per unit mass thickness. It has a strong nonlinear dependence on the proton energy, and is linearly dependent on the ratio Z/A . Thus, the energy loss of a proton beam of a given energy in a section of material of a given mass thickness will be very similar for all materials with the exception of highly hydrogenous materials (where $Z/A > 0.5$) and elements of very high Z (where $Z/A < 0.5$).

The finite range of protons is due to their almost continuous loss of energy as they traverse the material. This allows the computation of the continuous slowing-down approximation (see Section 3.4.1) range of a proton of given energy by the integration of the reciprocal of the stopping power along its entire path. (In practice, there is a distribution of penetrations due to statistical fluctuations in the energy-loss process.) As the range is inversely related to the stopping power, the penetration of a proton beam of a given energy, expressed in terms of mass thickness, is nearly independent of the material traversed (except near the end of range, where range straggling becomes important).

6.4.2.2.1 Water-equivalent density

To take into account the dependence of range and stopping power on the composition of the material, the concept of 'water-equivalent density' is used in heavy charged-particle radiation therapy. This can be defined as follows: let the thickness of a block of some material of interest and the energy loss in the block be represented by Δt and ΔE , respectively. Then, the water-equivalent density of the material of interest is equal to the density of a block of (fictional) material of the same elemental composition as water and of the same thickness, Δt , that produces the same energy loss, ΔE , of the protons passing through it.

The water-equivalent density, ρ_{eq} , can be estimated from range-energy tables by comparing the energy

²By 'range' is meant the depth to the distal 80 percent dose level, d_{80} , in accordance with the nomenclature of Section 3.4.2.2.

loss per unit mass thickness (*i.e.*, the mass stopping power) of the material in question with the energy loss per unit mass thickness of water, ρ_{water} (at an energy in about the mid-range of the energies of therapeutic interest). Or, it can be obtained by measuring the change in residual range in water, ΔR (a positive value of ΔR implies an increase in range), of protons passing through a water tank with and without a physical thickness, t , of the material in question inserted into the water tank in the path of the protons, in which case one has

$$\rho_{\text{eq}} = \left[1 - \left(\frac{\Delta R}{t} \right) \right] \cdot \rho_{\text{water}} = 1 - \left(\frac{\Delta R}{t} \right), \quad (6.1)$$

where the mass densities, ρ , are assumed to be in units of g cm^{-3} and ΔR and t are in the same units (*e.g.*, cm). Using the concept of water-equivalent density, one may, in practical cases, make the approximation that one can substitute for a given bulk sample of heterogeneous material of varying chemical composition and mass density a geometrically identical sample that is considered to be composed of material of the same chemical composition as water, and in which the actual mass density is everywhere replaced by the water-equivalent density. This approximation will generally allow sufficiently accurate estimates of energy losses, and hence penetration depth, but it will not give correct results for other important effects such as multiple Coulomb scattering.

6.4.2.3 Multiple Coulomb scattering

In addition to losing energy as they traverse matter through interactions with orbiting electrons, protons also experience numerous Coulomb interactions with the charged nuclei of the atoms in the material (see Section 3.4.1). Each of these interactions results in a usually very small deflection of the projectile proton. However, these interactions accumulate and result in the finite deflection of a proton from a straight path. An infinitesimal pencil beam of protons will be increasingly spread out in depth by multiple Coulomb scattering.

A near-monoenergetic proton beam traversing a thickness of material small relative to its range will be scattered with an approximately Gaussian distribution of angles for which sigma (standard deviation) is termed as the characteristic scattering angle, ϑ_0 . In contrast to the energy-loss process, the scattering of a proton beam has a significant dependence on the chemical composition of the material. The relation is complicated but, to within

5 percent, ϑ_0 varies as

$$\vartheta_0^2 \propto \left(\frac{\rho t}{X_0} \right) \approx \rho t \left(\frac{Z}{A} \right) Z^{0.7}, \quad (6.2)$$

where ρt is the mass thickness of the scattering material and X_0 is the characteristic length, termed the radiation length (Mustafa and Jackson, 1981; Tsai, 1974) of the material (in g cm^{-2}). The exponent of Z was obtained empirically by a fit to tabulated radiation-length data. Equation (6.2) implies that, in terms of mass thickness, a high- Z material scatters more strongly than a low- Z material, and in terms of thickness, the dependence is more like a power of 1.7. (For this reason, high- Z materials are preferentially used when it is desired to spread out a proton beam laterally.)

6.4.3 Bulk heterogeneity intersecting the full beam

The influence of interposing a uniform slab of material of composition other than that of the surrounding medium is entirely different for a proton beam than for a photon beam. x rays experience an intensity change in the shadow of such a slab heterogeneity; protons suffer virtually no change in intensity; only a change of penetration. This difference is illustrated schematically in Fig. 1.6. That is, the effect of interposing a slab of material of composition other than that of the surrounding medium is mainly to shorten or lengthen the proton depth-dose distribution, but not affect its shape or the intensity in the high-dose region distal to the heterogeneity. Indeed, plotted as a function of mass thickness along the beam path, the dose distribution would be little affected by the interposition of the slab. This is the case whether the beam is near-monoenergetic or involves a mixture of energies as is the case, for example, in an SOBP.

The change in the range, ΔR , of a beam in such a situation (measured in units of length and not water-equivalent density) is altered by an amount given by

$$\Delta R = \frac{t(\rho_{\text{eq}}^{\text{medium}} - \rho_{\text{eq}}^{\text{slab}})}{\rho_{\text{water}}}, \quad (6.3)$$

where t is the physical thickness of the interposed slab, $\rho_{\text{eq}}^{\text{slab}}$ is the water-equivalent density of the interposed slab, and $\rho_{\text{eq}}^{\text{medium}}$ is the water-equivalent density of the surrounding medium. The mass density of water, ρ_{water} , is taken to be unity when densities are expressed in units of g cm^{-3} . If the surrounding medium is water, or has a

water-equivalent density of 1, this reduces to Eq. (6.1).

These relations hold equally when the interposed slab replaces the entire surrounding medium. They describe the change in range (relative to the range in water) when the (homogenous) medium has a water-equivalent density different from water.

The proton beam will also be affected at its edges—*i.e.*, the beam penumbra will be affected by the interposed material, as the penumbra is largely caused by upstream multiple scattering and this scattering, as indicated above, is dependant on the chemical composition of the interposed material. However, when the materials involved are limited to those found in the human body, this is a small effect and is often ignored in practice.

6.4.4 Bulk heterogeneity partially intersecting the beam

When a slab of material of a mass density different from that of the surrounding medium is interposed over only part of the beam cross-section, then, away from the interface between the two media, the beam penetration is altered in the shadow of the heterogeneity just as for the case of a fully intersecting heterogeneity, and is unchanged in the region not shadowed by the heterogeneity. However, near and in the shadow of the interface region, an additional and quite different effect takes place because of the difference in the strengths of multiple scattering in the two adjacent materials. Namely, a dose enhancement (hot spot) occurs on the low-density side, and a dose reduction (cold spot) occurs on the high-density side (Goitein, 1978b; Goitein *et al.*, 1978). This is illustrated in Fig. 6.1a for the extreme case of a parallel beam of protons impinging on an air-tissue interface. Protons reach point P from both the unscattered beam impinging on the air side (I), and from protons initially impinging on the tissue side (II), but scattered laterally toward the point P. As a consequence, point P receives a greater fluence, and hence higher dose, than if the tissue heterogeneity were absent. Point Q, on the other hand, receives no dose from protons impinging on the air side, as air scatters them hardly at all, and a reduced dose from protons initially impinging on the tissue side, because a portion is scattered out to the air side. As a consequence of these effects, dose perturbations can be as high as 50 percent as illustrated in Fig. 6.1b.

The perturbation is substantially modified if the beam has significant angular confusion, such as would be induced by overlying material. For

example, when a layer of tissue of only one-half the thickness of the tissue in a tissue-air interface is interposed above the interface, the dose perturbation is reduced to ~12 percent (Goitein *et al.*, 1978).

If one side of the interface is not air, but rather the interface is between the two materials of different scattering powers, then the perturbation of fluence, and hence dose, is much reduced, *e.g.*, in the case of a bone-tissue interface, from 50 to ~9 percent (Goitein, 1978b).

6.4.5 Complexly structured heterogeneities

In practice, the patient usually presents a complex pattern of heterogeneities; this is perhaps most extreme in the region of the base of skull where protons may be directed along extended bone surfaces, or through a complex bone-tissue-air structure like the petrous ridge or paranasal sinuses. In consequence, a complex combination of range-penetration perturbations and scattering-induced dose non-uniformities takes place. The results of such complex situations are very hard to calculate analytically, although the preceding discussion of bulk heterogeneities gives some insight into the

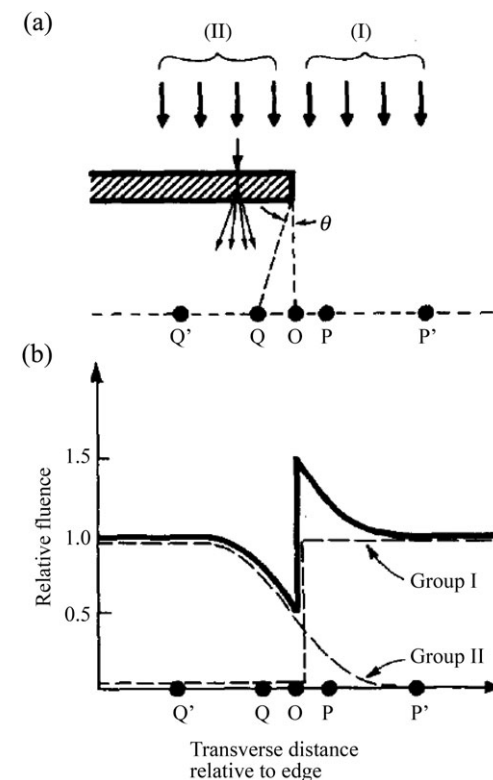


Figure 6.1. Illustration of edge-scattering effect (Goitein, 1978b; reproduced with permission). Schematic rendering of the geometry (a) and calculated fluence distribution along the dotted line of the upper figure (b). See Section 6.4.4 for discussion.

extent of the possible dose perturbations. Monte Carlo calculations (see Section 6.5.2.3) are presently the only way to obtain a reliable estimate in the case of highly complex geometries.

Figure 6.2 shows the degradation of the terminal region of an SOBP measured after passage through: (i) a relatively homogeneous region in the brain; and (ii) through highly heterogeneous regions of the base of the skull. These data demonstrate how the distal portion of the dose distribution can be substantially affected by a complex heterogeneity. The distal fall-off of the SOBP is not simply shifted in range. Rather, its slope is substantially less steep and less regular.

An uncertainty analysis, as seen in Goitein (1985) and in Section 8, can establish the confidence limits for the dose distribution. Figure 6.3 shows an example of the computed bounds for the penetration of a beam passing through the base of skull compared with the measured penetration (Urie *et al.*, 1986a). Such an analysis allows the design of beams that are assured (at a stated confidence level) to cover the target volume to full dose, with the price being that distal normal tissues receive a greater-than-desired dose.

6.4.6 Compensation for heterogeneities

6.4.6.1 Conversion from CT Hounsfield number to water-equivalent density

The advent of CT was, and remains, critical for the development of proton-beam therapy as it provided for the first time a spatially accurate mapping of the patient's anatomy together with a quantitative measurement of tissue properties. All CT values based on x-ray tomography are quoted in terms of Hounsfield numbers, H , and these measure a quantity related to the ratio of linear x-ray attenuation coefficients in the medium, μ^{tissue} , and in water, μ^{water} . Specifically,

$$H = 1000 \times \left(\frac{\mu^{\text{tissue}}}{\mu^{\text{water}}} - 1 \right), \quad (6.4)$$

The quantity H varies from -1000 for air to 0 for water and positive values for materials with greater attenuation than water. Linear x-ray attenuation coefficients are functions of electron density, atomic number, Z , and atomic mass number, A , of the material. This implies that they

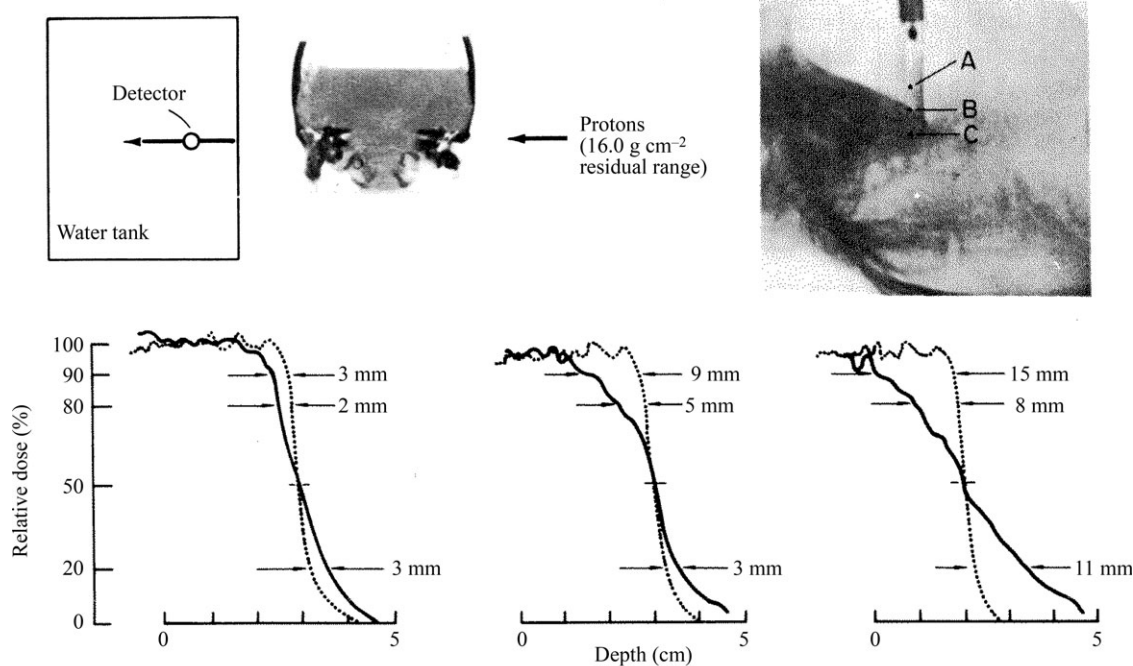


Figure 6.2. Measurement of the distal portion of the dose distribution of a spread-out Bragg peak (Urie *et al.*, 1986a; reproduced with permission). Upper left: experimental setup with the proton beam directed from the right and depth-dose measurements made in a water tank placed distal to the water-filled skull. Upper right: magnified portion of a radiograph showing the three locations for which depth-dose curves are shown. Lower panel: depth-dose curves in the shadow of point A (left graph), point B (middle graph), and point C (right graph). Point A has relatively few heterogeneities in the proton-beam path; protons passing through point C go through highly heterogeneous material, and point B is intermediate. The dotted curves show the distal portion of the depth-dose curves with the skull removed (*i.e.*, no heterogeneities).

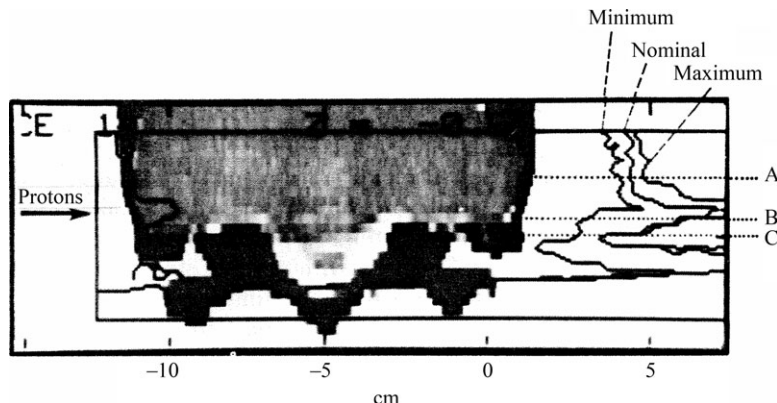


Figure 6.3. Calculated 90 percent isodose line distal to the skull of Fig. 6.2 showing the nominal and upper (maximum) and lower (minimum) bounds at the 85 percent confidence level (Urie *et al.*, 1986a; reproduced with permission). The dotted lines labeled A, B, and C correspond to the points with the same labels as in Fig. 6.2. The range of uncertainty is much less for the point A, as one would expect, because the proton beam traverses a relatively homogeneous section.

have a different dependence on the chemical composition of the medium than do proton-stopping powers. They are also, at typical diagnostic x-ray energies, fairly strong functions of the x-ray energy or energy spectrum, which means that the conversion from the Hounsfield number to the water-equivalent density must be established for each particular scanner and radiographic technique.

The theoretical relationship between proton-stopping powers and linear x-ray attenuation coefficients is complicated and, in practice, is not evaluated analytically. Rather, the relationship between the Hounsfield number and the mass stopping power of protons is derived from experiment, principally using one of two methods: direct-fit method and stoichiometric method.

6.4.6.1.1 Direct-fit method. In the simpler and more widely used approach, measurements are taken on each of a wide variety of tissue-equivalent materials, and possibly actual tissue samples, of two quantities, namely: the Hounsfield number (by measurement in a CT scanner) and the water-equivalent density (by measurement in a proton beam). When plotted against one another on a scatter plot, these data are approximately bi-linear and may be fit by a pair of straight lines (Chen *et al.*, 1979). Typically, one line covers the interval from -1000 to $+50$ Hounsfield numbers and the second line covers Hounsfield numbers above $+50$. The former range covers the soft tissues; in the latter range Hounsfield values >50 may be assumed to be caused by a mixture of compact bone and soft tissue. This method yields a calibration curve such as that shown in Fig. 6.4a. A similar approach, but using a set of three connected straight lines, has also been followed (Kanematsu *et al.*, 2003).

6.4.6.1.2 Stoichiometric method. A method proposed by Schneider *et al.* (1996) is based on the chemical composition of the test materials. The stopping power, and hence water-equivalent density, is determined using a simplified version of the Bethe–Bloch formula. The Hounsfield number is assumed to be represented by an equation with three terms corresponding to photoelectric effect, coherent scattering, and Compton scattering. Each term has a different Z dependence and includes a multiplicative constant. The goal of the calibration is to fit the equation to the measurements of the Hounsfield numbers, made in the CT scanner of concern, for a large variety of tissue-equivalent test materials of known chemical composition and to deduce the values of the three constants from the fit. Given the constants, it is then possible to predict the Hounsfield number for any other material, including tissue, of known chemical constitution. This is done for a wide variety of actual tissues and the results plotted on a chart of the water-equivalent density versus the Hounsfield number. These data points are then fitted by a series of straight lines, each of which extends over a limited range of Hounsfield numbers, and these lines provide the final conversion. Such a chart is shown in Fig. 6.4b. This approach has been verified for a number of biological tissue samples (Schaffner and Pedroni, 1998).

6.4.6.1.3 Confirmation of calibration. Confirmation of the calibration process can be obtained by means of proton radiography, in which the integrated water-equivalent density along any path through the patient can be measured, or by proton CT, in which case the local water-equivalent density at all points within the imaged volume can be measured (Schneider and Pedroni, 1995; Schneider *et al.*,

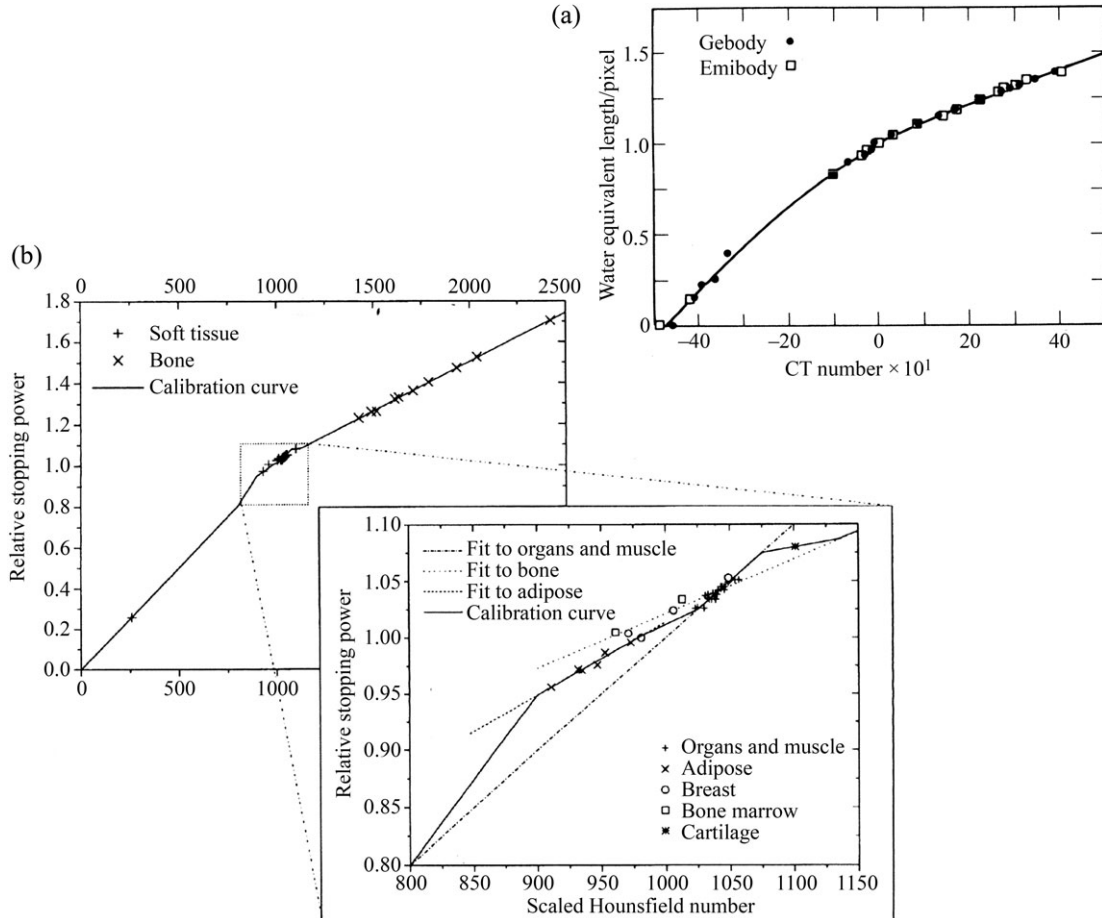


Figure 6.4. Conversion of Hounsfield numbers to water-equivalent density. (a) Direct-fit method (Chen *et al.*, 1979). Calibrations of two different scanners are shown. Here the results are fit with a polynomial curve. Usually, two straight lines are fit, one line to the region between -1000 and $+50$ Hounsfield numbers (in this figure the 'CT number' is equal to half of a Hounsfield number), and the other line to the region of higher Hounsfield numbers. (b) Calibration curve using the stoichiometric method (Schaffner and Pedroni, 1998). A magnified portion of the graph in the region of Hounsfield numbers close to zero (scaled to 1000 in this figure) is shown in the inset. Five line segments are used to fit the data. Reproduced with permission.

2005). In the latter case, the data could be used as input to the planning process. In the former case, the data are restricted to confirmation of the planning process.

6.4.6.1.4 Accuracy. Typically, the conversion from the Hounsfield number to water-equivalent density permits $\sim 1\text{--}2$ percent accuracy (1 SD) in calculating the effective range of near-monoenergetic protons within the patient. This leads to a 1–2 mm uncertainty in computing the effective range of a proton that penetrates some 10 cm into the patient. A more complete account may be found in Schaffner and Pedroni (1998) and Schneider *et al.* (1996). In addition, uncertainties in the CT measurements themselves, including effects due to beam-hardening effects, can add an additional 1–2 percent uncertainty (Constantinou *et al.*, 1992).

6.4.6.2 Design of compensators

For the high-dose volume to conform to the distal surface of the target over the entire field, some way of tailoring the proton penetration over the field area is required. The required penetration at any point in the field will depend on the location of the skin surface, the distal target surface, and the intervening heterogeneities. For scattered beams, the penetration is tailored by interposing a *compensator*, a piece of low-Z material (often PMMA), the thickness of which varies across the field, in the path of the beam.

In the simplest approach, one computes the radiological path lengths³ of protons over the entire field and then designs a variable-thickness

³Radiological path length is the integral along a straight line with respect to the path length of any material of water-equivalent density between the source and the distal point of interest.

compensator that is thin where the radiological path length is large, and thick where it is small, in such a manner that the radiological path lengths along all rays between the source and the distal target surface, including the contribution of the compensator, are equal. Figure 6.5a shows such a compensator (see also Section 3.2.1.1 and Fig. 3.3).

The above approach is deficient in several regards. First, it does not allow for possible misregistration between the compensator and the patient, *e.g.*, due to patient or organ motion or setup error. Secondly, it assumes that the protons travel along straight lines fanning out from the source of protons. That is, it ignores multiple scattering, which creates, in effect, a distribution of possible ranges for protons initially directed along a given line. A solution has been proposed to allow for these two effects (Urie *et al.*, 1984), namely, to expand or open up the compensator in such a manner that its thickness at any point in the field is the least thickness of the un-expanded compensator within some defined radius—which is typically at least a few millimeters. This is illustrated in Fig. 6.5b. The consequence of the expansion process is that the target is assured coverage, even in the face of setup error, patient motion, and scattering effects. However, on the downside, the beam will tend to overshoot in some places, thus increasing the dose to distal normal tissues.

6.4.6.2.1 Choice of range. The extent in depth of the high-dose region is determined by the maximum proton-beam energy. That energy could, in principle, be set so that the distal, say, 90 percent isodose surface just conforms to the distal target surface. However, such a prescription leaves no room for uncertainty. Just as is done laterally, one needs to allow some distal margin to allow for

setup uncertainties, patient motion, range uncertainties due to CT calibration errors and uncertainty in the Hounsfield number to water-equivalent density calibration, *etc*. The extent of this margin must be based, just as for lateral margins, on an analysis of these uncertainties. When a formal uncertainty analysis has been performed (see Section 8), the prescription is straightforward: one sets the maximum energy so that, for example, the 90 percent isodose surface just covers the target volume.

6.4.6.2.2 Compensator design close to, and outside, the projected target boundary. When the target volume is relatively spherical, the above design approach tends to lead to rather steep gradients in the thickness of the compensator near the edge of the projected target boundary because the target surface also has a steep gradient. This also leads to compensators being quite thick. One method used to reduce these effects is to taper the compensator in a region near its edge. That is, starting at, say, 1 cm from the edge of the projected target boundary and moving radially outwards, the compensator is not allowed to change thickness by more than a defined amount, typically, so that no gradient in the compensator is steeper than 60° (with respect to the direction of the beam axis) in that region.

In general, the beam extends somewhat beyond the projected target volume (often taken to be the CTV) in order to provide a lateral margin. The method of designing compensators outlined above does not work outside the projected target volume. There, in practice, one sets the compensator thickness equal to that of the closest point for which the compensator thickness can be calculated. This step is taken after the tapering process has been done.

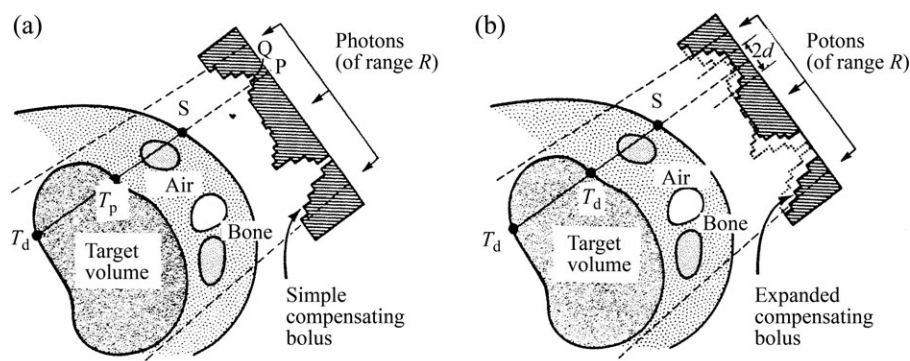


Figure 6.5. Design of a compensator (here labeled ‘bolus’) based on computing the radiological path length of protons along rays emanating from the source and stopping at the distal surface of the target (Urie *et al.*, 1984; reproduced with permission). (a) The calculation ignoring multiple-scattering effects and possible misregistration due to setup error and patient motion. (b) The technique of expanding the compensator so that the thickness of the new compensator at any point is replaced by the least thickness of the original compensator within a prescribed radius of the point.

6.4.6.2.3 Real and virtual compensators. The description of compensator design has, up to this point, assumed that the compensator is a physical device, such as that depicted in Fig. 6.5. This is, indeed, the case for scattered and wobbled proton beams. When a scanned pencil beam is used to form the treatment beam, a physical compensator could still be used. However, in practice, the variation in proton-beam penetration is achieved by upstream changes in the pencil-beam energies and hence penetrations. The compensator design described above should then be considered as a prescription of the way in which the pencil-beam energy needs to be modified over the field area. That is, the design is that of a virtual compensator, rather than an actual physical device. One advantage of virtual compensation using a scanned beam is that one has improved control over the proximal extent of the treated volume, and can thereby better spare proximal normal tissues (Goitein and Chen, 1983).

6.4.6.2.4 The effect of an air gap between compensator and patient. In the design process represented in Fig. 6.5, no account is made of the gap between a physical compensator and the patient. Indeed, the algorithm for designing a compensator implies that the compensator is in contact with the patient surface. However, in practice, an air gap is left between the compensator and the patient's skin surface. (Schemes have been proposed to shape the downstream face of compensators so that they can conform to, and be placed in juxtaposition with, the patient's skin surface. Such a compensator would

be termed a *bolus-compensator*.) Since the compensator induces multiple scattering of the protons in the beam, the air gap will result in both an increase of the beam penumbra and a blurring of the compensator's fine structure within the patient. The larger the air gap, the greater are these effects. This problem has been quantitatively explored (Sisterson *et al.*, 1989; Uriel *et al.*, 1986b). The amount of compensator expansion should be tailored to allow for beam spreading with depth, as well as misregistration effects. Obviously, one part of the strategy is to have the compensator induce as little scattering as possible by fabricating it from a low-*Z* material such as plastic.

One important advantage of pencil-beam scanning is that the air gap is less important because the change in beam penetration may be induced not by a physical compensator (which introduces scatter), but upstream by changes in the beam energy, which provide virtual compensation as mentioned above.

6.4.6.2.5 High-*Z* heterogeneities. The approaches to the compensation for heterogeneities described above work well for most tissues normally found in the human body. Not infrequently, however, one has to contend with man-made structures such as titanium rods used for vertebral body stabilization. The first approach to deal with such dense high-*Z* heterogeneities is to seek beam directions that do not require the beam to traverse the heterogeneity in order to cover the target. The use of IMPT can be helpful in this regard, allowing conformal avoidance of the structure. However, it is not always

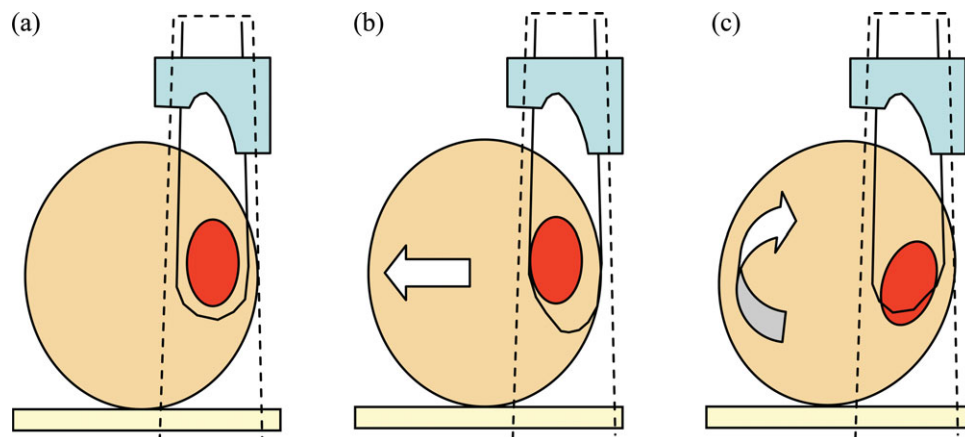


Figure 6.6. Schematic depiction of the situation when a near-tangential beam is employed. (a) Correct alignment of compensator (blue) and target volume (red) within a patient section (fawn). The dotted black lines depict the projection of the beam collimators into the patient. The continuous black line depicts the 90 percent isodose line that covers the target volume as intended. The very steep sides of the compensator are due to a combination of the shape of the target volume and of the patient's external contour. (b) The patient is shifted left. Now, the thickness from the skin surface to the intended distal 90 percent dose is reduced, so there is overshoot of the dose on the right-hand side. (c) The patient is rotated clockwise. Now, the thickness from the skin surface to the intended distal 90 percent dose is increased, so there is undershoot of the dose on the right-hand side.

possible to avoid having protons traverse the structure. In that case there are a number of problems: (i) the measured Hounsfield numbers may saturate and not be linear with absorption; (ii) owing to the high-Z of the material, the Hounsfield number-to-water-equivalent-density conversion schemes break down; and (iii) the structure usually induces heavy artifacts in the CT data outside the structure, making the computation of radiological path lengths questionable, even when the rays do not pass through the structure. For the last of these problems, there exist post-processing artifact-reduction techniques, and these can be used with advantage. Also, the region of heaviest artifacts can be edited and the Hounsfield numbers are replaced by the expected values for the tissue type in question. Since the composition of the heterogeneous structure is known, it is possible to edit the CT data and substitute a computed number for the Hounsfield numbers within the structure such that the Hounsfield number-to-water-equivalent-density conversion scheme used does correctly predict the energy loss of protons passing through the structure.

However, because the high-Z of the heterogeneity induces scattering not handled by conventional dose-computation techniques, it is highly desirable to use Monte Carlo dose computation techniques (see Section 6.5.2.3) to evaluate this situation.

6.5 DESIGN OF INDIVIDUAL PROTON BEAMS

A number of aspects of beam design in proton-beam therapy have already been touched on in Sections 6.2.2, 6.2.3, and 6.4, and will not be further elaborated here.

6.5.1 Compensation for heterogeneities

The design of compensators, whether real or virtual, has been fully described in Section 6.4.6.2. It takes into account the effects of compensator misregistration due to patient and/or organ motion or setup error, and of multiple scattering of the protons. This is necessary because lateral misregistration can, unlike the situation with x-ray beams, lead to changes in the designed beam penetration (Tatsuzaki and Urie, 1991; Urie *et al.*, 1984).

6.5.1.1 Choosing beam directions

In all radiation modalities, it is common to select the direction of a beam so as to entirely or partially avoid specific OARs. In charged-particle therapy, it is also desirable to avoid beam directions that bring

the beam in line with a substantial heterogeneity (e.g., the base of skull) or through very complexly structured regions (e.g., the petrous ridge). This is done deliberately by experienced treatment planners. However, the methods are also being investigated to provide quantitative measures to help assess when a beam is directed through a bad region (see Section 6.2.3.2).

6.5.1.2 Tangential irradiation

External skin surface is a special type of tangential heterogeneity. It can be hazardous to use a beam direction that requires one edge of the beam to be near-tangent to the patient's outer contour, as illustrated in Fig. 6.6. This figure shows situations in which the whole patient is shifted, but the patient's anatomy is stable. Figure 6.6a shows an ideal alignment of such a beam. Figure 6.6b and c demonstrates how normal-tissue-sparing and/or the target-volume coverage deteriorates as the patient is shifted, or rotated. However, it is common for the skin and underlying tissue to be differently distorted from day to day, owing to variable pressure from the immobilizing or supporting materials, for example. Such distortions may alter the skin-to-target-volume distances, and hence affect the dose distribution. Great care needs to be taken either to avoid tangential irradiation of the patient's surface or to control it carefully when it cannot be avoided.

6.5.2 Categories of models for dose computation

There are three primary models for the calculation of dose in a proton beam, namely,

- uniform-intensity beam algorithms (which can only be used for scattered and wobbled beams);
- pencil-beam algorithms (which can be used for any type of beam);
- Monte Carlo calculations (which can be used for any type of beam).

These are described⁴ here in the order of increasing accuracy.

All these calculation methods rely on having a three-dimensional description of the patient's anatomy in and near the region of interest, together with a map of the water-equivalent densities. The accuracy of this three-dimensional information, which may be compromised, for example, by artifacts in the CT images or the presence of contrast material, will affect the accuracy of the

⁴Adapted from Lomax and Goitein (1997).

calculations (see Section 8 regarding uncertainty analysis).

6.5.2.1 Uniform-intensity beam algorithms

Uniform-intensity beam algorithms provide the simplest, fastest, and least accurate approach to estimating dose. The input data to the dose calculation are either experimentally measured data, or numerical fits to experimentally measured data (of a variety of energies, field sizes, and so forth), which describe the dose distribution of various uniform-intensity beams irradiating a flat-surfaced water-equivalent phantom. Typically, for proton-beam therapy, these may consist of a depth-dose curve for an SOBP together with lateral dose profiles at representative depths. From these data, the dose at any point in the distribution can be derived by calculating its water-equivalent depth (the integral in depth of the water-equivalent densities, from the patient surface down to the point of interest), usually performed using a ray-tracing algorithm, and interpolating the resulting dose from the measured depth-dose data. The lateral fall-off due to collimation is usually fit by an error function in which the 50 percent level aligns with the projected edge of the collimator. The standard deviation of this error function is derived from measured lateral profiles in water (Petti, 1992).

Uniform-intensity beam algorithms can be used for both scattered and wobbled beams. In the latter case, a wobbled beam can be assumed to be equivalent to a scattered beam having the same beam-uniformity properties.

6.5.2.2 Pencil-beam algorithms

Although uniform-intensity beam algorithms are fast, the estimation of the effects of complex heterogeneities on the final dose distribution is rather inaccurate. More accurate modeling of dose can be achieved using pencil-beam algorithms (Hong *et al.*, 1996; Pedroni *et al.*, 2005; Petti, 1992; Scheib and Pedroni, 1992). Typically, the incident beam is modeled using a number of closely spaced finite pencil beams, with each pencil beam being assigned a weight that is directly proportional to the particle fluence of the beam for the pencil's position. Each pencil beam broadens because of multiple Coulomb scattering within the patient, and its lateral shape can be modeled using measured or calculated data, as can its depth-dose distribution in water. The resultant dose at any point is then computed by summing the contributions from each of the pencil beams, with each calculated point taken to be at its actual water-equivalent depth. Such approaches have a number of advantages.

First, because pencil beams passing outside of a collimator aperture are rejected, the penumbral effect of the collimator is automatically calculated. In addition, inhomogenous beam intensities can easily be modeled, which becomes important when intensity-modulated beams are to be designed or their dose distributions to be calculated. However, perhaps the greatest advantage of the pencil-beam approaches is that they more accurately model the effects of heterogeneities on the incident beam.

6.5.2.3 Monte Carlo algorithms

The most accurate, and hence desirable, dose-estimation algorithms are Monte Carlo models (Jiang and Paganetti, 2004; Paganetti *et al.*, 2005; Petti, 1996; 1997; Tourovsky *et al.*, 2005). In this approach, individual protons are tracked as they penetrate through the patient (and in some cases through the beam-delivery hardware as well) and interact with the material through which they pass. The likelihood of an interaction, and its consequences, is sampled using random numbers, from the best available probability distributions. Such random walks through the materials in the beam line and in the patient are followed for numerous proton interaction histories. The secondary particles produced in the interactions are also further traced through the material they encounter.

As well as estimating the Coulomb interactions that lead to energy loss and scattering of protons, Monte Carlo algorithms permit estimation of the nuclear interactions. These are responsible for the loss of primary protons along the beam path [~ 20 percent loss over the proton range for a 160 MeV beam (ICRU, 1998)]; for the production of secondary protons that produce a dose halo around the beam path; for the production of neutrons that largely escape from the patient, but may have some importance as regards somatic effects; and for the production of heavy secondary nuclei (e.g., alpha particles, deuterons, and other nuclear fragments) that deposit dose locally near the site of the nuclear interaction. The latter are heavily ionizing particles that are responsible in part for the elevated RBE observed throughout an SOBP and within the plateau region. The estimation of the dose contribution from nuclear interactions is an important element of absolute dosimetry in planning programs, especially for scanned pencil beams (Pedroni *et al.*, 2005).

To obtain sufficient statistical accuracy for useful dose distributions in practical situations (e.g., ~ 2 percent statistical accuracy (1 SD) within each dose-accumulation voxel of ~ 2 mm on a side

throughout a 1 l volume], tens of millions of histories usually must be traced. Such calculations can take hours or even days to process. For this reason, some Monte Carlo codes intended for proton-beam therapy simulation just follow analytically the primary protons and model contributions from secondary particles. In this case, calculation times can be substantially reduced by one to two orders of magnitude (Tourovsky *et al.*, 2005). As Monte Carlo methods model the fundamental physics of proton interactions, the resulting dose distributions can be considered to constitute the gold standard against which other dose-calculational algorithms should be compared. With the next generation of workstations and PCs, and with the aid of variance-reduction techniques, calculation times might be reduced sufficiently to make this approach applicable on a routine basis. One way to reduce the long computational time is to use a faster algorithm in the process of plan development and optimization, and then to use a Monte Carlo algorithm for recomputing, and perhaps fine-tuning, the final plan.

6.5.3 Normalization and the calculation of monitor units

Ideally, the dose distribution produced by a planning calculation provides a three-dimensional map of the absolute dose throughout the patient volume that would result from a specified beam-input intensity (*e.g.*, monitor units for a scattered beam, and pencil beam fluences for a scanned beam) without further normalization. This is not always the case, however. Some algorithms provide only a relative dose distribution. This is often normalized to some well-defined point (such as the ICRU reference point), which is said to receive ‘100 percent dose’, but it can be normalized in many other ways, for example, as 5 percent more than the minimum dose received by 95 percent of the PTV. While there are many possibilities for establishing the beam normalization (see Section 5.6.4), a nominal 100 percent value is generally not the maximum dose delivered.

6.6 DESIGN OF GROUPS OF BEAMS: THE TREATMENT PLAN

Before the planning of a radiation treatment can begin, the planning aims must be established (see Section 10); generally they include instructions as to the dose which is desired to be received by the target volume(s) (and, often, the desired dose uniformity within the tumor) together with dose or dose–volume constraints on the dose to be received

by all OARs of concern. More rarely, the prescription may include goals for TCPs, NTCPs, and/or EUDs (see Section 6.7.3).

A ‘treatment plan’, or simply ‘plan’, consists of two elements. First, it specifies a number of beams, each with all its defining parameters such as modality (protons, photons of a given energy, *etc.*); plans with mixed-modality beams are, of course, entirely possible), type (broad beam or scanned beam), size; open-field dose profile(s); direction, and energy, together with the weighting of each uniform-intensity beam or, for scanned beams, of all pencil beams. Secondly, it involves a simulation of the dose distribution within the patient that would result from the application of those beams. In addition, the plan defines the fractionation scheme (the list of beams and the dose per beam to be delivered in each treatment session and the time sequence of the sessions) to be used.

Sometimes a treatment is given in more than one segment, *e.g.*, a first segment that covers the primary tumor and potentially involved lymph nodes, and a second segment that covers just the primary tumor and takes it to a higher dose. Each segment will then be represented by an approved plan, and the treatment will consist of the set of such plans, which may be combined into an overall plan for purposes of assessing the treatment as a whole.

6.6.1 Treatment goals and constraints

6.6.1.1 Setting goal(s) and constraints

Generally, in this approach, a goal for the target-volume dose is established, and a plan is sought that meets that goal, subject to the requirement that it does not violate one or more constraints usually placed on the dose delivered to normal tissues. This is the traditional approach to manual treatment planning, and it is used in some approaches to optimized planning. If the goal for the target volume is to maximize some quantity such as the median PTV dose, then this approach guarantees that at least one constraint will be only just met. This is because, if one were not, the planner or optimization program would simply increase the weights of some or all beams until one constraint is just at its limit.

6.6.1.2 Establishing a score combining target-volume and normal-tissue effects

In this approach, the score is a single number composed of a number of components that represent

the plan's impact on the target volume or a normal tissue (or perhaps another factor such as some measure of plan complexity), each one weighted in some manner by an 'importance factor'. The planner or optimization algorithm then seeks to maximize the plan's score. This approach is used in many approaches to optimized planning. The factors that go into the score may be comprised of physical quantities, or quantities estimated by biophysical models, or some combination. There are many possible scoring schemes as reviewed by Bortfeld (2003) and by York (2003).

6.6.1.3 Target-volume goals and constraints

There is a wide variety of ways to specify the target-volume dose requirements, including the following:

- all of the PTV receive some specified fraction (*i.e.*, 95 percent) of the prescribed dose;
- at least 95 percent of the PTV receives the prescribed dose—and it might further be specified that the regions of lower dose should be in the PTV periphery (so that the CTV is minimally affected);
- the mean dose to the PTV be equal to the prescribed dose;
- the ICRU reference point receives the prescribed dose;
- the prescribed dose be the highest possible dose that can be delivered to the PTV, subject to the normal-tissue constraints;
- a biological model's estimate of the target-volume response (*e.g.*, EUD or TCP—see Section 6.7.3) be maximized.

In addition, a constraint might be placed on the target-volume dose homogeneity, for example, the dose everywhere within the PTV be within defined limits, *e.g.*, within -5 and $+7$ percent of the prescribed dose.

6.6.1.4 Normal-tissue constraints

Normal-tissue constraints tend to be either dose or dose–volume constraints. For example:

- the near-maximum ($D_{2\%}$) dose to a specified OAR not exceed some stated value;
- the mean or median dose to a specified OAR not exceed some stated value;
- the dose, D , received by some specified fractional volume, V , of a specified OAR not exceed some stated value ($D_V \leq$ some value);
- a biological model's estimate of the response of a normal tissue (*e.g.*, EUD or NTCP—see Section 6.7.3) not exceed some stated value.

6.6.2 Approaches to treatment design

There are two rather different approaches used for the planning and delivery of radiation.

6.6.2.1 Uniform-intensity radiation therapy

In radiation therapy with uniform-intensity beams, treatment is delivered using a number of uniform-intensity beams, generally cross firing on the target volume(s), and each delivering a close-to-uniform dose to the target volume. (In photon therapy, in contrast, there is an unavoidable gradient of dose with depth.)

The main art of treatment planning is to choose a set of parameters for each beam which, so far as is possible, lead to an overall dose distribution that spares adjacent critical normal tissues from receiving more dose than the treatment aims will allow, while delivering an adequate dose to the tumor. The direction of incidence of each beam is one important element in this and is often chosen to avoid critical structures to the extent possible. So far as beam intensities are concerned, in uniform-intensity-beam radiation therapy, one has only to adjust the weights of the individual beams. In manual optimization, the design of the individual beams is based on the planner's experience; computer tools such as the possibility of designing an aperture or the settings of a multi-leaf collimator automatically, on the basis of the beam's-eye view (BEV) of the PTV, can greatly assist in beam design (Goitein *et al.*, 1983b).

In proton-beam therapy, there is an additional consideration, namely, the desire to avoid metallic objects (*e.g.*, metal posts needed for spinal column stabilization or hip prostheses) that might have been implanted into the patient. These can perturb a beam's dose distribution to a very great degree, which is hard to estimate (see Section 6.4.6.2). The judgement as to whether a plan is satisfactory if one or more beams traverse such a metallic object is difficult. It depends on experience, and can be made much more accurate and objective by Monte Carlo simulations. To the extent possible, beams are chosen for which the metallic object is near the distal end of the beam, or preferably beyond it.

The development of a treatment plan involves a trial-and-error process in which a set of beams (including their weights) are proposed, evaluated as to their resulting dose distribution, and then, if necessary, modified. This process is repeated until a satisfactory plan is arrived at. In uniform-intensity-beam radiation therapy, the trial-and-error process is usually undertaken manually (in which case only a limited number of

rival plans can be considered). However, it may also be done automatically or semi-automatically, employing the same optimization techniques as are used in IMRT, as described below.

6.6.2.2 Intensity-modulated radiation therapy (IMRT)

In IMRT, the treatment employs a number of beams which together result in a near-uniform dose to the PTV, but each of which delivers a non-uniform dose within the PTV. To distinguish between IMRT, in general, and the radiation modality-specific implementations of it, the following terms and abbreviations are useful:

IMRT	Intensity-modulated treatment using any form(s) of radiation.
IMXT	Intensity-modulated treatment using x-ray (photon) beams specifically.
IMPT	Intensity-modulated treatment using proton beams specifically.

If intensity-modulated beams of different modalities were combined in a single treatment, the result would be described as IMRT.

In IMRT, the number of variables is too great for manual optimization to be viable since, in addition to all the variables needed to define beams in uniform-intensity-beam radiation therapy, the intensity profiles of the pencil beams that comprise each beam must also be determined, and this usually involves thousands of additional parameters. As a consequence, computer automation is essential in IMRT (see Section 6.9). This has the benefit that it is possible to generate and assess a very large number of rival plans. In IMPT, there are even more variables than in IMXT, which permit both depth and lateral modulation. This makes the computational task even more demanding than in IMXT.

With so many potential variables, the computational task of choosing the best value for each of them is very demanding. When all possible variables are included in the computer search, the process is said to be *automatic*. However, in order to reduce the computational task to a viable level, it is common to choose a number of the variables manually. These often include choice of the number of beams, the modality of each beam, and the placement and direction of each beam. When some variables are chosen manually, the process is said to be *semi-automatic*.

6.7 PLAN ASSESSMENT

Once a treatment plan has been decided, its impact on the patient must be assessed (Goitein, 1992). There are four basic elements in this: inspection of the resulting absorbed-dose distribution overlaid on the patient's anatomy, assessment of the clinical feasibility of delivering the plan, review of dose-summarizing quantities, and review of other measures of radiation effect. It should be emphasized that there is almost nothing specific to proton-beam therapy in this process. Comparable techniques are needed to assess treatment plans no matter what radiation modality they involve.

6.7.1 Inspection of the dose distribution

The dose distribution in any plane (generally a transverse, sagittal, or coronal section) can be displayed in a number of ways:

- as isodose contours overlaid on outlines of the patient's anatomy and tumor (without imaging data);
- as isodose contours overlaid on CT or MRI data; or
- as a color wash overlaid on CT or MRI data.

Of these, the color-wash display gives the most immediate qualitative impression of the dose distribution and its impact on the patient. However, unless efforts are made to divide the dose-to-color map into distinguishable bands, this display is somewhat less easy to assess quantitatively than the display of isodose contours.

It is very useful to be able to view, simultaneously on the screen, three orthogonal sections through the three-dimensional data (while being able to interactively adjust their intersection point), and to rapidly scan through a sequence of such images. A tool that allows a user to move interactively a pointer around in any image and display the dose (ideally with its uncertainty) at that point is also very helpful for the purpose of exploring a dose distribution in detail.

There are really no very satisfactory ways of gaining an impression of the full three-dimensional dose distribution in a single view. Dose bands, dose clouds, and dose on the surface of VOIs have all been investigated as possible approaches.

Although there are several other quantities that assist in the evaluation of plans (described in the immediately following sections), a final judgement about a plan should never be made without carefully inspecting its dose distribution.

6.7.2 Clinical feasibility

A plan might appear to make sense, but may be impractical or undesirable in practice. The number of beams might be deemed excessive, some beam angulations may be difficult to deliver the time to deliver the plan may be excessive, the patient's condition may constrain the plan in a number of ways, *etc.* The resolution of these largely subjective decisions can be affected by institutional policies.

6.7.3 Dose-summarizing quantities

In addition to graphical displays of the RBE-weighted absorbed dose distribution, the computer can present the numerical value of the dose or any quantity derived from the dose distribution. Dose-summarizing parameters are described in Section 5.6. Examples are the following:

- the dose at each of several points of interest;
- the mean, median, minimum, or near-minimum and/or maximum dose [D_{mean} , $D_{50\%}$ (D_{median}), $D_{98\%}$ ($D_{\text{near-min}}$), $D_{2\%}$ ($D_{\text{near-max}}$), respectively] to appropriate VOIs (such as the CTV, PTV, or OAR or PRV);
- the volume, or relative volume, of a VOI receiving at least a specified dose, D , represented as V_D ;
- the least dose received by a given volume, or relative volume, V , of a VOI, represented as D_V ;
- dose–volume histograms (either cumulative or differential).

A very useful capability is to present such dose-summarizing quantities in juxtaposition with the values specified in the treatment aims. For example, if a constraint on an OAR is that at most 20 percent of the OAR receives a dose in excess of 50 Gy, then juxtaposition of the actual value of $D_{20\%}$ together with the desired value of 50 Gy directly indicates whether or not the constraint was met. Equally, if several dose–volume constraints (or dose constraints such as constraints on D_{max} , D_{min} , or D_{median}) are superimposed on a DVH, the planner can immediately see whether any are violated and by how much.

In recent years, there has been much effort put into developing measures of the impact of radiation on both tumors and normal tissues. These include models to predict the following:

- the equivalent uniform dose (EUD)⁵ (Niemierko, 1997) for both tumor and normal tissues (Bortfeld, 2003);

- the tumor control probability (TCP) (Niemierko and Goitein, 1993; Webb, 1994; York, 2003);
- the normal-tissue complication probability (NTCP) of each of several normal tissues (Lyman, 1985; Schultheiss *et al.*, 1983; York, 2003);
- the probability of uncomplicated local control (preferably using importance weighting factors) (York, 2003).

All of these models involve assumptions (either explicit or implicit) about the response to radiation of tumors or normal tissues that are unlikely to fully represent their actual behavior. Moreover, the experimental and clinical data on dose–volume effects are rather sparse and the clinical data, in particular, have substantial uncertainties. The validity of all of these models is therefore in question. Nevertheless, they offer helpful aids, particularly in comparing plans (see Section 6.8), provided they are used cautiously and understood only to support, and not to replace, expert judgement.

The plan's 'score' is a summarizing quantity that attempts to quantitatively represent the quality of the plan by a single number, always subject to its meeting any constraints. This is of very limited use for the assessment of a single plan, but is useful in comparing a few plans, and is essential in computer optimization of very many plans—as discussed in the following section.

6.8 PLAN COMPARISON

One important goal of plan assessment is to support the comparison of alternative plans for a given patient (Goitein, 1992). This may be done for the purpose of deciding which of several possible plans should be used to treat a given patient, or for comparing rival approaches, including rival modalities (*e.g.*, protons versus photons), using a specific patient as a test case.

One can hardly compare two (or more) objects without some measure(s) of each. The principal tools for plan comparison have already been presented in the previous section on plan assessment. They may be used, however, in two rather different ways, one subjective and the other objective. Objective is meant a process that does not rely on human judgement and, if repeated, gives the same result.

⁵The equivalent uniform dose is that dose which, if applied uniformly to the entire volume of the tumor or a normal tissue, is judged on the basis of a simple biophysical model to be equivalent to the non-uniform dose distribution in terms of its clinical consequences.

6.8.1 Plan comparison by inspection

The comparison of plans through inspection by humans is a somewhat subjective matter. That is, two experts can disagree on which of a given pair of plans is the better. The comparison involves a multiplicity of factors. Experts can differ on the relative importance of different aspects of the plans (e.g., adequacy of tumor coverage versus avoidance of normal tissues), and can disagree on the most important measures to weight (e.g., D_{\min} or D_{mean} of the tumor). Nevertheless, in the end, an observer must be able to rank a pair of plans, with one of them being judged as being relatively 'better' or 'worse' than the other, or perhaps considering them as equally desirable clinically. The observer must also be able to judge whether a plan is adequate, or whether an alternative must be sought.

Although plan comparison might be subjective, it is greatly facilitated by the side-by-side comparison of objective measures, such as those already described for plan analysis. Thus, any platform that is intended to assist the planner in comparing plans should, for two or more plans, be able to do the following:

- display, side-by-side, the dose distributions overlaid over the identical anatomic image (i.e., the same slice) and to advance the slice being viewed rapidly in all panels;
- tabulate, side-by-side, the computed dose at each of several points of interest, preferably with confidence limits;
- tabulate, side-by-side, quantities such as the mean, median, (near-) minimum, and/or (near-) maximum dose (D_{mean} , D_{median} , $D_{\text{near-min}}$, D_{\min} , $D_{\text{near-max}}$, D_{\max} , respectively) to any VOI (such as the CTV, PTV, or OAR or PRV), preferably with confidence limits;
- tabulate, side-by-side, the computed volume, or relative volume, of a VOI receiving at least a specified dose, D (represented as V_D), preferably with confidence limits;
- tabulate, side-by-side, the minimum dose received by a given volume, or relative volume, V , of a VOI, represented as D_V , preferably with confidence limits;
- overlay on the same plot, for each of the plans being compared, the DVHs of any given VOI (either cumulative or differential); and
- present estimates of the uncertainties in the plans (at a minimum, where these differ between plans).

If a quantity has been specified in the treatment aims, it is very useful to indicate its desired value in the tabulation of the data being compared, so as

to assess whether an element of a plan satisfies the treatment aims. The first and the last in the above list of capabilities are probably the most useful in comparing plans. Optional features might allow the planner to:

- tabulate, side-by-side, the EUD for both tumor and normal tissues;
- tabulate, side-by-side, computation of the TCP; and
- tabulate, side-by-side, computation of the NTCP of each of several normal tissues.

A recent approach to planning is the use of the so-called Pareto optimization (Bortfeld *et al.*, 2004). This involves modification, neither of the usual input variables (e.g., gantry angle, beam weight, *etc.*), nor of importance factors but, rather, of measures of output quantities such as EUD or TCP/NTCP, which quantify the effect of the plan on the VOI (these measures may be called the 'output variables'). In this approach, a vast number of plans are generated by computer. Plans for which improvement of one of the output variables will inevitably result in the worsening of at least one other output variable are said to lie on the Pareto front. The planner views an interactive display that shows the values of all the output variables for the currently selected plan. He or she can then increase or decrease the value of any one output variable—thus moving to a neighboring plan on the Pareto front, and view, interactively, the consequences for all other output variables. For example, one might reduce the NTCP for the spinal cord and see what impact that would have on the TCP and the NTCPs of other critical structures. In this manner, the user can choose a plan that represents his or her best judgement of the most acceptable plan among those lying on the Pareto front. This approach in no way eliminates the problem of subjectivity in the comparison of plans. However, it has two attractive characteristics: it constrains the user to view only a productive subset of possible plans, and it allows the user to make adjustments in the space of clinically meaningful variables.

6.8.2 Automated plan comparison

It is now possible (and, for IMRT, necessary) for a computer to generate literally thousands of plans for a single patient. The selection of the most desirable of these is simply not possible through human inspection of each one, as it would be too burdensome. Therefore, some automated approach is necessary.

In order for a computer to rank plans, it must have a unique numerical measure of plan goodness.

That is, in spite of what has just been said about plan evaluation being a multi-faceted matter, the computer must be able to reduce several measures to one number; it is termed as the plan's 'score' (see Section 6.6.1.2). Without such a score, it cannot rank any two plans. And, without a choice of the better of any two plans, it cannot determine which of many plans is the best according to the chosen method of scoring. Once an objective method of scoring is decided upon, the process of determining the most acceptable of the plans is trivial: one must merely identify the plan with the highest score(s).

Obviously, being forced to use a single number to judge plans might not be a clinical advantage as the score may not faithfully reflect a given planner's judgement. It does have the advantage, however, of allowing a larger number of plans to be assessed than would be possible using manual-assessment techniques.

The heart of the comparison of plans by computer, then, is the development of a satisfactory algorithm for computing a plan's score. A number of such algorithms have been developed and used (Bortfeld, 2003; York, 2003). The rationale for some of them has more to do with computational simplicity than with their fidelity to the way an expert would judge a plan.

6.9 PLAN OPTIMIZATION

The process of iteratively generating and then automatically assessing a large number of plans and choosing the best among them is commonly termed plan optimization. This term has a precise mathematical meaning: the process of choosing those values for the treatment-delivery variables that would result in an *extremum of the score function*. However, given that usually only a subset of the variables has been adjusted, and that one can have at best only very limited confidence in the numerical measure of the plan's goodness (its score), the term optimization can be misleading.

A computer can be programmed to design a treatment plan automatically, given the following:

- a unique *goal* (e.g., $D_{95\%}$ for the tumor to be as high as possible); and a set of *constraints* (e.g., $V_{60\text{Gy}}$ for the kidney to be <30 percent, and/or the dose within the PRV not to exceed some stated dose);
- a *method of giving a score* to a plan;
- the definition of *what variables to adjust* (e.g., the pencil-beam weights that determine the intensity profiles); and
- an *initial guess* at a plan;
- a *method of searching* for that set of plan variables that maximizes the score.

The constraints and goals are given in the treatment aims and represent the clinician's instructions for the planning process. The constraints may be 'hard' constraints, in which case a minor violation is considered to be as bad as a severe violation, or they may be 'soft', in which case a small violation may be allowed, if necessary. Although the process of having a computer look for the best plan is fully automatic, it is not uncommon to modify the constraints or goals and try again, if the resulting plan is deemed by inspection to be unsatisfactory. Thus, even the automated approach to treatment planning usually has a manual (*i.e.*, user-guided) element to it.

A good optimization algorithm should be insensitive to the starting values used for the variables being adjusted. This is the case for some optimization algorithms being used in practice, but not for all. In any event, variables that are not adjusted in the iterative process do need to be specified with some care as they will remain in the final plan. Thus, for reasons of computational speed, it is common not to vary the number or the angle of entry of the beams. In that event, if one wishes to take advantage of the geometry, the beams must be pre-selected using expert judgement.

Optimization techniques have been reviewed by Censor (2003). A number of mathematical approaches has been used, including simplex methods (Dantzig, 1963; Nieder and Mead, 1965), various methods of conjugate-gradient search, and simulated annealing. It is important to point out that both the conduct of the search and the validity of the scoring method are susceptible to error. Some search methods are prone to find local *extrema* and get trapped in them, thus missing a possibly much better solution elsewhere in the parameter space; others force restrictions on the nature of the score function in order for them to work. Scores, while objective, can also be clinically misleading if the underlying algorithm does not adequately take into account the biology of the problem.

6.10 COMPARISON OF UNIFORM-INTENSITY VERSUS IMPT TREATMENT PLANS

As an example of plan comparison, a comparison of proton therapy using uniform-intensity beams versus uniform-intensity scanned beams versus intensity-modulated scanned beams is presented here.⁶ Side-by-side dose distributions in one transverse plane are shown in Fig. 6.7 for three plans, namely plans using uniform-intensity scattered

⁶This section has been prepared with the assistance of A. Lomax, Paul Scherrer Institute, Switzerland.

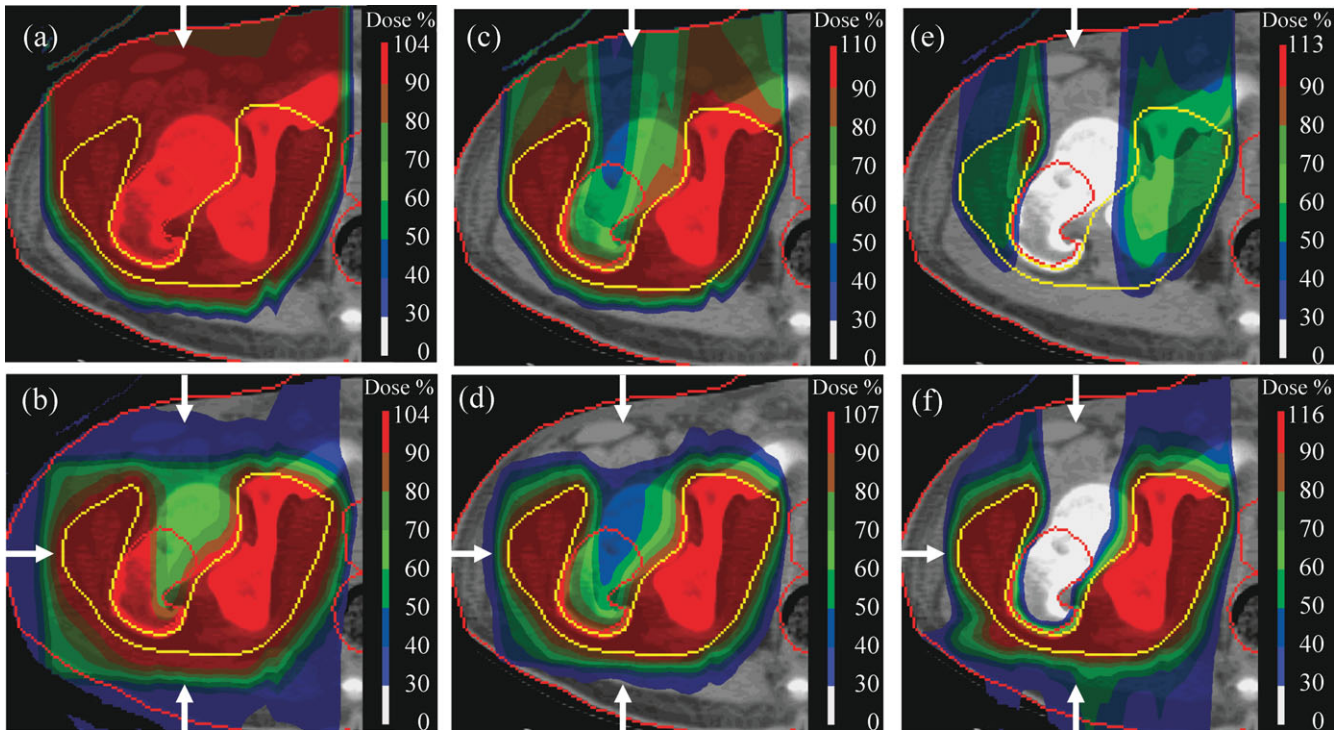


Figure 6.7. A comparison of various techniques of beam formation for a single beam (upper panels) and for a three-beam plan (lower panels) for a Ewing's sarcoma (the PTV is outlined in yellow). The three techniques are as follows: (a) and (b) passively scattered beam; (c) and (d) scanned beam(s), but with a uniform dose in the target volume from each beam; (e) and (f) IMPT, in which the individual beams irradiate the target volume non-uniformly, but the combined dose is uniform within the target volume. (e) The dose distribution from one of the three beams. (f) The combined dose distribution from all three beams, displaying excellent conformation of the dose to the target volume (see Section 6.10). (Figure courtesy of A. Lomax, Paul Scherrer Institute, Villigen, Switzerland.)

beams; uniform-intensity scanned beams with variable modulation across the field; and fully intensity-modulated and optimized scanned beams.

As can be seen in Fig. 6.7a, even a single uniform-intensity scattered beam can provide excellent conformation of dose to the distal end of the target and good lateral conformation. However, because of the fixed modulation of Bragg peaks in depth across the whole field, it provides little high-dose conformation of the dose to the proximal side of the target volume. In practice, the dose conformation to the target volume is enhanced through the application of multiple, angularly separated beams (Fig. 6.7b). Further improvements in the delivered dose can be achieved with beam-patching techniques. For example, the distal end of one or more beams can be directly abutted against the lateral edge of another beam, such that critical structures close to the tumor can be selectively avoided.

In contrast to a scattered beam, the treated volume of a scanned beam can be matched (at relatively high dose levels) to the proximal, as well as the distal, surface of the target volume, resulting in a beam that is near-uniform within the target volume, but provides some sparing of the tissues proximal to it as well as full sparing of distal

tissues. Figure 6.7c shows an example of the dose distribution of such a scanned beam for the identical beam geometry as shown for the uniform-intensity beam of Fig. 6.7a, and confirms that scanning can conform the high dose to the target volume in all three dimensions, significantly reducing the doses delivered to the tissues proximal to the target volume in comparison to use of a scattered beam. The dose distribution of three such scanned (but uniform within the PTV) beams, using the identical geometry as that of Fig. 6.7b, is shown in Fig. 6.7d. Although the difference between scanning and scattering in the three-beam plan is less marked than in the single-beam plan (comparing Fig. 6.7b and d), nevertheless scanning is seen to provide a method by which the high-dose conformation can be further improved, and by which doses outside of the target can be globally reduced.

A homogenous dose distribution, or indeed any desired dose distribution, can also be computed from a number of individually highly non-uniform proton beams (*i.e.*, IMPT). By removing the restriction that each beam must itself be homogenous, free rein is given to the optimization, allowing it to fully exploit all the degrees of freedom provided by the many thousands of individually weighted and

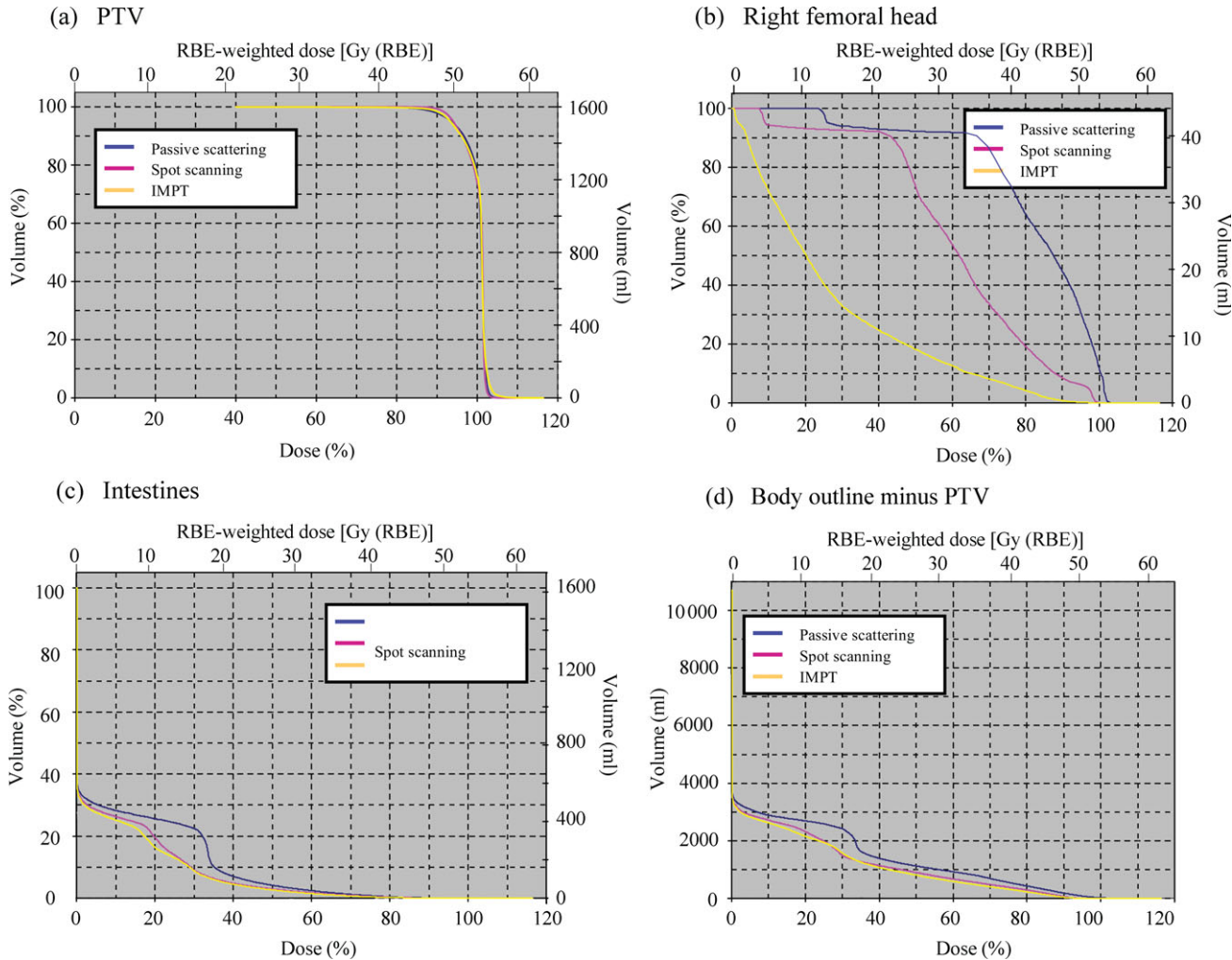


Figure 6.8. Dose–volume histograms for the 3 three-beam plans shown in the lower panels of Fig. 6.7 for (a) the PTV; (b) the right femoral head; (c) the intestines; and (d) the volume within the body outline, but excluding the PTV. (Figure courtesy of A. Lomax, Paul Scherrer Institute, Villigen, Switzerland.)

three-dimensionally distributed Bragg peaks incident from two or more different beam directions. The result is the possibility of conforming a dose distribution at different dose levels, using relatively few beams, while still selectively avoiding organs that are deeply embedded within the target volume. Figure 6.7e shows the dose distribution for just one of the three beams whose combined dose distribution is shown in Fig. 6.7f. When Fig. 6.7f is compared with either of Fig. 6.7d or b, the advantage of IMPT becomes clear.

The DVHs for the PTV, the right femoral head, the intestines, and the entire imaged patient volume minus the PTV are shown in Fig. 6.8 for the three plans. These histograms quantitatively capture the full three-dimensional dose distribution in these VOIs, but the images shown in Fig. 6.8 are by necessity two-dimensional images and cannot show how the dose distributions compare in other sections. From Fig. 6.8a, it is clear that the PTV is

well covered in all three plans. The DVH shown in Fig. 6.8 indicates that the femoral head is progressively better spared as one goes from passively scattered beams, to scanned but uniform beams, and to fully intensity-modulated beams, whereas the coverage of the intestines is worse with the passively scattered beams, but comparable for the other two beam-delivery systems. The DVH shown in Fig. 6.8d shows how much dose is distributed outside the PTV (the DVH for the RVR is not shown here as so much of the body is delineated). The volume axis in this DVH is shown only in absolute units as a relative volume would have little meaning (see Section 5.6.2.2). There is ~25 percent more dose delivered outside the PTV in the scattered beam plan than in the other two plans that are comparable with one another.

Dose statistics have an important quantitative role in comparing plans. Table 6.1 shows a representative set of such statistics. In principle, such

dose statistics (except D_{mean}) can be directly read off the DVHs. Displaying the data for the plans side-by-side, in tabular form, is very helpful.

6.11 SPECIAL TECHNIQUES

6.11.1 Intraocular treatments with protons

As described in Section 3.2.3.1, a specialized apparatus is usually used in the treatment of intraocular tumors. The treatment-planning programs used for such treatments are also specialized. They require the same elements as are required for general proton beam therapy, but these are differently implemented. The majority of eye-treatment programs use a program based on that reported by Goitein and Miller (1983). Further enhancements are being made (Dobler and Bendl, 2002) using CT and MRI. The main differences between the specialized eye-treatment-planning programs and those used in general radiation therapy are outlined in Sections 6.11.1.1–6.11.1.5.

6.11.1.1 Model of the patient anatomy

Rather than being based on a set of three-dimensional images from which pertinent anatomic features are extracted, either manually or automatically, the patient anatomy is generated by fitting a general library of two- and three-dimensional structures to a variety of parameters obtained in a variety of ways. Typically, the library includes the exterior of the eye, modeled as a pair of spheres or, better, ellipsoids; the optic axis; the iris; the lens; the *ora serrata*; the optic disc and nerve; the macula; *etc.* The tumor is modeled as a three-dimensional volume bounded by a tumor-base circumference; by a proximal-tumor high point and a distal deep point, both relative to the inner surface of the sclera; and by hyperbolic or near-hyperbolic sets of curves that connect both the high point and the deep point to the circumference. Figure 6.9a shows a lateral view of such a model.

6.11.1.2 Beam simulation

The beams used in intraocular treatments are uniform-intensity beams and, because of the simplicity of the beams and of the eye, they are usually simulated by simplistic models, *i.e.*, by a parameterized depth-dose curve, a measure of the lateral penumbra, and a cross-section determined by the geometric projection of the aperture. Dose heterogeneities are generally not taken into account; the tissues are taken to be equivalent to water. The treatment plan has to model a beam geometry that is, however, different in two ways. First, rather than the beam being rotated around the patient,

the beam is fixed in direction (usually horizontally) and it is the patient's eye that is displaced and rotated so as to gaze at a small-diameter fixation light with polar and axial location known to the planning program. The second difference is that, although the eye is rotated, the rest of the patient remains fixed. The patient's eyelid, then, remains fixed in space as the eye is rotated, and this must be modeled in the planning program.

6.11.1.3 Output of the planning process

As in treatment planning for general radiation therapy, the treatment-planning program generates the parameters needed to deliver a treatment. These include the shape and size of the beam collimator (designed in the BEV), the beam penetration and modulation, and the eye-fixation point. Very importantly, the planning program provides images that show how the radio-opaque clips sutured to the posterior scleral surface should appear in orthogonal radiographs (simulating the precise geometry of the alignment x-ray systems of the treatment apparatus). These clips are used both as an aid in the treatment setup and to demarcate the tumor circumference; they are an essential element of the treatment process.

6.11.1.4 Presentation of results

A number of specialized dose displays are provided. One of these is a plot of isodose contours on the curved retina, using the same projection as is provided by a fundus camera. This allows the dose display to be directly compared with the fundus pictures and, in principle, overlaid upon them (see Fig. 6.10b). The DVHs and dose-area histograms (the cumulative frequency of dose on the surface of a volume) are routinely employed. Indeed, their first use in treatment planning was for the planning of eye treatments (Goitein and Miller, 1983).

6.11.1.5 Treatment example

These concepts are illustrated⁷ by the example of a treatment of a uveal melanoma of the left eye. During a surgical intervention, four radio-opaque tantalum clips were sutured to the outside of the eye bulb around the base of the lesion, in order to make the location of the tumor visible in orthogonal x-ray images. Postoperative proton-radiation therapy was planned for four daily fractions of RBE-weighted absorbed doses of 15 Gy (RBE), for a total dose of 60 Gy (RBE).

⁷This case has been worked up by J. Verwey and A. Bölsi, Paul Scherrer Institute, Switzerland.

Table 6.1. Dose statistics for the three plans presented in Section 6.10 and Figs 6.7 and 6.8.

Volume	RBE-weighted absorbed dose [Gy (RBE)]		
	Scattered	Uniform scanned	IMPT
Target volume—PTV			
Dose to 98 percent of volume, $D_{98\%}$ (near-minimum dose)	48.5	49.7	48.9
Median dose, $D_{50\%}$	54.6	54.7	54.6
Dose to 2 percent of volume, $D_{2\%}$ (near-maximum dose)	55.5	55.4	56.2
Relative volume receiving 95 percent of the prescribed dose, $V_{95\%}$	93	93	92
Right femoral head			
Relative volume receiving 20 percent of the prescribed dose, $V_{20\%}$	54.0	50.3	27.3
Relative volume receiving 50 percent of the prescribed dose, $V_{50\%}$	49.8	39.7	9.8
Relative volume receiving 80 percent of the prescribed Dose, $V_{80\%}$	34.6	10.3	2.3
Dose to 2 percent of volume, $D_{2\%}$ (near-maximum dose)	102	98	85
Intestines			
Relative volume receiving 20 percent of the prescribed dose, $V_{20\%}$	13.8	10.6	8.9
Relative volume receiving 50 percent of the prescribed dose, $V_{50\%}$	2.2	1.6	1.4
Relative volume receiving 80 percent of the prescribed dose, $V_{80\%}$	0.2	0.2	0.1
Dose to 2 percent of volume, $D_{2\%}$ (near-maximum dose)	63	57	55
Body outline minus PTV			
Mean dose outside the PTV, D_{mean}	7.2	5.9	5.6

Volumes are relative volumes except for the 'body-outline—PTV', which is an absolute volume (in cm^3). The mean dose to the 'body-outline—PTV' is equal to the integral dose to that volume divided by its volume (which is 10.71).

Proton-beam treatment was planned using an enhanced version of the program developed by Goitein and Miller (1983). Reconstruction of the GTV was based on (i) for the tumor base: the position of the clips and the distance between the clips (measured intra-operatively) and the base of the tumor, as well as the measured distance between the tumor and the optic disc and macula; and (ii) for the tumor height and shape: an ultrasound study. The direction of gaze (both caudal and medial) was chosen to avoid irradiation of the optic disc, and as much as possible of the anterior segment. The beam aperture was designed (see Fig. 6.9a) around the GTV⁸ with a lateral margin of 2 mm to account for possible microscopic extension, motion uncertainty, and beam penumbra, and with a margin in depth of 3 mm to allow for range uncertainties. The dose distribution achieved is shown in sagittal section in Fig. 6.9b, as well as in a projection mimicking the fundus camera's geometry (Fig. 6.9c) to allow direct comparison with the fundus picture (Fig. 6.9d). Dose—volume histograms for a number of volumes of interest are shown in Fig. 6.9e.

The patient was treated in a seated position, the head fixed in a perforated thermoplastic mask with a bite block, and with the affected eye gazing at a light to achieve the desired orientation of gaze (Fig. 6.9f). Orthogonal radiographs were taken

before each treatment to compare the observed radio-opaque clip positions with their desired positions as calculated by the planning system. An accuracy of 0.2 mm can be achieved. Treatment was delivered as planned and was well tolerated, with mild conjunctivitis at the end of treatment.

6.11.2 Stereotactic treatments with protons

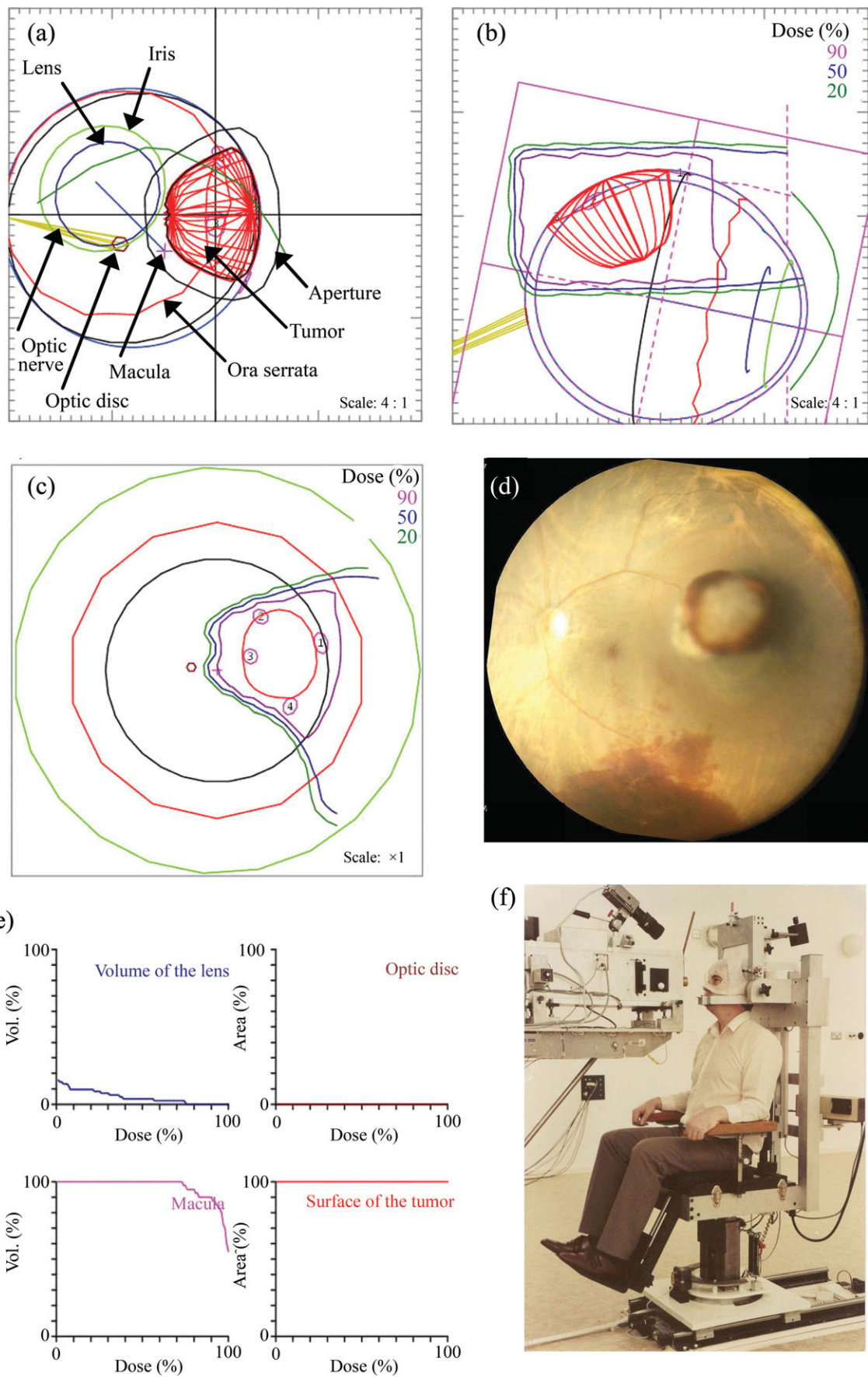
The process of proton radiosurgery is largely the same as for fractionated proton radiotherapy.⁹ What is different is the need to achieve a higher level of conformity because of the large doses prescribed, often administered in a single session, with the consequent lack of statistical averaging over multiple fractions. This increased accuracy must be incorporated throughout the whole planning and delivery process, including immobilization, planning, alignment, and radiation delivery. Specific implementations, such as using a gantry-based delivery system with a nonisocentric robotic bed, or using a custom isocentric patient positioner with a fixed horizontal beam line, introduce their own considerations when accounting for accuracy.

6.11.2.1 Immobilization

In principle, the conventional stereotactic fixation frames used for Gamma Knife and linac-based radiosurgery can also be used for proton radiosurgery.

⁸In this specialized treatment neither a CTV nor a PTV is explicitly drawn. Treatment margins are built into the aperture-design process.

⁹This section was prepared with the help of M. Bussière, Massachusetts General Hospital, Boston MA, USA.



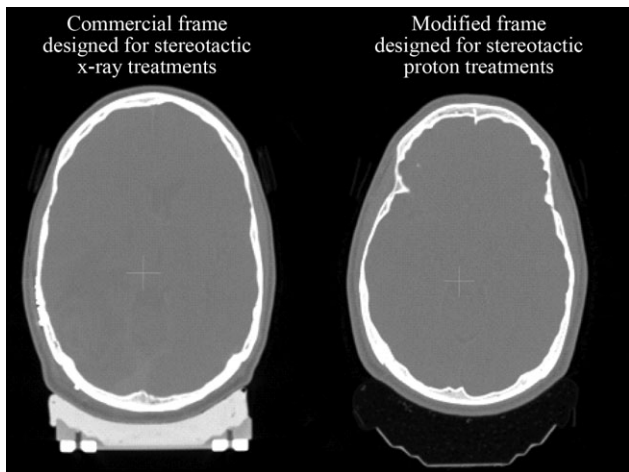


Figure 6.10. A CT scan of a commercially available stereotactic frame (left) that provides a secure fixation but would prevent the use of posterior and posterior-oblique beams because of the high-density occipital pad and plastic-aluminum support. A CT scan of a frame modified for use with protons (right) that uses a thin carbon support along with low-density cushion, enabling any portal direction with only small depth variations across individual treatment beams. (Figure courtesy of M. Bussière, Massachusetts General Hospital, Boston, MA, USA.)

These frames provide both immobilization and a reference coordinate system. The use of the 'built-in' coordinates implies that the processes associated with immobilization, CT scanning, treatment planning, and treatment can be accomplished on the same day. However, this may not be practical because of the time constraints involved with the overall quality-assurance program and the fabrication of custom devices such as apertures and compensators, or for fractionated treatments. The frames are also designed for isocentric-couch systems, and therefore additional effort is required when using nonisocentric beds. If invasive fixation is used, ceramic or aluminum pins, rather than stainless steel pins, will reduce artifacts that would otherwise change the CT densities necessary for range conversions. Commercially, available frames are likely to need modifications in order to control the type and amount of material that protons would encounter proximal to the patient (Fig. 6.10).

An alternative immobilization method is to use a reliable noninvasive frame with an independent coordinate system for alignment (Gall *et al.*, 1993b). Using three or more metallic spheres inserted in the outer table of the skull provides a reliable and accurate coordinate system when used

with a diagnostic-quality imaging platform for the treatment alignment. With this approach, minor changes in the patient's placement within the fixation frame that may occur between the patient being CT scanned and treated are not critical because the patient (not the frame) provides the reference coordinates. However, it is crucial that the frame keep the patient securely immobilized.

6.11.2.2 Imaging

A requirement for proton-therapy planning for stereotactic treatments is CT-based imaging. In order to maximize resolution, the scanner's field of view should be minimized while, nevertheless, encompassing any material that could potentially be traversed by the proton beams. The CT-slice thickness should also be minimized throughout the head (~ 1 mm), which requires the computer treatment-planning program to manage close to 200 axial slices.

For target visualization, a CT-angiography approach should be used, adjusting the time and rate of injection of the contrast agent to optimize the visualization of the area of interest. The presence of unaccounted-for contrast material would result in an incorrect estimate of the needed proton ranges. It is wise to obtain a baseline noncontrast scan to ensure proper conversion of the CT densities to proton ranges. When necessary, the contrast-enhanced CT study used to outline the target(s) and structure(s) of interest can be fused to the noncontrast CT study used for dose calculations. This is especially important when treating a vascular lesion such as an arteriovenous malformation (AVM). Other imaging modalities, such as MRI, PET, and planar angiography, can also be fused, to supplement the CT information.

6.11.2.3 Planning

Most plans use three or four beam directions; however, as many as six can be routinely used for a single target. The shape and location of the target will dictate the beam directions. This is especially true for AVMs, which tend to have irregular shapes and may be situated anywhere throughout the brain. Standard beam combinations can, however, be used for more routine targets such as pituitary adenomas and acoustic neuromas (Appendix B.4). For example, a standard approach for pituitary adenomas, with a typical prescription of

Figure 6.9. (a) Beam's-eye view of the eye, showing the design of the aperture. (b) Isodose lines in a plane through the tumor center. The portions of the eye structures behind the plane are suppressed. (c) Computer rendering of isodose lines on the curved retina. This image has the same scale as the fundus picture of the eye (d), with which it can be accurately compared. (e) Dose-volume histograms of the dose to various structures within the eye. (f) Photograph of a (different) patient in treatment position. (Figure courtesy of J. Verwey, Paul Scherrer Institute, Villigen, Switzerland.)

RBE-weighted absorbed doses of 18–20 Gy (RBE) to the PTV; <8 Gy (RBE) to the optic chiasm and nerves, and <12 Gy (RBE) to the brainstem, is to use four conformal beams: two lateral beams, one from the left, and one from the right, passing through the temporal lobes and avoiding the brainstem and optic structures; a posterior–superior–oblique approach passing through the brainstem but avoiding the temporal lobes and optic structures; and an anterior–superior–oblique approach, passing through the optic structures but avoiding the brainstem and temporal lobes.

Collimation is determined using a BEV approach. The exact margins will depend on the penumbra (a beamline-specific parameter) and the dose normalization. A standard practice is to normalize to the 90 percent isodose. Brass apertures provide the collimation, and compensators provide distal dose shaping. Modulation can be achieved using a variety of techniques including the use of a rotating absorber propeller, or the superposition of discrete Bragg peaks (lamination). Lateral dose equilibrium is lost for small beams, resulting in a change in the depth–dose profile (Fig. 6.11). This must be modeled in the planning algorithm and accounted for in the design of the SOBP.

Because the goal is to have tight margins, it is important to avoid to the extent possible having beams go through heterogeneous regions, as this has the effect of increasing the required modulation and broadening the penumbra. Also, unlike fractionated treatments, patching and abutting beam combinations are not used because of the resulting dose inhomogeneity that can result.

6.11.2.4 Treatment

Treatment sessions involve both alignment verification and dose delivery. Because of their weight,

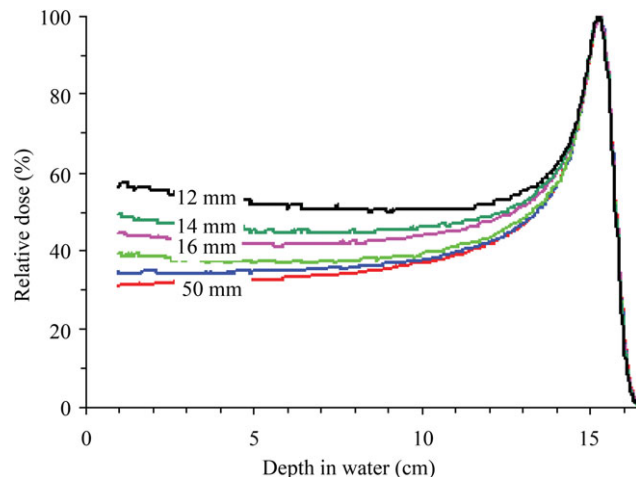


Figure 6.11. Depth–dose curves of 170 MeV protons for a number of circularly shaped beams of diameters 12, 14, 16, 20, 30, and 50 mm. Below 12 mm diameter, the peak-to-plateau ratio rapidly decreases. (Figure courtesy of M. Bussière, Massachusetts General Hospital, Boston, MA, USA.)

large gantries may have an isocentricity that is sub-optimal for radiosurgical tolerances. In such cases, the patient positioner can be adjusted to correct for the gantry-assembly deflections. Alignment verification will depend on the type of patient immobilization (stereotactic versus noninvasive with implanted markers) used, as well as the beam-delivery method (gantry versus fixed beam and isocentric bed versus nonisocentric robotic positioner). A practical approach is to use diagnostic-quality x-ray imaging to image the patient (with internal markers) or the frame with integrated markers. Alignment verification is usually done for every beam. Typical treatment sessions last from 30 to 40 min. The proton-beam dose rate is generally from 2 to 6 Gy min⁻¹.

7 MOTION MANAGEMENT

7.1 MOTION OF, AND WITHIN, THE PATIENT

The patient is not an inanimate object, but a living, breathing, and moving individual. The delivery of radiation to the target volume must involve first, an effort to minimize, to the extent reasonably possible, the motion and its uncertainties, and then taking the remaining motion and uncertainties into account.

Tumor and organ motion can be classified into three categories (Langen and Jones, 2001), namely, motion of the patient as a whole (relative to some reference object such as the couch top), inter-fraction motion of organs within the patient, and intra-fraction motion of organs within the patient during delivery of a single fraction.

7.2 SUPPORT AND IMMOBILIZATION

It is common to use some method of immobilization to better relate the patient to the treatment equipment. In some special cases (see, for example, Sections 3.2.3.1 and 3.2.3.2), the immobilization device is built into the equipment. Usually, a separate device is used and placed upon the couch top or treatment chair, often being indexed to it through the use of locating pins. Mechanisms for patient support have been described in Section 3.2.2.

An immobilization device is used to hold the patient as a whole in a stable and near-motionless position during both imaging and treatment. By doing so, the locations of internal organs and the tumor are also constrained. Immobilization devices also serve to minimize the problem that arises should the patient's position during treatment be different from the patient's position during the planning CT.

7.2.1. Proton-specific aspects of immobilization

Immobilization is particularly important in proton therapy for the following reasons:

- The goal of proton-beam therapy is to conform the treatment volume to the clinical target

volume (CTV) as closely as possible. Protons do this in the depth direction, and the dose is relatively insensitive to motion along the beam direction. However, the dose conformation in the plane perpendicular to the beam is sensitive to lateral motions; hence it needs immobilization.

- Heterogeneities are an issue for protons, much more than for photons (see Section 6.4). The registration of the compensator (either real or virtual) with the heterogeneities to be compensated for is important. If the potential misregistration is taken into consideration during compensator design (see Section 6.4.6.2), then, the greater the possibility of misregistration, the more the compensator has to be expanded and the greater the volume of distal tissue that is irradiated. If the potential misregistration is not taken into account, any mismatch between compensator and heterogeneities could lead to an under-dose within the target volume.

Immobilization has been used in x-ray therapy for many decades, and many techniques of moulage or other physical constraint have been developed. However, protons present two special issues:

- With passively spread beams, optimization of the penumbra demands that the aperture and compensator be as close to the patient as possible (consistent with avoiding hot spots due to aperture-edge scattering). This means that bulky immobilization devices can be problematic.
- With photons, material on the skin surface can spoil skin sparing. But, protons provide virtually no skin sparing, and hence there is no need to avoid material on the skin surface. On the other hand, all material in the beam path affects the beam penetration. Allowance for change in penetration requires knowledge of thickness and composition of such material. Whenever possible, having immobilization material in the path of a proton beam should be avoided.

7.2.2 Immobilization techniques

A review of immobilization methods in radiation oncology is given by Verhey and Bentel (1999). Many types of immobilization devices are available, including bite-block/head-rest combinations for stabilizing the head, partial-body casts for stabilizing the thorax or pelvis, and whole-body casts. Casts can be made *inter alia* from plaster of Paris, using conventional moulage techniques, from thermoplastic sheets that are draped over the patient while warm and become firm upon cooling, and from bags of foam pellets that are made rigid by being placed under vacuum once the bag is made to conform to the patient's surface. Immobilization techniques for special procedures are discussed in Section 3.2.3.

Many immobilization techniques were initially introduced in proton therapy, and have subsequently found a place in conventional x-ray therapy. These include the following:

Stereotactic head holder. The fixation of the head by attaching a stereotactic frame using pins set into burr-holes made in the skull was first used in external proton-beam radiotherapy for the irradiation of intracranial targets, *e.g.*, pituitary gland (Kjellberg *et al.*, 1962a).

Perforated thermoplastic head masks. A warm, perforated thermoplastic sheet is formed to the patient's head and allowed to set by cooling. The perforations serve to keep the head cool and to be less claustrophobic for the patient. The sheet is captured in a tennis racket-shaped frame that is attached to the couch top or chair with the use of indexing pins (Verhey *et al.*, 1982).

U-shaped 'pod', indexed to the treatment couch, supporting a foam-pellet bag. This technique was first developed for π -meson therapy, and then carried over to proton-beam therapy where it has been used at several proton therapy centers (von Essen *et al.*, 1982).

Vacuum-fixed bite block. The use of a bite block fixed to the treatment equipment (*e.g.*, the couch top), while usually providing good immobilization, suffers from the problem that it is of questionable value in the edentulous patient and can place some strain on the patient. This problem has been largely overcome though the use of vacuum suction on a bite block made to conform to the patient's palate (Schulte *et al.*, 2000).

7.3 LOCALIZATION

Once the patient has been adequately immobilized, the target volume in space is located, relative to the treatment equipment. This requires (i) that

the patient be located reproducibly relative to the treatment equipment and (ii) that the target volume be in a known spatial relationship to the patient. The latter is generally based on imaging studies, as discussed in Section 6.3. There are four general approaches to localization, which are described below.

7.3.1 Localization based on skin marks

In some circumstances (*e.g.*, cancers of the skin or lip), the target volume is best placed by the localization of overlying skin. The usual method of localization would then be to adjust the patient's position until a light field coincident with the radiation beam is aligned with the marks on the skin.

7.3.2 Localization based on bony anatomy

Because of the spatial accuracy desired in proton therapy, it is usual to relate the target volume to bony landmarks rather than to skin marks. For this reason, the use of laser beams in the treatment room, as is often done in conventional x-ray therapy, is used only as an initial step in the localization process.

The localization of the target volume relative to the treatment equipment based on bony anatomy proceeds in two steps: (i) the target volume is located relative to the bony anatomy and (ii) the bony anatomy is located relative to the treatment equipment. The first step is accomplished in the treatment-planning process, based on the planning CT study. Once the planning target volume (PTV) has been delineated, the planning process determines the beams to be used and the central axes of these are generally aimed toward a point in space, usually the isocenter. The planning process then establishes the location of the aiming point relative to selected features of the bony anatomy.

The most common way of locating the bony landmarks relative to the patient support system is to compare the alignment radiographs taken in the treatment room with digitally reconstructed radiographs (DRRs) (Goitein *et al.*, 1983b) computed for the same viewpoints. The DRR is a computer simulation, based on an imaging study (in this case, the planning CT study) that, by projecting and accumulating the CT voxel data onto a virtual film plane, simulates a radiograph, taken from any point of view, *e.g.*, from the beam's-eye view or from the viewpoint of an x-ray tube located at a well-defined point within the treatment room. The localization process generally consists of moving the patient until an orthogonal pair of radiographs has the same spatial relationship to the treatment equipment as the pair of corresponding DRRs. In

particular, the location of the bony anatomy relative to a cross hair (which establishes the coordinate system of the radiograph) is required to be the same in the alignment radiograph(s) as in the DRR(s). The process of establishing this correspondence can be done manually or, more objectively and in principle faster, by using a computer (Sharp *et al.*, 2005).

Alternatively, the radiographic information obtained just prior to treatment can be used to compare the patient's position relative to that required for the plan. This information could come from radiographs taken using a pair of (usually) orthogonal x-ray tubes, or from scout views from a CT scanner. In a recent development, a set of cone-beam CT images is acquired using an x-ray tube mounted on the treatment gantry (or a nearby cone-beam CT device) (Jaffray, 2003). These images can be compared with the CT image set used for planning, and the geometric differences between the bony (or other) anatomies in the two studies can be used to compute a positioning correction.

7.3.3 Localization relative to the immobilization device

When an immobilization device or localization frame (see Sections 7.2.2 and 3.2.3) is used, fiducial markers embedded in the localization device or frame can serve in the same fashion as bony landmarks as described in Section 7.3.2. Because fiducial markers can generally be located very accurately, localization in such cases can be more accurate than when using bony landmarks.

7.3.4 Localization based on identification of target-volume markers or the tumor itself

In some circumstances, radiographically visible objects such as gold seeds and surgical clips can be embedded in or close to the tumor; for example, gold seeds have been introduced into the prostate for tumor localization (Shipley *et al.*, 1979). In some cases, the gross tumor volume (GTV) itself may be visible, for example, when using ultrasound to locate the prostate just before treatments. Such techniques provide for accurate target-volume localization. The localization process in the case of radio-opaque markers follows that for bony landmarks.

7.4 VERIFICATION

Once the patient has been positioned for treatment, it is desirable to verify the alignment of the beam relative to the target volume. It may also be

desirable to verify, after the treatment has taken place, whether or by how much the patient has moved during treatment. This may provide valuable information on the efficacy of the immobilization techniques (Verhey and Bentel, 1999; Verhey *et al.*, 1982).

7.4.1 Verification using radiography

There is generally no analogy to the use of portal films in proton-beam therapy, because the proton beam usually does not penetrate the entire patient, and so it cannot be detected in an external detector. If protons are energetic enough to penetrate the patient, they cannot be imaged by a simple detector such as a film as their intensity is largely unchanged by the material through which they have passed (see Section 6.4). Thus, the radiographic verification of the patient's position is usually based on an x-ray radiograph taken along the central axis of the beam (either along the beam direction or, using an x-ray tube distal to the patient, pointing back toward the source of protons). The radiograph thus obtained is compared with a DRR computed from the radiographic viewpoint by the treatment-planning program. It is also feasible to employ a pair of x-ray tubes mounted in the treatment room and directed toward the isocenter to provide fluoroscopic imaging and hence real-time localization during treatment, which can be used for adjusting the position of the patient relative to the beam in real-time. These x-ray tubes need not necessarily be directed orthogonally to one another (Schweikard *et al.*, 2004).

Proton-beam radiography has been proposed, primarily for the verification of heterogeneities within the patient while in the treatment position but also, potentially, to assist in patient localization (Schneider and Pedroni, 1995). This technique requires highly specialized apparatus and has not yet found a place in clinical practice.

7.4.2 Verification using positron emission tomography

Energetic protons and other heavy charged particles undergo collisions with atomic nuclei, some of which result in the formation of a positron-emitting isotope. Positron emission tomography has been used to verify the location of light ion (^{12}C) beams (Enghardt *et al.*, 1999; 2004). Experimental and theoretical evaluations indicate that the same technique works for protons as well (Hishikawa *et al.*, 2002; Nishio *et al.*, 2005; Parodi and Enghardt, 2000; Parodi *et al.*, 2002; 2007a, 2007b; 2007c; Vynckier *et al.*, 1993). The technique

suffers from some disadvantages, the most fundamental of which is that there is usually a physiologic washout of the induced activity during the time period needed to collect the emission data (Maccabee *et al.*, 1969). Another problem is that the cross-section for the activation is not constant along the path length, and in fact there is a threshold energy such that there is no activation near the end of range. Thus the three-dimensional distribution, even with perfect beam delivery, does not exactly match the dose distribution; this is to some extent overcome by looking for any discrepancy between the observed and calculated distributions of activity.

7.5 ORGAN MOTION

Organs and tissues move within the body, both over the course of the entire therapy (inter-fraction motion) and during the delivery of a single fraction (intra-fraction motion). Inter-fraction movement of the tumor and/or organs on a day-to-day or week-to-week basis can, for example, be related to changes in bowel or bladder filling, tumor regression, or changes in the patient's weight. Inter-fraction motion is frequently a problem in treating pelvic tumor sites. It is a particular problem for proton-beam therapy because variable bowel or bladder filling can affect, by centimeters, the penetration of protons passing through those organs.

Intra-fraction motion can occur on a range of time scales. Motion caused by the beating of the heart is periodic in nature, with a cycle time of ~ 1 s; motion caused by respiration is periodic, with a cycle time of ~ 4 s; motion caused by peristalsis is aperiodic and can take place over time scales of up to 1 min. Of these motions, respiration is probably of greatest importance as it can produce quite large displacements and can affect the organs in the abdomen as well as in the thorax (Goitein, 2005; Langen and Jones, 2001). Respiration can sometimes result in excursions of organs of several centimeters, even if the organ is some distance from the diaphragm (e.g., kidney).

7.5.1 The measurement of organ motion

The problems caused by organ motion arise during imaging, simulation, and treatment. During simulation with plane films, the images might not be representative of the tumor position, as they are a single short exposure taken at one time point in the breathing cycle.

For many other forms of imaging, and for CT simulation, the scans can produce a distorted

reconstruction due to image blurring as has been demonstrated by Chen *et al.* (2004). CT techniques have been developed, using single- or multi-slice CT scanners, which have made it possible to obtain multiple sets of CT images that are correlated with well-defined phases of the respiratory cycle using an internal or external gating system (Ford *et al.*, 2003; Low *et al.*, 2003; Pan *et al.*, 2004). These so-called four-dimensional CT scans can provide basic data for planning treatments to largely overcome motion artifacts and to select phases of the breathing cycle when motion is at a minimum.

7.5.2 Organ motion in the absence of special measures

Motion of the patient as a whole will naturally result in motion of internal structures. This motion is minimized by adequate immobilization of the patient, as discussed in Section 7.2, and will not be further discussed here.

A number of studies have documented the extent of motion of several organs, and a comprehensive review has been given by Langen and Jones (2001). Typically, the extent of motion can vary from a negligible amount, to excursions of several centimeters or so in tissues near to, or influenced by, diaphragmatic movement. In the absence of special measures, the only way to deal with situations in which large excursions can occur is to allow generous margins in delineating both the PTV(s) and PRVs. It is likely that if the extent of motion or the artifacts that it produces are underappreciated, the probability of local control might be compromised (Ling *et al.*, 2004).

7.5.3 Organ motion under conditions of respiration gating

The most obvious and simplest way to handle respiratory motion is to track the respiratory cycle, identify the phase(s) when motion is least, and turn the beam off (gate the treatment) during the other phases.

Respiratory gating (Ohara *et al.*, 1989) uses an external breathing monitor to gate the radiation beam on and off at a well-defined phase of the breathing cycle, the external monitor reading having been previously correlated with tumor position. An example of a suitable monitor is a light-emitting diode placed on the patient's abdomen, the position of which is monitored by video cameras while the patient breathes freely. The diode movement is checked to ensure that its position is correlated with the phase of the breathing cycle and, hence, with the location of the target

volume. The diode position can be used to gate CT or fluoroscopic data acquisition, and can be used during treatment to gate the accelerator beam, thus reducing the effect of respiratory motion by synchronizing the dose delivery with the patient's breathing cycle. A wide variety of position-monitoring devices have been used, including a strain gauge or linear transducer attached to the abdomen or thorax, and a temperature-sensitive device inserted in the nostril (Ford *et al.*, 2003). The use of respiratory gating in particle therapy has been described by Minohara *et al.* (2000) and Tsunashima *et al.* (2004).

Deep breath hold at inspiration has been used to reduce the motion of lung tumors. In this technique, the patient is verbally coached to produce a reproducible level of deep inspiration, which is then used during treatment planning and dose delivery (Hanley *et al.*, 1999). The patient breathes through a mouthpiece connected to a spirometer, while nose breathing is restricted with a nose-clip. The coach observes the spirometer signal during treatment, instructs the patient to hold their breath at the appropriate time, and the accelerator is turned on (Mah *et al.*, 2000).

In active-breathing control, the patient breathes through a mouthpiece connected to a pair of flow monitors and valves. The device is used to monitor the patient's breathing pattern and is calibrated during simulation. By closing the valves at a pre-selected phase in the respiratory cycle, the patient's breathing motion can be temporarily halted (Wong *et al.*, 1999). The forced breath hold duration is 10–45 s, depending on the patient, and the sequence will usually need to be repeated several times during the dose delivery, with appropriate rest periods, until the desired dose has been delivered.

The various methods of breath control all have the advantage that the extent of motion of tumors and organs due to respiration can be substantially reduced.

7.5.4 Organ motion with tumor tracking

A problem with all the above techniques is that they reduce efficiency, as only a portion of the patient's breathing cycle can be used for irradiation, or the irradiation is interrupted between breath holds. In addition, they rely on measurements made well in advance of treatment that are assumed to apply at the time of treatment. A more elegant solution would be to track target motion during the treatment (*i.e.*, by imaging implanted seeds or surgical clips) and adjust the position of the beam appropriately relative to the

patient, while the accelerator runs continuously. The adjustment could be achieved by moving the patient couch as a function of time, or by moving the radiation beam. In the latter case, for scattered and wobbled proton beams the position of the aperture or settings of the multi-leaf collimator (but probably not the compensator) would be modified. In the case of scanned beams, the settings of individual pencil beams would be adjusted as they are delivered. Li *et al.* (2004) have simulated the time-dependent effects of target motion for a scanned ion beam. They have theoretically shown that online motion compensation with a scanned ion beam can yield a restoration of the dose homogeneity of >95 percent. However, such a tracking system has yet to be demonstrated practically.

7.6 COMPENSATION FOR PATIENT AND ORGAN MOTION

For any given set of patient immobilization and patient and organ localization techniques, there always remains some degree of residual motion and some uncertainties about the locations of patient, target volume(s), and organs at risk (OARs). These uncertainties must be taken into account in planning the treatment (Mageras *et al.*, 1996).

7.6.1 Margins at the periphery of the CTV or OARs: lateral margins

The first task is to add a lateral margin or margins to the beam in order to allow for uncertainties by: (i) defining a PTV (or PTVs) for the clinically determined CTV(s); and usually, (ii) the PRVs for all delineated OARs. The manner in which these margins should be established has been the matter of considerable study.

When delineating a PTV, the different types of margins must be added or combined. If margins are added linearly, the resulting PTV can often be too large, with a consequent risk of exceeding patient tolerance. A quadratic approach similar to that recommended by the Bureau International des Poids et Mesures (BIPM, 1981) can be employed. It provides a means to combine random and systematic, as well as correlated and uncorrelated uncertainties (Mijnheer *et al.*, 1987a). Utilizing this approach, in order to find the overall margin (*i.e.*, the internal margin and the set-up margin together), the overall systematic error can be derived by adding quadratically the separate

systematic errors:

$$\Sigma = \left(\Sigma_{\text{set-up}}^2 + \Sigma_{\text{organ motion}}^2 + \Sigma_{\text{delineation}}^2 \right)^{1/2}, \quad (7.1)$$

and similarly, the overall random error can be derived by adding the separate random errors quadratically:

$$\sigma = \left(\sigma_{\text{set-up}}^2 + \sigma_{\text{organ motion}}^2 \right)^{1/2}. \quad (7.2)$$

Several approaches have been published to quantify the CTV-to-PTV margin requirements (Austin-Seymour *et al.*, 1995; Balter *et al.*, 1996; Crook *et al.*, 1995; Goitein, 1985; Roeske *et al.*, 1995; Stroom *et al.*, 1999; van Herk *et al.*, 2000).

Stroom *et al.* (1999) presented a model that was tested for prostate, cervix, and lung cancer. A CTV-to-PTV set-up margin size, which ensures at least 95 percent of the dose is delivered to 99 percent of the CTV, is given by $2\Sigma + 0.7\sigma$, Σ being the standard deviation for the systematic error (average set-up deviations per patient in the group of patients) and σ the standard deviation for the random error (day-to-day set-up positions). Van Herk *et al.* (2000) came to a similar conclusion that the standard deviation for the systematic errors is three times larger than for the random errors. On the other hand, McKenzie (2000) pointed out that breathing-induced motion should be accounted for separately, with the breathing margin added linearly to the quadrature sum of the other contributing factors.

Unfortunately, this ideal approach can be applied only in situations in which one can identify the causes of errors and quantify the uncertainties (e.g., by standard deviations). Currently, this is not generally possible except for a few situations (e.g., some conformal therapy protocols).

However, it should be understood that the delineation of the PTV is a matter of compromise and is not simply a mathematical concept. It requires clinical judgement, and thus, is the responsibility of the radiation oncology team.

Note that the penumbra of the beam(s) is not considered when delineating the PTV. However, when selecting the beam sizes, the width of the penumbra has to be taken into account and the beam size must be enlarged accordingly. The beam sizes are defined by the 50 percent isodose (ICRU, 1976).

Studies have shown that intra- and inter-observer variability can be a large source of uncertainty in GTV and, especially, CTV delineation. The

uncertainty in the delineation should be included in margin considerations.

7.6.2 Margins at the periphery of the CTV or OARs: margin in depth

For protons, a margin in depth between the treated volume and the CTV must be provided to allow for uncertainties in proton-beam penetration. For reasons already given (see Section 5.1.4), the PTV may not be a very helpful tool for designing these margins. The correct approach is to assess the sources of uncertainty in the proton penetration (e.g., uncertainties concerning the precise location of patient's skin surface and internal organs, the effects of overlying heterogeneities, and the dose computation algorithm) and then design the compensator, so that the lower uncertainty bound of the treatment volume just covers the CTV (see Section 8).

Motions of internal organs transverse to the beam direction can, in addition to the possibility of causing under-dosing the tumor periphery, have a subtle influence on tissues distal to the moving organ or tumor. In the lung, for example, motion of a tumor transverse to the beam direction can affect the proton-beam penetration distal to the region of the tumor as changes in the shadowing of downstream tissues by the tumor will affect the penetration of protons reaching those tissues.

7.6.3 Dose variation within the CTV and OARs: interplay effects

With uniform beams produced by scattering, the beam is essentially delivered statically¹ and the dose internal to the target volume is, in practice, largely unaffected by organ motion or patient misregistration. The situation is different if the beam is applied dynamically, as with scanned beams.

When a scanned proton beam is applied, organ motion can cause both positive and negative fluctuations in the dose distribution due to what have been termed 'interplay effects' (Bortfeld *et al.*, 2002; Phillips *et al.*, 1992). Interplay effects arise because both the beam delivery and the target of that delivery are changing with time. A cell within an organ (Goitein, 2005) might move synchronously with the beam while it is being scanned in some direction and, as a result, receive either more dose (when the movement is in the scan direction) or less dose (when the movement is in the direction opposite to the scan) than was

¹In practice, even scattered beams are scanned in depth. However, the period of depth scanning is so much less than that for organ motion that this motion can be ignored.

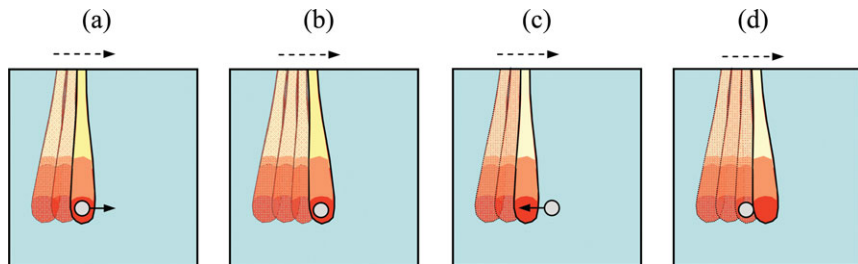


Figure 7.1. Schematic illustration of the interplay effect.

intended—giving rise to ‘dose mottle’. Because the total energy delivered by a beam is not appreciably affected by motion within the patient, the average dose within a volume of interest tends to be unaltered.

The interplay effect is shown schematically in Fig. 7.1. Pencil beams are being delivered from left to right, along the direction of the dotted arrow. Two situations are shown. In frames (a) and (b), a cell is moving to the right, in the same direction as the scan. At the time of frame (a), the cell is receiving dose from the third pencil beam; at the later time of frame (b), a fourth pencil beam has just been applied. The cell has now moved into the path of the fourth pencil beam, and so receives an additional unintended dose which could as much as double the dose it would have received if it were stationary. Frames (c) and (d) demonstrate the opposite case in which a cell is moving to the left—in the opposite direction to the scan. At the time of frame (c), the cell is receiving almost no dose; at the later time of frame (b), a fourth pencil beam has just been applied. Meanwhile, the cell has now moved out of the path of the fourth pencil beam, and so receives almost no dose—so that the total dose delivered to this cell is much less than had it been stationary.

With scanned beams, interplay effects arise when the frequencies of the beam scan and of organ motion are comparable. Typical organ motions have a period of between a fraction of a second to several seconds. Scanned-beam delivery, on the other hand, has three dimensions of scan, namely, the two lateral directions and penetration in depth, which are usually administered with a high, medium, and low frequency. Since the dose delivered by a beam should be deposited in ~ 1 min, it is almost guaranteed that at least one of the three motions will have a period on the order of that of organ motion.

The most direct way of mitigating the influence of motion on dose mottle within the CTV and/or OARs is by repeating the sequence of pencil beam delivery several times—a process termed

‘repainting’. This is further discussed in Sections 3.2.1.2.2 and 7.6.3.2.

Interplay effects occur with scanned beams regardless of the intensity profile of the beam. However, when the intensity varies spatially very rapidly within a beam, as can be the case in intensity-modulated radiation therapy (IMRT), the magnitude of the dose mottle may be greater than for a uniform intensity beam. This effect can be reduced by limiting the steepness of spatial changes in the beam intensity in IMRT.

7.6.3.1 *Experimental observation of interplay effects*

That the interplay effect is not merely a theoretical problem is evidenced by a radiobiological experiment performed by Gueulette *et al.* (2005). They were engaged in measuring the relative biological effectiveness (RBE) of protons by assessing crypt cell regeneration after whole-pelvis irradiation of experimental mice. The proton beam was a scanned beam, with a pencil width at the location of the animals of ~ 10 mm full width at half maximum. They observed a much greater fluctuation in their results than in the x-ray beam controls or in previous experiments on scattered-proton beams, and this effect was reproduced when they repeated the experiment. The scatter in the results was consistent with fluctuations in dose of approximately ± 13 percent (1 SD), while the measured beam profile was flat within a few percent. They ascribed the scatter to movements of the mice intestines during irradiation. Radiographs showed that the intestines of similarly-immobilized mice moved by up to ± 2 mm. Although there was wide scatter in the data, the RBE at the center of a spread-out Bragg peak, based on a fit to the data, was entirely consistent with values measured using the same animal model in several scattered proton beams (namely 1.16, but with wide confidence limits). This underlines the point that the mean dose might not be much altered, even though dose mottle may be quite large.

7.6.3.2 Repainting to reduce the influence of interplay effects

Phillips *et al.* (1992) have quantitatively analyzed the effects of organ motion and the need for repainting (termed 'multiplicity' by the authors), and Bortfeld *et al.* (2002) have demonstrated in a model that interplay effects can be substantial for scanned beams, namely dose variations of the order of ± 10 percent. They point out that, when multiple fractions are given, the effect tends to average out. However, one does not always give many fractions, and the safest and most straightforward way to overcome interplay effects is to repeat the dose delivery several times (obviously each application having a proportionately lower dose) during the application of a single scanned beam. Provided the repaintings occur asynchronously with respect to the organ motion, the reduction in dose fluctuations should be of the order of the inverse of the square root of the number of repaintings. This argument would suggest that something like 10 repaintings would be desirable. However, there is little need to repaint pencil beams that deliver relatively little dose, and therefore only a subset need to be repainted and one might conclude that only the few highest energy 'layers' need to be repainted. This would be the case when the PTV is approximately rectangular in shape as suggested in Fig. 7.2a. However, for a near-spherical tumor, which is a much more realistic case, the high-dose Bragg peaks are deposited in many layers, as shown in Fig. 7.2b. For example, when the spacing in depth is, say, ~ 5 mm in a target of, say, ≈ 15 cm diameter, pencil beams spread over something like 15 layers would need to be repainted.

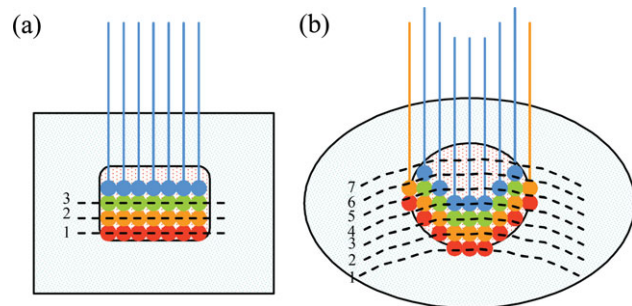


Figure 7.2. Schematic diagram of the application of a scanned beam in several energy layers. The highest weighted spots are colored red, followed by orange, green, and blue in decreasing order of weight. The dotted lines are iso-range lines, with the longest range labeled '1'. (a) If the target volume is near-rectangular, and only the distal three spots (red, orange, and green) need to be repainted, then only three energy layers need repainting. (b) For a near-spherical target volume, pencil-beam spots in many more energy layers need to be repainted (five or six in this schematic example). For a more realistic situation, from 10 to 20 layers would include at least some pencil beams that would need to be repainted.

7.7 CONCLUSION

Motion and misregistration of the target volume with respect to the radiation beams is, at some level, inevitable. If the target volumes are to be adequately irradiated, and adjacent OARs are to be protected: it is essential that the causes and possible magnitudes of motion and misregistration are understood; that their possible consequences are understood; that measures be taken to minimize motion and misregistration to the extent possible and clinically warranted; and that steps are taken to allow for the remaining degrees of motion and misregistration.

8 ESTIMATION AND PRESENTATION OF UNCERTAINTY IN THE DELIVERED DOSE

8.1 THE INEVITABILITY OF UNCERTAINTY

Radiation therapy is inherently probabilistic. One cannot be certain as to whether a tumor will be controlled, or whether any given normal tissue will be damaged. These outcomes can be stated only in terms of probabilities. In addition, the application of radiation involves very many factors, almost all of which have some level of associated uncertainty. For example, there are uncertainties regarding the following:

- the identification of the tumor and the designation of its histology and staging;
- the spatial extent of the tumor and of organs at risk (OARs; images may be incorrectly interpreted, they may be distorted, and so forth);
- for external-beam therapy, the immobilization and localization of the patient and of the tumor within the patient, and the effects of physiologic motions on the dose delivered to any point within the patient;
- the assessment of the distribution of heterogeneities, the effects of heterogeneities, and imperfections in the techniques to compensate for them;
- the algorithms used to estimate dose;
- the many parameters involved in the delivery of treatments.

Given such uncertainties, one seeks to understand the sources of uncertainty, to reduce them whenever practicable, and to evaluate the magnitude and implications. The mere exercise of identifying the sources and magnitudes of uncertainty can be a valuable aspect of developing and judging a plan.

In the practice of radiotherapy, the estimation and reporting of uncertainty has historically been at best implicit. Experienced physicians evaluating a treatment plan undoubtedly make some mental assessment of the magnitude of the known uncertainties and what the consequences may be. However, the current state-of-the-art treatment-delivery techniques seek greater geometric accuracy in dose delivery, and are more complex than those employed previously. Such methods have

many additional potential sources of uncertainty: interplay effects that, with beam scanning, can lead to a degree of dose inhomogeneity within the tumor that are not normally encountered in conventional radiotherapy (see Section 7.6.3), registration uncertainties (e.g., between a physical or virtual compensator and the patient) and, in charged-particle therapy, the effect of inhomogeneities within the patient that can strongly influence the dose distribution in their shadow. In this environment, it can be very difficult to assess the dose implications of the uncertainties through visual inspection, and some form of computational approach is required. Unfortunately, currently available radiotherapy-planning systems have yet to embrace uncertainty analysis.

Although, as just emphasized, there are many sources of uncertainty, some of them do not readily lend themselves to computational analysis. The following discussion is limited to the important question of the extent to which the prescribed dose distribution is a true representation of the distribution of dose the patient actually receives.

8.2 THE ESTIMATION OF UNCERTAINTY

In analyzing a radiation-treatment plan, there are at least two types of data whose uncertainties need to be estimated. The first involves the estimate of the uncertainty in the dose at selected points in three-dimensions within the patient. The second type involves the estimation of uncertainties in quantities such as $D_{98\%}$, $D_{50\%}$, EUD, TCP, and NTCP or in quantities used for constraints, such as the volume receiving greater than a certain dose D , V_D , or the minimum dose that is delivered to a given volume V , D_V . In this category is also the quantification of the adequacy of dose coverage of the planning target volume (PTV) and OARs.

The terminology of uncertainty analysis has been clarified in ISO (1995). However, little has been reported in the literature in relation to making estimates of uncertainty in radiotherapy. A general

review was presented in Urie *et al.* (1991). A method has been described (Goitein, 1985) to estimate the uncertainty limits associated with a particular treatment plan (see Section 8.3). Dose uncertainties in proton-beam therapy have also been estimated as suggested in Goitein (1978a; 1982a) and Lomax (2001).

At another level, a body of work has appeared in the last few years analyzing patient set-up uncertainties and motions from the point of view of determining the most appropriate safety margin around a tumor volume (van Herk, 2004), and more recently a number of authors have also begun to look into the problem of dealing with uncertainties at the optimization level, mainly from the point of view of organ motion (Beckham *et al.*, 2002; McShan *et al.*, 2002).

A confidence level (CL) must be associated with any uncertainty estimate. Without a statement of the CL, an uncertainty estimate is meaningless. It is common in reporting radiotherapy results to indicate the 95 percent (2 SD) confidence intervals. Goitein (1983) argued that, for many purposes in radiation therapy, 1 SD is too low a CL, and 2 SDs are too high, and that an 85 percent confidence interval, corresponding to ~ 1.5 SDs, is a more useful interval for many applications.

8.3 THE PRESENTATION OF UNCERTAINTY

The presentation of the uncertainty in a three-dimensional dose distribution presents a challenging problem because of the plethora of data. One approach is described by Goitein (1985) and by Urie *et al.* (1991), an example of which is shown in Fig. 8.1, taken from Urie *et al.* (1991). Three dose distributions are juxtaposed: the nominal (most likely) dose distribution, and, separately, the upper and lower bounds on the dose at each point (at the stated probability level). This highlights the scale of potential problems that can arise as a result of a beam juncture from possible treatment uncertainties and, in Fig. 8.1e, how these can be reduced by beam feathering (see Section 6.2.4.5).

An alternative approach is described in Lomax (2001). In this method, dose distributions are calculated for a number of translated (or rotated) CT datasets, and, potentially, from datasets with altered CT numbers to simulate density uncertainties. A hybrid dose distribution, which indicates the worst-case dose at any point, is then computed as follows. For points within the PTV and CTV, the dose is set to the lowest dose at that point in any of the calculated dose distributions. For those points

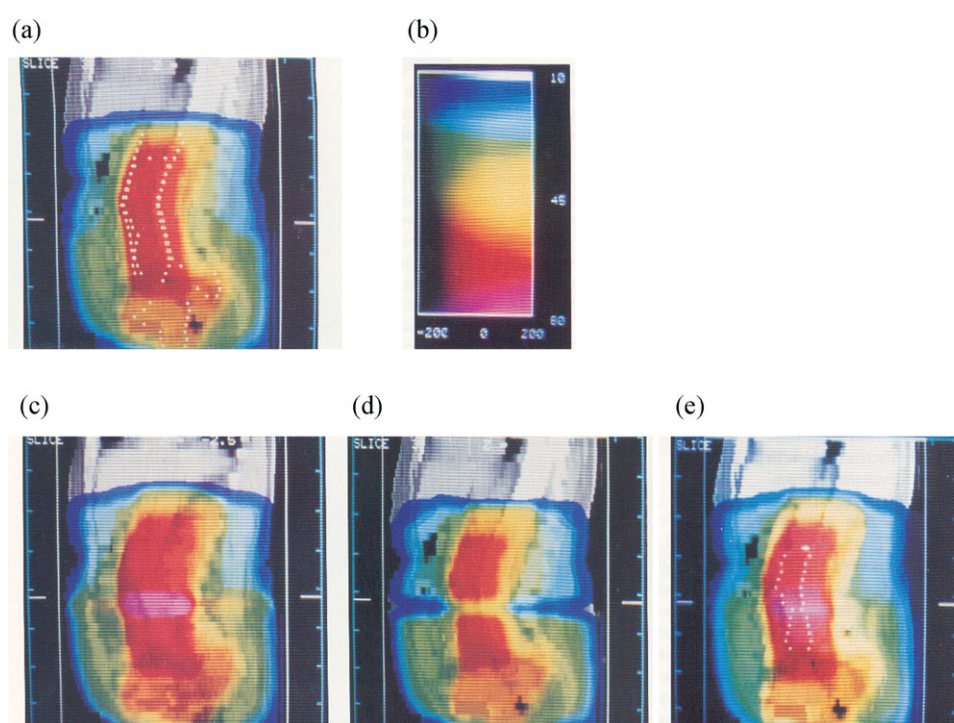


Figure 8.1. Display of the dose distribution in a sagittal section of a patient whose para-aortic nodes are being treated with parallel opposed x-ray beams, using beam junctioning (Urie *et al.*, 1991; reproduced with permission). (a) Nominal dose distribution; (b) absolute dose scale (color from 10 to 80 Gy; color gray < 10 Gy); (c) the upper-bound dose at the 85 percent CL, showing the possibility of a significant region of high dose; (d) the lower-bound dose at the 85 percent CL, showing the possibility of a significant region of low dose; (e) the upper-bound dose when the junction is feathered ($-1, 0, +1$ cm). A much smaller hot spot is seen in the overlap region [compare (e) with (c)].

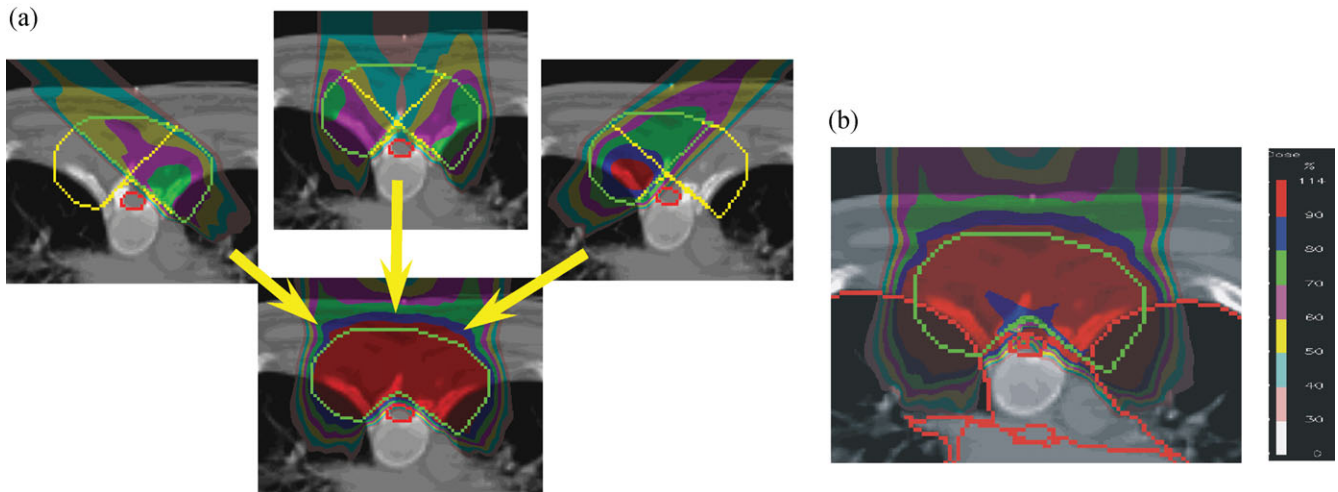


Figure 8.2. (a) The individual beams of a three-beam IMPT plan for a thoracic chordoma, with the nominal combined dose distribution at the bottom. (b) The ‘worst case’ distribution resulting from 5 mm shifts along each major axis of the patient. The worst-case distribution is calculated at each point by taking the minimum dose of these shifted doses within the CTV, and the maximum dose outside. Note the potential cold spots (blue areas) that could occur where beams abut (*i.e.*, along the patch lines of the oblique beams with the posterior beams). (Figure courtesy of A. Lomax, Paul Scherrer Institute, Villigen, Switzerland.)

outside the PTV (and, hence, within normal tissue), the dose is set to the highest in any of the calculated dose distributions. This then documents potential cold spots within the tumor and, in the same display, potential hot spots within normal tissues. Such an analysis is shown in Fig. 8.2; the potential cool regions in the tumor (colored blue corresponding to a 10–20 percent dose reduction) are because of possible junction problems with the three abutting beams. This form of data presentation has its origins in the display of ‘regions of regret’, which was suggested in Shalev *et al.* (1988).

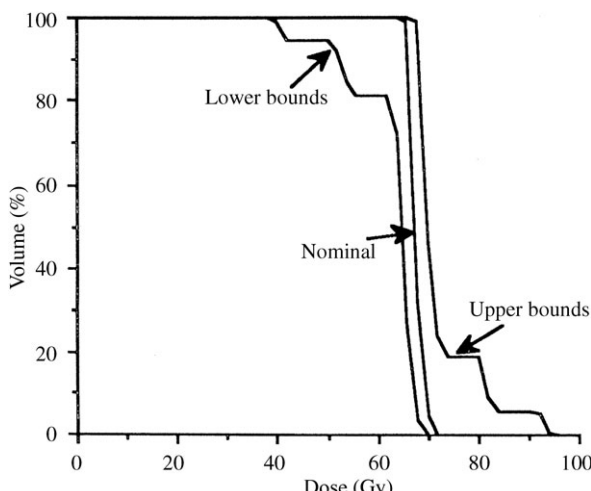


Figure 8.3. Dose–volume histogram with upper and lower bound limits (at the 85 percent CL) for the dose distributions shown in Fig. 8.1a, c, and d (Urie *et al.*, 1991; reproduced with permission). The potential hot and cold spots are very evident in the DVH, but their spatial locations, of course, cannot be inferred from the DVH.

Dose–volume histograms (DVHs) (Drzymala *et al.*, 1991; Shipley *et al.*, 1979) are also an important dose-summarizing tool. Techniques for estimating and displaying uncertainty bands for DVHs have been reported (Drzymala *et al.*, 1991; Niemierko and Goitein, 1994; Urie *et al.*, 1991). These techniques lead to the display of a band in dose–volume space, within which a given point of the true DVH lies (at a stated level of confidence). An example of this is shown in Fig. 8.3, which is reproduced from Urie *et al.* (1991). In this display, as with the uncertainty bounds of Figs 8.1 and 8.2, the uncertainties in the dose at points within the patient are generally highly correlated with one another so that a DVH following one of the uncertainty bounds is generally not physically realizable. Unfortunately, such displays are unable to exhibit this fact.

The PTV is defined largely to accommodate alignment and motion uncertainties, and the treatment plan is frequently designed such that the PTV receives a lower dose at its boundaries than in its interior. Because the CTV moment-to-moment or day-to-day is unlikely always to be located near the edge of the PTV, the DVH of the PTV will tend to underestimate the doses in the possible lower-dose regions in the CTV. On the other hand and for the same reasons, the DVH of the CTV will tend to overestimate the doses in the possible lower-dose regions in the CTV. Consequently, the DVHs of the PTV and CTV probably bracket the dose the tumor actually receives and, as such, can be used to estimate an uncertainty band about the ‘true’ (but unknowable) tumor DVH.

8.4 RECOMMENDATIONS FOR THE CONSIDERATION AND REPORTING OF UNCERTAINTY

- Those involved in designing radiation treatments should analyze the uncertainties; make an effort to minimize them to the extent practicable; ensure that a quality assurance program is in place to give assurance that the treatment can be given as prescribed; and document their assessment of the remaining uncertainties.
- Treatment planning systems should provide tools for the analysis, quantification, and display of uncertainties.
- For normal reporting purposes, in uncomplicated cases, the uncertainties in the full three-dimensional dose distribution need not be pre-

sented, but those in summarizing quantities (see Section 5.6.2) should be estimated, together with their corresponding confidence intervals. Such an estimate could be stated as follows: 'Doses are judged to be accurate to x percent of the prescription dose, or to be within y mm of the true location (at the z percent CL).' The uncertainty estimate might be based on generic analyses of the particular class of treatment, in which case it should be so-noted.

- For cases where unacceptably large uncertainties might exist, and for illustrative purposes in scientific reports: the uncertainties in the dose distribution(s), as well as those in summarizing quantities, should be estimated and presented, together with a statement of the corresponding confidence intervals.

9 QUALITY ASSURANCE

A comprehensive quality assurance (QA) program for a proton-beam therapy facility consists of procedures that ensure a consistent and safe fulfillment of the dose prescription as well as minimal radiation exposure to the personnel and the public. Practical implementation of a QA program depends on the details of the proton accelerator and the selected beam-delivery technique. In many cases, QA checks will be relevant only to the particular equipment or to the implemented technology. Very often the institution that has acquired a new proton-beam therapy facility plays the dual role of both manufacturer and user, and therefore the proposed checks are a result of research and development, and could be modified with accumulated experience.

The QA measurements described below follow the steps of the proton-therapy procedure and focus on dose delivery and treatment planning. Commissioning and validation of proton-beam delivery and treatment-planning systems (TPSs) include machine-specific beam-data acquisition, data entry into the treatment-planning system, validation of the calculations, development of operational procedures and constancy checks, as well as training of all staff concerned with the operation of the system. New types of proton-beam-delivery systems might also require biological assessment as a part of commissioning (Kagawa *et al.*, 2002; Pedroni *et al.*, 1995), whereas preclinical testing of commercially available facilities is usually limited to physics and dosimetry acceptance checks (Kooy, 2002). The data obtained during the commissioning and validation process are used later as benchmarks and thresholds for periodic QA checks. Acceptance, commissioning, as well as periodic engineering and maintenance checks of proton accelerators and multiple treatment room switchyards are not discussed, as the acceptance and quality control of particular proton accelerators and switchyards with vacuum beam lines, focusing, bending, and steering magnets, power supplies, and cooling equipment are usually based on the recommendations of the manufacturer and might not be relevant to another type of machine.

9.1 PROTON-BEAM DELIVERY SYSTEMS

Only a few publications and internal reports are available, which describe commissioning and periodic QA checks of different components of the beam-delivery systems (Chu *et al.*, 1993; JASTRO, 2004; Moyers, 1999; Pedroni *et al.*, 1995; Schreuder, 2002). The nozzle of a proton-beam-delivery system using dual scattering foils consists of a fixed section that contains various components for beam shaping and beam monitoring, and a movable snout that permits positioning of the patient-specific devices, such as aperture and compensator/bolus (see Section 3). The snouts are designed to minimize radiation leakage to the patient, and a part of quality control is focused on the radiation-protection issues. The integrity and quality of alignment of hardware components should be checked through the analysis of depth-dose curves and lateral profiles that are measured in a water phantom. Although measured results are needed to verify performance specifications and provide benchmarks for treatment-planning software (Moyers, 1999), the use of Monte Carlo simulation (Paganetti *et al.*, 2004) can also support dosimetry efforts in helping to define safety tolerances and to design QA procedures. The Monte Carlo simulation of an isocentric-gantry treatment nozzle described by Kooy (2002) and by Paganetti *et al.* (2004) allows the sensitivity of proton-dose distributions in a water phantom with respect to various beam parameters and geometrical misalignments, to be studied, and, as a result, the tolerance levels for these parameters might be established. Figure 9.1, for example, shows the high sensitivity of the Bragg peak to beam misalignment. Depending upon the amount of material in the beam, the pristine Bragg curve is characterized by either a low-energy tail or possibly by a secondary Bragg peak at a different depth. The upper part of Fig. 9.1 shows the effect on the depth-dose distribution of a beam scraping a frame used to support the first scatterer, whereas the lower part shows the proton energy distribution at a water phantom surface. On the basis of measurements and results of simulation, it is possible to calculate tolerances for the appropriate

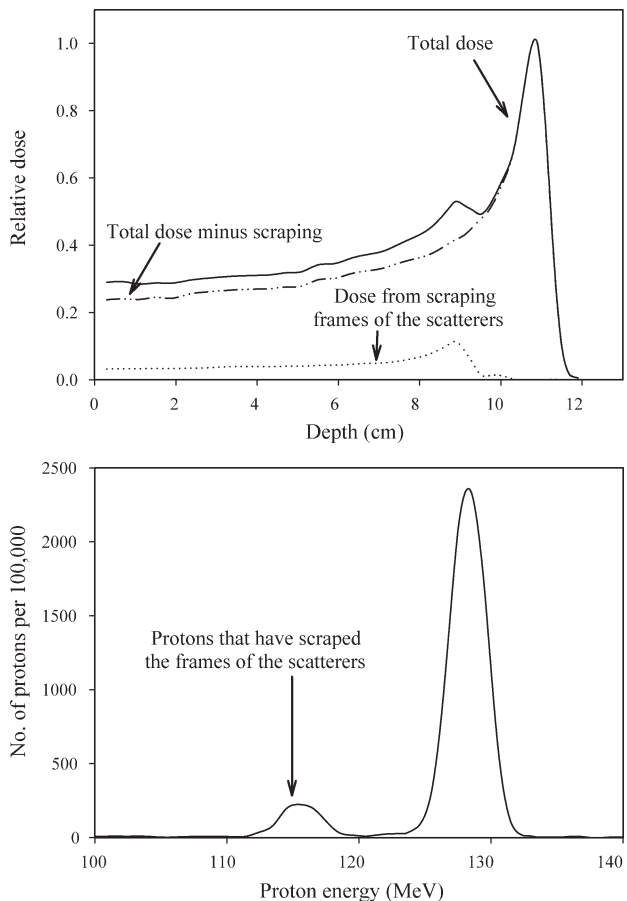


Figure 9.1. An example of the effect of beam misalignment on the pristine Bragg peak and on the proton spectrum (Paganetti *et al.*, 2004; reproduced with permission).

operational parameters for beam delivery and action levels that should be used in periodic checks. Characterization and periodic stability checks of the mechanical and radiation isocenter for proton gantries are important in order to facilitate better patient alignment from all beam directions. A procedure to determine the shape and size of the proton gantry isocenter to within 0.2 mm is given by Moyers and Lesyna (2004).

Periodic QA checks for wobbling and scanning delivery techniques are similar to those for the passive beam scattering technique. However, because these delivery systems are dynamic and accurate delivery of the planned dose depends on the accurate deposition of individually weighted pencil beams, additional QA methods are required for scanned-beam systems. Measuring procedures for the determination of the shape, position, and direction of individual pencil beams must be developed, together with methods for assessing the homogeneity of the dose and shape of complex fields, which can be delivered with such systems (Chu *et al.*, 1993; JASTRO, 2004; Pedroni *et al.*, 2005).

An important part of quality-control procedures is related to beam monitoring with multi-wire and multi-segment ionization chambers that control deviations in beam position, check the beam size and its uniformity, and control the dose delivered to the patient during the treatment. Usually, ratios of signals between various detectors are used to trigger safety control interlocks and terminate beam delivery. Tolerance values for beam termination should be specified to ensure proper settings of range-shifter devices, selection of scattering-foil positions, and rotational velocity of modulator propellers. The calibration of the primary dose monitor should be based on ionization-chamber measurements in a water phantom, and dose calculations using an established dosimetry code of practice (see Section 4). The monitor calibration is performed on a daily basis at many proton-therapy facilities. For daily checks of scanned-beam systems, an ionization chamber is positioned in the reference volume (often a $10 \times 10 \times 10 \text{ cm}^3$ cube) within a water phantom, which is irradiated so as to deliver a dose of 1 Gy to the reference volume (Coray *et al.*, 2002). Figure 9.2 shows an example of the relative doses measured daily in a homogeneous volume. The effect of the energy and the gantry angle on dosimetry should also be checked periodically. The relation between the proton-beam energy and the monitor-chamber response should be frequently checked (Coray *et al.*, 2002).

If a rotating gantry is used, multiple irradiations from different directions are often carried out with the patient in the same position. The monitor calibration value should be corrected at each gantry angle if the value varies as a function of gantry angle. The stability of the monitors with gantry angle and reproducibility of the beam from

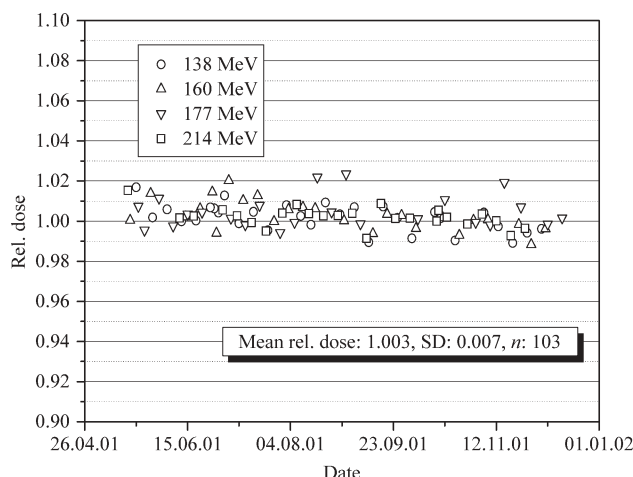


Figure 9.2. Dose measured daily in the center of a reference volume in a scanning beam (n is the number of data points) (Coray *et al.*, 2002; reproduced with permission).

the accelerator should be verified as a part of periodic QA checks (JASTRO, 2004; Moyers, 1999).

9.2 PATIENT POSITIONING AND IMMOBILIZATION

Accurate positioning of the patient in the proton beam requires location of the patient on the support system and precise operation and correct interaction of two systems: one that performs and controls the movements required to place the patient in the prescribed position, and another that verifies the position of the patient relative to the beam axis (see Section 7). The geometric/positioning measurements are performed to quantify the accuracy of the patient-positioning devices and the patient alignment with respect to the nozzle and gantry. The periodic checks of coincidence of the proton-beam isocenter and the patient setup-laser positions can be performed using a phosphor imaging plate (IP) (Terunuma *et al.*, 2003). When radiation is applied to an IP, an image of the radiation field is temporarily stored in the IP. The IP is then exposed to the patient position laser. As a result, the radiation field produces a 'positive' image while the patient setup laser creates a 'negative' image of its position. The advantages of this method are direct measurements in a short time, with high resolution.

The periodic QA checks of stereophotogrammetric positioning systems (Jones *et al.*, 1995) and digital x-ray imaging systems deal with the calibration of charge-coupled device (CCD) cameras and verification of the alignment of the axial x-ray imaging system (Schreuder, 2002; 2004). If automatic positioning based on comparison of digitally reconstructed radiographs (DRR) and x-ray data is employed, a check of the accuracy of the positioning algorithm should be done (JASTRO, 2004; Lesyna, 2004). Patient positioners can also include high-precision robotic systems (de Kock, 2002; Schreuder, 2004) that are capable, in combination with gantry angulations, of locating the treatment isocenter at any point within the patient so as to direct the beam from any angle through that point. The accuracy of robotic patient positioning depends mainly on the capability of the robot control and safety software rather than on the mechanical accuracy of the couch, and therefore periodic quality control involves a substantial amount of software and safety checks (de Kock, 2004).

9.3 TREATMENT-PLANNING SYSTEMS

The report of Fraass *et al.* (1998) contains recommendations from AAPM Task Group 53 (TG 53)

for QA of radiotherapy TPSs. This report and the recently published report from the IAEA, TRS 430 (IAEA, 2004), deal with an image-based three-dimensional TPS and can be generally applied to TPSs used in planning radiotherapy with protons. However, emphasis should be given to specific issues not covered by TG 53 (Fraass *et al.*, 1998) or TRS 430 (IAEA, 2004). The TPSs used at proton centers with a passive scattering beam-delivery system are mostly based on scatter-convolution algorithms (Moyers, 1999). This method employs as input data the measured depth-dose tables, off-axis profiles, and output factors for each energy and modulator combination. During commissioning, the dosimetric characteristics of the proton beams, such as depth doses, off-axis profiles, field-size factors, modulation factors for different field sizes, penumbra sizes, and beam ranges, should be measured and recorded for validation of the TPS and also stored in a database to be referenced in future periodic QA checks (JASTRO, 2004; Moyers, 1999). Again, for scanning systems, the beam data-acquisition procedure is somewhat different, and requires the measurement of depth-dose curves and lateral profiles of pencil beams, requiring small-field dosimetry equipment with a good spatial resolution (Pedroni *et al.*, 2005).

TG 53 (Fraass *et al.*, 1998) and TRS 430 (IAEA, 2004) do not cover the calibration of computed tomography (CT) images and conversion of CT Hounsfield units to proton stopping powers. The uncertainty in the range of protons due to inaccurate calibration of CT images and beam hardening artifacts is estimated by Schaffner and Pedroni (1998) to be 1.1 percent (1 SD) of the total range in soft tissue and 1.8 percent (1 SD) in cortical bone for the CT scanner that they used. Given the importance of the accuracy of the CT Hounsfield values, it is strongly recommended that regular checks of the consistency of the CT Hounsfield values be performed.

A proton-beam TPS usually has automated features to design aperture shapes from target-tissue outlines and to design compensator/boluses that provide distal-edge target coverage. Boluses that control penetration of the beam in non-uniform phantoms relative to the shape of the distal side of a specified target-tissue region are designed using preset margins. User-specified amounts of bolus expansion to account for lateral proton scatter and patient-position uncertainty are employed in bolus design (see Section 6). Tests using actual tissue samples to simulate typical treatments are performed as a final test to verify the design of a bolus intended to compensate for

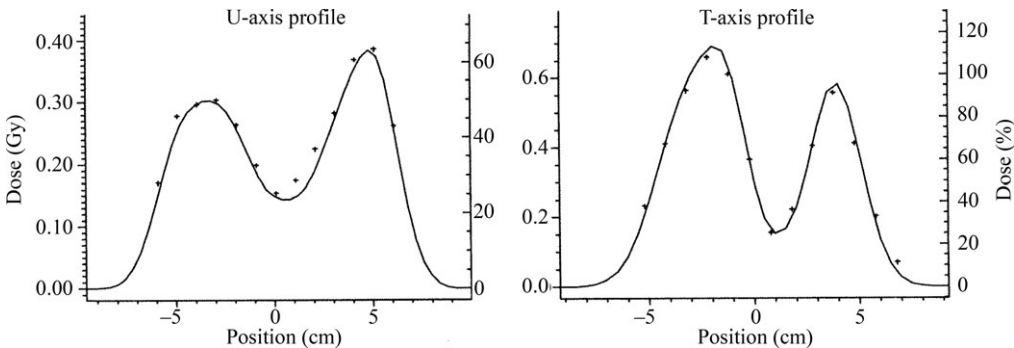


Figure 9.3. Verification of patient treatment in a scanning beam. The calculated orthogonal dose profiles (solid curves) and the measured data points (crosses) are shown (Coray *et al.*, 2002; reproduced with permission).

the tissue irregularities (Miller *et al.*, 1999; Schaffner and Pedroni, 1998).

Patient-specific periodic QA checks for a beam-delivery system using passive-scattering techniques include portal calibrations and verification of beam-shaping devices (apertures and compensators/boluses) (Heese *et al.*, 2002; iTL, 2001; JASTRO, 2004; Kacperek, 2003; Moyers, 1999). The TPS calculates the dose per monitor unit (MU) at the reference point in the patient but at present the dose per MU is individually verified in a phantom for each patient treatment portal at many facilities (iTL, 2001; JASTRO, 2004; Moyers, 1999). Precision in manufacturing the bolus directly affects the distal part of the depth-dose distribution, whereas the errors in the patient aperture impinge on the lateral-dose distribution. Although milling machines provide high manufacturing precision, the manufactured beam-shaping devices for each patient should be checked against TPS data files by comparing aperture shapes and bolus thicknesses at pre-selected points.

Improvement in quality control of dose delivery can be achieved through the use of proton radiography that provides verification in the relative range of protons *in vivo* in the patient (Schneider and Pedroni, 1995). The use of PET monitoring to check proton range, dose localization, and stability of the treatment during different fractions has been investigated (Enghardt *et al.*, 1999; 2004; Hishikawa *et al.*, 2002; Parodi *et al.*, 2002; 2007a; 2007b; 2007c). Real-time PET imaging could be considered a potentially useful tool for QA in proton therapy (see Section 7.4.2).

The TPS described by Lomax *et al.* (2004) calculates the dose distribution for a spot scanning-beam technique from a superposition of individual pencil beams, taking into account the density information from the corresponding CT slices. An empirical model of the pencil beam is used that takes into account the attenuation of the primary protons, effects of multiple Coulomb scattering, and losses

due to nuclear interactions. The model parameterization data are stored in lookup tables, and the therapy planning can predict absolute doses. There are no patient-specific devices; therefore the individual information on each patient treatment is in the control-point sequence (Chu *et al.*, 1993; Lomax *et al.*, 2004) that is used to calculate dose distributions in a water phantom. Patient-specific QA checks include manual calculations of the MU, range checks and, most importantly, independent dose calculations based on the control file itself, which is directly compared with that calculated by the TPS. In addition, as a weekly QA check, a field is quasi-randomly selected and the dose distribution checked in a water phantom with an array of ionization chambers. The thickness of the water column can be set to the required depth of measurement. The water phantom is irradiated, using the same control-point sequence as for the patient treatment. The measured dose profiles should be then compared with the dose distribution recalculated by the TPS using a homogeneous medium instead of the patient CT data. Figure 9.3 shows two orthogonal dose profiles taken during a routine patient verification (Coray *et al.*, 2002). The solid line represents the calculated profile; the crosses show the measured doses. As a quality check, the routine dosimetry with ionization chambers should agree with the expected dose from the treatment plan within the user-established tolerances. Verifications of dose delivery for a dynamic treatment technique using a fluorescent screen and CCD camera (Boon *et al.*, 2000) have shown good sensitivity with >1 mm spatial resolution that allowed the detection of deviations of a few percent from the calculated dose distribution.

If respiratory-synchronized irradiation is employed, CT images used for treatment planning must also be taken in respiratory-gating mode. The same specifications for irradiation gating, synchronizing timing and thresholds, should be applied for acquisition of treatment-planning CT images. As

Table 9.1. Quality-assurance procedures for passive beam-delivery systems.**Daily checks**

- Aperture alignment; room lasers, interlocks; communication; patient-positioning system
- Depth-dose and lateral profiles (range, entrance dose, uniformity of range modulation and Bragg-peak width, flatness, symmetry)
- Dose monitor calibration, check of MU value under standard condition
- Individual patient treatment calibration and range checks

Weekly checks

- Patient-positioning and imaging systems
- Beam-line apparatus
- Respiratory-gating equipment
- Dose delivered to randomly selected patients (comparison of planned dose distributions to those measured in a water phantom)

Annual or scheduled inspection checks

- x-ray patient positioning and alignment systems
- CT Hounsfield number calibration
- Comprehensive tests of therapy equipment
 - monitor chambers, timers, beam-delivery termination and control interlocks, stray radiation exposure to patients, gantry isocenter, depth-dose and lateral profiles, baseline data for daily QA checks

Table 9.2. Additional quality-assurance procedures for scanning beam-delivery systems.**Daily checks**

- Dose rate and monitor ratios for the pencil beam
- Performance of the beam-position monitors
- Depth-dose curve of a pencil beam in a water phantom
- Calibration of the primary dose monitor

Weekly checks

- Qualitative three-dimensional check of the outline and range of the dose distribution for one patient's irradiation field in a water phantom

Half-yearly checks

- Calibration of the primary dose monitor and the phase space of the beam tunes

Annual or scheduled inspection checks

- Check of the beam characteristics
 - calibration of the whole dosimetry system, performance of the scanning system in terms of dose linearity and dose-rate dependence

an example, the following issues should be investigated for respiratory-synchronized irradiation to serve as benchmarks for periodic QA checks (JASTRO, 2004):

- (1) differences between observed respiration signal and actual organ movement;
- (2) phase uncertainty at CT scanning for treatment planning to make reference images;
- (3) setting of the threshold level of the extent of the movement;
- (4) movement of organ during allowed period for irradiation.

9.4 EXAMPLES OF PERIODIC CHECKS

Each proton facility will have different QA requirements, and the items listed in Tables 9.1 and 9.2 are guidelines and suggestions and do not describe all tests that must be made at any particular facility. In Table 9.1, the procedures for passive scattering beam-delivery systems (iTL, 2001; JASTRO, 2004; Kacperek, 2003; Moyers, 1999; Schreuder, 2002) are listed, and in Table 9.2 additional procedures for spot-scanning beam-delivery systems (Chu *et al.*, 1993; Coray *et al.*, 2002) are given. The procedures for scanned beams are given mostly in terms of dosimetric issues, as the check of dose delivery is the most important task.

10 PRESCRIBING, RECORDING, AND REPORTING TREATMENT

10.1 INTRODUCTION

Previous sections of the present report have dealt with the development of planning aims, treatment plans, and treatment prescriptions. The present section summarizes some of this material and formulates suggestions concerning the process of prescribing, recording, and reporting of proton-therapy procedures. As discussed in Section 2, all doses should be specified as RBE-weighted absorbed doses in units of Gy (RBE).

10.2 GENERAL RECOMMENDATIONS FOR PRESCRIBING, RECORDING, AND REPORTING

10.2.1 The components of prescribing, recording, and reporting a patient's treatment

Once the goals of therapy have been determined, the information required to execute and document a patient's treatment must be accumulated and recorded. This information falls into seven categories:

1. Initial medical note	History of present illness, co-morbidities, physical examination, findings on imaging and pathological studies, and general management strategy.
2. Planning aims	All the information needed to plan the treatment of the patient.
3. Treatment planning	The process of simulating a number of delivery strategies for a radiation treatment and choosing the best one to use for treatment
4. Treatment prescription	Instructions for treatment delivery to achieve the planned dose distribution and authorization of the technical details to deliver the treatment plan
5. Technical data	Data required for treatment delivery according to the treatment plan (with the prescription, treatment plan, doses and technical data approved and fixed).
6. Record of the treatment	Storage of all data relevant to the patient's treatment.
7. Report(s) of the treatment	For example, completion note, report to the referring and other physician(s), publications.

The relation among these categories is shown schematically in Fig. 10.1.

10.2.2 Planning aims

The planning aims include the desired dose levels and the acceptable dose gradients to the target volume(s) and the organs at risk. The responsible radiation oncologist gives these aims to the planner as a basis for planning a treatment. They result from a medical decision-making process, based on the detailed evaluation of the patient, and diagnostic studies, consultation(s) when indicated, oncological concepts, delineation of volumes such as gross tumor volume (GTV), clinical target volume (CTV), planning target volume (PTV), and organ at risk (OAR). Consideration is commonly given to the use of one or more therapeutic modalities. In some cases, the initial planning aims cannot be achieved, and an iterative process takes place in which the aims are progressively adjusted until a plan is designed that is clinically acceptable or the patient is referred for management by other modalities. To develop the planning aims into an approved treatment plan requires involvement by a team of physicists, dosimetrists, technologists, and physician(s). It is recommended that the planning aims be part of the archived records, with notations describing any compromises between initial and final aims and the reasons for such compromises.

Setting planning aims and constraints and using new or developing tools for scoring the evolving treatment plans during optimization are discussed in Section 6 (planning aims and plans in Sections 6.1 and 6.6, plan assessment in Section 6.7, plan comparison and optimization in Sections 6.8 and 6.9, comparing uniform-intensity versus intensity-modulated proton therapy treatment plans in Section 6.10).

10.2.2.1 Specifying planning aims

As pointed out in Section 6.6.1.3, there is a wide variety of ways to specify the dose requirements for the tumor (PTV) and the dose constraints for normal tissues (PRV, RVR). In the case of both proton therapy and intensity-modulated radiation

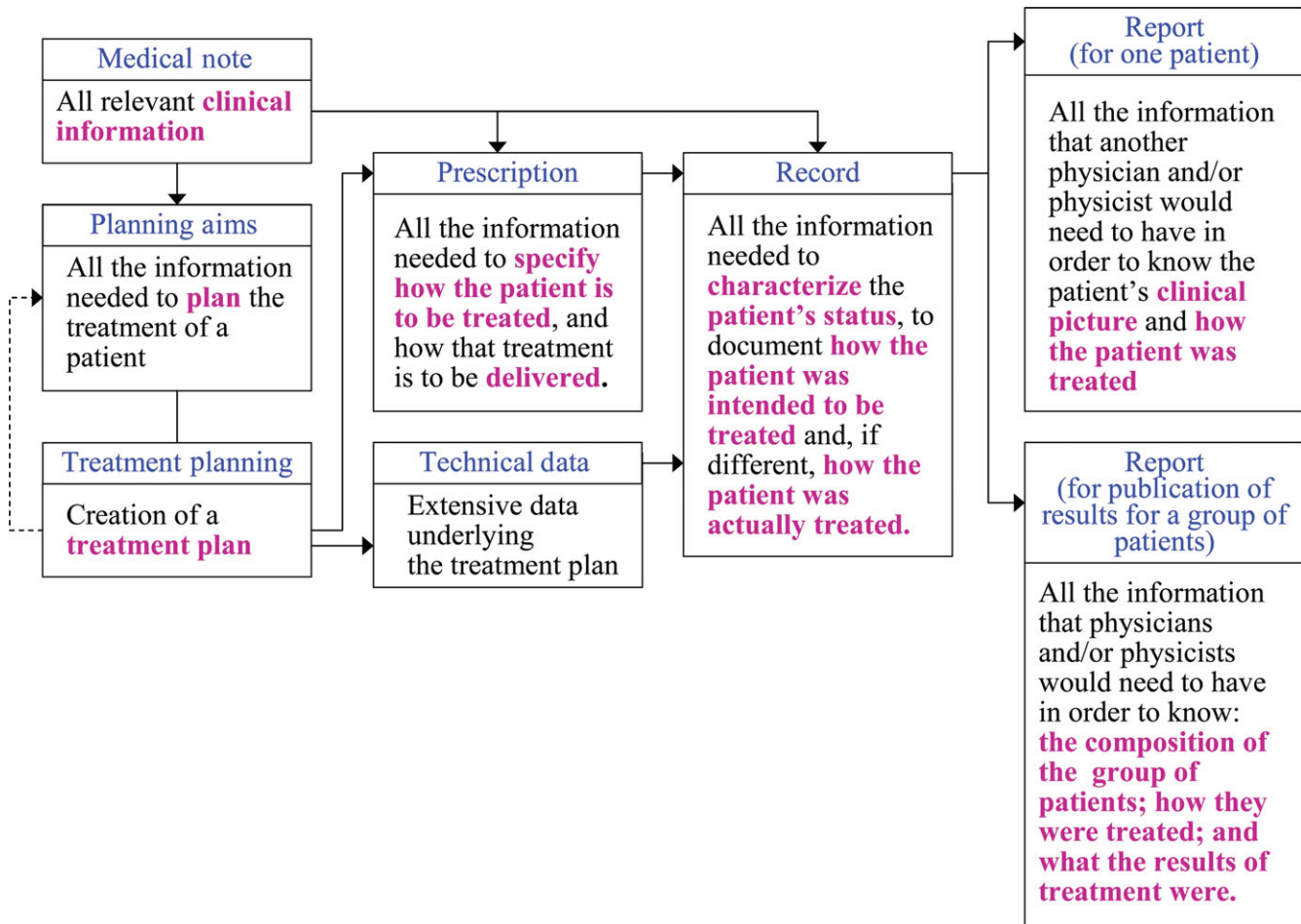


Figure 10.1. Block diagram, summarizing the relations among the planning aims, prescription, technical data, treatment record and reports.

therapy, when specifying dose to the PTV, there is an increasing trend away from specifying doses at a single point, *viz.*, the ICRU Reference Point, and toward specifying dose-summarizing quantities such as the dose delivered to 50 percent of the volume of interest (VOI) ($D_{50\%}$), the near-minimum dose or the dose delivered to 98 percent of the VOI ($D_{98\%}$), the near-maximum dose or the dose delivered to 2 percent of the VOI ($D_{2\%}$), the least dose delivered to a specified volume, V , of the VOI (D_V), *etc.* Additional information can be presented specifying the limits of dose inhomogeneities within the PTV and where minimum doses may be located. All of the pertinent information used in the definition of planning aims should be clearly recorded. Doses should be specified as RBE-weighted absorbed doses [in Gy (RBE)]. In Section 6.7.3, it is pointed out that there is also growing interest in the use of a variety of model-based parameters such as equivalent uniform dose (EUD), tumor control probability (TCP), and normal-tissue complication probability (NTCP) (Bortfeld, 2003; Lyman, 1985; Niemierko, 1997; Niemierko and Goitein, 1993; Schultheiss *et al.*,

1983; York, 2003) in the specification and evaluation of planning aims. When such models are used, the reference to the description of the model should be included in the record as well as the values of any selected parameters.

As stated in previous ICRU reports (ICRU, 1993b; 1999; 2004), the formulation of planning aims and hence the prescription of a treatment is the responsibility of the radiation oncologist. The goal of the present report and other ICRU reports is to suggest uniform approaches to the recording and reporting of pertinent treatment-related information.

10.2.2.2 Normal-tissue constraints

Normal-tissue constraints tend to be either dose or dose–volume constraints. In ‘serial-like’ organs (Withers *et al.*, 1988), the constraint will typically be the maximum dose to even a small volume, whereas for ‘parallel-like’ organs the relative size of the volume irradiated above the tolerance level might be the most important parameter (for further discussion see Section 5.6.1.3). In some instances,

specification of normal-tissue constraints might be based on predictions of NTCP derived from mathematical models. As noted above, all relevant parameter values of the model should be recorded.

10.2.2.3 Selection of treatment approach: the treatment plan

Having established the planning aims, the oncology team has two, rather different, approaches that can be used to deliver proton therapy, such as scattered-beam therapy and scanned-beam therapy with or without intensity modulation. If the necessary facilities are available, during the process of treatment planning, the team needs to evaluate which of these approaches and which plan would best achieve the planning aims. The process and available tools are described in Sections 6.7–6.10. Once a satisfactory treatment plan has been developed and accepted, the prescription and the plan, in sufficient detail to allow accurate reconstruction, become part of the prescription and should be recorded (see Table 10.1).

10.3 PRESCRIBING PROTON-BEAM THERAPY

10.3.1 General approaches to prescribing

As pointed out in Section 10.2.2.1, there is a variety of ways in which the oncology team can choose to express the planning aims for a given patient or group of patients, and indeed a variety of different approaches are currently in use in different centers. The general recommendations for prescribing, recording, and reporting conventional external-beam radiation therapy (ICRU, 1993b; 1999; 2004) largely apply to proton therapy. The major difference between prescribing for the former and the latter lies in the use of dose–volume reporting and the amount of technical data required for proton therapy.

10.3.2 The prescription

The prescription must give sufficient technical detail so that the radiation therapists/technologists can fully understand the prescription and deliver the dose according to the prescription. Approval of the final prescription means approval of all technical parameters chosen to implement the treatment plan.

10.3.3 General recommendations for prescribing

At a minimum, the prescription should include and record (see also Table 10.2):

1. the delineations of the volumes of interest (GTV, CTV, PTV, OAR, RVR, etc.);

2. the approved plan with its dose distribution(s);
3. the prescribed RBE-weighted absorbed doses and dose–volume constraints
 - a the intended reference dose, *e.g.*, D_{med} or dose at the ICRU Reference Point if specified
 - b near-minimum dose to the PTV ($D_{98\%}$) (see Section 5.6.1.3)
 - c near-maximum dose to the PTV ($D_{2\%}$) (see Section 5.6.1.3)
 - d V_D , *i.e.*, the largest volume of a specified VOI that receives a dose more than or equal to the dose, D_{RBE} (see Section 5.6.1.1);
4. the normal-tissue constraints, *e.g.*, the largest dose (D_V) to be received by a specified volume, *e.g.*, of normal tissues (see Section 5.6.1.2);
5. the fractionation scheme, *viz.*, the number of fractions, inter-fraction interval, and overall treatment time;
6. the medical aspects that affect how the treatment is to be performed;
7. all technical data required to perform the treatment (see Section 10.3.4. and Table 10.2).

10.3.4 Approval of the prescription and technical data

The execution of the prescribed treatment requires the specification and recording of a large volume of technical data for each treatment field, particularly for scanned-beam therapy. Table 10.2 lists the examples of data that should be recorded and reported. Examples of such technical data are as follows:

- for scattered-beam therapy, all appropriate beam-forming parameters such as the aperture shapes or multi-leaf collimator settings, the compensator design, and the range modulation;
- for wobbled-beam therapy, the scan pattern, the pencil beam size and spacing, the aperture shapes or multi-leaf collimator settings;
- for scanned-beam therapy (either for uniform-intensity or intensity-modulated therapy), the extensive files detailing the sequence of scanned pencil beams, each with their energy, weight, and position.

A physician's approval of a treatment prescription covers not only the specific treatment plan, but also the technical aspects required to implement the prescription. The technical factors can include extensive data files, which cannot be readily inspected by eye, nor can the compliance with the quality-assurance measures be assessed for each treatment plan. The reality is that the radiation oncologist accepts the calculations and statements of physicists and engineers. The responsibility for

PRESCRIBING, RECORDING, AND REPORTING PROTON-BEAM THERAPY

Table 10.1. Summary of the data required in each of the three areas: ‘planning aims’, ‘prescription’, and ‘treatment record’. Required items are identified by colored table cells. Items specific to, or that contain information concerning, proton-beam therapy are, in addition, crosshatched.

	Planning aims	Prescription	Treatment record	Note
Patient data				
Identifying information				<i>note 1</i>
Demographics				<i>note 2</i>
Contact information				<i>note 3</i>
Patient’s responsible physician				
Patient’s responsible physicist				
Disease data				
Tumor characteristics				<i>note 4</i>
History				<i>note 5</i>
Treatment intent				<i>note 6</i>
Volumes of interest				
Target volumes (GTV, CTV, and PTV)				
Organs at risk (OAR) and any PRVs				
Prescription (for the entire course of therapy)				<i>note 7</i>
Number of treatment segments				<i>note 8</i>
For all segments combined				
For target volume (usually PTV)				
Prescription dose				<i>note 9</i>
Goal dose				<i>note 10</i>
Margins				<i>note 11</i>
Fractionation scheme				<i>note 12</i>
For each organ at risk (OAR)				
Dose/dose–volume constraints, if any				<i>note 13</i>

Table 10.1. Continued

For each segment (if more than one)				
Modality				<i>note 14</i>
Target volume goal dose for segment				<i>note 15</i>
OAR constraints for segment (if any)				<i>note 16</i>
Treatment technique (e.g., IMRT or uniform)				<i>note 17</i>
Beam arrangements				<i>note 18</i>
Immobilization technique				<i>note 19</i>
Patient position (e.g., prone, supine, seated)				

Overall plan/beam arrangements

For the plan used for each segment:				
List of beams				
Beam weights				
For each beam in the plan				
Modality				
Maximum energy or penetration (protons)				
Beam direction relative to patient				

Dose information for overall plan

note 20

For the overall course and, if desired, for each segment separately				
Target volume dose/dose–volume statistics				<i>note 21</i>
OAR (PRV) dose/dose–volume statistics				<i>note 22</i>
Two-dimensional dose distributions in selected planes				<i>note 23</i>
DVHs for selected VOIs				<i>note 24</i>

Plan deviations (if any)

Explanation of, and remedial actions, if any				<i>note 25</i>
--	--	--	--	----------------

PRESCRIBING, RECORDING, AND REPORTING PROTON-BEAM THERAPY

note 1 For example, patient name, identifying code, and photograph (if any).

note 2 For example, age, sex, and race.

note 3 For example, patient's address, person to contact, and referring physician.

note 4 For example, site, histology, staging, TNM classification, and genetic characterization (if available).

note 5 For example, prior tumors, prior therapies, pertinent diagnostic-imaging results, and laboratory findings.

note 6 Curative/palliative intent; intention to use concomitant or subsequent courses of therapy (surgery, chemotherapy, other systemic therapies such as biological agents); identification of treatment protocol (if any).

note 7 A patient might receive one or more courses of treatment, in which one course might be a regime of chemotherapy, or radiation therapy for a primary tumor. Courses might be separated in time, or might be sequential or concurrent with the course of radiation therapy under consideration.

note 8 A course of radiation therapy might contain one or more sequential segments in which one segment, for example, might treat the primary tumor and regional nodes to a dose of 50 Gy (RBE), followed by a second segment in which the primary tumor is given a boost dose of 20 Gy (RBE) for a total tumor dose of 70 Gy (RBE). Each segment of a radiation therapy course is represented by one and only one plan. Generally, but not necessarily, each segment will involve a single modality (e.g., protons) that must be specified. If, however, mixed modalities are used (e.g., protons and photons), then the planning aims and the prescription need to supply separate information for each modality used.

note 9 See Section 5.6.3 for definition of the prescription dose.

note 10 The goal dose will usually be defined by a dose–volume requirement, phrased in terms of the prescription dose. For example 'the entire PTV is to receive at least 95 percent of the prescription dose'. It might also include some form of homogeneity requirement, for example, 'the dose within the PTV to be within -5 and +7 percent of the prescription dose' (see Section 6.6.1).

note 11 In some proton-planning approaches, because the lateral and depth margins need to be different, the beam is designed relative to the CTV, rather than the PTV, using the appropriate margins in each direction. In this case, the margins used should be individually specified.

note 12 In external-beam radiotherapy, one or more treatment fractions are delivered. A single fraction involves the delivery of radiation by (usually) several beams in sequence, usually over a short period of time (ranging from a minute to a fraction of an hour). More than one fraction might be delivered in a day. The fractionation scheme [e.g., $d_{\text{RBE}} = 2 \text{ Gy (RBE)}$ per fraction] must be specified for each segment of the treatment separately, if different. In addition, the beam sequencing must be specified (e.g., 'all beams delivered at each fraction').

note 13 See Section 6.6.1 for examples.

note 14 Generally, but not necessarily, each segment will involve a single modality (e.g., protons) that must be specified. If, however, mixed modalities are used (e.g., protons and photons), then the respective modality must be specified for the individual beams used in the segment.

note 15 Each segment will have its own target-volume goal dose, which must be established such that the target-volume dose for the overall course of radiation therapy is met.

note 16 As for the target volume, the dose received by each OAR (or PRV) within each segment must, when the segments are combined, meet the OARs' dose constraint(s) for the overall course of radiation therapy.

note 17 The type of plan (uniform-intensity or intensity-modulated), the type of equipment (e.g., gantry or fixed beam), the type of beam delivery (e.g., scattered or scanned), and the beam characteristics (e.g., pencil beam width in air for scanned beams) must all be specified.

note 18 If a particular beam arrangement (e.g., five-field prostate protocol plan) is required, it should be specified.

note 19 A photograph of the immobilized patient in the treatment position is highly desirable. Otherwise, a sketch is useful.

note 20 The two-dimensional dose displays and DVHs required in this category should be available either in hard-copy (i.e., printed on paper using a non-fading ink) or, in the case of an all-digital record, available as monitor displays.

note 21 At a minimum, in addition to the achieved RBE-weighted absorbed doses corresponding to the target-volume dose aims, the near-minimum ($D_{98\%}$), near-maximum ($D_{2\%}$), and median ($D_{50\%}$) RBE-weighted absorbed doses (see Section 5.6.1) to the PTV should be recorded.

note 22 At a minimum, for each OAR (and PRV) of clinical interest, the near-maximum RBE-weighted absorbed dose ($D_{2\%}$), and the achieved RBE-weighted doses corresponding to the normal-tissue dose constraints should be recorded.

note 23 The two-dimensional dose displays should be shown as RBE-weighted dose displays. When relative doses are displayed, the dose to which, say, the 100 percent level correspondence should be specified. The displays should have a clearly readable representation of the RBE-weighted absorbed dose levels corresponding either to RBE-weighted absorbed dose lines or to color-wash regions. The sections should be selected to sample adequately the target volume and clinically important normal tissues. If possible, the displays should feature sagittal and/or coronal sections as well as transverse sections.

note 24 Dose–volume histograms should be shown as RBE-weighted absorbed dose displays (see Section 5.6.2.2).

note 25 If any difference(s) between the delivered and intended treatments might be clinically significant, the explanation for the deviation and a description of the remedial action that was required should be recorded as well.

Table 10.2. List of some technical data that should be recorded. Items that are specific to or concerning, proton-beam therapy are shaded.

Patient data

Three-two-dimensional data for imaging studies (e.g., three-dimensional array of Hounsfield numbers for CT)
Delineation data of all VOIs, SOIs, and POIs

For each treatment segment

Segment name and/or identifying information
Segment dose
Plan identification

For each plan: non-dosimetric information

Plan name and/or identifying information
The list of beams used in the plan
The weight of each beam
List of SOIs, if any
List of POIs, if any

For each plan: dosimetric information

Three-dimensional dose distribution for the plan (three-dimensional array of values)
Selected two-dimensional dose sections (two-dimensional array of values)
Dose-volume (or dose-surface) histograms for each VOI (two-dimensional array of values)
Doses received by any SOIs (two-dimensional array of values)
Doses received by any POIs

For each beam

Beam name and/or identifying information
Modality: protons(energy), photons(energy), electrons(energy)
The equipment configuration used for the beam (gantry angle, couch settings, etc.)
Beam weights and monitor units

Continued

Table 10.2 Continued

For scattered beams	
	The settings of the collimator (if any)
	The angle of rotation of the nozzle or snout
	The name, and ID and quantitative description of the aperture or the multi-leaf collimator (MLC) (if any)
	The name, and ID and quantitative description of the compensator (if any)
	The name, and ID and quantitative description of other beam modifying devices (if any)
	The distance from the collimator or compensator to the patient's skin surface
	Extent in depth of SOBP and depth of beam penetration
For wobbled beams, in addition to data for scattered beams	
	Wobbled beam characteristics (spot size, wobbling pattern, <i>etc.</i>)
For scanned beams	
	Scan sequence(s) (e.g., Cartesian grid or contour-following, grid spacing(s))
	Pencil-beam characteristics (shape, FWHM at isocenter in air, <i>etc.</i>)
	Intensity and energy or penetration at each scan dwell-point

History of treatments

Record of dose(s) delivered per fraction
Full record of delivered treatments if record and verify system used

Patient-specific quality assurance

Before treatments begin	
	Methods used
	Results obtained
During treatments	
	Methods used
	Results obtained

Equipment identification

Make, type, and version number of therapy equipment used
Make, type, and version number of treatment-planning system(s) used

the existence and correctness of these data lies in the hands of the responsible physicist, who should formally approve these technical data that should be included in the treatment record (Table 10.2).

10.4 ADDITIONAL ASPECTS OF PRESCRIBING, RECORDING, AND REPORTING

10.4.1 Therapy equipment

In proton-beam therapy, several elements of the equipment need to be specifically prescribed, recorded, and reported. These include the following:

- the type of accelerator (e.g., cyclotron or synchrotron), as they may produce different beam characteristics (see Section 3);
- the treatment-delivery equipment (e.g., gantry or fixed beam);
- the beam-shaping configuration(s) used (e.g., scanning or scattering nozzle), including patient- and field-specific hardware such as collimators and compensators;
- motion tracking, if applicable.

In treatments using more than one radiation modality (e.g., protons and photons), the relevant details of the equipment of each modality used should be recorded.

10.4.2 Beam-shaping techniques

The patient's prescription and record must describe the beam-delivery technique used (e.g., scattered beam or scanned beam, in the latter case, uniform-intensity or intensity-modulated beam) (see Section 3). For scattered beams, the details of the beam-shaping system must be specified and documented (e.g., identification of the scattering devices, beam aperture, and compensator). For scanned beams, the details of the scanning system and pencil-beam parameters should be recorded (e.g., grid pattern, spacing of pencils, pencil widths, dwell times, and repainting specifications).

10.4.3 Techniques for dealing with heterogeneities

Heterogeneities in tissue densities penetrated by proton beams can substantially affect proton range and dose homogeneity. These heterogeneities can be compensated for using real (physical) or virtual (embedded in the scanning sequences) compensators (see Section 6.4.6.2). The details of the compensation scheme should be recorded.

10.4.4 Margins

Consideration of the plan is likely to include all the factors common to photon-beam therapy plus several

additional factors that are discussed in Sections 6 and 7: (i) allowance for dose uncertainties due to heterogeneities in tissue densities, and (ii) possible errors in registration of the real or virtual compensator with the patient's anatomy. As a result, the margins in depth and lateral must be documented.

10.5 RECORDING PROTON-BEAM THERAPY

10.5.1 The treatment record

Good recording is the basis for good reporting, and only recorded data can be analyzed. Records should be comprehensive enough to allow us to understand and validate components of the treatment and treatment outcome. In Tables 10.1 and 10.2 examples of data required for prescribing, recording, and reporting and examples of technical data, respectively, are given.

The treatment record should include all information needed to characterize the patient's status, to document how the patient was intended to be treated, and, if different, how the patient was treated. This includes, *inter alia*, the patient's demographic data and tumor status, the prescription and the underlying technical data, the details of how the therapy was delivered, and follow-up information. If difference(s) between the intended and delivered treatment are clinically significant, a description of the deviation and of any adjustments made should be recorded as well. The patient's radiation-therapy record is an archival document that should be retained for at least as long as the law prescribes.

10.5.2 The patient's record

The patient's record is usually a combination of a paper record (the patient's radiotherapy 'chart') and an electronic record containing a large volume of information (such as three-dimensional dose distributions and scan patterns of pencil beams). Hard copy is likely to remain highly prevalent for some time. However, the record may be entirely electronic, in which case provision should be made to ensure that changing technology does not render the records inaccessible.

10.6 REPORTING THE TREATMENT OF A SINGLE PATIENT

10.6.1 Reporting proton-beam therapy

In contrast to the prescription, in which some institutional freedom might be desirable, the reporting of treatments must be done using uniform terms

and concepts for all patients within each department and in all centers. If this is not followed, any useful exchange of scientific or clinical information between centers becomes difficult or even impossible. Without modifying the treatment techniques and the dose levels currently delivered in different centers, adopting the same concepts and definitions for both prescribing and reporting reduces the risks of confusion.

Reports normally have a focus either on a single patient, groups of patients, or on validation and comparison of technologies. The content of a report depends on the intended recipient and the purpose for which it is to be used. A completion of treatment note, a report to referring physician(s) (which might be a copy of the completion note), a report sent to a physician whom the patient has consulted, or a report sent to a radiation oncologist who may wish to evaluate the patient for re-treatment, all require different levels of detail and completeness.

The reporting of results is of special importance in proton radiation therapy, as the use of protons has only recently become widespread. Therefore, detailed recording and reporting is particularly needed. Otherwise the determination of the role of proton therapy as a component of modern cancer treatment will be very difficult. Previous ICRU reports have identified three levels of reporting, 1 through 3 (ICRU, 1999). For the most part, proton radiation therapy should be reported at level 3.

10.6.2 Patient-specific reports

There can be several types of patient-specific reports, depending on the intended audience. It would not be appropriate to enumerate all requirements for these reports as they should be tailored to the particular needs of each situation. However, some general points are followed for some common types of report.

10.6.2.1 The initial medical note

The initial medical note presents various categories of patient information. For example, history of present illness, including age, gender, race, symptoms, medical evaluations (including imaging studies and pathology, and treatments, if any), past medical history, especially autoimmune diseases; genetic diseases associated with increased radiation sensitivity; current medications; allergies; social history; family history; physical examination; review of imaging studies; review of pathological findings; and general management plan.

10.6.2.2 The completion note

The completion note is a summary report made by the treating physician and placed in the patient's chart and record. A copy is usually sent to the referring physician(s). It needs to include those aspects of the proton treatment that can become important base-line information for possible consecutive therapies (Grégoire *et al.*, 2004).

It should, at a minimum, include the following elements:

- diagnosis, pathological type and grade, stage of disease, and relevant prior history;
- a summary of the overall treatment plan;
- an appropriate summary of the RBE-weighted absorbed doses to the PTV, CTV, and GTV, as well as the near-minimum and near-maximum doses delivered to the CTV and GTV;
- RBE-weighted absorbed doses to PRVs or OARs, a statement of any complications, and deviations from the planned treatment;
- a statement of the patient's status upon completion of therapy and plans for future follow-up.

10.6.2.3 Summary report to the referring physician

The note to the referring physician(s) would in most cases be a copy of the completion or treatment note. In certain situations, the note might only be an abbreviation of the completion note.

10.6.2.4 Case report

A case report provides a detailed description of a patient's treatment suitable for case presentations at conferences or for written transmission of the details of an individual patient's treatment to knowledgeable professionals. Examples of Case Reports are provided in Appendix B.

10.6.2.5 Detailed report to a physician

Depending on their future role in the patient treatment, other physicians should be provided with all relevant information they might require, *e.g.*, for evaluation of a complication or for consideration of possible further therapy.

10.7 REPORTING PROTON-BEAM THERAPY FOR A SERIES OF PATIENTS

Reporting the results of proton-beam therapy is very similar to reporting any other radiation therapy modality. The reader is referred to ICRU Reports 50, 62, and 71 (ICRU, 1993b; 1999; 2004) for details.

APPENDIX A: IMPLEMENTATION OF THE TRS 398 CODE OF PRACTICE FOR IONIZATION CHAMBER DOSIMETRY

A.1 CALIBRATION OF IONIZATION CHAMBERS

When an ionization chamber or dosimeter is sent to a standards laboratory for calibration, stability-check measurements (using a suitable check device) should be carried out by the user before and after the calibration. This will ensure that the chamber response has not been affected by the transportation. A reference ionization chamber should be calibrated at a reference quality Q_0 at intervals not exceeding 2 or 3 years, or whenever the user suspects that the chamber has been damaged. If directly measured values of k_{Q,Q_0} (or N_{D,w,Q_0}) for the chamber have been obtained previously, a recalibration to verify the quality dependence of the chamber should be made at least every third time that the chamber is calibrated. The chamber should be recalibrated at all qualities at least every 6 years. It is the responsibility of the user to increase the frequency of the calibrations for chambers whose long-term stability has not been verified over a period exceeding 5 years.

A.1.1 Calibration in a ^{60}Co beam

Calibrations may be carried out either directly against a primary standard of absorbed dose

to water at a PSDL (Primary Standards Dosimetry Laboratory) or, more commonly, against a secondary standard at an SSDL (Secondary Standards Dosimetry Laboratory). Only the latter case will be discussed here. It is assumed that the absorbed dose to water, D_w , is known at a depth of 5 g cm^{-2} in a water phantom for ^{60}Co gamma rays. This is realized at the SSDL by means of a calibrated cavity-ionization chamber performing measurements in a water phantom. The user chamber is placed with its reference point at a depth of 5 g cm^{-2} in a water phantom, and its calibration factor $N_{D,w}$ is obtained from

$$N_{D,w} = \frac{D_w}{M}, \quad (\text{A.1})$$

where M is the dosimeter reading corrected for influence quantities, so as to correspond to the reference conditions for which the calibration factor is valid. Reference conditions recommended for the calibration of ionization chambers in ^{60}Co are given in Table A.1.

The text and tables in this Appendix are taken almost exclusively from sections of TRS 398 (IAEA, 2000), which is therefore not further referenced.

Table A.1. Reference conditions recommended for the calibration of ionization chambers in ^{60}Co gamma radiation at standards laboratories or for cross calibrations in user laboratories (IAEA, 2000).

Quantity	Reference value or reference characteristic
Phantom material	Water
Phantom size	$30 \times 30 \times 30 \text{ cm}^3$ (approximately)
Source-chamber distance ^a (SCD)	100 cm
Air temperature ^b	20°C
Air pressure	101.3 kPa
Reference point of the ionization chamber	For cylindrical chambers, on the chamber axis at the center of the cavity volume For plane-parallel chambers on the inner surface of the entrance window, at the center of the window
Depth in phantom of the reference point of the chamber ^a	5 g cm^{-2}
Field size at the position of the reference point of the chamber	$10 \times 10 \text{ cm}^2$
Relative humidity	50 percent
Polarizing voltage and polarity	No reference values are recommended, but the values used should be stated in the calibration certificate.
Dose rate	No reference values are recommended, but the dose rate used should always be stated in the calibration certificate. It should also be stated whether or not a recombination correction has been applied, and, if so, the value should be stated.

^aAfter a water phantom with a plastic window has been filled, its dimensions may slowly change with time. When using a horizontal beam, it may therefore be necessary to check the source–surface distance and the chamber depth every few hours.

^bThe temperature of the air in a chamber cavity should be taken to be that of the phantom, which should be measured; this is not necessarily the same as the temperature of the surrounding air.

^cIn some countries the reference air temperature is 22°C.

A.2 REFERENCE DOSIMETRY IN THE USER PROTON BEAM

A.2.1 Determination of the absorbed dose to water

It is assumed that the user has an ionization chamber or a dosimeter with a calibration factor N_{D,w,Q_0} in terms of absorbed dose to water at a reference-beam quality Q_0 . Following the formalism given in Section 4.4.2, the chamber is positioned according to the reference conditions and the absorbed dose to water in the proton beam is given by

$$D_{w,Q} = M_Q N_{D,w,Q_0} k_{Q,Q_0}, \quad (\text{A.2})$$

where M_Q is the reading of the dosimeter incorporating the product $\prod k_i$ of correction factors for influence quantities, and k_{Q,Q_0} is the correction factor that corrects for the difference between the reference-beam quality Q_0 and the actual quality Q being used.

A.2.2 Practical considerations for measurements in the proton beam

Unless the ionization chamber is designed so that it can be put directly into water, it must be used with a waterproof sleeve. The sleeve should be made of PMMA, with a wall sufficiently thin (preferably not >1.0 mm in thickness) to allow the chamber to achieve thermal equilibrium with the water in <10 min. The sleeve should be designed so as to allow the air pressure in the chamber to reach ambient air pressure quickly; an air gap of 0.1–0.3 mm between the chamber and the sleeve is adequate. To reduce the buildup of water vapor around the chamber, the waterproof sleeve should not be left in water longer than is necessary to carry out the measurements. Additional accuracy is gained if the same sleeve that was used for the calibration of the chamber in the standards laboratory is also used for all subsequent measurements.

Before measurements are made, the stability of the dosimeter should be verified using a check source. Enough time should be allowed for the dosimeter to reach thermal equilibrium. Some mains-powered electrometers are best switched on for at least 2 h before use to allow stabilization. It is always advisable to pre-irradiate an ionization chamber with 2–5 Gy to achieve charge equilibrium in the different materials. It is especially important to operate the measuring system under stable conditions whenever the polarity or polarizing voltage are modified, which, depending on the

chamber and sometimes on the polarity, might require several (up to 20) minutes. Indeed, failure to do so can result in errors that are larger than the effect for which one is correcting.

The leakage (and background) current is that generated by the complete measuring system in the absence of applied radiation. Leakage can also be radiation-induced, and chambers can show no leakage prior to irradiation yet have a significant leakage after irradiation. The leakage current should always be measured before and after irradiation, and should be small compared with the current obtained during the irradiation (less than ~ 0.1 percent of the measurement current and normally of the same sign). In some instances, for example, small-volume chambers used at low dose rates, the relative leakage current might be larger. If this is the case, the measurement current should be corrected for leakage, paying attention to the sign of the leakage current. Chambers with a leakage current that is larger than ~ 1 percent of the measurement current, or is variable in time, should not be used.

When relative measurements are carried out in accelerator beams, it is strongly recommended that an additional monitoring dosimetry system be used during the experimental procedure to account for fluctuations in the radiation output. This is especially important when ratios of dosimeter readings are used (e.g. for cross calibrations in different beams, for measurements using different polarities, or varying voltages, etc.). The external monitor should preferably be positioned within the phantom, along the major axis of the transverse plane, at the same depth as the chamber and at a distance of ~ 3 or 4 cm from the central axis. This might not be possible for a small beam such as an ocular beam. In that case the use of a transmission monitor chamber located downstream from the final collimator is recommended. If the monitor is positioned in air, the possible temperature drifts should be taken into account (IAEA, 2000).

A.2.3 Corrections for influence quantities

The calibration coefficient for an ionization chamber is valid only for the reference conditions that apply to the calibration. Any departure from the reference conditions when using the ionization chamber in the user beam should be corrected for using appropriate factors.

A.2.3.1 Temperature, pressure, and humidity

As all chambers recommended in the present report are open to ambient air, the mass of air in the cavity volume is subject to atmospheric

variations. The correction factor

$$k_{TP} = \frac{(273.2 + T)P_0}{(273.2 + T_0)P} \quad (\text{A.3})$$

should be applied to convert the cavity air mass to the reference conditions. In Eq. (A.3), T and P are the cavity temperature and air pressure at the time of the measurements, and T_0 and P_0 are the reference values (generally 20 or 22°C and 101.3 kPa). The temperature of the air in a chamber cavity should be taken to be that of the phantom, which should be measured; this is not necessarily the same as the temperature of the surrounding air. For measurements in a water phantom, the chamber waterproof sleeve should be vented to the atmosphere in order to obtain rapid equilibrium between the ambient air and the air in the chamber cavity.

No corrections for humidity are needed if the calibration coefficient was referred to a relative humidity of 50 percent and is used in a relative humidity between 20 and 80 percent. If the calibration factor is referred to dry air, a correction factor should be applied; for ^{60}Co calibrations, $K_{\text{hum}} = 0.997$ (ICRU, 1998).

A.2.3.2 Electrometer calibration

When the ionization chamber and the electrometer are calibrated separately, a calibration coefficient for each is given by the calibration laboratory. The electrometer calibration coefficient k_{elec} is an influence quantity and is included in the product Πk_i of correction factors. Typically, the calibration coefficient $N_{D,w}$ for the ionization chamber is given in units of Gy nC^{-1} and that for the electrometer k_{elec} either in units of nC rdg^{-1} (rdg = electrometer reading) or, if the electrometer readout is in terms of charge, as a dimensionless factor close to unity.

If the ionization chamber and the electrometer are calibrated together, then the combined calibration coefficient $N_{D,w}$ will typically be given in units of Gy rdg^{-1} or Gy nC^{-1} (depending on the electrometer readout) and no separate electrometer calibration factor k_{elec} is required. In this case, a value for k_{elec} of unity (dimensionless) should be recorded in the worksheets.

A.2.3.3 Polarity effect

The effect on a chamber reading of using polarizing potentials of opposite polarity must always be checked on commissioning. In charged-particle beams the effect can be significant (IAEA, 2000). When a chamber is used in a beam that produces a measurable polarity effect, the true reading is

taken to be the mean of the absolute values of readings taken at both polarities. For the routine use of a given ionization chamber, a single polarizing potential and polarity is normally adopted. However, the effect on the chamber reading of using polarizing potentials of opposite polarity for each user beam quality Q can be accounted for by using a correction factor

$$k_{\text{pol}} = \frac{|M_+| + |M_-|}{2M}, \quad (\text{A.4})$$

where M_+ and M_- are the electrometer readings obtained at positive and negative polarity, respectively, and M is the electrometer reading obtained with the polarity used routinely (positive or negative).

The readings M_+ and M_- should be made with care, ensuring that the chamber reading is stable following any change in polarity (some chambers can take up to 20 min to stabilize). To minimize the influence of fluctuations in the output of accelerators, it is preferable that all the readings be normalized to that of an external monitor. Ideally, the external monitor should be positioned approximately at the depth of measurement, but at a distance of 3–4 cm from the chamber center along the major axis in the transverse plane of the beam.

When the chamber is sent for calibration, a decision is normally made, either by the user or by the calibration laboratory, on the polarizing potential and polarity to be adopted for the routine use of the chamber. The calibration should be carried out at this polarizing potential (and polarity, if only one polarity is used for the calibration), or, if not, clearly stated. The calibration laboratory might or might not correct for the polarity effect at the calibration quality Q_0 . This should be stated in the calibration certificate.

If the calibration laboratory has already corrected for the polarity effect, then the user must apply the correction factor k_{pol} derived using Eq. (A.4) to all measurements made using the routine polarity. If the calibration laboratory has *not corrected* for the polarity effect, the subsequent treatment of the polarity effect depends on the facilities available to the user, and on what beam qualities must be measured.

A.2.3.4 Ion recombination

The incomplete collection of charge in an ionization-chamber cavity owing to the recombination of ions requires the use of a correction factor. Two separate effects take place: (i) the recombination of ions

APPENDIX A

formed by separate ionizing particle tracks, termed general (or volume) recombination, which is dependent on the density of ionizing particles and therefore on the dose rate; and (ii) the recombination of ions formed by a single ionizing particle track, referred to as initial recombination, which is independent of the dose rate. Both effects depend on the chamber geometry and on the applied polarizing voltage. For beams other than heavy ions, initial recombination is generally <0.2 percent.

For pulsed beams, it is recommended that the correction factor k_s be derived using the two-voltage method. This method assumes a linear dependence of $1/M$ on $1/V$ and uses the measured values of the collected charges M_1 and M_2 at the polarizing voltages V_1 and V_2 , respectively, measured using the same irradiation conditions. V_1 is the normal operating voltage and V_2 a lower voltage; the ratio V_1/V_2 should ideally be equal to or larger than 3. Strictly, the polarity effect will change with the voltage, and M_1 and M_2 should each be corrected for this effect using Equation (A.4). The recombination correction factor k_s at the normal operating voltage V_1 is obtained from

$$k_s = a_0 + a_1 \left(\frac{M_1}{M_2} \right) + a_2 \left(\frac{M_1}{M_2} \right)^2, \quad (\text{A.5})$$

where the constants a_i are given in Table A.2 for pulsed and for pulsed-scanned radiation. To minimize the influence of fluctuations in the output of accelerators, all the readings should preferably be normalized to that of an external monitor. The external monitor should preferably be positioned inside the phantom approximately at the depth of measurement, but at a distance of 3–4 cm away from the chamber center along the major axis in the transverse plane of the beam.

For $k_s < 1.03$, the correction can be approximated to within 0.1 percent using the relation:

$$k_s - 1 = \frac{M_1/M_2 - 1}{V_1/V_2 - 1}, \quad (\text{A.6})$$

that is, the percentage correction is the percentage change in reading divided by a number that is one less than the voltage ratio. This has the advantage of working for non-integral values of V_1/V_2 and serves as a check on the evaluation using Equation (A.5). Note that the correction factor k_s evaluated using the two-voltage method in pulsed beams corrects for both general and initial recombination.

A word of caution is required regarding the use of the two-voltage method for parallel-plane ionization chambers in pulsed beams. It has been shown

Table A.2. Quadratic-fit coefficients for the calculation of k_s by the two-voltage technique in pulsed and pulsed-scanned radiation, as a function of the voltage ratio V_1/V_2 (Weinhous and Meli, 1984).

V_1/V_2	Pulsed			Pulsed scanned		
	a_0	a_1	a_2	a_0	a_1	a_2
2.0	2.337	-3.636	2.299	4.711	-8.242	4.533
2.5	1.474	-1.587	1.114	2.719	-3.977	2.261
3.0	1.198	-0.875	0.677	2.001	-2.402	1.404
3.5	1.080	-0.542	0.463	1.665	-1.647	0.984
4.0	1.022	-0.363	0.341	1.468	-1.200	0.734
5.0	0.975	-0.188	0.214	1.279	-0.750	0.474

that for some plane-parallel chambers the expected linear dependence of $1/M$ on $1/V$ is not satisfied in the voltage interval used for the two voltage method. This effect can be compensated for by using the same two polarizing voltages for the dose determination in the user beam as are used for the chamber calibration at the standards laboratory, or by the user in the case of a cross calibration. Alternatively, the range of linearity of a chamber can be established in a pulsed beam by measuring the chamber response over a range of polarizing voltages up to the manufacturer's recommended maximum. This is a useful check on the performance of a chamber and should always be performed when commissioning a new chamber. If possible, the chamber should be used subsequently only at voltages within the linear range, in which case the use of the two-voltage method is valid.

In continuous radiation, the two-voltage method can also be used and a correction factor derived using the relation:

$$k_s = \frac{(V_1/V_2)^2 - 1}{(V_1/V_2)^2 - (M_1/M_2)}. \quad (\text{A.7})$$

Note that for making recombination corrections, proton-synchrotron beams of long-pulse duration and low-pulse-repetition frequency may be considered as continuous.

For relative measurements, for example, the determination of depth-dose distributions and the measurement of output factors, the recombination correction should be determined in a sufficient subset of conditions that appropriate corrections can be derived. In pulsed beams, for which general recombination is dominant, the recombination correction for a given chamber will scale approximately linearly with dose rate. In continuous beams, the recombination correction is small and approximately constant.

In scanned beams and other special beams of very high intensity, space-charge effects cannot be neglected, and the charge-collection efficiency should be assessed by calibration against a system that is independent of dose rate, such as a calorimeter.

It should be noted that for the calibration of ionization chambers in standards laboratories (see Table A.1), the calibration certificate should state whether or not a recombination correction has been applied. The preceding discussion and the worksheet is based on the assumption that the calibration laboratory has applied a recombination correction, and therefore the procedure given for the determination of k_s refers only to recombination in the user beam. If the calibration laboratory has not applied a recombination correction, the correction factor determined for the user beam quality Q must be divided by that appropriate to the calibration quality Q_0 , that is,

$$k'_s = \frac{k_{s,Q}}{k_{s,Q_0}}. \quad (\text{A.8})$$

If Q_0 is a continuous beam, k_{s,Q_0} will normally be close to unity, and the effect of not applying k_{s,Q_0} either at calibration or using Eq. (A.8) will be negligible in most cases. However, if Q_0 is a pulsed beam, failure by the standards laboratory to apply k_{s,Q_0} at the time of calibration is a potential source

of error, especially if the dose per pulse in the user beam is very different from that used at calibration. If this is the case, the user must determine k_{s,Q_0} in the clinic at a dose per pulse similar to that used at calibration (this might not be the dose per pulse normally used in the clinic). This determination does not need to be carried out at Q_0 ; it is the matching of the calibration dose per pulse that is important. To avoid a recurrence of this problem, the user should request that a recombination correction be applied, or at least measured, at the next calibration at a standards laboratory, especially for calibration in pulsed beams.

Although proton beams accelerated by an isochronous cyclotron are pulsed beams, the pulse repetition rate is so high (of the order of 20 MHz) that such proton beams ought to be treated as continuous beams. For modulated proton beams, the time-dependent dose can be regarded as pulsed due to the modulation process. However, even for the deepest points on the spread-out Bragg peak, the duration of each pulse is usually long compared with the ion-collection time and again the beam should be regarded as continuous in relation to recombination. It is important that the nature (pulsed or continuous) of each beam should be investigated. The ion-recombination correction factor can be overestimated by up to 2 per cent if a cyclotron beam is assumed to be pulsed (Palmans *et al.*, 2006).

APPENDIX A

A.3. DOSIMETRY WORKSHEET (IAEA, 2000).

Determination of the absorbed dose to water in a proton beam

User: _____ Date: _____

1. Radiation treatment unit and reference conditions for $D_{w,Q}$ determination

Proton therapy unit: _____ Nominal energy: _____ MeV
 Nominal dose rate: _____ MU min⁻¹ Practical range, R_p : _____ g cm⁻²
 Reference phantom: _____ water Width of the SOBP: _____ g cm⁻²
 Reference field size: _____ cm² Reference SSD: _____ cm
 Reference depth, z_{ref} : _____ g cm⁻² Beam quality, R_{res} : _____ g cm⁻²

2. Ionization chamber and electrometer

Ionization chamber model: _____ Serial no. _____ Type: cyl pp
 Chamber wall/window Material: _____ Thickness: _____ g cm⁻²
 Waterproof sleeve/cover Material: _____ Thickness: _____ g cm⁻²
 Phantom window Material: _____ Thickness: _____ g cm⁻²
Absorbed-dose-to-water calibration factor $N_{D,w}$ = _____ Gy nC⁻¹ Gy rdg⁻¹
 Reference conditions for calibration P_o : _____ kPa T_o : _____ °C Rel. humidity: _____ %
 Polarizing potential V_i : _____ V Calibration polarity: +ve -ve corrected for polarity effect
 User polarity: +ve -ve

Calibration Laboratory: _____ Date: _____
 Electrometer model: _____ Serial no.: _____
 Calibrated separately from chamber: yes no Range setting: _____
 If yes Calibration Laboratory: _____ Date: _____

3. Dosimeter reading^a and correction for influence quantities

Uncorrected dosimeter reading at V_i and user polarity: _____ nC rdg
 Corresponding accelerator monitor units: _____ MU
 Ratio of dosimeter reading and monitor units: $M_i =$ _____ nC MU⁻¹ rdg MU⁻¹
 (i) Pressure P : _____ kPa Temperature T : _____ °C Rel. humidity (if known): _____ %

$$k_{TP} = \frac{(273.2 + T)}{(273.2 + T_o)} \frac{P_o}{P} = \frac{1}{\frac{P_o}{P}}$$

 (ii) Electrometer calibration factor^b k_{elec} : _____ nC rdg⁻¹ dimensionless $k_{elec} =$ _____
 (iii) Polarity correction^c rdg at $+V_i$: M_+ = _____ rdg at $-V_i$: M_- = _____

$$k_{pol} = \frac{|M_+| + |M_-|}{2M} = \frac{|M_+|}{2M}$$

(iv) Recombination correction (two-voltage method) NATURE OF EACH BEAM SHOULD BE INVESTIGATED

Polarizing voltages: V_1 (normal) = _____ V V_2 (reduced) = _____ V

Readings^d at each V: M_1 = _____ M_2 = _____

Voltage ratio V_1/V_2 = _____ Ratio of readings M_1/M_2 = _____

Use Table A.2 for a beam of type: pulsed pulsed-scanned

a_0 = _____ a_1 = _____ a_2 = _____

$$k_s = a_0 + a_1 \left(\frac{M_1}{M_2} \right) + a_2 \left(\frac{M_1}{M_2} \right)^2 = \frac{1}{\frac{M_2}{M_1}} \quad \text{e, f}$$

Corrected dosimeter reading at the voltage V_1 :

$$M_Q = M_1 k_{TP} k_{elec} k_{pol} k_s = \underline{\hspace{100pt}} \quad \square \text{nC MU}^{-1} \quad \square \text{rdg MU}^{-1}$$

4. Absorbed dose to water at the reference depth, z_{ref}

Beam quality correction factor for user quality Q : $k_Q = \underline{\hspace{100pt}}$

taken from Table 4.11 Other, specify: _____

Absorbed-dose calibration of monitor at z_{ref} :

$$D_{u,Q}(Z_{ref}) = M_Q N_{D,W} k_Q = \underline{\hspace{100pt}} \quad \text{Gy MU}^{-1}$$

^aAll readings should be checked for leakage and corrected if necessary.

^bIf the electrometer is not calibrated separately set $k_{elec} = 1$.

^c M in the denominator of k_{pol} denotes reading at the user polarity. Preferably, each reading in the equation should be the average of the ratios of M (or M_+ or M_-) to the reading of an external monitor, M_{em} .

It is assumed that the calibration laboratory has performed a polarity correction. Otherwise k_{pol} is determined according to

$$\text{rdg at } +V_1 \text{ for quality } Q_0: M_+ = \underline{\hspace{100pt}} \quad \text{rdg at } -V_1 \text{ for quality } Q_0: M_- = \underline{\hspace{100pt}}$$

$$k_{pol} = \frac{\left[(|M_+| + |M_-|)/|M| \right]_Q}{\left[(|M_+| + |M_-|)/|M| \right]_{Q_0}} = \underline{\hspace{100pt}}.$$

^dStrictly, readings should be corrected for polarity effect (average with both polarities). Preferably, each reading in the equation should be the average of the ratios of M_1 or M_2 to the reading of an external monitor, M_{em} .

^eIt is assumed that the calibration laboratory has performed a recombination correction. Otherwise the factor $k_s' = k_s / k_{s,Q_0}$ should be used instead of k_s . When Q_0 is ^{60}Co , k_{s,Q_0} (at the calibration laboratory) will normally be close to unity and the effect of not using this equation will be negligible in most cases.

^fCheck that $k_s - 1 \approx \frac{M_1/M_2 - 1}{V_1/V_2 - 1}$.

APPENDIX B: CLINICAL EXAMPLES

DISCLAIMER

As in ICRU Reports 50, 62, and 71 (ICRU, 1993b; 1999; 2004), clinical examples are presented here with the aim of illustrating how the recommendations contained in the present report may be applied in practice. The six examples were obtained from different proton therapy centers in different countries. They should not be construed as ICRU recommendations for choosing given treatment techniques, volumes, or dose levels.

DOSE PRESCRIPTION

Absorbed doses (D) are given in Gy, whereas RBE-weighted absorbed doses (D_{RBE}) are given in Gy (RBE). Doses per fraction are stated as d and

d_{RBE} , respectively:

$$D_{RBE}[\text{Gy (RBE)}] = D(\text{Gy}) \times \text{RBE},$$
$$d_{RBE}[\text{Gy (RBE)}] = d(\text{Gy}) \times \text{RBE}.$$

A generic RBE value of 1.1 for the therapeutic use of protons is recommended (*i.e.*, for clinical proton-beam therapy, there is one value, and it is independent of total dose, dose per fraction, and tissue type).

CONTRIBUTORS

The contributions of the following to the compilations of the clinical examples are gratefully acknowledged: J. Adams, M. Bussière, H. Kooy, N. Liebsch, J. Loeffler, T. Sakae, N. Tarbell, and T. Yock.

CASE NUMBER B.1: UVEAL MELANOMA

General patient information

- a. Patient identification
- i. Name Confidential
 - ii. Age, gender, and race 85 year old
Japanese male
 - iii. Address Confidential
 - iv. Phone no. Confidential
 - v. E-mail address Confidential
 - vi. Hospital ID no. Confidential
 - vii. Person to notify Confidential
(with contact information)
were a problem to arise
- b. Medical team
- i. Radiation oncologist(s) Confidential
 - ii. Radiation physicist(s) Confidential
 - iii. Referring physician Confidential

Medical evaluation of presenting lesion

- a. Presenting complaint The patient presented with myodesopsia in the left eye.
- b. Clinical history He developed the myodesopsia, but decided to watch it without consulting with physicians. He visited a local ophthalmologist because the symptom had progressed over the following few months. He was referred to a University Hospital with diagnosis of retinal detachment.
- c. Physical examination Probable malignant melanoma in the nasal side of the left eye; otherwise non-contributory
- d. Imaging studies MRI: $9.5 \times 10.8 \text{ mm}^2$ tumor of left eye. Shown in Fig. B.1.1, and PET image in Fig. B.1.2
- e. Tumor site Left eye
- f. Diagnosis Uveal melanoma
- g. Grade No biopsy
- h. Stage Stage III, T3N0M0
- i. Prior therapy None
- j. Family history Noncontributory

General medical evaluation

- a. History, physical examination, and imaging No evidence of metastatic tumor in chest and abdominal CT
- b. Co-morbidities On medication for hypertension, gastritis and prostatic hypertrophy



Figure B.1.1. T2-weighted MRI image showing the tumor in the left eye.

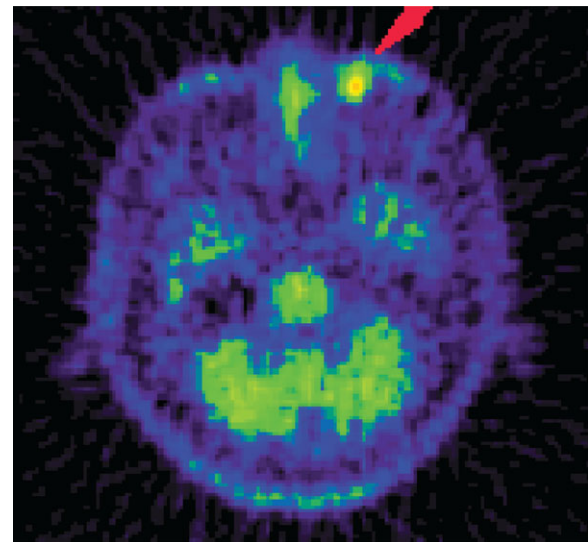


Figure B.1.2. Methionine-PET image demonstrates an increased uptake corresponding to the choroidal tumor (arrow).

Treatment intent

- a. Curative by proton therapy with $D_{RBE,50\%}$ of 70 Gy (RBE)
- b. No surgery or chemotherapy
- c. Probable outcome
 - i. Cure at 10 years: 95 percent
 - ii. Probability of distant metastasis: <5 percent
 - iii. Probability of visual loss: <5 percent

Treatment planning

- a. General plan
 - i. Single segment
 - ii. Single anterior beam
- b. Definitions of treatment volumes
 - i. One millimeter thick CT images throughout the orbit were taken and transferred to the treatment-planning system. The findings on MRI, ultrasound, and fundoscopic examination were utilized in the delineation of tumor margins for the GTV and CTV.
 - ii. GTV: GTV was delineated as demonstrated on CT scan.
 - iii. CTV: CTV was delineated as GTV + 0.5 mm, including the whole thickness of the sclera.
 - iv. PTV: PTV was delineated by adding 1 mm around CTV in all directions, to allow for any variation in beam set-up and potential movement of eye ball position during treatment.
- c. RBE = 1.10
- d. Dose fractionation: five fractions to the PTV of $d_{RBE,50\%} = 14$ Gy (RBE) or a total $D_{RBE,50\%} = 70$ Gy (RBE) over ~ 7 days
- e. Uncertainty in dose and patient position not quantified
- f. Organs at risk (OARs) and dose constraints or the dose producing major morbidity at ≤ 5 percent
Doses to optic disc and fovea were below the level of concern.
 - i. Optic disc $D_{RBE,2\%} < 1$ Gy (RBE)
 - ii. Fovea $D_{RBE,2\%} < 1$ Gy (RBE)
- g. The planned dose levels to other structures were also below the constraint levels.

Patient immobilization and positioning

- a. Supine position with individualized plastic cast was used for patient immobilization. There was supplemental immobilization of the head.
- b. Figure B.1.3a and b present the CT sections through the globe demonstrating the position of a metal clip (a) and the optic disc (b).
- c. Metal clips were not necessary to identify the tumor boundary in the treatment planning, but necessary for field positioning at each treatment session. For this purpose, a few clips were sutured on the sclera relatively near to the tumor margins before the acquisition of CT images.

Treatment prescription

- a. Prescribed dose
 - i. Beam energy: 70 MeV
 - ii. Dose is prescribed in D_{RBE} [Gy (RBE)]
 - iii. PTV: the dose at the center of the 2-cm wide spread-out Bragg peak (SOBP) on the central axis was 70 Gy (RBE). The minimum dose to the PTV was ≥ 90 percent of the prescribed dose or $D_{RBE,98\%} \geq 63$ Gy (RBE).
 - iv. Fractionation: five fractions over 7 days
- b. OAR: Dose constraints not exceeded by these prescribed doses



Figure B.1.3. Delineation of ROIs on CT images. Blue line indicates left eye ball. (a) red line indicates metal clip. (b) Yellow line indicates optic disc.

- c. Dose displays
 - i. Axial plane through center of eye in Fig. B.1.4
 - ii. Dose–volume histograms in Figs B.1.5 and B.1.6

Treatment technique

The patient was instructed to gaze at a point in space using a flickering light to achieve a fixed position of the ocular globe determined by the

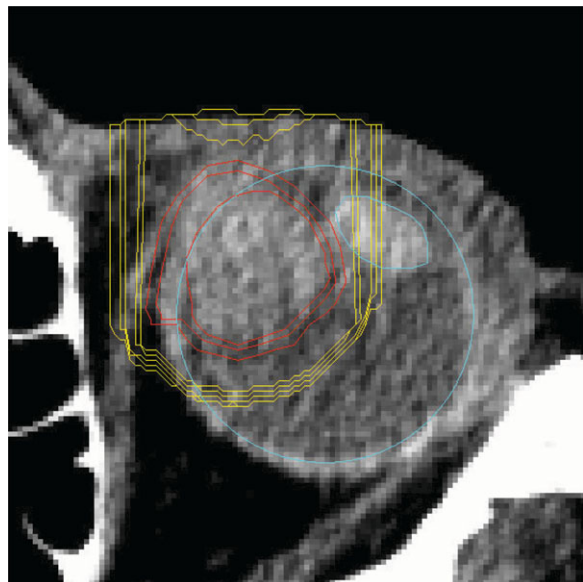


Figure B.1.4. Dose distribution in plane through the isocenter, where GTV, CTV, and PTV are indicated by red lines. Isodose distribution is indicated by yellow lines: from outside, 10, 30, 50, 90, and 95 percent of the prescribed dose, $D_{RBE} = 70$ Gy (RBE), respectively.

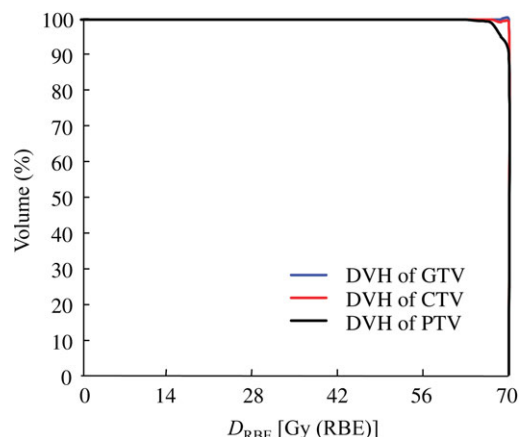


Figure B.1.5. Dose–volume histogram (DVH) of target volumes. GTV is indicated in blue, CTV in red, and PTV in black. The near-minimum dose to the CTV was $D_{RBE,98\%,CTV} = 67.4$ Gy (RBE). $D_{RBE,50\%,CTV} = D_{RBE,2\%,CTV} = 70$ Gy (RBE).

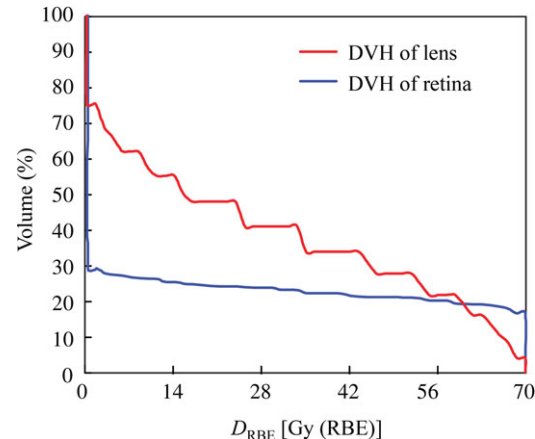


Figure B.1.6. Dose–volume histogram (DVH) of OARs. The x-axis indicates RBE-weighted absorbed dose (D_{RBE}) in Gy (RBE). The y-axis indicates cumulative volume in percentage. DVH of the lens is the red line and that of retina is the blue line. A part of the retina was included in the PTV.

planning process. The position of the flickering light was set in the treatment process to allow target volumes to be adequately irradiated with minimal dose to OARs. As the direction of the gaze and hence the position of the target was satisfactory in the first planning CT, a second CT was not taken in this case. Metal clips sutured on the sclera relatively near to the tumor were also used under fluoroscopy for accurate patient positioning.

Quality assurance

- a. Beam profiles (flatness and depth–dose) were checked prior to the start of the course of treatment.
- b. Determination of the dose at the reference point (center of the beam and SOBP) was performed.
- c. Transparent foils for beam’s eye view and lateral view were overlaid on orthogonal x-ray films to confirm the positioning. Beam’s eye view with collimator (Fig. B.1.7) was printed to compare with the corresponding positioning x-ray film (Fig. B.1.8). Eye position was monitored during each treatment session by a video camera with the cornea being marked directly on the video monitor. In case of detected movement of cornea of 1 mm the beam was immediately stopped manually.

Equipment

- a. Synchrotron-produced 70 MeV proton beam
- b. Broad-beam energy modulation
- c. Imaging system to position target on beam

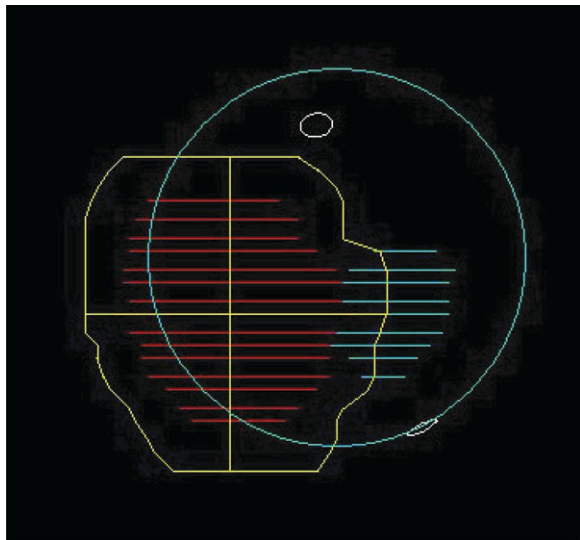


Figure B.1.7. Beam's eye view with the collimator. Structural images were printed on a transparent film. Blue circle indicates the eye ball, small white marks indicate the metal clips, red line stack indicates the tumor, blue line stack indicates the lens, and yellow line indicates the collimator. This image was used to set up the patient by comparison with a verification x-ray film.

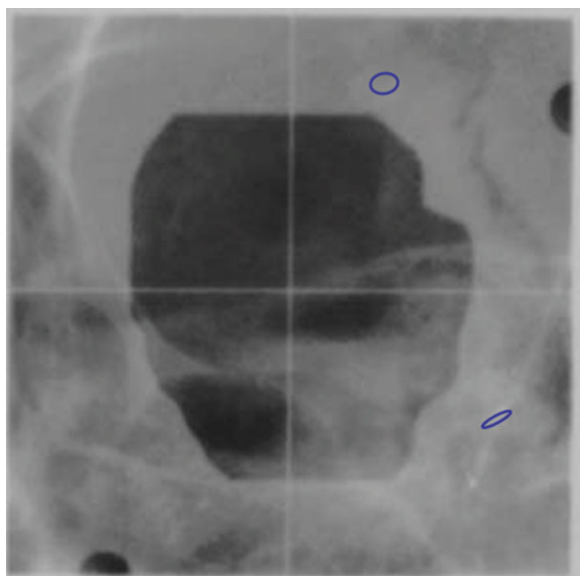


Figure B.1.8. Verification x-ray film showing the aperture outline. Metal clips are marked in blue for better visualization.

Total doses delivered

a. Total RBE-weighted absorbed doses, D_{RBE}

Volume/ structure	$D_{\text{RBE},50\%}$, Gy (RBE)	$D_{\text{RBE},98\%}$, Gy (RBE)	$D_{\text{RBE},2\%}$, Gy (RBE)
PTV	70	67.4	70
GTV	70	70	70

Continued

Continued

Lens	15.6		70
Retina	<1	<1	70
Ciliary body	<1		70
Iris	<1		70
Lid	<1		70
Fovea/ disc	<1		<1

Remaining volume at risk (RVR)

- Volume receiving $V_{30\text{Gy (RBE)}} = 2.9 \text{ ml}$
- Maximum dose outside PTV: $D_{\text{RBE},2\%} < 70 \text{ Gy (RBE)}$

b. Total absorbed doses, D

Volume/structure	$D_{50\%}$, Gy	$D_{98\%}$, Gy	$D_{2\%}$, Gy
PTV	63.6	61.3	63.6
GTV	63.6	63.6	63.6
Lens	14.2		63.6
Retina	<1	<1	63.6
Ciliary body	<1		63.6
Iris	<1		63.6
Lid	<1		63.6
Fovea/disc	<1		<1

Patient status at completion of treatment

- Response of tumor: none
- No interruptions
- No undue reactions

Addendum: technical information

Beam parameters and beam modification elements

- Rotating range modulator: SOBP width is 20.0 mm (H_2O)
- Beam course: C-9 (the ninth beam line)
- Lateral spreading: 0.04 mm gold foil scatterer and wobbler
- Penumbra (80–20 percent): 2.5 mm
- Range compensation and adjustment: compensating bolus made of polyethylene was used for conforming the distal edge of the beam to the shape of the PTV. The thickness of the compensating bolus at minimum thickness point was 12.97 mm.
- Multi-leaf collimator: not used
- Individualized collimator: brass

CASE NUMBER B.2: ADENOCARCINOMA OF PROSTATE

General patient information

a. Patient identification

- i. Name Confidential
 - ii. Age, gender, and race 78 year old
Japanese male
 - iii. Address Confidential
 - iv. Phone no. Confidential
 - v. E-mail address Confidential
 - vi. Hospital ID no. Confidential
 - vii. Person to notify Confidential
(with contact information)
were a problem to arise

b. Medical team

- i. Radiation oncologist(s) Confidential
 - ii. Radiation physicist(s) Confidential
 - iii. Referring physician Confidential

Medical evaluation of presenting lesion

- a. Medical history Asymptomatic, PSA of 5.4 ng ml⁻¹ (1998), 5.8 ng ml⁻¹ (2003)
 - b. Physical examination Prostate normal. Otherwise noncontributory
 - c. Imaging studies MRI: no tumor seen in prostate. CT, MRI, and bone scan: no metastatic tumors noted
 - d. Tumor site Prostate
 - e. Diagnosis Moderately differentiated adenocarcinoma.
 - f. Grade Ultrasound-guided biopsy Gleason 6
 - g. Stage T1cN0M0
 - h. Prior therapy None
 - i. Family history Noncontributory

General medical evaluation

- a. History, physical examination, Noncontributory and imaging
 - b. Co-morbidities None
 - c. Medications Noncontributory

Treatment intent

- a. Curative by proton radiation alone
 - b. No surgery or systemic therapy
 - c. Predicted outcome

- i. Local control probability at 10 years: 80 percent
 - ii. GIII/IV rectal injury: 5 percent
 - iii. GIII/IV bladder injury: 5 percent

Treatment planning

- a. General plan
 - i. One treatment segment
 - b. Definition of treatment volumes
 - i. The treatment planning CT was acquired with the patient in the same position, immobilization device, and conditions as used for treatment. 5 mm CT sections were used to define GTV, CTV and organs at risk (OARs).
 - ii. Definition of volumes
 - GTV: the prostate gland
 - CTV: GTV + 5 mm
 - PTV: not delineated (see Addendum)
 - c. $D_{RBE,50\%} = 76 \text{ Gy (RBE)}$ at 2.17 Gy (RBE) per fraction in 35 fractions over 7 weeks
 $D_{RBE,98\%} = 74 \text{ Gy (RBE)}$ or $D_{RBE,98\%} = 2.11 \text{ Gy (RBE)}$ per fraction
 - d. RBE = 1.10
 - e. Organs at risk with dose constraints
 - i. Anterior rectal wall: $D_{RBE,2\%} = 76 \text{ Gy (RBE)}$
 - ii. Bladder base: $D_{RBE,2\%} = 76 \text{ Gy (RBE)}$
 - iii. Right and left hip: $D_{RBE,2\%} = 32 \text{ Gy (RBE)}$
 - f. Delivery technique
 - i. Passive energy modulated 250 MeV proton beam
 - ii. Lateral opposed fields
 - iii. No allowance for prostate motion
 - g. Treatment-planning system
 - i. Doses were estimated with the three-dimensional dose calculation method based on CT images.
 - ii. Simple ray-line tracing method was used to calculate ranges and to design collimators.
 - iii. Accuracy of dose statement: not determined
 - h. RVR (Remaining Volume at Risk) receiving $V_{33 \text{ Gy (RBE)}} = 227 \text{ ml}$
 - i. Maximum dose outside PTV: $D_{RBE,2\%} = 76 \text{ Gy (RBE)}$
 - j. CTV and OARs are shown in Fig. B.2.1.
 - k. Beam's eye view of CTV is shown in Fig. B.2.2.

Patient immobilization and positioning

Supine with head on headrest. Patient immobilization was achieved by means of a cradle with polystyrene beads suctioned to conform to the contours of the patient's body. Position of the patient relative

APPENDIX B

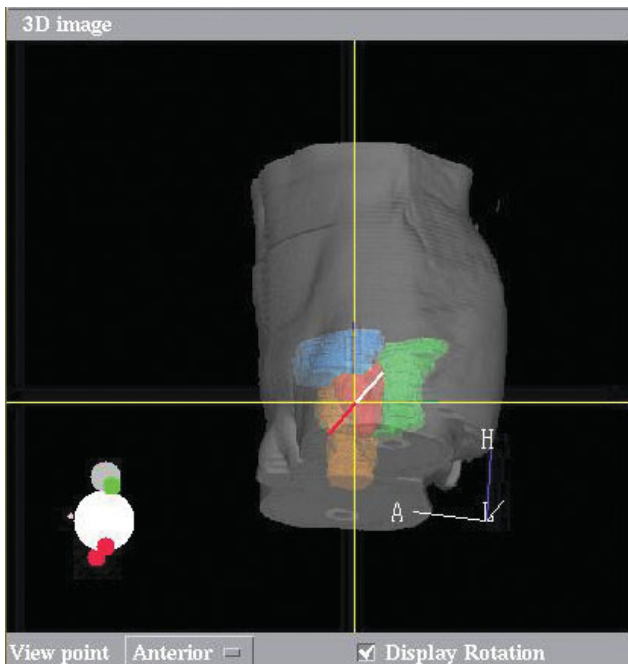


Figure B.2.1. The CTV (red), rectum (green), urinary bladder (blue), and right femur (orange) are shown in this three-dimensional reconstructed image. The left femur is not shown.

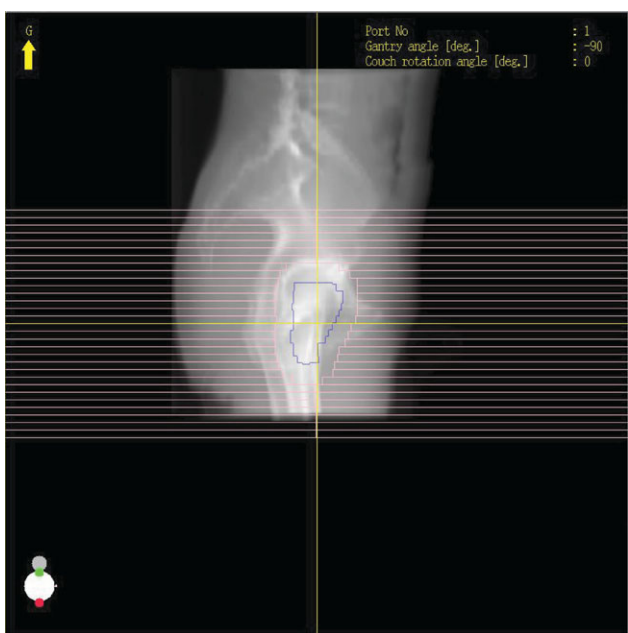


Figure B.2.2. The beam's eye view of the CTV and the beam aperture conformed to the tumor shape with the multi-leaf collimator.

to the beam was determined by laser alignment beams on markers on the cradle and patient skin.

Treatment prescription

- a. Proton-beam therapy: 250 MeV

- b. Total dose to CTV: $D_{RBE,50\%} = 76$ Gy (RBE) at 2.17 Gy per fraction, 35 fractions in 7 weeks $D_{RBE,98\%} = 74$ Gy (RBE), $D_{RBE,2\%} = 78$ Gy (RBE)
- c. RBE = 1.10
- d. $D_{RBE,2\%}$ to OARs. Anterior rectal wall: 76 Gy (RBE)
- e. Dose distributions are shown in Fig. B.2.3.
- f. Dose–volume histograms are shown in Fig. B.2.4.

Treatment technique

- a. Patient in immobilization devices.
- b. The positioning was confirmed using orthogonal simulator images referring to orthogonal digitally reconstructed radiograms (DRRs) generated in the treatment-planning computer program. It was confirmed using the orthogonal simulator images digitally stored and orthogonal fluoroscopic images during every treatment session.
- c. See Addendum for additional details.

Quality assurance

- a. The institutional standard dose monitor was calibrated once a year at the national standards center.
- b. The given dose at the reference point (the isocenter and/or the center of SOBP) was measured under the same conditions as for treatment for each patient before starting the irradiation.
- c. The dose-monitoring system and the beam-delivery system were checked every morning before the treatment.
- d. The beam position was evaluated during the irradiation by means of a beam-profile monitor.
- e. The beam current and the integral beam charge were measured with two independent sets of monitors. The ratio of doses measured by the two independent monitors was continuously evaluated during the irradiation so that any significant change of beam parameters could be instantly detected during the irradiation.
- f. The beam flatness was kept within $\pm 4\%$, and monitored during the irradiation by a special ion chamber.

Equipment

- a. 250 MeV proton beams were supplied by a slow extraction synchrotron. The average absorbed dose rate was 2 Gy min^{-1} at the isocenter.
- b. Rotating-gantry system
- c. Broad-beam energy modulation

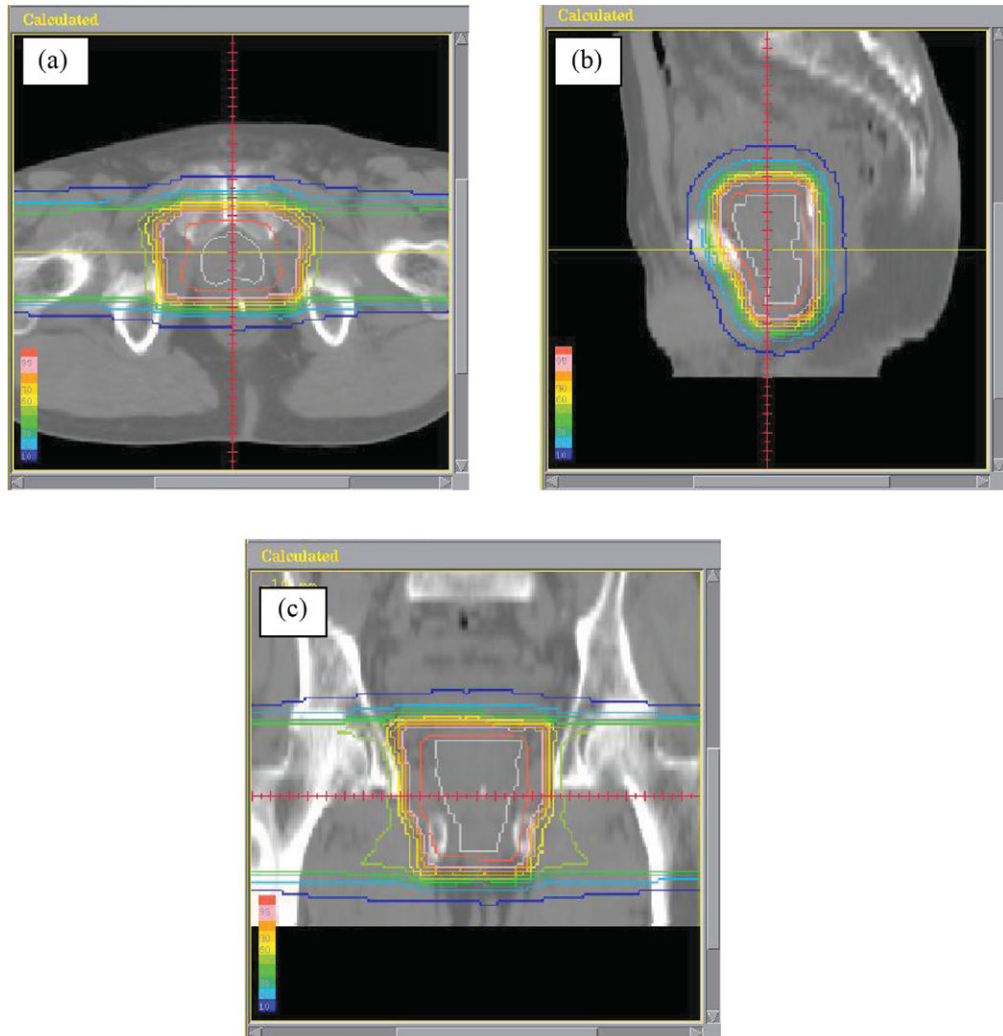


Figure B.2.3. Dose distributions in the axial (a), sagittal (b), and coronal (c) planes. The white contour represents the CTV. The red contour represents 95 percent of the prescribed dose, and that in blue represents 1 percent of the prescribed dose. The remaining contours represent the 10–80 percent isodoses in 10 percent steps.

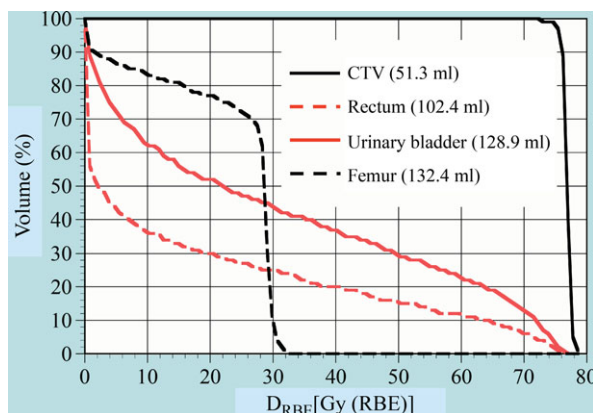


Figure B.2.4. Dose–volume histograms for the CTV and OARs. Note that the extent of rectum evaluated is from the caudal end of the sigmoid colon to the anal verge and that of the femur is 105 mm in length from the proximal end of the right femur, *i.e.*, from the proximal end of the right femur to a level 10 mm below the caudal end of the CTV.

Total doses delivered

a. Total RBE-weighted absorbed doses, D_{RBE}

Volume/structure	$D_{RBE,50\%}$, Gy (RBE)	$D_{RBE,98\%}$, Gy (RBE)	$D_{RBE,2\%}$, Gy (RBE)
CTV	76	74	78
Anterior rectal wall			76
Bladder base			76
Right hip/left hip			32

- RVR receiving V_{33} Gy (RBE) = 227 ml
- Maximum dose outside CTV: $D_{RBE,2\%} < 77$ Gy (RBE)
- No deviation from planned dose or dose fractionation

b. Total absorbed doses, D

Volume/structure	$D_{50\%}$, Gy	$D_{98\%}$, Gy	$D_{2\%}$, Gy
CTV	69.1	67.3	70.9
Anterior rectal wall			69.1
Bladder base			69.1
Right hip/left hip			29.1

Patient status at completion of treatment

- Response of tumor: none
- Change, if any, of patient symptoms: not applicable
- Planned follow-up appointment and imaging or other studies: 1 month after completion of the treatment

Addendum: technical information

Beam shaping

After delineating the CTV, the margins were added to the CTV by means of enlarging the beam aperture both laterally and cephalo-caudally in the beam's eye view, and the distal margin of the beam was extended by reducing the thickness of the range shifter for the beam. Shape of the inner surface of the bolus was enlarged according to the enlarged beam aperture. The margins covered uncertainty due to set-up errors, internal variability, and distal and lateral fall-offs of the irradiation fields.

Equipment

Proton beams of 250 MeV energy were supplied by a slow-extraction synchrotron with a

rotating gantry. Parameters of field preparation were computed with the simple ray-line-tracing method.

Treatment technique

The couch angle was 0° (parallel to the axis of gantry rotation). The patient was immobilized using a cradle with polystyrene beads suctioned to the contours of the patient's body. The position was aligned with laser pointers and markers on the cradle and the skin. The positioning was confirmed using orthogonal simulator images referring to orthogonal DRRs generated in the treatment-planning computer program. Beam directions with rotating gantry: (1) right lateral, 270° and (2) left lateral, 90°. The maximum depths were 207 and 212 mm in water-equivalent medium for beams (1) and (2), respectively. The beams were broadened by the dual-ring double-scattering method. A ridge filter was set for 60 mm spread-out Bragg peaks (SOBP). The beam apertures were shaped with a manually adjusted brass multi-leaf collimator with leaves 50 mm thick and 5 × 50 mm² in area. Boluses made of water-equivalent material were used to conform the distal edges of the beams to the tumor shapes. To account for various uncertainties the beam apertures were enlarged by 10 mm both laterally and cephalo-caudally in the beam's eye view and the beam ranges were extended 10 mm distally on the beam axes by means of reducing the thickness of the range shifter.

CASE NUMBER B.3: CARCINOMA OF LUNG

General patient information

a. Patient identification

- | | |
|---|---------------------------------|
| i. Name | Confidential |
| ii. Age, gender, and race | 81 year old
Japanese
male |
| iii. Address | Confidential |
| iv. Phone no. | Confidential |
| v. E-mail address | Confidential |
| vi. Hospital ID no. | Confidential |
| vii. Person to notify

(with contact information) | Confidential |
|
were a problem to arise | |

b. Medical team

- i. Radiation oncologist(s) Confidential
 - ii. Radiation physicist(s) Confidential
 - iii. Referring physician Confidential

Medical evaluation of presenting lesion

- a. Medical history Asymptomatic. Right lung mass on routine chest x-ray
 - b. Physical examination No abnormal findings
 - c. Imaging studies CT: 2.5 cm lesion in lateral segment of right medial lobe. No lymphadenopathy. PET [FDG] total body scan and MRI of brain: no evident distant metastases
 - d. Tumor site Right lung
 - e. Diagnosis Carcinoma. CT guided biopsy
 - f. Grade Poorly differentiated
 - g. Stage T1N0M0; Stage 1A
 - h. Prior therapy None
 - i. Family history Noncontributory

General medical evaluation

- a. History, physical examination, and imaging No important tumor findings
 - b. Co-morbidities None
 - c. Medications Noncontributory

Treatment intent

- a. Curative by proton radiation alone
 - b. No surgery or systemic therapy
 - c. Predicted outcome
 - i. Local control probability at 10 years: 80 percent

- ii. GIII/IV lung injury: \approx 5 percent
 - iii. Other thoracic structures judged to be at negligible risk

Treatment planning

- a. General plan
 - i. One treatment segment
 - b. Definition of treatment volumes
 - i. Treatment planning CT acquired with the patient in the same immobilization device and conditions as used for treatment. CT sections were used to define GTV, CTV, and organs at risk (OAR).
 - ii. Definition of volumes
 - GTV: gross primary tumor
 - CTV = GTV + 5 mm
 - PTV: not delineated (see Addendum)
 - The three-dimensional reconstructed image of the right lung and the CTV are presented in Fig. B.3.1. The beam's eye view of the targeted structures and the beam apertures are shown in Fig. B.3.2.
 - c. $D_{RBE,50\%} = 66$ Gy (RBE) at 6.6 Gy (RBE) per fraction, given in 10 fractions over 2 weeks.
 $D_{RBE,98\%} = 63$ Gy (RBE)
 - d. RBE = 1.10
 - e. Organs at risk with dose constraints: no thoracic structure was judged to be at significant risk of injury

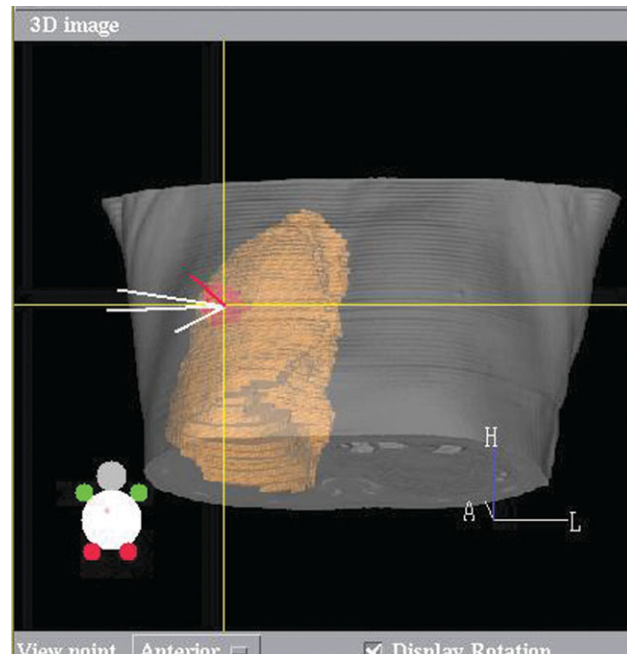


Figure B.3.1. The CTV (red) and the right lung (orange) are shown in this three-dimensional reconstructed image.

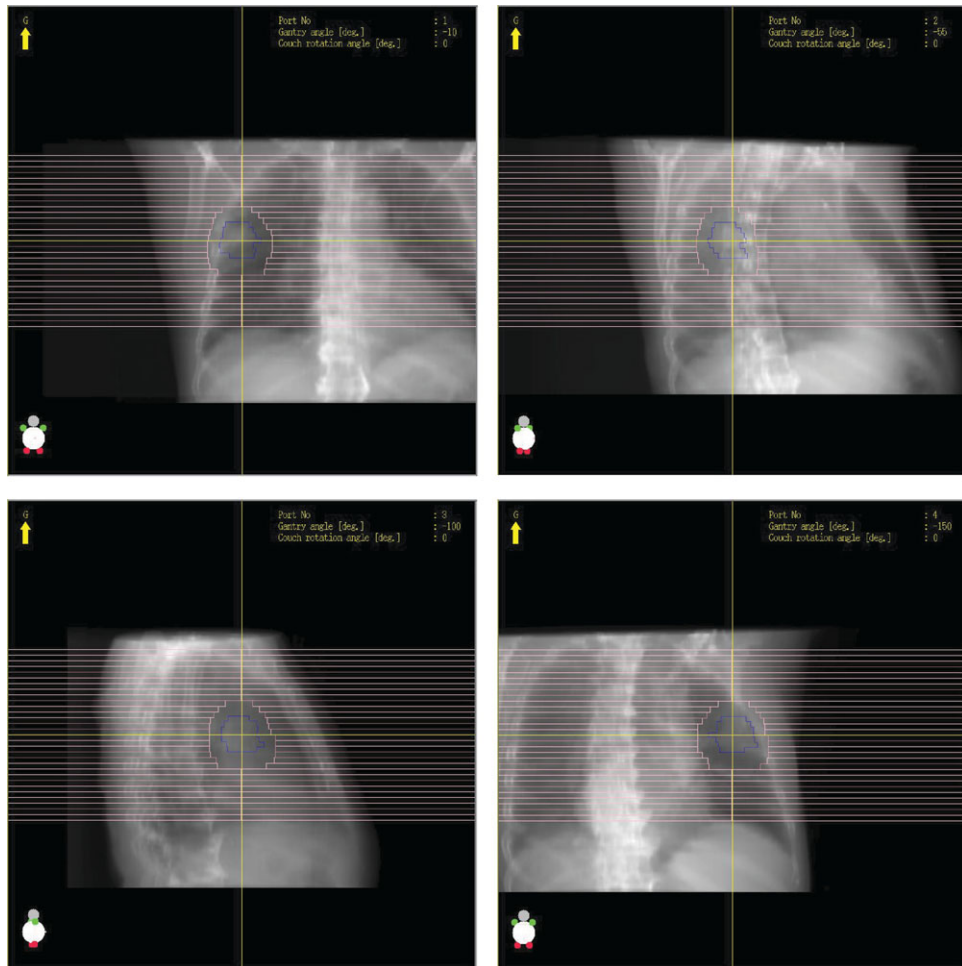


Figure B.3.2. The beam's eye view of the CTV and the beam apertures conformed with the multi-leaf collimators.

- f. Delivery technique
 - i. Passive energy modulated 155 and 200 MeV proton beams
 - ii. Four fields: isocentric and co-planar
 - iii. Respiration-gated treatment delivery
- g. Treatment-planning system
 - i. Doses were estimated with a three-dimensional dose calculation method based on CT images.
 - ii. Simple ray-line-tracing method was used for calculating ranges and designing collimators.
 - iii. Accuracy of dose statement: not determined.
- h. RVR (Remaining Volume at Risk) receiving $V_{30 \text{ Gy (RBE)}} = 25 \text{ ml}$
- i. Maximum dose outside PTV: $D_{\text{RBE}} < 66 \text{ Gy (RBE)}$

Patient immobilization and positioning

Supine with head on the headrest. Patient immobilization was achieved by means of a cradle with polystyrene beads suctioned to conform to the contours of the patient's body. Position of the patient

relative to the beam was determined by the use of laser alignment beams on markers on the cradle and patient skin.

Treatment prescription

- a. Proton-beam therapy: 155 and 200 MeV
- b. Total dose to CTV: $D_{\text{RBE,98\%}} = 63 \text{ Gy (RBE)}$ at 6.3 Gy (RBE) per fraction, given in 10 fractions over 2 weeks $D_{\text{RBE,50\%}} = 66 \text{ Gy (RBE)}$ $D_{\text{RBE,2\%}} = 67 \text{ Gy (RBE)}$
- c. Respiration-gated-beam delivery
- d. RBE = 1.10
- e. OAR—right lung: $D_{\text{RBE,2\%}} = 62 \text{ Gy (RBE)}$
- f. Dose distributions are presented in Fig. B.3.3
- g. Dose–volume histograms are shown in Fig. B.3.4

Treatment technique

- a. Patient in the immobilization devices
- b. Patient positioning was confirmed using orthogonal simulator images referring to orthogonal digitally reconstructed radiographs

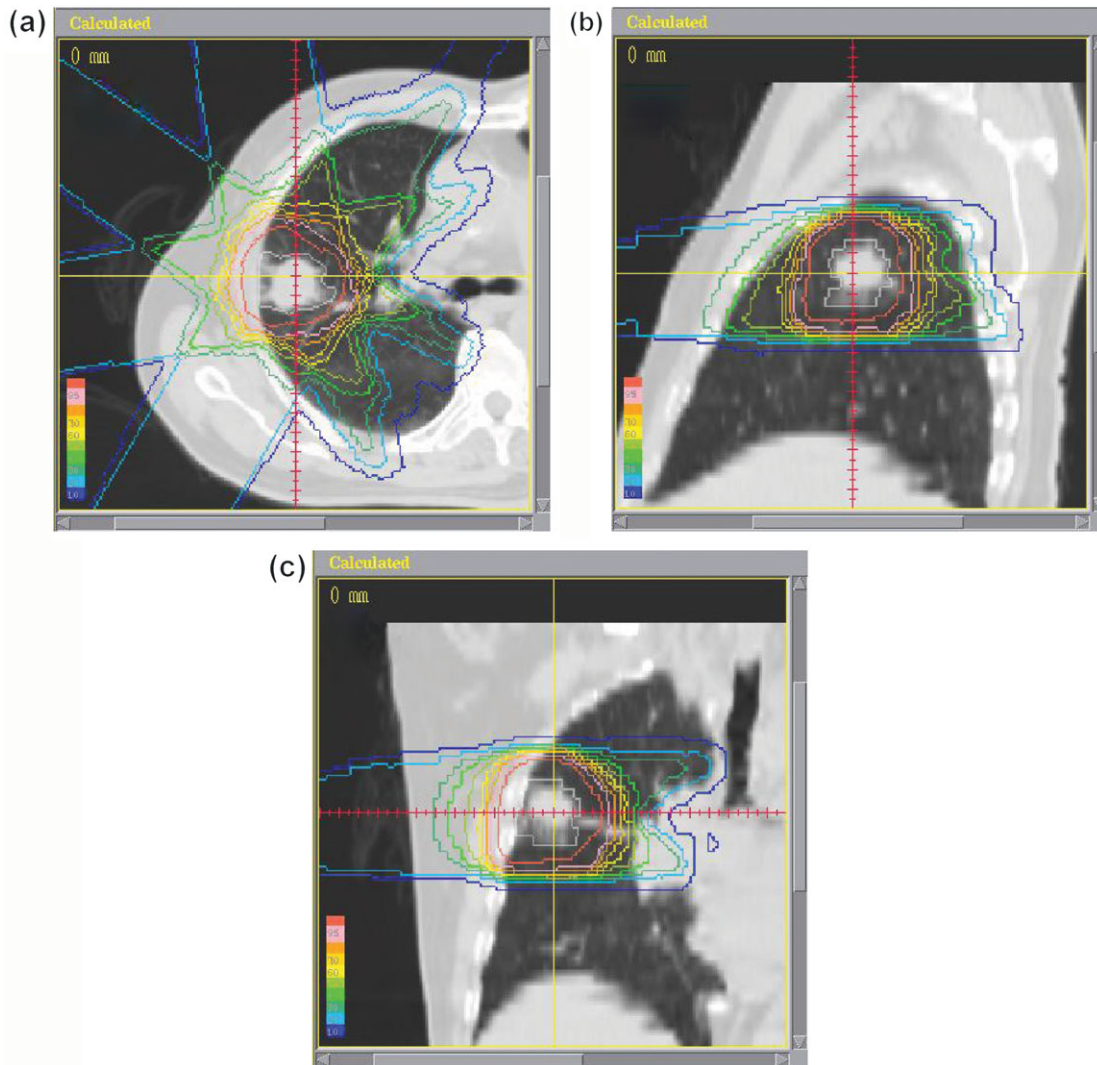


Figure B.3.3. Dose distributions on the axial (a), sagittal (b), and coronal (c) planes. The white contour represents the CTV. The red contour represents 95 percent of the prescribed dose and the blue contour represents 1 percent of the prescribed dose. The remaining contours represent the 10–80 percent isodoses in 10 percent steps.

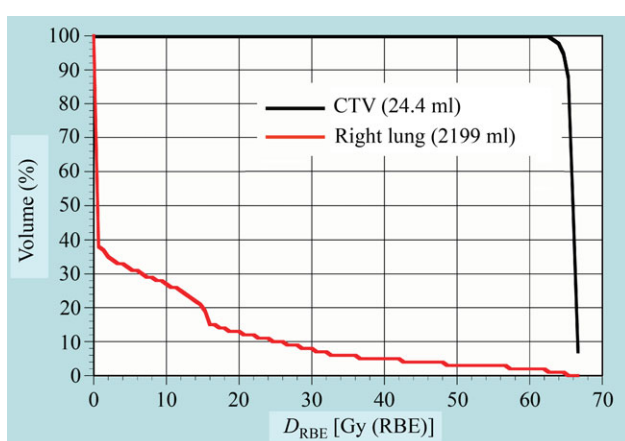


Figure B.3.4. Dose–volume histograms for the CTV and the right lung.

(DRRs) generated in the treatment planning computer program. It was confirmed using orthogonal simulator images digitally stored and orthogonal fluoroscopic images for every treatment session.

c. See Addendum for additional details

Quality assurance

- The institutional standard dose monitor was calibrated once a year at the national standards center.
- The given dose at the reference point (the isocenter and/or the center of the SOBP) was measured under the same conditions as for treatment before starting the irradiation.

- c. The dose-monitoring system and the beam-delivery system were checked every morning before the treatment.
- d. The beam position was evaluated during the irradiation by means of a beam profile monitor.
- e. The beam current and the integral beam charge were measured with two independent sets of monitors, from which signals were sent to the accelerator system when the irradiation was completed. The ratio of doses measured by the two independent monitors was continuously monitored during the irradiation so that a significant change of beam parameters could be instantly detected during the irradiation.
- f. The beam flatness was kept within ± 4 percent and was monitored during the irradiation by a special ion chamber.

Equipment

- a. Proton beams of 155 and 200 MeV were supplied by a slow extraction synchrotron. The average RBE-weighted absorbed dose rate was $2 \text{ Gy (RBE) min}^{-1}$ at the isocenter.
- b. Rotating gantry system
- c. Broad-beam energy modulation

Total doses delivered

- a. Total RBE-weighted absorbed doses, D_{RBE}

Volume/ structure	$D_{\text{RBE},50\%}$ Gy (RBE)	$D_{\text{RBE},98\%}$, Gy (RBE)	$D_{\text{RBE},2\%}$, Gy (RBE)
CTV	66	63	67
Right lung			62

- i. RVR receiving $V_{30 \text{ Gy (RBE)}} = 25 \text{ ml}$
- ii. Maximum dose outside CTV: $D_{\text{RBE},2\%} < 66 \text{ Gy (RBE)}$
- iii. No deviation from planned dose or fractionation

- b. Total absorbed doses, D

Volume/ structure	$D_{50\%}$, Gy	$D_{98\%}$, Gy	$D_{2\%}$, Gy
CTV	60	57.3	60.9
Right lung			56.4

Patient status at completion of treatment

- a. Response of tumor: none

- b. Asymptomatic at start of treatment and completion of therapy
- c. Planned follow-up appointment and imaging or other studies: 1 month after completion of the treatment

Addendum: technical information

Beam shaping

After delineating the CTV, the margins were added to the CTV both laterally and cephalo-caudally by means of enlarging the beam aperture in the beam's eye view, and the distal margin of the beam range was extended by reducing the thickness of the range shifter for the beam. The margins covered uncertainties due to setup errors, internal variability, distal and lateral fall-offs of the irradiation fields, the organ movement with breathing, and others (see Section 5.1.4.4).

Equipment

Proton beams of 250 MeV energy were supplied by a slow-extraction synchrotron with a rotating-gantry system for beam delivery. The average absorbed dose rate was 2 Gy min^{-1} at the isocenter. Doses were estimated with a three-dimensional dose calculation method based on CT images. Parameters of field preparation were computed with the simple ray-line-tracing method.

Treatment technique

The couch angle was 0° (parallel to the axis of gantry rotation). Beam directions with rotating gantry: (1) right anterior oblique, 350° ; (2) right anterior oblique, 305° ; (3) right posterior oblique, 260° ; and (4) right posterior oblique, 210° . The maximum depths were 89, 79, 102, and 138 mm in water-equivalent medium for beams (1), (2), (3), and (4), respectively. The beam was broadened by the dual-ring double-scattering method. A ridge filter was set for a 40 mm spread-out Bragg peak for all beams. The beam apertures were shaped with a manually adjusted brass multi-leaf collimator. Each leaf was 50 mm thick and $5 \times 50 \text{ mm}^2$ in area. The beam apertures were enlarged by 9 mm laterally, 9 mm in the cephalic direction, and 14 mm caudally in the beam's eye view. To take account of various uncertainties the beam ranges were extended 5 mm distally on the beam axes by reducing the thickness of the range shifters. Boluses were not used to conform the distal edge of the beam to the tumor shape.

CASE NUMBER B.4: ACOUSTIC NEUROMA

General patient information

a. Patient identification

- i. Name Confidential
 - ii. Age, gender, and race 72 year old Caucasian female
 - iii. Address Confidential
 - iv. Phone no. Confidential
 - v. E-mail address Confidential
 - vi. Hospital ID no. Confidential
 - vii. Person to notify Confidential
(with contact information)
were a problem to arise

b. Medical team

- i. Radiation oncologist(s) Confidential
 - ii. Radiation physicist(s) Confidential
 - iii. Referring physician Confidential

Medical evaluation of presenting lesion

- | | |
|-------------------------|--|
| a. Medical history | Seven years of decreasing auditory acuity and is now nearly deaf. Increasing size of tumor |
| b. Physical examination | Noncontributory |
| c. Imaging studies | 1.25 mm slice CT |
| d. Tumor site | Left cerebellopontine angle |
| e. Diagnosis | Acoustic neuroma: clinical and radiological diagnosis. Volume = 3.2 ml |
| f. Grade | No biopsy |
| g. Stage | No staging |
| h. Prior therapy | None |
| i. Family history | Noncontributory |

General medical evaluation

- a. History, physical examination, and imaging
 - b. Co-morbidities
 - c. Present status
 - d. Past surgery
 - e. Prior radiation

No evidence of other tumor detected

Spinal stenosis
Type II diabetes
Hypertension
Mastoid disease as child
Well controlled co-morbidities
C section
Mastoid surgery
None

Treatment intent

- a. Curative by single-dose proton radiation treatment.
 - b. No surgery or systemic therapy planned.
 - c. Predicted outcome
 - i. Local control probability at 7 years: 95 percent
 - ii. Hearing preservation: 50 percent
 - iii. Permanent facial nerve injury: 1 percent; temporary: 5 percent.

Treatment planning

- a. General plan
 - i. Standard stereotactic radiosurgery treatment for this tumor.
 - ii. Single dose
 - b. Definition of treatment volumes
 - i. Treatment-planning CT performed with the patient in the same immobilization device and conditions as used for treatment.
 - ii. GTV: GTV is defined as the demonstrable tumor relative to the fiducial markers for planning (Fig. B.4.1a–c). CTV was assumed to be identical to the GTV.
 - iii. Volume defined: 3.2 ml tumor visualized at the cerebellopontine angle on imaging studies.
 - iv. Fiducial markers (Fig. B.4.2a–c). Three SS316LVL 1/16 in. diameter micro-spheres inserted in the outer table of the patient's skull were used for patient alignment. Target position confirmation: with the patient in the fully immobilized position, orthogonal x-ray images were obtained for a standard set-up position as well as other coplanar fields prior to treatment. Single x-ray images were obtained for superior oblique or vertex fields prior to treatment. Implanted micro-spheres were automatically identified on the x-ray images with custom computer software which then compared them with expected projections as identified on planning DRR. Patient position corrections were made. This was repeated until the intended position was achieved, and reconfirmed prior to treatment.
 - v. PTV: PTV is defined as 1 mm beyond the GTV in all directions, to allow for all uncertainties included in the immobilization and setup. The PTV did abut the brainstem surface. The dose prescribed to the PTV was $D_{RBE,98\%} = 12.8$ Gy (RBE) and thus respected the dose constraint of 12 Gy

APPENDIX B

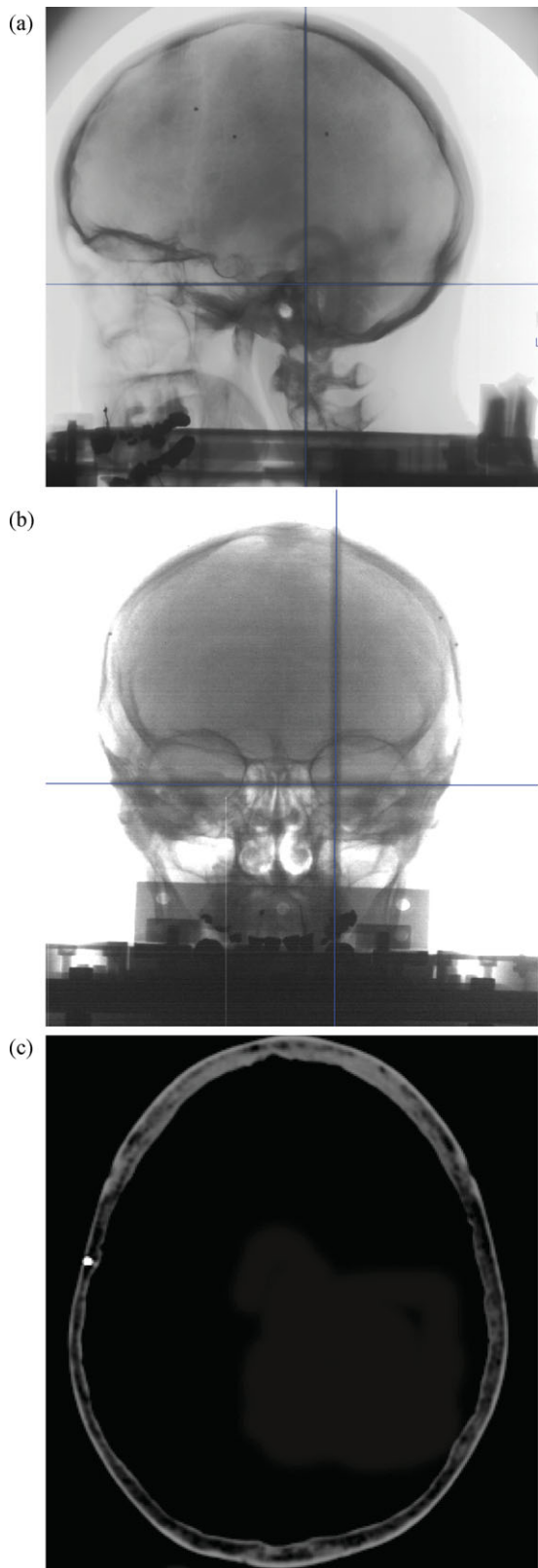


Figure B.4.1. Views (a) and (b) are lateral and AP fields, respectively, demonstrating the position of the fiducial markers placed in the skull. The diagnostic quality images were obtained for the positioning of the patient by the use of these markers. (c) CT slice at the level of one of the fiducial markers.

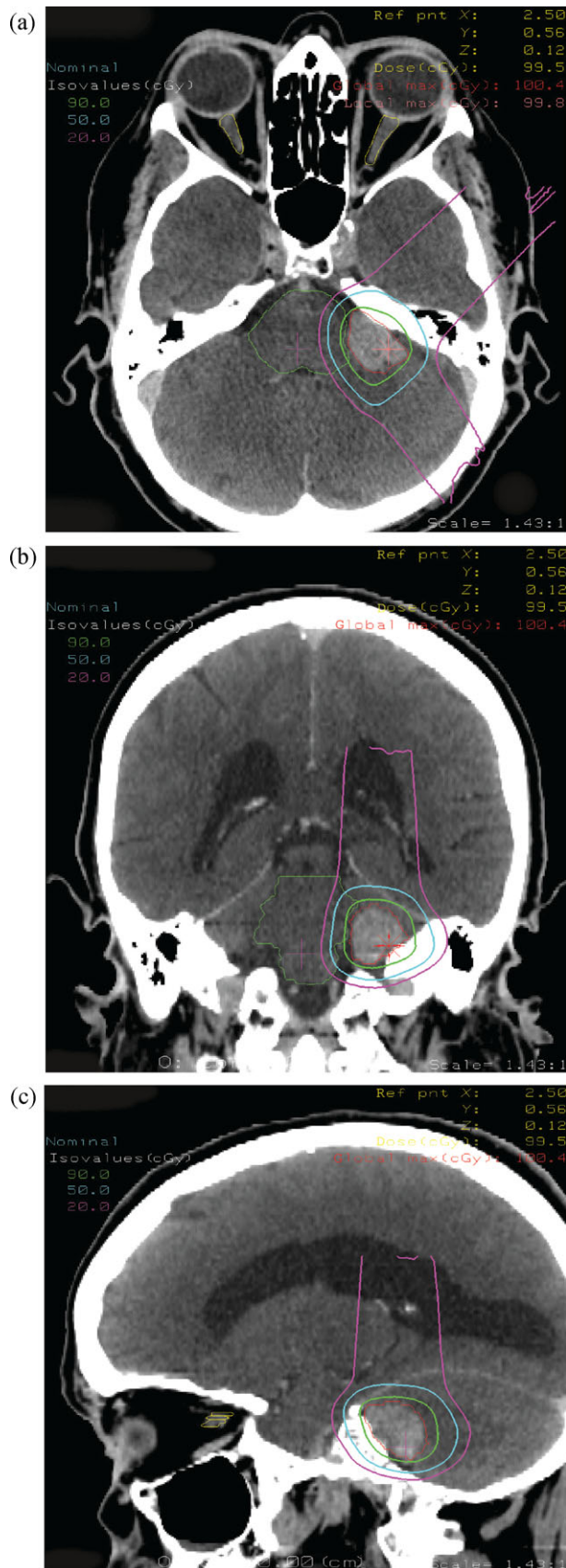


Figure B.4.2. Views (a), (b), and (c) are displays of the tumor and paths of the three beams employed.

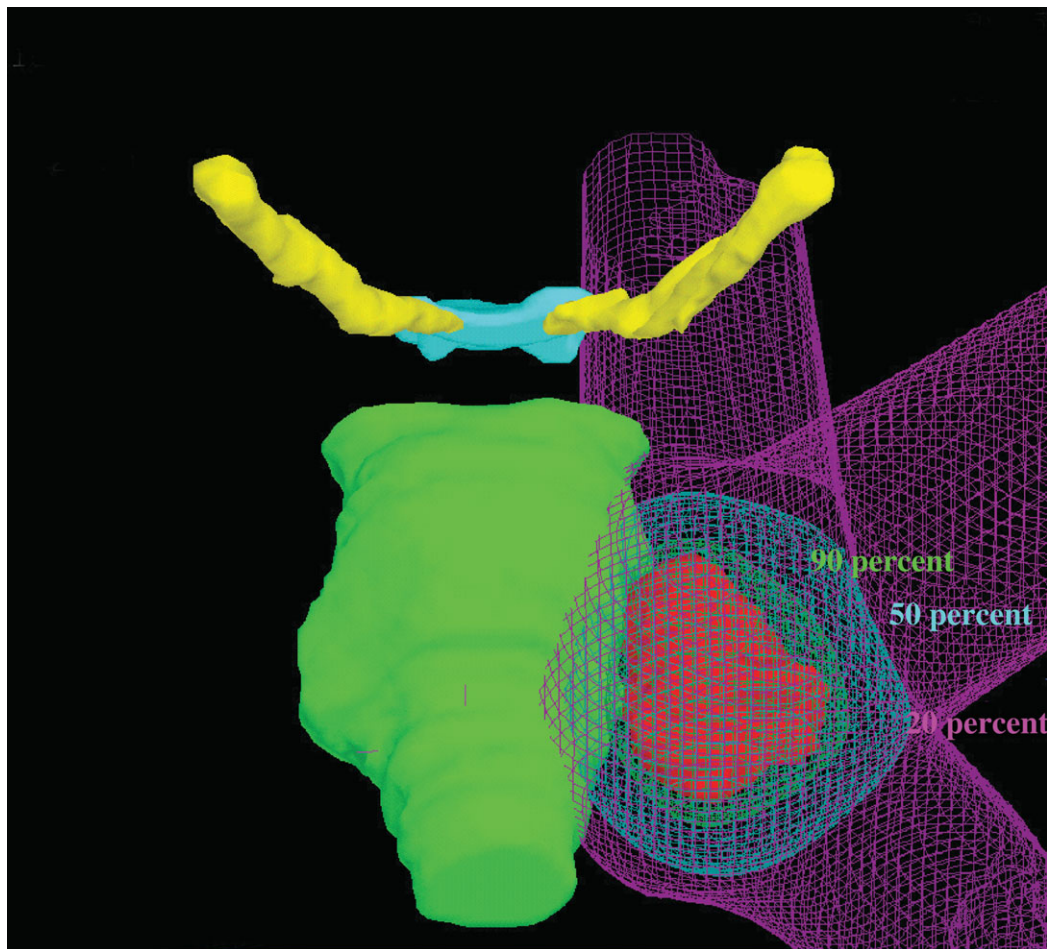


Figure B.4.3. Three-dimensional image of the tumor relative to the brainstem, chiasm, and the 90 and 50 percent dose volumes.

(RBE) to the brainstem surface. The aperture margin was 3.5 mm beyond the PTV to allow for the penumbra (Fig. B.4.3).

vi. Dose calculation

- Three-dimensional proton pencil beam algorithm based on 1.25 mm CT slices of the whole head (≈ 184 slices)
- Doses are stated with an accuracy of 2 percent.

vii. The XIO system was used for treatment planning

viii. Dose–volume histograms are given in Fig. B.4.4 for the tumor and brainstem.

c. Single dose: $D_{RBE,98\%} = 12.8$ Gy (RBE) to GTV.

d. RBE = 1.10

e. Organs at risk. Dose constraints

i. Brainstem surface: $D_{RBE,2\%} = 12$ Gy (RBE)

ii. Mid brainstem: $D_{RBE,2\%} = 6$ Gy (RBE)

Patient immobilization and positioning

Supine position with a modified Gill–Thomas–Cosman (GTC, Radionics Inc.) device.

Treatment prescription

a. RBE-weighted dose (D_{RBE}) is prescribed.

b. RBE = 1.10

c. Single dose

d. Brain-stem surface: $D_{RBE,2\%} = 12.0$ Gy (RBE), *viz.*, the near-maximum dose to the brainstem surface

e. $D_{RBE,98\%}$ and $D_{RBE,50\%}$ to the GTV are 12.8 and 13.3 Gy (RBE), respectively.

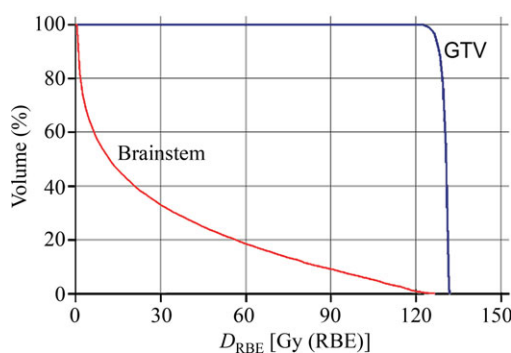


Figure B.4.4. Dose–volume histograms of the GTV and of the brainstem.

- f. OAR—brainstem surface: $D_{RBE,2\%} \leq 12$ Gy (RBE)

Treatment technique

- The patient was in the immobilization device.
- The target position relative to the fiducial markers was determined by study of the treatment-planning CT images. For the treatment, orthogonal x-ray images of the fiducial markers were compared with the digitally reconstructed radiographs for each beam path.
- The GTV was irradiated using a three-field approach. In this case of a left-sided acoustic neuroma, these comprised left anterior oblique, left posterior oblique, and superior vertex fields.
- Field range was defined with the distal 90 percent dose level of the SOBP at 2 mm beyond the calculated margin of the GTV.
- Field modulation was defined with the proximal 90 percent dose level of the SOBP at 2 mm proximal to the calculated margin of the GTV.
- The 80–20 percent penumbra was ≈ 5 mm and resulted from the use of a double-scattering gantry beam-modification system with a SAD of 220 cm.

Quality assurance

- Individual portal hardware consisted of custom brass apertures and PMMA range compensators. These underwent a thorough QA inspection, consisting of comparing various dimensions on the devices with those required by the treatment-planning system.
- Individual portals underwent range and modulation measurements as well as dose output verification, which were compared with the planned values.

Equipment

- Beam: cyclotron-produced 230 MeV proton beam
- Broad-beam energy modulation
- 360° isocentric gantry
- Beams: protons degraded to the planned range
- Ports: three ports (with projections close to orthogonal with respect to each other)

Total doses delivered

- a. Total RBE-weighted doses, D_{RBE}

Volume/structure	$D_{RBE,50\%}$, Gy (RBE)	$D_{RBE,98\%}$, Gy, (RBE)	$D_{RBE,2\%}$, Gy (RBE)
GTV	13.3	12.8	13.5
Anterior surface of brainstem ^a	1.1	0.09	11.9
Mid-brainstem	<0.5		

^aThe brainstem surface considered extends 4 mm beyond the GTV both superiorly and inferiorly.

- b. Total absorbed doses, D

Volume/structure	$D_{50\%}$, Gy	$D_{98\%}$, Gy	$D_{2\%}$, Gy
GTV	12.1	11.6	12.3
Anterior surface of brainstem ^a	1.0	0.082	10.8
Mid-brainstem	<0.5		

^aThe brainstem surface considered extends 4 mm beyond the GTV both superiorly and inferiorly.

Patient status at completion of treatment

- No change in auditory acuity
- General condition unchanged

Addendum: technical information*Quality-assurance checklist*

Patient	LP1A	LA1A	SU1A
Field			
Action	Verified	Verified	Verified
Construction	TR 5/18/2005	TR 5/18/2005	TR 5/18/2005
Aperture geometry check (against planning printout) and thickness	Ok	Ok	Ok
Range compensator shape and thicknesses	Ok	Ok	Ok
Patient and field identification	Ok	Ok	Ok
Calibration and dosimetry	SJR 5/18/2005	SJR 5/18/2005	SJR 5/18/2005
Range (g cm^{-2} ; treatment machine settings to achieve prescribed range)	8.48	10.27	13.65
Modulation (g cm^{-2} ; treatment machine settings to achieve prescribed modulation)	3.10	3.40	3.00
Calibration point (beam coordinates)	0,0,0	0,0,0	0,0,0
RBE-weighted absorbed dose [cGy (RBE)] ($D_{\text{RBE}} = 1200 \text{ cGy (RBE)}$, weighted 1:1:1 for three fields)	400.0	400.0	400.0
RBE	1.1	1.1	1.1
Absorbed dose (cGy)	363.6	363.6	363.6
Isodose normalization (%)	90	90	90
Output factor calculation Ψ [cGy MU^{-1} at STP]	1.272	1.336	1.444
Monitor units (MU at STP)	317.6	302.4	279.8
Equipment settings	SJR 5/18/2005	SJR 5/18/2005	SJR 5/18/2005
Treatment room	Gantry 1	Gantry 1	Gantry 1
Range modulator/scattering system ID	A3	A4	A5
Snout position (cm)	18.6	18.6	20.7

Maximum field sizes	
LAO: L45A	$3.0 \times 3.5 \text{ cm}^2$
LPO: L55P	$3.1 \times 3.1 \text{ cm}^2$
SUP	$3.1 \times 3.4 \text{ cm}^2$
Range/SOBP	
LAO	10.3 cm/3.4 cm
LPO	8.5 cm/3.1 cm
SUP	13.6 cm/3.0 cm

APPENDIX B

CASE NUMBER B.5: MEDULLOBLASTOMA (PEDIATRIC)

General patient information

a. Patient identification	
i. Name	Confidential
ii. Age, gender, and race	10 year old Caucasian male
iii. Address	Confidential
iv. Phone no.	Confidential
v. E-mail address	Confidential
vi. Hospital ID no.	Confidential
vii. Person to notify (with contact information) were a problem to arise	Confidential
b. Medical team	
i. Radiation oncologist(s)	Confidential
ii. Radiation physicist(s)	Confidential
iii. Referring physician	Confidential

Medical evaluation of presenting lesion

a. Medical history	Four week headache and emesis
b. Physical examination	Normal neurological and general examination
c. Imaging studies	Pre-surgical CT and MRI: partially calcified $5.5 \times 3.5 \times 3.5 \text{ cm}^3$ mass within fourth ventricle extending into lateral recess; obstructive hydrocephalus
d. Tumor site	Posterior fossa
e. Diagnosis	Medulloblastoma
f. Grade	WHO grade IV
g. Stage	Preoperative. CSF negative.
h. Prior therapy	Standard risk patient
i. Family history	Near total resection; minimal residual tumor Paternal grandmother, lung cancer. Multiple maternal breast cancers

General medical evaluation

a. History, physical examination, and imaging	No evident non-tumor disease
b. Co-morbidities	None
c. Current medications	Anti-emetic and pain medication

Treatment intent

- a. Curative by combined modality therapies: surgery, chemotherapy, and radiation. Radiation to be given postoperatively.

- b. Patient was standard risk and was to receive standard doses of $D_{\text{RBE,98\%},\text{CTV}} = 23.4 \text{ Gy (RBE)}$ to cerebrospinal axis and total $D_{\text{RBE,98\%},\text{CTV}} = 54 \text{ Gy (RBE)}$ to posterior fossa.
- c. RBE = 1.10
- d. Probabilities of outcome:
 - i. Cure at 5 years: 85 percent
 - ii. Probability of treatment-related morbidity
 - Late hearing loss: 20 percent
 - Neuro-cognitive partial loss at 10 years: approaches 100 percent
 - Measurable loss of IQ at 10 years: approaches 100 percent.

Treatment planning

- a. General plan
 - i. The patient was treated according to Institutional Protocol No. 99271.
 - ii. Patient was post near complete resection.
 - iii. Postoperative proton radiation treatment, in two segments.
 - iv. VCR chemotherapy given concurrent with, and following, the radiation therapy.
- b. Definitions of treatment volumes
 - i. For Segments 1 and 2, there was no GTV.
 - ii. For Segment 1, the CTV-1 was defined as the entirety of the CNS, *i.e.*, the brain and the thecal sac (to bottom of S3).
 - iii. For Segment 2, the CTV-2 was defined as the posterior fossa.
 - iv. Treatment planning CT images were obtained with the patient in the treatment position.
 - For Segment 1, the patient was in the prone position and 3.75 mm CT slices were used to scan from the superior aspect of cranium to the coccyx.
 - For Segment 2 the patient was in the supine position and 2.5 mm CT slices were used to scan from the superior aspect of cranium to the level of C4.
 - v. PTV: not delineated for Segments 1 or 2.
 - 2. Field sizes were defined to assure delivery of the planned dose to the CTV.
- c. Dose fractionation: $D_{\text{RBE,98\%}} = 1.8 \text{ Gy (RBE)}$ per fraction and five fractions per week.
- d. RBE is 1.10
- e. Organs at risk and dose constraints defined as the dose producing major morbidity, *viz.*, Grade III/IV severity of complications at <5 percent. This pertains to radiation combined with chemotherapy.

- i. Cochlea: $D_{RBE,2\%} = 40$ Gy (RBE)
- ii. Spinal cord: $D_{RBE,2\%} = 45$ Gy (RBE)

There was no need to reduce the dose to CTV-1 or CTV-2 at any point to respect the defined dose constraints

- f. The XIO treatment planning system was employed
 - i. Dose statement accuracy: 2 percent
 - ii. Position accuracy: 2 mm

- g. Isodose and color wash displays of dose distributions are shown in Figs B.5.1–B.5.3 and dose–volume histograms are shown in Fig. B.5.4.

Patient immobilization and positioning

- a. For each treatment session of Segment 1, the patient was anesthetized and then placed in the prone position in the immobilization device, which consisted of a base plate, rocker device and face

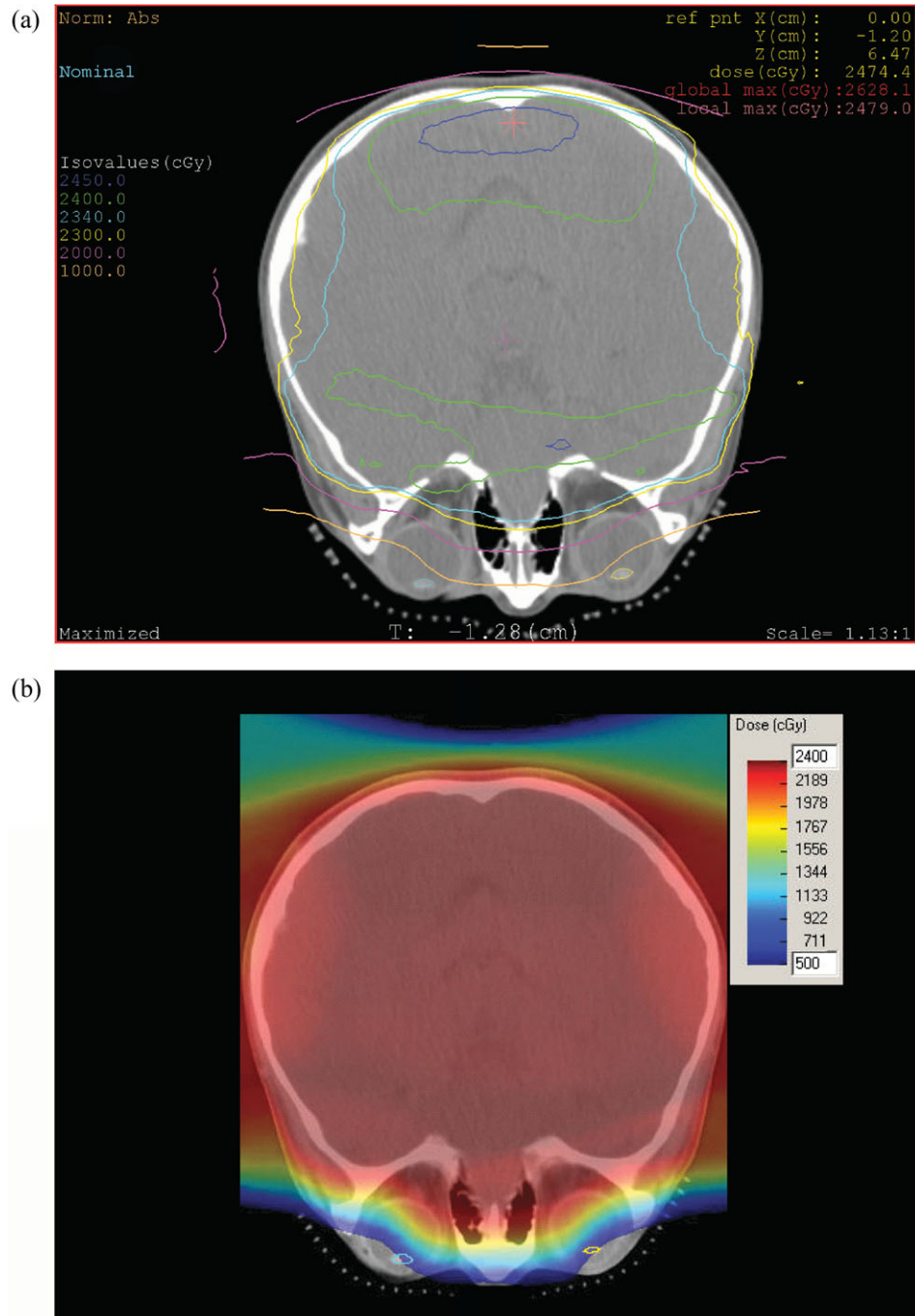


Figure B.5.1. Segment 1. Axial section through cerebellum and eyes: isodose contour display (a) and color-wash display (b) of dose distributions.



Figure B.5.2. Segment 1. Spinal axis (sagittal section): isodose-contour display (a) and color-wash display (b) of dose distributions. For the Segment 1 treatment the patient was prone.

mask (Med-Tec, Inc.). Orthogonal x-ray images were obtained for a standard set-up position as well the treatment fields prior to treatment. These images were then compared and analyzed in the digital-imaging positioning system. Patient position corrections were made. This was repeated until the intended position was achieved, applied, and reconfirmed prior to each treatment.

- b. For Segment 2, the patient was supine in the immobilization device. Anesthesia was not required.
- c. Orthogonal x-ray images were obtained for a standard set-up position as well the treatment fields prior to each treatment. These images were then compared and analyzed in the digital-imaging positioning system. Patient position corrections were made. This was repeated until the intended position was achieved, applied, and reconfirmed prior to each treatment.

Treatment prescription

- a. Prescribed dose
 - i. Proton radiation treatment.
 - ii. Doses were prescribed in RBE-weighted doses, D_{RBE} [Gy (RBE)].
 - iii. RBE = 1.10
 - iv. Doses were specified as $D_{RBE,50\%}$, $D_{RBE,98\%}$ and $D_{RBE,2\%}$
 - v. Fractionation: $D_{RBE,98\%} = 1.8$ Gy (RBE) for five fractions per week for 30 fractions over a time of 6 weeks.
 - vi. Segment 1
 - To CTV-1, $D_{RBE,98\%} = 23.4$ Gy (RBE) in 13 equal fractions of $d_{RBE,98\%} = 1.8$ Gy (RBE).
 - vii. Segment 2
 - To CTV-2, $D_{RBE,98\%} = 30.6$ Gy (RBE) given in 17 equal fractions of $d_{RBE,98\%} = 1.8$ Gy (RBE).

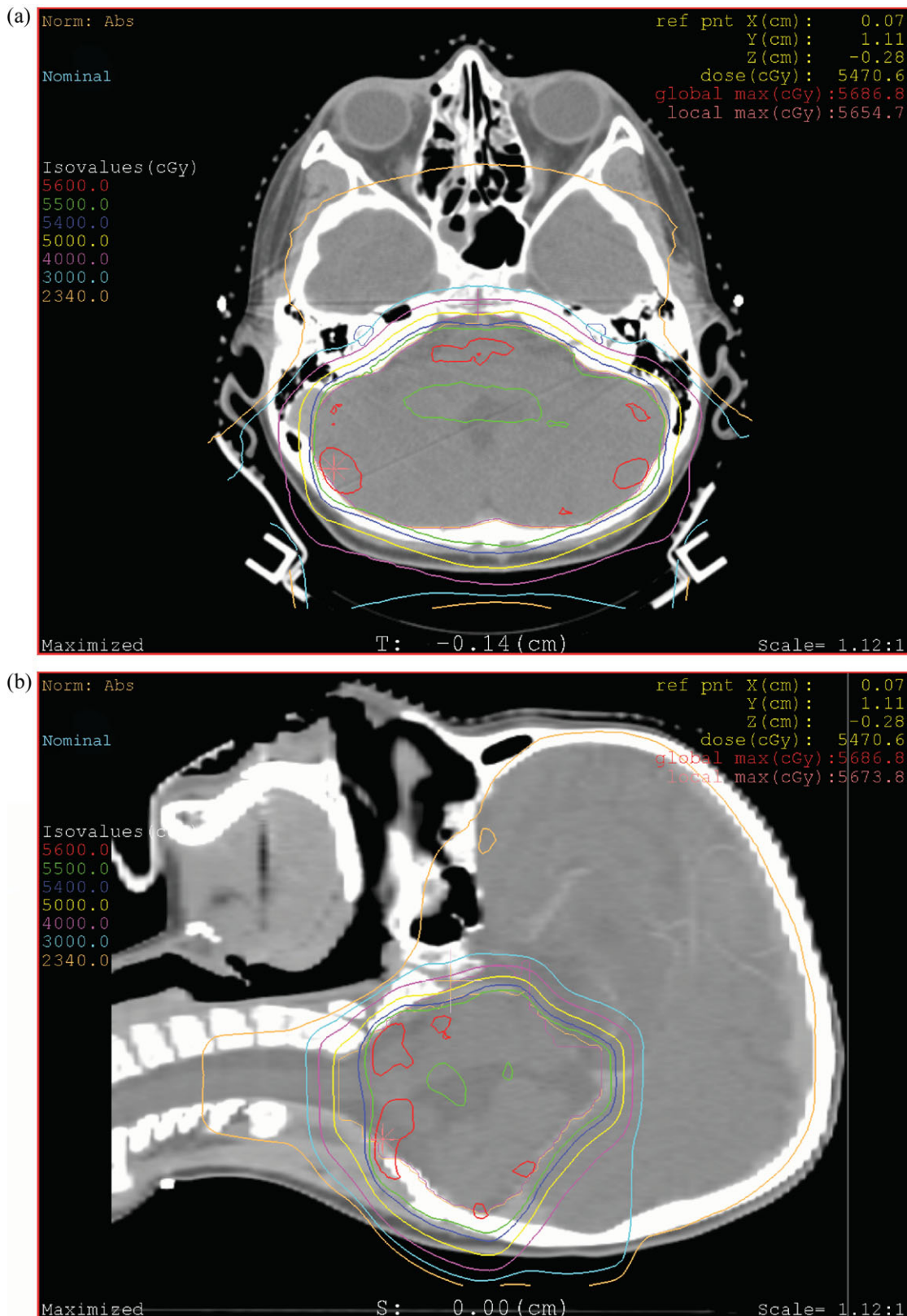


Figure B.5.3. Total dose to posterior fossa: Segments 1 and 2. Patient in supine position for Segment 2. Axial (a) and sagittal (b) sections through posterior fossa with isodose contours.

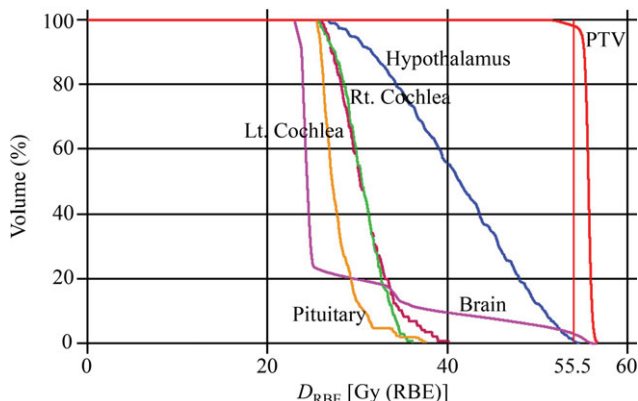


Figure B.5.4. Dose–volume histograms for (from left to right) brain (posterior fossa) (pink), pituitary gland (yellow), right cochlea (green), left cochlea (red), hypothalamus (blue), and PTV (cerebrum) (red). $D_{RBE,PTV,98\%} = 55.5$ Gy (RBE) as indicated by the vertical red line.

- b. Total dose to posterior fossa: $D_{RBE,98\%} = 54.0$ Gy (RBE) in 30 fractions in 6 weeks.
- c. OAR: Dose constraints were not exceeded by these prescribed doses.

Treatment technique

- a. Proton beam
- b. Segment 1.
 - i. Spinal axis (the target was the thecal sac)
 - Two matching posterior–anterior proton fields were used to treat the spinal axis to the inferior border of the thecal sac. The SOBP for the spine field was designed for the distal 75 percent isodose of the SOBP to be at the anterior edge of the vertebral bodies, to enhance esophagus sparing. This resulted in delivery of $D_{RBE,98\%}$ of ~ 20 – 22 Gy (RBE) to vertebral bodies, intending to produce uniform growth modification. The proximal 90 percent isodose of the SOBP was set at the posterior edge of the spinous processes.
 - A moving-junction technique was employed.
 - ii. Whole brain
 - Treated with right and left posterior oblique fields to $D_{RBE,98\%} = 23.4$ Gy (RBE) and with sparing of the lenses.
 - Field ranges for all the brain fields were defined with the distal 100 percent of the SOBP conforming to the brain surface.

- Field modulations for the brain fields were defined with the proximal 98 percent of the SOBP at the brain surface.

c. Segment 2. Posterior fossa

- i. Dose by Segment 1, $D_{RBE,98\%}$ was 23.4 Gy (RBE)
- ii. Dose by Segment 2, $D_{RBE,98\%}$ was 30.6 Gy (RBE), delivered by a posterior, a right posterior and a left posterior oblique fields, *viz.*, a boost treatment.

Quality assurance

- a. Individual portal hardware consisted of custom brass apertures and PMMA range compensators. These underwent a thorough QA inspection before treatment. This consisted of measuring various dimensions on the devices and comparing them with the output of the treatment-planning system.
- b. Range modulation and absorbed-dose verification measurements were made for individual treatment portals and were compared with planned values.

Equipment

- a. Cyclotron-produced 230 MeV proton beam
- b. Broad-beam passive energy modulation
- c. 360° rotational gantry
- d. Digital imaging system for patient position verification
- e. 80–20 percent penumbra was ≈ 5 mm with passive double-scattering gantry beam-delivery system with SAD of 220 cm.

Total doses delivered

- a. Total RBE-weighted absorbed doses, D_{RBE}
 - i. Spinal axis
 - $D_{RBE,2\%} = 25.7$ Gy (RBE) at the anterior vertebral body matchline.
 - $D_{RBE,98\%} = 22.2$ Gy (RBE) at the posterior thecal sac matchline
 - ii. Posterior fossa by Segments 1 and 2 was $D_{RBE,98\%} = 54$ Gy (RBE) in 30 fractions
 - iii. There were no interruptions in the treatment.
 - iv. Dose to OARs
 - Dose to the cochlea was reduced by only several percent for the whole brain fields, but significantly more for the posterior fossa boost. The total dose to the cochlea was $D_{RBE} = 30.4$ – 36.7 Gy (RBE) and below the dose constraint of $D_{RBE} = 40$ Gy (RBE). This

compares to an absorbed dose of 54–55 Gy for photon treatment in this department that results in deafness in 50 percent of patients in this age group.

- Lens dose: $D_{\text{RBE}} = 3\text{--}5$ Gy (RBE) with oblique proton fields
- Scalp dose: $D_{\text{RBE}} \approx 16$ Gy (RBE)

Target/ structure	D_{RBE} , Gy (RBE)			Dose per fraction (d_{RBE}), Gy (RBE)	Number of fractions
	$D_{98\%}$	$D_{50\%}$	$D_{2\%}$		
CTV1 (CSI) ^a	23.4	23.4	25.7	1.8	13
CTV2 (posterior fossa)	54.3	55.6	56.4	1.8	30
Pituitary	25.6	27.1	36.5		
Hypothalamus	3.0	5.3	7.8		
Cochlea	26.2	30.4	36.7		
Lens	3.6	5.4	7.6		
Esophagus	0.1	2.3	12.4		
Thyroid	0	0	2.6		

^aCraniospinal irradiation.

b. Total absorbed doses, D

Target/ structure	D , Gy			Dose per fraction (d), Gy	Number of fractions
	$D_{98\%}$	$D_{50\%}$	$D_{2\%}$		
CTV1 (CSI)	21.3	21.3	23.4	1.64	13
CTV2 (posterior fossa)	49.4	50.5	51.3	1.64	30
Pituitary	23.3	24.6	33.2		
Hypothalamus	2.7	4.8	7.1		
Cochlea	23.8	27.6	33.4		
Lens	3.2	4.9	6.9		
Esophagus	0.09	2.1	11.3		
Thyroid	0	0	2.4		

Patient status at completion of treatment

- Persistent emesis
- To continue chemotherapy
- Follow-up appointment in 4 weeks

APPENDIX B

Addendum: technical information

Quality-assurance checklist

Patient	—	—	—	—	—	—	—
Field	LP2A	RP2A	SS2A	IS2A	PA1A	RP4B	LP4B
Action	Verified						
Construction	TR 5/18/2005						
Aperture geometry check (against planning printout) and thickness	Ok						
Range compensator shape and thicknesses	Ok						
Patient and field identification	Ok						
Calibration and dosimetry	SJR 5/18/2005						
Range (g cm^{-2})	17.50	17.50	7.35	8.30	10.5	13.55	13.25
Modulation (g cm^{-2})	17.92 (full)	17.92 (full)	7.20	7.90	8.80	12.0	11.9
Calibration point (beam coordinates)	0,0,0	0,0,0	0,0,0	0,0,0	0,0,0	0,0,0	0,0,0
DRBE [cGy (RBE)] (RX dose of 1200 cGy (RBE) weighted 1:1 for three fields)	90	90	180	180	180	90	90
RBE factor	1.1	1.1	1.1	1.1	1.1	1.1	1.1
Absorbed dose (cGy)	82	82	164	164	164	82	82
Isodose normalization (%)	98	98	98	99	98	98	98
Output factor calculation Ψ (cGy MU $^{-1}$ at STP)	0.819	0.819	0.814	0.840	0.962	0.877	0.866
Monitor units (MU at STP)	102.2	102.2	205.6	197.2	174	95.4	96.6
Equipment settings	SJR 5/18/2005						
Treatment room	Gantry 1						
Range modulator/scattering system ID	A6	A6	A2	A3	A2	A5	A5
Snout position (cm)	26.9	26.8	22.5	21.0	22.5	15.7	15.5

Beams for Segment 1 (cranial spinal axis treatment)

	Beam number			
	1	2	3	4
Description	L1 L15P WB	L1 R15P WB	L1 SS	L1 IS
Machine ID	1G protons	1G protons	1G protons	1G protons
Collimator	Sym	Sym	Sym	Sym
Set up/dist (cm)	SAD/227.0	SAD/227.0	SAD/227.0	SAD/227.0
SSD/Wt fan SSD (cm)	217.5/217.5	217.6/217.6	219.0/219.0	221.2/221.2
Field defined at	Isocenter	Isocenter	Isocenter	Isocenter
Width (cm, L/R if asym)	27.0	27.0	26.4	26.2
Length (cm, U/L if asym)	27.0	27.0	26.4	26.2
Gantry/collimator angle (deg)	285/-0	75/-0	0/-0	0/-0
Couch/pitch/roll angle (deg)	0/0/0	0/0/0	0/0/0	0/0/0
Isocenter/beam entry	Iso	Iso	Iso	Iso
x/y/z (cm)	0.20/-1.50/1.00	0.20/-1.50/1.00	0.20/-21.50/1.00	0.20/-42.50/1.00
Tx aids				
Customized port ID	L1v1LWB	L1v1RWB	L1v1SS	L1v1IS
Iso-to-port dist (cm)	26.91	26.83	22.46	20.95
Compensator	LWBv1RC	RWBv1RC	SSv1RC	ISv1RC
Iso-to-RC dist (cm)	15.52	15.44	18.04	15.81
Taper angle (deg)/margin (cm)	30.0/1.00	30.0/1.00	0.0/0.00	0.0/0.00
Snout ID	250	250	250	250
Degrader ID				

Continued

Continued

	Beam number			
	1	2	3	4
Compensating block ID	—	—	—	—
Calculation algorithm	Pencil beam	Pencil beam	Broad beam	Broad beam
Weight (cGy)/no. of fractions	365.0/4	365.0/4	707.0/4	716.0/4
<i>x, y, z</i> (cm)	0.00/0.00/0.00	0.00/0.00/0.00	0.00/0.00/0.00	0.00/0.00/0.00
Target	Brain PTV	Brain PTV	Vertebra RC	Vertebra RC
Beam spreading	Passive	Passive	Passive	Passive
Air gap (cm)	6	6	10	10
Prescribed range (g cm ⁻²)	17.5	17.5	7.2	8.2
Raw, w/uncert	16.64/17.32	16.59/17.27	7.17/7.52	8.18/8.56
Prescribed modulation (g cm ⁻²)	17.92	17.92	7.2	7.9
Raw, smr, smr w/uncert	15.70/15.83/16.82	15.56/15.70/16.74	6.08/6.21/6.69	6.72/6.85/7.38
Smearing distance (cm)	0.3	0.3	0.3	0.3
Uncertainty parameters	Nominal	Nominal	Nominal	Nominal
Density (%)	3.5	3.5	3.5	3.5
Range (cm)	0.1	0.1	0.1	0.1
Dose (cGy MU ⁻¹)	0.811	0.811	0.821	0.815

Beams for Segment 1 (posterior fossa treatment).

	Beam number					
	1	2	3	4	5	6
Description	PA PF	PA PF offcord	R30P PF	L25P PF	L15P WB	R15P WB
Machine ID	1G protons	1G protons	1G protons	1G protons	1G protons	1G protons
Collimator	Sym	Sym	Sym	Sym	Sym	Sym
Setup/dist (cm)	SAD/227.0	SAD/227.0	SAD/227.0	SAD/227.0	SAD/227.0	SAD/227.0
SSD/Wt fan SSD (cm)	219.0/219.0	219.0/219.0	219.3/219.3	219.2/219.2	218.1/218.1	217.9/217.9
Field defined at	Isocenter	Isocenter	Isocenter	Isocenter	Isocenter	Isocenter
Width (cm, L/R if asym)	12.5	12.5	12.5	12.5	26.7	26.8
Length (cm, U/L if asym)	12.5	12.5	12.5	12.5	26.7	26.8
Gantry/coll angle (deg)	180/0	180/0	240/0	115/0	105/0	255/0
Couch/pitch/roll angle (deg)	0/0/0	0/0/0	0/0/0	0/0/0	0/0/0	0/0/0
Isocenter/beam entry	Iso	Iso	Iso	Iso	Iso	Iso
<i>x/y/z</i> (cm)	0.35/ 0.58/ -3.31	0.35/ 0.58/ -3.31	0.35/ 0.58/ -3.31	0.35/0.58/ -3.31	0.20/2.50/ -1.50	0.20/2.50/ -1.50
Tx aids						
Customized port ID	PAv1PF	PAv2PF	R30Pv1PF	L25Pv1PF	L15PsupWB	R15PsupWB
Iso-to-port dist (cm)	15.53	15.53	15.69	15.48	24.68	25.3
Compensator	PAv1PF	PAv1PF	R30Pv1PF	L25Pv1PF	L15PsupWB	R15PsupWB
Iso-to-RC dist (cm)	9.99	9.99	9.71	9.81	14.92	15.12
Taper angle (deg)/margin (cm)	15.0/0.50	15.0/0.50	15.0/0.50	30.0/1.00	30.0/1.00	30.0/1.00
Snout ID	124	124	124	124	250	250
Degrader ID						
Compensating block ID	—	—	—	—	—	—
Calculation algorithm	Pencil beam	Pencil beam	Pencil beam	Pencil beam	Pencil beam	Pencil beam
Weight (cGy)/no. of fractions	742.0/4	370.0/2	1018.0/11	1019.0/11	1236.0/13	1236.0/13
<i>x/y/z</i> (cm)	0.00/0.00/0.00	0.00/0.00/0.00	0.00/0.00/0.00	0.00/0.00/0.00	0.00/0.00/0.00	0.00/0.00/0.00
Target	GTV	Post fossa BF	Post fossa BF	Post fossa BF	Brain PTV	Brain PTV
Beam spreading	Passive	Passive	Passive	Passive	Passive	Passive
Air gap (cm)	2	2	2	2	6	6
Prescribed range (g cm ⁻²)	10.5	10.5	13.5	13.2	17.7	17.9
Raw, w/uncert	10.03/10.48	10.03/10.48	12.88/13.43	12.57/13.11	16.85/17.54	17.01/17.70
Prescribed modulation (g cm ⁻²)	8.8	8.8	11.98	11.98	17.92	17.92
Raw, smr, smr w/uncert	7.38/7.70/8.35	7.38/7.70/8.35	9.87/10.95/11.74	10.33/10.59/ 11.39	15.69/15.91/ 16.90	15.63/16.18/ 17.21
Smearing distance (cm)	0.3	0.3	0.3	0.3	0.3	0.3
Uncertainty parameters	Nominal	Nominal	Nominal	Nominal	Nominal	Nominal
Density (%)	3.5	3.5	3.5	3.5	3.5	3.5
Range (cm)	0.1	0.1	0.1	0.1	0.1	0.1
Dose (cGy MU ⁻¹)	0.994	0.994	0.940	0.929	0.809	0.809

CASE NUMBER B.6: SKULL-BASE CHORDOMA

CASE NUMBER B.6: SKULL-BASE CHORDOMA

General patient information

a. Patient identification

i. Name	Confidential
ii. Age, gender, and race	61 year old Caucasian male
iii. Address	Confidential
iv. Phone no.	Confidential
v. E-mail address	Confidential
vi. Hospital ID no.	Confidential
vii. Person to notify (with contact information) were a problem to arise	Confidential

b. Medical team

i. Radiation oncologist(s)	Confidential
ii. Radiation physicist(s)	Confidential
iii. Referring physician	Confidential

Medical evaluation of presenting lesion

a. Medical history	Six months, binocular oblique double vision on downgaze, drooping of left upper eyelid
b. Physical examination	Left CN III, IV palsies
c. Imaging studies	MRI: 3 cm (maximum dimension) extradural tumor of left lateral clivus
d. Tumor site	Clivus, invading left cavernous sinus, encasing left cavernous carotid artery, displacing left mesial temporal lobe, effacing prepontine cistern, elevating left limb of optic chiasm. Figure B.6.1 is the T2 MRI image of the residual lesion at start of radiation treatment.
e. Diagnosis	Chordoma (pathological study of surgical specimen)
f. Grade	No grade
g. Stage	No staging system
h. Prior therapy	Left pterional craniotomy, trans-sylvian approach, partial tumor removal. No irradiation
i. Family history	Mother: throat cancer

General medical evaluation

a. History, physical examination, and imaging	Impairment of short-term memory since surgery, left CN III palsy, KPS = 90
b. Co-morbidities	Obesity

- c. Current medications None
- d. Prior radiation therapy None

Treatment intent

- a. Curative
- b. No systemic therapy
- c. Predicted outcome at 10 years
 - i. Tumor control probability: 60 percent
 - ii. Blindness: <1 percent
 - iii. Temporal lobe injury (symptomatic): <5 percent
 - iv. Brainstem injury (symptomatic): <5 percent
 - v. Pituitary dysfunction: 100 percent

Treatment planning

- a. General plan: postoperative combined proton and photon radiation therapy
- b. Definition of treatment volumes
 - i. The treatment-planning CT study was performed with the patient in the treatment position and immobilized with a custom-made thermoplastic head mask.
 - ii. CT sections of 2.5 mm were employed in the definition of the GTV, CTV and OARs in the treatment planning system.
 - iii. The GTV was the gross residual tumor as seen on the imaging studies. The CTV was delineated to include possible microscopic tumor extensions (see Fig. B.6.2). PTV was not delineated.
- c. Combined radiation beams.
 - i. 10 MV x-ray beams were to be employed for the initial 2 weeks of treatment and then treatment completed by 230 MeV proton beams.
- d. Dose constraints
 - i. Brainstem $D_{RBE,2\%} = 55.0$ Gy (RBE) at center/67.0 Gy (RBE) at surface
 - ii. Optic chiasm and nerves: $D_{RBE,2\%} = 62$ Gy (RBE)
 - iii. For treatment of skull base sarcoma, no constraints are formally applied for the temporal lobes and the pituitary gland.
- e. Dose calculation
 - i. Three-dimensional proton pencil-beam algorithm based on 2.5 mm CT slices of the whole head
 - ii. Clarkson algorithm for the photon component
 - iii. Dose is stated with an accuracy of 2 percent.
 - iv. Treatment planning used the XIO system

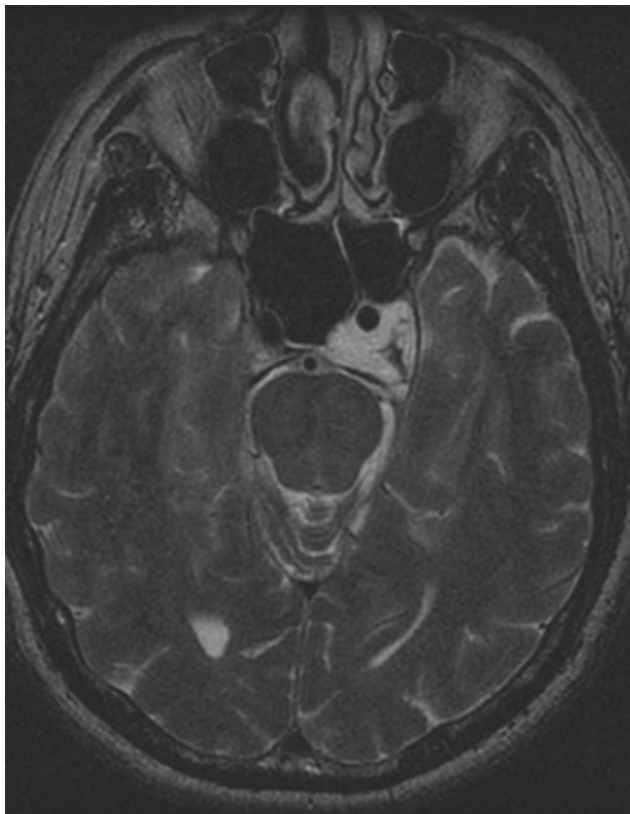


Figure B.6.1. Axial T2 MRI demonstrating the residual chordoma encasing the cavernous carotid artery.

f. $D_{RBE,50\%} = 76$ Gy (RBE) to the GTV at 2 Gy (RBE) per fraction, five fractions per week

dose-volume histograms are shown in Fig. B.6.3.

Treatment technique

- The CTV was irradiated using a combination of photons and protons. The photon component was three fields: right and left lateral and a superior anterior oblique.
- The proton component to the CTV was also three fields: right anterior and left anterior oblique and a posterior.
- The GTV was irradiated using five proton beams, a vertex field and two patched-field combinations: a left superior posterior oblique paired with a right lateral patch and a right inferior oblique paired with a left posterior patch.
- Field range was defined with the distal 99 percent of the SOBP at the distal margin of the CTV and GTV, respectively.
- Field modulation was defined with the proximal 98 percent dose of the SOBP at the proximal margin of the CTV and GTV, respectively.
- Penumbra: 80–20 percent dose gradient was ≈ 5 mm and resulted from use of the double-scattering gantry beam with SAD of 227 cm.
- See Addendum for additional technical details.

Patient immobilization and positioning

- Supine position with a thermoplastic mask
- The positions of the defined bony landmarks (fiducials) relative to the beam were determined by bi-planar radiographs. The patient position was adjusted and the imaging repeated; this continued until the desired target position was achieved.

Treatment prescription

- 10 MV x-ray and 230 MeV proton beams
- Prescribed doses
 - GTV: $D_{RBE,50\%} = 76.0$ Gy (RBE) administered at $d_{RBE,50\%} = 2$ Gy (RBE) per fraction, five fractions per week
 - Anterior surface of brainstem: $D_{RBE,98\%} = 62$ Gy (RBE)
 - RBE = 1.10
- Isodose contours in the axial, coronal, and sagittal planes are shown in Fig. B.6.2 and

Quality assurance

- Individual portal hardware consisted of custom brass apertures and PMMA range compensators. These underwent a thorough QA inspection consisting of measuring various points on the devices using reference points from the computer planning system.
- Individual portals underwent range and modulation measurements as well as dose output verification, which were compared with planned values.

Equipment

- Protons: cyclotron-produced 230 MeV beam
 - Broad-beam energy modulation
 - 360° isocentric gantry
 - Protons degraded to the planned range
- Photons: 10 MV linear accelerator
 - Isocentric setup
- Ports: three-field photon technique, 4 proton ports and 2 proton patch combinations

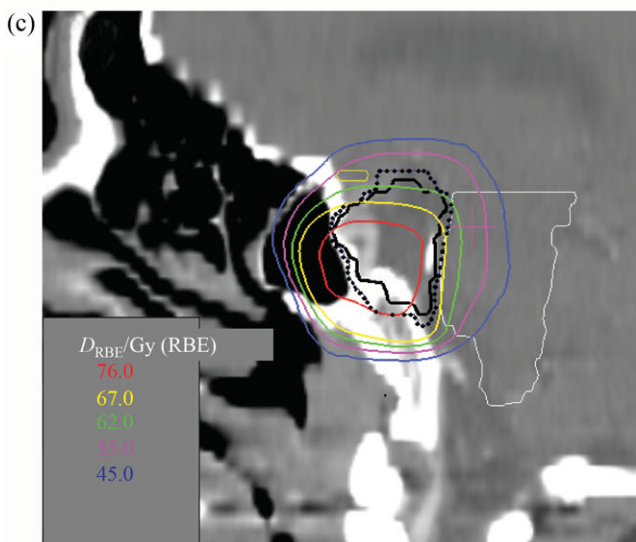
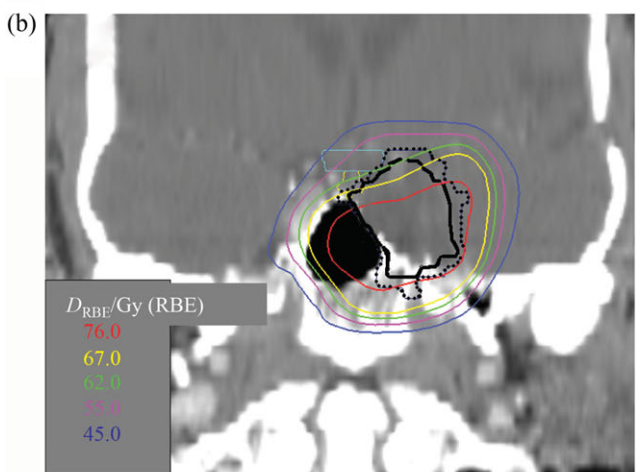
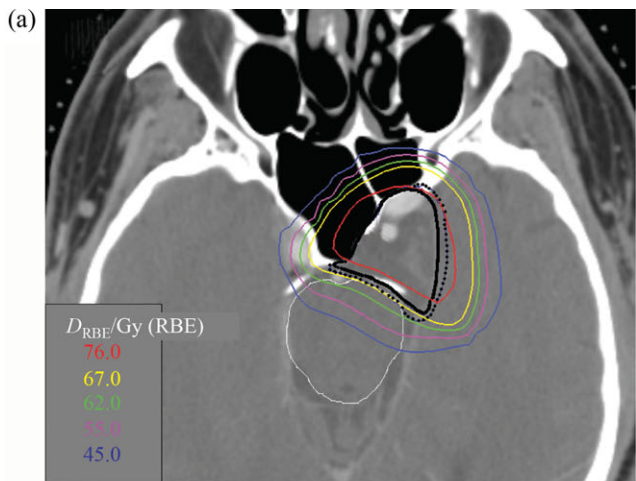


Figure B.6.2. Isodose contours in the axial (a), coronal (b), and sagittal (c) planes. GTV and CTV are represented by solid black and dotted black lines, respectively.

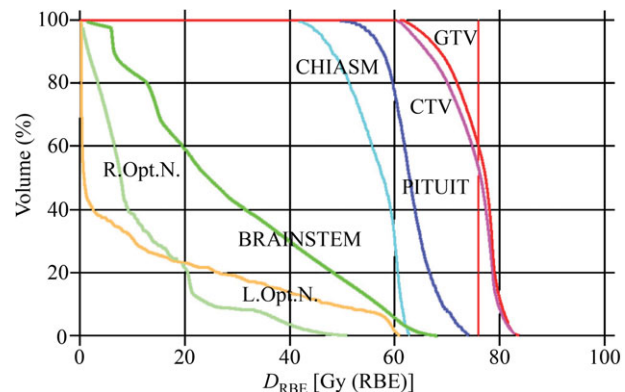


Figure B.6.3. Dose–volume histograms for GTV, CTV, brainstem, chiasm, right and left optic nerve, and pituitary gland.

Total doses delivered

a. Total RBE-weighted absorbed doses, D_{RBE}

Volume/structure	Volume, ml	$D_{RBE,50\%}$, Gy (RBE)	$D_{RBE,98\%}$, Gy (RBE)	$D_{RBE,2\%}$, Gy (RBE)
GTV	9.5	77.3 (20.4)	63.2 (20.2)	82.3 (20.6)
CTV	14.3	76.3 (20.4)	61.8 (20.2)	82.3 (20.6)
Brainstem	32.5	24.7 (13.9)	24.7 (0.6)	62.8 (20.6)
Optic chiasm	0.5	57.8 (20.4)	44.0 (20.4)	62.4 (20.4)
Right optic nerve	1.3	7.8 (0.6)	0.5 (0.2)	42.2 (20.2)
Left optic nerve	1.2	0.7 (0.6)	0.2 (0.2)	59.8 (20.3)
Pituitary	0.5	62.9 (20.4)	53.5 (20.4)	72.8 (20.4)

The numbers in parentheses are the doses administered by photon beams.

i. $D_{RBE,50\%} = 77.3$ Gy (RBE) was delivered to the GTV in 38 fractions, one fraction per day, five fractions per week. The treatment was not interrupted during the 54 days. That the delivered RBE-weighted absorbed dose exceeded the prescribed dose by 1.3 Gy (RBE) was the consequence of the need to employ patch fields.

ii. Dose constraint to the anterior surface of the brainstem was exceeded by <1.5 percent.

b. Total absorbed dose, D

Volume/structure	Volume, ml	$D_{50\%}$, Gy	$D_{98\%}$, Gy	$D_{2\%}$, Gy
GTV	9.5	72.1	59.2	76.7
CTV	14.3	71.2	58.0	76.7
Brainstem	32.5	23.7	22.5	59.0
Optic chiasm	0.5	54.4	41.9	58.6
Right optic nerve	1.3	7.2	–	40.2
Left optic nerve	1.2	–	–	56.2
Pituitary	0.5	62.9	53.5	72.8

Patient status at completion of treatment

- a. No acute reactions
- b. General condition unchanged.
- c. The patient lives some 12 000 miles distant.
In partnership with the referring physician,

follow-up evaluations are to be conducted and appropriate imaging studies undertaken in 6 months, 12 months and annually thereafter.

Addendum: technical information

Quality-assurance checklist

Patient Field	— RA1A	— PA1A	LA1A	SU1A	LS1A	RI1A	LP1A	— RL1A
Action	Verified							
Construction	TR 6/18/2005							
Aperture geometry and thickness	Ok							
Range compensator shape and thicknesses	Ok							
Patient and field identification	Ok							
Calibration and dosimetry	HK 6/18/2005							
Range (g cm^{-2})	13.4	15.7	11.5	14.5	12.7	9.9	15.6	11.0
Modulation (g cm^{-2})	6.7	5.4	5.4	5.4	4.8	3.4	8.3	5.4
Calibration point (beam coordinates)	0,0,0	0,0,0	0,0,0	0,0,0	0,0,0	0,0,0	0,0,0	0,0,0
Fraction RBE-weighted dose [cGy (RBE)]	100	100	100	100	200	200	200	200
RBE factor	1.1	1.1	1.1	1.1	1.1	1.1	1.1	1.1
Fraction absorbed dose (cGy)	90.9	90.9	90.9	90.9	181.8	181.8	181.8	181.8
Isodose normalization (%)	100	100	100	100	100	100	100	100
Output factor (cGy MU^{-1} at STP)	1.053	1.227	1.184	1.181	1.340	1.134	1.064	1.207
Monitor units (MU at STP)	86.3	74.1	76.8	77.0	139.8	160.3	171.0	150.7
Equipment settings	HK 6/18/2005							
Treatment room	Gantry 1							
Range modulator/scattering system ID	A5	A6	A4	A5	A5	A4	A6	A5
Snout position (cm)	16.3	17.5	13.7	15.4	13.7	15.2	16.6	20.4

REFERENCES

- AAPM (1980) American Association of Physicists in Medicine: Task Group 18. *Protocol for Neutron Beam Dosimetry*, AAPM Report No. 7 (American Association of Physicists in Medicine: New York).
- AAPM (1983) American Association of Physicists in Medicine. 'A protocol for the determination of absorbed dose from high-energy photon and electron beams.' *Med. Phys.* **10**, 741–771.
- AAPM (1986) American Association of Physicists in Medicine: Task Group 20. *Protocol for Heavy Charged-Particle Therapy Beam Dosimetry*, AAPM Report No. 16 (American Association of Physicists in Medicine: New York).
- Agosteo, S., Birattari, C., Caravaggio, M., Silari, M. and Tosi, G. (1998) 'Secondary neutron and photon dose in proton therapy.' *Radiother. Oncol.* **48**, 293–305.
- AJCC (2002) American Joint Committee on Cancer. In *Cancer Staging Manual*, 6th edn, Greene, F. L., Page, D. L., Fleming, I. D., Fritz, A. G., Balch, C. M., Haller, D. G. and Morrow, M. Eds. (Springer: New York).
- Almond, P. R. and Smathers, J. B. (1977) 'Physics intercomparisons for neutron radiation therapy.' *Int. J. Radiat. Oncol. Biol. Phys.* **3**, 169–176.
- Amaldi, U., Arduini, G., Cambrai, R., Campi, D., Gerardi, F., Gramatica, R., Leone, R., Manfredi, G., Ninis, M., Petrucci, G., Rossi, S., Sangaletti, L., Silari, M., Tosi, G., Vecchi, L. and Weiss, M. (1994) 'A hospital-based hadrontherapy facility for Italy,' pp. 329–339 in *Hadrontherapy in Oncology*, Amaldi, U. and Larsson, B. Eds (Elsevier Science B.V.: Amsterdam).
- Amerio, S., Boriano, A., Bourhaleb, F., Cirio, R., Donetti, M., Fidanzio, A., Garelli, E., Giordanengo, S., Madon, E., Marchetto, F., Nastasi, U., Peroni, C., Piermattei, A., Sanz Freire, C. J., Sardo, A. and Trevisiol, E. (2004) 'Dosimetric characterization of a large area pixel-segmented ionization chamber.' *Med. Phys.* **31**, 414–420.
- Ando, K., Koike, S., Kawachi, K., Hiraoka, T., Ohara, H., Yokota, M., Inada, T., Hirokawa, Y., Sato, S. and Eguchi, K. (1985) 'Relative biological effectiveness of the therapeutic proton beams at NIRS and Tsukuba University.' *Nippon Igaku Hoshasen Gakkai Zasshi, (Nippon Acta Radiologica)* **45**, 531–535.
- Andreo, P. (1992) 'Absorbed dose beam quality factors for the dosimetry of high-energy photon beams.' *Phys. Med. Biol.* **37**, 2189–2211.
- Andreo, P. (2002) 'Role of the IAEA codes of practice in the radiation dosimetry chain,' pp. 21–33 in *Proc. Int. Symp. on Standards and Codes of Practice in Medical Radiation Dosimetry*. IAEA-CN-96 (International Atomic Energy Agency, Vienna).
- Andreo, P., Nahum, A. and Brahme, A. (1986) 'Chamber-dependent wall correction factors in dosimetry.' *Phys. Med. Biol.* **31**, 1189–1199.
- Archambeau, J. O., Bennett, G. W., Levine, G. S., Cowen, R. and Akanuma, A. (1974) 'Proton radiation therapy.' *Radiology* **110**, 445–457.
- Attix, F. H. (1986) *Introduction to Radiological Physics and Radiation Dosimetry* (John Wiley: New York).
- Austin-Seymour, M., Kalet, I., McDonald, J., Kromhout-Schiros, S., Jacky, J., Hummel, S. and Unger, J. (1995) 'Three dimensional planning target volumes: A model and a software tool.' *Int. J. Radiat. Oncol. Biol. Phys.*, **33**, 1073–1080.
- Bacher, R., Blattmann, H., Boehringer, T., Coray, A., Egger, E., Pedroni, E., Phillips, M. and Scheib, S. (1989) 'Development and first results of discrete dynamic spot scanning with protons,' pp. 9–12 in *Proc. Int. Heavy Particle Therapy Workshop (PTCOG/EORTC/ECNEU)*, PSI Report No. 69 (Paul Scherrer Institute, Villigen, Switzerland).
- Balter, J. M., Ten Haken, R. K. and Lamm, K. L. (1996) 'Treatment setup verification,' pp. 471–493 in *Teletherapy: Present and Future*, Mackie, T. R. and Palta, J. R. Eds. (Advanced Medical Publishing: Madison, WI).
- Bartolotta, A., Indovina, P. L., Onori, S. and Rosati, A. (1984) 'Dosimetry for Cobalt-60 gamma rays with alanine.' *Radiat. Prot. Dosim.* **9**, 277–281.
- Bartolotta, A., Onori, S. and Pantaloni, M. (1990) 'Alanine EPR dosimetry as a traveling dosimetric system for intercomparison purposes.' *Radiat. Phys. Chem.* **35**, 708–712.
- Bartolotta, A., Fattibene, P., Onori, S., Pantaloni, M. and Petetti, E. (1993) 'Sources of uncertainty in therapy level alanine dosimetry.' *Appl. Radiat. Isot.* **44**, 13–17.
- Baumert, B. G., Lomax, A. J., Miltchev, V. and Davis, J. B. (2001) 'A comparison of dose distributions of proton and photon beams in stereotactic conformal radiotherapy of brain lesions.' *Int. J. Radiat. Oncol. Biol. Phys.* **29**, 1439–1449.
- Baumert, B. G., Norton, I. A., Lomax, A. J. and Davis, J. B. (2004) 'Dose conformation of intensity-modulated stereotactic photon beams, proton beams, and intensity-modulated proton beams for intracranial lesions.' *Int. J. Radiat. Oncol. Biol. Phys.* **60**, 1314–1324.

- Beckham, W. A., Keall, P. J. and Siebers, J. V. (2002) 'A fluence-convolution method to calculate radiation therapy dose distributions that incorporate random set-up error.' *Phys. Med. Biol.* **47**, 3465–3473.
- Beeckman, W., Jongen, Y., Laisne, A. and Lannoye, G. (1991) 'Preliminary design of a reduced-cost proton therapy facility using a compact high field isochronous cyclotron.' *Nucl. Instrum. Methods Phys. Res. B* **56/57**, 1201–1204.
- Belli, M., Cera, F., Cherubini, R., Haque, A. M. I., Ianzini, F., Moschini, G., Sapora, O., Simone, G., Tabocchini, M. A. and Tivero, P. (1993) 'Inactivation and mutation induction in V79 cells by low energy protons: re-evaluation of the results at the LNL facility.' *Int. J. Radiat. Biol.* **63**, 331–337.
- Bettega, D., Calzolari, P., Chauvel, P., Courdi, A., Herault, J., Iborra, N., Marchesini, R., Massariello, P., Poli, G. L. and Tallone, L. (2000) 'Radiobiological studies on the 65 MeV therapeutic proton beam at Nice using human tumour cells.' *Int. J. Radiat. Biol.* **76**, 1297–1303.
- Bichsel, H. (1995) 'Calculated Bragg curves for ionization chambers of different shapes.' *Med. Phys.* **22**, 1721–1726.
- Bilski, P., Budzanowski, M., Hoffmann, W., Molokanov, A., Olko, P. and Waligórski, M. P. R. (1997) 'Investigation of efficiency of thermoluminescence detectors for particle therapy beams.' *Radiat. Prot. Dosim.* **70**, 501–504.
- Binns, P. J. and Hough, J. H. (1997) 'Secondary dose exposures during 200 MeV proton therapy.' *Radiat. Prot. Dosim.* **70**, 441–444.
- Binns, P. J., Hough, J. H., Jones, D. T. L. and Schreuder, A. N. (1993) 'Microdose Spectra for Protons of Different LET.' In *NAC Annual Report, NAC/AR/93–01* (National Accelerator Centre: Faure, South Africa 88).
- BIPM (1981) Bureau International des Poids et Mesures. *Recommendation R(I)-1, page R(I) 15 in BIPM Com. Cons. Étalons Mes. Ray. Ionisants* (Section I) 6, (Offilib, Paris, France).
- BIPM (2006) Bureau International des Poids et Mesures. *The International System of Units (SI)*, 8th edn. (BIPM, Pavillon de Breteuil, Sèvres Cedex, France).
- Björk, P., Knöös, T. and Nilsson, P. (2000) 'Comparative dosimetry of diode and diamond detectors in electron beams for intraoperative radiation therapy.' *Med. Phys.* **27**, 2580–2588.
- Blomquist, E., Russell, K. R., Stenerlöw, B., Montelius, A., Grusell, E. and Carlsson, J. (1993) 'Relative biological effectiveness of intermediate energy protons. Comparisons with ^{60}Co gamma-radiation using two cell lines.' *Radiother. Oncol.* **28**, 44–51.
- Blosser, H., Johnson, D., Lawton, D., Ronningen, R., Burleigh, R. and Gottschalk, B. (1991) *Preliminary Design Study Exploring Building Features Required for a Proton Therapy Facility for Ontario Cancer Institute*, Report MSUCL 76a (National Superconducting Cyclotron Laboratory, Michigan State University, East Lansing, MI).
- Blosser, H. G., Gelbke, G. K., Lawton, D., Marti, F., Vincent, J., York, R. C. and Zeller, A. (1993) *Proposal to Construct a 250 MeV Superconducting Isochronous Cyclotron to Serve as an Advanced Cancer Treatment Facility and as a Manufacturing Prototype for Commercial Productions of such Cyclotrons*, Report MSUCL-874 (National Superconducting Cyclotron Laboratory, Michigan State University, East Lansing, MI).
- Boag, J. W. (1966) 'Ionization Chambers,' pp. 1–72 in *Radiation Dosimetry*, Vol. II, Attix, F. H. and Roesch, W. C. Eds. (Academic Press: New York).
- Boag, J. W. and Wilson, T. (1952) 'The saturation curve at high ionization intensity.' *Br. J. Appl. Phys.* **3**, 222–229.
- Bolsi, A., Fogliata, A. and Cozzi, L. (2003) 'Radiotherapy of small intracranial tumours with different advanced techniques using photon and proton beams: a treatment planning study.' *Radiother. Oncol.* **68**, 1–14.
- Bonnett, D. E. (1993) 'Current developments in proton therapy: A review.' *Phys. Med. Biol.* **38**, 1371–1392.
- Boon, S. N. (1998) *Dosimetry and quality control of scanning proton beams*. Doctoral Thesis, Mathematics and Natural Sciences (Rijksuniveriteit Groningen, The Netherlands).
- Boon, S. N., van Luijk, P., Schippers, J. M., Meertens, H., Denis, J. M., Vynckier, S., Medin, J. and Grusell, E. (1998) 'Fast 2D phantom dosimetry for scanning proton beams.' *Med. Phys.* **25**, 464–475.
- Boon, S. N., van Luijk, P., Böhringer, T., Coray, A., Lomax, A., Pedroni, E., Schaffner, B. and Schippers, J. M. (2000) 'Performance of a fluorescent screen and CCD camera as a two-dimensional dosimetry system for dynamic treatment techniques.' *Med. Phys.* **27**, 2198–2208.
- Bortfeld, T. (2003) 'Physical optimization.' In *Intensity-Modulated Radiation Therapy: The State of the Art*, Palta, J. R. and Mackie, T. R. Eds. (Medical Physics Publishing: Madison, WI).
- Bortfeld, T., Jokivarsi, K., Goitein, M., Kung, J. and Jiang, S. B. (2002) 'Effects of intra-fraction motion on IMRT dose delivery: Statistical analysis and simulation.' *Phys. Med. Biol.* **47**, 2203–2220.
- Bortfeld, T., Trofimov, A., Shipley, W. U., Chan, W. F. A., Adams, J., DeLaney, T. F., Kooy, H., Küfer, K.-H. and Monz, M. (2004) 'Advances in comparative proton therapy treatment planning at NPTC in Boston.' *Proc. ESTRO* **23**, S122.
- Boutillon, M. (1987) *Values of g for photon energies*. CCEMRI, Offilib Report (I) 85–18 (Comité Consultatif pour les Étalons de Mesures des Rayonnements Ionisants, Offilib, Paris, France).
- Boutillon, M. (1989) 'Gap correction for the calorimetric measurement of absorbed dose in graphite with a ^{60}Co beam.' *Phys. Med. Biol.* **34**, 1809–1821.
- Boutillon, M. and Perroche-Roux, A. M. (1987) 'Re-evaluation of the W value for electrons in dry air.' *Phys. Med. Biol.* **32**, 213–219.
- Boyd, T. J., Crandall, K. R., Hamm, R. W., Hansborough, L. D., Hoeberling, R. F., Jameson, R. A., Knapp, E. A., Mueller, D. W., Potter, J. M., Stokes, R. H., Stovall,

REFERENCES

- J. E. Sturgess, R. G., Swenson, D. A., Tallerico, P. J., Wangler, T. P. and Wilkerson, L. C. (1982) 'The PIGMI linear accelerator technology,' pp. 3–22 in *Pion and Heavy Ion Radiotherapy: Pre-Clinical and Clinical Studies*, Skarsgard, L. D. Ed. (Elsevier Science Publishing Co., Inc.: New York).
- Bradshaw, W. W., Cadena, D. G., Jr., Crawford, G. W. and Spetzler, H. A.W. (1962) 'The use of alanine as a solid dosimeter.' *Radiat. Res.* **17**, 11–21.
- Brahme, A. (1984) 'Dosimetric precision requirements in radiation therapy.' *Acta Radiol. Oncol.* **23**, 379–391.
- Brahme, A., Källman, P. and Lind, B. K. (1989) 'Optimization of proton and heavy ion therapy using an adaptive inversion algorithm.' *Radiother. Oncol.* **15**, 189–197.
- Brede, H. J., Hecker, O. and Selbach, H. J. (1994) 'Measurement principles and experimental setup for determining the heat defect of water for high-energy protons, deuterons and alpha particles.' In *Proc. NPL Calorimetry Workshop* (National Physical Laboratory, Teddington, UK).
- Brede, H. J., Hecker, O. and Hollnagel, R. (1997) 'Measurement of the heat defect in water and A-150 plastic for high-energy protons, deuterons, and alpha particles.' *Radiat. Prot. Dosim.* **70**, 505–508.
- Brede, H. J., Heinemann, E., Binns, P. J., Langen, K. M., Jones, D. T. L. and Schreuder, A. N. (1999) 'Water calorimetry and ionization chamber dosimetry in the proton therapy beam,' pp. 123–124 in *National Accelerator Annual Report, March 1999* (National Accelerator Centre, Faure, South Africa).
- Brede, H. J., Hecker, O. and Hollnagel, R. (2000) 'An absorbed dose to water calorimeter for collimated radiation fields.' *Nucl. Instrum. Methods Phys. Res.* **A455**, 721–732.
- Brede, H. J., Greif, K-D., Hecker, O., Heeg, P., Heese, J., Jones, D. T. L., Kluge, H. and Schardt, D. (2006) 'Absorbed dose to water determination with ionization chamber dosimetry and calorimetry in restricted neutron, photon, proton and heavy-ion radiation fields.' *Phys. Med. Biol.* **51**, 3667–3682.
- Breuer, H. and Smit, B. J. (2000) *Proton Therapy and Radiosurgery* (Springer-Verlag: Berlin).
- Broerse, J. J., Coppola, M. and Burger, G. (1978) *A European Neutron Dosimetry Intercomparison Project (ENDIP): Results and Evaluation*. EUR 6004 EN (Commission of the European Communities: Luxembourg).
- Broerse, J. J., Mijnheer, B. J., Eenma, J. and Wootton, P. (1979) 'Dosimetry intercomparisons and protocols for therapeutic applications of fast neutron beams,' in pp. 117–123 *High LET Radiations in Clinical Radiotherapy*, Barendsen, G. W., Broerse, J. J. and Breur, K. Eds. (Pergamon Press: Oxford).
- Broerse, J. J., Mijnheer, B. J. and Williams, J. R. (1981) 'European protocol for neutron dosimetry for external beam therapy. European Neutron Dosimetry Group (ECNEU).' *Br. J. Radiol.* **54**, 882–898.
- Brusasco, C., Cattai, A., Cirio, R., Dellacasa, G., Donetti, M., Isoardi, P., Marchetto, F., Peroni, C., Rolando, V., Ruspa, M., Solano, A. and Zambernardi, C. (1997) 'Strip ionization chambers as 3-D detector for hadron therapy.' *Nucl. Instrum. Methods Phys. Res.* **A389**, 499–512.
- Brusasco, C., Voss, B., Schardt, D., Krämer, M. and Kraft, G. (2000) 'A dosimetry system for fast measurement of 3D depth-dose profiles in charged-particle tumor therapy with scanning techniques.' *Nucl. Instrum. Methods Phys. Res.* **B168**, 578–592.
- Bucciolini, M., Cuttome, G., Egger, E., Guasti, A., Mazzocchi, S., Raffaele, L. and Sabini, M. G. (1999) 'A comparison of the TLD-100 response to ^{60}Co beam and 62 MeV protons.' *Phys. Med.* **XV**, 71–77.
- Bucciolini, M., Cuttome, G., Guasti, A., Lo Nigro, S., Mazzocchi, S., Raffaele, L., Sabini, M. G., Kacperek, A. and Egger, E. (2000) 'Check on the use of thermoluminescence detectors for proton dose distribution measurements.' *Phys. Med.* **XVI**, 117–120.
- Bucciolini, M., Banci Buonamici, F., Mazzocchi, S., De Angelis, C., Onori, S. and Cirrone, G. A. P. (2003) 'Diamond detector versus silicon diode and ion chamber in photon beams of different energy and field size.' *Med. Phys.* **30**, 2149–2154.
- Bush, D. A., Slater, J. D., Shin, B. B., Cheek, G., Miller, D. W. and Slater, J. M. (2004a) 'Hypofractionated proton beam radiotherapy for stage I lung cancer.' *Chest* **126**, 1198–1203.
- Bush, D. A., Hillebrand, D. J., Slater, J. M. and Slater, J. D. (2004b) 'High-dose proton beam radiotherapy of hepatocellular carcinoma: preliminary results of a phase II trial.' *Gastroenterol.* **127** (Suppl. 1), S189–S193.
- Butson, M. J., Cheung, T. and Yu, P. K. N. (2001) 'Radiochromic film dosimetry in water phantoms.' *Phys. Med. Biol.* **46**, N27–N31.
- Cambria, R., Héault, J., Brassart, N., Silari, M. and Chauvel, P. (1997) 'Proton beam dosimetry: A comparison between the Faraday cup and an ionization chamber.' *Phys. Med. Biol.* **42**, 1185–1196.
- Carlsson, C. A. and Carlsson, G. A. (1970) 'Proton dosimetry: measurement of depth doses from 185-MeV protons by means of thermoluminescent LiF.' *Radiat. Res.* **42**, 207–219.
- Case, J. A., von Goeler, F., Rabin, M. S. Z. and Wagner, M. (1994) 'Effects of detector geometry and sensitivity on the shape of the Bragg peak.' *Proton Therapy Co-Operative Group Meeting, Cambridge, MA*.
- Castro, J. R., Quivey, J. M., Lyman, J. T., Chen, G. T. Y., Phillips, T. L., Tobias, C. A. and Alpen, E. L. (1980) 'Current status of clinical particle radiotherapy at Lawrence Berkeley Laboratory.' *Cancer* **46**, 633–641.
- Caumes, J., Ostrowski, A., Steinschaden, K., Mancaux, M., Cance, M., Simeon, J. P., Sabattier, R. and Breteau, N. (1984) 'Direct calibration of ionization chambers with a TE calorimeter at the Orleans cyclotron neutron facility.' *Strahlenther.* **160**, 127–128.
- CCEMRI (1977) Comité Consultatif pour les Étalons de Mesures des Rayonnements Ionisants (Section I). *Correction d'Humidité*. CCEMRI R(I)-30 (Bureau International des Poids et Mesures, Sèvres, France).
- CCEMRI (1985) Comité Consultatif pour les Étalons de Mesures des Rayonnements Ionisants (Section I).

- Effect of a change of stopping-power values on the W values recommended by ICRU for electrons in dry air.* CCEMRI (I)/85-8 (Bureau International des Poids et Mesures, Sèvres, France).
- Cella, L., Lomax, A. and Miralbell, R. (2001) 'Potential role of intensity modulated proton beams in prostate cancer radiotherapy.' *Int. J. Radiat. Oncol. Biol. Phys.* **49**, 217-223.
- Censor, Y. (2003) 'Mathematical optimization for the inverse problem of intensity-modulated radiation therapy.' In *Intensity Modulated Radiation Therapy: The State of the Art*, Palta, J. R. and Mackie, T. R. Eds. (Medical Physics Publishing: Madison, WI).
- Chadwick, M. B., Jones, D. T. L., Arendse, G. J., Cowley, A. A., Richter, W. A., Lawrie, J. J., Newman, R. T., Pilcher, J. V., Smit, F. D., Steyn, G. F., Koen, J. W. and Stander, J. A. (1999) 'Nuclear interaction cross sections for proton radiotherapy.' *Nucl. Phys.* **A654**, 1051c-1057c.
- Chandna, S., Dwarakanath, B. S., Khaitan, D., Lazar Mathew, T. and Jain, V. (2002) 'Low-dose radiation hypersensitivity in human tumor cell lines: Effects of cell-cell contact and nutritional deprivation.' *Radiat. Res.* **157**, 516-525.
- Chapman, P. H., Ogilvy, C. S. and Butler, W. E. (1993) 'A new stereotactic alignment system for charged particle radiosurgery at the Harvard Cyclotron Laboratory, Boston,' pp. 105-108 in *Stereotactic Radiosurgery*, Alexander, E., III, Loeffler, J. S. and Lunsford, L. D. Eds. (McGraw-Hill: New York).
- Char, D. H., Quivey, J. M., Castro, J. R., Kroll, S. and Phillips, T. (1993) 'Helium ions versus iodine 125 brachytherapy in the management of uveal melanoma. A prospective, randomized, dynamically balanced trial.' *Ophthalmology* **100**, 1547-1554.
- Charpak, G. (1970) 'Evolution of the automatic spark chambers.' *Ann. Rev. Nucl. Sci.* **20**, 195-254.
- Chauvenet, B., Baltès, D. and Delaunay, F. (1997) 'Comparison of graphite-to-water absorbed-dose transfers for ^{60}Co photon beams using ionometry and Fricke dosimetry.' *Phys. Med. Biol.* **42**, 2053-2063.
- Chen, G. T. (1988) 'Dose volume histograms in treatment planning.' *Int. J. Radiat. Oncol. Biol. Phys.* **14**, 1319-1320.
- Chen, G. T., Singh, R. P., Castro, J. R., Lyman, J. T. and Quivey, J. M. (1979) 'Treatment planning for heavy ion radiotherapy.' *Int. J. Radiat. Oncol. Biol. Phys.* **5**, 1809-1819.
- Chen, G. T. Y., Kung, J. H. and Beaudette, K. P. (2004) 'Artifacts in computed tomography scanning of moving objects.' *Semin. Radiat. Oncol.*, **14**, 19-26.
- Cheung, T., Butson, M. J. and Yu, P. K. N. (2005) 'Post-irradiation colouration of GafChromic EBT radiochromic film.' *Phys. Med. Biol.* **50**, N281-N285.
- Chiba, T., Tokuyue, K., Matsuzaki, Y., Sugahara, S., Chuganji, Y., Kagei, K., Shoda, J., Hata, M., Abei, M., Igaki, H., Tanaka, N. and Akine, Y. (2005) 'Proton beam therapy for hepatocellular carcinoma: A retrospective review of 162 patients.' *Clin. Cancer Res.* **11**, 3799-3805.
- Chu, W. T. (1995a) 'Ion beams for cancer treatment - a perspective.' *Nucl. Instrum. Methods Phys. Res.* **B99**, 835-838.
- Chu, W. T. (1995b) 'Radiation detectors', pp. 234-245 in *Ion Beams in Tumor Therapy*, Linz, U. Ed. (Chapman and Hall: Weinheim, Germany).
- Chu, W., McEvoy, M., Nyman, M., Renner, T., Gonzales, B., Singh, R. P. and Stradner, R. (1985) 'Wobbler dosimetry for the biomedical program at the LBL BEVALAC.' *IEEE Trans. Nucl. Sci.* **NS-32**, 3324-3326.
- Chu, W. T., Renner, T. R. and Ludewigt, B. A. (1989) 'Dynamic beam delivery for three-dimensional conformal therapy,' pp. 295-328 in *EULIMA Workshop on the Potential Value of Light Ion Beam Therapy*, Nice, France, Chauvel, P. and Wambersie, A. Eds. EUR 12165 EN (Commission of the European Communities: Luxembourg).
- Chu, W. T., Ludewigt, B. A. and Renner, T. R. (1993) 'Instrumentation for treatment of cancer using proton and light-ion beams.' *Rev. Sci. Instrum.* **64**, 2055-2122.
- Ciesielski, B. and Wielopolski, L. (1994) 'The effects of dose and radiation quality on the shape and power saturation of the EPR signal in alanine.' *Radiat. Res.* **140**, 105-111.
- Cirio, R., Garelli, E., Schulte, R., Amerio, S., Boriano, A., Bourhaleb, F., Coutrakon, G., Donetti, M., Giordanengo, S., Koss, P., Madon, E., Marchetto, F., Nastasi, U., Peroni, C., Santuari, D., Sardo, A., Scielzo, G., Stasi, M. and Trevisiol, E. (2004) 'Two-dimensional and quasi-three-dimensional dosimetry of hadron and photon beams with the Magic Cube and the Pixel Ionization Chamber.' *Phys. Med. Biol.* **49**, 3713-3724.
- Cole, F., Livdahl, P. V., Mills, F. and Teng, L. (1987) 'Design and application of a proton therapy accelerator,' pp. 1985-1987 in *Proc. 1987 IEEE Particle Accelerator Conference*, Lindstrom, E. R. and Taylor, L. S. Eds. (IEEE Press, Piscataway, NJ).
- Constable, I. J., Goitein, M., Koehler, A. M. and Schmidt, R. A. (1976) 'Small-field irradiation of monkey eyes with protons and photons.' *Radiat. Res.* **65**, 304-314.
- Constantinou, C., Harrington, J. C. and DeWerd, L. A. (1992) 'An electron density calibration phantom for CT-based treatment planning computers.' *Med. Phys.*, **19**, 325-327.
- Coray, A., Pedroni, E., Boehringer, T., Lin, S., Lomax, A. and Goitein, G. (2002) 'Dosimetry with the scanned proton beam on the Paul Scherrer Institute gantry,' pp. 295-302 in *Proc. Int. Symp. on Standards and Codes of Practice in Medical Radiation Dosimetry*. IAEA-CN-96 (International Atomic Energy Agency, Vienna.).
- Courant, E. D., Livingston, M. S. and Snyder, H. S. (1952) 'The strong-focusing synchrotron-a new high energy accelerator.' *Phys. Rev.* **88**, 1190-1196.
- Courdi, A., Brassart, N., Herault, J. and Chauvel, P. (1994) 'The depth-dependent radiation response of human melanoma cells exposed to 65 MeV protons.' *Br. J. Radiol.* **67**, 800-804.

REFERENCES

- Coutrakon, G., Miller, D., Wong, J., Gere, L. and Binns, R. (1990) 'Characterization of the Loma Linda proton beam using a plastic scintillator and CCD camera readout.' *Med. Phys.* **17**, 543 (Abstract).
- Coutrakon, G., Miller, D., Kross, B. J., Anderson, D. F., DeLuca, P. M. Jr. and Siebers, J. (1991a) 'A beam intensity monitor for the Loma Linda cancer therapy proton accelerator.' *Med. Phys.* **18**, 817–820.
- Coutrakon, G., Bauman, M., Lesyna, D., Miller, D., Nusbaum, J., Slater, J., Johanning, J., Miranda, J., DeLuca, P. M. Jr., Siebers, J. and Ludewigt, B. (1991b) 'A prototype beam delivery system for the proton medical accelerator at Loma Linda.' *Med. Phys.* **18**, 1093–1099.
- Coutrakon, G., Hubbard, J., Johanning, J., Maudsley, G., Slaton, T. and Morton, P. (1994) 'A performance study of the Loma Linda proton medical accelerator.' *Med. Phys.* **21**, 1691–1701.
- Coutrakon, G., Cortese, J., Ghebremedhin, A., Hubbard, J., Johanning, J., Koss, P., Maudsley, G., Slater, C. R. and Zuccarelli, C. (1997) 'Microdosimetry spectra of the Loma Linda proton beam and relative biological effectiveness comparisons.' *Med. Phys.* **24**, 1499–1506.
- Cox, R., Thacker, J., Goodhead, D. T. and Munson, R. J. (1977) 'Mutation and inactivation of mammalian cells by various ionising radiations.' *Nature* **267**, 425–427.
- Crook, J. M., Raymond, Y., Salhani, D., Yang, H. and Esche, B. (1995) 'Prostate motion during standard radiotherapy as assessed by fiducial markers.' *Radiother. Oncol.* **37**, 35–42.
- Cumming, J. B. (1963) 'Monitor reactions for high energy proton beams.' *Ann. Rev. Nucl. Sci.* **13**, 261–286.
- Cuttone, G., Raffaele, L., Barone Tonghi, L., Rovelli, A., Sabini, M. G., Egger, E., Kacperek, A., Brai, M., Bartolotta, A., Teri, G., Onori, S. and Fattibene, P. (1999) 'First dosimetry intercomparison results for the CATANA Project.' *Phys. Med.* **19**, 121–130.
- Daftari, I., Castenadas, C., Petti, P. L., Singh, R. P. and Verhey, L. J. (1999) 'An application of GafChromic MD-55 film for 67.5 MeV clinical proton beam dosimetry.' *Phys. Med. Biol.* **44**, 2735–2745.
- Dantzig, G. B. (1963) *Linear Programming and Extensions* (Princeton University Press, Princeton, NJ).
- Daures, J., Chauvenet, B. and Ostrowski, A. (1994) 'State-of the-art of calorimetry at LPRI.' In *Proc. NPL Calorimetry Workshop* (National Physical Laboratory, Teddington, UK).
- De Angelis, C., Onori, S., Pacilio, M., Cirrone, G. A. P., Cuttone, G., Raffaele, L., Bucciolini, M. and Mazzocchi, S. (2002) 'An investigation of the operating characteristics of two PTW diamond detectors in photon and electron beams.' *Med. Phys.* **29**, 248–254.
- Debus, J., Schulz-Ertner, D., Schad, L., Essig, M., Rhein, B., Thillmann, C. O. and Wannenmacher, M. (2000) 'Stereotactic fractionated radiotherapy for chordomas and chondrosarcomas of the skull base.' *Int. J. Radiat. Oncol. Biol. Phys.*, **47**, 591–596.
- de Kock, E. A. (2002) 'The robot-based patient positioning system for high precision radiotherapy at iThemba LABS.' In *Particles 32, Abstracts of the 37th Proton Therapy Co-Operative Group Meeting, Cape Town, South Africa*.
- Deasy, J. O., Chao, K. S. C. and Markman, J. (2001) 'Uncertainties in model-based outcome predictions for treatment planning.' *Int. J. Radiat. Oncol. Biol. Phys.* **51**, 1389–1399.
- Delacroix, S., Bridier, A., Mazal, A., Daures, J., Ostrowsky, A., Nauraye, C., Kacperek, A., Vynckier, S., Brassard, N. and Habrand, J. L. (1997) 'Proton dosimetry comparison involving ionometry and calorimetry.' *Int. J. Radiat. Oncol. Biol. Phys.* **37**, 711–718.
- Dendale, R., Lumbroso-Le Rouic, L., Noel, G., Feuvret, L., Levy, C., Delacroix, S., Meyer, A., Nauraye, C., Mazal, A., Mammar, H., Garcia, P., D'Hermies, F., Frau, E., Plancher, C., Asselain, B., Schlienger, P., Mazeran, J. J. and Desjardins, L. (2006) 'Proton beam radiotherapy for uveal melanoma: Results of Curie Institut-Orsay Proton Therapy Center (ICPO).' *Int. J. Radiat. Oncol. Biol. Phys.* **65**, 780–787.
- Dieckmann, K., Georg, D., Bogner, J., Zehetmayer, M., Petersch, B., Chorvat, M., Weitmann, H. and Potter, R. (2006) 'Optimizing linac-based stereotactic radiotherapy of uveal melanomas: 7 years clinical experience.' *Int. J. Radiat. Oncol. Biol. Phys.* **66**, S47–S52.
- Dobler, B. and Bendl, R. (2002) 'Precise modelling of the eye for proton therapy of intra-ocular tumours.' *Phys. Med. Biol.* **47**, 593–613.
- Domen, S. R. (1980) 'Absorbed dose water calorimeter.' *Med. Phys.* **7**, 157–159.
- Domen, S. R. (1987) 'Advances in calorimetry for radiation dosimetry,' pp. 245–320 in *The Dosimetry of Ionizing Radiation, Vol. II*, Kase, K. R., Bjarnegard, B. E. and Attix, F. H. Eds. (Academic Press: Orlando, FL).
- Domen, S. R. (1994) 'A sealed water calorimeter for measuring absorbed dose.' *J. Res. Natl. Inst. Stand. Technol.* **99**, 121–141.
- Domen, S. R. and Lamperti, P. J. (1974) 'A heat-loss compensated calorimeter: Theory, design, and performance.' *J. Res. Natl. Bur. Stand.* **78A**, 595–610.
- Drzymala, R. E., Mohan, R., Brewster, L., Chu, J., Goitein, M., Harms, W. and Uriel, M. (1991) 'Dose-volume histograms.' *Int. J. Radiat. Oncol. Biol. Phys.* **21**, 71–78.
- Dudley, R. A. (1966) 'Dosimetry with photographic emulsions,' pp. 325–387. in *Radiation Dosimetry, Vol. II*, Attix, F. H. and Roesch, W. C. Eds. (Academic Press: New York).
- DuSautoy, A. R. (1996) 'The UK primary standard calorimeter for photon-beam absorbed dose measurement.' *Phys. Med. Biol.* **41**, pp. 137–151.
- Ebert, P. J., Hardy, K. A. and Cadena, J. D. G. (1965) 'Energy dependence of free radical production in alanine.' *Radiat. Res.* **26**, 178–197.
- Egger, E., Schalenbourg, A., Zografas, L., Bercher, L., Boehringer, T., Chamot, L. and Goitein, G. (2001) 'Maximizing local tumor control and survival after proton beam radiotherapy of uveal melanoma.' *Int. J. Radiat. Oncol. Biol. Phys.* **51**, 138–147.

- Enghardt, W., Debus, J., Haberer, T., Hasch, B. G., Hinz, R., Jäkel, O., Krämer, M., Lauckner, K., Pawelke, J. and Pönisch, F. (1999) 'Positron emission tomography for quality assurance of cancer therapy with light ion beams.' *Nucl. Phys.* **A654**, 1047c–1050c.
- Enghardt, W., Crespo, P., Fiedler, F., Hinz, R., Parodi, K., Pawelke, J. and Pönisch, F. (2004) 'Charged hadron tumour therapy monitoring by means of PET.' *Nucl. Instrum. Methods Phys. Res.* **A525**, 284–288.
- Falkmer, S., Fors, B., Larsson, B., Lindell, A., Naeslund, J. and Stenson, S. (1962) 'Pilot study on proton irradiation of human carcinoma.' *Acta Radiol.* **58**, 33–51.
- Fattibene, P., Calicchia, A., d'Errico, F., De Angelis, C., Egger, E. and Onori, S. (1996) 'Preliminary assessment of LiF and alanine detectors for the dosimetry of proton therapy beams.' *Radiat. Prot. Dosim.* **66**, 305–309.
- Fidanzio, A., Azario, L., De Angelis, C., Pacilio, M., Onori, S. and Piermattei, A. (2002) 'Radiochromic film dosimetry for a 62 MeV clinical proton beam.' *Phys. Med.* **XV11**, 15–23.
- Field, S. B. (1977) 'Early and late normal tissue damage after fast neutrons.' *Int. J. Radiat. Oncol. Biol. Phys.* **3**, 203–210.
- Fitzek, M. M., Thornton, A. F., Rabinov, J. D., Lev, M. H., Pardo, F. S., Munzenrider, J. E., Okunieff, P., Bussiere, M., Braun, I., Hochberg, F. H., Hedley-Whyte, E. T., Liebsch, N. J. and Harsh, G. R. (1999) 'Accelerated fractionated proton/photon irradiation to 90 cobalt gray equivalent for glioblastoma multiforme: results of a phase II prospective trial.' *J. Neurosurg.* **91**, 251–260.
- Fleming, D. M. and Glass, W. A. (1969) 'Endothermic processes in tissue-equivalent plastic.' *Radiat. Res.* **37**, 316–322.
- Fogliata, A., Bolsi, A. and Cozzi, L. (2002) 'Critical appraisal of treatment techniques based on conventional photon beams, intensity modulated photon beams and proton beams for therapy of intact breast.' *Radiother. Oncol.* **62**, 137–145.
- Fong, P. M., Keil, D. C., Does, M. D. and Gore, J. C. (2001) 'Polymer gels for magnetic resonance imaging of radiation dose distributions at normal room atmosphere.' *Phys. Med. Biol.* **46**, 3105–3113.
- Fontenot, J. D., Newhauser, W. D. and Titt, U. (2005) 'Design tools for proton therapy nozzles based on the double-scattering foil technique.' *Radiat. Prot. Dosim.* **116**, 211–215.
- Ford, E. C., Mageras, G. S., Yorke, E. and Ling, C. C. (2003) 'Respiration-correlated spiral CT: A method of measuring respiratory-induced anatomic motion for radiation treatment planning.' *Med. Phys.* **30**, 88–97.
- Fowler, J. F. (1981) *Nuclear Particles in Cancer Treatment* (Adam Hilger Ltd.: Bristol, UK).
- Fraass, B., Doppke, K., Hunt, M., Kutcher, G., Starkschall, G., Stern, R. and Van Dyke, J. (1998) 'American Association of Physicists in Medicine Radiation Therapy Committee, Task Group 53: Quality assurance for clinical radiotherapy treatment planning.' *Med. Phys.* **25**, 1773–1829.
- Fukumoto, S., Endo, K., Muto, K., Akisada, M., Kitagawa, T., Inada, T., Tsujii, H., Maruhashi, A., Hayakawa, Y., Takada, Y. and Tada, J. (1989) 'Tsukuba Medical Proton Synchrotron,' p. 70 in *Heavy Particle Therapy Workshop (PTCOG, EORTC, ECNEU)*, PSI Report No. 69 (Paul Scherrer Institute, Villigen, Switzerland).
- Fukumura, A., Kanai, T., Kanematsu, N., Yusa, K., Maruhashi, A., Nohtomi, A., Nishio, T., Shimbo, M., Akagi, T., Yanou, T., Fukuda, S., Hasegawa, T., Kusano, Y. and Masuda, Y. (2002) 'Proton beam dosimetry: protocol and intercomparison in Japan,' pp. 321–326 in *Proc. Int. Symp. on Standards and Codes of Practice in Medical Radiation Dosimetry*, IAEA-CN-96 (International Atomic Energy Agency, Vienna).
- Gall, K. P., Verhey, L., Alonso, J., Castro, J., Collier, J. M., Chu, W., Daftari, I., Goitein, M., Kubo, H., Ludewigt, B., Munzenrider, J., Petti, P., Renner, T., Rosenthal, S., Smith, A., Staples, J., Suit, H. and Thornton, A. (1993a) 'State of the art? New proton medical facilities for the Massachusetts General Hospital and the University of California Davis Medical Center.' *Nucl. Instrum. Methods Phys. Res.* **B79**, 881–884.
- Gall, K. P., Verhey, L. J. and Wagner, M. (1993b) 'Computer-assisted positioning of radiotherapy patients using implanted radiopaque fiducials.' *Med. Phys.* **20**, 1153–1159.
- Gall, K., Rosenthal, S. K. and Smith, A. R. (1994) 'Proton dosimetry protocol comparisons,' pp. 231–233 in *Proc. NIRS International Seminar on the Application of Heavy Ion Accelerators to Radiation Therapy of Cancer in Connection with XXI PTCOG Meeting*, Kanai, T. and Takada, E. Eds. NIRS-M-103/HIMAC-008 (National Institute of Radiological Sciences, Chiba, Japan. 231–233).
- Gastorf, R., Humphries, L. and Rozenfeld, M. (1986) 'Cylindrical chamber dimensions and the corresponding values of A_{wall} and $N_{\text{gas}}/(N_x A_{\text{ion}})$.' *Med. Phys.* **13**, 751–754.
- Geso, M., Ackerly, T. and Patterson, W. (2004) 'Improving radiochromic film's sensitivity by wrapping it with UV phosphor.' *Med. Phys.* **31**, 1014–1016.
- Glimelius, B., Ask, A., Bjelkengren, G., Bjork-Eriksson, T., Blomquist, E., Johansson, B., Karlsson, M. and Zackrisson, B. (2005) 'Number of patients potentially eligible for proton therapy.' *Acta Oncol.* **44**, 836–849.
- Goitein, M. (1977) 'The measurement of tissue heterogeneity to guide charged particle radiotherapy.' *Int. J. Radiat. Oncol. Biol. Phys.* **3**, 27–33.
- Goitein, M. (1978a) 'Compensation for inhomogeneities in charged particle radiotherapy using computed tomography.' *Int. J. Radiat. Oncol. Biol. Phys.* **4**, 499–508.
- Goitein, M. (1978b) 'A technique for calculating the influence of thin inhomogeneities on charged particle beams.' *Med. Phys.* **5**, 258–264.
- Goitein, M. (1980) 'Calculation of the uncertainty in the dose delivered in radiation therapy.' *J. Am. Med. Assoc.* **244**, 1347–1350.

REFERENCES

- Goitein, M. (1982a) 'Limitations of two-dimensional treatment planning programs.' *Med. Phys.* **9**, 580–586.
- Goitein, M. (1982b) 'Applications of computed tomography in radiotherapy treatment planning,' pp. 195–293 in *Progress in Medical Radiation Physics*, Vol. I, Orton, C. G. Ed. (Plenum Press, New York).
- Goitein, M. (1983) 'Non standard deviations.' *Med. Phys.* **10**, 709–711.
- Goitein, M. (1985) 'Calculation of the uncertainty in the dose delivered in radiation therapy.' *Med. Phys.* **12**, 608–612.
- Goitein, M. (1992) 'The comparison of treatment plans.' *Semin. Radiat. Oncol.*, **2**, 246–256.
- Goitein, M. (1995) 'Lessons to be learned from proton beam therapy,' pp. 667–672 in *Proc. 5th Int. Meeting on Progress in Radio-Oncology (ICRO, ÖGRO 5), Salzburg, Austria* (Monduzzi Editore S. P. A., Bologna, Italy).
- Goitein, M. (2005) 'The cell's-eye view: Assessing dose in four dimensions.' *Int. J. Radiat. Oncol. Biol. Phys.* **62**, 951–953.
- Goitein, M. and Abrams, M. (1983) 'Multi-dimensional treatment planning: I. Delineation of anatomy.' *Int. J. Radiat. Oncol. Biol. Phys.* **9**, 777–787.
- Goitein, M. and Chen, G. T. Y. (1983) 'Beam scanning for heavy charged particle radiotherapy.' *Med. Phys.* **10**, 831–840.
- Goitein, M. and Miller, T. (1983) 'Planning proton therapy of the eye.' *Med. Phys.* **10**, 275–283.
- Goitein, M. and Schultheiss, T. E. (1985) 'Strategies for treating possible tumor extensions: Some theoretical considerations.' *Int. J. Radiat. Oncol. Biol. Phys.* **11**, 1519–1528.
- Goitein, M., Gentry, R. and Koehler, A. M. (1983a) 'Energy of proton accelerator necessary for treatment of choroidal melanomas.' *Int. J. Radiat. Oncol. Biol. Phys.* **9**, 259–260.
- Goitein, M., Abrams, M., Rowell, D., Pollari, H. and Wiles, J. (1983b) 'Multi-dimensional treatment planning: II. Beam's-eye view, back projection, and projection through CT sections.' *Int. J. Radiat. Oncol. Biol. Phys.* **9**, 789–797.
- Goitein, M., Chen, G. T. Y., Ting, J. Y., Schneider, R. J. and Sisterson, J. M. (1978) 'Measurements and calculations of the influence of thin inhomogeneities on charged particle beams.' *Med. Phys.* **5**, 265–273.
- Goitein, M., Lomax, A. J. and Pedroni, E. S. (2002) 'Treating cancer with protons.' *Phys. Today* **55**, 45–51.
- Goitein, M., Suit, H. D., Gragoudas, E., Koehler, A. M. and Wilson, R. (1985) 'Potential for low-LET charged-particle radiation therapy in cancer.' *Radiat. Res.* **104**, S297–S309.
- Gore, J. C., Kang, Y. S. and Schulz, R. J. (1984) 'Measurement of radiation dose distributions by nuclear magnetic resonance (NMR) imaging.' *Phys. Med. Biol.* **29**, 1189–1197.
- Gottschalk, B. (1983) 'Charge-balancing current integrator with large dynamic range.' *Nucl. Instrum. Methods* **207**, 417–421.
- Gottschalk, B. (2003) 'On the characterization of spread-out Bragg peaks and the definition of 'Depth' and "Modulation".' <http://huhepl.harvard.edu/~gottschalk/BGdocs.zip/SOBP.pdf>.
- Gottschalk, B., Platais, R. and Paganetti, H. (1999) 'Nuclear interactions of 160 MeV protons stopping in copper: A test of Monte Carlo nuclear models.' *Med. Phys.* **26**, 2597–2601.
- Graffman, S. (1975) *On the Evaluation of New Irradiation Modalities in Tumor Therapy: An Experimental and Clinical Study with Special Reference to High Energy Protons*, Umeå University Medical Dissertations, New Series No. 1 (Umeå University, Sweden).
- Graffman, S., Brahme, A. and Larsson, B. (1985) 'Proton radiotherapy with the Uppsala cyclotron. Experience and plans.' *Strahlenther.* **161**, 764–770.
- Gragoudas, E. S., Goitein, M., Koehler, A. M., Verhey, L., Tepper, J., Suit, H. D., Brockhurst, R. and Constable, I. J. (1977) 'Proton irradiation of small choroidal malignant melanomas.' *Am. J. Ophthalmol.* **83**, 665–673.
- Gragoudas, E. S., Goitein, M., Verhey, L., Suit, H. D. and Koehler, A. M. (1980) 'Proton beam irradiation: An alternative to enucleation for intraocular melanomas.' *Ophthalmol.* **87**, 571–581.
- Gragoudas, E. S., Lane, A. M., Egan, K. M. and Li, W. (2002a) 'Long term risk of local failure after proton therapy for choroidal/ciliary body melanoma.' *Trans. Am. Ophthalmol. Soc.* **100**, 43–49.
- Gragoudas, E., Li, W., Goitein, M., Lane, A. M. and Egan, K. M. (2002b) 'Evidence-based estimates of outcome in patients irradiated for intraocular melanoma.' *Arch. Ophthalmol.* **120**, 1665–1671.
- Grégoire, V., Coche, E., Cosnard, G., Hamoir, M. and Reyhler, H. (2000) 'Selection and delineation of lymph node target volumes in head and neck conformal radiotherapy. Proposal for standardizing terminology and procedure based on the surgical experience.' *Radiother. Oncol.* **56**, 135–150.
- Grégoire, V., Pötter, R. and Wambersie, A. (2004) 'General principles for prescribing, recording and reporting a therapeutic irradiation.' *Radiother. Oncol.* **73** (Suppl. 2), S57–S61.
- Grusell, E. and Medin, J. (2000) 'General characteristics of the use of silicon diode detectors for clinical dosimetry in proton beams.' *Phys. Med. Biol.* **45**, 2573–2582.
- Grusell, E., Montelius, A., Brahme, A., Rikner, G. and Russell, K. (1994) 'A general solution to charged particle beam flattening using an optimized dual-scattering-foil technique, with application to proton therapy beams.' *Phys. Med. Biol.* **39**, 2201–2216.
- Grusell, E., Isacsson, U., Montelius, A. and Medin, J. (1995) 'Faraday cup dosimetry in a proton beam without collimation.' *Phys. Med. Biol.* **40**, 1831–1840.
- Guerra, A. S., Laitano, R. F. and Pimpinella, M. (1996) 'Characteristics of the absorbed dose to water standard at ENEA.' *Phys. Med. Biol.* **41**, 657–674.
- Gueulette, J., Grégoire, V., Octave-Prignot, M. and Wambersie, A. (1996) 'Measurements of radiobiological effectiveness in the 85 MeV proton beam produced at the cyclotron CYCLONE of Louvain-la-Neuve, Belgium.' *Radiat. Res.* **145**, 70–74.

- Gueulette, J., Böhm, L., Slabbert, J. P., De Coster, B. M., Rutherford, G. S., Ruifrok, A., Octave-Prignot, M., Binns, P. J., Schreuder, A. N., Symons, J. E., Scalliet, P. and Jones, D. T. L. (2000) 'Proton relative biological effectiveness (RBE) for survival in mice after thoracic irradiation with fractionated doses.' *Int. J. Radiat. Oncol. Biol. Phys.* **47**, 1051–1058.
- Gueulette, J., Octave-Prignot, M., De Coster, B-M., Wambersie, A. and Grégoire, V. (2004) 'Intestinal crypt cell regeneration in mice: a biological system for quality assurance in non-conventional radiation therapy.' *Radiother. Oncol.* **73** (Suppl. 2), 148–154.
- Gueulette, J., Blattmann, H., Pedroni, E., Coray, A., De Coster, B. M., Mahy, P., Wambersie, A. and Goitein, G. (2005) 'Relative biologic effectiveness determination in mouse intestine for scanning proton beam at Paul Scherrer Institute, Switzerland. Influence of motion.' *Int. J. Radiat. Oncol. Biol. Phys.* **62**, 838–845.
- Gulbrandsen, T. and Madsen, C. B. (1962) 'Radiation dosimetry by means of semiconductor.' *Acta Radiol.* **58**, 226–232.
- Guo, P. Y., Adamovics, J. A. and Oldham, M. (2006) 'Characterization of a new radiochromic three-dimensional dosimeter.' *Med. Phys.* **33**, 1338–1345.
- Guru Prasad, S., Parthasaradhi, K. and Bloomer, W. D. (1997) 'Effective atomic numbers of composite materials for total and partial interaction processes for photons, electrons, and protons.' *Med. Phys.* **24**, 883–885.
- Gustavsson, H., Bäck, S. Å. J., Medin, J., Grusell, E. and Olsson, L. E. (2004) 'Linear energy transfer dependence of a normoxic polymer gel dosimeter investigated using proton beam absorbed dose measurements.' *Phys. Med. Biol.* **49**, 3847–3855.
- Haberer, T., Becher, W., Schardt, D. and Kraft, G. (1993) 'Magnetic scanning system for heavy ion therapy.' *Nucl. Instrum. Methods Phys. Res. A* **330**, 296–305.
- Hall, E. J. (2006) 'Intensity-modulated radiation therapy, protons, and the risk of second cancers.' *Int. J. Radiat. Oncol. Biol. Phys.* **65**, 1–7.
- Hamm, R. W., Crandall, K. R. and Potter, J. (1991) 'Preliminary design of a dedicated proton therapy linac,' p. 2583 in *IEEE Particle Accelerator Conference: Accelerator Science and Technology, Lawrence Berkeley Laboratory, Berkeley, CA*, Lizama, L. and Chew, J. Eds. (IEEE Press, Piscataway, NJ).
- Hanley, J., Debois, M. M., Mah, D., Mageras, G. S., Raben, A., Rosenzweig, K., Mychalczak, B., Schwartz, L. H., Gloeggler, P. J., Lutz, W., Ling, C. C., Leibel, S. A., Fuks, Z. and Kutcher, G. J. (1999) 'Deep inspiration breath-hold technique for lung tumors: The potential value of target immobilization and reduced lung density in dose escalation.' *Int. J. Radiat. Oncol. Biol. Phys.* **45**, 603–611.
- Hansen, J. W. and Olsen, K. J. (1985) 'Theoretical and experimental radiation effectiveness of the free radical dosimeter alanine to irradiation with heavy charged particles.' *Radiat. Res.* **104**, 15–27.
- Hansen, J. W. and Olsen, K. J. (1989) 'Predicting decay in free-radical concentration in L- α -alanine following high-LET radiation exposure.' *Appl. Radiat. Isot.* **40**, 935–939.
- Hashemian, R., Foster, C. C., Murray, K. M., Landolt, R. L., Shaw, S. M. and Bloch, C. (2003) 'Measurement of W/e for protons in air.' *39th Meeting of the Particle Therapy Co-Operative Group, San Francisco, CA*.
- Harsh, G. R., Thornton, A. F., Chapman, P. H., Bussière, M. R., Rabinov, J. D. and Loeffler, J. S. (2002) 'Proton beam stereotactic radiosurgery of vestibular schwannomas.' *Int. J. Radiat. Oncol. Biol. Phys.* **54**, 35–44.
- Hayakawa, Y. and Schechtman, H. (1988) 'Comments on the value of the average energy per ion pair formed in air for a proton beam recommended by the American Association of Physicists in Medicine.' *Med. Phys.* **15**, 778.
- Hazle, J. D., Hefner, L., Nyerick, C. E., Wilson, L. and Boyer, A. L. (1991) 'Dose-response characteristics of a ferrous-sulfate-doped gelatin system for determining radiation absorbed dose distribution by magnetic resonance imaging (Fe MRI).' *Phys. Med. Biol.* **36**, 1117–1125.
- Heese, J., Kluge, H., Fuchs, H., Heufelder, J., Cordinil, D., Morgenstern, H., Nausner, M., Bechrakis, M., Hinkelbein, J. and Foerster, M. H. (2002) 'The proton facility at HMI.' *Particles 32, Abstracts of the 37th Proton Therapy Co-Operative Group Meeting, Cape Town*.
- Hilts, M., Jirasek, A., Audet, C. and Duzenli, C. (2000) 'X-ray CT polymer gel dosimetry: Applications in stereotactic radiosurgery and proton therapy.' *Radiother. Oncol.* **56**, (Suppl. 1), S80 (Abstract).
- Hiraoka, T., Omata, K., Fukumura, A. and Takeshita, M. (1997) 'Dosimetry of particle beams with different walled ionization chambers.' *Med. Phys.* **24**, 1051 (Abstract).
- Hiramoto, K. and Nishi, M. (1992) 'Resonant beam extraction scheme with constant separatrix.' *Nucl. Instrum. Meth. Phys. Res. A* **322**, 154–160.
- Hishikawa, Y., Kagawa, K., Murakami, M., Sakai, H., Akagi, T. and Abe, M. (2002) 'Usefulness of positron-emission tomographic images after proton therapy.' *Int. J. Radiat. Oncol. Biol. Phys.* **53**, 1388–1391.
- Hohlfield, K. (1988) 'The standard DIN 6800: Procedures for absorbed dose determination in radiology by the ionization method,' pp. 13–22 in *Dosimetry in Radiotherapy*, IAEA-SM-298/31 (International Atomic Energy Agency, Vienna) pp. 13–22.
- Hong, L., Goitein, M., Bucciolini, M., Comiskey, R., Gottschalk, B., Rosenthal, S., Serago, C. and Urie, M. (1996) 'A pencil beam algorithm for proton dose calculations.' *Phys. Med. Biol.* **41**, 1305–1330.
- Hong, T. S., Ritter, M. A., Tome, W. A. and Harari, P. M. (2005) 'Intensity-modulated radiation therapy: Emerging cancer treatment technology.' *Br. J. Cancer* **92**, 1819–1824.
- Hoppe, B. S., Stegman, L. D., Zelefsky, M. J., Rosenzweig, K. E., Wolden, S. L., Patel, S. G., Shah, J. P., Kraus, D. H. and Lee, N. Y. (2007) 'Treatment of nasal cavity and paranasal sinus cancer with modern radiotherapy techniques in the postoperative setting:

REFERENCES

- the MSKCC experience.' *Int. J. Radiat. Oncol. Biol. Phys.* **67**, 691–702.
- Hoyer, M., Roed, H., Hansen, A. T., Ohlhuis, L., Petersen, J., Nellemann, H., Berthelsen, A. K., Grau, C., Engelholm, S. A. and von der Masse, H. (2006) 'Prospective study on stereotactic radiotherapy of limited-stage non-small-cell lung cancer.' *Int. J. Radiat. Oncol. Biol. Phys.* **66**, S128–S135.
- Hsiung-Stripp, D. C., McDonough, J., Masters, H. M., Levin, W. P., Hahn, S. M., Jones, H. A. and Metz, J. M. (2001) 'Comparative treatment planning between proton and x-ray therapy in pancreatic cancer.' *Med. Dosim.* **26**, 255–259.
- Hug, E. B., Fitzek, M. M., Liebsch, N. J. and Munzenrider, J. E. (1995) 'Locally challenging osteo- and chondrogenic tumors of the axial skeleton: Results of combined proton and photon radiation therapy using three-dimensional treatment planning.' *Int. J. Radiat. Oncol. Biol. Phys.* **31**, 467–476.
- IAEA (1997a) International Atomic Energy Agency. *Absorbed Dose Determination in Photon and Electron Beams: An International Code of Practice*, Technical Report Series No. 277, 2nd edn (International Atomic Energy Agency: Vienna).
- IAEA (1997b) International Atomic Energy Agency. *The Use of Plane Parallel Ionization Chambers in High Energy Electron and Photon Beams: An International Code of Practice for Dosimetry*, Technical Reports Series No. 381 (International Atomic Energy Agency: Vienna).
- IAEA (2000) International Atomic Energy Agency. *Absorbed Dose Determination in External Beam Radiotherapy. An International Code of Practice for Dosimetry Based on Standards of Absorbed Dose to Water*, Technical Reports Series No. 398 (International Atomic Energy Agency: Vienna). Revised and updated version (V.11b, 23 April, 2004): http://wwwnaweb.iaea.org/nahu/dmrp/pdf_files/COPV11b.pdf.
- IAEA (2004) International Atomic Energy Agency. *Commissioning and Quality Assurance of Computerized Planning Systems for Radiation Treatment of Cancer*, Technical Reports Series No. 430 (International Atomic Energy Agency: Vienna).
- ICRP (1991) International Commission on Radiological Protection. *1990 Recommendations of the International Commission on Radiological Protection*, ICRP Publication 60, *Anns. ICRP* **21**, 1–3 (Elsevier Science B. V.: Amsterdam).
- ICRU (1976) International Commission on Radiation Units and Measurements. *Determination of Absorbed Dose in a Patient Irradiated by Beams of X or Gamma Rays in Radiotherapy Procedures*, ICRU Report 24 (International Commission on Radiation Units and Measurements: Bethesda, MD).
- ICRU (1977) International Commission on Radiation Units and Measurements. *Neutron Dosimetry for Biology and Medicine*, ICRU Report 26 (International Commission on Radiation Units and Measurements: Bethesda, MD).
- ICRU (1978) International Commission on Radiation Units and Measurements. *An International Neutron Dosimetry Intercomparison*, ICRU Report 27 (International Commission on Radiation Units and Measurements: Bethesda, MD).
- ICRU (1979) International Commission on Radiation Units and Measurements. *Average Energy Required to Produce an Ion Pair*, ICRU Report 31 (International Commission on Radiation Units and Measurements: Bethesda, MD).
- ICRU (1984) International Commission on Radiation Units and Measurements, *Stopping Powers for Electrons and Positrons*, ICRU Report 37 (International Commission on Radiation Units and Measurements: Bethesda, MD).
- ICRU (1989) International Commission on Radiation Units and Measurements. *Clinical Neutron Dosimetry Part 1: Determination of Absorbed Dose in a Patient Treated by External Beams of Fast Neutrons*, ICRU Report 45 (International Commission on Radiation Units and Measurements: Bethesda, MD).
- ICRU (1993a) International Commission on Radiation Units and Measurements, *Stopping Powers and Ranges for Protons and Alpha Particles*, ICRU Report 49 (International Commission on Radiation Units and Measurements: Bethesda, MD).
- ICRU (1993b) International Commission on Radiation Units and Measurements. *Prescribing, Recording, and Reporting Photon Beam Therapy*, ICRU Report 50, (International Commission on Radiation Units and Measurements: Washington, DC).
- ICRU (1998) International Commission on Radiation Units and Measurements. *Clinical Proton Dosimetry Part 1: Beam Production, Beam Delivery and Measurement of Absorbed Dose*, ICRU Report 59 (International Commission on Radiation Units and Measurements: Bethesda, MD).
- ICRU (1999) International Commission on Radiation Units and Measurements. *Prescribing, Recording, and Reporting Photon Beam Therapy (Supplement to ICRU Report 50)*, ICRU Report 62 (International Commission on Radiation Units and Measurements: Bethesda, MD).
- ICRU (2000) International Commission on Radiation Units and Measurements. *Nuclear Data for Neutron and Proton Radiotherapy and for Radiation Protection*, ICRU Report 63 (International Commission on Radiation Units and Measurements: Bethesda, MD).
- ICRU (2001) International Commission on Radiation Units and Measurements. *Dosimetry of High-Energy Photon Beams Based on Standards of Absorbed Dose to Water*, ICRU Report 64 (Nuclear Technology Publishing: Ashford, UK).
- ICRU (2004) International Commission on Radiation Units and Measurements. *Prescribing, Recording, and Reporting Electron Beam Therapy*, ICRU Report 71, *J. ICRU* **4**(1) (Oxford University Press: Oxford, UK).
- ISO (1995) International Organization for Standardization. *Guide to the Expression of Uncertainty in Measurement*, 2nd edn. Published by ISO in the name of BIPM, IEC, IFCC, IUPAC, IUPAP and OIML (International Organization for Standardization: Geneva).

- iTL (2001) iThemba Laboratory for Accelerator-Based Sciences. *The Quality Control Programme for the iThemba LABS Proton Therapy Facility*, Internal Report (iThemba LABS: Somerset West, South Africa).
- Jaffray, D. A. (2003) 'X-ray-guided IMRT.' In *Intensity Modulated Radiation Therapy: The State of the Art*, Palta, J. R. and Mackie, T. R. Eds. (Medical Physics Publishing: Madison, WI).
- JASTRO (2004) Japanese Association of Therapeutic Radiation Oncology. *Guidelines of Physical and Technological Quality Assurance for Particle Beam Therapy*.
- Jesse, W. P. and Sadauskis, J. (1952) 'Alpha-particle ionization in mixtures of the noble gases.' *Phys. Rev.* **88**, 417–418.
- Jesse, W. P. and Sadauskis, J. (1953) 'Alpha-particle ionization in pure gases and the average energy to make an ion pair.' *Phys. Rev.* **90**, 1120–1121.
- Jiang, H. and Paganetti, H. (2004) 'Adaptation of GEANT4 to Monte Carlo dose calculations based on CT data.' *Med. Phys.*, **31**, 2811–2818.
- Jiang, H., Wang, B., Xu, X. G., Suit, H. D. and Paganetti, H. (2005) 'Simulation of organ-specific patient effective dose due to secondary neutrons in proton radiation treatment.' *Phys. Med. Biol.* **50**, 4337–4353.
- Jirasek, A. and Duzenli, C. (2002) 'Relative effectiveness of polyacrylamide gel dosimeters applied to proton beams: Fourier transform Raman observations and track structure calculations.' *Med. Phys.* **29**, 569–577.
- Jones, A. Z., Bloch, C. D., Hall, E. R., Hashemian, R., Klein, S. B., von Przewoski, B., Murray, K. M. and Foster, C. C. (1999) 'Comparison of Indiana University Cyclotron Facility Faraday cup proton dosimetry with radiochromic films, a calorimeter, and a calibrated ion chamber.' *IEEE Trans. Nucl. Sci.* **46**, 1762–1765.
- Jones, D. T. L. (1995) 'The NAC particle therapy facilities,' pp. 350–359 in *Ion Beams in Tumor Therapy*, Linz, U. Ed. (Chapman and Hall: Weinheim, Germany).
- Jones, D. T. L. (1996) 'Proton dosimetry intercomparison performed at the NAC,' p. 116 in *National Accelerator Centre Annual Report, March* (National Accelerator Centre: Faure, South Africa).
- Jones, D. T. L. (1999) 'Present status and future trends of heavy particle therapy,' pp. 13–20 in *Proc. 15th Int. Conf. on Cyclotrons and their Applications*, Baron, E. and Lievin, M. Eds. (Institute of Physics Publishing: Bristol, UK).
- Jones, D. T. L. (2001a) 'Overview of hadron therapy: rationales, present status and future prospects.' *Radiochim. Acta* **89**, 235–244.
- Jones, D. T. L. (2001b) 'Fast neutron and proton therapy sources.' *Radiochim. Acta* **89**, 265–277.
- Jones, D. T. L. (2001c) 'Proton therapy: the promise of precision.' *Bull. Int. Radiat. Phys. Soc.* **15** (3/4), 4–13.
- Jones, D. T. L. (2001d) 'Reference dosimetry for fast neutron and proton therapy.' *Radiochim. Acta* **89**, 279–287.
- Jones, D. T. L. (2006) 'The w -value in air for proton therapy beams.' *Radiat. Phys. Chem.* **75**, 541–550.
- Jones, D. T. L. and Schreuder, A. N. (2001) 'Magnetically scanned proton therapy beams: rationales and principles.' *Radiat. Phys. Chem.* **61**, 615–618.
- Jones, D. T. L., Kacperek, A., Vynckier, S., Mazal, A., Delacroix, S. and Nauraye, C. (1992) 'A European proton dosimetry intercomparison,' pp. 61–63 in *National Accelerator Centre Annual Report*, NAC/AR/92–01 (National Accelerator Centre: Faure, South Africa).
- Jones, D. T. L., Schreuder, A. N., Symons, J. E., Vynckier, S., Hayakawa, Y. and Maruhashi, A. (1994a) 'Proton dosimetry intercomparison at NAC,' pp. 94–95 in *National Accelerator Centre Annual Report*, NAC/AR/94–01 (National Accelerator Centre: Faure, South Africa).
- Jones, D. T. L., Schreuder, A. N., Symons, J. E., Vynckier, S., Kacperek, A., Mazal, A., Delacroix, S., Nauraye, C., Bridier, A., Wagner, M., Beatty, J., Gall, K. and Hayakawa, Y. (1994b) 'National Accelerator Centre: proton dosimetry protocol intercomparisons,' p. 230 in *Proc. NIRS International Seminar on the Application of Heavy Ion Accelerator to Radiation Therapy of Cancer in Connection with XXI PTCOG Meeting*, Kanai, T. and Takada, E. Eds. NIRS-M-103/HIMAC-008 (National Institute of Radiological Sciences: Chiba, Japan).
- Jones, D. T. L., Schreuder, A. N. and Symons, J. E. (1995) 'Use of stereophotogrammetry in proton radiation therapy,' pp. 138–153 in *Proc. Int. Symp. on Photogrammetry in Engineering Surveying*, Rüther, H. Ed. (University of Cape Town: South Africa).
- Kacperek, A. (2003) 'Low-energy proton therapy: QA protocol.' *Internal Report* (Douglas Cyclotron, Clatterbridge Centre for Oncology: Clatterbridge, UK).
- Kacperek, A. and Bonnett, D. E. (1990) 'Development of a Faraday cup for proton beam dosimetry at the MRC Cyclotron Unit at Clatterbridge Hospital,' pp. 53–56 in *Proc. Int. Heavy Particle Therapy Workshop (PTCOG/EORTC/ECNEU)*, Blattmann, H. Ed. PSI-Bericht Nr. 69 (Paul Scherrer Institute: Villigen, Switzerland).
- Kacperek, A., Egger, E., Barone Tonghi, L., Cuttone, G., Raffaele, L., Rovelli, A., Sabini, M. G., Tabarelli De Fatis, P., Luraschi, F. and Marzoli, L. (2002) 'Proton dosimetry intercomparison using parallel-plate ionization chambers in a proton eye therapy beam,' pp. 311–319 in *Proc. Int. Symp. on Standards and Codes of Practice in Medical Radiation Dosimetry*. IAEA-CN-96 (International Atomic Energy Agency: Vienna).
- Kacperek, A., Vynckier, S., Bridier, A., Héault, J. and Bonnett, D. E. (1991) 'A small scale European proton dosimetry intercomparison,' pp. 76–79 in *Proc. Proton Radiotherapy Workshop*, Blattmann, H. Ed. PSI-Bericht Nr. 111 (Paul Scherrer Institute, Villigen, Switzerland).
- Kagawa, K., Murakami, M., Hishikawa, Y., Abe, M., Akagi, T., Yanou, T., Kagiya, G., Furusawa, Y., Ando, K., Nojima, K., Aoki, M. and Kanai, T. (2002) 'Preclinical biological assessment of proton and carbon

REFERENCES

- ion beams at Hyogo Ion Beam Medical Center.' *Int. J. Radiat. Oncol. Biol. Phys.* **54**, 928–938.
- Kanai, T., Kawachi, K., Kumamoto, Y., Ogawa, H., Yamada, T. and Matsuzawa, H. (1980) 'Spot scanning system for proton radiotherapy.' *Med. Phys.* **7**, 365–369.
- Kanai, T., Kawachi, K., Matsuzawa, H. and Inada, T. (1983) 'Three-dimensional beam scanning for proton therapy.' *Nucl. Instrum. Methods* **214**, 491–496.
- Kanai, T., Endo, M., Minohara, S., Miyahara, N., Koyama-ito, H., Tomura, H., Matsufuji, N., Futami, Y., Fukumura, A., Hiraoka, T., Furusawa, Y., Ando, K., Suzuki, M., Soga, F. and Kawachi, K. (1999) 'Biophysical characteristics of HIMAC clinical irradiation system for heavy-ion radiation therapy.' *Int. J. Radiat. Oncol. Biol. Phys.* **44**, 201–210.
- Kanai, T., Fukumura, A., Kusano, Y., Shimbo, M. and Nishio, T. (2004) 'Cross-calibration of ionization chambers in proton and carbon beams.' *Phys. Med. Biol.* **49**, 771–781.
- Kanematsu, N., Matsufuji, N., Kohno, R., Minohara, S. and Kanai, T. (2003) 'A CT calibration method based on the polybinary tissue model for radiotherapy treatment planning.' *Phys. Med. Biol.* **48**, 1053–1064.
- Kapchinskii, I. M. and Teplyakov, V. A. (1970) 'Linear ion accelerator with spatially homogeneous strong focusing.' *Prib. Tekh. Eksp.* **19**, 19–22.
- Karzmark, C. J. (1964) 'Secondary emission monitor as a linear accelerator electron beam dose monitor.' *Rev. Sci. Instrum.* **35**, 1646–1652.
- Kavanaugh, B. D., Schefter, T. E., Cardenes, H. R., Stieber, V. W., Raben, D., Timmerman, R. D., McCarter, M. C., Burri, S., Nedzi, L. A., Sawyer, T. E. and Gaspar, L. E. (2006) 'Interim analysis of a prospective phase I/II trial of SBRT for liver metastases.' *Acta Oncol.* **45**, 848–855.
- Khoroshkov, V. S., Goldin, L. L., Onosovsky, K. K. and Klenov, G. I. (1991) 'Soviet project of proton therapy facility with several treatment rooms,' pp. 37–42 in *Proc. Proton Radiotherapy Workshop*, Blattmann, H. Ed. PSI-Bericht Nr. 111 (Paul Scherrer Institute: Villigen, Switzerland).
- Khrunov, V. S., Martynov, S. S., Vatnitsky, S. M., Ermakov, I. A., Chervjakov, A. M., Karlin, D. L., Fominych, V. I. and Tarbeyev, Yu. V. (1990) 'Diamond detectors in relative dosimetry of photon, electron and proton radiation fields.' *Radiat. Prot. Dosim.* **33**, 155–157.
- Kjellberg, R. N. (1979) 'Stereotactic Bragg peak proton radiosurgery results,' pp. 233–241 in *Stereotactic Cerebral Irradiation: INSERM Symposium No. 12*, Szikla, G. Ed. (Elsevier/North Holland Press: Amsterdam).
- Kjellberg, R. N., Koehler, A. M., Preston, W. M. and Sweet, W. H. (1962a) 'Stereotaxic instrument for use with the Bragg peak of a proton beam.' *Confin. Neurol.* **22**, 183–189.
- Kjellberg, R. N., Sweet, W. H., Preston, W. M. and Koehler, A. M. (1962b) 'The Bragg peak of a proton beam in intracranial therapy of tumors.' *Trans. Am. Neurol. Soc.* **87**, 216–218.
- Kjellberg, R. N., Shintani, A., Frantz, A. G. and Kliman, B. (1968) 'Proton-beam therapy in acromegaly.' *New Eng. J. Med.* **278**, 689–695.
- Kjellberg, R. N., Hanamura, T., Davis, K. R., Lyons, S. L. and Adams, R. D. (1983) 'Bragg-peak proton-beam therapy for arteriovenous malformations of the brain.' *N Engl. J. Med.* **309**, 269–274.
- Klassen, N. V. and Ross, C. K. (1991) 'Absorbed dose calorimetry using various aqueous solutions.' *Radiat. Phys. Chem.*, **38**, 95–104.
- Klevenhagen, S. C. (1977a) 'The non-linearity of the temperature response of silicon p-n junction radiation detectors operated in the DC mode.' *Phys. Med. Biol.* **22**, 353–358.
- Klevenhagen, S. C. (1977b) 'Transient processes in the DC circuit of p-n junction silicon radiation detectors.' *Phys. Med. Biol.* **22**, 773–779.
- Knoll, G. F. (1989) *Radiation Detection and Measurement* (John Wiley, New York).
- Knöös, T., Kristensen, I. and Nilsson, P. (1998) 'Volumetric and dosimetric evaluation of radiation treatment plans: Radiation conformity index.' *Int. J. Radiat. Oncol. Biol. Phys.* **42**, 1169–1176.
- Koehler, A. M. (1967) 'Dosimetry of proton beams using small silicon diodes.' *Radiat. Res. (Suppl. 7)*, 53–63.
- Koehler, A. M. (1987) 'Preliminary design study for a corkscrew gantry,' pp. 147–158 in *Proc. Fifth Proton Therapy Co-Operative Group Meeting: International Workshop on Biomedical Accelerators. Lawrence Berkeley Laboratory, Dec 1–2, 1986*, Publication LBL-22962 (Lawrence Berkeley Laboratory: Berkeley, CA).
- Koehler, A. M. and Preston, W. M. (1972) 'Protons in radiation therapy. Comparative dose distributions for protons, photons, and electrons.' *Radiology* **104**, 191–195.
- Koehler, A. M., Schneider, R. J. and Sisteron, J. M. (1975) 'Range modulators for protons and heavy ions.' *Nucl. Instrum. Methods* **131**, 437–440.
- Koehler, A. M., Schneider, R. J. and Sisteron, J. M. (1977) 'Flattening of proton dose distributions for large-field radiotherapy.' *Med. Phys.* **4**, 297–301.
- Kogelnik, H. D. (1997) 'Hadrontherapy – do we need it?,' pp. 12–27 in *Advances in Hadrontherapy*, Amaldi, U., Larsson, B. and Lemoigne, Y. Eds. (Elsevier Science B.V.: Amsterdam).
- Kooy, H. M. (2002) 'Clinical commissioning of Gantry 1 at the Northeast Proton Therapy Center,' in *Particles 31: Abstracts of the 36th Proton Therapy Co-Operative Group Meeting, Catania, Italy*.
- Kooy, H. M., Schaefer, M., Rosenthal, S. and Bortfeld, T. (2003) 'Monitor unit calculations for range-modulated spread-out Bragg peak fields.' *Phys. Med. Biol.* **48**, 2797–2808.
- Kostjuchenko, V. and Nichiporov, D. (1993) 'Measurement of the $^{12}\text{C}(\text{p},\text{pn})^{11}\text{C}$ reaction from 95 to 200 MeV.' *Int. J. Appl. Radiat. Isot.* **44**, 1173–1175.
- Kostjuchenko, V., Nichiporov, D. and Luckjashin, V. (2001) 'A compact ridge filter for spread out Bragg peak production in pulsed proton clinical beams.' *Med. Phys.* **28**, 1427–1430.

- Kubo, H. and Brown, D. E. (1984) 'Calorimeter dose determinations by direct voltage measurements on a Wheatstone-type bridge circuit.' *Phys. Med. Biol.* **29**, 885–889.
- Kubo, H. and Brown, D. E. (1986) 'Absorbed dose calorimetry: Bridge nulling and voltage analysis techniques.' *Phys. Med. Biol.* **31**, 242–247.
- Kubo, H., Kageyama, Y. and Kai Lo, K. (1989) 'Construction of a calorimeter prototype with a high sensitivity pulsed signal detection circuit.' *Phys. Med. Biol.* **34**, 1119–1123.
- Laitano, R. F. (1997) 'Reference dosimetry of proton beams for radiotherapy.' *Phys. Med.* **XII** (Suppl. 1), 75–79.
- Laitano, R. F. (1998) 'Absolute measurement methods for proton beam dosimetry.' *Riv. Nuovo Cimento* **21**, 1–58.
- Laitano, R. F. and Rosetti, M. (2000) 'Proton stopping powers averaged over beam energy spectra.' *Phys. Med. Biol.* **45**, 3025–3043.
- Laitano, R. F., Rosetti, M. and Frisoni, M. (1996) 'Effects of nuclear interactions on energy and stopping power in proton beam dosimetry' *Nucl. Instrum. Meth. Phys. Res. A* **376**, 466–476.
- Langen, K. M. and Jones, D. T. L. (2001) 'Organ motion and its management.' *Int. J. Radiat. Oncol. Biol. Phys.* **50**, 265–278.
- Larsson, B. (1961) 'Pre-therapeutic physical experiments with high energy protons.' *Br. J. Radiol.* **34**, 143–151.
- Larsson, B. (1967) 'Radiological properties of beams of high-energy protons.' *Radiat. Res.* (Suppl. 7), 304–311.
- Larsson, B. and Sarby, B. (1987) 'Equipment for radiation surgery using narrow 185 MeV proton beams. Dosimetry and design.' *Acta Oncol.* **26**, 143–158.
- Larsson, B., Leksell, L., Rexed, B., Sourander, P., Mair, W. and Andersson, B. (1958) 'The high-energy proton beam as a neurosurgical tool.' *Nature* **182**, 1222–1223.
- Larsson, B., Leksell, L., Rexed, B. and Sourander, P. (1959) 'Effect of high energy protons on the spinal cord.' *Acta Radiol.* **51**, 52–64.
- Larsson, B., Leksell, L. and Rexed, B. (1963) 'The use of high energy protons for cerebral surgery in man.' *Acta Chir. Scand.* **125**, 1–7.
- Larsson, B., Graffman, S. and Jung, B. (1965) 'Fixation of Carbon-11 in the cells of proton-irradiated blood.' *Nature* **207**, 543–544.
- Laughlin, J. S. and Jenna, S. (1966) 'Calorimetry,' pp. 389–441 in *Radiation Dosimetry*, Vol. II, Attix, F. H. and Roesch, W. C. Eds. (Academic Press: New York).
- Lawrence, J. H. (1957) 'Proton irradiation of the pituitary.' *Cancer* **10**, 795–798.
- Leksell, L. (1951) 'The stereotaxic method and radiosurgery of the brain.' *Acta Chir. Scand.* **102**, 316–319.
- Leksell, L., Larsson, B., Andersson, B., Rexed, B., Sourander, P. and Mair, W. (1960) 'Lesions in the depth of the brain produced by a beam of high energy protons.' *Acta Radiol.* **54**, 251–264.
- Lesyna, D. (2004) 'An automated patient registration system for precision daily set-up for proton beam therapy,' in *Particles 34, Abstracts of the 40th Proton Therapy Co-Operative Group Meeting Proton Therapy, Paris, France*.
- Li, Q., Groeziinger, S. O., Haberer, T., Rietzel, E. and Kraft, G. (2004) 'Online compensation for target motion with scanned particle beams: Simulation environment.' *Phys. Med. Biol.* **49**, 3029–3046.
- Lin, R., Hug, E. B., Schaefer, R. A., Miller, D. W., Slater, J. M. and Slater, J. D. (2000) 'Conformal proton radiation therapy of the posterior fossa: A study comparing protons with three-dimensional planned photons in limiting dose to auditory structures.' *Int. J. Radiat. Oncol. Biol. Phys.* **48**, 1219–1226.
- Lin, S., Blattmann, H., Boehringer, T., Coray, A., Kohli, M. and Pedroni, E. (1994) 'Preparatory work for proton therapy beam dosimetry system at PSI,' pp. 481–487 in *Hadrontherapy in Oncology*, Amaldi, U. and Larsson, B. Eds. (Elsevier Science B. V.: Amsterdam).
- Ling, C. C., Yorke, E., Amols, H., Mechakos, J., Erdi, Y., Leibel, S., Rosenzweig, K. and Jackson, A. (2004) 'High-tech will improve radiotherapy of NSCLC: A hypothesis waiting to be validated.' *Int. J. Radiat. Oncol. Biol. Phys.* **60**, 3–7.
- Lomax, A. (1999) 'Intensity modulated methods for proton therapy.' *Phys. Med. Biol.* **44**, 185–205.
- Lomax, A. J. (2001) 'Methods for assessing the effects of inter- and intra-fraction position errors in radiotherapy.' *Radiother. Oncol.* **61** (Suppl. 1), S22 (abstract).
- Lomax, A. J., Boehringer, T., Coray, A., Egger, E., Goitein, G., Grossmann, M., Juelke, P., Lin, S., Pedroni, E., Rohrer, B., Roser, W., Rossi, B., Siegenthaler, B., Stadelmann, O., Stauble, H., Vetter, C. and Wisser, L. (2001) 'Intensity modulated proton therapy: A clinical example.' *Med. Phys.* **28**, 317–324.
- Lomax, A. J., Goitein, M. and Adams, J. (2003) 'Intensity modulation in radiotherapy: photons versus protons in the paranasal sinus.' *Radiother. Oncol.* **66**, 11–18.
- Lomax, A. J., Böhringer, T., Bolisi, A., Coray, D., Emert, F., Goitein, G., Jermann, M., Lin, S., Pedroni, E., Rutz, H., Stadelmann, O., Timmermann, B., Verwey, J. and Weber, D. C. (2004) 'Treatment planning and verification of proton therapy using spot scanning: Initial experiences.' *Med. Phys.* **31**, 3150–3157.
- Loncol, T., Cosgrove, V., Denis, J. M., Guelette, J., Mazal, A., Menzel, H. G., Pihet, P. and Sabattier, R. (1994) 'Radiobiological effectiveness of radiation beams with broad LET spectra: Microdosimetric analysis using biological weighting factors.' *Radiat. Prot. Dosim.* **52**, 347–352.
- Loncol, Th., Vynckier, S. and Wambersie, A. (1996) 'Thermoluminescence in proton and fast neutron therapy beams.' *Radiat. Prot. Dosim.* **66**, 299–304.
- Lorin, S., Grusell, E., Tilly, N., Medin, J., Blom, M., Ziemann, V., Reistad, D. and Glimelius, B. (2000) 'Development of a compact proton scanning system in Uppsala with a moveable second magnet.' *Phys. Med. Biol.* **45**, 1151–1163.
- Low, D. A., Nystrom, M., Kalinin, E., Parikh, P., Dempsey, J. F., Bradley, J. D., Mutic, S., Wahab, S. H., Islam, T., Christensen, G., Politte, D. G. and Whiting, B. R. (2003) 'A method for the reconstruction of four-dimensional synchronized CT scans acquired during free breathing.' *Med. Phys.* **30**, 1254–1263.

REFERENCES

- Luchin, Y. I., Vatnitsky, S. M., Miller, D. W., Kostyuchenko, V. I., Nichiporov, D. F., Slater, J. D. and Slater, J. M. (2000) 'The use of radiochromic film in treatment verification of proton radiosurgery.' *J. Radiosurg.* **3**, 69–75.
- Lyman, J. (1985) 'Complication probability as assessed from dose-volume histograms.' *Radiat. Res.* **104**, S13–S19.
- Maccabee, H. D., Madhvanath, U. and Raju, M. R. (1969) 'Tissue activation studies with alpha-particle beams.' *Phys. Med. Biol.* **14**, 213–224.
- Mageras, G. S., Kutcher, G. J., Leibel, S. A., Zelefsky, M. J., Melian, E., Mohan, R. and Fuks, Z. (1996) 'A method of incorporating organ motion uncertainties into three-dimensional conformal treatment plans.' *Int. J. Radiat. Oncol. Biol. Phys.* **35**, 333–342.
- Mah, D., Hanley, J., Rosenzweig, K. E., Yorke, E., Braban, L., Ling, C. C., Leibel, S. A. and Mageras, G. (2000) 'Technical aspects of the deep inspirational breath-hold technique in the treatment of thoracic cancer.' *Int. J. Radiat. Oncol. Biol. Phys.* **48**, 1175–1185.
- Martin, R. L. (1987) 'A proton accelerator for medical applications.' *Nucl. Instrum. Meth. Phys. Res.* **B24/25**, 1087–1091.
- Martinez-Monge, R., Fernandes, P. S., Gupta, N. and Gahbauer, R. (1999) 'Cross-sectional nodal atlas: a tool for the definition of clinical target volumes in three-dimensional radiation therapy planning.' *Radiol.* **211**, 815–828.
- Maruhashi, A. (1977) 'Characteristics of a miniature dosimeter developed for measurement of electrons.' *Nucl. Instrum. Meth.* **141**, 87–92.
- Maryanski, M. J., Schulz, R. J., Ibbott, G. S., Gatenby, J. C., Xie, J., Horton, D. and Gore, J. C. (1994) 'Magnetic resonance imaging of radiation dose distributions using a polymer-gel dosimeter.' *Phys. Med. Biol.* **39**, 1437–1455.
- Matsumura, S., Jikko, A., Ozeki, S., Tang, J. T., Fukushima, S., Yamazaki, H., Inoue, T., Hatanaka, K., Inoue, T. and Fuchihata, H. (1999) 'Differences in the biological effects of in vitro irradiation by 65 MeV protons and 137 cesium gamma-rays.' *Anticancer Res.* **19**, 477–480.
- McDonald, J. C. (1987) 'Calorimetric measurement of the carbon kerma factor for 14.6 MeV neutrons.' *Radiat. Res.* **109**, 28–35.
- McDonald, J. C. and Goodman, L. J. (1982) 'Measurements of the thermal defect of A-150 plastic (tissue-equivalent plastic).' *Phys. Med. Biol.* **27**, 229–233.
- McDonald, J. C. and Domen, S. R. (1986) 'A-150 plastic radiometric calorimeter for charged particles and other radiations.' *Nucl. Instrum. Methods. Phys. Res.* **A252**, 35–40.
- McDonald, J. C., Laughlin, J. S. and Freeman, R. E. (1976) 'Portable tissue equivalent calorimeter.' *Med. Phys.* **3**, 80–86.
- McEwen, M. R. and Duane, S. (2000) 'A portable calorimeter for measuring absorbed dose in the radiotherapy clinic.' *Phys. Med. Biol.* **45**, 3675–3691.
- McKenzie, A. L. (2000) 'How should breathing motion be combined with other errors when drawing margins around clinical target volumes?' *Br. J. Radiol.* **73**, 973–977.
- McShan, D., Lynn, K., Vineberg, K. and Fraass, B. (2002) 'Radiotherapy plan optimization accounting for set-up and motion uncertainty using a multiple instance geometry approximation.' *Med. Phys.* **29**, 1257 (abstract).
- Medin, J. (1997) *Studies of Clinical Proton Dosimetry Using Monte Carlo Simulation and Experimental Techniques*, Doctoral Dissertation (Department of Medical Radiation Physics, University of Stockholm).
- Medin, J. and Andreo, P. (1992) 'Stopping powers for the ion-chamber dosimetry of radiotherapeutic heavy-particle beams.' *Nucl. Instrum. Methods. Phys. Res.* **B69**, 64–75.
- Medin, J. and Andreo, P. (1997a) *PETRA: A Monte Carlo Code for the Simulation of Proton and Electron Transport in Water*, Report MSF 1997–01 (Department of Medical Radiation Physics, University of Stockholm).
- Medin, J. and Andreo, P. (1997b) 'Monte Carlo calculated stopping-power ratios water/air for clinical proton dosimetry (50–250 MeV).' *Phys. Med. Biol.* **42**, 89–105.
- Medin, J., Andreo, P., Grusell, E., Mattsson, O., Montelius, A. and Roos, M. (1995) 'Ionization chamber dosimetry of proton beams using cylindrical and plane parallel chambers. N_w versus N_K ion chamber calibrations.' *Phys. Med. Biol.* **40**, 1161–1176.
- Medin, J., Andreo, P. and Vynckier, S. (2000) 'Comparison of dosimetry recommendations for clinical proton beams.' *Phys. Med. Biol.* **45**, 3195–3211.
- Medin, J., Ross, C. K., Klassen, N. V., Grusell, E. and Grindborg, J.-E. (2005) 'Comparison between water calorimetry and ionization chamber dosimetry in two photon beam qualities and a clinical proton beam.' *Biomed. Tech* **50** (Suppl. 1), 760–761.
- Medin, J., Ross, C. K., Klassen, N. V., Palmans, H., Grusell, E. and Grindborg, J.-E. (2006) 'Experimental determination of beam quality factors, k_Q , for two types of Farmer chamber in a 10 MV photon and a 175 MeV proton beam.' *Phys. Med. Biol.* **51**, 1503–1521.
- Meer, D., Pedroni, E., Bula, C., Hilbes, C. and Zenklusen, S. (2007) 'Progress on advanced scanning in the Gantry 2 test area,' in *PSI Scientific Report 2006*, (Paul Scherrer Institute: Villigen, Switzerland) pp. 5–6.
- Méndez Romero, A., Wunderink, W., Hussain, S. M., De Pooter, J. A., Heijmen, B. J., Nowak, P. C., Nuyttens, J. J., Brandwijk, R. P., Verhoef, C., Ijzermans, J. N. and Levendag, P. C. (2006) 'Stereotactic body radiation therapy for primary and metastatic liver tumors: A single institution phase i-ii study.' *Acta Oncol.* **45**, 831–837.
- Menzel, H. G., Pihet, P. and Wambersie, A. (1990) 'Microdosimetric specification of radiation quality in

- neutron radiation therapy.' *Int. J. Radiat. Biol.* **57**, 865–883.
- Mesoloras, G., Sandison, G. A., Stewart, R. D., Farr, J. B. and Hsi, W. C. (2006) 'Neutron scattered dose equivalent to a fetus from proton radiotherapy of the mother.' *Med. Phys.* **33**, 2479–2490.
- Mijnheer, B. J. and Williams, J. R. (1985) 'Comments on dry air or humid air values for physical parameters used in the AAPM protocol for photon and electron dosimetry.' *Med. Phys.* **12**, 656–658.
- Mijnheer, B. J., Battermann, J. J. and Wambersie, A. (1987a) 'What degree of accuracy is required and can be achieved in photon and neutron therapy?' *Radiother. Oncol.* **8**, 237–252.
- Mijnheer, B. J., Wootton, P., Williams, J. R., Eenmaa, J. and Parnell, C. J. (1987b) 'Uniformity in dosimetry protocols for therapeutic applications of fast neutron beams.' *Med. Phys.* **14**, 1020–1026.
- Miller, D. W. (1995) 'A review of proton beam radiation therapy.' *Med. Phys.* **22**, 1943–1954.
- Miller, D., Moyers, M. and Vatnitsky, S. (1999) 'QA and commissioning of treatment planning system for radiotherapy with heavy-charged particles.' *Radiother. Oncol.* **51** (Suppl. 1), S3 (abstract).
- Minohara, S., Kanai, T., Endo, M., Noda, K. and Kanazawa, M. (2000) 'Respiratory gated irradiation system for heavy-ion radiotherapy.' *Int. J. Radiat. Oncol. Biol. Phys.* **47**, 1097–1103.
- Miralbell, R., Lomax, A., Cella, L. and Schneider, U. (2002) 'Potential reduction of the incidence of radiation-induced second cancers by using proton beams in the treatment of pediatric tumors.' *Int. J. Radiat. Oncol. Biol. Phys.* **54**, 824–829.
- Mobit, P. N., Sandison, G. A. and Bloch, C. (2000) 'Depth ionization curves for an unmodulated proton beam measured with different ionization chambers.' *Med. Phys.* **27**, 2780–2787.
- Mock, U., Georg, D., Bogner, J., Auberger, T. and Pötter, R. (2004) 'Treatment planning comparison of conventional, 3D conformal, and intensity-modulated photon (IMRT) and proton therapy for paranasal sinus carcinoma.' *Int. J. Radiat. Oncol. Biol. Phys.* **58**, 147–154.
- Moyers, M. F. (1999) 'Proton therapy,' pp. 823–869 in *The Modern Technology of Radiation Oncology*, Van Dyk, J. Ed. (Medical Physics Publishing: Madison, WI).
- Moyers, M. F. and Lesyna, W. (2004) 'Isocenter characteristics of an external ring proton gantry.' *Int. J. Radiat. Oncol. Biol. Phys.* **60**, 1622–1630.
- Moyers, M. F., Vatnitsky, S. M., Miller, D. W. and Slater, J. M. (2000) 'Determination of the air *w*-value in proton beams using ionization chambers with gas flow capability.' *Med. Phys.* **27**, 2363–2368.
- Müller, J. W. (2000a) *Weighted Medians*, Report BIPM-2000/6 (Bureau International des Poids et Mesures, Sèvres).
- Müller, J. W. (2000b) 'Possible advantages of a robust evaluation of comparisons.' *Res. Natl. Inst. Stand. Technol.* **105**, 551–555.
- Munzenrider, J. E. (1999) 'Proton therapy for uveal melanoma and other eye lesions.' *Strahlenther. Onkol.* **175** (Suppl. II), 68–73.
- Munzenrider, J. E., Shipley, W. U. and Verhey, L. J. (1981) 'Future prospects of radiation therapy with protons.' *Semin. Oncol.* **8**, 110–124.
- Mustafa, A. A. M. and Jackson, D. F. (1981) 'Small-angle multiple scattering and spatial resolution in charged particle tomography.' *Phys. Med. Biol.* **26**, 461–472.
- Myers, I. T. (1968) 'Ionization,' pp. 317–330 in *Radiation Dosimetry*, Vol. 1, Attix, F. H., Roesch, W. and Tochilin, E. Eds. (Academic Press: New York).
- Nahum, A. E. and Glimelius, B. (2001) 'Biological models applied to the comparison of proton and photon treatments.' *Phys. Med.* **XV11**, 126–130.
- Nahum, A. E. and Sanchez-Nieto, B. (2001) 'Tumor control probability modelling: Basic principles and applications in treatment planning.' *Phys. Med.* **XV11**, 13–23.
- Nahum, A. E., Dearnaley, D. P. and Steel, G. G. (1994) 'Prospects for proton-beam radiotherapy.' *Eur. J. Cancer* **30A**, 1577–1583.
- Nath, R. and Schulz, R. J. (1981) 'Calculated response and wall correction factors for ionization chambers exposed to ⁶⁰Co gamma-rays.' *Med. Phys.* **8**, 85–93.
- Nauraye, C., Mazal, A., Delacroix, S., Bridier, A., Chavaudra, J. and Rosenwald, J.-C. (1995) 'An experimental approach to the design of a scattering system for a proton therapy beam line dedicated to ophthalmological applications.' *Int. J. Radiat. Oncol. Biol. Phys.* **32**, 1177–1183.
- Nemoto, K., Pickles, T., Minchinton, A. I. and Lam, G. K. (1998) 'The relative biological effectiveness of the modulated proton beam at TRIUMF.' *Radiat. Med.* **16**, 43–46.
- Newhauser, W. D., Burns, J. and Smith, A. R. (2002a). 'Dosimetry for ocular proton beam therapy at the Harvard Cyclotron Laboratory based on the ICRU Report 59.' *Med. Phys.* **29**, 1953–1961.
- Newhauser, W. D., Myers, K. D., Rosenthal, S. J. and Smith, A. R. (2002b). 'Proton beam dosimetry for radiosurgery: Implementation of the ICRU Report 59 at the Harvard Cyclotron Laboratory.' *Phys. Med. Biol.* **47**, 1369–1389.
- Newhauser, W. D., Koch, N., Hummel, S., Ziegler, M. and Titt, U. (2005) 'Monte Carlo simulations of a nozzle for the treatment of ocular tumours with high-energy proton beams.' *Phys. Med. Biol.* **50**, 5229–5249.
- Niatel, M. T. (1969) 'Étude expérimentale de l'influence de la vapeur d'eau sur l'ionisation produite dans l'air.' *C. R. Acad. Sci. Paris* **B268**, 1650–1653.
- Niatel, M. T., Perroche-Roux, A. M. and Boutilhon, M. (1985) 'Two determinations of *W* for electrons in dry air.' *Phys. Med. Biol.* **30**, 67–75.
- Nichiporov, D. (2003) 'Verification of absolute ionization chamber dosimetry in a proton beam using carbon activation measurements.' *Med. Phys.* **30**, 972–978.
- Nichiporov, D., Kostjuchenko, V., Puhl, J. M., Bensen, D. L., Desrosiers, M. F., Dick, C. E., McLaughlin, W. L., Kojima, T., Coursey, B. M. and Zink, S. (1995) 'Investigation of applicability of alanine and'

REFERENCES

- radiochromic detectors to dosimetry of proton clinical beams.' *Appl. Radiat. Isot.* **46**, 1355–1362.
- Nichiporov, D., Luckjashin, V. and Kostjuchenko, V. (2004) 'Measurement of the activity of ^{11}C and ^{22}Na sources using 4π - β - γ coincidence system.' *Appl. Radiat. Isot.* **60**, 703–716.
- Nieder, J. A. and Mead, R. (1965) 'A simplex method for function minimization.' *Comp. J.* **7**, 308–313.
- Niemierko, A. (1997) 'Reporting and analyzing dose distributions: A concept of equivalent uniform dose.' *Med. Phys.* **24**, 103–110.
- Niemierko, A. and Goitein, M. (1993) 'Implementation of a model for estimating tumor control probability for an inhomogeneously irradiated tumor.' *Radiother. Oncol.* **29**, 140–147.
- Niemierko, A. and Goitein, M. (1994) 'Dose-volume distributions: A new approach to dose-volume histograms in three-dimensional treatment planning.' *Med. Phys.* **21**, 3–11.
- Niroomand-Rad, A., Blackwell, C. R., Coursey, B. M., Gall, K. P., Galvin, J. M., McLaughlin, W. L., Meigooni, A. S., Nath, R., Rodgers, J. E. and Soares, C. G. (1998) 'Radiochromic film dosimetry: Recommendations of AAPM Radiation Therapy Committee Task Group 55.' *Med. Phys.* **25**, 2093–2115.
- Nishio, T., Sato, T., Kitamura, H., Murakami, K. and Ogino, T. (2005) 'Distributions of β^+ decayed nuclei generated in the CH_2 and H_2O targets by target nuclear fragment reaction using therapeutic MONO and SOBP proton beams.' *Med. Phys.* **32**, 1070–1082.
- Noel, G., Ferrand, R., Feuvert, L., Boissarie, G., Meyroneinc, S. and Mazeron, J. J. (2003) 'Automatization and robotics of the set-up and treatment of patients irradiated for brain and base of the skull tumors.' *Cancer Radiother.* **7** (Suppl. 1), 33s–41s.
- Noel, G., Feuvert, L., Ferrand, R., Boissarie, G., Mazeron, J. J. and Habrand, J. L. (2004) 'Radiotherapeutic factors in the management of cervical-basal chordomas and chondrosarcomas.' *Neurosurgery* **55** 1252–1262.
- Noel, G., Feuvert, L., Calugaru, V., Dhermain, F., Mammar, H., Haie-Meder, C., Ponvert, D., Hasboun, D., Ferrand, R., Nauraye, C., Boissarie, G., Beaudre, A., Gaboriaud, G., Mazal, A., Habrand, J. L. and Mazeron, J. J. (2005) 'Chordomas of the base of the skull and upper cervical spine. One hundred patients irradiated by a 3D conformal technique combining photon and proton beams.' *Acta Oncol.* **44**, 700–708.
- Nohtomi, A., Sakae, T., Tsunashima, Y. and Kohno, R. (2001) 'Dosimetry of pulsed clinical proton beams by a small ionization chamber.' *Med. Phys.* **28**, 1431–1435.
- Oelfke, U. and Bortfeld, T. (2001) 'Inverse planning for photon and proton beams.' *Med. Dosim.* **26**, 113–124.
- Ohara, K., Okumura, T., Akisada, M., Inada, T., Mori, T., Yokota, H. and Calaguas, M. J. (1989) 'Irradiation synchronized with respiration gating.' *Int. J. Radiat. Oncol. Biol. Phys.* **17**, 853–857.
- Onori, S., d'Errico, F., De Angelis, C., Egger, E., Fattibene, P. and Janovsky, I. (1997) 'Alanine dosimetry of proton therapy beams.' *Med. Phys.* **24**, 447–453.
- Onori, S., De Angelis, C., Fattibene, P., Pacilio, M., Petetti, E., Azario, L., Miceli, R., Piermattei, A., Barone Tonghi, L., Cuttone, G. and Lo Nigro, S. (2000) 'Dosimetric characterization of silicon and diamond detectors in low-energy proton beams.' *Phys. Med. Biol.* **45**, 3045–3058.
- Ozzeer, R., Mazal, A., Rosenwald, J. C., Belshi, R., Nauraye, C., Ferrand, R. and Biensan, S. (1997) 'A model for the lateral penumbra in water of a 200-MeV proton beam devoted to clinical applications.' *Med. Phys.* **24**, 1599–1604.
- Pacilio, M., De Angelis, C., Onori, S., Azario, L., Fidanzio, A., Miceli, R., Piermattei, A. and Kacperek, A. (2002) 'Characteristics of silicon and diamond detectors in a 60 MeV proton beam.' *Phys. Med. Biol.* **47**, N107–N112.
- Paganetti, H. (1998) 'Monte Carlo method to study the proton fluence for treatment planning.' *Med. Phys.* **25**, 2370–2375.
- Paganetti, H. (2002) 'Nuclear interactions in proton therapy: Dose and relative biological effect distributions originating from primary and secondary particles.' *Phys. Med. Biol.* **47**, 747–764.
- Paganetti, H. and Goitein, M. (2000) 'Radiobiological significance of beam line dependent proton energy distributions in a spread-out Bragg peak.' *Med. Phys.* **27**, 1119–1126.
- Paganetti, H. and Gottschalk, B. (2003) 'Test of GEANT3 and GEANT4 nuclear models for 160 MeV protons stopping in CH_2 .' *Med. Phys.* **30**, 1926–1931.
- Paganetti, H., Niemierko, A., Ancukiewicz, M., Gerweck, L. E., Goitein, M., Loeffler, J. S. and Suit, H. D. (2002) 'Relative biological effectiveness (RBE) values for proton therapy.' *Int. J. Radiat. Oncol. Biol. Phys.* **53**, 407–421.
- Paganetti, H., Jiang, H., Lee, S.-Y. and Kooy, H. M. (2004) 'Accurate Monte Carlo simulations for nozzle design, commissioning and quality assurance for a proton radiation therapy facility.' *Med. Phys.* **31**, 2107–2118.
- Paganetti, H., Jiang, H. and Trofimov, A. (2005) '4D Monte Carlo simulation of proton beam scanning: Modeling of variations in time and space to study the interplay between scanning pattern and time-dependent patient geometry.' *Phys. Med. Biol.* **50**, 983–990.
- Palmans, H. (2003) 'Effect of alanine energy response and phantom material on depth dose measurements in ocular proton beams.' *Technol. Cancer Res. Treatment* **2**, 579–586.
- Palmans, H. and Verhaegen, F. (1997) 'Calculated depth dose distributions for proton beams in some low-Z materials.' *Phys. Med. Biol.* **42**, 1175–1183.
- Palmans, H. and Verhaegen, F. (1998) 'Monte Carlo study of fluence perturbation effects on cavity dose response in clinical proton beams.' *Phys. Med. Biol.* **43**, 65–89.
- Palmans, H. and Vynckier, S. (2002) 'Reference dosimetry for clinical proton beams,' pp. 157–194 in *Recent Developments in Accurate Radiation Dosimetry*,

- Seuntjens, J. and Mobit, P. N. Eds. (Medical Physics Publishing: Madison, WI).
- Palmans, H., Seuntjens, J., Verhaegen, F., Denis, J.-M., Vynckier, S. and Thierens, H. (1996) 'Water calorimetry and ionization chamber dosimetry in an 85-MeV clinical proton beam.' *Med. Phys.* **23**, 643–650.
- Palmans, H., Verhaegen, F., Denis, J.-M., Vynckier, S. and Thierens, H. (1999) 'Experimental study of perturbation correction factors for ionization chambers in a 75 MeV clinical proton beam.' *Radiother. Oncol.* **51** Suppl. 1, S39 (abstract).
- Palmans, H., Verhaegen, F., Denis, J.-M., Vynckier, S. and Thierens, H. (2001) 'Experimental p_{wall} and p_{cel} correction factors for ionization chambers in low-energy clinical proton beams.' *Phys. Med. Biol.* **46**, 1187–1204.
- Palmans, H., Verhaegen, F., Denis, J.-M. and Vynckier, S. (2002a). 'Dosimetry using plane-parallel ionization chambers in a 75 MeV clinical proton beam.' *Phys. Med. Biol.* **47**, 2895–2905.
- Palmans, H., Symons, J. E., Denis, J.-M., de Kock, E. A., Jones, D. T. L. and Vynckier, S. (2002b) 'Fluence correction factors in plastic phantoms for clinical proton beams.' *Phys. Med. Biol.* **47**, 3055–3071.
- Palmans, H., Thomas, R., Simon, M., Duane, S., Kacperek, A., DuSautoy, A. and Verhaegen, F. (2004) 'A small-body portable graphite calorimeter for dosimetry in low-energy clinical proton beams.' *Phys. Med. Biol.* **49**, 3737–3749.
- Palmans, H., Thomas, R. and Kacperek, A. (2006) 'Ion recombination correction in the Clatterbridge Centre of Oncology clinical proton beam.' *Med. Phys.* **21**, 3–11.
- Pan, T., Lee, T. Y., Rietzel, E. and Chen, G. T. Y. (2004) '4D-CT imaging of a volume influenced by respiratory motion on multi-slice CT.' *Med. Phys.* **31**, 333–340.
- Parodi, K. and Enghardt, W. (2000) 'Potential application of PET in quality assurance of proton therapy.' *Phys. Med. Biol.* **45**, N151–N156.
- Parodi, K., Enghardt, W. and Haberer, T. (2002) 'In-beam PET measurements of β^+ -radioactivity induced by proton beams.' *Phys. Med. Biol.* **47**, 21–36.
- Parodi, K., Ferrari, A., Sommerer, F. and Paganetti, H. (2007a) 'Clinical CT-based calculations and positron emitter distributions in proton therapy using the FLUKA Monte Carlo code.' *Phys. Med. Biol.* **52**, 3369–3387.
- Parodi, K., Paganetti, H., Cascio, E., Flanz, J., Bonab, A., Alpert, N., Lohmann, K. and Bortfeld, T. (2007b) 'PET/CT imaging for treatment verification after proton therapy—a study with plastic phantoms and metallic implants.' *Med. Phys.* **34**, 419–435.
- Parodi, K., Paganetti, H., Loeffler, J. S., DeLaney, T. F., Liebsch, N. J., Munzenrider, J., Fischman, A. J., Knopf, A. and Bortfeld, T. (2007c) 'Patient study of *in vivo* verification of beam delivery and range, using positron emission tomography and computed tomography imaging after proton therapy.' *Int. J. Radiat. Oncol. Biol. Phys.* **68**, 920–934.
- Pedroni, E., Bacher, R., Blattmann, H., Böhringer, T., Coray, A., Egger, E., Phillips, M. and Scheib, S. (1990) 'The 200 MeV proton therapy project at PSI: A status report,' pp. 1–8 in *Proc. Int. Heavy Particle Therapy Workshop (PTCOG/EORTC/ECNEU)*, Blattmann, H. Ed. PSI-Bericht Nr. 69 (Paul Scherrer Institute: Villigen, Switzerland).
- Pedroni, E., Bacher, R., Blattmann, H., Böhringer, T., Coray, A., Lomax, A., Lin, S., Munkel, G., Scheib, S., Schneider, U. and Tourovsky, A. (1995) 'The 200-MeV proton therapy project at the Paul Scherrer Institute: Conceptual design and practical realization.' *Med. Phys.* **22**, 37–53.
- Pedroni, E., Bearpark, R., Böhringer, T., Coray, A., Duppich, J., Forss, S., Gearge, D., Grossman, M., Goitein, G., Hilbes, C., Jermann, M., Lin, S., Lomax, A., Negrazus, M., Schippers, M. and Kotle, G. (2004) 'The PSI gantry 2: a second generation proton scanning gantry.' *Z. Med. Phys.* **14**, 25–34.
- Pedroni, E., Scheib, S., Böhringer, T., Coray, A., Grossmann, M., Lin, S. and Lomax, A. (2005) 'Experimental characterization and physical modelling of the dose distribution of scanned proton pencil beams.' *Phys. Med. Biol.* **50**, 541–561.
- Petti, P. L. (1992) 'Differential-pencil-beam dose calculations for charged particles.' *Med. Phys.* **19**, 137–149.
- Petti, P. L. (1996) 'Evaluation of a pencil-beam dose calculation technique for charged particle radiotherapy.' *Int. J. Radiat. Oncol. Biol. Phys.* **35**, 1049–1057.
- Petti, P. L. (1997) 'New compensator design options for charged-particle radiotherapy.' *Phys. Med. Biol.*, **42**, 1289–1300.
- Petti, P. L. and Lennox, A. J. (1994) 'Hadronic radiotherapy.' *Ann. Rev. Nucl. Part. Sci.* **44**, 155–197.
- Phillips, M. H., Pedroni, E., Blattmann, H., Böhringer, T., Coray, A. and Scheib, S. (1992) 'Effects of respiratory motion on dose uniformity with a charged particle scanning method.' *Phys. Med. Biol.* **37**, 223–233.
- Piermattei, A., Miceli, R., Azario, L., Fidanzio, A., delle Canne, S., de Angelis, C., Onori, S., Pacilio, M., Petetti, E., Raffaele, L. and Sabini, M. G. (2000) 'Radiochromic film dosimetry of a low energy proton beam.' *Med. Phys.* **27**, 1655–1660.
- Podgorsak, M. B. and Schreiner, L. J. (1992) 'Nuclear magnetic relaxation characterization of irradiated Fricke solution.' *Med. Phys.* **19**, 87–95.
- Polf, J. C. and Newhauser, W. D. (2005) 'Calculations of neutron dose equivalent exposures from range-modulated proton therapy beams.' *Phys. Med. Biol.* **50**, 3859–3873.
- Polf, J. C., Newhauser, W. D. and Titt, U. (2005) 'Patient neutron dose equivalent exposures outside of the proton therapy treatment field.' *Radiat. Prot. Dosim.* **115**, 154–158.
- Pommier, P., Liebsch, N. J., Deschler, D. G., Lin, D. T., McIntyre, J. F., Barker, F. G., II, Adams, J. A., Lopes, V. V., Varvares, M., Loeffler, J. S. and Chan, A. W. (2006) 'Proton beam radiation therapy for skull base adenoid cystic carcinoma.' *Arch. Otolaryngol. Head Neck Surg.* **132**, 1242–1249.
- Rabin, M. S. W. (1987) 'Skin/tumor dose ratio as a function of source to isocenter distance for a 250 MeV

REFERENCES

- proton beam.' *Proton Therapy Co-Operative Group Meeting, Boston, MA.*
- Raju, M. R. (1966) 'The use of the miniature silicon diode as a radiation dosimeter.' *Phys. Med. Biol.* **11**, 371–376.
- Raju, M. R. (1980) *Heavy Particle Radiotherapy* (Academic Press, Inc.: New York).
- Raju, M. R. (1994) 'Hadrontherapy in a historical and international perspective,' pp. 67–79 in *Hadrontherapy in Oncology*, Amaldi, U. and Larsson, B. Eds. (Elsevier Science B. V.: Amsterdam).
- Raju, M. R. (1995a) 'The history of ion beam therapy,' pp. 3–32 in *Ion Beams in Tumor Therapy*, Linz, U. Ed (Chapman and Hall, Weinheim, Germany).
- Raju, M. R. (1995b) 'Proton radiobiology, radiosurgery and radiotherapy.' *Int. J. Radiat. Biol.* **67**, 237–259.
- Raju, M. R. (1996) 'Particle radiotherapy: historical developments and current status.' *Radiat. Res.* **145**, 391–407.
- Raju, M. R., Bain, E., Carpenter, S. G., Cox, R. A. and Robertson, J. B. (1978) 'A heavy particle comparative study. Part II: Cell survival versus depth.' *Br. J. Radiol.* **51**, 704–711.
- Ramm, U., Weber, U., Bock, M., Krämer, M., Bankamp, A., Damrau, M., Thilmann, C., Böttcher, H. D., Schad, L. R. and Kraft, G. (2000) 'Three-dimensional BANG™ gel dosimetry in conformal carbon ion radiotherapy.' *Phys. Med. Biol.* **45**, N95–N102.
- Regulla, D. F. and Deffner, U. (1982) 'Dosimetry by ESR spectroscopy of alanine.' *Int. J. Appl. Radiat. Isot.* **33**, 1101–1114.
- Renner, T. R., Chu, W. T., Ludewigt, B., Nyman, M. A. and Stradtner, R. (1989) 'Multisegmented ionization chamber dosimetry system for light ion beams.' *Nucl. Instr. Meth. Phys. Res. A* **281**, 640–648.
- Rexed, B., Mair, W., Sourander, P., Larsson, B. and Leksell, L. (1960) 'Effect of high energy protons on the brain of the rabbit.' *Acta Radiol.* **53**, 289–299.
- Rikner, G. (1983) *Silicon diodes as detectors in relative dosimetry of photon, electron and proton radiation fields*, PhD Dissertation (Uppsala University, Sweden).
- Rikner, G. (1985) 'Characteristics of a p-Si detector in high energy electron fields.' *Acta Radiol. Oncol.* **24**, 71–74.
- Rikner, G. and Grusell, E. (1987) 'General specifications for silicon semiconductors for use in radiation dosimetry.' *Phys. Med. Biol.* **32**, 1109–1117.
- Robertson, J. B., Williams, J. R., Schmidt, R. A., Little, J. B., Flynn, D. F. and Suit, H. D. (1975) 'Radiobiological studies of a high-energy modulated proton beam utilizing cultured mammalian cells.' *Cancer* **35**, 1664–1677.
- Roeske, J. C., Forman, J. D., Mesina, C. F., He, T., Pelizzari, C. A., Fontenla, E., Vijayakumar, S. and Chen, G. T. Y. (1995) 'Evaluation of changes in the size and location of the prostate, seminal vesicles, bladder, and rectum during a course of external beam radiation therapy.' *Int. J. Radiat. Oncol. Biol. Phys.* **33**, 1321–1329.
- Rogers, D. W. O. (1992) 'The advantages of absorbed-dose calibration factors.' *Med. Phys.* **19**, 1227–1239.
- Rogers, D. W. O. and Ross, C. K. (1988) 'The role of humidity and other correction factors in the AAPM TG-21 dosimetry protocol.' *Med. Phys.* **15**, 40–48.
- Rosenberg, A. E., Nielsen, G. P., Keel, S. B., Renard, L. G., Fitzek, M. M., Munzenrider, J. E. and Liebsch, N. J. (1999) 'Chondrosarcoma of the base of the skull: a clinicopathological study of 200 cases with emphasis on its distinction from chordoma.' *Am. J. Surg. Pathol.* **23**, 1370–1378.
- Ross, C. K. and Klassen, N. V. (1996) 'Water calorimetry for radiation dosimetry.' *Phys. Med. Biol.* **41**, 1–29.
- Ross, C. K., Klaasen, N. V., Shortt, K. R. and Smith, G. D. (1989) 'A direct comparison of water calorimetry and Fricke dosimetry.' *Phys. Med. Biol.* **34**, 23–42.
- Rosser, K. E. (1994) 'An ice calorimeter for photon dosimetry.' *Phys. Med. Biol.* **39**, 293–298.
- Roy, S. C. and Sandison, G. A. (2004) 'Scattered neutron dose equivalent to a fetus from proton therapy of the mother.' *Radiat. Phys. Chem.* **71**, 997–998.
- Rutz, H-P. and Lomax, A. (2005) 'Donut-shaped high-dose configuration for proton beam radiation therapy.' *Strahlenther. Onkol.* **181**, 49–53.
- Ryneveld, S. (1998) *Measurement of Proton Beam Dose Profiles Using a Sensitive Scintillation Screen Observed with a CCD Camera*, Master of Science thesis (Department of Physics, The University of British Columbia, Vancouver, Canada).
- Säbel, M., Schmidt, Th. and Pauly, H. (1973) 'Heat defect of low energy x-rays absorbed in carbon and various plastics.' *Health Phys.* **25**, 519–521.
- Safai, S., Lin, S. and Pedroni, E. (2004) 'Development of an inorganic scintillating mixture for proton beam verification dosimetry.' *Phys. Med. Biol.* **49**, 4637–4655.
- Sankar, A., Ayyangar, K., Nehru, R., Gopalakrishna Kurup, P., Murai, E., Enke, C. and Velmurugan, J. (2006) 'Comparison of Kodak EDR2 and GafChromic EBT film for intensity-modulated radiation therapy dose distribution verification.' *Med. Dosim.* **31**, 273–282.
- Sauli, F. (1977) *Principles of Operation of Multiwire Proportional and Drift Chambers*, CERN Report 77–09 (CERN, Geneva, Switzerland).
- Sauli, F. (1992) 'Applications of gaseous detectors in astrophysics, medicine and biology.' *Nucl. Instrum. Meth. Phys. Res. A* **323**, 1–11.
- Schaffner, B. and Pedroni, E. (1998) 'The precision of proton range calculations in proton radiotherapy treatment planning: experimental verification of the relation between CT-HU and proton stopping power.' *Phys. Med. Biol.* **43**, 1579–1592.
- Scheib, S. and Pedroni, E. (1992) 'Dose calculations and optimization for 3D conformal voxel scanning.' *Radiat. Environ. Biophys.* **31**, 251–256.
- Schneider, U. and Pedroni, E. (1995) 'Proton radiography as a tool for quality control in proton therapy.' *Med. Phys.* **22**, 353–363.
- Schneider, U., Pedroni, E. and Lomax, A. (1996) 'The calibration of CT Hounsfield units for radiotherapy treatment planning.' *Phys. Med. Biol.* **41**, 111–124.
- Schneider, U., Pemler, P., Besserer, J., Dellert, M., Moosburger, M., de Boer, J., Pedroni, E. and

- Boehringer, T. (2002a) 'The water equivalence of solid materials used for dosimetry with small proton beams.' *Med. Phys.* **29**, 2946–2951.
- Schneider, U., Agosteo, S., Pedroni, E. and Besserer, J. (2002b) 'Secondary neutron dose during proton therapy using spot scanning.' *Int. J. Radiat. Oncol. Biol. Phys.* **53**, 244–251.
- Schneider, U., Pemler, P., Besserer, J., Pedroni, E., Lomax, A. and Kaser-Hotz, B. (2005) 'Patient specific optimization of the relation between CT-Hounsfield units and proton stopping powers with proton radiography.' *Med. Phys.* **32**, 195–199.
- Schreuder, A. N. (2002) *Proton Therapy Operations and Treatment Procedure Manual*. Internal Report (iThemba LABS, Somerset West, South Africa).
- Schreuder, A. N. (2004) 'The MPRI robotic patient positioner,' in *Particles 34, Abstracts of the 40th Proton Therapy Co-Operative Group Meeting, Paris, France*.
- Schreuder, A. N., Jones, D. T. L. and Kiefer, A. (1997) 'A small ionization chamber for dose distribution measurements in a clinical proton beam,' pp. 284–289 in *Advances in Hadrontherapy*, Amaldi, U., Larsson, B. and Lemoigne, Y. Eds (Elsevier Science B. V: Amsterdam).
- Schreuder, A. N., Mazal, A., Nauraye, C., Delacroix, S., Bridier, A., Gall, K., Wagner, M. and Beatty, J. (1994) 'Proton dosimetry intercomparisons at CPO, France and HCL, USA,' pp. 95–97 in *National Accelerator Centre Annual Report, NAC/AR/94-01* (National Accelerator Centre: Faure, South Africa).
- Schreuder, A. N., Tourovsky, A., Kiefer, A. and van der Merwe, J. (2001) 'The development of a multi-layer Faraday cup to characterize the NAC proton therapy beam,' in *NAC Annual Report, March 2001*.http://www4.tlabs.ac.za/annualreport/development_of_a_multi.htm.
- Schulte, R. W., Fargo, R. A., Meinass, H. J., Slater, J. D. and Slater, J. M. (2000) 'Analysis of head motion prior to and during proton beam therapy.' *Int. J. Radiat. Oncol. Biol. Phys.* **47**, 1105–1110.
- Schultheiss, T. E., Orton, C. G. and Peck, R. A. (1983) 'Models in radiotherapy: Volume effects.' *Med. Phys.* **10**, 410–415.
- Schulz, R. J., Almond, P. R., Kutcher, G., Loevinger, R., Nath, R., Rogers, D. W. O., Suntharalingam, N., Wright, K. A. and Kahn, F. M. (1986) 'Clarification of the AAPM Task Group 21 protocol.' *Med. Phys.* **13**, 755–759.
- Schulz, R. J., Wuu, C. S. and Weinhous, M. S. (1987) 'The direct determination of dose-to-water using a water calorimeter.' *Med. Phys.* **14**, 790–796.
- Schulz, R. J., Venkataraman, N. and Huq, M. S. (1990) 'The thermal defect of A-150 plastic and graphite for low-energy protons.' *Phys. Med. Biol.* **35**, 1563–1574.
- Schulz, R. J., Huq, M. S., Venkataraman, N. and Motakabir, K. A. (1991) 'A comparison of ionization-chamber and water-calorimeter dosimetry for high-energy x rays.' *Med. Phys.* **18**, 1229–1233.
- Schulz, R. J., Verhey, L. J., Huq, M. S. and Venkataraman, N. (1992) 'Water calorimeter dosimetry for 160 MeV protons.' *Phys. Med. Biol.* **37**, 947–953.
- Schweikard, A., Shiomi, H. and Adler, J. (2004) 'Respiration tracking in radiosurgery.' *Med. Phys.* **31**, 2738–2741.
- Seltzer, S. M. (1993) *An Assessment of the Role of Charged Secondaries from Nonelastic Nuclear Interactions by Therapy Proton Beams in Water*, NISTIR 5221 (National Institute of Standards and Technology, Gaithersburg, MD).
- Seuntjens, J. and Palmans, H. (1999) 'Correction factors and performance of a 4°C sealed water calorimeter.' *Phys. Med. Biol.* **44**, 627–646.
- Seuntjens, J. P. and DuSautoy, A. R. (2002) 'Review of calorimeter based absorbed dose to water standards,' pp. 37–66 in *Proc. Int. Symp. on Standards and Codes of Practice in Medical Radiation Dosimetry*. IAEA-CN-96 (International Atomic Energy Agency: Vienna).
- Seuntjens, J., Palmans, H., Verhaegen, F., Denis, J.-M., Vynckier, S. and Thierens, H. (1994) 'Water calorimetry for clinical proton beams,' in *Proc. NPL Calorimetry Workshop* (National Physical Laboratory: Teddington, UK).
- Shalev, S., Bartel, L., Therrien, P., Hahn, P. and Carey, M. (1988) 'The objective evaluation of alternative treatment plans: I. Images of regret.' *Int. J. Radiat. Oncol. Biol. Phys.* **15**, 763–767.
- Sharp, G. C., Kollipara, S., Madden, T., Jiang, S. B. and Rosenthal, S. (2005) 'Anatomic feature-based registration for patient setup in head and neck cancer radiotherapy.' *Phys. Med. Biol.* **50**, 4667–4679.
- Sheng, K., Jeraj, R., Shaw, R., Mackie, T. R. and Paliwal, B. R. (2005) 'Imaging dose management using multi-resolution in CT-guided radiation therapy.' *Phys. Med. Biol.* **50**, 1205–1219.
- Shipley, W. U., Tepper, J. E., Prout, G. R., Verhey, L. J., Mendiondo, O. A., Goitein, M., Koehler, A. M. and Suit, H. D. (1979) 'Proton radiation as boost therapy for localized prostatic carcinoma.' *J. Am. Med. Assoc.* **241**, 1912–1915.
- Shipley, W. U., Verhey, L. J., Munzenrider, J. E., Suit, H. D., Urie, M. M., McManus, P. L., Young, R. H., Shipley, J. W., Zietman, A. L., Biggs, P. J., Heney, N. M. and Goitein, M. (1995) 'Advanced prostate cancer: The results of a randomized comparative trial of high dose irradiation boosting with conformal protons compared with conventional dose irradiation using photons alone.' *Int. J. Radiat. Oncol. Biol. Phys.* **32**, 3–12.
- Siebers, J. V., DeLuca, P. M. Jr., Awschalom, M. and Coutrakon, G. (1988) 'Performance of a prototype range ionization chamber bombarded by 160 MeV protons.' Paper MPWP9.7, *World Congress on Medical Physics and Biomedical Engineering, San Antonio, TX*.
- Siebers, J. V., Vatnitsky, S. M., Miller, D. W. and Moyers, M. F. (1995) 'Deduction of the air w value in a therapeutic proton beam.' *Phys. Med. Biol.* **40**, 1339–1356.
- Sisterson, J. M. (2005) *Particles Newsletter*, Vol. **37** (Northeast Proton Therapy Center, Boston, MA).
- Sisterson, J. M., Urie, M. M., Koehler, A. M. and Goitein, M. (1989) 'Distal penetration of proton beams: the

REFERENCES

- effects of air gaps between compensating bolus and patient.' *Phys. Med. Biol.* **34**, 1309–1315.
- Sisterson, J. M., Cascio, E., Koehler, A. M. and Johnson, K. N. (1991) 'Proton beam therapy: Reliability of the synchrocyclotron at the Harvard Cyclotron Laboratory.' *Phys. Med. Biol.* **36**, 285–290.
- Skarsgard, L. D. (1998) 'Radiobiology with heavy charged particles: a historical review.' *Phys. Med.* **XIV** (Suppl. 1), 1–19.
- Slabbert, J. P., Jones, D. T. L., Schreuder, A. N., Jones, H. L., Symons, J. and Hough, J. H. (1994) 'Variations in biological effectiveness with depth in a 200 MeV proton beam,' pp. 103–106 in *NAC Annual Report, NAC/AR/94-1* (National Accelerator: Faure, South Africa).
- Slater, J. D., Slater, J. M. and Schulte, R. W. (1995) 'Proton beam therapy at Loma Linda University Medical Center: clinical experience of the first four years,' pp. 673–679 in *Proc. 5th Int. Meeting on Progress in Radio-Oncology (ICRO, OGRO 5), Salzburg, Austria* (Monduzzi Editore S.p.A.: Bologna, Italy).
- Slater, J. D., Rossi, C. J., Yonemoto, L. T., Bush, D. A., Jabola, B. R., Levy, R. P., Grove, R. I., Preston, W. and Slater, J. M. (2004) 'Proton therapy for prostate cancer: The initial Loma Linda University experience.' *Int. J. Radiat. Oncol. Biol. Phys.* **59**, 348–352.
- Smith, A. R. (2006) 'Proton therapy.' *Phys. Med. Biol.* **51**, R491–R504.
- Smith, A. R., Rosen, I. I. and Hogstrom, K. R. (1977) 'The silicon diode as an *in vivo* dosimeter for fast neutrons.' *Int. J. Radiat. Oncol. Biol. Phys.* **2**, 111–116.
- Soares, C. G. (2006) 'New developments in radiochromic film dosimetry.' *Radiat. Prot. Dosim.* **120**, 100–106.
- Spielberger, B., Scholz, M., Krämer, M. and Kraft, G. (2001) 'Experimental investigations of the response of films to heavy-ion irradiation.' *Phys. Med. Biol.* **46**, 2889–2897.
- Spielberger, B., Scholz, M., Krämer, M. and Kraft, G. (2002) 'Calculation of the x-ray film response to heavy charged particle irradiation.' *Phys. Med. Biol.* **47**, 4107–4120.
- Stavrev, P., Niemierko, A., Stavreva, N. and Goitein, M. (2001) 'The application of biological models to clinical data.' *Phys. Med.* **XV11**, 71–82.
- Stroom, J. C., de Boer, H. C. J., Huizenga, H. and Visser, A. G. (1999) 'Inclusion of geometrical uncertainties in radiotherapy treatment planning by means of coverage probability.' *Int. J. Radiat. Oncol. Biol. Phys.* **43**, 905–919.
- Suit, H. (2002) 'The Gray Lecture 2001: Coming technical advances in radiation oncology.' *Int. J. Radiat. Oncol. Biol. Phys.* **53**, 798–809.
- Suit, H. D. and Goitein, M. (1974) 'Dose-limiting tissues in relation to type and location of tumors: implications for efforts to improve radiation dose distributions.' *Eur. J. Cancer* **10**, 217–224.
- Suit, H. and Urie, M. (1992) 'Proton beams in radiation therapy.' *J. Natl. Cancer Inst.* **84**, 155–164.
- Suit, H. D. and Krengli, M. (1997) 'Basis for interest in proton beam radiation therapy,' pp. 29–37 in *Advances in Hadrontherapy*, Amaldi, U., Larsson, B. and Lemoigne, Y. Eds (Elsevier Science B. V: Amsterdam).
- Suit, H. D., Goitein, M., Tepper, J., Koehler, A. M., Schmidt, R. A. and Schneider, R. (1975) 'Exploratory study of proton radiation therapy using large field techniques and fractionated dose schedules.' *Cancer* **35**, 1646–1657.
- Suit, H., Goitein, M., Munzenrider, J., Verhey, L., Blitzer, P., Gragoudas, E., Koehler, A. M., Urie, M., Gentry, R., Shipley, W., Urano, M., Duttenhaver, J. and Wagner, M. (1982) 'Evaluation of the clinical applicability of proton beams in definitive fractionated radiation therapy.' *Int. J. Radiat. Oncol. Biol. Phys.* **8**, 2199–2205.
- Suit, H., Urie, M. and Efird, J. T. (1992) 'Proton beams in clinical radiation therapy.' *Principles Practice Oncol.* **6**, 1–15.
- Suit, H., Goldberg, S., Niemierko, A., Trofimov, A., Adams, J., Paganetti, H., Chen, G. T. Y., Bortfeld, T., Rosenthal, S., Loeffler, J. and Delaney, T. (2003) 'Proton beams to replace photon beams in radical dose treatments.' *Acta. Oncol.* **42**, 800–808.
- Sunaga, H., Agematsu, T., Tanaka, R., Yosida, K. and Kohno, I. (1988) 'Dosimetry by cellulose triacetate film dosimetry in proton-beam irradiation.' *Radioisotopes* **37**, 84–87 (in Japanese).
- Szymanowski, H. and Oelfke, U. (2003) 'CT calibration for two-dimensional scaling of proton pencil beams.' *Phys. Med. Biol.* **48**, 861–874.
- Tang, J. T., Inoue, T., Yamazaki, H., Fukushima, S., Fournier-Bidoz, N., Koizumi, M., Ozeki, S. and Hatanaka, K. (1997) 'Comparison of radiobiological effective depths in 65 MeV modulated proton beams.' *Br. J. Cancer* **76**, 220–225.
- Tatsuzaki, H. and Urie, M. (1991) 'Importance of precise positioning for proton beam therapy in the base of skull and cervical spine.' *Int. J. Radiat. Oncol. Biol. Phys.* **21**, 757–765.
- Tatsuzaki, H., Inada, T., Arimoto, T., Shimizu, T., Sato, S., Yaguchi, M. and Akisada, M. (1991) 'Early and late effects of fractionated 250 MeV proton beam irradiation on murine legs.' *J. Jpn. Soc. Ther. Radiat. Oncol.* **3**, 171–179.
- Tautfest, G. W. and Fechter, H. R. (1955) 'A nonsaturable high-energy beam monitor.' *Rev. Sci. Instrum.* **26**, 229–231.
- Terahara, A., Niemierko, A., Goitein, M., Finkelstein, D., Hug, E., Liebsch, N., O'Farrell, D., Lyons, S. and Munzenrider, J. (1999) 'Analysis of the relationship between tumor dose inhomogeneity and local control in patients with skull base chordoma.' *Int. J. Radiat. Oncol. Biol. Phys.* **45**, 351–358.
- Terunuma, T., Sakae, T., Nohtomi, A. and Tsunashima, Y. (2003) 'The direct measurement using an imaging plate for coincidence of radiation centre and laser position in external radiation therapy.' *Phys. Med. Biol.* **48**, N59–N63.
- Thomas, L. H. (1938) 'The paths of ions in the cyclotron. I. Orbits in the magnetic field.' *Phys. Rev.* **54**, 580–588.

- Tobias, C. A., Anger, H. O. and Lawrence, J. H. (1952) 'Radiological use of high energy deuterons and alpha particles.' *Am. J. Roentgenol. Rad. Ther. Nucl. Med.* **67**, 1–27.
- Tobias, C. A., Van Dyke, D. C., Simpson, M. E., Anger, H. O., Huff, R. L. and Koneff, A. A. (1954) 'Irradiation of the pituitary of the rat with high energy deuterons.' *Am. J. Roentgenol. Rad. Ther. Nucl. Med.* **72**, 1–21.
- Tobias, C. A., Roberts, J. E., Lawrence, J. H., Low-Beer, B. V. A., Anger, H. O., Born, J. L., McCombs, R. and Huggins, C. (1955) 'Irradiation hypophysectomy and related studies using 340-MeV protons and 190-MeV deuterons,' pp. 95–105 in *Proc. Int. Conf. on Peaceful Uses of Atomic Energy, Geneva, Switzerland*.
- Tobias, C. A., Lawrence, J. H., Born, J. L., McCombs, R. K., Roberts, J. E., Anger, H. O., Low-Beer, B. V. A. and Huggins, C. B. (1958) 'Pituitary irradiation with high-energy proton beams: A preliminary report.' *Cancer Res.* **18**, 121–139.
- Tourovsky, A., Lomax, A. J., Schneider, U. and Pedroni, E. (2005) 'Monte Carlo dose calculations for spot scanned proton therapy.' *Phys. Med. Biol.* **50**, 971–981.
- Trump, M. A. and Pinkerton, A. P. (1967) 'Application of PN junction diodes to the measurement of dose distribution of high energy radiation.' *Phys. Med. Biol.* **12**, 573–576.
- Tsai, Y.-S. (1974) 'Pair production and bremsstrahlung of charged leptons.' *Rev. Mod. Phys.* **46**, 815–851.
- Tsunashima, Y., Sakae, T., Shioyama, Y., Kagei, K., Terunuma, T., Nohtomi, A. and Akine, Y. (2004) 'Correlation between the respiratory waveform measured using a respiratory sensor and 3D tumor motion in gated radiotherapy.' *Int. J. Radiat. Oncol. Biol. Phys.* **60**, 951–958.
- UICC (1997) International Union against Cancer. *TNM Classification of Malignant Tumors*, 5th edn, Sabin, L. H. and Wittekind, C. Eds (Wiley-Liss and Sons, Inc.: New York).
- Ulmer, W. and Kaissl, W. (2003) 'The inverse problem of a Gaussian convolution and its application to the finite size of the measurement chambers/detectors in photon and proton dosimetry.' *Phys. Med. Biol.* **48**, 707–727.
- Urie, M. M. and Goitein, M. (1989) 'Variable versus fixed modulation of proton beams for treatments in the cranium.' *Med. Phys.* **16**, 593–601.
- Urie, M., Goitein, M. and Wagner, M. (1984) 'Compensating for heterogeneities in proton radiation therapy.' *Phys. Med. Biol.* **29**, 553–566.
- Urie, M., Goitein, M., Holley, W. R. and Chen, G. T. Y. (1986a) 'Degradation of the Bragg peak due to inhomogeneities.' *Phys. Med. Biol.* **31**, 1–15.
- Urie, M. M., Sisteron, J. M., Koehler, A. M., Goitein, M. and Zoesman, J. (1986b) 'Proton beam penumbra: Effects of separation between patient and beam modifying devices.' *Med. Phys.* **13**, 734–741.
- Urie, M., Goitein, M., Doppke, K., Kutcher, J. G., LoSasso, T., Mohan, R., Munzenrider, J. E., Sontag, M. and Wong, J. W. (1991) 'The role of uncertainty analysis in treatment planning.' *Int. J. Radiat. Oncol. Biol. Phys.* **21**, 91–107.
- Uusi-Simola, J., Savolainen, S., Kangasmäki, A., Heikkinen, S., Perkiö, J., Abo Ramadan, U., Seppälä, T., Karila, J., Serén, T., Kotiluoto, P., Sorvari, P. and Auterinen, I. (2003) 'Study of the relative dose-response of BANG-3® polymer gel dosimeters in epithermal neutron irradiation.' *Phys. Med. Biol.* **48**, 2895–2906.
- van Herk, M. (2004) 'Errors and margins in radiotherapy.' *Semin. Radiat. Oncol.* **14**, 52–64.
- van Herk, M., Remeijer, P., Rasch, C. and Lebesque, J. V. (2000) 'The probability of correct target dosage: dose population histograms for deriving treatment margins in radiotherapy.' *Int. J. Radiat. Oncol. Biol. Phys.* **47**, 1121–1135.
- van Luijk, P., van't Veld, A. A., Zelle, H. D. and Schippers, J. M. (2001) 'Collimator scatter and 2D dosimetry in small proton beams.' *Phys. Med. Biol.* **46**, 653–670.
- van Luijk, P., Delvigne, T. C., Schilstra, C. and Schippers, J. M. (2003) 'Estimation of parameters of dose-volume models and their confidence limits.' *Phys. Med. Biol.* **48**, 1863–1884.
- van't Riet, A., Mak, A. C., Moerland, M. A., Elders, L. H. and van der Zee, W. (1997) 'A conformation number to quantify the degree of conformality in brachytherapy and external beam irradiation: Application to the prostate.' *Int. J. Radiat. Oncol. Biol. Phys.* **37**, 731–736.
- Vatnitsky, S. M. (1997) 'Radiochromic film dosimetry for clinical proton beams.' *Appl. Radiat. Isot.* **48**, 643–651.
- Vatnitsky, S. and Järvinen, H. (1993) 'Application of a natural diamond detector for the measurement of relative dose distributions in radiotherapy.' *Phys. Med. Biol.* **38**, 173–184.
- Vatnitsky, S. M. and Andreo, P. (2002) 'Codes of practice and protocols for the dosimetry in reference conditions of proton and ion beams,' pp. 279–294 in *Proc. Int. Symp. on Standards and Codes of Practice in Medical Radiation Dosimetry*. IAEA-CN-96 (International Atomic Energy Agency, Vienna).
- Vatnitsky, S. M., Khrunov, V. S., Fominych, V. I. and Schuele, E. (1993) 'Diamond detector dosimetry for medical applications.' *Radiat. Prot. Dosim.* **47**, 515–518.
- Vatnitsky, S. M., Miller, D. W., Siebers, J. and Moyers, M. (1995) 'Application of solid state detectors for dosimetry of therapeutic proton beams.' *Med. Phys.* **22**, 469–473.
- Vatnitsky, S. M., Siebers, J. V. and Miller, D. W. (1996a) ' k_Q factors for ionization chamber dosimetry in clinical proton beams.' *Med. Phys.* **23**, 25–31.
- Vatnitsky, S., Siebers, J., Miller, D., Moyers, M., Schaefer, M., Jones, D., Vynckier, S., Hayakawa, Y., Delacroix, S., Isacsson, U., Medin, J., Kacperek, A., Lomax, A., Coray, A., Kluge, H., Heese, J., Verhey, L., Daftari, I., Gall, K., Lam, G., Beck, T. and Hartmann, G. (1996b) 'Proton dosimetry intercomparison.' *Radiother. Oncol.* **41**, 169–177.

REFERENCES

- Vatnitsky, S. M., Schulte, R. W. M., Galindo, R., Meinass, H. J. and Miller, D. W. (1997) 'Radiochromic film dosimetry for verification of dose distributions delivered with proton-beam radiosurgery.' *Phys. Med. Biol.* **42**, 1887–1898.
- Vatnitsky, S. M., Miller, D. W., Moyers, M. F., Levy, R. P., Schulte, R. W., Slater, J. D. and Slater, J. M. (1999a) 'Dosimetry techniques for narrow proton beam radiosurgery.' *Phys. Med. Biol.* **44**, 2789–2801.
- Vatnitsky, S., Moyers, M., Miller, D., Abell, G., Slater, J. M., Pedroni, E., Coray, A., Mazal, A., Newhauser, W., Jaekel, O., Heese, J., Fukumura, A., Futami, Y., Verhey, L., Daftari, I., Grusell, E., Molokanov, A. and Bloch, C. (1999b) 'Proton dosimetry intercomparison based on the ICRU Report 59 protocol.' *Radiother. Oncol.* **51**, 273–379.
- Vatnitsky, S. M., Moyers, M. F. and Vatnitsky, A. S. (2002) 'Parallel-plate and thimble ionization chamber calibrations in proton beams using the TRS 398 and ICRU 59 recommendations,' pp. 327–336 in *Proc. Int. Symp. on Standards and Codes of Practice in Medical Radiation Dosimetry*. IAEA-CN-96 (International Atomic Energy Agency, Vienna).
- Verhaegen, F. and Palmans, H. (2001) 'A systematic Monte Carlo study of secondary electron fluence perturbation in clinical proton beams (70–250 MeV) for cylindrical and spherical ion chambers.' *Med. Phys.* **28**, 2088–2095.
- Verhey, L. J. and Munzenrider, J. E. (1982) 'Proton beam therapy.' *Ann. Rev. Biophys. Bioeng.* **11**, 331–357.
- Verhey, L. J. and Lyman, J. T. (1992) 'Some considerations regarding w values for heavy charged-particle radiotherapy.' *Med. Phys.* **19**, 151–153.
- Verhey, L. and Bentel, G. (1999) 'Patient immobilization,' pp. 53–94 in *The Modern Technology of Radiation Oncology*, Van Dyk, J. Ed. (Medical Physics Publishing: Madison, WI).
- Verhey, L. J., Koehler, A. M., McDonald, J. C., Goitein, M., Ma, I-C., Schneider, R. J. and Wagner, M. (1979) 'The determination of absorbed dose in a proton beam for purposes of charged-particle radiation therapy.' *Radiat. Res.* **79**, 34–54.
- Verhey, L. J., Goitein, M., McNulty, P., Munzenrider, J. E. and Suit, H. D. (1982) 'Precise positioning of patients for radiation therapy.' *Int. J. Radiat. Oncol. Biol. Phys.* **8**, 289–294.
- von Essen, C. F., Blattmann, H., Crawford, J. F., Fessenden, P., Pedroni, E., Perret, C., Salzmann, M., Shortt, K. and Walder, E. (1982) 'The PIOTRON, initial performance, preparation and experience with pion therapy.' *Int. J. Radiat. Oncol. Biol. Phys.* **8**, 1499–1509.
- Vynckier, S. (1995) 'Dosimetry techniques for ion beams,' in *Ion Beams in Tumor Therapy*, Linz, U. Ed. (Chapman and Hall: Weinheim, Germany) pp. 246–255.
- Vynckier, S. (2004) 'Dosimetry of clinical neutron and proton beams: an overview of recommendations.' *Radiat. Prot. Dosim.* **110**, 565–572.
- Vynckier, S., Meulders, J.-P., Robert, P. and Wambersie, A. (1984) 'The protontherapy program at the cyclotron 'Cyclone' of Louvain-la-Neuve (first dosimetric results).' *J. Eur. Radiother.* **3**, 245–247.
- Vynckier, S., Bonnett, D. E. and Jones, D. T. L. (1991) 'Code of practice for clinical proton dosimetry.' *Radiother. Oncol.* **20**, 53–63.
- Vynckier, S., Derreumaux, S., Richard, F., Bol, A., Michel, C. and Wambersie, A. (1993) 'Is it possible to verify directly a proton-treatment plan using positron emission tomography?' *Radiother. Oncol.* **26**, 275–277.
- Vynckier, S., Bonnett, D. E. and Jones, D. T. L. (1994) 'Supplement to the code of practice for clinical proton dosimetry.' *Radiother. Oncol.* **32**, 174–179.
- Wagner, M. S. (1982) 'Automated range compensation for proton therapy.' *Med. Phys.* **9**, 749–752.
- Wagner, W. and Pruss, A. (2002) 'The IAPWS formulation 1995 for the thermodynamic properties of ordinary water substance for general and scientific use.' *J. Phys. Chem. Ref. Data* **31**, 387–535.
- Waligórski, M. P. R., Dania, G., Loh, K. S. and Katz, R. (1989) 'The response of the alanine detector after charged-particle and neutron irradiations.' *Appl. Radiat. Isot.* **40**, 923–933.
- Wambersie, A. and Battermann, J. J. (1995) 'Socio-economic aspects of ion beam therapy,' pp. 24–32 in *Ion Beams in Tumor Therapy*, Linz, U. Ed (Chapman and Hall: Weinheim, Germany).
- Wambersie, A., Auberger, T., Gahbauer, R. A., Jones, D. T. L. and Pötter, R. (1999) 'A challenge for high-precision radiation therapy: the case for hadrons.' *Strahlenther. Onkol.* **175** (Suppl. II), 122–128.
- Wambersie, A., Menzel, H., Gahbauer, R., DeLuca, P. and Whitmore, G. (2002) 'RBE and harmonization in prescribing, recording and reporting hadron therapy,' pp. 361–371 in *Progress in Radiation Oncology VII*, Kogelnik, H. D., Lukas, P. and Sedlmayer, F. Eds (Mondazzi Editore S.p.A.: Bologna, Italy).
- Wambersie, A., Gahbauer, R. A. and Menzel, H. G. (2004a) 'RBE and weighting of absorbed dose in ion-beam therapy.' *Radiother. Oncol.* **73** (Suppl. 2), S176–S182.
- Wambersie, A., Guelette, J., Jones, D. T. L. and Gahbauer, R. (2004b) 'Ion-beam therapy: rationale, achievements, and expectations,' pp. 743–784 in *Charged Particle and Photon Interactions with Matter*, Mozumder, A. and Hatano, Y. Eds (Marcel Dekker, Inc.: New York).
- Wambersie, A., Hendry, J. H., Andreo, P., DeLuca, P. M., Gahbauer, R., Menzel, H. and Whitmore, G. (2006) 'The RBE issues in ion-beam therapy: conclusions of a joint IAEA/ICRU working group regarding quantities and units.' *Radiat. Prot. Dosim.* **122**, 463–470.
- Webb, S. (1994) 'Optimum parameters in a model for tumour control probability including inter-patient heterogeneity.' *Phys. Med. Biol.* **39**, 1895–1914.
- Weber, D. C., Trofimov, A. V., Delaney, T. F. and Bortfeld, T. (2004) 'A treatment planning comparison of intensity modulated photon and proton therapy for paraspinal sarcomas.' *Int. J. Radiat. Oncol. Biol. Phys.* **58**, 1596–1606.

- Weinhous, M. S. and Meli, J. A. (1984) 'Determining P_{ion} , the correction factor for recombination losses in an ionization chamber.' *Med. Phys.* **11**, 846–849.
- Welsh, J. S., Patel, R. R., Ritter, M. A., Harari, P. M., Mackie, T. R. and Mehta, M. P. (2002) 'Helical tomotherapy: an innovative technology and approach to radiation therapy.' *Technol. Cancer Res. Treat.* **1**, 311–316.
- Weyrather, W. K., Ritter, S., Scholz, M. and Kraft, G. (1999) 'RBE for carbon track-segment irradiation in cell lines of differing repair capacity.' *Int. J. Radiat. Biol.* **75**, 1357–1364.
- Wieser, A., Lettau, C., Fill, U. and Regulla, D. F. (1993) 'The influence of non-radiation induced ESR background signal from paraffin-alanine probes for dosimetry in the radiotherapy dose range.' *Appl. Radiat. Isot.* **44**, 59–65.
- Wilkins, D., Li, X. A., Cygler, J. and Gerig, L. (1997) 'The effect of dose rate dependence of *p*-type silicon detectors on linac relative dosimetry.' *Med. Phys.* **24**, 879–891.
- Wilson, R. R. (1946) 'Radiological use of fast protons.' *Radiol.* **47**, 487–491.
- Withers, H. R., Taylor, J. M. and Maciejewski, B. (1988) 'Treatment volume and tissue tolerance.' *Int. J. Radiat. Oncol. Biol. Phys.* **14**, 751–759.
- Wong, J. W., Sharpe, M. B., Jaffray, D. A., Kini, V. R., Robertson, J. M., Stromberg, J. S. and Martinez, A. A. (1999) 'The use of active breathing control (ABC) to reduce margin for breathing motion.' *Int. J. Radiat. Oncol. Biol. Phys.* **44**, 911–919.
- Wouters, B. G., Lam, G. K. Y., Oelfke, U., Gardey, K., Durand, R. E. and Skarsgard, L. D. (1996) 'Measurements of relative biological effectiveness of the 70 MeV proton beam at TRIUMF using Chinese hamster V79 cells and the high-precision cell sorter assay.' *Radiat. Res.* **146**, 159–170.
- Wroe, A. J., Cornelius, I. M. and Rosenfeld, A. B. (2005) 'The role of nonelastic reactions in absorbed dose distributions from therapeutic proton beams in different medium.' *Med. Phys.* **32**, 37–41.
- Wroe, A., Rosenfeld, A. and Schulte, R. (2007) 'Out-of-field dose equivalents delivered by proton therapy of prostate cancer.' *Med. Phys.* **34**, 3449–3456.
- Wulf, J., Guckenberger, M., Haedinger, U., Oppitz, U., Mueller, G., Baier, K. and Flentje, M. (2006) 'Stereotactic radiotherapy of primary liver cancer and hepatic metastases.' *Acta Oncol.* **45**, 838–847.
- Yamada, Y., Lovelock, D. M., Yenice, K. M., Bilsky, M. H., Hunt, M. A., Zatcky, J. and Leibel, S. A. (2005) 'Multifractionated image-guided and stereotactic intensity-modulated radiotherapy of paraspinal tumors: A preliminary report.' *Int. J. Radiat. Oncol. Biol. Phys.* **62**, 53–61.
- Yan, X., Titt, U., Koehler, A. M. and Newhauser, W. D. (2002) 'Measurements of neutron dose equivalent to proton therapy patients outside of the proton radiation field.' *Nucl. Instrum. Methods Phys. Res.* **A476**, 429–434.
- York, E. D. (2003) 'Biological indices for evaluation and optimization of IMRT,' in *Intensity Modulated Radiation Therapy: The State of the Art*, Palta, J. R. and Mackie, T. R. Eds (Medical Physics Publishing, Madison, WI).
- Zankowski, C., Vatnitsky, S., Siebers, J. and Podgorsak, E. B. (1998) 'Proton beam output measurement with an extrapolation chamber.' *Med. Dosim.* **23**, 288–291.
- Zeidan, O. A., Stephenson, S. A. L., Meeks, S. L., Wagner, T. H., Willoughby, T. R., Kupelian, P. A. and Langen, K. M. (2006) 'Characterization and use of EBT radiochromic film for IMRT dose verification.' *Med. Phys.* **33**, 4064–4072.
- Zelefsky, M. J., Chan, H., Hunt, M., Yamada, Y., Shippy, A. M. and Amols, H. (2006) 'Long-term outcome of high dose intensity modulated radiation therapy for patients with clinically localized prostate cancer.' *J. Urol.* **176**, 1415–1419.
- Ziegler, J. F., Saunders, P. A. and Zabel, T. H. (1996) 'Portable Faraday cup for non vacuum proton beams.' *IBM J. Res. Develop.* **40**, 73–76.
- Zietman, A. L., DeSilvio, M. L., Slater, J. D., Rossi, C. J. Jr., Miller, D. W., Adams, J. A. and Shipley, W. U. (2005) 'Comparison of conventional-dose vs. high-dose conformal radiation therapy in clinically localized adenocarcinoma of the prostate: a randomized controlled trial.' *J. Am. Med. Assoc.* **294**, 1233–1239.
- Zurlo, A., Lomax, A., Hoess, A., Bortfeld, T., Russo, M., Goitein, G., Valentini, V., Marucci, L., Capparella, R. and Loasses, A. (2000) 'The role of proton therapy in the treatment of large irradiation volumes: A comparative planning study of pancreatic and biliary tumors.' *Int. J. Radiat. Oncol. Biol. Phys.* **48**, 277–288.